

Exploring the Molecular Mechanisms of Aphid and Thrips Perception in *Arabidopsis thaliana*

Joshua Robert Joyce

A thesis submitted for the degree of Doctor of Philosophy
University of East Anglia
John Innes Centre
March 2023

This copy of the thesis has been supplied on condition that anyone who consults it is understood to recognise that its copyright rests with the author and that use of any information derived therefrom must be in accordance with current UK Copyright Law. In addition, any quotation or extract must include full attribution.

This page is intentionally left blank.

Abstract

Plants have evolved sophisticated mechanisms to perceive biotic stresses and launch appropriate defence responses that safeguard their health. Aphids and thrips can threaten plant health both as herbivores and as vectors of plant viruses. Despite this, the mechanisms by which plants perceive localised feeding from these insects are not well characterised. Therefore, the work described in this thesis aimed to investigate how plants perceive feeding by aphids and thrips. To achieve this goal, methods were developed to investigate plant responses to localised stimuli by visualising fluorescent reporters expressed in *Arabidopsis thaliana*. These methods revealed that feeding from the aphid species *Myzus persicae* induces intracellular Ca^{2+} concentration ($[\text{Ca}^{2+}]$) increases which are altered in *A. thaliana* carrying mutations in both *GLUTAMATE RECEPTOR-LIKE (GLR) 3.3* and *3.6*. Reporter imaging with localised wound and touch stimuli explored how the GLR3.3 and 3.6 Ca^{2+} -permeable channels might function in damage or mechanical stress perception during localised insect feeding. GLR3.3 alone contributed to the wound-induced $[\text{Ca}^{2+}]$ elevations whilst neither channel functioned in responses to touch. Further reporter imaging of wound- and touch-induced responses investigated the role of apoplastic pH and glutamate in regulating GLR3.3 and revealed that localised GLR3.3 activation promotes jasmonate-mediated defence gene expression. GLR3.3 also functioned in responses to feeding by a thrips species, *Frankliniella occidentalis*, as well as by the aphid species *M. persicae*, *Rhopalosiphum padi* and *Brevicoryne brassicae*. The contribution of GLR3.3 to the responses induced by each species appeared to differ, potentially due to differences in insect feeding behaviour or effector activity. A reverse genetics approach evaluated additional candidate genes for their potential to contribute to aphid or thrips perception in *A. thaliana*. Through characterising GLR3.3 function in responses to localised wounding, touch, aphid feeding and thrips feeding, this thesis significantly advances the understanding of how plants perceive aphids and thrips.

Access Condition and Agreement

Each deposit in UEA Digital Repository is protected by copyright and other intellectual property rights, and duplication or sale of all or part of any of the Data Collections is not permitted, except that material may be duplicated by you for your research use or for educational purposes in electronic or print form. You must obtain permission from the copyright holder, usually the author, for any other use. Exceptions only apply where a deposit may be explicitly provided under a stated licence, such as a Creative Commons licence or Open Government licence.

Electronic or print copies may not be offered, whether for sale or otherwise to anyone, unless explicitly stated under a Creative Commons or Open Government license. Unauthorised reproduction, editing or reformatting for resale purposes is explicitly prohibited (except where approved by the copyright holder themselves) and UEA reserves the right to take immediate 'take down' action on behalf of the copyright and/or rights holder if this Access condition of the UEA Digital Repository is breached. Any material in this database has been supplied on the understanding that it is copyright material and that no quotation from the material may be published without proper acknowledgement.

Table of Contents

Abstract	3
Table of Contents	4
List of Figures	9
List of Tables	13
List of Accompanying Material	14
Common Abbreviations	15
Definitions for Key Terms	17
Acknowledgements	19
1. General Introduction	20
1.1. Plant defence responses to biotic stresses	21
1.1.1. Introduction to plant immunity.....	21
1.1.2. Diversity in biotic stresses and specificity in responses.....	22
1.1.3. Perceiving biotic stress at the plasma membrane	23
1.1.4. Communicating the perception of a biotic stress	27
1.1.5. Hormone signalling in plant responses to biotic attackers	35
1.1.6. Effectors and ETI.....	41
1.1.7. Plant defence outputs	44
1.1.8. Summary of general plant defence responses to biotic stress	45
1.2. Plant defence responses to insect pests	45
1.2.1. Lepidopteran larvae: Chewing insects that cause large-scale damage.....	45
1.2.2. Thrips: Minute pests that exhibit damage-based feeding on a local scale	48
1.2.3. Aphids: Phloem feeding pests that minimise cell damage for sustained feeding	53
1.3. Investigations of this thesis	60
1.4. Contributions to this thesis	61
2. Materials and Methods	63
2.1. Plant materials, growth conditions and generation of new material	64
2.1.1. Plant materials and growth conditions	64
2.1.2. Crossing <i>A. thaliana</i>	65
2.1.3. Methyl-jasmonate treatment.....	70
2.1.4. DNA extractions and genotyping.....	70
2.1.5. Protein extractions and visualisation of GCaMP3	73
2.2. Insect rearing and resistance assays	73
2.2.1. Stock insect colony maintenance.....	74
2.2.2. <i>Myzus persicae</i> fecundity assays.....	74
2.2.3. <i>B. brassicae</i> fecundity assays	74

2.2.4. <i>R. padi</i> survival assays.....	74
2.2.5. Thrips damage assays	75
2.2.6. Insect rearing for microscopy experiments	75
2.3. Assessing stimulus-induced responses in <i>A. thaliana</i> by imaging genetically encoded fluorescent reporters.....	76
2.3.1. Plant preparation for fluorescence microscopy	76
2.3.2. Aphid and thrips treatment	77
2.3.3. Micropipette wounding	78
2.3.4. Touch treatment.....	78
2.3.5. Fluorescence microscopy imaging.....	79
2.3.6. Microscopy data analyses – Signalling reporters	81
2.3.7. Microscopy data analyses – Expression reporters	85
2.4. Assessing aphid extract-induced <i>A. thaliana</i> responses by plate reader measurements of genetically encoded fluorescent reporters.....	86
2.4.1. Preparation of aphid extract.....	86
2.4.2. Plant preparation.....	86
2.4.3. Treatment, fluorescence intensity measurements and analyses.....	86
2.5. Data handling and presentation	87
2.6. Reporter signal modelling.....	88
3. Developing the Foundations for Exploring the Perception of Aphid and Thrips Feeding in <i>A. thaliana</i> with Genetically Encoded Fluorescent Reporters	89
3.1. Introduction	90
3.1.1. Considerations for genetically encoded reporter imaging	90
3.1.2. Insights into aphid feeding-induced [Ca ²⁺] elevations established with GECs	92
3.1.3. Current investigations.....	93
3.2. Results.....	94
3.2.1. Previous conclusions implicating BAK1, GLR3.3/3.6 and TPC1 in aphid feeding-induced [Ca ²⁺] elevations are compromised by differences in reporter expression	94
3.2.2. Empirically assessing the effect of variation in reporter expression on normalised GCaMP3 signals and whether background corrections can offset any effects	96
3.2.3. Modelling highlights the benefit of background corrections in limiting the effects of variable intensimetric and ratiometric reporter expression on normalised signals	104
3.2.4. <i>M. persicae</i> feeding-induced [Ca ²⁺] elevations are not altered in <i>tpc1-2 A. thaliana</i>	111
3.2.5. <i>M. persicae</i> feeding-induced [Ca ²⁺] elevations are not altered in <i>bak1-5</i> mutant <i>A. thaliana</i>	113

3.2.6. <i>M. persicae</i> feeding-induced [Ca ²⁺] elevations are partially dependent on GLR3.3/GLR3.6	115
3.3. Discussion	117
3.3.1. Causes and lessons: What has been learnt from investigating the effects of variation in fluorescent reporter expression on normalised reporter signals?	117
3.3.2. Reassessing the role of BAK1, TPC1 and GLR3.3/3.6 in aphid-plant interactions.....	120
4. Exploring the Mechanisms of Localised Wound and Touch Perception and the Contributions of GLR3.3/3.6	123
4.1. Introduction.....	124
4.1.1. GLR3.3/3.6 contribute to various biological processes including responses to large-scale damage and touch.....	124
4.1.2. What factors determine GLR3.3/3.6 activation?	125
4.1.3. How do GLR3.3/3.6 contribute to plant defence responses?	127
4.1.4. Current investigations	128
4.2. Results	130
4.2.1. The dynamics of wound-induced [Ca ²⁺] elevations are altered on <i>glr3.3a</i> mutants	130
4.2.2. Water infiltration perturbs wound-induced [Ca ²⁺] elevations and provides insights into the underlying signalling mechanisms.....	133
4.2.3. Micropipette wounding induces iGluSnFR and apo-pHusion signals that are spatiotemporally correlated with GCaMP3 reporter signals	135
4.2.4. Wound-induced apo-pHusion and iGluSnFR signals are altered in <i>glr3.3a</i> mutants	140
4.2.5. Wounding induces JA marker gene expression that shows partial dependency on GLR3.3	143
4.2.6. Touch induces GLR3.3-independent [Ca ²⁺] elevations similar to those induced by wounding in <i>glr3.3a</i> mutants	148
4.2.7. Touch can induce iGluSnFR and apo-pHusion signals that are associated with the touch-induced GCaMP3 signals.....	151
4.2.8. Localised touch treatment does not induce <i>JAZ10</i> or <i>AOS</i> expression.....	156
4.3. Discussion	157
4.3.1. How could mechanical stress trigger burst [Ca ²⁺] elevations?.....	158
4.3.2. How is GLR3.3 permeability regulated in localised wound-induced responses?.....	159
4.3.3. What determines the extent of GLR3.3 activation in localised responses?	161
4.3.4. What drives secondary [Ca ²⁺] elevations?.....	163
4.3.5. Do localised GLR3.3-dependent responses contribute to plant defences?	164
4.3.6. A model for mechanical stress perception and GLR3.3 activation in responses to localised wounding and touch.....	165

5. Exploring the Role of GLR3.3 in the Perception of Aphid and Thrips Feeding	168
5.1. Introduction	169
5.2. Results.....	172
5.2.1. GLR3.3 contributes to [Ca ²⁺] elevations induced by <i>M. persicae</i> feeding	172
5.2.2. <i>R. padi</i> and <i>B. brassicae</i> feeding induces localised [Ca ²⁺] elevations in <i>A. thaliana</i> that are altered in <i>glr3.3a</i> mutants.....	176
5.2.3. <i>F. occidentalis</i> feeding induces localised GLR3.3-dependent [Ca ²⁺] elevations in <i>A. thaliana</i>	179
5.2.4. Localised feeding from aphids and thrips induces iGluSnFR and apo-pHusion reporter signals associated with the GCaMP3 signals	181
5.2.5. Localised feeding from the aphid and thrips species differentially induces JA marker gene expression	185
5.2.6. GLR3.3 contributes to limiting <i>R. padi</i> survival and <i>F. occidentalis</i> feeding but does not impact <i>M. persicae</i> or <i>B. brassicae</i> fecundity	190
5.3. Discussion.....	193
5.3.1. How is GLR3.3 activity regulated in responses to localised insect feeding?	194
5.3.2. Why does localised feeding from the different insect species differentially activate GLR3.3?	194
5.3.3. How could GLR3.3 contribute to <i>A. thaliana</i> resistance against aphids and thrips?	196
5.3.4. A piece in the puzzle of aphid and thrips perception in <i>A. thaliana</i>	197
6. Screening Candidate Genes for Their Potential to Contribute to the Perception of Aphid or Thrips Feeding in <i>A. thaliana</i>	200
6.1. Introduction	201
6.1.1. Candidate genes selected for their potential to regulate GLR3.3 activity.....	201
6.1.2. Candidate genes investigated for their contributions to large-scale wound-induced rapid systemic signalling	202
6.1.3. Candidate genes for perceiving mechanical stress during thrips or aphid feeding..	204
6.1.4. Candidates genes selected for their role in damage perception.....	205
6.1.5. Candidate genes that function in perceiving putative aphid HAMPs.....	207
6.1.6. Screening components for their potential to contribute to aphid or thrips feeding-induced responses	208
6.2. Results.....	210
6.2.1. Screening candidate mutants for a phenotype in wound- or touch-induced responses	210
6.2.2. Aphid extract induces [Ca ²⁺] elevations in <i>A. thaliana</i>	217

6.2.3. BAK1 and SOBIR1 contribute to aphid extract-induced [Ca ²⁺] elevations which are GLR3.1/3.3/3.6-independent	218
6.2.4. BAK1 does not appear to contribute to <i>M. persicae</i> feeding-induced [Ca ²⁺] elevations in the <i>glr3.3a</i> background	222
6.2.5. SOBIR1 does not appear to contribute to <i>M. persicae</i> feeding-induced [Ca ²⁺] elevations in the Col-0 or <i>glr3.3a</i> background	224
6.3. Discussion	227
6.3.1. Outstanding candidates components for functioning in localised damage or mechanical stress perception in <i>A. thaliana</i>	228
6.3.2. Limitations of the reverse genetics approach.....	230
6.3.3. Alternative approaches to reverse genetics	232
6.3.4. The search can continue.....	233
7. General Discussion	234
7.1. Summary and Discussion of Research Findings.....	235
7.1.1. Developing methods for investigating plant responses to localised stimuli.....	235
7.1.2. GLR3.3 functions in localised wound-induced responses	237
7.1.3. GLR3.3 functions in responses to localised feeding from aphids and thrips	241
7.1.4. The search for additional components involved in the perception of aphid or thrips feeding.....	245
7.2. Focus for future investigations.....	246
7.2.1. What determines GLR3.3 activation <i>in planta</i> ?	246
7.2.2. How significant is GLR3.3 in promoting JA-mediated defence responses to localised stimuli?	249
7.2.3. What is the contribution of GLR3.3 to the perception of feeding from other insect pests?	249
7.2.4. What other components contribute to the perception of aphid and thrips feeding?	250
7.3. Conclusions.....	250
Appendix I	252
Reference List	284

List of Figures

Figure 1.1 Zig-zag model of plant immunity.	22
Figure 1.2 Examples of the mechanisms for plasma membrane perception of pests and pathogens.	27
Figure 1.3 Generalised overview of plant Ca ²⁺ signalling components.	33
Figure 1.4 Model for large-scale wound-induced rapid systemic signalling upstream of <i>de novo</i> JA biosynthesis.	40
Figure 1.5 Model of resistosome and Ca ²⁺ -permeable channel formation by NLRs.	43
Figure 1.6 Thrips feeding model and scar damage.	50
Figure 1.7 Model of aphid feeding.	55
Figure 2.1 Arrangement of isolated <i>A. thaliana</i> leaves for Axio Zoom.V16 imaging.	79
Figure 2.2 Demonstration of signalling reporter analyses in response to micropipette wounding and <i>M. persicae</i> feeding.	83
Figure 3.1 Mutant <i>35S::GCaMP3 A. thaliana</i> lines investigated in Vincent <i>et al.</i> (2017a) had reduced baseline fluorescence intensities compared to their wild-type counterparts.	95
Figure 3.2 Selected Col-0 and <i>tpc1-2 A. thaliana</i> lines expressing <i>GCaMP3</i> with different expression levels and fluorescence intensities.	98
Figure 3.3 Assessing the effect of <i>GCaMP3</i> reporter expression differences on wound-induced non-corrected normalised reporter signals in the Col-0 and <i>tpc1-2</i> lines.	100
Figure 3.4 Background correction offsets the effects of differences in <i>GCaMP3</i> expression on $\Delta F/F_0$ amplitude.	102
Figure 3.5 Local wound-induced <i>GCaMP3</i> signals display similar properties in Col-0 and <i>tpc1-2 A. thaliana</i> leaves.	103
Figure 3.6 Modelling the effect of variation in reporter expression on non-corrected $\Delta F/F_0$ values.	105
Figure 3.7 Modelling how background corrections can offset the effects of variation in reporter expression on $\Delta F/F_0$ traces.	106
Figure 3.8 The effect of variation in reporter expression on the underestimation of $\Delta F/F_0$	107
Figure 3.9 Background correction does not alter the signal-to-noise ratio but does amplify variation in $\Delta F/F_0$	108

Figure 3.10 Modelling the effects of variation in reporter expression on signals detected from the ratiometric apo-pHusion reporter.	110
Figure 3.11 Properties of <i>M. persicae</i> feeding-induced GCaMP3 signals in Col-0 and <i>tpc1-2 A. thaliana</i>	112
Figure 3.12 Properties of <i>M. persicae</i> feeding-induced GCaMP3 signals in Col-0 and <i>bak1-5 A. thaliana</i>	114
Figure 3.13 Properties of <i>M. persicae</i> feeding-induced GCaMP3 signals in Col-0 and <i>glr3.3a glr3.6a A. thaliana</i>	116
Figure 4.1 <i>glr3.3a</i> mutants display altered wound-induced GCaMP3 signals.....	132
Figure 4.2 Wound-induced GCaMP3 signals are perturbed in water-infiltrated Col-0 and <i>glr3.3a</i> mutant <i>A. thaliana</i>	134
Figure 4.3 Wound-induced reporter signals in <i>A. thaliana</i> expressing <i>35S::iGluSnFR</i>	136
Figure 4.4 Wound-induced reporter signals in <i>A. thaliana</i> expressing <i>35S::Apo-pHusion</i>	137
Figure 4.5 Comparisons of wound-induced reporter signal properties in Col-0 <i>A. thaliana</i> expressing <i>UBQ10::GCaMP3</i> , <i>35S::iGluSnFR</i> or <i>35S::Apo-pHusion</i>	139
Figure 4.6 Wound-induced iGluSnFR signals are altered in <i>glr3.3a</i> mutants.....	141
Figure 4.7 Wound-induced apo-pHusion signals are altered in <i>glr3.3a</i> mutants	142
Figure 4.8 Wounding of <i>A. thaliana</i> induces JA, but not SA or Et, marker gene expression.....	144
Figure 4.9 Developing and wounding <i>glr3.3a pAOS::NLS-3xVENUS A. thaliana</i> revealed that wound-induced AOS marker gene expression is not GLR3.3-dependent.	146
Figure 4.10 Developing and wounding <i>glr3.3a pJAZ10::NLS-3xVENUS A. thaliana</i> revealed that wound-induced JAZ10 marker gene expression is reduced in <i>glr3.3a</i> mutants.	147
Figure 4.11 Touch induces GCaMP3 signals with burst and secondary signal dynamics that appear GLR3.3-independent.	149
Figure 4.12 Touch-induced GCaMP3 signals in <i>A. thaliana</i> leaves are unaltered in the <i>glr3.1a glr3.3a glr3.6a</i> mutant.	150
Figure 4.13 Touch can induce detectable iGluSnFR reporter signals in <i>A. thaliana</i> leaves.	152
Figure 4.14 Touch can induce detectable apo-pHusion reporter signals in <i>A. thaliana</i> leaves.	153
Figure 4.15 Comparisons of touch-induced reporter signal properties in Col-0 <i>A. thaliana</i> expressing <i>UBQ10::GCaMP3</i> , <i>35S::iGluSnFR</i> or <i>35S::Apo-pHusion</i>	155

Figure 4.16 Touch treatment does not induce <i>AOS</i> or <i>JAZ10</i> marker gene expression within 8 h of treatment.....	156
Figure 4.17 Hypothetical model for how mechanical stress perception and <i>GLR3.3</i> could function in wound- and touch-induced responses.	167
Figure 5.1 <i>glr3.3a</i> mutants are partially impaired in <i>M. persicae</i> feeding-induced GCaMP3 signals.....	173
Figure 5.2 <i>glr3.1a glr3.3a</i> mutants are partially impaired in <i>M. persicae</i> feeding-induced GCaMP3 signals.....	175
Figure 5.3 <i>R. padi</i> feeding induces GCaMP3 signals that are partially dependent on <i>glr3.3a</i>	177
Figure 5.4 <i>B. brassicae</i> feeding induces <i>A. thaliana</i> GCaMP3 signals that are partially dependent on <i>GLR3.3</i>	178
Figure 5.5 <i>F. occidentalis</i> feeding induces <i>A. thaliana</i> GCaMP3 signals that are partially dependent on <i>GLR3.3</i>	180
Figure 5.6 Localised feeding from aphids and thrips induces iGluSnFR reporter signals.	182
Figure 5.7 Localised feeding from aphids and thrips induces apo-pHusion reporter signals... ..	184
Figure 5.8 <i>pAOS::NLS-3xVENUS</i> expression in responses to feeding from different aphid species.....	186
Figure 5.9 <i>pJAZ10::NLS-3xVENUS</i> expression in responses to feeding from different aphid species.....	187
Figure 5.10 Feeding from <i>F. occidentalis</i> induces <i>AOS</i> and <i>JAZ10</i> JA marker gene expression.	189
Figure 5.11 The <i>glr3.3a</i> mutation does not affect <i>M. persicae</i> or <i>B. brassicae</i> fecundity on <i>A. thaliana</i> but does increase <i>R. padi</i> survival.	191
Figure 5.12 <i>F. occidentalis</i> feeding is increased on <i>glr3.3a A. thaliana</i>	192
Figure 5.13 Hypothetical model for the contribution of <i>GLR3.3</i> to aphid and thrips feeding-induced responses.	199
Figure 6.1 Aphid extract from <i>M. persicae</i> induces GCaMP3 signals in <i>A. thaliana</i> seedlings.	217
Figure 6.2 Aphid extract-induced GCaMP3 signals are not altered in <i>glr3.1 glr3.3a glr3.6a</i> mutants.....	219
Figure 6.3 Aphid extract-induced GCaMP3 signals are reduced in <i>bak1-5</i> mutant <i>A. thaliana</i>	220

Figure 6.4 Aphid extract-induced GCaMP3 signals are severely reduced in <i>sobir1-12</i> mutant <i>A. thaliana</i>	221
Figure 6.5 BAK1 does not appear to contribute to <i>M. persicae</i> feeding-induced GCaMP3 signals in <i>glr3.3a</i> mutant <i>A. thaliana</i>	223
Figure 6.6 The <i>sobir1-12</i> mutation does not affect <i>M. persicae</i> feeding-induced GCaMP3 signals in Col-0 <i>A. thaliana</i>	225
Figure 6.7 SOBIR1 does not appear to contribute to <i>M. persicae</i> feeding-induced GCaMP3 signals in the <i>glr3.3a</i> background.....	226
Figure 7.1 Proposed model for the function of mechanical stress perception and GLR3.3 in responses to localised wounding, touch, aphid feeding, and thrips feeding.....	244

List of Tables

Table 2.1 Details of donated <i>Arabidopsis thaliana</i> lines used in this study.	66
Table 2.2 <i>A. thaliana</i> lines produced by crossing.	69
Table 2.3 Genotyping primers used in this study	71
Table 2.4 Conditions used to image <i>A. thaliana</i> fluorescent reporter lines with a Zeiss Axio Zoom.V16 microscope and a Lumenacor Spectra III Light Engine.....	80
Table 2.5 Background correction values used for signalling reporter analyses.	82
Table 4.1 Properties of wound-induced GCaMP3 signals in <i>A. thaliana</i> with mutations in <i>GLR3.1</i> , <i>GLR3.3</i> and/or <i>GLR3.6</i> alongside wildtype Col-0 controls.....	130
Table 5.1 The relative presence of GLR3.3-dependent and associated responses in <i>A. thaliana</i> following feeding from the aphid and thrips species investigated.....	193
Table 6.1 Properties of wound- and touch-induced reporter signals in mutant <i>A. thaliana</i> lines.	213

List of Accompanying Material

This thesis is accompanied by supplementary videos. The videos are formed from time-series images of *Arabidopsis thaliana* leaves expressing genetically fluorescent reporters and subjected to various stimuli.

- Video S4.1 Wound-induced GCaMP3 signals are perturbed in *glr3.3a* mutant *A. thaliana*.
- Video S4.2 Wound-induced GCaMP3 signals are perturbed in water-infiltrated Col-0 and *glr3.3a A. thaliana*.
- Video S4.3 Micropipette wounding induces iGluSnFR reporter signals in *A. thaliana*.
- Video S4.4 Micropipette wounding induces apo-pHusion reporter signal increases in *A. thaliana*.
- Video S4.5 Touch-induced GCaMP3 signals in Col-0 and *glr3.3a A. thaliana*.
- Video S5.1 *M. persicae* feeding-induced GCaMP3 signals in Col-0 and *glr3.3a A. thaliana*.
- Video S5.2 *F. occidentalis* feeding-induced GCaMP3 signals in Col-0 and *glr3.3a A. thaliana*.

Common Abbreviations

- AHA - H⁺-ATPase
- [Ca²⁺] - Intracellular Ca²⁺ concentration
- [Ca²⁺]_{cyt} - Cytosolic Ca²⁺ concentration
- CAX - Ca²⁺-H⁺ exchanger
- CICR - Calcium-induced calcium release
- DAMP - Damage-associated molecular pattern
- Et – Ethylene
- ETI - Effector-triggered immunity
- ETS - Effector-triggered susceptibility
- F - Fluorescence intensity
- F0 - Baseline fluorescence intensity
- FP - Fluorescent protein
 - C prefix - Cyan
 - cp prefix - Circularly permuted
 - e or E prefix – Enhanced
 - G prefix - Green
 - R prefix - Red
 - Y prefix - Yellow
- FRET - Förster resonance energy transfer
- GECl - Genetically encoded calcium indicators
- GLR3.3/3.6 - GLR3.3 and/or GLR3.6
- Glu - Glutamate
- GS - Glucosinolate
- HAMP - Herbivore-associated molecular pattern
- HR - Hypersensitive response
- JA - Jasmonic acid
- JAs - Jasmonates
- LRR - Leucine rich-repeat
- OGs - Oligogalacturonides
- MAPK - Mitogen-activated protein kinase
- MeJA - Methyl jasmonate
- PAMP - Pathogen-associated molecular pattern
- PI - Proteinase inhibitor
- PRR - Pattern recognition receptor

- PTI - Pattern-triggered immunity
- R - Ratio of fluorescence intensities
- RLK - Receptor-like kinase
- RLP - Receptor-like protein
- ROI - Region of interest
- ROS - Reactive oxygen species
- SA - Salicylic acid
- SEM - Standard error of the mean
- SNR - Signal-to-noise ratio
- TSWV – Tomato spotted wilt virus
- VOC - Volatile organic compound
- YC - Yellow cameleon

Definitions for Key Terms

Abiotic stress: An environmental stress caused by any stimulus other than a living organism.

Biotic stress: An environmental stress caused by a living organism.

Cell wall damage: The degradation of cell wall components that is caused directly by a stress stimulus.

(Cell) damage: Irreversible rupture of the plasma membrane resulting from stress.

Effector: A pest- or pathogen-derived molecule that promotes the performance of a biotic attacker by modifying plant physiology.

Effector-Triggered Immunity (ETI): Defence responses that are triggered by the recognition of a pest- or pathogen-derived effector.

Elicitor: A pest- or pathogen-derived molecule that triggers the induction of early plant defence responses. Elicitors are typically conserved between many species and form molecular patterns that are often perceived by plasma membrane-localised receptors.

Insect feeding: Any insect behaviour that directly facilitates the ingestion of a substrate. For thrips and aphids, these behaviours include any contact of insect mouth parts with the host plant, any navigation of mouth parts within the host plant, and the ingestion of plant material. Feeding behaviours for thrips and aphids are described in detail in Sections 1.2.2. and 1.2.3., respectively. This broad definition of insect feeding does not discriminate between different feeding behaviours, which are complex for many insects and challenging to differentiate.

Large scale stimuli: Any stimulus that directly affects many cells across several tissues or organs. These stimuli often cause systemic signalling responses.

Localised/local stimulus: Any stimulus that directly affects only a relatively small number of cells and tissues with limited effect beyond the range of the stimulated region.

Mechanical stress: A stress event that causes changes in the tension or pressure experienced.

Mechanosensing/mechanical stress perception: The perception of changes in the tension or pressure experienced.

Pattern-Triggered Immunity (PTI): Rapid defence responses triggered by a pest or pathogen elicitor.

Resistance: The extent to which plant defence responses limit the ability of the pest or pathogen to colonise or feed from the plant.

Stress: Any environmental condition that negatively impacts plant physiology.

Touch stimulus: A mechanical stress event that occurs without cell damage.

Wound: A stress event that directly causes cell damage.

Acknowledgements

Firstly, I would like to acknowledge the supervisory dream team of Professors Saskia Hogenhout, Dale Sanders and Tony Miller. They have all offered invaluable guidance and have always been ready to provide support however it may be required.

On the ground, all the members of the Hogenhout and Sanders/Miller groups that I have worked alongside have greatly supported this PhD and deserve recognition. Sam Mugford, you truly are the do-it-all scientist that represents everything good about research. Thank you Sam for chatting science and always being on hand with some words of wisdom. James Canham, thank you for being an excellent mentor and friend. Your perseverance, generosity and kindness are an inspiration and collaborating with you has been an immense pleasure. Emma Turley, thank you for being an incredible student and outstanding company. Matteo and Qun, you are simply the best. Sylvain, Captain Rolie, Sigi, Thomas, Millie, Reuben and George, it has been a delight to stumble through a PhD with you all.

The John Innes Centre Entomology, Biolmaging, and Horticulture Platforms have been fundamental to this PhD. Thank you to Ian, Victor, Mike, Anna, Darryl, Will, Susie, Eva, Sergio, Tim and Sophie. Without you all, this thesis would not have been possible.

Outside of the lab, I have been blessed with some top-tier friends who have helped me through this PhD. José, Baz, Conal and Weller, it is always a pleasure to have you around. Melissa, your support and positivity have been uplifting from the very start of this PhD. Alan, Lauren, Tom, Johnny and Ocean, it never fails to amaze me how lovely and supportive you all are. Thank you all.

Most importantly, the biggest thanks must go to my family. To my parents and sister, your strength, guidance, and friendship underpin everything that I do. I don't always make the best decisions or even know what I am doing but I know that I can always count on you to help me figure it out. To Oti (the dog), thanks for always bringing good energy, no questions asked. To the Minters & Co., hanging out is always a delight. Thanks for welcoming me with open arms and always guaranteeing a joyful break from the PhD. To all my family, I love you unreservedly and wouldn't make it far without you all.

To my partner and best friend, Francesca, my life has transformed for the better since you came into it. Your loving support and empathy have carried me through this PhD. Our best adventures lie ahead.

1. General Introduction

To survive, plants must defend themselves against a diverse range of biotic stresses including pests and pathogens. To do so, plants possess an array of constitutive defences such as waxy cuticles and trichomes (War *et al.*, 2012). However, with limited resources, those allocated to defence come at the cost of growth and reproduction (Huot *et al.*, 2014). Therefore, plants have evolved inducible defences that they can initiate on perception of a biotic stress. Understanding the mechanisms of inducible plant defence responses is crucial for appreciating plant-pest/pathogen interactions. Moreover, this understanding may aid efforts to enhance plant resistance to pests and pathogens and limit the significant crop yields lost to these biotic stresses each year (Savary *et al.*, 2019). This thesis explores how the model organism, *Arabidopsis thaliana*, perceives feeding from some significant pest species in the Aphidoidea (aphid) superfamily and in the Thysanoptera (thrips, singular and plural) order.

1.1. Plant defence responses to biotic stresses

Inducible plant defence responses against biotic stresses comprise of perception events, signalling events and then defence outputs. The molecular mechanisms of inducible plant defence responses are most well characterised for microbial pathogens in 'plant immunity'. Many elements of plant immunity are applicable more broadly to plant defence responses including those to aphids and thrips. Section 1.1 will explore the general mechanisms of plant immunity and defence responses to provide a foundation for considering molecular insect-plant interactions. Section 1.2 will then consider the existing knowledge of the molecular interactions between plants and relevant insects to frame the investigations of this thesis into how plants perceive aphid and thrips feeding.

1.1.1. Introduction to plant immunity

Plant immunity can be described by a two-tier 'zig-zag' model (Figure 1.1)(Jones and Dangl, 2006). In this model, biotic stresses are perceived by the presence of conserved molecular patterns that bind plasma membrane Pattern Recognition Receptors (PRRs). These patterns, or elicitors, induce effective defence responses in Pattern-Triggered Immunity (PTI) including rapid and transient Ca^{2+} and reactive oxygen species (ROS) signalling, transcriptional changes and callose deposition. However, pathogens and pests can deliver effector proteins that manipulate the host plant to promote colonisation and some of these may do so by suppressing PTI in Effector-Triggered Susceptibility (ETS). Plants may possess intracellular Nucleotide-Binding Leucine-Rich Repeat (NB-LRR or NLR) receptors that perceive effectors or their activity to induce an enhanced defence response of Effector-Triggered Immunity (ETI). ETI often involves similar signalling to PTI but with a greater amplitude and duration. Additionally, ETI can include a

programmed cell death defence response called the hypersensitive response (HR). The ETS-ETI interactions can result in a co-evolutionary arms race. Overall, these molecular interactions become significant determinants of how resistant a plant is to a pest or pathogen meaning the extent to which the plant defences limit colonisation of the pest or pathogen. Additionally, these molecular interactions can differ for different genotypes and species of plant, pest, and pathogen. As PTI confers effective resistance in the absence of effectors, most pests and pathogens can only colonise hosts with which they have co-evolved, resulting in ‘specialist’ pests and pathogens with relatively narrow host ranges. However, some pests and pathogens can evolve broader host ranges as ‘generalists’, though the mechanisms of generalism are largely enigmatic. Whilst the classifications within the zig-zag model can be blurred (Thomma *et al.*, 2011), this model provides the foundations for exploring molecular plant-pathogen and -pest interactions and understanding plant resistance to biotic stresses.

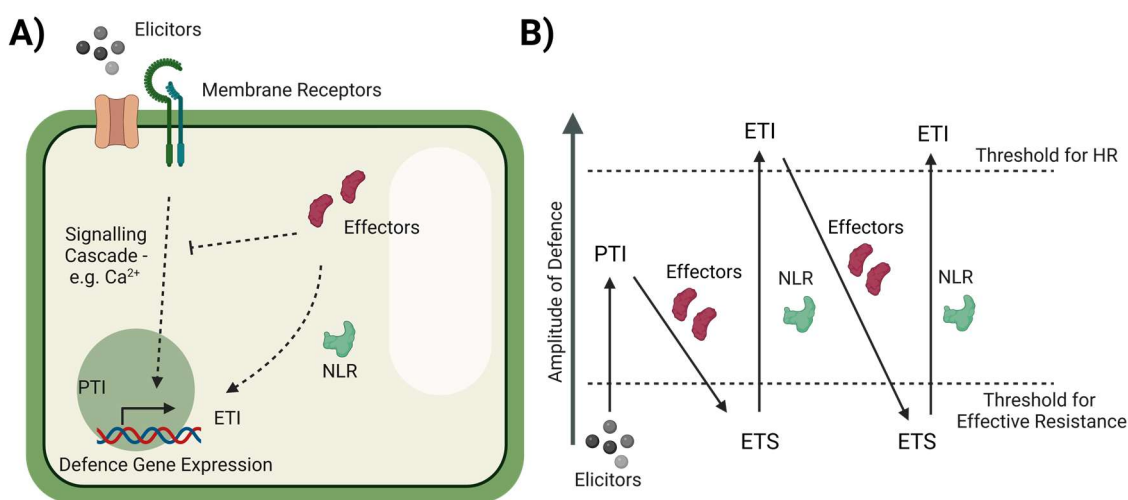


Figure 1.1 Zig-zag model of plant immunity.

(A) Model of plant immunity in which molecular patterns or elicitors are perceived by plasma membrane receptors to initiate signalling upstream of defence gene expression. The defences triggered in this way are termed Pattern-Triggered Immunity (PTI). Effector proteins introduced by the pest or pathogen can manipulate the host to promote infection or colonisation and may do so by suppressing PTI in Effector-Triggered Susceptibility (ETS). However, if effectors are recognised by plant nucleotide-binding leucine-rich repeat (NLR) receptors, then the plant can trigger enhanced defence responses in Effector-Triggered Immunity (ETI). (B) The model outlined in (A) but arranged to highlight the amplitude of the defence responses. PTI can confer effective resistance against a biotic stress. ETS can suppress defences making them insufficient for pathogen/pest resistance. ETI bolsters plant defence responses and can trigger the hypersensitive response. A co-evolutionary arms race between ETS and ETI may result. Model adapted from Jones and Dangl (2006). Created with BioRender.com.

1.1.2. Diversity in biotic stresses and specificity in responses

Plant pests and pathogens can have diverse feeding mechanisms or infection strategies. For example, pathogens can be grouped by their infection strategies as: biotrophic pathogens

which extract nutrients from living cells with limited cell death, necrotrophic pathogens which require cell death to access nutrients and hemi-biotrophic pathogens which initially exhibit biotrophic infection before switching to necrotrophic infection (McCombe *et al.*, 2022). To be effective, plants must tailor the defence responses to the specific pest or pathogen present. For instance, cell death in HR is effective against biotrophs but can promote necrotrophic infection by improving access to plant nutrients (Morel and Dangl, 1997; Pitsili *et al.*, 2020). Therefore, specificity in the perception and signalling mechanisms can be important for ensuring the inducible defence responses are appropriate for the biotic stress present.

1.1.3. Perceiving biotic stress at the plasma membrane

Plasma membrane perception mechanisms are key in the early and specific recognition of biotic stresses. Here, elicitors and PRRs are considered along with other mechanisms that underpin this perception.

Pattern Recognition Receptors (PRRs): Class and activity

Plants have evolved hundreds of PRRs that can facilitate the perception of biotic stresses. The most common PRR forms are the Receptor-Like Kinases (RLKs) and the Receptor-Like Proteins (RLPs) with RLKs containing a cytoplasmic kinase domain but RLPs not (Roudaire *et al.*, 2020; McCombe *et al.*, 2022). RLPs and RLKs can be further categorised by their extracellular domains which could include a leucine-rich repeat (LRR), lysin motif (LysM), epidermal growth factor (EGF)-like domain, lectin (lec), malectin-like domain, galacturonan-binding wall-associated-kinase (GubWAK) domain or a WAK-associated C-terminal domain (McCombe *et al.*, 2022; Albert *et al.*, 2020; Jose *et al.*, 2020). There are various other forms that PRRs can take such as ion channel receptors. The presence of diverse PRRs facilitates the perception of a wide range of elicitors and biotic stresses.

Activation of PRRs by elicitors initiates signal transduction events. For the large family of LRR-RLK PRRs, this involves receptor complex formation usually with co-receptor Somatic Embryogenesis Receptor Kinase (SERK) RLKs (Albert *et al.*, 2020). The SERK BRI1-ASSOCIATED KINASE1 (BAK1) is a co-receptor for many RLKs functioning in defence responses and development (Chinchilla *et al.*, 2009). Following complex formation, phosphorylation events occur between RLK receptors, co-receptors and interacting partners (Wang *et al.*, 2014b; Schwessinger *et al.*, 2011). For example, BAK1 and the Receptor-Like Cytoplasmic Kinase (RLCK), BOTRYTIS-INDUCED KINASE 1 (BIK1), can undergo transphosphorylation that initiates BIK1 migration to the nucleus to phosphorylate downstream signalling components (Lu *et al.*, 2010; Lal *et al.*, 2018; Albert *et al.*, 2020). Through such activity, RLCKs are key in defence signalling following RLK activation and complex formation (Liang and Zhou, 2018). RLP PRRs initiate

signalling processes similarly to RLKs. However, as RLPs lack an intracellular kinase domain, downstream phosphorylation events are often mediated by the co-receptor RLK SUPPRESSOR OF BIR1 (SOBIR1), with which many RLPs constitutively interact (Liebrand *et al.*, 2013; Liebrand *et al.*, 2014). The PRRs, co-receptors, signalling proteins and phosphorylation sites involved vary in response to different elicitors (Albert *et al.*, 2020). Through this mechanism of complex formation and phosphorylation, RLPs and RLKs can transduce the perception of diverse extracellular elicitors into intracellular signalling events upstream of appropriate plant defence responses.

Elicitors and modulators of defence responses perceived at the plasma membrane

Different forms of elicitor molecules are perceived at the plasma membrane along with other molecules and stimuli that can induce or modulate plant defence responses. These elicitors can be categorised based upon their origin and function.

Pathogen-associated molecular patterns (PAMPs) and **herbivore-associated molecular patterns (HAMPs)** are elicitors that derive from pathogens and herbivores, respectively. Many PAMPs have been identified and some have been well characterised (Albert *et al.*, 2020). For example, apoplastic plant enzymes, including β -galactosidase 1, liberate the flg22 peptide PAMP from bacterial flagellin which then binds the FLS2 LRR-RLK to induce FLS2-BAK1 complex formation and PTI signalling (Felix *et al.*, 1999; Gómez-Gómez *et al.*, 1999; Chinchilla *et al.*, 2006; Sun *et al.*, 2013; Buscaill *et al.*, 2019). Additionally, nlp20 is a peptide PAMP that can derive from many proteins in the NLP superfamily of microbial proteins (Böhm *et al.*, 2014; Oome and Van den Ackerveken, 2014). The RLP23 LRR-RLP binds nlp20 resulting in RLP23-SOBIR1-BAK1 complex formation and defence signalling (Albert *et al.*, 2015). Finally, oligomers of the chitin aminopolysaccharide found in fungal cell walls and insects can bind the LysM-RLKs CERK1 and LYK5 to initiate immune signalling (Cao *et al.*, 2014; Xue *et al.*, 2019; Iizasa *et al.*, 2010; Petutschnig *et al.*, 2010; Miya *et al.*, 2007). In contrast to PAMPs, relatively few HAMPs have been identified and characterised with those for caterpillars, aphids and thrips explored in sections 1.2.1-1.2.3.

Damage-associated molecular patterns (DAMPs) are elicitors released by cell or cell wall damage without processing by plant enzymes (Hou *et al.*, 2021a; Rzemieniewski and Stegmann, 2022). Unless cell wall damage is specified, damage in this thesis refers to cell damage meaning an event that includes irreversible plasma membrane rupture. There are various DAMPs thought to operate in plant damage responses including extracellular nicotinamide adenine dinucleotide (eNAD) and eNAD phosphate (eNADP) (Wang *et al.*, 2017a), extracellular DNA (eDNA) (Rassizadeh *et al.*, 2021) and the HMG-box domain containing protein, HMGB3 (Choi *et al.*, 2016). For example, the DAMP extracellular ATP (eATP) induces defence responses of $[Ca^{2+}]$

elevations, gene expression changes and pathogen resistance via the lectin RLKs, DOES NOT RESPOND TO NUCLEOTIDES 1 (DORN1, P2K1) and P2K2 (Choi *et al.*, 2014b; Choi *et al.*, 2014a; Matthus *et al.*, 2020; Bouwmeester *et al.*, 2011; Pham *et al.*, 2020). Amino acids and small amino acid derivatives, such as glutamate (Glu) and glutathione, can also act as DAMPs. These DAMPs can be perceived by the GLUTAMATE RECEPTOR-LIKE (GLR) ion channels with a clear role for GLR3.3 in this perception (Qi *et al.*, 2006; Li *et al.*, 2013; Goto *et al.*, 2020; Gao *et al.*, 2023). Apoplastic [Glu] elevations are thought to occur passively with damage (Toyota *et al.*, 2018; Bellandi *et al.*, 2022; Grenzi *et al.*, 2023) whilst glutathione levels can increase in pathogen-infected cells and be released by transporters or damage (Vanacker *et al.*, 2000; Parisy *et al.*, 2007). GLR-activating ligands, such as Glu and glutathione, can induce a range of defence responses that promote resistance against biotic attackers (Wingate *et al.*, 1988; Qi *et al.*, 2006; Goto *et al.*, 2020; Toyota *et al.*, 2018; Li *et al.*, 2013). Homogalacturonan-derived oligosaccharides (OGs) are DAMPs released with the partial degradation of cell wall pectin during pathogen infection or cell wall damage (Benedetti *et al.*, 2015). OGs induce various immune responses including resistance against multiple pathogens with the RLK WAK1 contributing to OG perception (Gravino *et al.*, 2017; Bellincampi *et al.*, 2000; Galletti *et al.*, 2011; Galletti *et al.*, 2008; Ferrari *et al.*, 2007; Brutus *et al.*, 2010; Decreux and Messiaen, 2005). These DAMPs demonstrate how cell wall or cell damage can induce plant defence responses.

Phytocytokines are plant-derived signalling peptides that are perceived at the plasma membrane and stored as inactive precursor peptides often extracellularly. Some phytocytokines are processed during biotic stresses and modulate plant defence responses (Hou *et al.*, 2021a; Rzemieniewski and Stegmann, 2022). The serine-, glycine- and proline-rich (SGP-rich) PLANT ELICITOR PEPTIDES (PEPs) are phytocytokines which trigger defence responses. They are released from their precursors (PROPEPs) by METACASPASE (MC) activity and can bind the PEPR1 and/or PEPR2 RLKs (Yamaguchi *et al.*, 2010; Yamaguchi *et al.*, 2006; Shen *et al.*, 2019; Huffaker *et al.*, 2006; Bartels *et al.*, 2013). Damage can induce PEP1 release by MC4 because a loss of membrane integrity causes a Ca²⁺ influx which can activate MC4 (Hander *et al.*, 2019). Other defence promoting SGP-rich phytocytokines include the SERINE-RICH ENDOGENOUS PEPTIDES (SCOOPs), perceived by the MIK2 receptor, and the PAMP-INDUCED PEPTIDES (PIPs) (Rhodes *et al.*, 2021; Hou *et al.*, 2021b; Hou *et al.*, 2014). Some phytocytokines can negatively regulate plant defence responses. For example, RAPID ALKALINISATION FACTOR (RALF) 23 and 33 are phytocytokines rapidly released from PRORALFs by SITE-1 PROTEASE (S1P) with the initiation of PTI (Stegmann *et al.*, 2017). RALF23 and 33 then bind to the FERONIA (FER) RLK inducing complex formation with LORELEI-LIKE GPI-ANCHORED PROTEIN 1 (LLG1) (Xiao *et al.*, 2019). This complex formation impairs the ability of FER and LLG1 to promote PRR activity and PTI signalling, thus suppressing PTI (Stegmann *et al.*, 2017; Shen *et al.*, 2017). Other

phytoytokines which suppress defence responses include PHYTOSULFOKINE (PSK) and PLANT PEPTIDE CONTAINING SULFATED TYROSINE1 (PSY1), which are perceived by the LRR-RLKs PSKR1/2 (Matsubayashi *et al.*, 2006) and PSYR1 (Amano *et al.*, 2007), respectively (Mosher *et al.*, 2013). Whilst many phytoytokines exist with diverse functions (Rzemieniewski and Stegmann, 2022), these members display how phytoytokines can modulate plant defence signalling.

Mechanosensing or mechanical stress perception involves the perception of mechanical perturbations without requiring any cell wall or cell damage. Such perception can contribute to plant defence responses against pests and pathogens (Jayaraman *et al.*, 2014). For example, mechanosensing guides microtubule reorganisation during *Sclerotinia sclerotiorum* infection of *A. thaliana* which activates plant defences (Léger *et al.*, 2022). Moreover, touch stimuli can induce defence responses against various pests and pathogens (Tomas-Grau *et al.*, 2018; Markovic *et al.*, 2014; Benikhlef *et al.*, 2013; Matsumura *et al.*, 2022). Mechanical stress perception can occur by several mechanisms. Mechanosensitive membrane ion channels can be gated by tension changes in the membrane or between the channels and extracellular or intracellular components to initiate signalling responses (Hamant and Haswell, 2017). Mechanosensitive ion channels which could contribute to the perception of biotic stresses include the plasma membrane localised MID1-COMPLEMENTING ACTIVITY 1 & 2 (MCA1 & 2) (Yoshimura *et al.*, 2021) and the 10 *A. thaliana* MscS-LIKE (MSL) channels (Basu and Haswell, 2017). MSL10 has been implicated in modulating *A. thaliana* resistance against the pathogen *Pseudomonas syringae* (Basu *et al.*, 2022). An alternative mechanism for mechanical stress perception is by receptors that perceive cell wall physicochemical properties (Hamant and Haswell, 2017; Rui and Dinneny, 2020). The *Catharanthus roseus* RLK1-LIKE (CrRLK1L) family of RLKs contain two extracellular malectin-like domains which may bind cell wall carbohydrates and confer mechanosensing activity to the receptors (Rui and Dinneny, 2020). FER is a CrRLK1L which can bind de-methylesterified homogalacturonan which is found in the cell wall (Feng *et al.*, 2018; Lin *et al.*, 2018). This binding could explain the function of FER in root mechanosensing (Shih *et al.*, 2014). By these mechanisms, mechanical stress perception can contribute to the initiation of plant defence responses.

PAMPs, HAMPs, DAMPs, phytoytokines and mechanical stress can be perceived at the plasma membrane to initiate or modulate plant defence responses to biotic attackers (Figure 1.2). The presence of many perception mechanisms and components provides a framework for plants to specifically respond to diverse biotic stresses with appropriate defence responses.

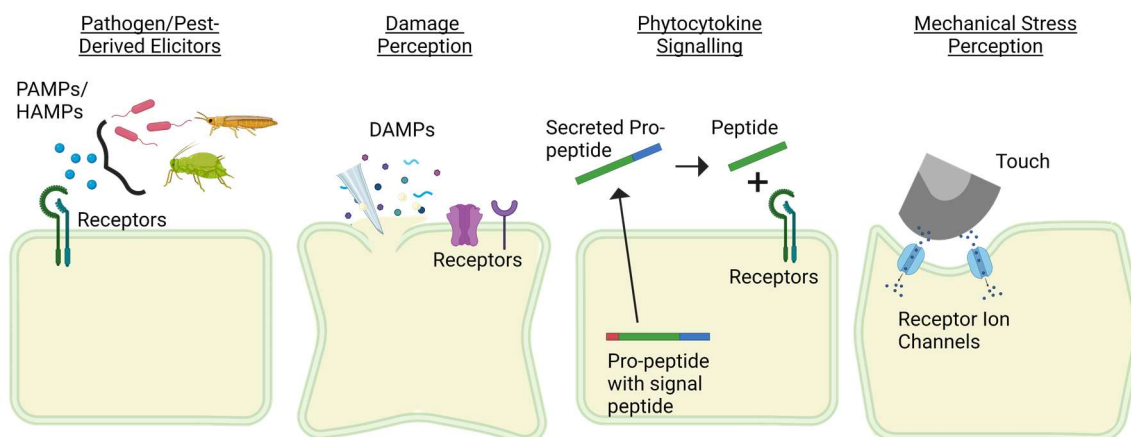


Figure 1.2 Examples of the mechanisms for plasma membrane perception of pests and pathogens.

Biotic stress perception at the plasma membrane can include the perception of pathogen- and pest-derived elicitors as pathogen- and herbivore-associated molecular patterns (PAMPs and HAMPs), respectively. Additionally, damage-associated molecular patterns (DAMPs) can be released passively with cell damage and perceived as elicitors to induce plant defence responses. Phytoytokine signalling peptides can be processed with biotic stress to modulate defence responses. Additionally, the perception of mechanical stresses can initiate plant defence responses. Created with BioRender.com.

1.1.4. Communicating the perception of a biotic stress

Rapid and transient signalling events transduce the perception of a biotic stress at the plasma membrane into a defence response. These early signalling events function largely to drive transcriptional changes that promote further defence signalling as well as defence outputs. The signal properties and the combination of signalling events that occur can communicate information about the specific stress perceived to help coordinate an appropriate defence response. Whilst not all the mechanisms that comprise early plant defence signalling can be explored here, those with particular relevance to the plant-insect interactions discussed in Section 1.2 and the content of this thesis are considered.

Calcium signalling

Changes in intracellular Ca^{2+} concentrations ($[\text{Ca}^{2+}]$) are a versatile and ubiquitous eukaryotic signalling mechanism (Edel *et al.*, 2017). As Ca^{2+} ions form cytotoxic precipitates with phosphate, free Ca^{2+} concentrations in the cytosol are maintained low at approximately 100 - 200 nM. Ca^{2+} is instead sequestered in stores of the apoplast, vacuole and endoplasmic reticulum by the action of membrane localised Ca^{2+} transporters. Resultingly, a steep $[\text{Ca}^{2+}]$ gradient exists between stores and their surroundings. Controlled release of Ca^{2+} from the stores via Ca^{2+} -permeable channels creates transient cytosolic $[\text{Ca}^{2+}]$ increases of up to 1 - 2 μM (Rudd

and Franklin-Tong, 1999; Dodd *et al.*, 2010). These $[Ca^{2+}]$ elevations can regulate various processes through Ca^{2+} sensor proteins, including defence responses (Ranf *et al.*, 2014; Bigeard *et al.*, 2015; Peng *et al.*, 2018; Li *et al.*, 2016a; Jiang and Ding, 2023). To ensure $[Ca^{2+}]$ elevations regulate the appropriate responses, specificity is encoded into the elevations through variation in the amplitude, duration and frequency of the $[Ca^{2+}]$ changes, known as 'Ca²⁺ signatures' (McAinsh and Pittman, 2009). Spatial specificity can also occur because Ca^{2+} diffusion is limited in the intracellular environment (Stael *et al.*, 2012) and as $[Ca^{2+}]$ elevations can be confined to within organelles. For example, transient $[Ca^{2+}]$ elevations have been identified in nuclei (Charpentier *et al.*, 2016; Lecourieux *et al.*, 2005; Leitão *et al.*, 2019) and mitochondria (Logan and Knight, 2003; Loro *et al.*, 2012; Loro *et al.*, 2013; Manzoor *et al.*, 2012). Such properties of $[Ca^{2+}]$ elevations allow them to specifically coordinate responses to diverse stimuli including biotic stresses.

A. thaliana possesses many Ca^{2+} -permeable channels that can contribute to Ca^{2+} signalling. These include several families that are relevant to *A. thaliana* defence responses:

- **The CYCLIC-NUCLEOTIDE-GATED CHANNEL (CNGC) family** includes 20 members that form homo- or hetero-tetrameric channel complexes largely at the plasma membrane (Zelman *et al.*, 2012; Jarratt-Barnham *et al.*, 2021). Regulation of CNGC activity can involve complex formation, phosphorylation, Ca^{2+} signalling and the cyclic nucleotide monophosphates (cNMPs) adenosine 3',5'-cyclic monophosphate (cAMP) and guanosine 3',5'-cyclic monophosphate (cGMP) (Jarratt-Barnham *et al.*, 2021). CNGCs implicated in plant immunity and defence responses include CNGC2 and 4 (Chin *et al.*, 2013; Wang *et al.*, 2022a; Tian *et al.*, 2019), CNGC11 and 12 (Yoshioka *et al.*, 2006) and CNGC19 and 20 (Yu *et al.*, 2019b; Zhao *et al.*; Meena *et al.*, 2019). Interestingly, cGMP and PEP can both induce CNGC2-dependent $[Ca^{2+}]$ elevations and the PEPR1 PEP receptor has guanylyl cyclase activity capable of catalysing cGMP production (Qi *et al.*, 2010). Therefore, some defence receptors may produce cNMPs that induce CNGC-dependent $[Ca^{2+}]$ elevations and signalling.
- **TWO-PORE CHANNEL 1 (TPC1)** is a tonoplast-localised Na^{+} -, K^{+} - and Ca^{2+} -permeable channel regulated by voltage and $[Ca^{2+}]$ with increased cytosolic $[Ca^{2+}]$ promoting opening and increased vacuolar $[Ca^{2+}]$ suppressing opening (Guo *et al.*, 2016; Beyhl *et al.*, 2009; Allen and Sanders, 1996; Hedrich and Neher, 1987). TPC1 contributes to various processes including tonoplast excitability (Jašlan *et al.*, 2019) and propagating $[Ca^{2+}]$ elevations in root salt stress responses (Choi *et al.*, 2014c; Evans *et al.*, 2016). Moreover, TPC1 functions in systemic $[Ca^{2+}]$ elevations induced by large-scale damage (Kiep *et al.*, 2015).

- **MCA1 and MCA2** form homo-tetrameric Ca^{2+} -permeable plasma membrane channels gated by membrane tension and voltage (Nakagawa *et al.*, 2007; Yoshimura *et al.*, 2021; Yamanaka *et al.*, 2010; Nakano *et al.*, 2011; Kamano *et al.*, 2015; Shigematsu *et al.*, 2014). The functions of MCA1 and 2 include in responses to hypergravity (Hattori *et al.*, 2020), chilling and freezing (Mori *et al.*, 2018) and root sensing of media hardness (Yamanaka *et al.*, 2010; Nakagawa *et al.*, 2007). Moreover, MCA1 has been implicated in responses to cell wall damage (Engelsdorf *et al.*, 2018a) that can occur with biotic attack.
- **ANNEXINS (ANNs)** comprise an 8-member family thought to act as ion channels permeable to Ca^{2+} (Laohavisit and Davies, 2011; Cantero *et al.*, 2006). ANNs are atypical membrane proteins as their subcellular localisation and membrane binding can dynamically change in a $[\text{Ca}^{2+}]$ -dependent manner (Laohavisit and Davies, 2011; Tichá *et al.*, 2020). ANNs are proposed to have diverse functions including in plant immunity. For example, ANN1 contributes to ROS- and eATP-induced $[\text{Ca}^{2+}]$ elevations in roots (Laohavisit *et al.*, 2012; Richards *et al.*, 2014; Mohammad-Sidik *et al.*, 2021), chitin-induced CERK1 signalling (Espinoza *et al.*, 2017) and systemic responses to large-scale wounding or herbivory (Malabarba *et al.*, 2021). Additionally, ANN1 and ANN4 are targets of a nematode effector (Zhao *et al.*, 2019) and ANN8 negatively regulates HR-like cell death and resistance mediated by *A. thaliana* RESISTANCE TO POWDERY MILDEW 8.1 (RPW8.1) (Zhao *et al.*, 2021b)
- **REDUCED HYPEROSMOLARITY-INDUCED $[\text{Ca}^{2+}]$ INCREASE (OSCA) channels** form a 15-member family with some members demonstrated to be Ca^{2+} -permeable (Murthy *et al.*, 2018; Yuan *et al.*, 2014). OSCA1.1, 1.2 and 3.1 form channels as homo-dimers (Liu *et al.*, 2018; Zhang *et al.*, 2018; Jojoa-Cruz *et al.*, 2018) and OSCA1.2 is known to be mechanosensitive (Murthy *et al.*, 2018). Whilst many OSCA functions remain unknown, *osca1.3 osca1.7* double mutants are impaired in PAMP-induced stomatal closure and $[\text{Ca}^{2+}]$ elevations in guard cells as well as resistance against *P. syringae* (Thor *et al.*, 2020). During PAMP-induced responses, BIK1 can phosphorylate OSCA1.3 and increase its activity as a Ca^{2+} -permeable channel (Thor *et al.*, 2020).
- **PIEZO1** is a tonoplast-localised mechanosensitive ion channel that is widely expressed in *A. thaliana* and is thought to be Ca^{2+} -permeable (Mousavi *et al.*, 2021; Radin *et al.*, 2021; Fang *et al.*, 2021). PIEZO1 functions in mechanical stress-induced $[\text{Ca}^{2+}]$ elevations in *A. thaliana* roots (Mousavi *et al.*, 2021; Fang *et al.*, 2021) and can suppress the systemic movement of plant viruses (Zhang *et al.*, 2019).

- GLUTAMATE RECEPTOR-LIKES (GLRs)** are a 20-member family of channels split across three clades (I, II, III) that are homologous to animal ionotropic glutamate receptors (iGluRs) (Wudick *et al.*, 2018a; Chiu *et al.*, 2002). *A. thaliana* GLRs are thought to function as homo- or hetero-tetramers with a homo-tetrameric structure of GLR3.4 demonstrated (Green *et al.*, 2021; Wudick *et al.*, 2018a). Many GLRs are considered to be Ca²⁺ channels *in planta* with GLR1.1, 1.4 and 3.3 demonstrated to form channels permeable to Ca²⁺, Na⁺ and K⁺ (Tapken and Hollmann, 2008; Shao *et al.*, 2020; Alfieri *et al.*, 2020). GLRs can display various intracellular localisations (Wudick *et al.*, 2018a) with some members, including GLR3.3, reported at the plasma membrane (Alfieri *et al.*, 2020; Bellandi *et al.*, 2022). GLR gating is not well resolved but can involve ligand binding and pH (Simon *et al.*, 2023; Shao *et al.*, 2020). For example, GLR3.3 can be regulated by extracellular pH and has a broad agonist profile that includes various amino acids, such as glutamate which is thought to act as a DAMP (Alfieri *et al.*, 2020; Qi *et al.*, 2006; Grenzi *et al.*, 2023; Bellandi *et al.*, 2022). GLR3.1, 3.2, 3.3, 3.5 and 3.6 have all been implicated in large-scale wound-induced responses thought to be induced by chewing herbivores (Nguyen *et al.*, 2018; Mousavi *et al.*, 2013; Salvador-Recatalà, 2016; Toyota *et al.*, 2018; Bellandi *et al.*, 2022; Shao *et al.*, 2020; Grenzi *et al.*, 2023). Additionally, GLRs have been implicated in plant immunity with *glr2.7 glr2.8 glr2.9* mutants impaired in PAMP-induced [Ca²⁺] elevations and resistance to *P. syringae* (Bjornson *et al.*, 2021). GLR3.3 also promotes resistance to *Hyaloperonospora arabidopsidis* (Manzoor *et al.*, 2013) and *P. syringae* (Li *et al.*, 2013).

[Ca²⁺] elevations are also shaped by Ca²⁺ transporters that use ATP or cation gradients to transport Ca²⁺ against its concentration gradient back into stores. Whilst some of this Ca²⁺ efflux is mediated by the chloroplast PI-ATPase HMA1 and the mitochondrial Ca²⁺ uniporter complex (MCUC) proteins, most of this efflux is driven by PII Ca²⁺-ATPases and Ca²⁺ exchangers (Moreno *et al.*, 2008; Seigneurin-Berny *et al.*, 2006; Teardo *et al.*, 2019; Ghosh *et al.*, 2022). PII Ca²⁺-ATPases form two clades: PII-A ER-type ATPases (ECAs), which are mainly found at the endoplasmic reticulum (ER) membrane, and PII-B autoinhibited Ca²⁺-ATPases (ACAs), primarily located at the plasma membrane but with some members present in the ER and vacuole membranes (García Bossi *et al.*, 2019). Some Ca²⁺-ATPases have been implicated in plant defence responses. For example, the tonoplast-localised ACA4 and ACA11 negatively regulate flg22-induced PTI responses (Hilleary *et al.*, 2020) as well as *P. syringae* resistance (Boursiac *et al.*, 2010). Furthermore, plants lacking the plasma membrane-localised ACA8 and ACA10 proteins are impaired in flg22-induced [Ca²⁺] elevations, PTI responses, pathogen resistance and ATP-induced responses (Frei dit Frey *et al.*, 2012; Behera *et al.*, 2018). The Ca²⁺-exchangers comprise five families that display different cation specificities, including the vacuolar cation/H⁺ exchangers (CAXs) (Zheng *et al.*, 2021). Whilst the contribution of Ca²⁺-exchangers to plant

immunity is poorly characterised, CAX1 and CAX3 have been proposed to contribute to plant immunity through the regulation of stomatal aperture by Ca²⁺ transport (Hocking *et al.*, 2017). The combined activity of Ca²⁺ transporters can help shape [Ca²⁺] elevations important in the specific regulation of downstream responses.

Ca²⁺ sensor proteins with variation in Ca²⁺-binding capacity, Ca²⁺ affinity, structure, and localisation function to decode Ca²⁺ signatures and regulate downstream responses (Jiang and Ding, 2023). There are four main Ca²⁺ sensor families in *A. thaliana* and all contain members that can regulate biotic stress responses (Singh and Pandey, 2020; Ghosh *et al.*, 2022). Calmodulin (CaM) and CaM-like (CML) proteins bind Ca²⁺ via EF-hand motifs with four EF-hands in CaMs and between one and six EF-hands in CMLs (Ghosh *et al.*, 2022). Ca²⁺-bound CaMs and CMLs can interact with diverse proteins, including transcription factors and ion channels, to regulate their activities. Ca²⁺-dependent protein kinases (CDPKs) mediate responses via kinase activity following Ca²⁺ binding to a CaM-like domain (Singh and Pandey, 2020). CDPKs can then phosphorylate various substrates to regulate responses (Bredow and Monaghan, 2019) including in flg22-induced PTI (Boudsocq *et al.*, 2010). In contrast to CDPKs, calcineurin B-like (CBL) proteins require interaction with CBL-interacting protein kinases (CIPKs) to mediate phosphorylation events (Tang *et al.*, 2020). The CBL-CIPK association is regulated by Ca²⁺ binding to CBLs via four EF-hands. Some CBL-CIPKs have been implicated in plant defence responses (Ma *et al.*, 2020b) including CIPK6 which negatively regulates resistance against *P. syringae* (Sardar *et al.*, 2017). Thus, various Ca²⁺ sensor proteins can function to decode [Ca²⁺] elevations in plant defence responses.

Visualising [Ca²⁺] elevations can provide unique insights into plant responses to biotic stresses (Jiang and Ding, 2023). There are various approaches for [Ca²⁺] visualisation (reviewed in Grenzi *et al.*, 2021). These include imaging fluorescent [Ca²⁺] indicator dyes which were applied to plants early on but are challenging to load reproducibly (Bush and Jones, 1987; Bush and Jones, 1990). Genetically encoded [Ca²⁺] indicators (GECIs) were therefore developed. The first GECI established in plants was aequorin which exhibits [Ca²⁺]-dependent bioluminescence and revealed fungal elicitor-induced [Ca²⁺] elevations in *Nicotiana plumbaginifolia* (Knight *et al.*, 1991). Aequorin remains a useful tool but is limited by the need for pre-treatment with its co-factor and its relatively low quantum yield efficiency (Grenzi *et al.*, 2021). Since the development of aequorin, the GECI toolbox has rapidly expanded to include a wide range of bioluminescent and fluorescent GECIs with properties appropriate for different applications. Some fluorescent GECIs are intensimetric and report [Ca²⁺] by a single emission signal whilst others are ratiometric and report [Ca²⁺] via a ratio of two emission signals. Ratiometric reporters can be based on Förster resonance energy transfer (FRET) between two fluorescent proteins (FPs). The

Yellow Cameleon (YC) family of reporters display $[Ca^{2+}]$ -dependent FRET between a cyan FP (CFP) and a yellow FP (YFP). This is regulated by Ca^{2+} binding to an incorporated CaM which then interacts with an M13 peptide to reduce the distance between the two fluorescent entities (Miyawaki *et al.*, 1997). YC reporters have been widely used in *A. thaliana* including to reveal the dependency of flg22-induced stomatal $[Ca^{2+}]$ elevations on OSCA1.3/1.7 (Thor *et al.*, 2020). GCaMPs are intensimetric fluorescent GECIs. The GCaMP GECIs are also based on $[Ca^{2+}]$ -dependent interactions between a CaM and an M13 but these are attached to the termini of a single circularly permuted enhanced green FP (GFP) (Nakai *et al.*, 2001; Kostyuk *et al.*, 2019). GCaMPs, such as GCaMP3 (Tian *et al.*, 2009), have been expressed in *A. thaliana* and utilised for a range of experiments including investigations into plant-insect interactions (Vincent *et al.*, 2017a; Nguyen *et al.*, 2018; Toyota *et al.*, 2018). In summary, the GECI toolbox can be useful for investigating plant responses to stimuli including biotic stresses.

Pharmacological manipulations of $[Ca^{2+}]$ elevations can help generate insights into how plants respond to biotic stresses. For example, Ca^{2+} signalling can be non-selectively manipulated by the direct blocking of Ca^{2+} permeable channels by La^{3+} or Gd^{3+} ions, chelation of extracellular Ca^{2+} by EGTA or by CaM binding and inhibition (De Vriese *et al.*, 2018). Moreover, some processes can be selectively targeted. For instance, 6,7-dinitroquinoxaline-2,3-dione (DNQX) and 2-amino-5-phosphonopentanoic acid (AP5) can antagonise GLR activity by competitively binding to the ligand binding sites (De Vriese *et al.*, 2018; Dubos *et al.*, 2003). DNQX was used to identify a role for GLRs in OG-induced $[Ca^{2+}]$ elevations that led to GLR3.3 being implicated in resistance against *H. arabidopsidis* (Manzoor *et al.*, 2013). Whilst such pharmacological manipulation can cause off-target effects (De Vriese *et al.*, 2018), these approaches can inform on the mechanisms and significance of $[Ca^{2+}]$ elevations in plant defence responses.

In summary, $[Ca^{2+}]$ elevations in plants can act as signals that communicate the perception of a biotic stress to specifically regulate defence responses. This signalling includes the action of Ca^{2+} channels, transporters, and sensor proteins (Figure 1.3). Studying $[Ca^{2+}]$ elevations can provide significant insights into the plant perception and signalling mechanisms that operate in response to a biotic stress.

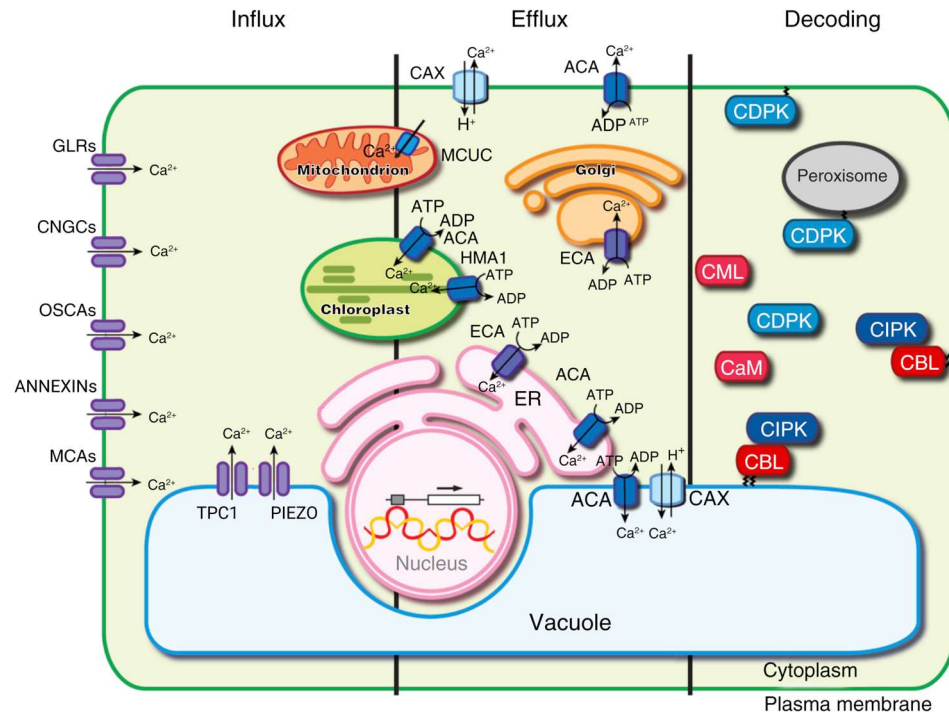


Figure 1.3 Generalised overview of plant Ca^{2+} signalling components.

Generalised model of plant Ca^{2+} signalling components with Ca^{2+} influx from Ca^{2+} stores mediated by Ca^{2+} channels, Ca^{2+} efflux mediated by Ca^{2+} pumps and transporters, and the decoding of Ca^{2+} signals mediated by Ca^{2+} sensor proteins. Model adapted from Edel *et al.* (2017) with permissions. Figure modified with BioRender.com.

Reactive oxygen species signalling

The production of apoplastic ROS contributes to plant defence responses by damaging the biotic attacker, by promoting cell wall cross-linking and strengthening, and as a signalling species (Lamb and Dixon, 1997). This ROS is predominantly produced by plasma membrane RESPIRATORY BURST OXIDASE HOMOLOGs (RBOHs). These enzymes catalyse the production of superoxide which is then converted to H_2O_2 spontaneously or through superoxide dismutase activity (Qi *et al.*, 2017). The most prominent RBOHs in plant defence responses are RBOHD and F, which mediate plant immune responses to many pathogens (Kadota *et al.*, 2015; Otulak-Koziet *et al.*, 2020; Torres *et al.*, 2002). These RBOHs have overlapping but distinct expression profiles and activities (Morales *et al.*, 2016). Multiple mechanisms regulate RBOHD and F activity. For example, following the perception of eATP, flg22 or elf18, RBOHD activity can be promoted by phosphorylation (Li *et al.*, 2014; Kadota *et al.*, 2014; Chen *et al.*, 2017). $[\text{Ca}^{2+}]$ elevations can also promote ROS production from RBOHD through binding to its EF-hand motifs (Ogasawara *et al.*, 2008) or by promoting its phosphorylation by CPK5 (Dubiella *et al.*, 2013). In contrast, phosphorylation of RBOHD by PBS1-LIKE KINASE 13 (PBL13) can promote RBOHD ubiquitination and degradation suppressing plant resistance against bacterial infection (Lee *et al.*, 2020). Through regulation of RBOHs, ROS production and signalling can be tightly regulated in plant defence responses.

Identifying proteins regulated by ROS elevations can be challenging as direct ROS effects often manifest as changes in redox state resulting in altered protein conformation or interactions which can be difficult to detect (Qi *et al.*, 2017). However, there are notable proteins in plant defence responses that may be regulated by ROS. For instance, NON-EXPRESSION OF PR GENES 1 (NPR1) is thought to be regulated by redox reactions and is a central regulator of resistance mediated by the hormone, salicylic acid (Section 1.1.5)(Mou *et al.*, 2003). Additionally, an *A. thaliana* quiescin sulfhydryl oxidase, QSOX1, negatively regulates plant immunity and functions as a redox sensor activated by ROS (Chae *et al.*, 2021). Identifying ROS-regulated components can help reveal how ROS signalling regulates plant defence responses.

MAPK signalling

Mitogen-activated protein kinase (MAPK) cascades are key in plant signalling responses to biotic attackers (Zhang and Zhang, 2022). These cascades in *A. thaliana* typically consist of a MAPK (20 genes), a MAPK kinase (MAPKK, 10 genes) and a MAPKK kinase (MAPKKK, approximately 70 genes). Often, more than one kinase can operate at each level with redundant or partially overlapping functions. When active, each member of a cascade is phosphorylated and activated in turn starting with the MAPKKK and ending on the MAPK which phosphorylates target proteins to regulate their activity. In PTI signalling, two cascades dominate (Tang *et al.*, 2017; Erickson *et al.*, 2022). One cascade is comprised of MEKK1 (MAPKKK), MKK1/2 (MAPKKs) and MPK4/11 (MAPKs). The second and more significant cascade is comprised of MKKK3/5 (MAPKKK), MKK4/5 (MAPKK) and MPK3/6 (MAPK). The elicitors flg22, elf18 and chitin can all induce MKKK3/5 phosphorylation by PRR-associated RLCKs upstream of plant immune responses (Bi *et al.*, 2018; Yamada *et al.*, 2016). Following the cascade, MAPK targets can include transcription factors, protein kinases and structural proteins. One immune related target is the repressor of defence gene expression, CaM-BINDING TRANSCRIPTION FACTOR 3 (CAMTA3) (Galon *et al.*, 2008). flg22 induces MPK3/6 phosphorylation of CAMTA3 promoting its nuclear export and de-repression of defence gene expression (Jiang *et al.*, 2020). Therefore, MAPK signalling is significant in transducing the perception of a biotic stress into a defence response.

G-protein signalling

Membrane-bound G proteins are guanine nucleotide-binding proteins formed of 3 subunits ($G\alpha$, $G\beta$ and $G\gamma$) which can contribute to plant defence signalling. In *A. thaliana*, there is one $G\alpha$ subunit (GPA1), one $G\beta$ subunit (AGB1) and three $G\gamma$ subunits (AGG1-3) as well as three atypical $G\alpha$ -like subunits (XLG1-3) (Zhang *et al.*, 2021b). In the inactive state, $G\alpha$ -GDP is associated with $G\beta\gamma$. Active $G\alpha$ binds GTP and dissociates from $G\beta\gamma$. Promoted by GTPase activity-accelerating proteins (GAPs), the GTP is then hydrolysed reforming inactive $G\alpha$ -GDP (Zhang *et al.*, 2021b). One GTPase accelerating protein, REGULATOR OF G-PROTEIN SIGNALLING

1 (RGS1), maintains XLG2 in an inactive state until flg22-induced phosphorylation of RGS1 de-represses G-protein signalling (Liang *et al.*, 2018; Tunc-Ozdemir and Jones, 2017). Similarly, elf18, chitin and PEP2 can all regulate RGS1 activity (Liang *et al.*, 2018). GPA1 positively regulates responses to flg22 (Xue *et al.*, 2020) along with AGB1, AGG1 and AGG2, which are also implicated in responses to chitin and elf18 (Liu *et al.*, 2013a). G-protein signalling can regulate immune responses by various processes including by regulating MAPK signalling (Meng *et al.*, 2015; Su *et al.*, 2015) and RBOHD activity (Xu *et al.*, 2017; Zhang *et al.*, 2021b).

Apoplastic pH changes

Apoplastic pH changes occur in plant defence responses and could function as signalling events that regulate these responses (Geilfus, 2017). Various elicitors, including flg22, induce apoplastic alkalinisations (Gust *et al.*, 2007; Jeworutzki *et al.*, 2010; Felix *et al.*, 1999). In support of a signalling role for apoplastic pH changes, plasma membrane H⁺-ATPases (AHAs), which regulate apoplastic pH, have been implicated in plant defence responses (Elmore and Coaker, 2011). For example, overactive *AHA1* mutants display reduced flg22-induced ROS production (Keinath *et al.*, 2010) whilst *aha5* null mutants have enhanced PTI against *P. syringae* (Zhao *et al.*, 2022). Furthermore, flg22 induces phosphorylation status changes in AHA1, 2 and 3, which may regulate their activity (Nühse *et al.*, 2007). As GLR3.3 and 3.6 can be gated by apoplastic pH, apoplastic pH changes could regulate their function in defence signalling (Shao *et al.*, 2020). Interestingly, many pathogens have evolved to manipulate apoplastic pH to promote colonisation (Elmore and Coaker, 2011; Havshøi and Fuglsang, 2022; Kesten *et al.*, 2019). Moreover, beneficial microbes in the plant rhizosphere appear to reduce apoplastic pH to limit PTI responses important in subsequent root colonisation (Yu *et al.*, 2019a). Therefore, it is possible that apoplastic pH changes act as signalling events in plant defence responses.

1.1.5. Hormone signalling in plant responses to biotic attackers

Following the rapid signal transduction events, phytohormone signalling helps drive plant defence responses. Salicylic acid (SA) is the dominant phytohormone for signalling responses to biotrophs. In contrast, jasmonic acid/jasmonates (JA/JAs) and ethylene (Et) dominate phytohormone signalling responses against necrotrophs and damage-based stresses, such as wounding or chewing insects (Bürger and Chory, 2019). Here, the synthesis and signalling of these hormones will be explored along with their role in systemic defence responses.

Salicylic acid: Synthesis and signalling

SA biosynthesis and regulation has recently been well reviewed by Huang *et al.* (2020). Briefly, there are two SA biosynthesis pathways which both begin in chloroplasts from chorismate (CA). In the isochorismate synthase (ICS) pathway, ICS enzymes mediate

isochorismate (IC) synthesis in the chloroplast before export to the cytosol. In the cytosol, glutamate is conjugated to IC before spontaneous degradation to SA which can be promoted by ENHANCED PSEUDOMONAS SUSCEPTIBILITY 1 (EPS1) (Torrens-Spence *et al.*, 2019; Rekhter *et al.*, 2019). The phenylalanine ammonia-lyase (PAL) pathway begins by converting CA to phenylalanine which is used then to produce trans-CA in the cytosol by PAL enzymes. ABNORMAL INFLORESCENCE MERISTEM 1 (AIM1) then converts trans-CA to benzoic acid (BA) before an unknown enzyme converts BA to SA (Huang *et al.*, 2020).

Many of the genes that mediate SA biosynthesis in plant immune responses are transcriptionally regulated (Huang *et al.*, 2020). For example, *ICS1* expression is regulated by SAR-DEFICIENT 1 (SARD1) and CaM-BINDING PROTEIN 60 g (CBP60g) (Zhang *et al.*, 2010; Wang *et al.*, 2011; Wang *et al.*, 2009). CBP60g and SARD1 expression is also regulated in plant immunity including by certain CAMTA transcription factors, such as CAMTA3 which negatively regulates their expression (Sun *et al.*, 2020). CAMTA3 repressive activity can be reduced by flg22-induced phosphorylation of CAMTA3 by MPK3/6 (Jiang *et al.*, 2020). Through such regulation, SA biosynthesis can be enhanced in defence or immune responses.

SA is perceived by the NON-EXPRESSOR OF PATHOGENESIS-RELATED GENES (NPR) 1, 3 and 4 which directly regulate defence gene expression (Fu *et al.*, 2012; Wu *et al.*, 2012). NPR1 acts as a transcriptional co-activator of SA-dependent gene expression whilst NPR3 and 4 function independently of NPR1 and are transcriptional co-repressors (Ding *et al.*, 2018). SA binding to NPR3 or 4 relieves their repressive activity whilst SA binding to NPR1 causes monomerization and subsequent translocation to the nucleus (Mou *et al.*, 2003; Wu *et al.*, 2012). The TGACG SEQUENCE-SPECIFIC BINDING PROTEIN (TGA) transcription factors, TGA2, 5 and 6, then interact with NPR1 to induce transcriptional changes key to SA-induced defence responses (Kesarwani *et al.*, 2007; Zhang *et al.*, 2003; Després *et al.*, 2000; Zhang *et al.*, 1999; Zhou *et al.*, 2000). SA treatments can cause differential expression of over 2400 genes (Ding *et al.*, 2018). Some of these genes can promote further defence signalling and defence responses such as cell wall strengthening by lignin production and the synthesis of antimicrobial secondary metabolites (van Butselaar and Van den Ackerveken, 2020). Therefore, SA signalling is a key regulator of plant defence responses.

Systemic SA signalling

Following the local perception of a biotic threat, SA signalling can contribute not only to local responses but also to systemic defence responses in systemic acquired resistance (SAR) (Sun and Zhang, 2021). Whilst many candidate signalling species have been proposed to mediate SAR, it is currently thought that *N*-hydroxyphenylacetic acid (NHP) is the dominant systemic signal with transport likely via the phloem (Chen *et al.*, 2018; Hartmann *et al.*, 2018). NHP derives from

lysine in the plastid with additional biosynthetic steps in the chloroplast and cytosol (Sun and Zhang, 2021). As with SA biosynthesis, NHP biosynthetic enzymes are transcriptionally regulated with SARD1 and CBP60g promoting their expression following local immune signalling (Sun *et al.*, 2020; Sun *et al.*, 2015; Sun *et al.*, 2018). NHP treatment induces the expression of various defence genes including SA and NHP biosynthetic genes (Chen *et al.*, 2018; Hartmann *et al.*, 2018). Resultingly, NHP systemic signalling activates SAR through promoting NHP and SA signalling in systemic tissues.

Jasmonic acid: Synthesis and signalling

Biosynthesis of JAs can occur via three pathways all split across the chloroplasts, peroxisomes, and cytosol (Ruan *et al.*, 2019). The octadecane pathway is a major contributor to JA synthesis in plant defence responses. This pathway can start from α -linolenic acid (18:3) released from chloroplast phospholipids. α -linolenic acid then undergoes reactions catalysed by a 13-LIPOXYGENASE (LOX), ALLENE OXIDE SYNTHASE (AOS) and an ALLENE OXIDE CYCLASE (AOC) to produce *cis* (+)-12-oxo-phytodienoic acid (OPDA) (Bürger and Chory, 2019; Griffiths, 2020). OPDA is exported from the chloroplasts and can itself function as a signalling species in plant defence responses (Taki *et al.*, 2005; Gleason *et al.*, 2016). Additionally, OPDA can be reduced by OPDA REDUCTASE 3 (OPR3) in the peroxisome before three rounds of β -oxidation to produce jasmonic acid which is released into the cytosol (Griffiths, 2020). In the cytosol, jasmonic acid can be converted to various forms including the bioactive jasmonic acid-isoleucine (JA-Ile) (Staswick and Tiryaki, 2004; Fonseca *et al.*, 2009).

JA biosynthesis in plant defence responses can be transcriptionally regulated. For example, in the absence of defence signalling, the JAV1-JAZ8-WRKY51 complex represses the expression of JA biosynthetic genes including AOS and OPR3. Damage that occurs with insect herbivory leads to $[Ca^{2+}]$ elevations perceived by a CaM that promotes the phosphorylation and disassembly of this complex, thus promoting expression of JA biosynthetic genes and JA accumulation (Yan *et al.*, 2018). Similarly, CaM1 is thought to perceive $[Ca^{2+}]$ elevations in response to herbivory to release WRKY52 repression of (13-)LOX gene expression promoting JA biosynthesis (Jiao *et al.*, 2022). Whilst other mechanisms exist for regulating JA levels, this demonstrates how JAs can accumulate in plant defence responses.

JA-Ile signalling is transduced via an SCF complex containing CORONATINE INSENSITIVE 1 (COI1) as a JA-Ile receptor (Yan *et al.*, 2009; Griffiths, 2020). In the absence of JA-Ile, JA ZIM domain (JAZ) proteins function as transcriptional repressors of JA-regulated transcription factors along with the TPL co-repressor and NINJA adaptor proteins (Acosta *et al.*, 2013; Pauwels *et al.*, 2010). JA-Ile binding to the SCF-COI1 complex triggers JAZ ubiquitination and subsequent proteasomal degradation (Griffiths, 2020). This signalling therefore de-represses various JA-

regulated transcription factors with two major branches identified: the MYC branch which is largely active against damage-based stimuli and the ERF branch which is predominantly active in responses to necrotrophic pathogens (Gupta *et al.*, 2020). In the MYC branch, MYC2 is a master regulator transcription factor that can function as a homo-dimer or in hetero-dimers with MYC3 or MYC4 (Dombrecht *et al.*, 2007; Kazan and Manners, 2013; Lorenzo *et al.*, 2004; Fernández-Calvo *et al.*, 2011). The ERF branch involves the ETHYLENE-INSENSITIVE 3 (EIN3) and EIN3-LIKE 1 (EIL1) transcription factors which are stabilised by Et signalling and induce various defence genes including *ETHYLENE RESPONSE FACTOR 1 (ERF1)* and *PLANT DEFENSIN 1.2 (PDF1.2)* (Gupta *et al.*, 2020). These two branches of JA-mediated defence signalling are mutually antagonistic helping to tailor the transcriptional changes and defence responses to the prevailing biotic stress (Song *et al.*, 2014).

Systemic JA signalling: Mobile JAs and *de novo* JA biosynthesis

JA signalling can also contribute to systemic responses following biotic attack or damage (Hilleary and Gilroy, 2018). In part, this systemic JA signalling can be mediated by mobile JA species. For instance, cotyledon wounding induces LOX2-dependent root JA signalling mediated by mobile JA oxylipins (Gasperini *et al.*, 2015). Moreover, systemic wound responses in adult plants are thought to involve mobile jasmonates produced by LOX6 that travel radially away from the vasculature into the leaf blade (Gasperini *et al.*, 2015). OPDA and its derivatives, but not JA-Ile, can translocate from shoots into roots following wounding. This transport is thought to occur by the phloem with OPDA then converted into JA and JA-Ile to mediate responses (Schulze *et al.*, 2019). JAT3 and JAT4 are plasma membrane-localised JA importers that function in the phloem to promote long distance JA translocation in wound responses (Li *et al.*, 2020; Li *et al.*, 2021b). Moreover, JAT1, could contribute to this process as a transporter that mediates JA efflux from cells (Li *et al.*, 2017; Wang *et al.*, 2019a). In summary, mobile JAs can contribute to systemic JA signalling in plant defence responses.

Large-scale wounding triggers rapid systemic JA accumulations within 120 s which are thought occur by *de novo* JA biosynthesis and contribute to plant defence responses (Mousavi *et al.*, 2013; Chauvin *et al.*, 2013; Glauser *et al.*, 2009; Koo *et al.*, 2009; Glauser *et al.*, 2008). A model is evolving for the mechanisms that may underpin this rapid systemic JA biosynthesis (Figure 1.4)(Suda and Toyota, 2022). In this model, large-scale wound events, including primary vascular tissue, trigger rapid systemic signalling that propagates via the vascular tissue to connected organs. This signalling includes membrane depolarisations, $[Ca^{2+}]$ elevations, ROS elevations and hydraulic waves, which are thought to be interconnected (Mousavi *et al.*, 2013; Fichman and Mittler, 2021a; Fichman *et al.*, 2019; Toyota *et al.*, 2018; Nguyen *et al.*, 2018; Bellandi *et al.*, 2022; Grenzi *et al.*, 2023; Salvador-Recatalà, 2016; Gao *et al.*, 2023). The Ca^{2+} -

permeable GLR3.3 and 3.6 channels both significantly contribute to all these large-scale wound-induced signalling events with roles also reported for GLR3.1, GLR3.5, RBOHD, AHA1, MSL10, ANNEXIN1 and plasmodesmata (Mousavi *et al.*, 2013; Salvador-Recatalà, 2016; Toyota *et al.*, 2018; Nguyen *et al.*, 2018; Kumari *et al.*, 2019; Fichman and Mittler, 2021a; Moe-Lange *et al.*, 2021; Malabarba *et al.*, 2021; Bellandi *et al.*, 2022; Grenzi *et al.*, 2023; Gao *et al.*, 2023). GLR3.3 and GLR3.6 are primarily expressed in the phloem and xylem contact cells, respectively (Nguyen *et al.*, 2018). Various mechanisms are thought to contribute to GLR3.3 and 3.6 activation in systemic responses to large-scale wounding. Some mechanisms involve the rapid transport of mobile signals via the xylem. Glutamate has been proposed to be passively released from the phloem with large-scale wounding and to travel by bulk flow in the xylem to systemically activate GLR3.3 (Toyota *et al.*, 2018; Bellandi *et al.*, 2022; Grenzi *et al.*, 2023). The thioglucosidase (TGG) enzymes, TGG1 and 2, are also released with large-scale wounding and can travel systemically via the xylem to induce rapid membrane depolarisations, $[Ca^{2+}]$ elevations, and JA defence signalling (Gao *et al.*, 2023). TGG1 appears to activate GLR3.3 and 3.6 because TGG1-induced systemic responses are impaired in *glr3.3* mutants and abolished in *glr3.6* mutants. It is unclear how TGG1 could activate GLRs, though reactive aglycones produced from glucosinolates by TGG1 are required for the systemic signalling. Other proposed mechanisms for the large-scale wound-induced rapid systemic signalling include the systemic perception of turgor pressure changes in the vascular tissue (Farmer *et al.*, 2014). The MSL10 mechanosensitive anion channel is thought to perceive these pressure changes and contribute to systemic membrane depolarisations which promote the full activation of GLR3.3 and 3.6 (Moe-Lange *et al.*, 2021). Moreover, turgor pressure changes may activate GLRs by causing systemic elevations in apoplastic glutamate concentrations by unknown mechanisms (Grenzi *et al.*, 2023). Finally, there may be a role for pH in the systemic activation of GLR3.3 and 3.6 because the AHA1 plasma membrane H^+ -ATPase is implicated in large-scale wound-induced systemic signalling and because pH can gate GLR3.3 and 3.6 (Kumari *et al.*, 2019; Shao *et al.*, 2020). Whilst the activation of GLR3.3 and 3.6 in large-scale wound-induced systemic signalling is not well resolved, these channels are heavily implicated in the rapid systemic accumulation of JAs and subsequent defence responses.

phosphorylate and inactivate CONSTITUTIVE TRIPLE RESPONSE 1 (CTR1) which liberates EIN2 from suppression by CTR1. EIN2 then enters the nucleus and stabilises EIN3 and EIL transcription factors which promote the expression of *ERF* transcription factor genes that can induce defence gene expression. Et signalling can thereby integrate into the ERF branch of JA defence signalling.

Interactions between SA and JA signalling

As SA signalling promotes defences against biotrophs and JA signalling promotes defences against necrotrophs, SA and JA signalling often interact antagonistically to ensure appropriate defence responses (Hou and Tsuda, 2022). These interactions can be regulated in several ways. SA signalling can suppress JA-induced gene expression to promote SA-dependent pathogen resistance by SA-activated NPR1 binding and inhibiting JA-activated MYC2 (Nomoto *et al.*, 2021). Moreover, CATALASE2 promotes JA biosynthesis and is suppressed by SA signalling (Yuan *et al.*, 2017). During JA signalling, MYC2 and its homologues promote the expression of specific ANAC genes and ZAT18. The ANAC transcription factors suppress the expression of *ICS1* whilst ZAT18 inhibits EDS1 both leading to reduced SA accumulation and SA signalling (Zheng *et al.*, 2012; Gao *et al.*, 2022). This SA-JA antagonism can help tailor plant defence responses to be appropriate for the pest or pathogen present. However, there are cases when SA and JA signalling operate synergistically, especially if SA and JA are applied at relatively low concentrations (Mur *et al.*, 2006). In ETI, SA signalling via NPR3 and 4 may promote JA signalling by JAZ degradation (Liu *et al.*, 2016). SA signalling promoting JA signalling could act to limit the risk of necrotrophic pathogen infection after cell death in HR against biotrophic pathogens. However, this may not be true synergy between the signalling pathways as the SA and JA signalling domains appear to be spatially separated (Betsuyaku *et al.*, 2018). In any case, SA and JA signalling interact and can tailor plant defence responses for the biotic stress present.

1.1.6. Effectors and ETI

Pest or pathogen effectors can manipulate a broad range of host processes to promote infection or colonisation including elicitor perception, defence signalling and defence outputs (Wang *et al.*, 2022c). NLRs may recognise effectors directly by binding them or through monitoring and 'guarding' effector targets or 'decoy' proteins (Chen *et al.*, 2022). NLR signalling is an important determinant of plant resistance to pests and pathogens and will therefore be considered here.

NLR classification and activity

The understanding of NLR structure, function and signalling is rapidly advancing and has recently been well reviewed by Wang *et al.* (2023). In brief, most NLRs consist of three domains: a variable N-terminal domain, a central conserved nucleotide-binding and oligomerization

domain (NOD) and a C-terminal LRR domain. Plant NLRs can largely be categorised into groups by their N-terminal domains: coiled-coil (CC) NLRs (CNLs), Toll/interleukin-1 receptor (TIR) NLRs (TNLs), and CC_R-NLRs (RNLs). Finally, NLRs can be categorised by their functions as either sensor NLRs or helper NLRs which perceive effectors or mediate signalling responses, respectively (Feehan *et al.*, 2020). However, some NLRs can mediate both the perception of effectors and downstream signalling such as the CNL HOPZ-ACTIVATED RESISTANCE 1 (ZAR1). When sensor and helper NLRs are required, they may be genetically linked as paired NLRs.

Oligomerisation of NLRs into a 'resistosome' complex is important for signalling from many NLRs and can involve nucleotide switching. The ZAR1 resistosome typifies this mechanism and is one of the most well characterised NLRs. ZAR1 constitutively interacts with the RLCK RESISTANCE-RELATED KINASE 1 (RKS1) which allows 'guarding' of another RLCK, PBS1-LIKE 2 (PBL2). The *Xanthomonas campestris* effector AvrAC uridylates PBL2 to form PBL2^{UMP} which is recruited to ZAR1-RKS1. This recruitment causes a ZAR1 conformational change which releases ADP and results in the formation of the pentameric wheel-like ZAR1 resistosome stabilised by ATP binding (Wang *et al.*, 2019c; Wang *et al.*, 2019b; Hu *et al.*, 2020). Not all NLRs show nucleotide switching in oligomerisation with the TNL RECOGNITION OF *Peronospora parasitica* 1 (RPP1) remaining ADP bound in a tetrameric resistosome (Ma *et al.*, 2020a). Appreciating the mechanisms of NLR oligomerisation will help understand how effector recognition initiates plants defence signalling.

Following oligomerisation, NLRs trigger signalling events that drive defence responses. The structure of the ZAR1 resistosome contains a central pore required for its function (Wang *et al.*, 2019b). This pore creates a plasma membrane Ca²⁺-permeable channel allowing Ca²⁺ influxes that are required for HR activation (Bi *et al.*, 2021). Whilst it is not yet resolved how the Ca²⁺ fluxes regulate immunity, Ca²⁺ channel formation is thought to be a conserved mechanism for CNL signalling (Wang *et al.*, 2023). TNL oligomerisation into a tetrameric resistosome is also thought to induce Ca²⁺-permeable channel formation to regulate responses (Wang *et al.*, 2023). Firstly, the TIR domains of activated TNL tetramers form two composite NADase active sites from each TIR dimer (Ma *et al.*, 2020a; Wan *et al.*, 2019; Horsefield *et al.*, 2019; Martin *et al.*, 2020). Small molecules generated by this activity then regulate the interactions of the lipase-like protein ENHANCED DISEASE SUSCEPTIBILITY 1 (EDS1) with either PHYTOALEXIN DEFICIENT 4 (PAD4) or SENESCENCE-ASSOCIATED GENE 101 (SAG101). Subsequently, EDS1-PAD4 and EDS1-SAG101 complexes promote the formation of Ca²⁺-permeable resistosome channels by the RNLs, ACTIVATED DISEASE RESISTANCE 1 (ADR1) and N REQUIREMENT GENE 1 (NRG1), respectively (Jacob *et al.*, 2021; Dongus and Parker, 2021; Wang *et al.*, 2023). In this way, it is

thought that NLR activation converges on Ca^{2+} channel formation and signalling that promotes ETI responses including large scale transcriptional reprogramming (Figure 1.5).

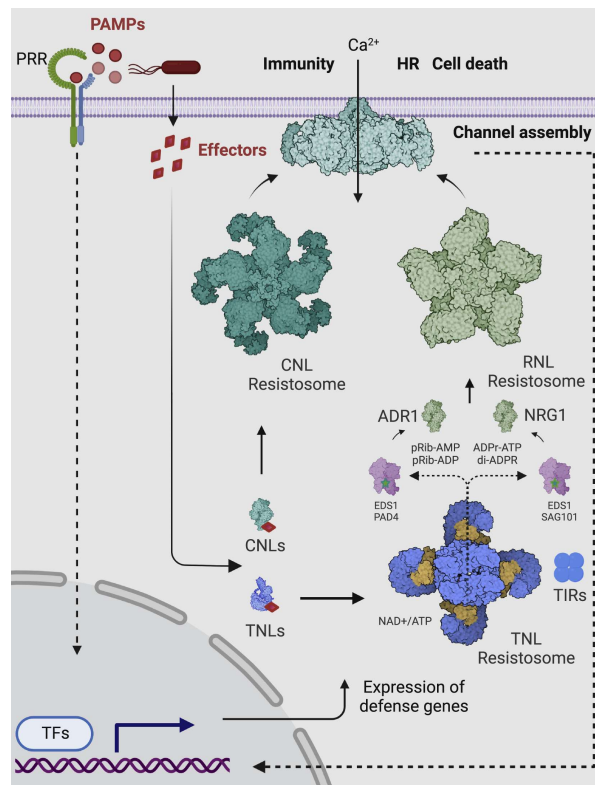


Figure 1.5 Model of resistosome and Ca^{2+} -permeable channel formation by NLRs.

Pathogen recognition involves PAMP-perception and signalling to mediate defence responses including transcriptional changes. Effector recognition by NLRs can also occur. Following this perception, coiled coil domain NLRs (CNLs) form resistosome oligomers that can insert into the plasma membrane as Ca^{2+} -permeable channels. Effector recognition by toll/interleukin-1 receptor domain NLRs (TNLs) results in resistosome oligomers that have NADase activity and produce small nucleotide-based molecules. These small molecules activate either EDS1-PAD4 or EDS1-SAG101 that then activate the helper NLRs, ADR1 and NRG1, respectively. The helper NLR resistosomes can then form Ca^{2+} -permeable channels in the plasma membrane. Channel formation allows Ca^{2+} influx and promotes signalling to induce effector-triggered immunity. Model adapted from Wang *et al.* (2023) with permissions.

ETI signalling and the interactions with PTI

ETI and PTI signalling appear to be overlapping and interacting. For example, PTI and ETI responses both involve MAPK signalling, $[\text{Ca}^{2+}]$ and ROS elevations, transcriptional reprogramming, and hormone signalling (Thulasi Devendrakumar *et al.*, 2018; Peng *et al.*, 2018; Tsuda and Katagiri, 2010). Whilst there are differences in the dynamics of the responses induced by PTI and ETI, this overlap suggests PTI and ETI signalling could act synergistically in immune responses (Yuan *et al.*, 2021). Indeed, recent work has revealed that NLR-activated responses potentiate those induced by PRR activation including ROS elevations, MAPK activation, gene

expression and callose deposition (Ngou *et al.*, 2021). Moreover, ETI activation induces the expression of various PTI signalling components including BAK1 and SOBIR1 (Ngou *et al.*, 2021; Yuan *et al.*, 2020). PRR signalling can also promote ETI-associated responses to ectopically expressed effectors and the pathogen *P. syringae* carrying the AvrRpt2 or AvrRps4 effectors (Ngou *et al.*, 2021; Yuan *et al.*, 2020). Whilst there are some cases in which PRR signalling suppresses ETI responses (Hatsugai *et al.*, 2017), these recent findings suggest that PTI and ETI are largely mutually potentiating. Subsequently, the 'zig zag' model of plant immunity (Figure 1.1) has been adapted to incorporate this mutual potentiation (Yuan *et al.*, 2021). An improved understanding of ETI signalling will help evolve the understanding of plant defence responses.

1.1.7. Plant defence outputs

Plant perception and signalling of a biotic stress ultimately functions to tailor inducible defences against the specific pest or pathogen. Some inducible defences can be structural such as reinforcement of the cell wall and callose deposition (Voigt, 2014; Rasool *et al.*, 2017). Additionally, plants can express pathogenesis related (PR) proteins with diverse and direct defence related functions, such as chitinases that can attack fungal or insect chitin and defensins that have antibacterial and antifungal activities (Loon *et al.*, 2006). Against herbivorous insects, plant defence responses can include the expression of proteinase inhibitors (PIs) which can impair insect protein digestion (War *et al.*, 2012; Arnaiz *et al.*, 2018). Secondary metabolites are diverse compounds that primarily function in plant-environment interactions including plant defence responses (Erb and Kliebenstein, 2020; Piasecka *et al.*, 2015). Inducible defensive secondary metabolites can include cyanogenic glycosides, terpenes, and alkaloids and can have diverse defensive effects including membrane disruption, inhibition of ion or nutrient transport and disruption of DNA replication (Piasecka *et al.*, 2015; Divekar *et al.*, 2022). Some secondary metabolites form volatile organic compounds (VOCs) which can be toxic to insect herbivores, repel them or attract natural predators of the insect (Zhou and Jander, 2021). Pathogen infection and aphid feeding can both promote increases in the amino acid-derived glucosinolate secondary metabolite, 4-methoxyindole-3-yl-methylglucosinolate, that functions in plant defence responses (Kim and Jander, 2007; Xu *et al.*, 2016). Glucosinolates can act as defences following their enzymatic break down into toxic products during pathogen or pest attack (Piasecka *et al.*, 2015). In summary, diverse inducible defences are deployed following the perception and signalling of a biotic stress to limit pest or pathogen colonisation or infection.

1.1.8. Summary of general plant defence responses to biotic stress

Here, the mechanisms by which plants recognise and respond to biotic stresses have been explored. Perception at the plasma membrane can include the recognition of PAMPs, HAMPs, DAMPs, phytochemicals and mechanical stress. This perception triggers a series of rapid signalling events, including $[Ca^{2+}]$ elevations. Together with phytohormone signalling, these signalling events coordinate defence outputs. Whilst effectors may function to suppress defence signalling, NLR recognition of pest or pathogen effectors can trigger further signalling to enhance plant defence responses. The defence outputs can take many forms. To ensure defence responses are appropriate to resist diverse pests and pathogens, there is specificity built into the perception and signalling mechanisms. The molecular interactions between plants and their biotic attackers can determine how resistant the plant is to the pest or pathogen present.

1.2. Plant defence responses to insect pests

Using the understanding of general plant defence responses laid out in Section 1.1, plant defence responses to insect pests can be explored. Molecular insect-plant interactions are heavily influenced by how the insect colonises and/or feeds from the plant. These interactions are relatively well characterised for the chewing insects of lepidopteran larvae (caterpillars) but much less well characterised for aphids and thrips which feed on a more localised scale. To lay the foundations for the upcoming investigations into how plants perceive aphid and thrips feeding, the knowledge of the plant molecular interactions with caterpillars, aphids and thrips will be considered here.

In considering the plant-insect interactions, stimuli will be categorised based on spatial scales. A large-scale stimulus will refer to any stimulus that influences many cells across different tissues (e.g. cutting or crushing a leaf and caterpillar feeding). Such stimuli may induce rapid systemic signalling. A localised/local stimulus will refer to any stimulus that affects only a few cells in direct contact with the stimulus or closely neighbouring cells (e.g. localised wounding or aphid feeding). These stimuli generally do not trigger rapid systemic signalling responses.

1.2.1. Lepidopteran larvae: Chewing insects that cause large-scale damage

Caterpillar feeding and plant perception

Phytophagous lepidopteran larvae (caterpillars) are usually multiple millimetres in length. They can form significant pests through using their chewing mandibles to fracture and remove relatively large quantities of plant tissue for consumption. During this feeding process,

caterpillars can produce oral secretions (OS), comprised of regurgitant from the anterior gut, and salivary secretions, produced from labial and mandibular glands (Acevedo *et al.*, 2015).

Plant responses to caterpillar feeding have been heavily studied. To mimic caterpillar feeding in investigations, stimuli that cause large-scale damage are often applied with or without OS treatments (Malabarba *et al.*, 2021; Meena *et al.*, 2019). Moreover, robotics has been used to recapitulate caterpillar feeding patterns with MecWorm (Bricchi *et al.*, 2010) and with salivary components added using SpitWorm (Li *et al.*, 2019). These investigations have revealed that the pattern of damage and the OS both contribute to the plant perception of caterpillar feeding.

Perception of caterpillar HAMPs

Various HAMPs that induce plant defences have been identified from lepidopteran larvae (Jones *et al.*, 2022; Snoeck *et al.*, 2022). For example, volicitin, a fatty acid-amino acid conjugate (FAC), was the first purified HAMP and was identified from *Spodoptera exigua*. Volicitin induces VOC emissions in damaged maize leaves that can attract parasitic wasps of *S. exigua* (Turlings *et al.*, 2000). Similar FAC HAMPs have been identified in the OS of many lepidopteran species (Yoshinaga *et al.*, 2010). For some lepidopteran larvae, bacterial endosymbionts can modulate the extent of defence elicitation suggesting that endosymbionts may influence HAMP production or perception (Wang *et al.*, 2017b; Acevedo *et al.*, 2017; Yamasaki *et al.*, 2021). There is limited knowledge of receptors that perceive lepidopteran HAMPs. However, recently a receptor for the HAMP, inceptin, was identified (Steinbrenner *et al.*, 2020). Inceptins are present in the OS of several lepidopteran species and are produced by caterpillars as disulfide-bridged peptides derived from plant chloroplastic ATP synthase γ -subunits (Schmelz *et al.*, 2006; Schmelz *et al.*, 2012). Inceptins can induce many defence responses including JA signalling, volatile emissions, and PI production (Schmelz *et al.*, 2006). The RLP INCEPTIN RECEPTOR (INR) was demonstrated in tobacco species to bind inceptins, facilitate inceptin-induced defence responses and enhance *S. exigua* resistance (Steinbrenner *et al.*, 2020). In summary, plant perception of caterpillar feeding can include HAMP perception.

Damage perception and signalling during lepidopteran larval feeding

Large-scale damage is an integral part of caterpillar feeding. Therefore, the mechanism of large-scale wound-induced rapid systemic signalling that leads to *de novo* JA biosynthesis may operate in responses to caterpillar feeding (Section 1.1.5 – Systemic JA Signalling). In support of this notion, when the primary vascular tissue is damaged, both large-scale wounding and caterpillar feeding induce rapid systemic $[Ca^{2+}]$ elevations, membrane depolarisations and JA marker gene expression (Kiep *et al.*, 2015; Salvador-Recatalà *et al.*, 2014; Nguyen *et al.*, 2018; Toyota *et al.*, 2018; Gao *et al.*, 2023). Moreover, resistance against *Spodoptera* spp. is altered in several *A. thaliana* mutants (*glr3.3*, *aha1*, *isi1*, *aca10* *aca12* and *ann1*) that are impaired in the

large-scale wound-induced rapid systemic signalling (Kumari *et al.*, 2019; Nguyen *et al.*, 2018; Wu *et al.*, 2022; Malabarba *et al.*, 2021; Fotouhi *et al.*, 2022). As proposed for the large-scale wound-induced responses (Toyota *et al.*, 2018; Bellandi *et al.*, 2022; Grenzi *et al.*, 2023), the caterpillar-feeding induced rapid systemic signalling may be regulated by GLR3.3 and 3.6 following the perception of the DAMP glutamate. Thus, the perception of damage or DAMPs with caterpillar feeding appears to trigger rapid systemic signalling upstream of JA-mediated plant defence responses.

Other damage perception mechanisms also appear to contribute to local and systemic responses to caterpillar feeding, including various phytoytokine signalling pathways. For example, the systemin phytoytokine found in many solanaceous plant species is thought to be released from pro-systemin with wounding and caterpillar feeding as a mobile signal (Zhang *et al.*, 2020). Systemin is perceived locally and systemically by the RLK SYSTEMIN RECEPTOR 1 (SYR1) to promote defence responses against chewing insects including ROS and ethylene production, JA signalling and PI accumulation (Wang *et al.*, 2018; Coppola *et al.*, 2019; Pearce *et al.*, 1991; Green and Ryan, 1972; Orozco-Cardenas *et al.*, 1993). Similar molecules in hydroxyproline-rich systemins have also been implicated as phytoytokines in responses to lepidopteran larvae as well as to some pathogens (Pearce, 2011; Hou *et al.*, 2021a). The PEP-PEPR phytoytokine signalling system that can be induced by damage can also promote resistance against chewing insects. For example, *pepr1 pepr2* mutant *A. thaliana* displays reduced resistance against *S. littoralis* (Klauser *et al.*, 2015). The SCOOP-MIK2 phytoytokine signalling system that can be induced by wounding is also induced following *S. littoralis* feeding and contributes to plant defences against this pest (Stahl *et al.*, 2022). Therefore, various damage-associated phytoytokine signalling pathways operate in plant defence responses to lepidopteran larvae.

Hormone signalling responses to caterpillars

JA signalling is largely considered to be the dominant hormone signalling pathway that operates in responses to chewing insect herbivory in both local and systemic tissues (Bürger and Chory, 2019; Erb *et al.*, 2012; Wang *et al.*, 2021a). Indeed, many investigations report that caterpillar feeding induces the accumulation of JAs and JA-regulated defence compounds as well as the expression of JA responsive genes (Weech *et al.*, 2008; Reymond *et al.*, 2004; De Vos *et al.*, 2005; Schweizer *et al.*, 2013; Mewis *et al.*, 2006; Meena *et al.*, 2019). Moreover, *A. thaliana* mutants defective in JA biosynthesis or signalling often display reduced resistance to chewing insect herbivores (Schweizer *et al.*, 2013; Fernández-Calvo *et al.*, 2011; Mewis *et al.*, 2006; Meena *et al.*, 2019; Havko *et al.*, 2020). The dominance of JA signalling in responses to caterpillar feeding is consistent with damage being a major contributor to the plant perception of

caterpillar feeding because JA signalling also dominates hormone signalling responses to large-scale damage (Koo and Howe, 2009; Mousavi *et al.*, 2013; Meena *et al.*, 2019; Toyota *et al.*, 2018). However, treatment with caterpillar OS can also induce JA accumulation (Klauser *et al.*, 2015). Thus, the perception of both damage and HAMPs may induce JA defence signalling in responses to caterpillar feeding.

Effectors from lepidopteran larvae

Lepidopteran larval secretions are considered to contain effector proteins that can manipulate host defences. In support of this, the OS of some caterpillars species can suppress wound-induced responses in plants (Consales *et al.*, 2011; Kinoshita and Betsuyaku, 2018) including the large-scale wound-induced systemic $[Ca^{2+}]$ elevations (Kiep *et al.*, 2015). Moreover, some effectors have been identified in caterpillar OS. In contrast to the inceptin elicitor from the generalist *S. frugiperda*, the *Anticarsia gemmatalis* specialist caterpillar produces a truncated inceptin peptide effector that antagonises full length inceptin-induced defence responses (Schmelz *et al.*, 2012). Additionally, *Helicoverpa armigera* produces the HARP1 effector protein that is delivered into plants with feeding. HARP1 limits JA-induced JAZ repressor degradation and JA-mediated defence responses thus promoting *H. armigera* feeding (Chen *et al.*, 2019). Many caterpillar species are relatively mobile and quickly consume large amounts of plant tissue. Therefore, effectors may play a relatively minor role in determining whether a caterpillar can feed from a plant. However, *S. frugiperda* feeding occurs over extended periods of time in enclosed whorls where frass can accumulate near feeding sites. Interestingly, when feeding from maize, this frass can contain maize chitinases that are induced with feeding and that suppress host defences against *S. frugiperda* (Ray *et al.*, 2016). These examples reveal that caterpillars can deliver effectors to suppress plant defence responses and promote feeding.

Summary of plant responses to lepidopteran larvae

Feeding from caterpillars causes significant damage which can be perceived along with HAMPs from OS. The perception of caterpillar feeding in *A. thaliana* induces local and systemic defence responses which can include rapid systemic signalling and *de novo* JA biosynthesis. Effectors can also be delivered with feeding to suppress plant defence responses. The ability to mimic caterpillar feeding by wounding and OS treatments has greatly facilitated investigations into the mechanisms that underpin the plant perception of caterpillar feeding.

1.2.2. Thrips: Minute pests that exhibit damage-based feeding on a local scale

There are over 5500 described species of thrips (order: Thysanoptera). These insects are usually less than 1.5 mm in length and display characteristic fringed wings that help them remain airborne despite being poor flyers (Mound, 2005). Phytophagous thrips species can form plant

pests by direct damage during feeding or by transmitting economically significant plant viruses, such as tospoviruses (Riley *et al.*, 2011; Steenbergen *et al.*, 2018; Rotenberg and Whitfield, 2018; Jones, 2005). For example, the thrips *Frankliniella occidentalis* poses a significant threat as both a generalist pest, feeding on host plants from over 60 families, and as the primary vector of the devastating tomato spotted wilt virus (TSWV) (Wijkamp *et al.*, 1995; Riley *et al.*, 2011; Steenbergen *et al.*, 2018; Mouden *et al.*, 2017). Thrips pests are challenging to control due to several factors, including their complex lifecycles, rapidly evolving pesticide resistance and ability to evade pesticides or detection (Gao *et al.*, 2012; Steenbergen *et al.*, 2018; Rotenberg and Whitfield, 2018). Understanding and enhancing plant defences against thrips would help to limit thrips damage to plants and thrips-vectoring virus transmission.

Thrips interactions with plants

Thrips detect suitable host plants through pre- and post-alighting cues which occur before and after making physical contact with the plant, respectively (Steenbergen *et al.*, 2018). Pre-alighting selection involves the detection of various stimuli including volatile molecules and colour (Childers and Brecht, 1996; Koschier *et al.*, 2007; Teulon *et al.*, 1999; Koschier *et al.*, 2000). Post-alighting selection can involve sensing plant nutritional quality and the presence of plant defences (Leiss *et al.*, 2013; Wang *et al.*, 2014a; Pobożniak and Koschier, 2014; Leiss *et al.*, 2009; Baez *et al.*, 2011). For example, potato overexpressing defensive PIs can deter *F. occidentalis* (Outchkourov *et al.*, 2004).

Thrips display a complex lifecycle on host plants (Steenbergen *et al.*, 2018). This involves a haplodiploid sex-determination system with diploid females emerging from fertilised eggs and haploid males emerging from unfertilised eggs. Adult female thrips lay eggs into or on host plant tissue from which larvae emerge and develop through two larval stages (L1 then L2) that actively feed on the plant. Following this, thrips larvae develop into prepupae and then pupae, both of which do not feed and are soil-dwelling. Adults form from pupae with adult females of *F. occidentalis* being notably larger than adult males. Viral acquisition occurs by L1 and early L2 thrips with later L2 larvae and adult thrips able to deposit viruses (Steenbergen *et al.*, 2018; Riley *et al.*, 2011). The thrips lifecycle generally takes two to three weeks to complete with females capable of laying between 40 and 100 eggs (Cloyd, 2009; Steenbergen *et al.*, 2018). As a result, thrips populations can rapidly expand to colonise a host plant.

Phytophagous thrips can often feed on leaves, petals, fruits and pollen (Steenbergen *et al.*, 2018). Thrips feeding uses the mouth cone which contains two paired, interlocking maxillary stylets and a single mandibular stylet which are all innervated supporting chemosensory functions (Hunter and Ullman, 1994; Hunter and Ullman, 1992). At its distal point, the *F. occidentalis* mandibular stylet is approximately 1-2 μm in diameter as is the maxillary stylet

bundle (Hunter and Ullman, 1992). The mandibular stylet protrudes from the mouth cone by a maximum of approximately 20 μm whilst the maxillary stylets protrude to a maximum of approximately 60 μm (Chisholm and Lewis, 1984). These stylet properties result in highly localised feeding events that are limited to a few cell layers at the leaf surface (Figure 1.6A). To initiate feeding, the mandibular stylet macerates epidermal and mesophyll cells by a downward and backward thrust of the head taking only a fraction of a second. Following this, the mandibular stylet is rapidly withdrawn and replaced by the maxillary stylets. The food canal formed by the maxillary stylets is then used to suck up the released cell contents (Kindt *et al.*, 2006; Kindt *et al.*, 2003; Hunter and Ullman, 1992; Hunter and Ullman, 1989; Chisholm and Lewis, 1984). The maxillary stylets also form a salivary canal which can deliver watery or gelling saliva from the salivary glands during feeding (Hunter and Ullman, 1992; Stafford *et al.*, 2011; Heming, 1978). Whilst the functions of thrips saliva are poorly characterised, saliva is thought to contribute to virus delivery, lubrication of mouth parts, digestion, and effector delivery (Stafford-Banks *et al.*, 2014; Rotenberg *et al.*, 2020). Individual feeding events often last between a few seconds and 30 min with more damage caused by longer duration feeding events (Chisholm and Lewis, 1984). Following feeding, pierced cells collapse and fill with air causing silvery 'scars' to form (Figure 1.6B) (Steenbergen *et al.*, 2018). This feeding behaviour means individual thrips feeding events cause highly localised damage of epidermal and mesophyll cells with limited penetration towards vascular tissue.

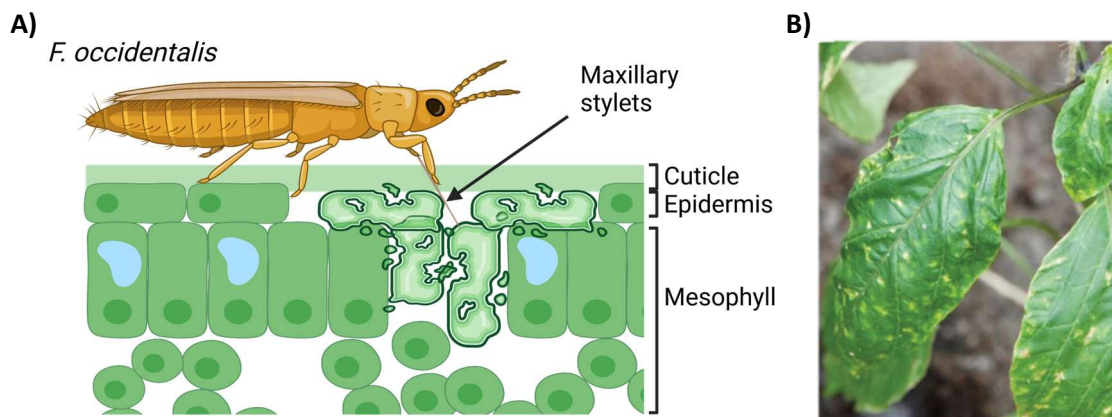


Figure 1.6 Thrips feeding model and scar damage.

(A) Model of feeding for the thrips *Frankliniella occidentalis*. During feeding, *F. occidentalis* pierces and macerates epidermal and mesophyll cells with the mandibular stylet before sucking up cell contents with the maxillary stylets. This feeding and cell damage is largely restricted to a few cell layers at the leaf surface. Created with BioRender.com. (B) Scar damage that results from cell collapse following thrips feeding. Image from Steenbergen *et al.* (2018) with permissions.

Plant perception of thrips feeding

The plant perception of thrips feeding is not well characterised. Partly, this results from thrips being difficult to culture, handle and contain safely without the risk of virus transmission. High throughput methods for assessing thrips resistance are emerging through the automated measurement of thrips feeding-induced damage or plant choice (Thoen *et al.*, 2016; Visschers *et al.*, 2018; Jongsma *et al.*, 2019). However, these approaches have not yet been used to search for components involved in thrips perception in plants and cannot directly provide insights into the initial plant responses to thrips feeding. It is also challenging to recapitulate thrips feeding experimentally without using live insects as can be done for caterpillar feeding. This is because thrips feeding is highly intricate and localised with micrometre or sub-micrometre scale feeding structures and small volumes of saliva which have not yet been collected. Whilst thrips feeding can induce the transcription of *PEPR1*, *PEPR2* and *PROPEP3* (Klauser *et al.*, 2015), it is unknown if these components contribute to thrips perception. In summary, there are currently no known receptors that perceive thrips feeding or elicitors implicated in this plant perception.

Phytohormone signalling in responses to thrips feeding

Since localised damage is a major component of thrips feeding, it is unsurprising that JA signalling dominates phytohormone responses to thrips (Steenbergen *et al.*, 2018). In *A. thaliana*, thrips treatment has been shown to induce JA accumulation and the expression of many JA responsive genes (De Vos *et al.*, 2005; Steenbergen, 2022; Santamaria *et al.*, 2021; Sarde, 2019; Abe *et al.*, 2009; Abe *et al.*, 2008). Moreover, JA pre-treatment of *A. thaliana* increases resistance to *F. occidentalis* whilst *coi1* mutants defective in JA signalling have reduced *F. occidentalis* resistance (Kato *et al.*, 2022; Abe *et al.*, 2009; Abe *et al.*, 2008). *F. occidentalis* treatment can also induce the expression of JA responsive genes in the pepper, *Capsicum annuum* (Sarde, 2019), and in *Solanum lycopersicum* with JA-deficient *S. lycopersicum* mutants impaired in the production of thrips-induced defensive VOCs (Escobar-Bravo *et al.*, 2017). Interestingly, TSWV can suppress JA defence signalling against *F. occidentalis* by inducing antagonistic SA signalling (Abe *et al.*, 2012) and by the viral NSs protein binding JA-activated MYC transcription factors (Wu *et al.*, 2019). This viral manipulation of JA signalling further demonstrates the importance of JA-mediated defence responses in plant resistance to thrips.

It is unclear whether JA signalling in responses to thrips feeding operates systemically. Since thrips feed from epidermal and mesophyll cell layers in leaves, they are not expected to damage the primary vascular tissue as is required to induce rapid systemic $[Ca^{2+}]$ signalling and membrane depolarisations (Kiep *et al.*, 2015; Salvador-Recatalà *et al.*, 2014; Toyota *et al.*, 2018; Gao *et al.*, 2023). Because these rapid systemic signalling mechanisms are thought to regulate *de novo* JA biosynthesis (Johns *et al.*, 2021), it is unlikely that thrips could trigger systemic JA

signalling in this way. However, thrips treatment of *A. thaliana* has been demonstrated to cause the systemic induction of JA marker gene expression in *LOX2*, *3* and *4* and *PDF1.2* (Steenbergen, 2022). These JA-induced responses could be regulated by migratory JA species activating systemic responses. Further investigations are required to appreciate the local and systemic hormone signalling responses to thrips feeding.

Thrips effectors

Whilst thrips effectors may be present in saliva, no *bona fide* thrips effectors have yet been identified and characterised. A salivary gland transcriptome of *F. occidentalis* has been used to predict salivary proteins and has revealed some candidate effectors including regulacin, a Ca²⁺-binding protein hypothesised to disrupt host Ca²⁺ signalling (Stafford-Banks *et al.*, 2014). Recently, a *F. occidentalis* genome has also been produced which facilitated improved characterisation of proteins that may be secreted into saliva on the basis of displaying enriched expression in the salivary glands, predicted signal peptides and no apparent transmembrane domains (Rotenberg *et al.*, 2020). These genes form candidate effectors that could suppress plant defence responses. Methods have been developed to identify whether putative salivary proteins influence thrips resistance by assaying thrips reproduction on tomato leaf discs transiently expressing candidate effector genes (Abd-El-Haliem *et al.*, 2018). This method yielded a putative effector, Foc238, which has not yet been further characterised. Because *F. occidentalis* gene expression can be knocked down by RNA interference (RNAi) (Badillo-Vargas *et al.*, 2015), the contribution of putative effectors to thrips-plant interactions could be assessed through RNAi. Identifying any thrips effectors will be significant in understanding the molecular interactions between plants and thrips.

Summary of plant responses to thrips feeding

Plant responses to thrips feeding are challenging to investigate. In contrast to caterpillars, there are no known elicitors or plant receptors for the recognition of thrips feeding. Moreover, thrips effectors that suppress plant defence responses have not yet been identified. Like caterpillar feeding, damage is likely significant in the plant perception of thrips feeding and the subsequent JA defence signalling. However, unlike caterpillars, thrips feeding-induced damage is highly localised and focussed in epidermal and mesophyll cells. Nonetheless, various DAMPs could be significant for thrips perception in plants as could mechanosensory components and HAMPs that may exist in thrips saliva. Understanding how plants perceive thrips feeding will be significant for appreciating thrips resistance in plants.

1.2.3. Aphids: Phloem feeding pests that minimise cell damage for sustained feeding

Aphids are small hemipteran insects with adult body lengths typically between 1 and 3 mm. Aphids use stylets to feed and primarily feed from plant phloem tissue. With over 4700 species and a presence on all continents except Antarctica, aphids are highly pervasive and diverse (Dixon, 2012; Remaudiere and Remaudiere, 1997). Most of these species are specialists with relatively few aphid species forming generalists (Dixon, 2012). *Myzus persicae* is a model generalist aphid that can colonise more than 100 different plant species including *A. thaliana* (Blackman and Eastop, 2000). Aphid colonisation of plants can directly deplete nutrients, reduce light availability for photosynthesis, promote pathogen infection and cause gall formation (Guerrieri and Digilio, 2008; Kranti *et al.*, 2021). Additionally, aphids can transmit a multitude of economically significant plant viruses (Ng and Perry, 2004). For example, *M. persicae* can transmit over 100 different viruses (CABI, 2015; Blackman and Eastop, 2000). For these reasons, aphid species that can colonise crop plants can be devastating pests (Valenzuela and Hoffmann, 2015; Watanabe *et al.*, 2018; Rabbinge *et al.*, 1981; Khan *et al.*, 2012; Blackman and Eastop, 2017). Whilst pesticide application has been the major strategy for controlling aphid pests, pesticide resistance and legislation to reduce pesticide use make this control strategy less effective (Dewar, 2017; Dedryver *et al.*, 2010; Bass *et al.*, 2014; Silva *et al.*, 2012). Moreover, alternative control strategies for insect pests, such as plant-mediated RNAi and Bt toxins, are of limited use against aphids (Yu *et al.*, 2016; Porcar *et al.*, 2009; Zhao *et al.*, 2016). Therefore, efforts to control aphid pests focus on understanding and enhancing aphid resistance in plants.

Aphid lifecycle and host selection

Aphid colonisation of plants differs throughout a complex lifecycle which is influenced by environmental conditions and varies between species (Hardy *et al.*, 2015; Simon *et al.*, 2002). Despite this, a generalised lifecycle can be described that applies to *M. persicae* in temperate climates and includes cyclic parthenogenesis (Blackman, 1974). In winter, short day lengths and low temperatures result in a single sexual generation of aphids that produce overwintering eggs on a primary host (Le Trionnaire *et al.*, 2008). This phase helps avoid winter food shortages, allows genetic mixing and confers a better ability to tolerate harsh winter conditions (Simon *et al.*, 2002). Following winter, female nymphs emerge from eggs and develop to begin viviparous asexual reproduction producing nymphs which develop through 4 instar stages to become reproductive adults. These asexual or parthenogenetic aphids soon migrate to a suitable secondary host and can continue asexual reproduction until autumn. Asexual populations can expand rapidly as females display relatively short generation times, high fecundities and give birth to individuals with the next generation already developing within them (Kranti *et al.*, 2021; Hong *et al.*, 2019). Aphids can develop as winged (alate) or wingless (apterous). Alates can

develop to promote migration between host plants especially in unfavourable conditions such as on overpopulated leaves (Ogawa and Miura, 2014; Le Trionnaire *et al.*, 2008). Aphid host selection involves a series of cues including pre-alighting cues such as visual and volatile stimuli (Döring, 2014), and post-alighting cues including tactile (Powell *et al.*, 2006) and gustatory cues (Powell *et al.*, 2006; Dixon, 2012; Leybourne *et al.*, 2018; Phelan and Miller, 1982; Escudero-Martinez *et al.*, 2021). These lifecycle properties and behaviours can allow aphids to identify and rapidly colonise secondary host plants.

Aphid feeding structures and behaviour

Like thrips, aphids feed using stylets. However, the aphid stylets and feeding behaviours are significantly different from those of thrips (Figure 1.7). Aphids possess two innervated mandibular stylets that surround two maxillary stylets to form a stylet bundle typically 400 – 700 μm in length (Forbes, 1966; Forbes, 1969). The maxillary stylets interlock and form a food canal and a smaller salivary canal, which fuse into a single common canal towards the distal point of the stylet bundle (Forbes, 1969). The entire stylet bundle tapers from a diameter of approximately 4.5 μm at the head to 2.7 μm near the tip, with each stylet also tapering to a finer point (Forbes, 1969). Both the mandibular and maxillary stylets have several barb-like projections in series towards the distal tip that may aid with clamping stylets in plant tissue or with tissue penetration (Forbes, 1966; Klingauf, 1987). In the common canal, the acrostyle exists as a distinct anatomical region on the inner face of the maxillary stylet cuticle (Uzest *et al.*, 2010). The acrostyle appears to bind effectors and viruses and may therefore promote effector delivery and virus transmission (Deshoux *et al.*, 2022; Webster *et al.*, 2017). The stylets lie in part within a groove along the segmented labium which is extended under the body towards the posterior when aphids are not feeding (Forbes, 1977). These stylets differ significantly from thrips stylets and allow aphids to feed on plant vascular tissue.

To initiate feeding, the aphid labium taps and explores the leaf surface before contracting to allow stylet emergence (Forbes, 1977). A drop of gelling saliva is secreted onto the leaf surface and solidifies to provide a holdfast for feeding initiation as the stylets penetrate into the leaf intercellular spaces (Pollard, 1973; Tjallingii, 2006). Gelling saliva secretion then continues in the plant apoplast producing a sheath that surrounds the stylets (Tjallingii, 2006). This stylet sheath may help lubricate and guide stylet movement and protect stylets from mechanical or chemical damage (Tjallingii, 2006; Will *et al.*, 2012). This sheath remains in the plant after stylet retraction allowing the path of aphid stylets to be visualised. Before reaching the phloem for feeding, aphids perform probes of approximately 5 – 10 s on most of the cells that they encounter, including epidermal and mesophyll cells (Tjallingii and Esch, 1993). During these probes, they secrete a small amount of a watery saliva and ingest a small volume of the

cell contents (Martín *et al.*, 1997). Though some cell death can result from this probing, most cells show no signs of damage or necrosis with gelling saliva helping to plug probed sites (Tjallingii and Esch, 1993; Walling, 2008). The process of probing with limited cell death may promote virus transmission and limit plant defence responses (Martín *et al.*, 1997). Probing mesophyll cells may also allow aphids to sense sugar concentrations and vacuolar pH, both lower than that of phloem sieve elements, to help guide stylets to the phloem (Hewer *et al.*, 2010; Hewer *et al.*, 2011). Once aphids locate the phloem, there is an initial salivation of watery saliva before ingestion coupled with salivation, which is thought to limit the coagulation of phloem proteins during ingestion (Tjallingii, 2006). The watery saliva likely contains proteins that limit phloem occlusion in response to aphid feeding (Will *et al.*, 2009). Subsequent sustained feeding from the phloem can occur and last for hours or even days (Tjallingii, 1995) with phloem sap forming a high carbon and nitrogen substrate which is relatively low in plant defence molecules (Douglas, 2006).

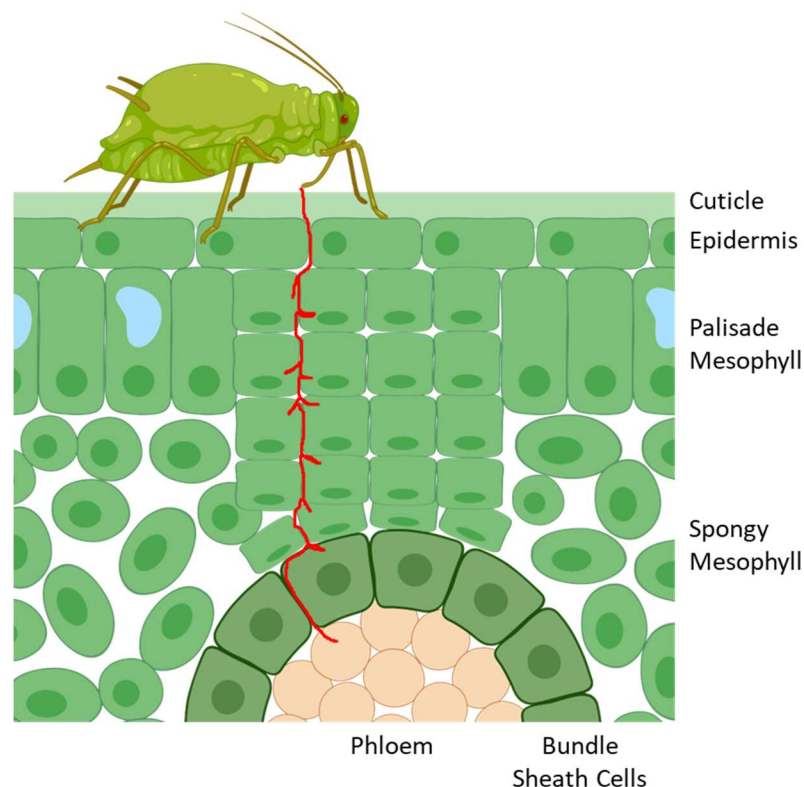


Figure 1.7 Model of aphid feeding.

Model for aphid feeding from a leaf with the path of the aphid stylets demonstrated in red. The aphid stylets extend from the aphid mouthparts and penetrate the leaf cuticle to enter the intercellular space. The stylets are then navigated through the apoplast and probe most cells that they encounter. The probes are short, 5 – 10 s long events that involve secreting a small amount of watery saliva and consuming a small amount of cell contents. Very few cells die because of the probing. The probing process helps guide the stylets to the vascular bundle which includes the phloem and the xylem tissue. When the stylets reach the vascular bundle, they can penetrate the phloem cells and aphids can begin sustained feeding from the phloem sap. Created with BioRender.com.

Plant perception of aphids at the plasma membrane

Aphid feeding interactions are intricate. The cell damage caused is highly localised and limited and the aphid saliva is complex with different types present. Thus, aphid feeding is challenging to recapitulate for investigations into how plants perceive aphid feeding. Nonetheless, aphid feeding is known to induce plant defence responses, including $[Ca^{2+}]$ elevations and gene expression changes, within 30 minutes of feeding initiation or probing (Vincent *et al.*, 2017a; Giolai, 2019). Other inducible defence responses also occur with aphid feeding including ROS production, secondary metabolite accumulation and callose deposition (Nalam *et al.*, 2019; Moran and Thompson, 2001; Jaouannet *et al.*, 2015). Therefore, plants can perceive the early phases of aphid feeding to trigger defence responses.

With limited damage caused by aphid feeding, it is thought that HAMPs play a more major role in the plant perception of aphid feeding than damage or DAMPs. Such HAMPs could be present in aphid saliva. Indeed, the less than 10 kDa fraction of *M. persicae* saliva appears to contain a proteinaceous component that induces plant defence responses against *M. persicae* (De Vos and Jander, 2009). Some candidate HAMPs in aphid saliva have been identified. For example, the *M. persicae* salivary proteins, Mp56, 57 and 58, are considered putative elicitors because they promote aphid resistance when expressed in *A. thaliana* and *N. benthamiana* (Elzinga *et al.*, 2014). Additionally, a salivary pectinase from *Sitobian avenae* can elicit the production of VOCs in wheat that attract the aphid parasitoid, *Aphidius avenae* (Liu *et al.*, 2009). GroEL, a protein derived from the *Buchnera aphidicola* endosymbiont, is a candidate elicitor found in *Macrosiphum euphorbiae* saliva (Chaudhary *et al.*, 2014). GroEL can induce PTI-like ROS bursts, callose deposition, gene expression changes and resistance to aphids (Chaudhary *et al.*, 2014; Elzinga *et al.*, 2014). Extracts produced from whole aphids may also contain HAMPs that function in aphid-plant interactions. *M. persicae* aphid extract can induce the PTI-like responses of ROS bursts, MAPK activation, gene expression changes and aphid resistance (Prince *et al.*, 2014; Canham, 2022). However, the identity of any specific elicitors in *M. persicae* aphid extract remains unknown. Whilst putative aphid HAMPs exist, none have yet been demonstrated to be active in plant-insect interactions without exogenous application or ectopic expression. As such, there is a limited understanding of HAMPs that function in the plant perception of aphid feeding.

Receptors for aphid HAMPs at the plasma membrane have also not yet been identified. The BAK1 RLK co-receptor is required for the full induction of responses to GroEL and *M. persicae* aphid extract (Chaudhary *et al.*, 2014; Prince *et al.*, 2014; Canham, 2022). Whilst *M. persicae* resistance is unaltered on *bak1-5* mutant *A. thaliana* (Prince *et al.*, 2014; Drurey *et al.*, 2019), this may be explained by *M. persicae* effectors suppressing BAK1-dependent defence responses (Drurey *et al.*, 2019). In support of BAK1 contributing to the perception of aphid feeding, *M.*

persicae feeding induces $[Ca^{2+}]$ elevations that are thought to be BAK1-dependent (Vincent *et al.*, 2017a). Moreover, resistance against the pea aphid, *Acyrtosiphon pisum*, is reduced on *bak1-5* mutant *A. thaliana* suggesting that BAK1 can contribute to defences against certain aphid species (Prince *et al.*, 2014). Similarly to BAK1, the SOBIR1 co-receptor contributes to aphid extract-induced PTI-like responses but does not contribute to *M. persicae* resistance (Canham, 2022). The AGB1 G-protein is another plasma membrane signalling component that contributes to *M. persicae* aphid extract-induced responses (Drurey, 2015). As *M. persicae* fecundity and *A. pisum* survival is increased on *agb1-2* mutants (Drurey, 2015), it may be that an aphid HAMP receptor activates a G-protein signalling response that contributes to defence induction. Nonetheless, whilst receptors for aphid HAMPs in *A. thaliana* may exist, none have yet been identified.

A role for damage sensing in the perception of aphid feeding is often overlooked due to the small amount of cell damage and death caused by aphid feeding. Despite this, there is some evidence that damage perception might contribute to aphid feeding-induced responses in *A. thaliana*. Firstly, *M. persicae* feeding induces rapid $[Ca^{2+}]$ elevations around the feeding site that are thought to be dependent on the glutamate DAMP receptors, GLR3.3/3.6 (GLR3.3 and/or GLR3.6) (Vincent *et al.*, 2017a). In addition, these $[Ca^{2+}]$ elevations are considered partially dependent on TPC1 (Vincent *et al.*, 2017a), which has been implicated in plant responses to large-scale wounding (Kiep *et al.*, 2015). The ROS producing RBOHD enzyme, also implicated in systemic responses to large-scale wounding (Fichman and Mittler, 2021a; Fichman and Mittler, 2021b; Fichman *et al.*, 2019; Miller *et al.*, 2009), has also been implicated in *M. persicae* resistance (Miller *et al.*, 2009). However, this role for RBOHD is unclear with RBOHF reported to function in *M. persicae* resistance instead (Jaouannet *et al.*, 2015). Nonetheless, several components implicated in responses to *M. persicae* feeding also function in responses to wounding suggesting that cell damage may contribute to aphid perception. Cell wall damage during aphid feeding could also lead to the release of DAMPs, such as OGs, that induce plant defence responses. In support of this, aphid saliva can contain cell wall modifying enzymes including pectin methylesterases (PMEs) and polygalacturonases (PGs) (Dreyer and Campbell, 1987; Ma *et al.*, 1990; McAllan and Adams, 1961). Moreover, PME activity in *A. thaliana* increases in response to *M. persicae* feeding (Silva-Sanzana *et al.*, 2020) and OGs can induce *M. persicae* resistance (Silva-Sanzana *et al.*, 2022). Therefore, whilst damage perception has not been directly reported during aphid feeding, this perception could contribute to the induction of plant defence responses following aphid feeding.

Whilst there are plasma membrane co-receptors and signalling components implicated in aphid perception, there are no HAMPs, DAMPs or plasma membrane receptors that have

been demonstrated to function at the aphid feeding site. Moreover, mechanical stress caused by stylet navigation may contribute to the plant perception of aphid feeding, but no mechanosensory components have yet been implicated in this perception. Characterising how plants perceive aphid feeding will be critical for understanding plant defence responses against aphids.

JA and SA signalling in responses to aphids

Compared with thrips and caterpillar feeding, the roles of phytohormone signalling pathways in responses to aphid feeding are less clear. For example, *M. persicae* has been demonstrated to induce the expression of various SA and JA marker genes including *PR1* and *PDF1.2*, respectively (Moran and Thompson, 2001; Moran *et al.*, 2002; De Vos *et al.*, 2005). Additionally, the Brassica specialist aphid, *Brevicoryne brassicae*, can induce *PR1* and *JAZ10* expression around feeding sites (Rubil *et al.*, 2022) along with the expression of over 800 JA-regulated transcripts following colonisation (Kusnierczyk *et al.*, 2011). Interestingly, *A. thaliana* genotypes impaired in SA signalling or accumulation have often been shown to have unaltered resistance against *M. persicae* (Pegadaraju *et al.*, 2005; Moran and Thompson, 2001). Additionally, *M. persicae* colonisation is reduced on *A. thaliana npr1* mutants and *NahG* expressing plants that have impaired SA perception and enhanced SA degradation, respectively (Mewis *et al.*, 2006). Therefore, SA signalling may promote *M. persicae* colonisation of *A. thaliana*. In contrast, *M. persicae* resistance is reduced in the *coi1* and *aos* mutants, which are defective in JA signalling, and enhanced in the *cev1* and *fou2* mutants, which over-accumulate JAs (Ellis *et al.*, 2002; Vincent *et al.*, 2017a; Archer *et al.*, 2022). With JA signalling likely therefore to promote aphid resistance, it has been proposed that aphid feeding may induce SA signalling to antagonise JA signalling and promote aphid colonisation (Züst and Agrawal, 2016). The plant responses to aphids vary with different aphid species (Jaouannet *et al.*, 2015). Therefore, the hormone signalling pathways active may differ in different aphid-plant interactions and may be influenced by the balance of plant perception, defence signalling and aphid effector activity.

Hormone signalling and defence responses induced by aphid feeding and colonisation are thought to remain localised to the feeding sites and colonised leaves, respectively. This is evidenced by aphid resistance induced by prior aphid treatments only occurring in the challenged leaves and not in systemic leaves (De Vos *et al.*, 2005). Moreover, $[Ca^{2+}]$ elevations induced by individual aphid feeding events remain localised and do not propagate systemically in *A. thaliana* or *N. benthamiana* (Then *et al.*, 2021; Vincent *et al.*, 2017a; Wang *et al.*, 2022b). Similarly, aphid feeding-induced defence gene expression in *A. thaliana* remains localised around feeding sites (Rubil *et al.*, 2022; Giolai, 2019; Kettles *et al.*, 2013). However, it seems that heavy aphid infestation can trigger systemic transcriptional changes, JA and glucosinolate

accumulation, and aphid resistance (Xue *et al.*, 2022). As GLR3.3/3.6 are required for the full activation of these systemic responses (Xue *et al.*, 2022), these responses may be regulated by the rapid systemic signalling mechanism proposed to underpin systemic JA biosynthesis (Section 1.1.5 – Systemic JA Signalling). It may be, therefore, that aphid infestation triggers such systemic responses when the colonisation pressure is sufficiently high. In contrast, individual feeding events appear to primarily induce responses that remain localised to the feeding sites.

Aphid effectors and plant NLRs

Aphids produce effectors that can promote aphid colonisation. These effectors are primarily delivered into plants in the watery saliva (Mondal, 2020). Aphid effector proteins may be recognised by NLRs to trigger enhanced defence responses against aphids. To appreciate how plants perceive aphids and the molecular aphid-plant interactions, it is important to characterise any aphid effectors and cognate NLRs.

Many aphid effectors have been identified. Examples of aphid effector proteins include COO2 (Mutti *et al.*, 2008; Bos *et al.*, 2010; Pitino and Hogenhout, 2013; Elzinga *et al.*, 2014; Coleman *et al.*, 2015; Escudero-Martinez *et al.*, 2020), PlntO1 and PlntO2 (Pitino and Hogenhout, 2013; Coleman *et al.*, 2015; Rodriguez *et al.*, 2017), Mp42 (Bos *et al.*, 2010; Rodriguez *et al.*, 2014), Me10 (Atamian *et al.*, 2013; Chaudhary *et al.*, 2018), MIF (Naessens *et al.*, 2015), Mp55 (Elzinga *et al.*, 2014) and Armet (Cui *et al.*, 2019; Wang *et al.*, 2015). Aphid effectors can influence aphid colonisation ability through diverse mechanisms. Some of the earliest proposed aphid effector activity was in Ca²⁺-binding proteins in the watery saliva. When stylets penetrate the phloem, a Ca²⁺ influx drives phloem occlusion to limit sap loss. Salivary Ca²⁺-binding proteins are thought to prevent and reverse that process allowing aphids to continue feeding (Will *et al.*, 2009; Will *et al.*, 2007; Mondal, 2020). Saliva from the cowpea aphid, *Aphis craccivora*, contains a DCXR enzyme effector. This effector is thought to promote *A. craccivora* colonisation of cowpea by catalysing the release of carbohydrate energy sources and limiting the production of a defence signalling molecule and toxin (MacWilliams *et al.*, 2020). The *M. persicae* Mp1 effector interacts with *A. thaliana* VACUOLAR SORTING ASSOCIATED PROTEIN 52 (VPS52) and promotes its relocalisation and degradation which reduces *M. persicae* resistance (Rodriguez *et al.*, 2017). Some effectors are immunosuppressive such as *M. persicae* Mp10 (Bos *et al.*, 2010). Mp10 suppresses ROS bursts induced by flg22 and aphid extract with RNAi of Mp10 reducing *M. persicae* fecundity on *A. thaliana* (Bos *et al.*, 2010; Drurey *et al.*, 2019). Moreover, Mp10 is delivered into plant mesophyll cells with aphid feeding suggesting that it could suppress plant defence signalling during aphid feeding (Mugford *et al.*, 2016). Aphid effectors can also be non-proteinaceous such as the Ya1 RNA effector which migrates systemically from *M. persicae* feeding sites and promotes aphid colonisation (Chen *et al.*, 2020). Interestingly, aphid effectors

can display species specificity in their activity. For example, the *M. persicae* COO2, but not *A. pisum* COO2, suppresses resistance against *M. persicae* (Pitino and Hogenhout, 2013). Characterising aphid effector activities will help appreciate how aphids can colonise host plants.

With aphid effectors promoting colonisation, plants have likely evolved NLRs capable of detecting aphid effectors to initiate enhanced ETI-like defence responses. This notion is supported with evidence that some putative aphid effectors induce aphid resistance instead of suppressing it. For example, Mp10 reduces *M. persicae* fecundity when expressed in *N. benthamiana* and induces chlorosis dependent on the ETI-associated co-chaperone SGT1 (Bos *et al.*, 2010). Moreover, there are various NLRs that can confer resistance to certain aphid species in specific plant species. For example, the Mi 1.2 sensor NLR can confer resistance to the potato aphid, *Macrosiphum euphorbiae*, in tomato but not eggplant (Rossi *et al.*, 1998; Vos *et al.*, 1998; Goggin *et al.*, 2006). Mi 1.2 functions with the helper NLR, NRC4 (Wu *et al.*, 2017). The Vat NLR confers resistance to *Aphis gossypii* in the melon species, *Cucumis melo*, as well as resistance to *A. gossypii*-vectored viruses (Dogimont *et al.*, 2014). The Adnr1 NLR in wheat can confer resistance against the specialist aphid, *Diuraphis noxia* (Nicolis and Venter, 2018). Other NLR-encoding loci are also implicated in aphid resistance. Such loci include *RAP1* that contains NLR encoding genes and confers resistance to *A. pisum* in *Medicago truncatula* (Stewart *et al.*, 2009; Kanvil *et al.*, 2015; Kamphuis *et al.*, 2016). Though no effector-NLR pairs have been identified for aphid-plant interactions, it seems that some plant NLRs can recognise aphid effectors or effector activity and promote plant defence responses.

Aphid-plant interactions summary

Aphid feeding establishes a highly intricate and localised interaction with host plants that can be sustained for hours. Whilst damage is thought to play a minor role in aphid-plant interactions, plants could perceive HAMPs, DAMPs, and mechanical stress to trigger defence responses. With sustained feeding events, aphid effectors and plant NLRs may be particularly influential in determining whether certain aphid species can feed from specific plant species. Molecular plant-aphid interactions are challenging to investigate and remain enigmatic. Improving the knowledge of these interactions will be important for understanding aphid resistance in plants.

1.3. Investigations of this thesis

The early perception of pests and pathogens is crucial for initiating plant defence signalling and resistance against biotic stresses. Whilst these perception mechanisms are well characterised for some pests and pathogens, for insects with highly localised feeding mechanisms, such as aphids and thrips, the early perception mechanisms are poorly resolved.

This thesis focusses therefore on investigating how the model plant species, *A. thaliana*, recognises and responds to localised feeding from aphids and thrips. Whilst these insects both feed using stylets, they differ significantly in their feeding mechanisms and the extent of damage that they cause.

In Chapter 3, I report methods developed for utilising genetically encoded fluorescent reporters to visualise early plant responses to localised stimuli such as aphid and thrips feeding. These methods are applied to investigate the reported contributions of BAK1, TPC1 and GLR3.3/3.6 to *M. persicae* feeding-induced $[Ca^{2+}]$ elevations.

In Chapter 4, I describe investigations aimed to characterise the role of GLR3.3 and 3.6 in responses to localised damage through wounding and in responses to localised mechanical stress through touch. These investigations reveal a role for GLR3.3 in responses to localised wounding and explore its activation and its contribution to JA signalling. Furthermore, these investigations explore the nature of touch-induced $[Ca^{2+}]$ elevations in *A. thaliana*.

In Chapter 5, I describe investigations that utilise the findings of Chapter 4 to explore whether and how GLR3.3 contributes to localised aphid and thrips feeding-induced responses and insect resistance. These investigations include three different aphid species and the thrips species, *F. occidentalis*. The work reported provides insights into how the relationship of the aphid species to *A. thaliana* and the insect feeding mechanisms influence GLR3.3 activation.

In Chapter 6, I report investigations that use a reverse genetics approach coupled with genetically encoded fluorescent reporter imaging to test whether candidate genes are likely to contribute to aphid or thrips perception in *A. thaliana*. The candidate genes investigated include genes involved in the perception of HAMPs, DAMPs, mechanical stress or phytochemicals.

In Chapter 7, I consider the contributions of this thesis to the understanding of how *A. thaliana* perceives aphid and thrips feeding as well as localised wound and touch stimuli. Furthermore, I consider future experiments which can complement the work reported in this thesis to advance the understanding of how *A. thaliana* perceives these localised stimuli.

1.4. Contributions to this thesis

All experiments reported in this thesis were designed and undertaken by me. In Chapter 3, some data are presented from Vincent *et al.* (2017a) and this is acknowledged in the text and figure legends. Additionally, the modelling of reporter signals in Chapter 3 was performed in collaboration with Dr Sergio Lopez (BioImaging Platform, John Innes Centre) and this contribution is acknowledged in the relevant figure legends. In Chapter 4, experiments revealing

local wound-induced iGluSnFR signals and GLR3.3-dependent $[Ca^{2+}]$ elevations in *A. thaliana* leaves were performed in collaboration with Dr Annalisa Bellandi (formerly Faulkner lab, John Innes Centre). Dr Bellandi obtained similar results in *A. thaliana* cotyledons, which are cited in the text as appropriate. Experiments in Chapter 6 regarding aphid HAMP perception were performed in collaboration with Dr James Canham (formerly Hogenhout lab, John Innes Centre). Dr Canham produced the aphid extract and repeated any experiments with the extract for the independent verification of results.

2. Materials and Methods

2.1. Plant materials, growth conditions and generation of new material

2.1.1. Plant materials and growth conditions

A. thaliana plants were grown for many purposes including crossing, seed collection, insect rearing and experimentation. Seeds were either germinated on Levington F2 compost (Scotts, UK) or Murashige and Skoog (MS) media (Murashige and Skoog, 1962) with the option of seedlings later being transferred from MS to compost. All *A. thaliana* seeds were stratified in dH₂O at 4°C in dark conditions for 2 - 5 days before germination. Those grown with MS media were also surface sterilised before stratification. For sterilisation, seeds were immersed in a solution of 1 mL 0.01% v/v sodium dodecyl sulphate (SDS) and 1.6% v/v NaClO with 30 rpm at 4°C for 10 min. Sterilised seeds then underwent three sterile dH₂O washes before resuspension in 1 mL dH₂O with 10 min, 30 rpm at 4°C before stratification. *A. thaliana* seeds for fluorescence selection or microscopy experiments were germinated on ¼-strength MS media (w/v in dH₂O: 0.11% MS + vitamins, 0.75% sucrose, 1% Formedium agar, NaOH adjusted to pH 5.8) in 100 mm square plastic plates (ThermoFisher Scientific) and grown vertically with three rows of 9-12 seeds per plate. *A. thaliana* seeds grown for plate reader experiments were germinated in 96-well plates in 200 µL ½-strength liquid MS (w/v in dH₂O: 0.22% MS + vitamins, 0.5% sucrose, NaOH adjusted to pH 5.8) with a single seed per well. Plants growing with MS media were in conditions of 22°C for cycles of 16 h light (90 µmol m⁻² sec⁻¹) and 8 h dark. *A. thaliana* grown in compost for seed collection or crossing was grown in 15- or 24-cell trays in cycles of 16 h light (120 µmol m⁻² sec⁻¹) at 22°C and 8 h dark at 20°C. *A. thaliana* plants used for rearing age-standardised insect populations were grown in 7.5 cm diameter, 8 cm high pots at 22°C with 10 h light (125 µmol m⁻² sec⁻¹) and 14 h dark cycles. For *A. thaliana* used in insect resistance assays, plants were grown identically but instead in 15-cell trays. *A. thaliana* lines used that were donated, made available or ordered from the Nottingham Arabidopsis Stock Centre (NASCC) (Scholl *et al.*, 2000) are listed in Table 2.1. Additional mutant *A. thaliana* lines containing reporter transgenes were generated by crossing and are listed in Table 2.2.

Avena sativa (Aspen Spring Oat, Senova, UK) for *R. padi* rearing was grown directly on Levington F2 compost (Scotts, UK) in 9 cm diameter, 9 cm high pots. Approximately 10 seeds were sown 1 mm deep in each pot and then grown with cycles of 22°C for 14 h light (90 µmol m⁻² s⁻¹) and 20°C for 10 h dark.

Chrysanthemum spp. for thrips rearing were purchased as bouquets from supermarkets and maintained in beakers containing dH₂O with plants replaced whenever they deteriorated. Plants were kept at 21°C with cycles of 10 h light (90 µmol m⁻² s⁻¹) and 14 h dark at 70% relative humidity.

2.1.2. Crossing *A. thaliana*

All *A. thaliana* crosses described in this thesis were made to introduce a fluorescent reporter transgene into a mutant background for investigation and are shown in Table 2.2. For each cross, the reporter line was used as the male component or pollen donor. To cross plants, first the largest fully closed buds of several inflorescences on the receiving plant were opened using sharp forceps and all but the carpel and stigma tissue was removed. Fully open flowers from the pollen donor were then removed and the stamens exposed. Pollination was performed by brushing the stamens and pollen against the receiving stigmas. Successfully pollinated stigmas on the recipient plant were then left to develop to maturation. Resulting seeds were germinated on ¼-strength MS before using an Axio Zoom.V16 microscope (Zeiss) to assess reporter fluorescence and identify seeds from successful crosses. Such seeds were grown to maturation on soil and the next generation grown and genotyped to identify individuals homozygous for any mutations. These plants were also screened for fluorescence to assess the presence of the reporter transgene. As resting reporter fluorescence was not always clear for crosses with *pAOS/JAZ10::NLS-3xVENUS A. thaliana*, reporter expression was induced in this generation by crushing a single leaf with forceps. Identified lines homozygous for mutations and possessing the reporter transgene, were assessed for reporter homozygosity and expression levels by fluorescence in the next generation. To do this for the *pAOS/pJAZ10::NLS-3xVENUS A. thaliana* lines, plants were first treated with methyl-jasmonate (MeJA) to induce reporter expression. Lines subsequently selected for experiments were homozygous for desired mutations and reporter transgenes and ideally displayed uniform and consistent reporter expression that was approximately equal to the parental or control reporter line. If no such lines were detected, more seed or additional generations were screened. Seed used in experiments was from the earliest possible generation following crossing.

Table 2.1 Details of donated *Arabidopsis thaliana* lines used in this study.All *Arabidopsis thaliana* lines are of the Col-0 ecotype. JA – jasmonic acid, SA – salicylic acid, Et – ethylene.

Genotype	Description	AGI Locus Code	Mutant Reference	Source	Reference
Col-0 UBQ10::GCaMP3	Intensiometric GFP-based intracellular [Ca ²⁺] reporter line				
glr3.1a UBQ10::GCaMP3	T-DNA mutant in <i>GLR3.1</i> with <i>UBQ10::GCaMP3</i>	AT2G17260	SALK_063873		
glr3.3a UBQ10::GCaMP3	T-DNA mutant in <i>GLR3.3</i> with <i>UBQ10::GCaMP3</i>	AT1G42540	SALK_099757		
glr3.6a UBQ10::GCaMP3	T-DNA mutant in <i>GLR3.6</i> with <i>UBQ10::GCaMP3</i>	AT3G51480	SALK_091801		
glr3.1a glr3.3a UBQ10::GCaMP3	T-DNA mutant in <i>GLR3.1</i> and <i>GLR3.3</i> with <i>UBQ10::GCaMP3</i>	AT2G17260, AT1G42540	SALK_063873, SALK_099757	Edward Farmer, University of Lausanne	Nguyen <i>et al.</i> (2018)
glr3.3a glr3.6a UBQ10::GCaMP3	T-DNA mutant in <i>GLR3.3</i> and <i>GLR3.6</i> with <i>UBQ10::GCaMP3</i>	AT1G42540, AT3G51480	SALK_099757, SALK_091801		
glr3.1a glr3.3a glr3.6a UBQ10::GCaMP3	T-DNA mutant in <i>GLR3.1</i> , <i>GLR3.3</i> and <i>GLR3.6</i> with <i>UBQ10::GCaMP3</i>	AT2G17260, AT1G42540, AT3G51480	SALK_063873, SALK_099757, SALK_091801		
aha1-7 UBQ10::GCaMP3	T-DNA mutant in <i>AHA1</i> with <i>UBQ10::GCaMP3</i>	AT2G18960	SALK_065288		Kumari <i>et al.</i> (2019)
Col-0 35S::CHIB-iGluSnFR	Intensiometric GFP-based apoplastic [Glu] reporter line			Murray Grant, University of Warwick	Toyota <i>et al.</i> (2018)
Col-0 35S::Apo-pHusion	Ratiometric GFP/RFP-based apoplastic pH reporter line			Anja Thoe Fuglsang, University of Copenhagen	Gjetting <i>et al.</i> (2012)
Col-0 pAOS::NLS-3xVENUS	YFP-based expression reporter line for JA signalling				
Col-0 pJAZ10::NLS-3xVENUS	YFP-based expression reporter line for JA signalling				
Col-0 pACS6::NLS-3xVENUS	YFP-based expression reporter line for Et signalling			Niko Geldner, University of Lausanne	Marhavý <i>et al.</i> (2019)
Col-0 pPR4::NLS-3xVENUS	YFP-based expression reporter line for Et signalling				
Col-0 pPR1::NLS-3xVENUS	YFP-based expression reporter line for SA signalling				
					Poncini <i>et al.</i> (2017)

Table 2.1 Continued

Col-0 35S::GCaMP3	Intensiometric GFP-based intracellular [Ca ²⁺] reporter line			Simon Gilroy, University of Wisconsin-Madison	Vincent <i>et al.</i> (2017a)
Col-0 UBQ10::NES-YC3.6	Ratiometric YFP/CFP-based cytosolic [Ca ²⁺] reporter line				Krebs <i>et al.</i> (2012)
aca8 aca10	T-DNA mutant in <i>ACA8</i> and <i>ACA10</i>	AT5G57110, AT4G29900	GK-688H09, GK-044H01	Alex Costa, University of Milan	Behera <i>et al.</i> (2018)
aca8 aca10 UBQ10::NES-YC3.6	T-DNA mutant in <i>ACA8</i> and <i>ACA10</i> with <i>UBQ10::NES-YC3.6</i>	AT5G57110, AT4G29900	GK-688H09, GK-044H01		
gl1 35S::GCaMP3	Deletion mutant in <i>GL1</i> with <i>35S::GCaMP3</i>	AT3G27920	Oppenheimer <i>et al.</i> (1991)	Masatsugu Toyota, Saitama University	Matsumura <i>et al.</i> (2022)
Col-0 UBQ10::GCaMP6s	Intensiometric GFP-based intracellular [Ca ²⁺] reporter line				Shao <i>et al.</i> (2020)
piezo-1 UBQ10::GCaMP6s	T-DNA mutant in <i>PIEZO1</i> with <i>UBQ10::GCaMP6s</i>	AT2G48060	SALK_003005	Kai He, Lanzhou University	Fang <i>et al.</i> (2021)
tpc1-2 35S::GCaMP3	T-DNA mutant in <i>TPC1</i> with <i>35S::GCaMP3</i>	AT4G03560	SALK_145413	Dale Sanders, John Innes Centre	Vincent <i>et al.</i> (2017a)
bak1-5	Missense point mutant in <i>BAK1</i>	AT4G33430	Schwessinger <i>et al.</i> (2011)	Ben Schwessinger, The Sainsbury Laboratory	Schwessinger <i>et al.</i> (2011)
dorn1-3	T-DNA mutant in <i>P2K1/DORN1</i>	AT5G60300	SALK_042209	NASC, Nottingham, U.K.	Scholl <i>et al.</i> (2000)
fer-4	T-DNA mutant in <i>FER</i>	AT3G51550	GABI_106A06	Jack Rhodes, The Sainsbury Laboratory	Duan <i>et al.</i> (2010)
glr3.2a	T-DNA mutant in <i>GLR3.2</i>	AT4G35290	SALK_150710	NASC, Nottingham, U.K.	Scholl <i>et al.</i> (2000)
isi1-3	T-DNA mutant in <i>ISI1</i>	AT4G27750	SALK_045849	NASC, Nottingham, U.K.	Scholl <i>et al.</i> (2000)

Table 2.1 Continued

<i>mca1 mca2</i>	T-DNA mutant in <i>MCA1</i> and <i>MCA2</i>	AT4G35920, AT2G17780	T-DNA-tag line of Kazusa DNA Research Institute (Chiba, Japan); SALK_129208	Hidetoshi Iida, Tokyo Gakugei University	Yamanaka <i>et al.</i> (2010)
<i>mik2-6</i>	T-DNA mutant in <i>MIK2</i>	AT4G08850	SAIL_264_A08	Jack Rhodes, The Sainsbury Laboratory	Unpublished
<i>msl10-1</i>	T-DNA mutant in the <i>MSL10</i>	AT5G12080	SALK_076254	Elizabeth Haswell, Washington State University	Basu and Haswell (2020)
<i>MSL10-3G</i>	Gain-of-function point mutant in <i>MSL10</i>	AT5G12080	Zou <i>et al.</i> (2016)		
<i>pepr1-1 pepr2-3</i>	T-DNA mutant in <i>PEPR1</i> and <i>PEPR2</i>	AT1G73080, AT1G17750	SALK_059281, SALK_098161	Cyril Zipfel, The Sainsbury Laboratory	Krol <i>et al.</i> (2010)
<i>rbohD rbohF</i>	T-DNA mutant in <i>RBOHD</i> and <i>RBOHF</i>	AT5G47910, AT1G64060	Tissier <i>et al.</i> (1999)	Jonathon Jones, The Sainsbury Laboratory	Torres <i>et al.</i> (2002)
<i>sobir1-12</i>	T-DNA mutant in <i>SOBIR1</i>	AT2G31880	SALK_050715	Cyril Zipfel, The Sainsbury Laboratory	Gao <i>et al.</i> (2009)
<i>tpc1-2</i>	T-DNA mutant in <i>TPC1</i>	AT4G03560	SALK_145413	Dale Sanders, John Innes Centre	Peiter <i>et al.</i> (2005)
<i>tpk1-1 tpk3-2</i>	T-DNA mutant in <i>TPK1</i> and <i>TPK3</i>	AT5G55630, AT4G18160	SALK_146903, SALKseq_61131	Rainer Hedrich, University of Würzburg	Jašlan <i>et al.</i> (2019)

Table 2.2 A. *thaliana* lines produced by crossing.

Donor refers to the male component and pollen donor. Recipient refers to the female component.

Donor Genotype	Recipient Genotype	Homozygous Product	Published
Col-0 <i>UBQ10::GCaMP3</i>	<i>bak1-5</i>	<i>bak1-5 UBQ10::GCaMP3</i>	-
<i>glr3.3a UBQ10::GCaMP3</i>	<i>bak1-5</i>	<i>bak1-5 glr3.3a UBQ10::GCaMP3</i>	-
<i>glr3.3a UBQ10::GCaMP3</i>	<i>dorn1-3</i>	<i>dorn1-3 UBQ10::GCaMP3</i>	-
<i>glr3.3a UBQ10::GCaMP3</i>	<i>dorn1-3</i>	<i>dorn1-3 glr3.3a UBQ10::GCaMP3</i>	-
Col-0 <i>35S::apo-pHusion</i>	<i>fer-4</i>	<i>fer-4 35S::apo-pHusion</i>	-
<i>glr3.3a UBQ10::GCaMP3</i>	<i>fer-4</i>	<i>fer-4 UBQ10::GCaMP3</i>	-
<i>glr3.3a UBQ10::GCaMP3</i>	<i>fer-4</i>	<i>fer-4 glr3.3a UBQ10::GCaMP3</i>	-
Col-0 <i>UBQ10::GCaMP3</i>	<i>glr3.2a</i>	<i>glr3.2a UBQ10::GCaMP3</i>	-
Col-0 <i>35S::apo-pHusion</i>	<i>glr3.3a</i>	<i>glr3.3a 35S::apo-pHusion</i>	-
Col-0 <i>35S::CHIB-iGluSnFR</i>	<i>glr3.3a</i>	<i>glr3.3a 35S::CHIB-iGluSnFR</i>	-
Col-0 <i>pAOS::NLS-3xVENUS</i>	<i>glr3.3a</i>	<i>glr3.3a pAOS::NLS-3xVENUS</i>	-
Col-0 <i>pJAZ10::NLS-3xVENUS</i>	<i>glr3.3a</i>	<i>glr3.3a pJAZ10::NLS-3xVENUS</i>	-
Col-0 <i>UBQ10::GCaMP3</i>	<i>isi1-3</i>	<i>isi1-3 UBQ10::GCaMP3</i>	-
Col-0 <i>UBQ10::GCaMP3</i>	<i>mca1 mca2</i>	<i>mca1 mca2 UBQ10::GCaMP3</i>	-
<i>glr3.3a UBQ10::GCaMP3</i>	<i>mik2-6</i>	<i>mik2-6 UBQ10::GCaMP3</i>	-
<i>glr3.3a UBQ10::GCaMP3</i>	<i>mik2-6</i>	<i>mik2-6 glr3.3a UBQ10::GCaMP3</i>	-
Col-0 <i>UBQ10::GCaMP3</i>	<i>msl10-1</i>	<i>msl10-1 UBQ10::GCaMP3</i>	-
Col-0 <i>UBQ10::GCaMP3</i>	<i>MSL10-3G</i>	<i>MSL10-3G UBQ10::GCaMP3</i>	-
Col-0 <i>UBQ10::GCaMP3</i>	<i>pepr1-1 pepr2-3</i>	<i>pepr1-1 pepr2-3 UBQ10::GCaMP3</i>	-
Col-0 <i>35S::GCaMP3</i>	<i>rbohD rbohF</i>	<i>rbohD rbohF 35S::GCaMP3</i>	Bellandi et al. (2022)
Col-0 <i>35S::GCaMP3</i>	<i>rbohD rbohF</i>	<i>rbohD 35S::GCaMP3</i>	Bellandi et al. (2022)
Col-0 <i>35S::GCaMP3</i>	<i>rbohD rbohF</i>	<i>rbohF 35S::GCaMP3</i>	-
<i>glr3.3a UBQ10::GCaMP3</i>	<i>sobir1-12</i>	<i>sobir1-12 UBQ10::GCaMP3</i>	-
<i>glr3.3a UBQ10::GCaMP3</i>	<i>sobir1-12</i>	<i>sobir1-12 glr3.3a UBQ10::GCaMP3</i>	-
Col-0 <i>UBQ10::GCaMP3</i>	<i>tpc1-2</i>	<i>tpc1-2 UBQ10::GCaMP3</i>	-
<i>glr3.3a UBQ10::GCaMP3</i>	<i>tpc1-2</i>	<i>tpc1-2 glr3.3a UBQ10::GCaMP3</i>	-
Col-0 <i>35S::GCaMP3</i>	<i>tpk1-1 tpk3-2</i>	<i>tpk1-1 35S::GCaMP3</i>	-

2.1.3. Methyl-jasmonate treatment

pAOS/pJAZ10::NLS-3xVENUS A. thaliana lines were treated with MeJA to induce reporter expression and aid screening of reporter homozygosity and expression levels following crosses. For this, a solution of 1 mM MeJA (Sigma-Aldrich), 10% v/v EtOH and 0.1% v/v TWEEN 20 (Merck) was sprayed onto 15-day-old seedlings on ¼-strength MS plates alongside equivalent plants treated with an equivalent mock solution without MeJA. Plates were then resealed and left vertically at room temperature for 48 h. Leaves from these plants were prepared in 96-well plates and reporter expression and homozygosity was assessed via fluorescence as by the methods in 2.3.

2.1.4. DNA extractions and genotyping

DNA extractions and genotyping were performed on individuals from segregating populations after crosses as well as on all populations used in experiments for which there were no obvious reported developmental phenotypes. DNA extractions were in either single 2 mL tubes or, for higher throughput extractions, in 96-well collection microtube plates with caps (Qiagen). In both, samples were contained with a single 4 mm stainless steel ball and flash frozen in liquid nitrogen before grinding with a Geno/Grinder 2010 (Spex SamplePrep) or TissueLyser LT (Qiagen). 250 µL DNA extraction buffer (10mM Tris HCl pH 7.0, 1mM EDTA, 0.4M NaCl) was then added and samples vortexed before 10 min centrifugation at 3200 x g for 96-well plates or 16000 x g for single tubes. 200 µL of the supernatant was transferred into 200 µL isopropanol for a 30 min incubation at -20°C to promote DNA precipitation. Samples were then centrifuged with the same conditions before the DNA pellet was washed with 500 µl 70% v/v ethanol and air dried. DNA was resuspended in 50 µl sterile dH₂O and 1 µL was used as the PCR template for genotyping with the primers outlined in Table 2.3. PCRs used Phusion polymerase in HF buffer (New England BioLabs) according to the manufacturer's guidance and annealing temperatures calculated using the T_m calculator (New England BioLabs). Sequencing was performed as required using the Eurofins Genomics TubeSeq service (Eurofins Genomics).

Table 2.3 Genotyping primers used in this study

Where Left and Right Primers are given, the Right Primer amplified with the Left Border primer.

Mutant	Primer	Mutant Code	Method	Primer Sequence (5'-3')	Reference
-	LBb1.3	-	PCR - SALK Left Border	ATTTTGCCGATTTGCGAAC	Alonso <i>et al.</i> (2003)
-	GABI-LB -	-	PCR - GABI- Kat Left Border	TTGGACGTGAATGTAGACAC	Huep <i>et al.</i> (2014)
-	GABI-LB2 -	-	PCR - GABI- Kat Left Border 2	ATATTGACCATCATACTCATTGC	Guo <i>et al.</i> (2018)
-	SAIL LB2 -	-	PCR - SAIL Left Border 2	GCTTCCTATTATATCTTCCCAAATT ACCAA	Sessions <i>et al.</i> (2002)
-	dSpm1 -	-	PCR - dSpm Border	CTTATTTAGTAAGAGTGTGGGG TTTTGG	Torres <i>et al.</i> (2002)
aca8	Forward Primer Reverse Primer	GK-688H09	PCR with GABI-LB	GAGTTTCTTCACCATTGTCT GACATAGTGGTGGGTGATGT	Yu <i>et al.</i> (2018)
aca10	Forward Primer Reverse Primer	GK-044H01	PCR with GABI-LB	GAACCTGAGGCCAATAGTG CAAGACCATGTCATACTGC	Yu <i>et al.</i> (2018)
aha1-7	Left Primer Right Primer	SALK_065288	PCR with LBb1.3	GCGTTGTAACCTTGCAGTTTG TCTTTCTGGTTGTGAAAGCG	SALK Institute Genomic Analysis Laboratory
bak1-5	Forward Primer Reverse Primer	-	PCR and dCAPs with RsaI	AAGAGGGCTTGCGTATTTACATG ATCAGT GAGGCGAGCAAGATCAAAG	Schwessinger <i>et al.</i> (2011)
bak1-5	Forward Primer Reverse Primer	-	PCR and sequencing	CATGACTCCAACCGAAA CATGACTCCATACCCAAA	Unpublished
dorn1-3	Left Primer Right Primer	SALK_042209	PCR with LBb1.3	CTGAATACTTGCCTCTCTGTC CAGCTTGCAGGTTATGATTC	SALK Institute Genomic Analysis Laboratory
fer-4	Forward Primer Reverse Primer	GABI_106A06	PCR with GABI-LB2	GGAAAATGAGAGAACAGAGAAC AA CTTCTGTGAGTTCCTTGTCTCTCT C	Guo <i>et al.</i> (2018)
glr3.1a	Left Primer Right Primer	SALK_063873	PCR with LBb1.3	AGATGAACAAACGTGACCACC TGGCTTTTTGTGGTTCTGATC	Mousavi <i>et al.</i> (2013)
glr3.2a	Left Primer Right Primer	SALK_150710	PCR with LBb1.3	TTTTGGATCCAGCATTAGTCG TTTTGCGTTTTGTTTGTAGG	Mousavi <i>et al.</i> (2013)
glr3.3a	Left Primer Right Primer	SALK_099757	PCR with LBb1.3	GATGCTGCATATGGTTGTGTG GTTGAACGATAAGCTTGCAG	Mousavi <i>et al.</i> (2013)
glr3.6a	Left Primer Right Primer	SALK_091801	PCR with LBb1.3	TTCGTTCAAAGGTGGCATAAC CGACTATGAGGAAAGACGCAG	Mousavi <i>et al.</i> (2013)
isi1-3	Left Primer	SALK_045849	PCR with LBb1.3	ATCCTTCCCATTACGTGTCC	

Table 2.3 Continued

	Right Primer			CTCCATCCTCAGAGCACTGTC	SALK Institute Genomic Analysis Laboratory
mca1	Left Primer	-	PCR with Border Primer	TCTCTATCAACAATGCCGTCC	Hidetoshi Iida, Tokyo Gakugei University
	Right Primer			GCTGCACGAGTACTGCTTTTC	
	Border Primer			CAACATTTGCCCGAGCTTC	
mca2	Left Primer	SALK_129208	PCR with Border Primer	CAAGGTTCTGAACAACAATCCAG C	
	Right Primer			ACAAGTACCATCTCTGTAATTCTT GAC	
	Border Primer			ATTTTGCCGATTTTCGGAAC	
mik2-6	Left Primer	SAIL_264_A08	PCR with SAIL LB2	TGGATGCTCTCCTTTGATCAC	Jack Rhodes, The Sainsbury Laboratory
	Right Primer			AAGCTACCAAACGCAATCATG	
msl10-1	Left Primer	SALK_076254	PCR with LBb1.3	GTTGGTTTCTGGGTTTAAGCC	Basu and Haswell (2020)
	Right Primer			TACTTGGAGTAACCGGTGCTG	
MSL10-3G	Forward Primer	-	PCR and CAPs with Taq1	GCAACGACTAAGGTTTTGCTG	Basu and Haswell (2020)
	Reverse Primer			AGGAGAGTGTAGTCGATGTGAA	
pepr1-1	Left Primer	SALK_059281	PCR with LBb1.3	TTTCACCTGTCAATCCGTTTC	SALK Institute Genomic Analysis Laboratory
	Right Primer			TCGTTTCGGATCACCTAATTG	
pepr2-3	Left Primer	SALK_098161	PCR with LBb1.3	AGCGTCCAAAGAAGCTTTCTC	SALK Institute Genomic Analysis Laboratory
	Right Primer			TGCCTATCTCAGGTGGAACAC	
rbohD	Forward Primer	-	PCR with dSpm1	TTGCAAGCGGGATAGTCGTC	Morales Bello (2015)
	Reverse Primer			TTAACCGGAAAAAGGAAAGAAA AT	
rbohF	Forward Primer	-	PCR with dSpm1	CTCCGATATCCTTCAACCAACTC	Hsu <i>et al.</i> (2018)
	Reverse Primer			CGAAGAAGATCTGGAGACGAGA	
sobir1-12	Left Primer	SALK_050715	PCR with LBb1.3	GGAGCCATAGGAGGAACAATC	SALK Institute Genomic Analysis Laboratory
	Right Primer			TGACATCTTTACTGTTCGGCC	
tpc1-2	Left Primer	SALK_145413	PCR with LBb1.3	ATATCGAAGAAAGCTCGGCTC	Vincent (2016)
	Right Primer			GGGAAATAGAACCCGTGAGAG	
tpk1-1	Left Primer	SALK_146903	PCR with LBb1.3	AAATGTCGAGTGATGCAGCTC	SALK Institute Genomic Analysis Laboratory
	Right Primer			TCAAGTTGCTCGAACTCATCC	
tpk3-2	Left Primer	SALKseq_61131	PCR with LBb1.3	GTTTTGGATCGGTGAAGAGC	Jašlan <i>et al.</i> (2019)
	Right Primer			ACGTTTCACGTTCTCTCT	

2.1.5. Protein extractions and visualisation of GCaMP3

To assess GCaMP3 protein levels in *A. thaliana* lines, protein was first extracted from the aerial tissue of single 15-day-old seedlings grown vertically on ¼-strength MS. For this, the tissue was harvested into a 2 mL tube containing a 4 mm stainless steel ball. Samples were snap frozen and ground using a TissueLyser LT (Qiagen). Ground tissue was then thawed in 120 µL 1 x NuPAGE™ LDS Sample Buffer (Invitrogen) before boiling for 5 min. The proteins within were resolved alongside a broad range colour prestained protein standard (New England BioLabs) on 12-well 12% TruPAGE™ precast gels (Sigma-Aldrich) by SDS-PAGE with 1 x TruPage™ SDS Running Buffer (Merck Life Science UK Ltd) in a mini-PROTEAN Tetra Electrophoresis Cell (Bio-Rad). Protein was then transferred by Western blot to a 0.45 µm polyvinylidene difluoride membrane (PVDF, Thermo Scientific) at 4°C overnight in the same cell but with 1 x TruPage™ Transfer Buffer. Membrane blocking was performed with 5% w/v powdered milk solution in 1 x phosphate-buffered saline (PBS) for 30 min shaking at room temperature. To probe the membrane, this solution was replaced with the same solution but containing 1:1000 GFP (B-2) HRP monoclonal antibody (anti-GFP-HRP, sc-9996 HRP, Santa Cruz Biotechnology) for 1 h shaking at room temperature. The membrane was then washed twice for 10 min with 1 x PBS 0.1% v/v triton before three 10 min washes with 1 x PBS. Immunodetection of proteins was on the ImageQuant™ LAS-500 (GE Healthcare Life Science) with the Immobilon Western Chemiluminescent HRP substrate (Millipore). Total protein staining was performed with 1 x amido black staining solution (Sigma-Aldrich). GCaMP3 quantities were compared across samples against the total protein stain visually.

2.2. Insect rearing and resistance assays

All aphid populations of *Myzus persicae* (US1L), *Brevicoryne brassicae* and *Rhopalosiphum padi* were kept in cycles of 22°C for 14 h light (90 µmol m⁻² s⁻¹) and 20°C for 10 h dark. *M. persicae* (Clone O) was reared under similar conditions but with light temperatures of 24°C and dark temperatures of 20°C. Aphid colonies were maintained as asexual females. All *Frankliniella occidentalis* populations were kept at 21°C with cycles of 10 h light (90 µmol m⁻² s⁻¹) and 14 h dark at 70% relative humidity.

The *F. occidentalis* thrips were donated by Professor Kirk (Keele University, U.K.) and the *B. brassicae* aphids were donated by Professor Carr (Cambridge University, U.K.).

2.2.1. Stock insect colony maintenance

Stock colonies of *M. persicae* (US1L & Clone O), *B. brassicae*, *R. padi* and *F. occidentalis* were maintained separately in cages (52 cm x 52 cm x 50 cm). *M. persicae* and *B. brassicae* were reared on *Brassica rapa* (subsp. *chinensis*) whilst *R. padi* was reared on *A. sativa* (Aspen Spring Oat, Senova, UK). *F. occidentalis* was reared on *Chrysanthemum* spp. Stock plants were replaced and new colonies started as required. Stock colonies were the only source of insects used in these experiments and were maintained by the Entomology Facility at the John Innes Centre.

2.2.2. *Myzus persicae* fecundity assays

M. persicae (US1L) resistance was assessed through fecundity assays performed on four-week-old *A. thaliana* plants that were double caged in microperforated bread bags (160 holes per square inch, SNAPPY). Age-standardised *M. persicae* (US1L) nymphs were produced by adding approximately 15 female apterous *M. persicae* adults to two individual *A. thaliana* plants of each genotype to be investigated. After 24 h, one resulting nymph was transferred by paintbrush to each of the remaining *A. thaliana* plants of the corresponding genotypes and the plants were caged. This was defined as Day 0 with aphid fecundity scored on Days 7, 9, 11 and 13 by counting and removing the nymphs. For any nymphs that did not survive transfer from the aged population, samples were discarded. The total number of nymphs per aphid (fecundity) was compared between genotypes at each time point.

2.2.3. *B. brassicae* fecundity assays

Resistance assays for *B. brassicae* were performed as for *M. persicae* fecundity assays. However, as *B. brassicae* produced fewer nymphs throughout these experiments than *M. persicae*, fecundity was scored for *B. brassicae* on Days 11, 13, 15 and 17.

2.2.4. *R. padi* survival assays

R. padi resistance was assessed through survival assays performed on four-week-old *A. thaliana* plants. Age-standardised *R. padi* aphids were first produced on 10-day-old *A. sativa* by adding multiple adult female apterous aphids to several pots each containing multiple plants and leaving them for 24 h before removing the adults. The resulting nymphs were left to develop for 4 additional days. *R. padi* was caged on *A. sativa* during this time by clear plastic tubing (10 cm diameter x 30 cm high) with a thrips-proof mesh window in the base and top caps. After this, 10 of the aphids were transferred by paintbrush to each four-week-old *A. thaliana* plant. These plants were then double caged in microperforated bread bags (160 holes per square inch,

SNAPPY) and the number of nymphs alive on *A. thaliana* was scored each day for the subsequent 6 days. Survival was then compared between genotypes.

2.2.5. Thrips damage assays

Thrips resistance was assessed through *F. occidentalis* damage assays performed using adult female *F. occidentalis* harvested from the stock colony into groups of 4 in 2 mL tubes. Two of these tubes (8 thrips) were placed open into the soil either side of individual 4-week-old *A. thaliana* plants allowing the thrips to emerge. These thrips treated plants were then caged by clear plastic tubing (10 cm diameter x 20 cm high) with a thrips-proof mesh window in the base and top caps. Control plants did not have thrips added but were still caged. After 8 days, all the leaves from each plant were removed and placed flat on a white PVC foam board containing a 10 cm scalebar. Samples were then scanned using a CanoScan LiDE 300 scanner (Canon) and IJ Scan Utility (Canon) software with a ScanGear setting of 720 dpi. Scans were opened in Fiji Image J 1.53j (Schindelin *et al.*, 2012) and the scale was set. All the scar damage on the leaves from each plant was then outlined using the polygon ROI tool and the ROI manager. Measuring all the ROIs from each plant revealed the total area (mm²) of thrips scar damage across each plant and this was compared between genotypes and treatments.

2.2.6. Insect rearing for microscopy experiments

Age-standardised populations were reared for assessing aphid feeding-induced responses in *A. thaliana* reporter plants by microscopy. For *M. persicae* (US1L) and *B. brassicae*, these populations were reared on individual four-week-old *A. thaliana* (Col-0) plants. *R. padi* aged populations were reared on multiple 10-day-old *A. sativa* plants grouped within single pots. These plants were caged by clear plastic tubing (10 cm diameter x 30 cm high) with a thrips-proof mesh window in the base and top caps. Approximately, 15 - 20 adult female apterous aphids were added to each *A. thaliana* plant or to each group of *A. sativa* plants. These were left for 24 h before removing all the adult aphids to leave just the nymphs that had been produced. Nymphs were then left to develop into adult female aphids and apterous aphids were used for microscopy 7 days later for *M. persicae*, 8 days later for *B. brassicae* and 6 days later for *R. padi*. The differences in timing were designed to ensure adult aphids only were used for microscopy experiments as detected by the consistent appearance of nymphs within aged populations. For each day of microscopy, two age-standardised populations were used.

For microscopy investigations using *F. occidentalis*, individual flower heads were removed from the stock colony. Adult female thrips were selected from these flower heads and used for microscopy experiments.

2.3. Assessing stimulus-induced responses in *A. thaliana* by imaging genetically encoded fluorescent reporters

A. thaliana plants expressing genetically encoded fluorescent reporters were imaged to investigate responses to aphids, thrips, micropipette wounding and touch. Reporters were split into two categories and investigated differently. 'Signalling reporters' were those that reported relative changes in analyte concentration by binding the analyte (e.g. Ca^{2+} , H^+ (pH), glutamate), whilst 'expression reporters' reported increases in phytohormone-mediated marker gene expression. The methods used to treat and image reporter samples here are outlined below and were developed around existing methods for investigating aphid feeding-induced Ca^{2+} signalling (Vincent *et al.*, 2017b; Vincent *et al.*, 2017a).

2.3.1. Plant preparation for fluorescence microscopy

For fluorescence microscopy experiments, *A. thaliana* reporter plants were grown vertically on ¼-strength MS media for 15 days. Using an established leaf numbering system (Farmer *et al.*, 2013), the first or second true leaf was detached from healthy seedlings of an appropriate size. Individual leaves were then placed abaxial surface up on 300 μL dH_2O within a well of a flat bottomed clear 96-well plate (Alpha Laboratories). For MeJA treated plants, plates were imaged immediately after this preparation. For all other experiments, plates were covered tightly with cling film and kept in the dark overnight at room temperature before use.

For vacuum infiltration of *A. thaliana* leaves, the leaves were removed from the 96-well plate after the overnight incubation. The leaves were then placed in a 20 mL syringe and submerged in 15 mL of the desired infiltration solution. The plunger was used to expel air in the syringe before the syringe was sealed. The plunger was then fully retracted to create negative pressure within the syringe. This negative pressure was held for 5 s before slowly releasing the plunger and repeating this process 4 more times. All leaves were then visibly infiltrated with the solution. Infiltrated leaves were returned to the 96-well plate, abaxial surface up, and covered with cling film in the dark for 2 h before use to allow samples to recover intracellular $[\text{Ca}^{2+}]$ to a resting state.

As samples in 96-well plates would later be imaged in groups of four (2 x 2 wells), samples from each group (e.g. genotype) were distributed to ensure an approximately equal number of samples would be in each of the four relative positions. This was designed to limit the impact of any position effects on data though there were no indications that such effects were influential. Where mentioned, position was also included as a variable in statistical

analyses to assess, and account for, any variation in data that was due to the position of samples in the plate.

2.3.2. Aphid and thrips treatment

Signalling reporter leaves were treated with aphids or thrips by adding a single adult female insect using a fine paintbrush. For aphids, individuals were preferentially chosen that were feeding as these were deemed more likely to feed again. The treated leaf was imaged alongside a control leaf with no insect added and this pair represented one biological replicate (n). Plates were covered with cling film to maintain humidity and contain insects with treated leaves throughout the imaging period. Leaves were imaged until a suitable stimulus event was recorded or until one was deemed unlikely. For aphids, this was a single feeding event defined by the aphid remaining stationary for ≥ 5 min and presenting a visible feeding site. For thrips, this was an isolated feeding initiation event that occurred from the head of the thrips usually with a downward motion that corresponds to a piercing of the cuticle and/or epidermis (Kindt *et al.*, 2003). Suitable thrips feeding events for analyses had no further feeding after feeding initiation. In this thesis, these aphid and thrips events are referred to as 'feeding' events as they form part of the insect's feeding behaviours. The aphid and thrips feeding events ideally had 5 min directly pre-stimulus and 30 min directly post-stimulus to measure baseline fluorescence and any stimulus-induced reporter signals, respectively. However, feeding events with ≥ 2.5 min directly prior to feeding and ≥ 10 min directly post-feeding were retained for further analyses. Samples not meeting these criteria were discarded. Each experiment ideally had 30 or more replicates with data collected over 9 – 18 imaging days.

For the imaging of expression reporters in response to insect treatments, images were first taken of samples before insect treatment giving a pre-treatment reference. A single aphid or thrips was then added to a leaf alongside a control leaf with no insect added with the pair of leaves forming one biological replicate (n). Once all treatment leaves had received an insect, plates were covered with clingfilm and left for 30 min. In this time, aphid feeding events were monitored and events of ≥ 5 min were noted along with their location on the leaf. The location of thrips feeding events could not easily be monitored. All insects were then removed and another image was taken as the 0 h time point. Following this, images were taken hourly for 8 h. Between time points, plates were sealed with clingfilm and kept in the dark at room temperature.

All insects used in microscopy experiments were used only once and were discarded after use.

2.3.3. Micropipette wounding

Localised wounds were administered to leaves based on methods modified from Bellandi *et al.* (2022). The wounds were inflicted by glass micropipette needles produced from Drummond Microcap glass microcapillaries (Sigma-Aldrich) using a Narishige PE-2 (Japan) glass microelectrode puller (magnet setting: 5.15; heater setting: 4.35). Needle points were measured at 65 x magnification on an Axio Zoom.V16 and had a mean \pm S.E.M. diameter of $6.46 \pm 0.61 \mu\text{m}$ ($n = 6$). The needle was controlled by a manual micromanipulator under an Axio Zoom.V16. To inflict wounds, the needle point was briefly pressed against the abaxial leaf surface away from the main vein and edge to produce a highly localised wound without deep penetration into the leaf. This marked time point 0 and the location of this event as the wound site. The needle and apparatus were only introduced into the imaging area for the wound event and were then completely removed for further imaging. Control sites were untreated representative sites on the same leaf with each wound and control site pair forming one biological replicate (n). Any samples in which reporter signals clearly propagated through vascular networks, or in which micropipette wounding penetrated deep into the leaf, were discarded. Wounding experiments were performed over 1 - 3 imaging days. Unless otherwise specified, wound or wounding in this thesis will refer to this method.

For wounding of *A. thaliana* expressing signalling reporters, the cling film was first removed from covering the samples. After imaging for at least 5 min to allow for baseline measurements, these samples were wounded. The wounding was performed during continuous imaging in the dark and was followed by 30 min imaging to record any wound-induced responses.

For wounding of expression reporter plants, plates were uncovered before wounding and wound sites were recorded by their location on the leaf. Images were then taken immediately after wounding and at hourly intervals for 8 h to allow change in signal intensity over time to be analysed. Between time points, plates were sealed with cling film in the dark.

2.3.4. Touch treatment

For localised touch treatments, the same methods were used as for wounding but the micropipette needle was first blunted by brief exposure to a flame. Blunted needle ends were measured at 65 x magnification on an Axio Zoom.V16 and had a mean \pm S.E.M. diameter of $333 \pm 13 \mu\text{m}$ ($n = 7$). Touch experiments were performed over one or two imaging days. Unless otherwise specified, a touch stimulus in this thesis will refer to this method.

2.3.5. Fluorescence microscopy imaging

Leaves of stimulus treated *A. thaliana* reporter expressing lines were imaged in groups of four in 96-well plates (Figure 2.1). All images were taken in a dark room maintained at $21 \pm 2^\circ\text{C}$. An Axio Zoom.V16 epifluorescence microscope was used for the imaging and controlled via the ZEN Blue software (ZEISS). Unless otherwise stated, a Lumenacor Spectra III Light Engine (ZEISS) was used and provided 15% intensity excitation light for imaging. The additional conditions used for this imaging are outlined in Table 2.4 for each reporter. Where stated in figure legends, an alternative light source of a HXP 120 V metal halide lamp (ZEISS) was used at 50% intensity with otherwise equal imaging conditions. For dual fluorescent protein (FP) reporters, the two FPs were imaged sequentially at each time point. All images were taken at 100% aperture and 7 x magnification and were exported as .CZI files. The John Innes Centre BioImaging platform provided the imaging equipment and support for these experiments.

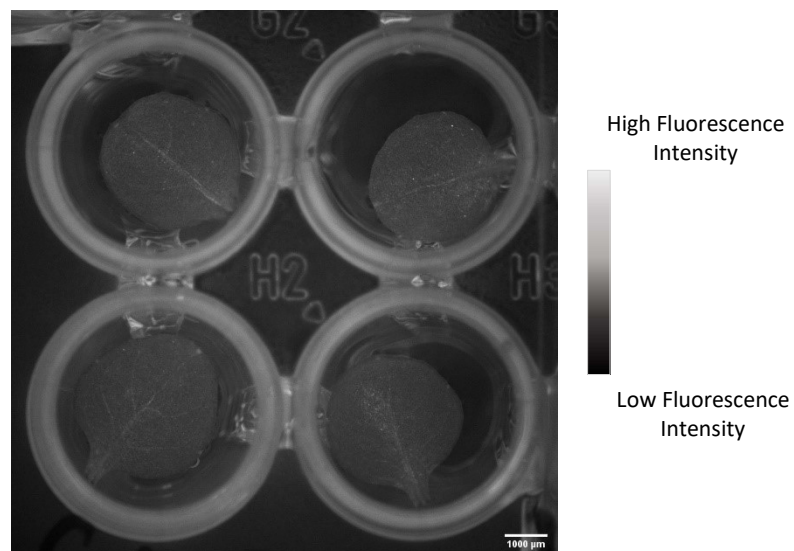


Figure 2.1 Arrangement of isolated *A. thaliana* leaves for Axio Zoom.V16 imaging.

An example of the arrangement of *A. thaliana* leaves for imaging. Leaf 1 or 2 was removed from 15-day old Col-0 *A. thaliana* plants expressing *UBQ10::GCaMP3* and floated abaxial side up on 300 μl dH_2O in wells of a clear, flat bottom 96-well plate. Plates were sealed in cling film and left overnight at room temperature in the dark before imaging. Samples were imaged in groups of four using an Axio Zoom.V16 at 7 x magnification. Fluorescence intensity from the GFP channel is shown in greyscale with higher intensities represented by lighter colours.

Table 2.4 Conditions used to image *A. thaliana* fluorescent reporter lines with a Zeiss Axio Zoom.V16 microscope and a Lumenacor Spectra III Light Engine.

White background – Signalling reporters. Grey background – expression reporters. Modified FS47 does not contain an excitation filter. Modified FS108 contains an FS47 excitation filter and a HC YFP emission filter. Subscript cyt – cytosolic, subscript apo – apoplasmic, FP – fluorescent protein. Filter wavelengths (nm) are shown as ‘central wavelength/full bandwidth’.

Reporter Transgene	Analyte	Reporter Type	FP(s)	LED Colour	Excitation Filter (nm)	Emission Filter (nm)	Filter Cube	Exposure (s)	Reference for <i>A. thaliana</i> material
<i>UBQ10::GCaMP3</i>	[Ca ²⁺]	Intensiometric	cpEGFP	Cyan	470/40	525/50	38 HE GFP	1.5	Nguyen <i>et al.</i> (2018)
<i>35S::GCaMP3</i>	[Ca ²⁺]	Intensiometric	cpEGFP	Cyan	470/40	525/50	38 HE GFP	1.5	Vincent <i>et al.</i> (2017a)
<i>UBQ10::GCaMP6s</i>	[Ca ²⁺]	Intensiometric	cpEGFP	Cyan	470/40	525/50	38 HE GFP	1.5	Shao <i>et al.</i> (2020)
<i>35S::CHIB-iGluSnFR</i>	[Glu] _{apo}	Intensiometric	cpGFP	Cyan	470/40	525/50	38 HE GFP	1.5	Toyota <i>et al.</i> (2018)
<i>35S::Apo-pHusion</i>	Apoplastic pH	Ratiometric – non-FRET	eGFP	Cyan	470/40	525/50	38 HE GFP	1.5	Gjetting <i>et al.</i> (2012)
			mRFP1	Green	545/25	605/70	43 DsRed	1.5	
<i>UBQ10::NES-YC3.6</i>	[Ca ²⁺] _{cyt}	Ratiometric - FRET	eCFP	Blue	438/29	480/40	Modified FS47 - CFP	1	Krebs <i>et al.</i> (2012)
			cpVENUS	Blue	436/24	544/24	Modified FS108 - CFP/YFP	1	
<i>pAOS::NLS-3xVENUS</i>	AOS expression		mVENUS	Teal	509/22	544/24	HC YFP	1	Marhavý <i>et al.</i> (2019)
<i>pJAZ10::NLS-3xVENUS</i>	JAZ10 expression		mVENUS	Teal	509/22	544/24	HC YFP	1	
<i>pACS6::NLS-3xVENUS</i>	ACS6 expression		mVENUS	Teal	509/22	544/24	HC YFP	1	
<i>pPR4::NLS-3xVENUS</i>	PR4 expression		mVENUS	Teal	509/22	544/24	HC YFP	1	
<i>pPR1::NLS-3xVENUS</i>	PR1 expression		mVENUS	Teal	509/22	544/24	HC YFP	1	

For all signalling reporter samples, imaging was performed at 5 s intervals. Wherever possible, at least 5 min (60 frames) imaging was performed pre-stimulus for baseline analyses and 30 min (360 frames) after for analysing any reporter signals. For insect treatments, the feeding events could not be easily standardised to meet these criteria. Instead, image sequences were retained for further analyses if they had images available for ≥ 2.5 min directly pre-stimulus and ≥ 10 min directly post-stimulus. To acquire background correction values for signalling reporters, single images were taken of non-transgenic *A. thaliana* (Col-0) leaves with equivalent set ups. The conditions used for imaging signalling reporter samples were selected to allow clear and consistent visualisation of reporter responses without inducing significant reporter signals.

For aphid, thrips, touch or wound treated expression reporter samples, images were taken hourly starting immediately after treatment. To ensure the first time point was not influenced by the insect treatment, a pre-treatment reference image was also taken for thrips and aphid treated expression reporter samples. For expression reporter samples treated with MeJA for screening purposes, images were taken only at 48 h post-treatment.

2.3.6. Microscopy data analyses – Signalling reporters

For analysing image sequences of signalling reporter samples, .CZI files were opened in Fiji Image J 1.53j (Schindelin *et al.*, 2012) with Bio-Formats 6.10.0 (Linkert *et al.*, 2010). Regions of interest (ROIs) were outlined with the polygon or circular ROI tool with the ROI manager.

For Col-0 non-transgenic samples used to obtain background correction values, ROIs were drawn within the area of leaves to cover most of the leaf surface. The measure function was then used to obtain the mean fluorescence intensity (A.U.) across each sample. The background correction values for each experiment and reporter are shown in Table 2.5 and these were the values used for background corrections unless otherwise specified.

For signalling reporter analyses, the treatment site was first identified and any associated reporter signals were considered to assess whether they were induced by the treatment stimulus. If reporter signals were present, a single dominant signal was identified as that which gave the most significant changes in fluorescence intensity across the signalling area. The maximum visible area of this dominant signal was outlined by a ROI and measured to give the 'signal area' (μm^2). Additionally, the mean propagation rate for the dominant reporter signal was measured using the MTrackJ 1.5.1 plugin (Meijering *et al.*, 2012). For this, the origin of the dominant signal was identified and marked with another mark placed at a representative region on the maximum signal area perimeter when the dominant signal first stopped propagating radially outwards. The 'signal rate' ($\mu\text{m s}^{-1}$) was then calculated from the distance (μm) and time

(s) between these marks. In the absence of any reporter signal, these values were omitted from data. Instead, circular ROIs were placed at the stimulus treated sites of a size comparable to other reporter responses induced by the same stimulus. These ROIs had areas and radii of 320000 μm^2 (0.32 mm^2) and 319.15 μm for wounding, 150000 μm^2 (0.15 mm^2) and 218.51 μm for aphids and 130000 μm^2 (0.13 mm^2) and 203.42 μm for touch, respectively. The ROI at the stimulus treated site was then duplicated to a representative untreated control site on the same leaf for wounding or touch stimuli, or on an untreated leaf for insect stimuli. The mean fluorescence intensity across ROIs for each frame was extracted using the Time Series Analyzer 3.0 plugin (RRID:SCR_014269). These values represented the non-corrected fluorescence intensity (F) values and were further analysed in Microsoft Excel Version 2202 (Microsoft). This method for analysing signalling reporters is demonstrated for wounding (Figure 2.2A) and *M. persicae* feeding (Figure 2.2B). In some cases, characterising reporter dynamics required additional analyses. Therefore, additional measurements using these same approaches were performed on specific components of the reporter signals as described in results.

Table 2.5 Background correction values used for signalling reporter analyses.

The background intensity or correction value is a mean shown alongside the standard error of the mean (S.E.M) for the number of samples, *n*, measured. e/E – enhanced, cp – circularly permuted. All correction values were calculated from images taken with an AxioZoom.V16.

Stimulus	Reporters	Fluorescent Protein	Background Intensity (A.U.)	S.E.M.	<i>n</i>
Aphid or Thrips	GCaMP3	cpEGFP	1908.35	16.61	10
	GCaMP6s	cpEGFP			
	iGluSnFR	cpGFP			
	Apo-pHusion	eGFP			
Wound	Apo-pHusion	mRFP1	1787.41	11.42	18
			9312.59	142.76	18
	GCaMP3	cpEGFP	2062.56	12.56	21
	GCaMP6s	cpEGFP			
	iGluSnFR	cpGFP	1973.84	43.53	10
	YC3.6	eCFP	2360.68	56.67	8
		cpVENUS	1170.90	12.93	8
Water Infiltrated Wound	Apo-pHusion	eGFP	1822.90	6.58	48
		mRFP1	1598.87	4.61	48
	GCaMP3	cpEGFP	1838.86	8.45	24
	iGluSnFR	cpEGFP			

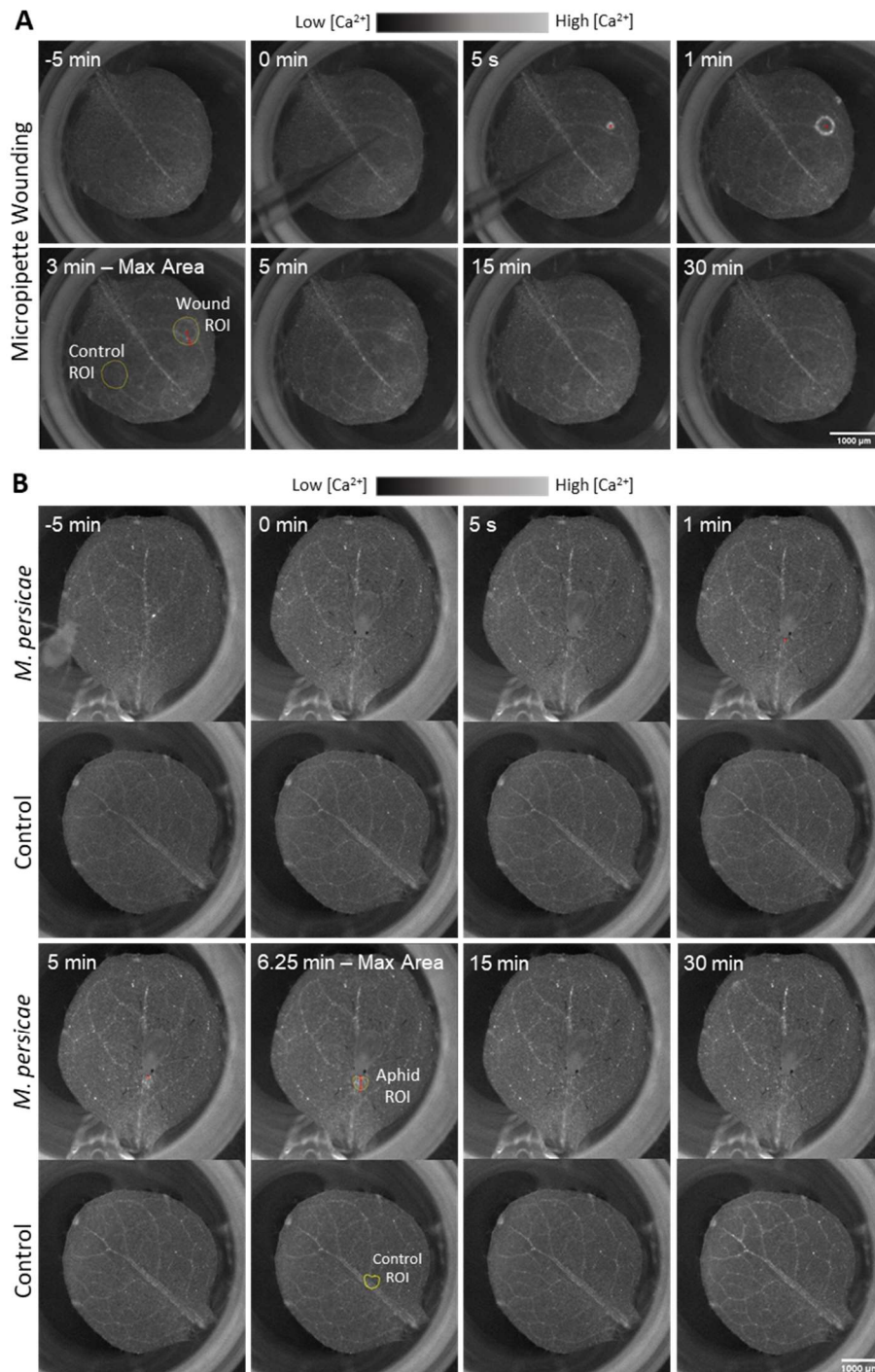


Figure 2.2 Demonstration of signalling reporter analyses in response to micropipette wounding and *M. persicae* feeding.

Axio Zoom.V16 time series images from (A) micropipette wound-induced and (B) *M. persicae* feeding-induced GCaMP3 fluorescent reporter signals in *A. thaliana*. Analyses performed in Fiji Image J 1.53j (Schindelin *et al.*, 2012) with stimuli onset at 0 min. The ROIs for the stimulus and control sites used to measure mean fluorescence intensity over time are shown in yellow in the frame that the dominant signal first reached its maximum area (Max Area). This ROI outlines the dominant signal at this point and was used to measure signal area. MTrackJ 1.5.1 (Meijering *et al.*, 2012) was used to measure the signal rate. This was the rate of dominant signal propagation from its origin marked by the first red dot to when the signal first stopped propagating at the max area marked by a second red dot at a representative site. The rate was calculated as the length of the red line divided by the time between these points.

Unless otherwise specified, non-corrected fluorescence intensity values from signalling reporters first underwent a background correction in Excel. For this, the relevant value in Table 2.5 was subtracted from every fluorescence intensity value to produce background corrected fluorescence intensity values (F). For intensimetric signalling reporters, corrected or non-corrected F values were normalised using the formula $\Delta F/F_0$ where F_0 is the baseline fluorescence calculated as the mean F over a resting period of the 5 min prior to stimulus application and $\Delta F = F - F_0$. For ratiometric signalling reporters, the ratio (R) of the F values from the two emission wavelengths was first calculated at each time point before this was normalised by $\Delta R/R_0$. R_0 was the baseline R calculated as the mean R over the resting period of the 5 min prior to stimulus application and $\Delta R = R - R_0$. For all signalling reporters, stimuli occurred at time point 0 with time plotted from -5 min to 30 min. Often data presented for $\Delta F/F_0$ or $\Delta R/R_0$ are for the difference between treated and control ROI pairs. Taking this difference further normalised reporter signals to their control, removed variation caused by fluctuations in background or excitation light intensity and efficiently incorporated untreated controls into analyses. These values are referred to as normalised $\Delta F/F_0$ or $\Delta R/R_0$ values and were compared between groups over time to assess reporter signal dynamics. As required, reporter signals were also compared by maximum (peak) normalised $\Delta F/F_0$ or $\Delta R/R_0$ values and these values at selected times, signal areas and signal propagation rates. F_0 values for stimulus-treated sites were compared as a measure of reporter expression. To test if reporter signals were induced in response to certain stimuli, the approximate time of the normalised $\Delta F/F_0$ or $\Delta R/R_0$ trace peaks were identified and the $\Delta F/F_0$ or $\Delta R/R_0$ values at these times were compared between control and treated groups.

To ensure data were representative and accurate, strict criteria were applied during analyses which resulted in some data points or samples being removed. Unrepresentative data points which were removed were often due to stimuli, especially insect stimuli, interfering with treatment or control ROIs. If a second insect feeding event caused another signal which interfered with the signal being analysed, all data points after that time were discarded. Occasionally, data points were removed due to spikes in light intensity caused by either light intensity increases in the imaging environment or errors in the microscopy equipment. Following this step, to ensure data were based around an accurate F_0 value, samples were discarded if they did not have ≥ 30 data points in the 60 possible directly prior to stimulus application for baseline calculations. Additionally, to give accurate measurements of the stimulus-induced responses, samples were discarded if they did not have ≥ 120 data points from the 180 (15 min) directly post stimulus for measuring reporter signals. Most samples used significantly exceeded these criteria. To avoid measuring responses to non-treatment stimuli, samples were discarded in the rare case that both the treated and control samples gave reporter signals with a sustained

normalised intensity greater than that of a typical stimulus induced response. Any discarded samples were excluded from all analyses.

2.3.7. Microscopy data analyses – Expression reporters

Images of expression reporter samples were opened and managed as for signalling reporter images.

In response to micropipette wounding, touch or aphid treatment, images of expression reporter samples were analysed with the knowledge of where the stimulus events occurred. For each sample, if there was a clear elevation in this area of the reporter fluorescence through the imaging period, a fitted ROI was drawn around the signal area. The signal area was then measured. In the absence of any reporter signal, a circular ROI was drawn at the stimulus treated site with an area based on the signal area recorded for responses to the same stimulus in other reporters. These ROIs had areas and radii of 320000 μm^2 (0.32 mm^2) and 319.15 μm for wounding, 150000 μm^2 (0.15 mm^2) and 218.51 μm for aphids and 130000 μm^2 (0.13 mm^2) and 203.42 μm for touch, respectively. As thrips feeding events could not easily be recorded during treatment, ROIs were first drawn around the whole leaf for all samples allowing measurements of whether the reporter expression was induced by the thrips treatment. Additionally, if reporter signal responses were clear, one signal for each sample was outlined with an ROI and analysed allowing responses to presumed individual feeding events to be measured. For all treatments, the ROIs were duplicated or reproduced at an equivalent control site in every image. This was in the same leaf for wounding and touch and in a control leaf for insect treatments. Next, the fluorescence intensity (F, A.U.) was measured for every ROI across the time points adjusting the ROI position as necessary to ensure measurements represented the same region of the leaf. The change in fluorescence intensity, ΔF , was then calculated for each ROI at each time point from the fluorescence intensity in the earliest image, F_0 , as $\Delta F = F - F_0$. ΔF values were compared between groups at each time point along with signal areas as required.

For MeJA treatments and screening of *pAOS/JAZ10::NLS-3xVENUS A. thaliana* lines, ROIs were drawn around the whole abaxial surface of MeJA- or mock-treated leaves. Intensity values were measured and compared for the treatments and genotypes being assessed.

2.4. Assessing aphid extract-induced *A. thaliana* responses by plate reader measurements of genetically encoded fluorescent reporters

2.4.1. Preparation of aphid extract

Aphid extract used to investigate aphid HAMP-induced responses was prepared by James Canham (formerly Hogenhout Group, J.I.C.) from *M. persicae* (Clone O) as described in Canham (2022). Approximately 50 mg of mixed instar adult *M. persicae* (Clone O) aphids were collected into 2 mL tubes and snap frozen in liquid nitrogen with a 4 mm stainless steel ball before grinding in a TissueLyser LT (Qiagen). 820 μ L 4°C extraction buffer (50 mM Tris-HCl pH 7, 1 mM EDTA) was added to tubes and vortexed prior to sonication twice for 20 s with a Soniprep 150 Plus (MSE) at amplitude 8. To remove insoluble material, samples were centrifuged for 10 min at 10000 x g and 4°C. The supernatant was collected and the protein within precipitated with 60% v/v 4.1 M ammonium sulphate solution with constant agitation for 1 h at 4°C. The precipitate was isolated by centrifugation at 12000 x g for 20 min before being resuspended in 400 μ L 1 X PBS at 4°C overnight with 30 rpm. Samples were then treated with 80% v/v acetonitrile and mixed before incubation on ice for 1 h and subsequent centrifugation for 10 min at 12000 x g and 4°C. The low molecular weight enriched supernatant was snap frozen and lyophilised using a Centrifugal Quattro Concentrator (Genevac). 400 μ L 1 X PBS was added to the resulting powder which was then passed with other batches of extract through a 15 mL < 3 kDa low molecular weight filter (Amicon) according to the manufacturer's guidance. Filtrates were then treated with 200 μ M proteinase k (Merck) and incubated for 2 h at 50°C before deactivation by heat treatment at 95°C for 10 min. Filtrate was stored at 4°C for up to 3 weeks prior to use as 'aphid extract'.

2.4.2. Plant preparation

A. thaliana seedlings for experiments with aphid extract were grown in 96-well plates for 9 days before the 200 μ L ½-strength MS media was replaced with 150 μ L of dH₂O. Plates were sealed with cling film and kept dark overnight at room temperature before experimentation on day 10.

2.4.3. Treatment, fluorescence intensity measurements and analyses

To measure fluorescence intensity from samples in 96-well plates, plates were uncovered and placed in the FLUOstar Omega plate reader (BMG LABTECH) controlled by the Omega software (BMG LABTECH). As reporters investigated in this way were all GFP-based, wells

were successively excited, going between treatment groups, using a high energy xenon flash lamp with a GFP filter set (emission: 485/12 nm, excitation: 520/30 nm) and a gain of 1000. A cycle of the entire plate took 40 s and was repeated at 1 min intervals. 30 min recording was performed prior to treatment to acquire baseline intensities for normalisation. Elicitor treatment was then performed by quickly replacing 50 μ L from each well with a 3 x elicitor solution with minimal agitation of seedlings. Treatments applied were dH₂O, 0.75% v/v 1 x PBS, 0.75% v/v aphid extract and 60 nM flg22 in dH₂O (EZBiolab, Carmell, USA). After elicitation, plates were quickly returned for a further 90 min recording of plant fluorescent reporter intensity. Intensity measurements for each sample and time point were exported into Microsoft Excel Version 2202 (Microsoft). Every fluorescence intensity value was then background corrected by subtracting a mean background intensity value collected over 60 min from non-transgenic seedlings under equal conditions (background value: 348.01 ± 0.94 A.U., $n = 55$). The resulting background-corrected fluorescence intensity, F , values were normalised by $\Delta F/F_0$ where F_0 was the mean F over the 30 min baseline period prior to elicitation and $\Delta F = F - F_0$. F_0 values were compared between the genotypes and treatments to assess for equal reporter expression. Mean $\Delta F/F_0$ traces and maximum $\Delta F/F_0$ values were also compared between treatments and genotypes to evaluate responses to the treatments applied.

2.5. Data handling and presentation

All numerical data were recorded and handled in Microsoft Excel Version 2202 (Microsoft). Where measures of central tendency and variation are given, these are the mean and the standard error of the mean (S.E.M.), respectively. For each variable investigated, data is reported to a consistent number of decimal places throughout the thesis to aid the comparison of results. Repeated measures were not performed to assess the precision to which each variable should be reported. However, the precision to which each variable is reported was deemed reasonable for the equipment and approaches used.

For data presented in line graphs, data points represent the mean at each time point with the mean \pm S.E.M. presented as a shaded region around the mean. For data presented in a boxplot, horizontal lines indicate the lower quartile, median and upper quartile. Individual data points are indicated by black dots on boxplots. Data points that fell outside of the interquartile range by more than 1.5 x the interquartile range were deemed to be outliers. These data points are highlighted on boxplots by the addition of a grey dot in the centre line of the boxplot at the same vertical position as the data point. Whiskers on boxplots extend from the lower and upper quartile lines to the minimum and maximum data points that are not outliers, respectively.

All statistical analyses were performed using RStudio Version 1.2.5033 (RStudio Team, 2020). The assumptions for all statistical tests were assessed before tests were implemented. Data were assessed for normality using Shapiro-Wilks tests. A Levene's test was used for assessing the equality of variances between compared groups. Further statistical tests used are referenced in the relevant results text and figure legends. For each statistical test, all data points were included in the analysis, including data points that were identified as outliers.

2.6. Reporter signal modelling

Modelling of reporter fluorescence intensity values and normalised reporter signals was performed in Python using the Jupyter notebook (Kluyver *et al.*, 2016), as described in results. Scripts for the models were originally written by Sergio Lopez (BioImaging Platform, John Innes Centre) as part of a collaboration and were subsequently modified here to meet the desired parameters.

3. Developing the Foundations for Exploring the Perception of
Aphid and Thrips Feeding in *A. thaliana* with Genetically Encoded
Fluorescent Reporters

3.1. Introduction

To investigate how *A. thaliana* perceives aphid and thrips feeding, it will be beneficial to develop methods that allow the visualisation of early plant responses to localised stimuli. $[Ca^{2+}]$ reporter imaging can provide a foundation for these methods as Ca^{2+} signalling is fundamental in plant biotic stress responses and as $[Ca^{2+}]$ reporter imaging is well established with various genetically encoded Ca^{2+} indicators (GECIs) available (Grenzi *et al.*, 2021; Jiang and Ding, 2023; Patra *et al.*, 2021). Moreover, GECI imaging has previously been performed to investigate *A. thaliana* responses to aphid feeding (Vincent *et al.*, 2017a; Vincent *et al.*, 2017b; Then *et al.*, 2021; Wang *et al.*, 2022b; Xue *et al.*, 2022). In Section 3.1.1., I will explore key considerations for developing methods to image genetically encoded fluorescent reporters. In Section 3.1.2., I will summarise the knowledge of aphid feeding-induced responses in plants that has been established by GECI imaging. Section 3.1.3. will then outline the aims of this chapter.

3.1.1. Considerations for genetically encoded reporter imaging

Many genetically encoded reporters are based on fluorescent proteins (FPs). Intensiometric FP-based reporters indicate relative analyte concentrations by the absolute intensity of a single emission wavelength. In contrast, ratiometric reporters indicate analyte levels by the ratio of two emission wavelengths. Ratiometric reporters may be based on a single FP, two FPs displaying FRET, or two linked FPs with a reporter FP that indicates analyte concentration and an analyte-insensitive reference FP (Walia *et al.*, 2018). Reporters differ in their properties including their signal-to-noise ratios (SNRs), dynamic ranges, and detection ranges (Grenzi *et al.*, 2021). Selecting appropriate reporters based on their properties and rigorously implementing them can determine the success and reliability of investigations using genetically encoded reporters.

Intensiometric reporters, such as the GFP-based GCaMP GECIs, are relatively simple to implement and have comparatively broad dynamic ranges and high SNRs compared to ratiometric FRET-based reporters (Hilleary and Gilroy, 2018; Grenzi *et al.*, 2021). However, using absolute intensities to report relative analyte concentrations with intensiometric reporters can elevate the risk of producing artefactual results (Grenzi *et al.*, 2021). For example, intensiometric reporter fluorescence is often sensitive to pH as has been demonstrated for the R-GECO1 (Zhao *et al.*, 2011; Keinath *et al.*, 2015) and GCaMP3 GECIs (Cho *et al.*, 2017). As a result, pH changes can influence intensiometric reporter signals and cause artefacts in data. Assessing and controlling for the limitations of intensiometric reporters is therefore important. For example, complementary measurements to assess for pH changes could be conducted with a genetically

encoded pH reporter such as the ratiometric dual FP reporter, pHusion (Gjetting *et al.*, 2012). Additionally, to assess for pH changes, intensimetric GECIs could be replaced by dual Ca^{2+} -pH reporters such as CapHensor (Li *et al.*, 2021a) or R-GECO1-GSL-E²GFP (Waadt *et al.*, 2020). Because reference proteins can indicate changes in variables such as pH, non-FRET ratiometric reporters can limit the risk of artefacts in results going unnoticed. For the FRET-based YC-Nano 65 and YC3.6 GECIs, it is thought that both FPs are similarly responsive to pH and thus pH changes should not significantly influence signals detected with these reporters (Behera *et al.*, 2018; Grenzi *et al.*, 2021; Nagai *et al.*, 2004). Therefore, compared to other reporters, intensimetric reporters require additional care to ensure that background variables, such as pH, do not influence the reporter signals detected or resulting conclusions.

Intensimetric reporter signals can also be heavily influenced by variation in reporter expression levels (Grenzi *et al.*, 2021; Rudolf *et al.*, 2003; Bootman *et al.*, 2013). To control for expression levels, intensimetric reporter signals are normalised to their baseline intensity. This normalisation is often performed by a $\Delta F/F_0$ calculation where F is fluorescence intensity, F_0 represents the baseline F over a resting period and $\Delta F = F - F_0$. However, changes in fluorescence (ΔF) are only directly proportional to F_0 or reporter expression when F represents solely the reporter signal and does not include any background intensity. The inclusion of a constant background intensity in F leads to $\Delta F/F_0$ underestimations. This underestimation effect would be greater with lower reporter expression or F_0 than with higher reporter expression. Resultingly, if background signal is included in F, expression differences can cause artefactual differences in $\Delta F/F_0$ comparisons. To avoid this issue, the background intensity, representing that of a sample in the absence of the reporter, should be removed from all F values in a 'background correction'. The use of a background correction is mentioned in some guidance for, or descriptions of, using genetically encoded fluorescent reporters (Bootman *et al.*, 2013; Gjetting *et al.*, 2012; Shkryl, 2020). Nonetheless, this risk of expression artefacts highlights the need for extra caution when using intensimetric reporters.

Ratiometric reporters can help avoid expression artefacts and aid comparisons of reporter signals between tissues, samples and material (Grenzi *et al.*, 2021). This is as two emission intensities are used for ratiometry and these usually originate from components with linked expression. Expression levels can therefore be gauged by the two intensities and the ratio can help control for variation in expression (Rudolf *et al.*, 2003; Grenzi *et al.*, 2021). GEX-GECO1 provides an example of a single FP-based ratiometric GECI derived from GCaMP3 that reports $[\text{Ca}^{2+}]$ via the $[\text{Ca}^{2+}]$ -dependent excitation ratio at 400 and 488 nm (Zhao *et al.*, 2011). However, this reporter has relatively low emission intensity compared to intensimetric GCaMPs (Grenzi *et al.*, 2021). To keep the benefits of existing intensimetric GECIs but with an added reference

FP for ratiometry, dual FP non-FRET reporters have been developed around single FP GECIs. For instance, the R-GECO1-mTurquoise reporter utilises R-GECO1 for $[Ca^{2+}]$ reporting and mTurquoise as a reference FP (Waadt *et al.*, 2017). Based on a similar principle but with only one excitation wavelength required, Ast *et al.* (2017) developed MatryoshCaMP6s around GCaMP6s. Such reporters are not without challenges as they are often more complex to image and of a larger size than intensimetric reporters (Grenzi *et al.*, 2021). With the benefits of ratiometric reporters in controlling for expression, background correction may be deemed less important. However, having a background intensity contributing to fluorescence measurements and ratios may still influence results, thereby maintaining a risk of expression artefacts emerging. The extent to which this is a problem has not been well demonstrated for ratiometric reporters used in *A. thaliana*. Therefore, it seems important to maintain care for expression with ratiometric reporters and consider background corrections that remove all signal extraneous to the reporter to improve the accuracy of results.

3.1.2. Insights into aphid feeding-induced $[Ca^{2+}]$ elevations established with GECIs

Despite their limitations, the benefits of intensimetric GECIs have made those such as GCaMPs popular for studying whole plant or organ Ca^{2+} signalling responses to stimuli and especially those less reproducible like insect feeding (Toyota *et al.*, 2018; Vincent *et al.*, 2017a; Nguyen *et al.*, 2018; Xue *et al.*, 2022; Shao *et al.*, 2020; Hagihara *et al.*, 2022; Parmagnani and Maffei, 2022). Whilst GECIs have not yet been used to investigate thrips-plant interactions, live aphid-plant interactions have been investigated with GECIs on several occasions (Then *et al.*, 2021; Vincent *et al.*, 2017a; Xue *et al.*, 2022; Wang *et al.*, 2022b). GCaMP3 imaging revealed that *M. persicae* feeding induces $[Ca^{2+}]$ elevations in epidermal and mesophyll cell layers that are restricted around the feeding site and do not travel systemically (Vincent *et al.*, 2017a). Additionally, these $[Ca^{2+}]$ elevations appear to be fully dependent on BAK1 and GLR3.3/3.6 (GLR3.3 and/or GLR3.6) as well as partially dependent on TPC1 (Vincent *et al.*, 2017a). This localised response is consistent with *M. persicae* being thought not to induce significant systemic signalling or defence responses in *A. thaliana* (De Vos and Jander, 2009; Vincent, 2016). However, Xue *et al.* (2022) utilised GCaMP6s to reveal that heavy *M. persicae* infestation can induce systemic GLR3.3/3.6-dependent $[Ca^{2+}]$ elevations and JA-mediated aphid resistance. As Ca^{2+} -permeable receptor channels, GLR3.3/3.6 therefore appear to function in both localised and systemic aphid-induced responses. Overall, it is largely unknown how plants initially perceive aphid feeding with only a few candidate elicitors described and PRRs remaining elusive (Chaudhary *et al.*, 2014; Elzinga *et al.*, 2014; Bos *et al.*, 2010; Nalam *et al.*, 2019; Prince *et al.*, 2014; Canham, 2022). As such, intensimetric $[Ca^{2+}]$ reporter imaging has helped provide key

insights into the plant perception of live aphid feeding by implicating BAK1, TPC1 and GLR3.3/3.6.

3.1.3. Current investigations

Imaging genetically encoded reporters will be valuable here for investigations into how plants recognise and respond to aphid or thrips feeding. For this, approaches can build on the existing knowledge of aphid-induced Ca^{2+} signalling (Vincent *et al.*, 2017a; Xue *et al.*, 2022) and the established protocols for imaging aphid-induced $[\text{Ca}^{2+}]$ elevations using GCaMP3 (Vincent *et al.*, 2017b). However, considering the limitations of the intensimetric reporters used for previous investigations into aphid feeding-induced $[\text{Ca}^{2+}]$ elevations, it is important that the existing methods and results are reassessed and that any findings inform the methods and rationales of this thesis. As such, the research aims of this chapter are to:

1. Identify whether differences in intensimetric reporter expression between compared lines could have influenced the conclusions of Vincent *et al.* (2017a) regarding aphid feeding-induced $[\text{Ca}^{2+}]$ elevations.
2. Explore how differences in reporter expression between compared groups could cause differences in normalised intensimetric and ratiometric non-FRET reporter signals and whether background corrections can adequately control for this effect. Utilise any findings to develop methods for imaging and analysing genetically encoded reporter signals induced by localised stimuli.
3. Using the updated methods, investigate whether *M. persicae* feeding-induced $[\text{Ca}^{2+}]$ elevations are dependent on BAK1, TPC1 and GLR3.3/3.6.

3.2. Results

3.2.1. Previous conclusions implicating BAK1, GLR3.3/3.6 and TPC1 in aphid feeding-induced $[Ca^{2+}]$ elevations are compromised by differences in reporter expression

Vincent *et al.* (2017a) investigated *M. persicae* feeding-induced $[Ca^{2+}]$ elevations using *A. thaliana* expressing *35S::GCaMP3* but analyses did not include background corrections. Compared to Col-0 controls, the $\Delta F/F_0$ measurements suggested a loss of $[Ca^{2+}]$ elevations in *bak1-5* and *glr3.3b glr3.6a* mutants with reduced amplitude elevations in the *tpc1-2* mutant. To assess if variation in GCaMP3 expression influenced these results, I reanalysed the raw data from Vincent *et al.* (2017a). In these data, non-corrected fluorescence intensity, F, was measured at 5 s intervals with the baseline fluorescence, F_0 , being the mean F for the 5 min before feeding. F_0 values from the *M. persicae* feeding sites were used as an indicator of reporter expression. Compared to its Col-0 control samples, the F_0 values from *bak1-5 35S::GCaMP3 A. thaliana* samples were significantly reduced (Figure 3.1A, Kruskal-Wallis, $W = 619$, $p = 0.011$). Similarly, compared to Col-0 control samples, F_0 values were significantly lower in *glr3.3b glr3.6a 35S::GCaMP3* samples (Figure 3.1B Kruskal-Wallis, $W = 1148$, $p < 0.0001$) and *tpc1-2 35S::GCaMP3* samples (Figure 3.1C, Kruskal-Wallis, $W = 515$, $p < 0.0001$). The difference between F_0 values in the Col-0 and mutant samples was much more pronounced for the comparisons with *glr3.3b glr3.6a* and *tpc1-2* than with *bak1-5* (Figure 3.1). Given these data, GCaMP3 expression differences may have influenced the results implicating BAK1, GLR3.3/3.6 and TPC1 in *M. persicae* feeding-induced $[Ca^{2+}]$ elevations thereby warranting further investigation.

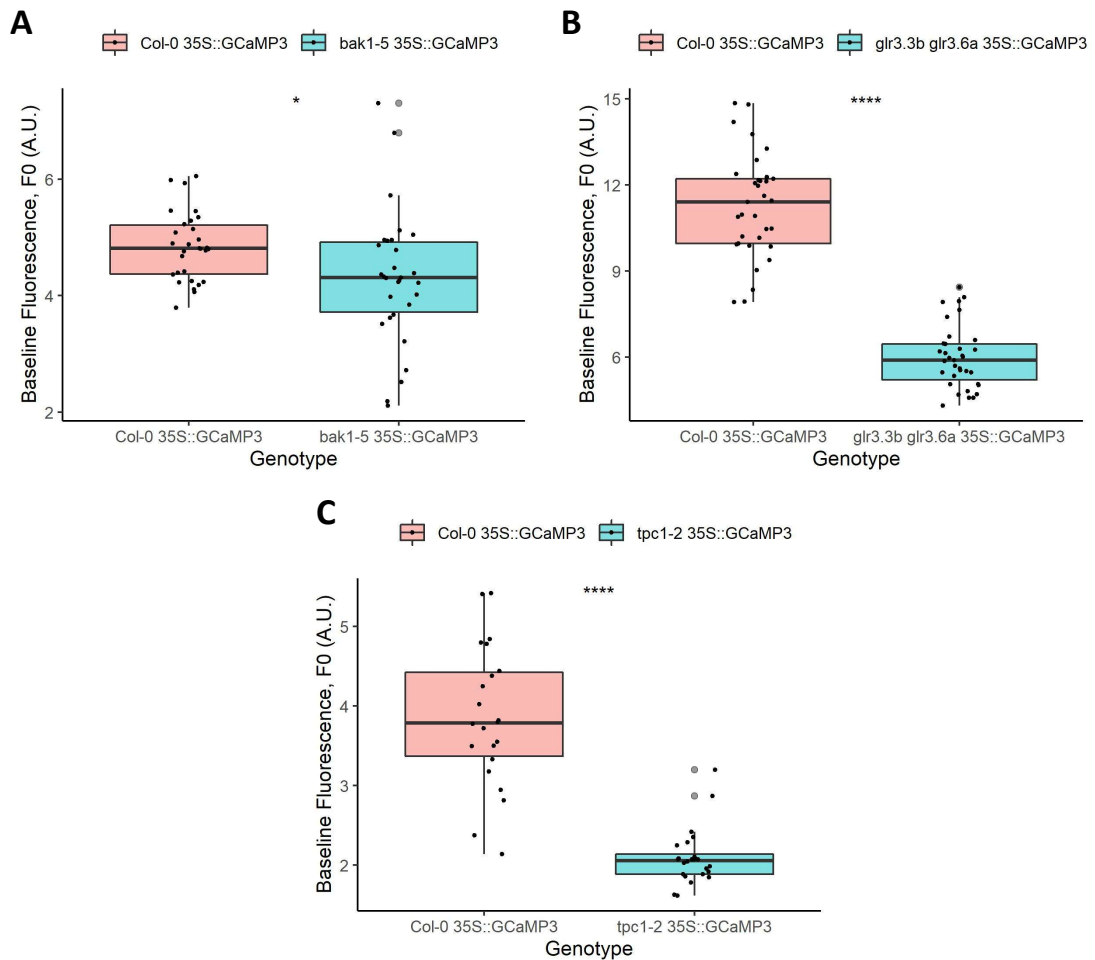


Figure 3.1 Mutant 35S::GCaMP3 *A. thaliana* lines investigated in Vincent *et al.* (2017a) had reduced baseline fluorescence intensities compared to their wild-type counterparts.

Boxplots of non-corrected baseline fluorescence (F0, arbitrary units: A.U.) at feeding sites calculated as the mean of the non-corrected fluorescent intensity (F, A.U.) values over the 5 min prior to *M. persicae* feeding. Data taken from Vincent *et al.* (2017a) with imaging on a Leica M205FA microscope. *A. thaliana* lines were (A) Col-0 35S::GCaMP3 ($n = 30$) and *bak1-5* 35S::GCaMP3 ($n = 30$), (B) Col-0 35S::GCaMP3 ($n = 33$) and *glr3.3b glr3.6a* 35S::GCaMP3 ($n = 35$) and (C) Col-0 35S::GCaMP3 ($n = 22$) and *tpc1-2* 35S::GCaMP3 ($n = 24$). Grey dots are associated with outliers. Statistical significance, tested using Kruskal-Wallis tests, shown by *: $p \leq 0.05$, ****: $p \leq 0.0001$.

3.2.2. Empirically assessing the effect of variation in reporter expression on normalised GCaMP3 signals and whether background corrections can offset any effects

Next, I investigated the impact of variation in intensimetric reporter expression on $\Delta F/F_0$ comparisons and whether background corrections can limit any effects. To do so, I first identified *A. thaliana* lines with different *GCaMP3* expression levels by screening GFP fluorescence intensities in seedlings on an Axio Zoom.V16 microscope. Selected lines were then subjected to localised micropipette wounding to induce reporter signals that could be compared between lines by normalised $\Delta F/F_0$ values before and after background corrections. For this, fluorescence intensity, F , was measured over the responding areas and at control sites at 5 s intervals with baseline intensity, F_0 , values being the mean F over the 5 min prior to wounding. After wounding, a further 30 min imaging was performed to measure the wound-induced responses. Background-corrected F values were produced by subtracting from all F values a mean intensity value obtained from across equivalent non-transgenic *A. thaliana* leaves imaged under equivalent conditions. As the wounding experiments were conducted over two occasions, there were two background intensity values of 1974.90 ± 14.91 A.U. ($n = 13$) and 2036.57 ± 12.69 A.U. ($n = 39$). The corrected F_0 values were compared between lines to compare reporter expression levels (Figure 3.2A, B, C). Additionally, *GCaMP3* expression was assessed by Western blots of the aerial tissue from whole seedlings with an anti-GFP-HRP antibody that probes *GCaMP3* (Figure 3.2D, E, F). This allowed comparisons to be established between *A. thaliana* lines with different fluorescence intensities and attribution of that variation to differences in reporter expression before comparing non-corrected and corrected normalised $\Delta F/F_0$ values.

Various wildtype and mutant *GCaMP3* lines were assessed for their fluorescence intensities. First identified was a Col-0 *35S::GCaMP3 A. thaliana* line with a relatively high and uniform reporter fluorescence within and between seedlings and only occasional low intensity seedlings that were discarded. This 'high expression line' was a descendant of the one used in Vincent *et al.* (2017a) which was crossed to produce the *tpc1-2 35S::GCaMP3 A. thaliana* line. This Col-0 high expression line was identified as containing two copies of the *35S::GCaMP3* transgene (iDna Genetics, Norwich, U.K.). Notable variation between *tpc1-2 35S::GCaMP3 A. thaliana* lines allowed selection for different fluorescence intensities and revealed that the *tpc1-2* mutation did not explain this variation. I identified a *tpc1-2 35S::GCaMP3* line with greatly reduced F_0 values compared to the wildtype (Figure 3.2A, Wilcoxon rank-sum, $W = 477$, $p < 0.0001$) and very low, almost unidentifiable, *GCaMP3* concentrations (Figure 3.2D). This was termed the 'low expression line'. A parental line to this was a *tpc1-2 35S::GCaMP3* line which, compared to the wildtype, had moderately reduced F_0 values (Figure 3.2B, t-test, $t = 5.60$, $p < 0.0001$) and *GCaMP3* concentrations (Figure 3.2E). This was termed the 'moderate expression

line'. The low and moderate expression lines yielded some seedlings with no clear reporter expression and some with older leaves that displayed localised lower expression that developed after approximately 7 days post-germination and seemed to expand with development. These seedlings were discarded. To produce Col-0 and *tpc1-2* lines with equal reporter expression, Col-0 *UBQ10::GCaMP3 A. thaliana* (Nguyen *et al.*, 2018) was crossed with the *tpc1-2* mutant to produce a homozygous *tpc1-2 UBQ10::GCaMP3* line. The Col-0 and *tpc1-2 UBQ10::GCaMP3 A. thaliana* lines had F0 values that were not statistically different (Figure 3.2C, Wilcoxon rank-sum, $W = 295$, $p = 0.70$) and displayed similar GCaMP3 concentrations (Figure 3.2F). As these lines had GCaMP3 expression levels that seemed slightly lower than that of the Col-0 *35S::GCaMP3* line, they were termed 'intermediate expression' lines. As a result, the selection process established three comparisons between Col-0 and *tpc1-2* lines based on GCaMP3 fluorescence and expression levels: a high vs low expression, a high vs moderate expression and an intermediate vs intermediate expression comparison. These comparisons provided a background to investigate the effect of variation in reporter expression on non-corrected and background-corrected normalised $\Delta F/F_0$ values.

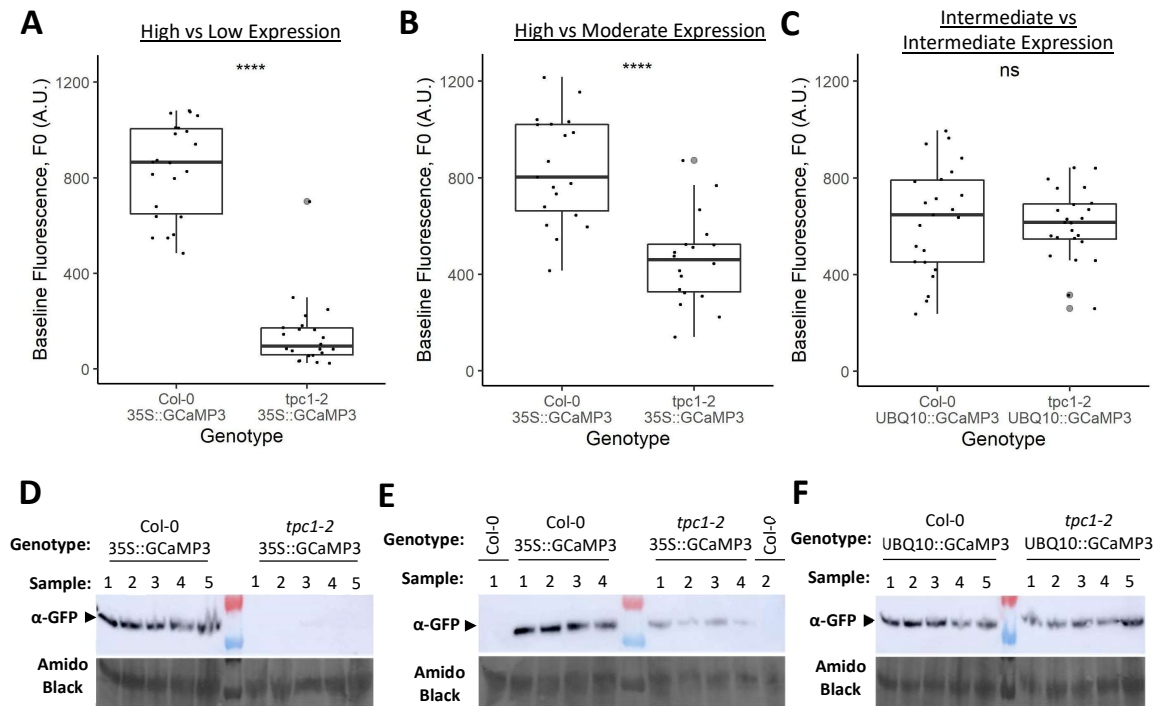


Figure 3.2 Selected Col-0 and *tpc1-2* *A. thaliana* lines expressing *GCaMP3* with different expression levels and fluorescence intensities.

Baseline fluorescence and *GCaMP3* levels in selected Col-0 and *tpc1-2* *A. thaliana* lines expressing *GCaMP3*. Lines assessed were (A, D) Col-0 35S::GCaMP3 (high expression, $n = 22$) and *tpc1-2* 35S::GCaMP3 (low expression, $n = 22$), (B, E) Col-0 35S::GCaMP3 (high expression, $n = 19$) and *tpc1-2* 35S::GCaMP3 (moderate expression, $n = 18$) and (C, F) Col-0 UBQ10::GCaMP3 (intermediate expression, $n = 22$) and *tpc1-2* UBQ10::GCaMP3 (intermediate expression, $n = 24$). (A-C) Boxplots of corrected baseline fluorescence (F0, A.U.) values calculated as the mean of the background corrected fluorescence intensity (F, A.U.) values over the 5 min prior to wounding for the responding areas in Col-0 and *tpc1-2* *A. thaliana* samples expressing *GCaMP3*. The background correction values were (A) 1974.90 A.U. and (B, C) 2036.57 A.U. Grey dots are associated with outliers. Statistical significance, tested using (A, C) a Wilcoxon rank-sum test or (B) a t-test, is shown by ns: $p > 0.05$, ****: $p \leq 0.0001$. (D-F) Western blots displaying *GCaMP3* protein levels across the selected Col-0 and *tpc1-2* *GCaMP3* expressing *A. thaliana* lines with (E) two non-transgenic Col-0 samples included. Blots were performed on aerial tissue samples from representative 16-day-old seedlings and were probed with an anti-GFP-HRP antibody before a 10 min exposure for immunodetection and then total protein staining with 1 x Amido Black.

To test the effect of the expression differences on non-corrected $\Delta F/F_0$ values for each comparison, I compared the normalised $\Delta F/F_0$ traces and the peak normalised $\Delta F/F_0$ values in the absence of a background correction (Figure 3.3A, C, E). Compared to the high expression Col-0 *35S::GCaMP3* line, the peak normalised $\Delta F/F_0$ values were significantly lower in the low expression *tpc1-2 35S::GCaMP3* line (Figure 3.3A, Wilcoxon rank-sum, $W = 479$, $p < 0.0001$) and in the moderate expression *tpc1-2 35S::GCaMP3* line (Figure 3.3C, t-test, $t = 9.04$, $p < 0.0001$). In contrast, the intermediate expression Col-0 and *tpc1-2 UBQ10::GCaMP3* lines with equal expression had statistically indifferent peak normalised $\Delta F/F_0$ values (Figure 3.3E, Wilcoxon rank-sum, $W = 281$, $p = 0.9244$). The differences in leaf fluorescence intensities in the three comparisons were clear in images from 2 min post-wounding (Figure 3.3B, D, F). These data revealed that the significantly reduced peak normalised $\Delta F/F_0$ values in the moderate and low expression lines compared to the high expression wildtype was a direct effect of reduced reporter expression. As such, differences in reporter expression can produce artefactual differences in non-corrected $\Delta F/F_0$ values.

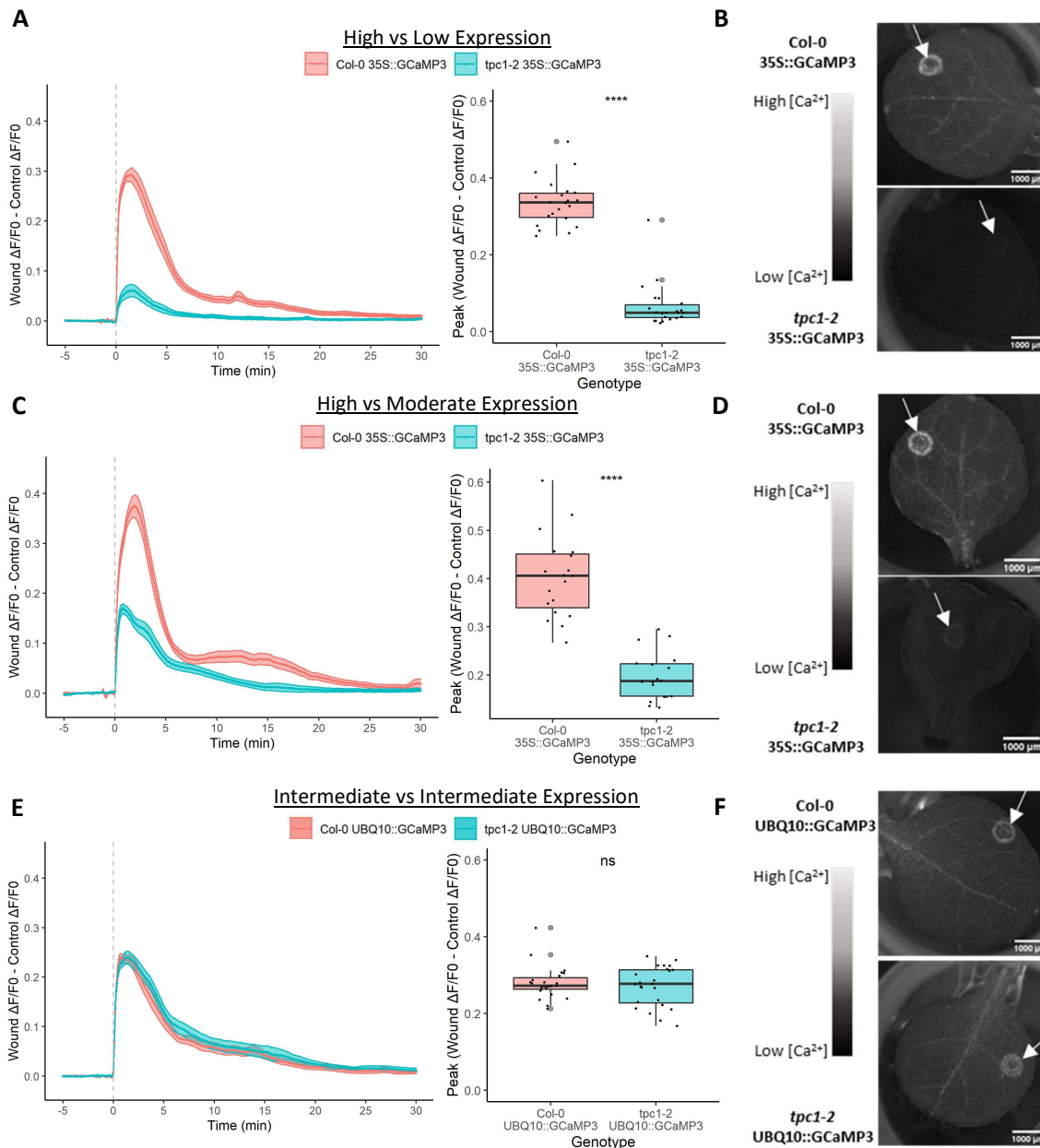


Figure 3.3 Assessing the effect of GCaMP3 reporter expression differences on wound-induced non-corrected normalised reporter signals in the Col-0 and *tpc1-2* lines.

Comparisons of wound-induced non-corrected reporter signals in *A. thaliana* lines between (A, B) high expression Col-0 35S::GCaMP3 ($n = 22$) and low expression *tpc1-2* 35S::GCaMP3 ($n = 22$), (C, D) high expression Col-0 35S::GCaMP3 ($n = 19$) and moderate expression *tpc1-2* 35S::GCaMP3 ($n = 18$) and (E, F) the intermediate expression lines of Col-0 ($n = 22$) and *tpc1-2* UBQ10::GCaMP3 ($n = 24$). Non-corrected fluorescence intensity values (F, A.U.) were detected at 5 s intervals over the area of wound-induced reporter signals and at comparable control sites with the baseline (F0, A.U.) values being the mean F over the 5 min before wounding at 0 min. F values were not corrected for background intensity. (A, C, E) Traces for the mean \pm S.E.M. normalised $\Delta F/F_0$ values (Wound $\Delta F/F_0$ – Control $\Delta F/F_0$) over time with wounding at 0 min (grey dashed line) alongside boxplots for the peak normalised $\Delta F/F_0$ values with grey dots associated with outliers. Statistical significance, tested using (A, C) a Wilcoxon rank-sum test or (B) a t-test, shown by ns: $p > 0.05$, ****: $p \leq 0.0001$. Representative images for samples 2 min post-wounding in the (B) low vs high expression comparison, (D) the moderate vs high expression comparison and (F) the intermediate vs intermediate expression comparison. Arrows indicate wound-induced reporter signals.

Next, I tested the ability of background corrections to prevent differences in reporter expression giving rise to artefactual differences in $\Delta F/F_0$ values. To do so, background corrections were applied using the correction values of 1974.90 A.U. for the high vs low expression comparison and 2036.57 A.U. for the other comparisons. Following this, compared to the high expression Col-0 *35S::GCaMP3* line, the peak normalised $\Delta F/F_0$ values were not statistically different for the low expression *tpc1-2 35S::GCaMP3* line (Figure 3.4A, Wilcoxon rank-sum, $W = 282$, $p = 0.36$) or for the moderate expression *tpc1-2 35S::GCaMP3* line (Figure 3.4B, t-test, $t = 1.83$, $df = 33.25$, $p = 0.077$). There were also no statistically significant differences between peak normalised $\Delta F/F_0$ values for the equally expressing, intermediate expression Col-0 and *tpc1-2 UBQ10::GCaMP3* lines (Figure 3.4C, Wilcoxon rank-sum, $W = 267$, $p = 0.86$). Wound-induced GCaMP3 signal areas were also not statistically different between the Col-0 and *tpc1-2 UBQ10::GCaMP3* samples with mean values of $0.574 \pm 0.032 \text{ mm}^2$ and $0.577 \pm 0.029 \text{ mm}^2$, respectively (Figure 3.5A, t-test, $t = -0.073$, $p = 0.94$). Similarly, there were no statistically significant differences in the signal propagation rates for these lines with a mean value of $2.40 \pm 0.10 \mu\text{m s}^{-1}$ for Col-0 and $2.24 \pm 0.10 \mu\text{m s}^{-1}$ for *tpc1-2* (Figure 3.5B, t-test, $t = 1.14$, $p = 0.26$). It was clear however, that background correction on the low expression *tpc1-2 35S::GCaMP3* line led to notably larger variation in normalised $\Delta F/F_0$ values compared to the other lines (Figure 3.4A). Some of the increased variation likely derived from noise within each sample being amplified with background correction. However, Figure 3.4A revealed that some of the low expression samples had high peak corrected normalised $\Delta F/F_0$ values that contributed significantly to the increased variation. This resulted from some samples having such low reporter expression and intensity that they were only marginally brighter than a non-transgenic sample. As the background correction value is an estimate of the true background value for each sample, any error in the background value leads to a misestimation of the $\Delta F/F_0$ values. For lower expression lines, this effect is more significant as the background correction error is larger relative to the fluorescence intensity from the reporter. As such, low expression lines appear to be problematic for analyses with a background correction. Nonetheless, an appropriate background correction can offset the effects of differences in reporter expression on the amplitude of $\Delta F/F_0$ and is therefore, important for analyses of intensimetric reporters.

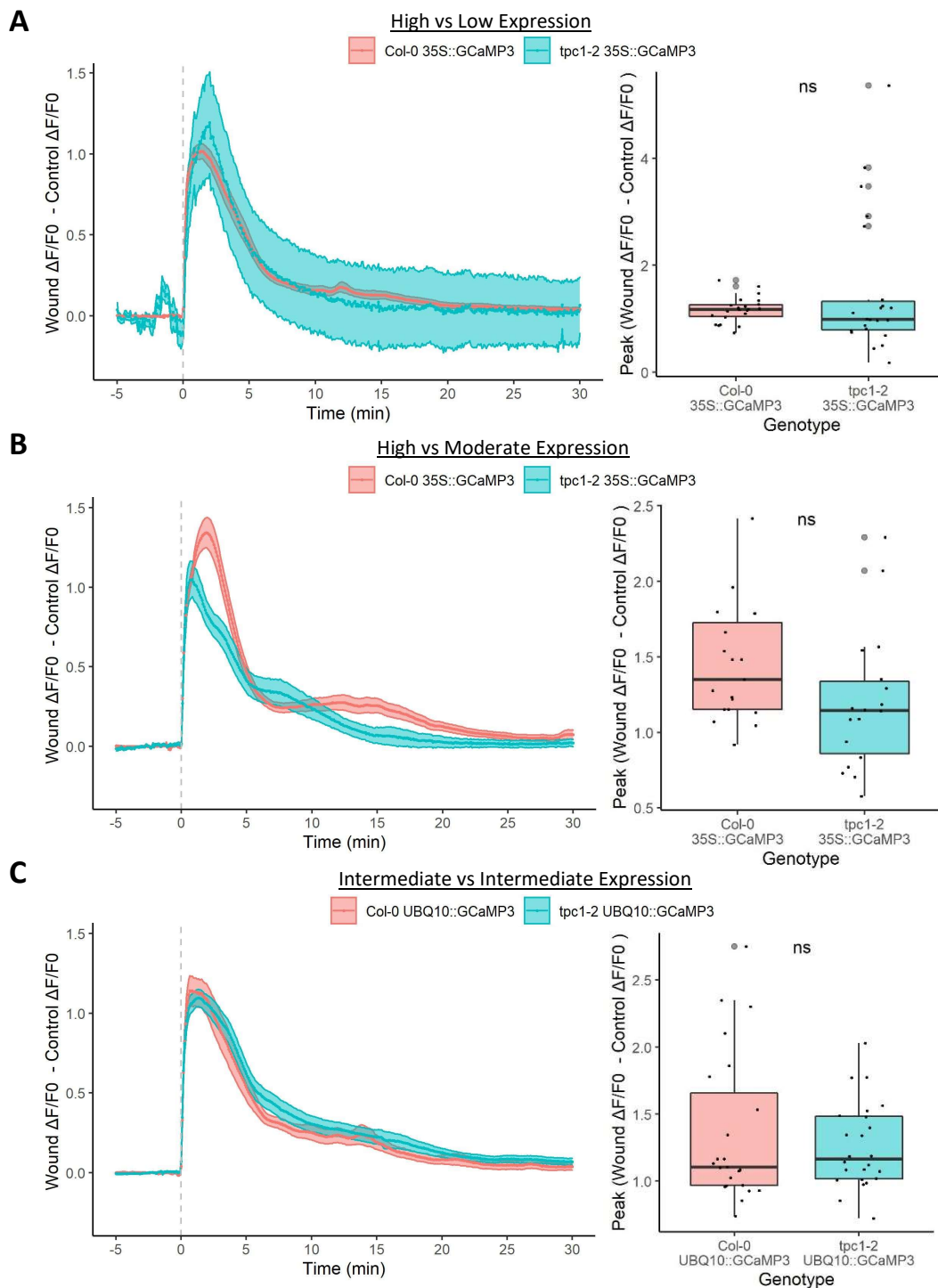


Figure 3.4 Background correction offsets the effects of differences in GCaMP3 expression on $\Delta F/F_0$ amplitude.

Comparisons of background-corrected reporter signals in *A. thaliana* lines between (A) high expression Col-0 35S::GCaMP3 ($n = 22$) and low expression *tpc1-2* 35S::GCaMP3 ($n = 22$), (B) high expression Col-0 35S::GCaMP3 ($n = 19$) and moderate expression *tpc1-2* 35S::GCaMP3 ($n = 18$) and (C) the intermediate expression lines of Col-0 ($n = 22$) and *tpc1-2* UBQ10::GCaMP3 ($n = 24$). Fluorescence intensity (F, A.U.) values were detected over the area of wound-induced reporter signals and at comparable control sites and background corrected with values of (A) 1974.90 A.U. or (B, C) 2036.57 A.U. Baseline intensity (F_0 , A.U.) was the mean corrected F over the 5 min before wounding at 0 min for each sample. (A-C) Traces for the mean \pm S.E.M. normalised $\Delta F/F_0$ values (Wound $\Delta F/F_0$ - Control $\Delta F/F_0$) with wounding at 0 min (grey dashed line) alongside boxplots for the peak normalised $\Delta F/F_0$ values with grey dots associated with outliers. Statistical significance, tested by (A, C) a Wilcoxon rank-sum test or (B) a t-test, shown by ns: $p > 0.05$.

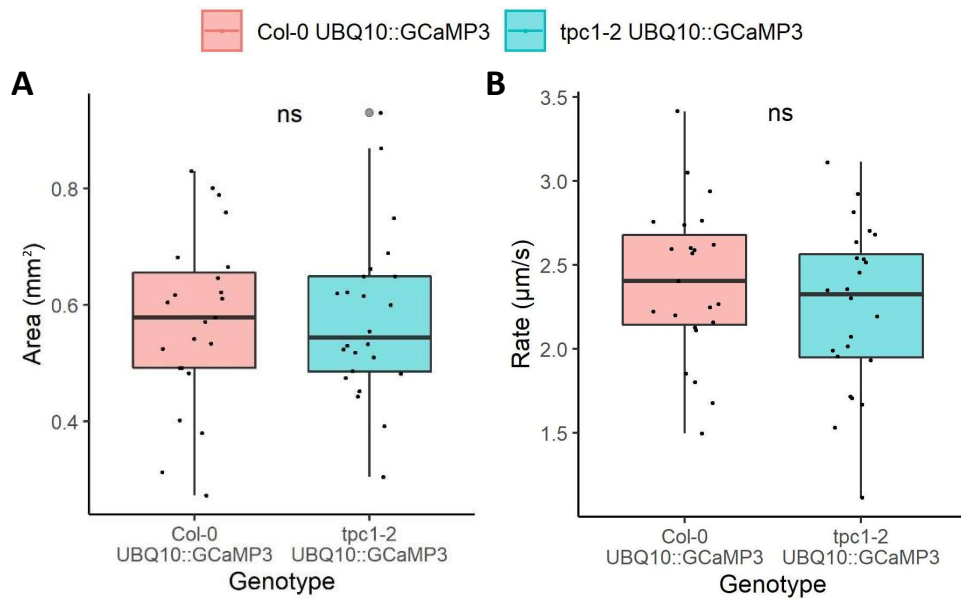


Figure 3.5 Local wound-induced GCaMP3 signals display similar properties in Col-0 and *tpc1-2 A. thaliana* leaves.

Boxplots comparing (A) the maximum signal areas (mm²) and (B) the signal propagation rates (µm s⁻¹) in wound-induced GCaMP3 reporter signals from Col-0 *UBQ10::GCaMP3* and *tpc1-2 UBQ10::GCaMP3 A. thaliana*. Grey dots are associated with outliers. Sample sizes were Col-0 $n = 22$, *tpc1-2* $n = 24$. Statistical significance, tested using a t-test, shown by ns: $p > 0.05$.

3.2.3. Modelling highlights the benefit of background corrections in limiting the effects of variable intensiometric and ratiometric reporter expression on normalised signals

To further demonstrate how variation in reporter expression can influence $\Delta F/F_0$ values, and how background corrections can counter these effects, the experimental data were used to produce a model. This model included *A. thaliana* GCaMP3 reporter lines with high (10 units GCaMP3/pixel), moderate (5 units GCaMP3/pixel) and low GCaMP3 expression (3 units GCaMP3/pixel) along with two intermediate expression lines (7 units GCaMP3/pixel). Reporter signals were modelled over 1653 pixels or 0.57 mm² which equalled the mean area of the wound induced GCaMP3 signals in the *UBQ10::GCaMP3* lines. Background intensity values were 1974.90 A.U./pixel for the high vs low expression comparison and 2036.56 A.U./pixel for the other comparisons. Using these values, I modelled GCaMP3 intensity to range from 83.00 A.U. unbound to 183.43 A.U. when fully Ca²⁺-bound. The non-corrected fluorescence intensity, F, values were calculated as the mean intensity across the area including the intensity of the background, the free GCaMP3 and the Ca²⁺-bound GCaMP3. F₀ was the mean F over the baseline period from -5 to 0 min. A wound event started at 0 min and peaked at 5 min with 80% of the GCaMP3 molecules Ca²⁺-bound at the peak. For the lines with different expression levels, this modelling facilitated comparisons of non-corrected and background-corrected $\Delta F/F_0$ values.

Firstly, the non-corrected F and $\Delta F/F_0$ values were modelled. This revealed that, compared to the high expression line, the low expression (Figure 3.6A) and moderate expression (Figure 3.6B) lines had reduced peak $\Delta F/F_0$ values. The lines with equal, intermediate expression had equal $\Delta F/F_0$ values (Figure 3.6C). The background correction, which subtracted the appropriate background value from all F values, eliminated these differences for the low (Figure 3.7A) and moderate expression lines (Figure 3.7B). After background correction, the equal intermediate expression lines were again equal in their $\Delta F/F_0$ values (Figure 3.7C). Modelling also clarified that $\Delta F/F_0$ amplitude is underestimated without background corrections and that this underestimation is greater in lines with lower expression as it depends on the reporter baseline intensity/background intensity ratio (Figure 3.8). Background correction eliminates this underestimation. In summary, this modelling demonstrated that differences in intensiometric reporter expression in comparisons can produce artefactual differences in $\Delta F/F_0$ values. Moreover, background correction can prevent these differences by eliminating the underestimation of $\Delta F/F_0$ caused by the presence of background signal intensity.

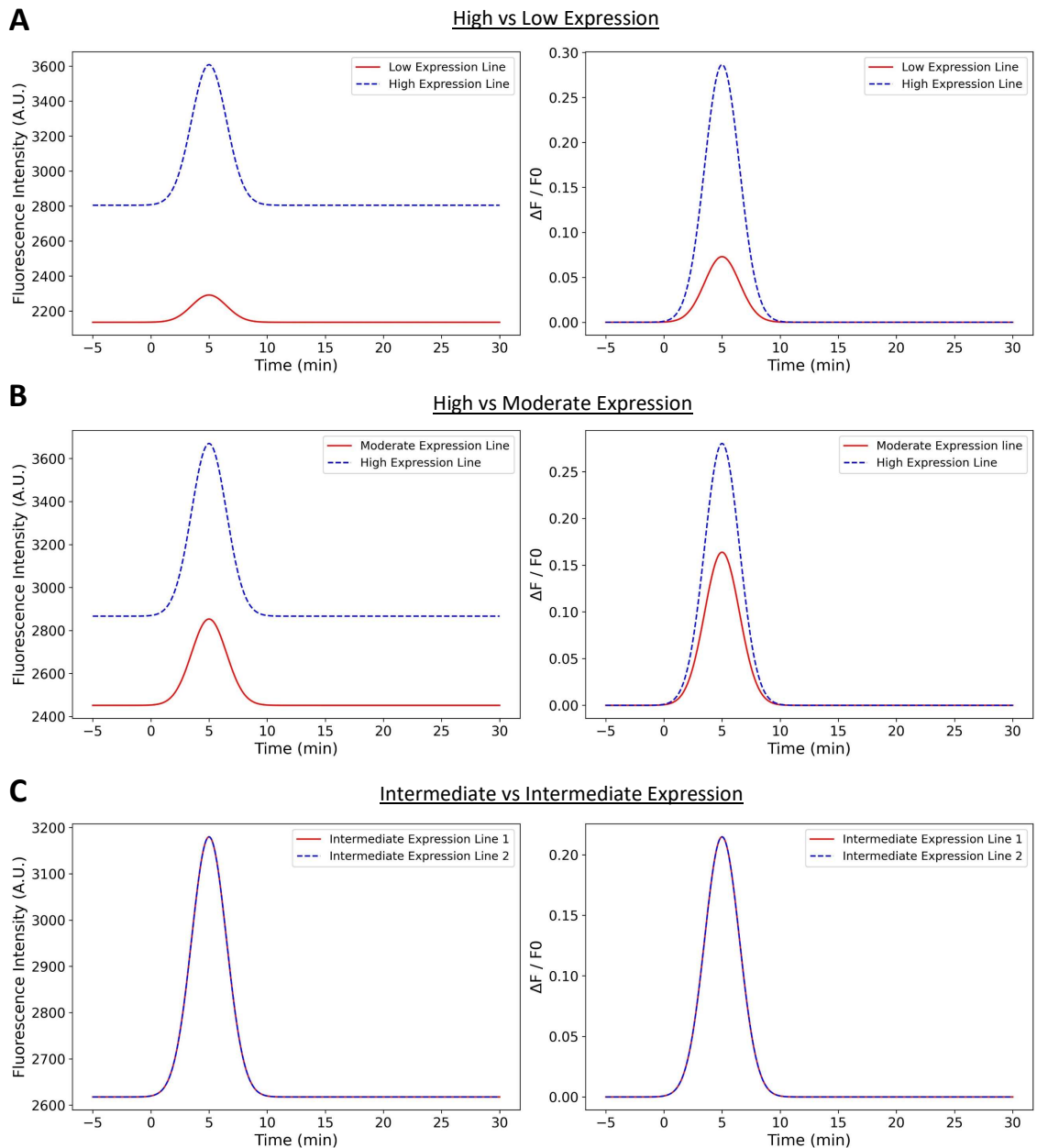


Figure 3.6 Modelling the effect of variation in reporter expression on non-corrected $\Delta F/F_0$ values.

Modelled representations of non-corrected fluorescence intensity values (F , A.U., left) and $\Delta F/F_0$ traces (right) for *A. thaliana* plants expressing the $[Ca^{2+}]$ reporter, GCaMP3, and responding to a wounding stimulus at 0 min. Comparisons were modelled for samples with (A) high (10 units GCaMP3/pixel) vs low expression (3 units GCaMP3/pixel), (B) high vs moderate expression (5 units GCaMP3/pixel) and (C) intermediate (7 units GCaMP3/pixel) vs intermediate expression. Modelling based on values obtained from experimental data with background intensities of (A) 1974.90 A.U. and (B, C) 2036.56 A.U., free GCaMP3 intensity of 83.00 A.U. increasing to 183.43 A.U. when bound to Ca^{2+} , and signals peaking at 5 min with 80% of the GCaMP3 bound to Ca^{2+} . Datapoints are plotted at 5 s intervals. Signals were modelled over 1653 pixels. F values were the mean intensities across the area including the intensities of the background and GCaMP3. F_0 values were the mean of the F values from -5 min to 0 min. Modelling performed in Python (Van Rossum and Drake Jr, 2009) with assistance from Sergio Lopez (Bioimaging Platform, John Innes Centre).

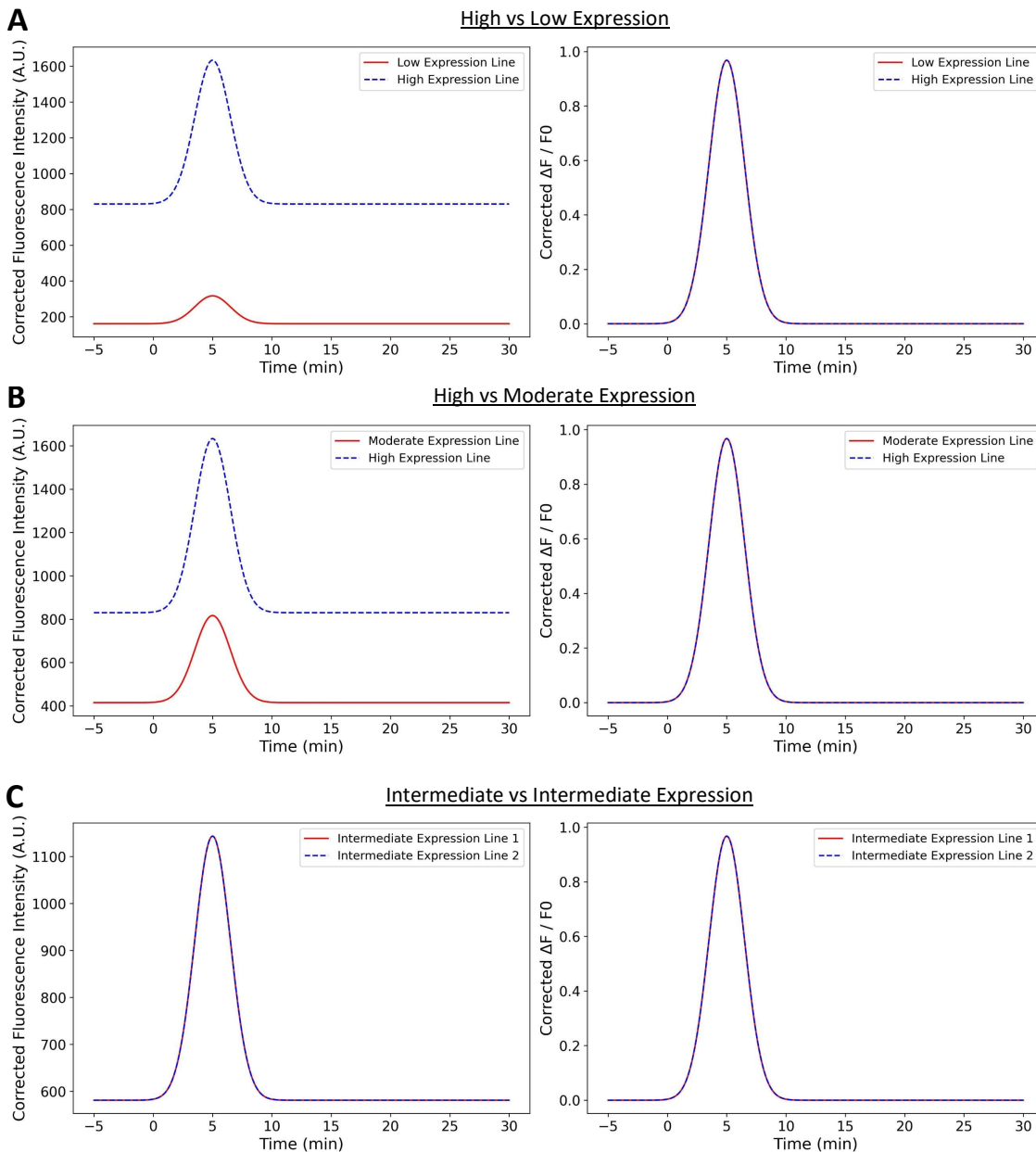


Figure 3.7 Modelling how background corrections can offset the effects of variation in reporter expression on $\Delta F/F_0$ traces.

Modelled representations of background-corrected fluorescence intensity values (F , A.U., left) and $\Delta F/F_0$ traces (right) for *A. thaliana* plants expressing the $[Ca^{2+}]$ reporter, GCaMP3, and responding to a wounding stimulus at 0 min. Comparisons were modelled for plants with (A) high (10 units GCaMP3/pixel) vs low expression (3 units GCaMP3/pixel), (B) high vs moderate expression (5 units GCaMP3/pixel) and (C) intermediate (7 units GCaMP3/pixel) vs intermediate expression. Modelling based on values obtained in experimental data with background intensities of (A) 1974.90 A.U. and (B, C) 2036.56 A.U., free GCaMP3 having an intensity of 83.00 A.U. increasing to 183.43 A.U. when Ca^{2+} bound, and signals peaking at 5 min with 80% of GCaMP3 bound to Ca^{2+} at the peak. Datapoints are plotted at 5 s intervals. Signals were modelled over 1653 pixels. F values were the mean GCaMP3 intensities across the area and F_0 values were the mean of the F values from -5 min to 0 min. Modelling was performed in Python (Van Rossum and Drake Jr, 2009) with assistance from Sergio Lopez (Bioimaging Platform, John Innes Centre).

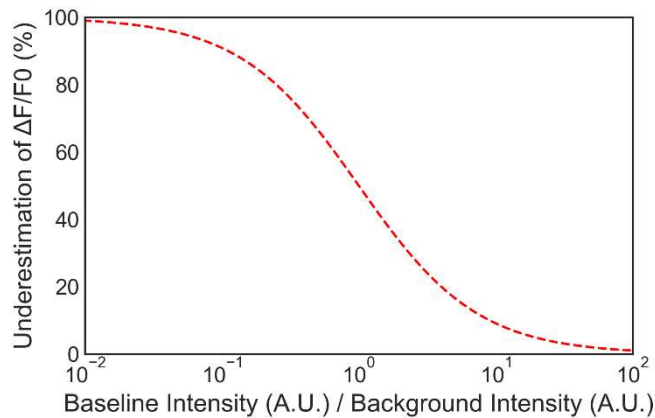


Figure 3.8 The effect of variation in reporter expression on the underestimation of $\Delta F/F_0$.

Modelling of the effect of reporter expression (baseline intensity, A.U.), indicated relative to background intensity (A.U.), on the underestimation of $\Delta F/F_0$ for a GCaMP3 expressing *A. thaliana* sample analysed without background correction. Baseline intensity represents the background-corrected F_0 of the sample (i.e. GCaMP3 fluorescence intensity) whilst background intensity represents the intensity of the sample in the absence of any reporter expression. Underestimation of $\Delta F/F_0$ is calculated as the percentage difference between the peak $\Delta F/F_0$ in background-corrected and non-corrected models. Background intensity was taken as 1974.90 A.U. with the baseline intensity ranging from 1 to 197490 A.U. GCaMP3 intensity (A.U.) increased by 2.21x at the signal peak. Modelling performed in Python (Van Rossum and Drake Jr, 2009) with assistance from Sergio Lopez (Bioimaging Platform, John Innes Centre).

Though background correction limited the effect of GCaMP3 expression differences on $\Delta F/F_0$ amplitude in responses to micropipette wounding, the low expression reporter line displayed greater variation in corrected $\Delta F/F_0$ than the high expression line (Figure 3.4). As background correction amplifies peak $\Delta F/F_0$, and as this effect is greater in lower expression lines (Figure 3.8), I hypothesised that this increased variation came in part from amplifying noise in $\Delta F/F_0$ more in low expression lines than in high expression lines. To test this, I added a fixed degree of noise to the high and low expression line models. The noise comprised values randomly sampled from a normal distribution with a standard deviation equal to the square root of the background intensity. As the noise came from a constant distribution that was the same for both lines, this noise represented non-biological noise. The signal-to-noise ratio (SNR) was then calculated as $SNR = A/(1.96 * SD)$ where A is the amplitude of the $\Delta F/F_0$ peak and SD is the standard deviation of the $\Delta F/F_0$ values over the last 35% of time points. This measure of signal peak relative to noise revealed that the low expression line had a lower SNR than the high expression line and that background correction did not change the SNR values (Figure 3.9). Therefore, these results provide evidence that background correction does not alter SNR properties but instead, amplifies variation in $\Delta F/F_0$ and does so more in lower expression lines contributing to greater variation in $\Delta F/F_0$ values.

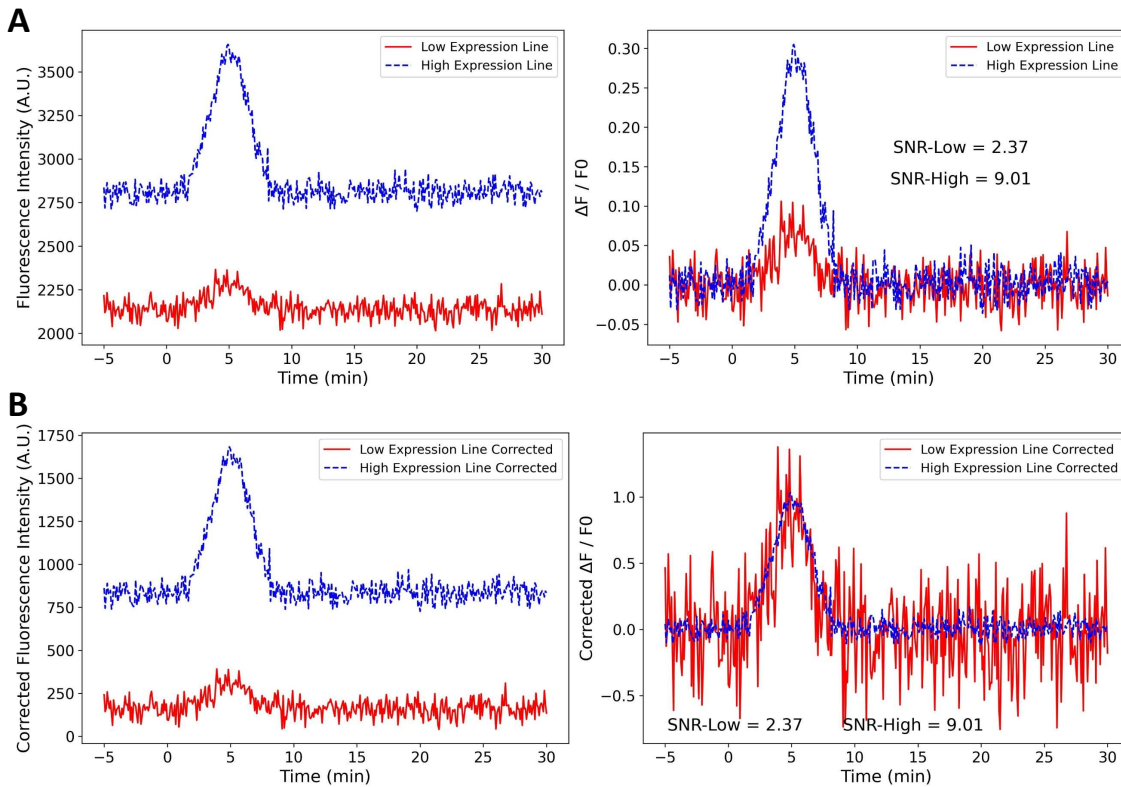


Figure 3.9 Background correction does not alter the signal-to-noise ratio but does amplify variation in $\Delta F/F_0$.

Modelled representations of (A) non-corrected and (B) background-corrected fluorescence intensity values (F , A.U., left) and $\Delta F/F_0$ traces (right) over time with noise for *A. thaliana* plants expressing the $[Ca^{2+}]$ reporter, GCaMP3, and responding to a typical wounding stimulus at 0 min. Modelling was of a low expression (3 units of GCaMP3/pixel) and a high expression line (10 units of GCaMP3/pixel). Values based on those obtained in previous experiments with intensities being 1974.90 A.U./pixel for the background, 83.00 A.U. for free GCaMP3 and 183.43 A.U. for Ca^{2+} -bound GCaMP3. Signals peaked at 5 min with 80% of the GCaMP3 bound to Ca^{2+} . Signals were modelled over 1653 pixels. Datapoints were plotted at 5 s intervals. Noise was added to the model at a fixed rate for both lines. This noise was randomly sampled from a normal distribution with a standard deviation equal to the square root of the background intensity. Signal/Noise (SNR) was calculated using $SNR = \frac{A}{1.96 \cdot SD}$ where A is the amplitude of the signal at its peak and SD is the standard deviation of the $\Delta F/F_0$ values in the last 35% of time points. Modelling performed in Python (Van Rossum and Drake Jr, 2009) with assistance from Sergio Lopez (Bioimaging Platform, John Innes Centre).

Ratiometric reporters are often established with reference proteins or wavelengths to help control for variation in reporter expression levels. Using ratiometric reporters could eliminate the need for background corrections. To test if this is the case, I modelled the effects of reporter expression differences with and without background corrections on signals reported from the ratiometric non-FRET reporter, apo-pHusion (Figure 3.10, Gjetting *et al.*, 2012). Apo-pHusion uses linked GFP and RFP, and the GFP/RFP intensity ratio, to report apoplasmic pH. The raw fluorescence intensity (F) of GFP and RFP, the GFP/RFP intensity ratio (R) and the normalised R ($\Delta R/R_0$) were modelled for time frames -60 to 360 A.U. $\Delta R/R_0$ was calculated as $(R-R_0)/R_0$ where R_0 represents the mean R for frames -60 to 0. A signal elevation was introduced to occur just after frame 0 and peak at frame 90 in which GFP, the pH reporter FP, increased in brightness by 4 x to its maximum whilst the reference FP, RFP, maintained a constant brightness. The model included a 'low expression' line (baseline intensity: GFP = 40 A.U., RFP = 60 A.U.) and a 2.5x greater expression 'high expression' line (baseline intensity: GFP = 100 A.U., RFP = 150 A.U.). Background intensities were kept constant at 100 A.U. for both GFP and RFP. Results demonstrated that, in the absence of a background correction, peak R and $\Delta R/R_0$ were lower in the low expression line than in the high expression (Figure 3.10A, C, E). Upon background correction, the high and low expression lines were equal in their R and $\Delta R/R_0$ traces (Figure 3.10B, D, F). Therefore, background corrections are necessary to limit the risk of differences in reporter expression impacting comparisons of reporter signals with ratiometric non-FRET reporters as well as intensimetric reporters.

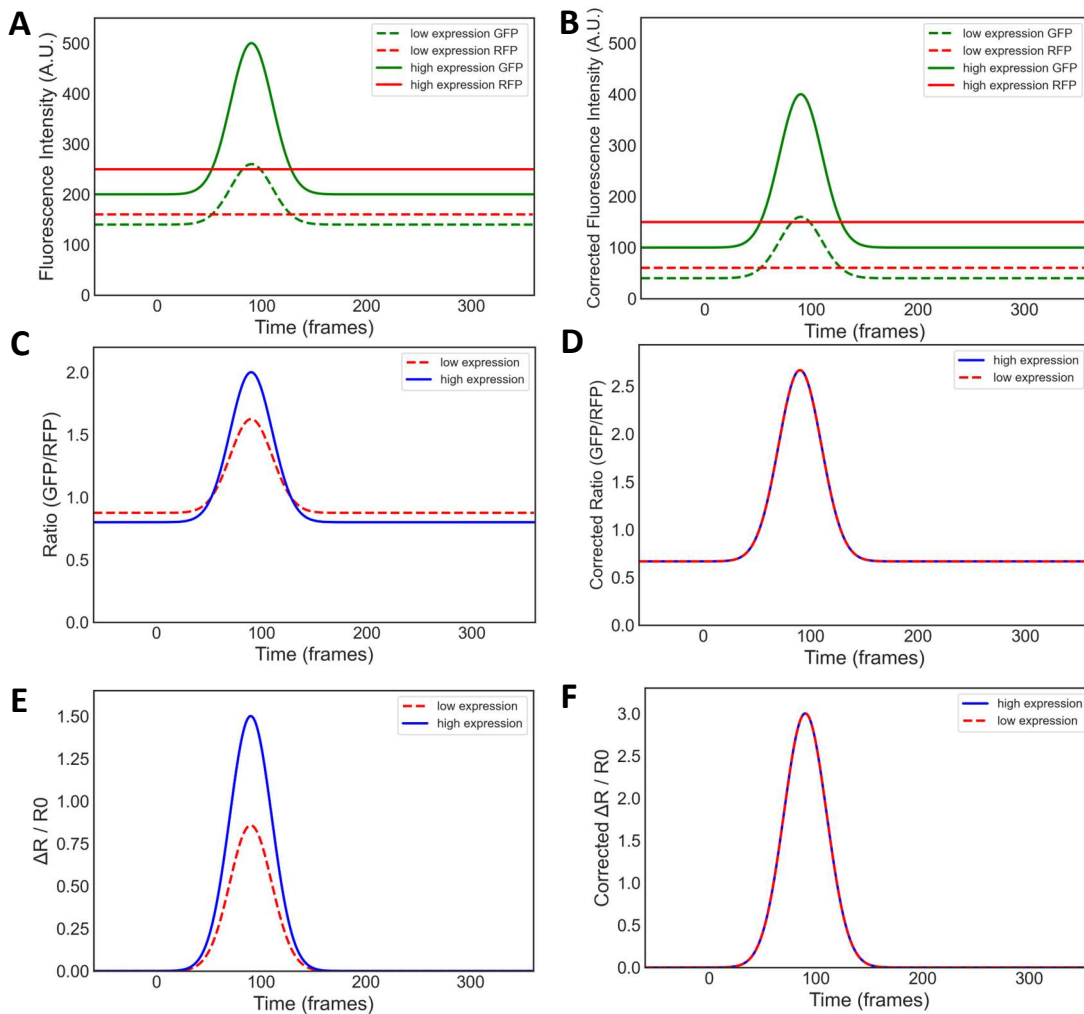


Figure 3.10 Modelling the effects of variation in reporter expression on signals detected from the ratiometric apo-pHusion reporter.

Modelled representation of *A. thaliana* samples expressing the apo-pHusion pH reporter. Apo-pHusion contains a GFP and RFP which display pH-dependent and pH-independent fluorescence, respectively. Reporter signals were modelled over time (frames, A.U.) from -60 to 360 frames with a signal peak at frame 90 which represented a pH elevation. Traces are for the (A, B) raw fluorescence intensity values (F, A.U.), (C, D) the GFP/RFP intensity ratio (R) values and (E, F) the $\Delta R/R_0$ values. R_0 values were the mean of the R values from -60 to 0. The model was comprised of two lines: a low expression line (RFP intensity = 60 A.U., GFP baseline intensity = 40 A.U., GFP peak intensity = 160 A.U.) and a high expression line (RFP intensity = 150 A.U., GFP baseline intensity = 100 A.U., GFP peak intensity = 400 A.U.). Modelling was for non-corrected (left) and background-corrected (right) values in which the non-corrected F values for GFP and RFP had a constant background value of 100 A.U. added. Modelling was performed in Python (Van Rossum and Drake Jr, 2009) with assistance from Sergio Lopez (Bioimaging Platform, John Innes Centre).

3.2.4. *M. persicae* feeding-induced $[Ca^{2+}]$ elevations are not altered in *tpc1-2 A. thaliana*

Previously, *M. persicae* feeding-induced $[Ca^{2+}]$ elevations were found to be impaired in *tpc1-2* mutants (Vincent *et al.*, 2017a). I reassessed the contribution of TPC1 to these elevations with updated methods from those used previously (Vincent *et al.*, 2017b). These methods included checks for equal reporter expression, background corrections to offset any effects from variation in reporter expression and higher resolution imaging with the Axio Zoom.V16. With the higher resolution imaging, stricter criteria could be applied of only retaining samples if the aphid feeding site was visible. An additional change from the methods previously used was to utilise ROIs fitted to the reporter signal areas instead of fixed circular ROIs. This meant that intensity values only represented regions displaying reporter signals and that these values were less heavily affected by variation in signal shape or size or the region in which the signal occurred. The Col-0 and *tpc1-2 UBQ10::GCaMP3* lines were used for this investigation as they appeared to display equal expression levels with no statistically significant differences detected in the corrected F0 values at feeding sites (Figure 3.11A, t-test, $t = -0.65$, $df = 56.89$, $p = 0.52$). Assessing *M. persicae* feeding-induced GCaMP3 signals by corrected normalised $\Delta F/F0$ traces revealed reporter signals in both the Col-0 and *tpc1-2* lines with no clear differences in reporter signal dynamics between the genotypes (Figure 3.11B). These reporter signals were localised around the feeding sites. Furthermore, there were no statistically significant differences between the genotypes in the peak normalised $\Delta F/F0$ values (Figure 3.11C, Wilcoxon rank-sum test, $W = 418$, $p = 0.64$), the reporter signal areas (Figure 3.11D, Wilcoxon rank-sum, $W = 542$, $p = 0.18$), or the signal propagation rates (Figure 3.11E, Wilcoxon rank-sum, $W = 395$, $p = 0.42$). These data indicate that *M. persicae* feeding-induced $[Ca^{2+}]$ elevations in *A. thaliana* leaves are not dependent on TPC1.

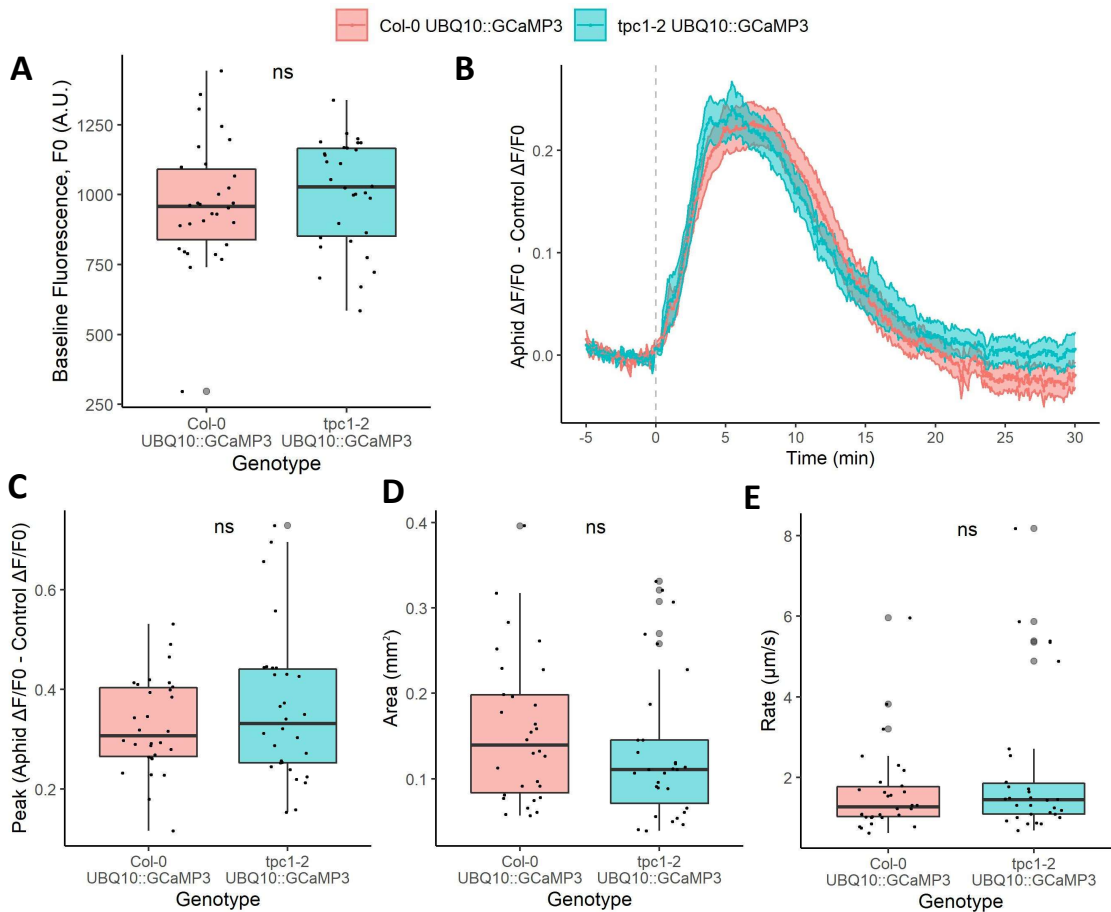


Figure 3.11 Properties of *M. persicae* feeding-induced GCaMP3 signals in Col-0 and *tpc1-2* *A. thaliana*.

Properties of *M. persicae* feeding-induced reporter signals in Col-0 and *tpc1-2* *UBQ10::GCaMP3* *A. thaliana* ($n = 30$). Elevations were recorded by imaging *A. thaliana* leaves subjected to *M. persicae* or no aphid control treatments. Background-corrected fluorescence intensity (F , A.U.) values were recorded over the area of the feeding-induced responses and at comparable control sites and transformed into $\Delta F/F_0$ values with F_0 being the mean F over the 5 min prior to feeding. (B) Traces for the mean \pm S.E.M. normalised $\Delta F/F_0$ values (Aphid $\Delta F/F_0$ - Control $\Delta F/F_0$) over time with feeding beginning at 0 min (grey dashed line). Boxplots are displayed for the (A) feeding site F_0 values (A.U.), (C) peak normalised $\Delta F/F_0$ values (Aphid $\Delta F/F_0$ - Control $\Delta F/F_0$), (D) signal areas (mm^2) and (E) signal propagation rates ($\mu\text{m s}^{-1}$), with grey dots associated with outliers. Statistical significance, tested using (A) a t-test or (C, D, E) a Wilcoxon rank-sum test, shown by ns: $p > 0.05$.

3.2.5. *M. persicae* feeding-induced $[Ca^{2+}]$ elevations are not altered in *bak1-5* mutant *A. thaliana*

As with TPC1, BAK1 was previously implicated in *M. persicae* feeding-induced $[Ca^{2+}]$ elevations (Vincent *et al.*, 2017a). With the improved methods, I reassessed this contribution. For this, Col-0 *UBQ10::GCaMP3 A. thaliana* was crossed with the *bak1-5* mutant to produce a homozygous *bak1-5 UBQ10::GCaMP3 A. thaliana* line. I then investigated *M. persicae* feeding-induced GCaMP3 signals in these lines. The feeding site F0 values were not statistically different between the Col-0 and *bak1-5* lines indicating that they had comparable GCaMP3 expression levels (Figure 3.12A, t-test, $t = -1.277$, $df = 57.011$, $p = 0.21$). *M. persicae* feeding induced GCaMP3 reporter signals in both Col-0 and *bak1-5* with no clear differences in the normalised $\Delta F/F_0$ traces between the genotypes (Figure 3.12B). Furthermore, there were no statistically significant differences between Col-0 and *bak1-5* samples in peak normalised $\Delta F/F_0$ values (Figure 3.12C, Wilcoxon rank-sum, $W = 434$, $p = 0.82$), signal areas (Figure 3.12D, Wilcoxon rank-sum, $W = 416$, $p = 0.62$) or signal propagation rates (Figure 3.12E, Wilcoxon rank-sum, $W = 437$, $p = 0.85$). Therefore, these data indicate that *M. persicae* feeding-induced $[Ca^{2+}]$ elevations in *A. thaliana* leaves are not altered in *bak1-5* mutants.

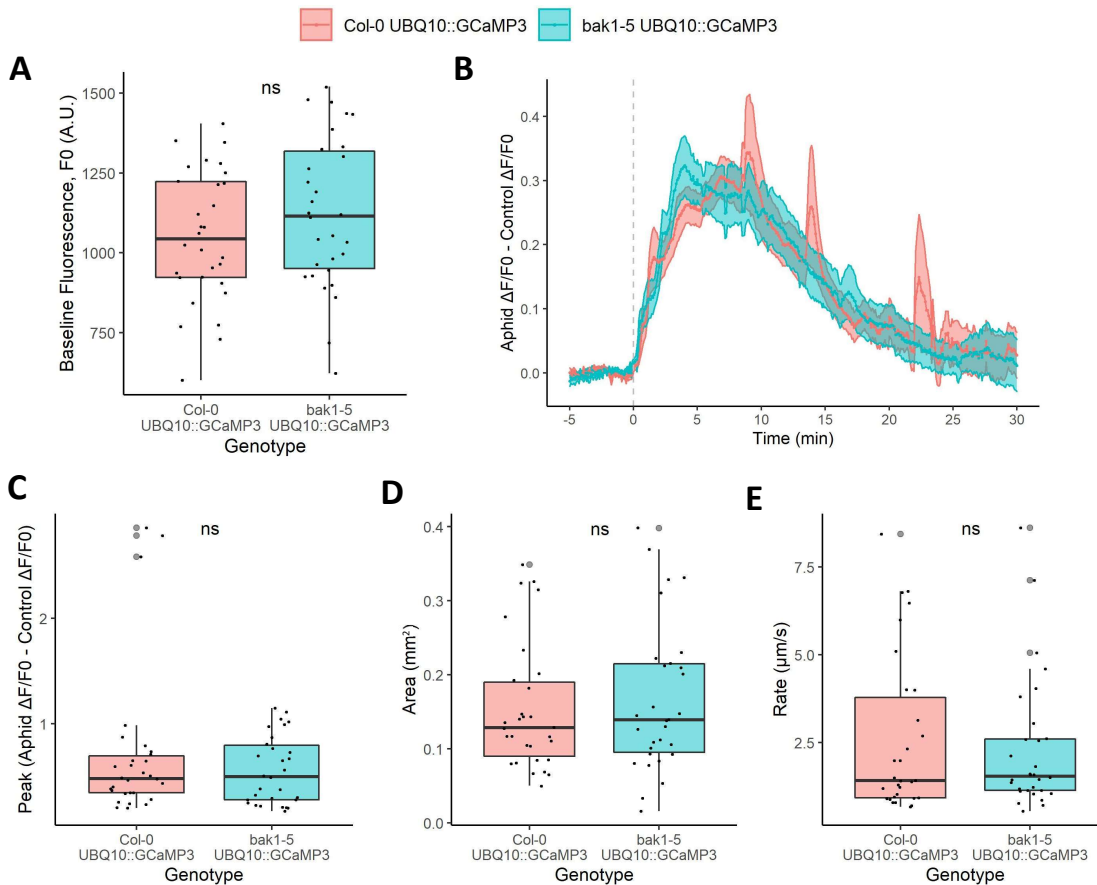


Figure 3.12 Properties of *M. persicae* feeding-induced GCaMP3 signals in Col-0 and *bak1-5 A. thaliana*.

Properties of *M. persicae* feeding-induced reporter signals in Col-0 and *bak1-5 UBQ10::GCaMP3 A. thaliana* ($n = 30$). Elevations were recorded by imaging *A. thaliana* leaves subjected to *M. persicae* or no aphid control treatments. Background-corrected fluorescence intensity (F , A.U.) values were recorded over the area of the feeding-induced responses and at comparable control sites and transformed into $\Delta F/F_0$ values with F_0 being the mean F over the 5 min prior to feeding. (B) Traces for the mean \pm S.E.M. normalised $\Delta F/F_0$ values (Aphid $\Delta F/F_0$ - Control $\Delta F/F_0$) over time with feeding beginning at 0 min (grey dashed line). Boxplots are displayed for the (A) feeding site F_0 values (A.U.), (C) peak normalised $\Delta F/F_0$ values (Aphid $\Delta F/F_0$ - Control $\Delta F/F_0$), (D) signal areas (mm²) and (E) signal propagation rates ($\mu\text{m s}^{-1}$), with grey dots associated with outliers. Statistical significance, tested using (A) a t-test or (C, D, E) a Wilcoxon rank-sum test, shown by ns: $p > 0.05$.

3.2.6. *M. persicae* feeding-induced $[Ca^{2+}]$ elevations are partially dependent on GLR3.3/GLR3.6

In previous work, *glr3.3 glr3.6* double mutants lacked detectable *M. persicae* feeding-induced $[Ca^{2+}]$ elevations (Vincent *et al.*, 2017a). I reassessed this phenotype using the improved methods and the Col-0 and *glr3.3a glr3.6a UBQ10::GCaMP3 A. thaliana* lines from Nguyen *et al.* (2018). These investigations were performed using an Axio Zoom.V16 microscope with a metal halide HXP 120 V light source but did not include imaging of suitable background control samples before the light source was replaced at the BioImaging Platform (John Innes Centre, Norwich). As a result, background corrections were absent here. Nonetheless, these lines were deemed sufficiently comparable as the feeding site F0 values were not statistically different (Figure 3.13A, t-test, $t = 47.90$, $p = 0.47$). The normalised $\Delta F/F_0$ traces were superficially similar between the genotypes with clear reporter signals in both (Figure 3.13B). However, the mutant trace was smoother than the wildtype trace. Moreover, the Col-0 samples gave statistically larger peak normalised $\Delta F/F_0$ values than the *glr3.3a glr3.6a* samples (Figure 3.13C, Wilcoxon rank-sum, $W = 435$, $p = 0.017$). There were 11 Col-0 samples with peak normalised $\Delta F/F_0$ values greater than the maximum value of 0.30 A.U. detected for the *glr3.3a glr3.6a* samples. The peak normalised $\Delta F/F_0$ values of the other 14 Col-0 samples were comparable to those of the *glr3.3a glr3.6a* samples (Figure 3.13C). There were no significant differences in signal areas between Col-0 and *glr3.3a glr3.6a* samples with mean values of $0.169 \pm 0.013 \text{ mm}^2$ and $0.181 \pm 0.019 \text{ mm}^2$, respectively (Figure 3.13D, Wilcoxon rank-sum, $W = 318$, $p = 0.92$). There were also no statistically significant differences in the reporter signal propagation rates between Col-0 and *glr3.3a glr3.6a* samples with mean values of $2.01 \pm 0.29 \mu\text{m s}^{-1}$ and $1.20 \pm 0.09 \mu\text{m s}^{-1}$, respectively (Figure 3.13E, Wilcoxon rank-sum, $W = 389$, $p = 0.14$). However, 6 out of the 25 Col-0 reporter signals had propagation rates greater than the maximum rate of $2.24 \mu\text{m s}^{-1}$ detected for the *glr3.3a glr3.6a* samples (Figure 3.13E). These 6 were in the group of 11 Col-0 samples with peak normalised $\Delta F/F_0$ values beyond the maximum value detected for *glr3.3a glr3.6a* samples. The signal propagation rates for the other 19 Col-0 samples were comparable to those for the *glr3.3a glr3.6a* samples. Taken together, these data suggest that *glr3.3a glr3.6a* mutants are impaired in *M. persicae* feeding-induced GCaMP3 signals that give relatively high peak intensities and/or propagation rates. As such, *M. persicae* feeding-induced $[Ca^{2+}]$ elevations are partially dependent on GLR3.3/3.6 (GLR3.3 and/or GLR3.6).

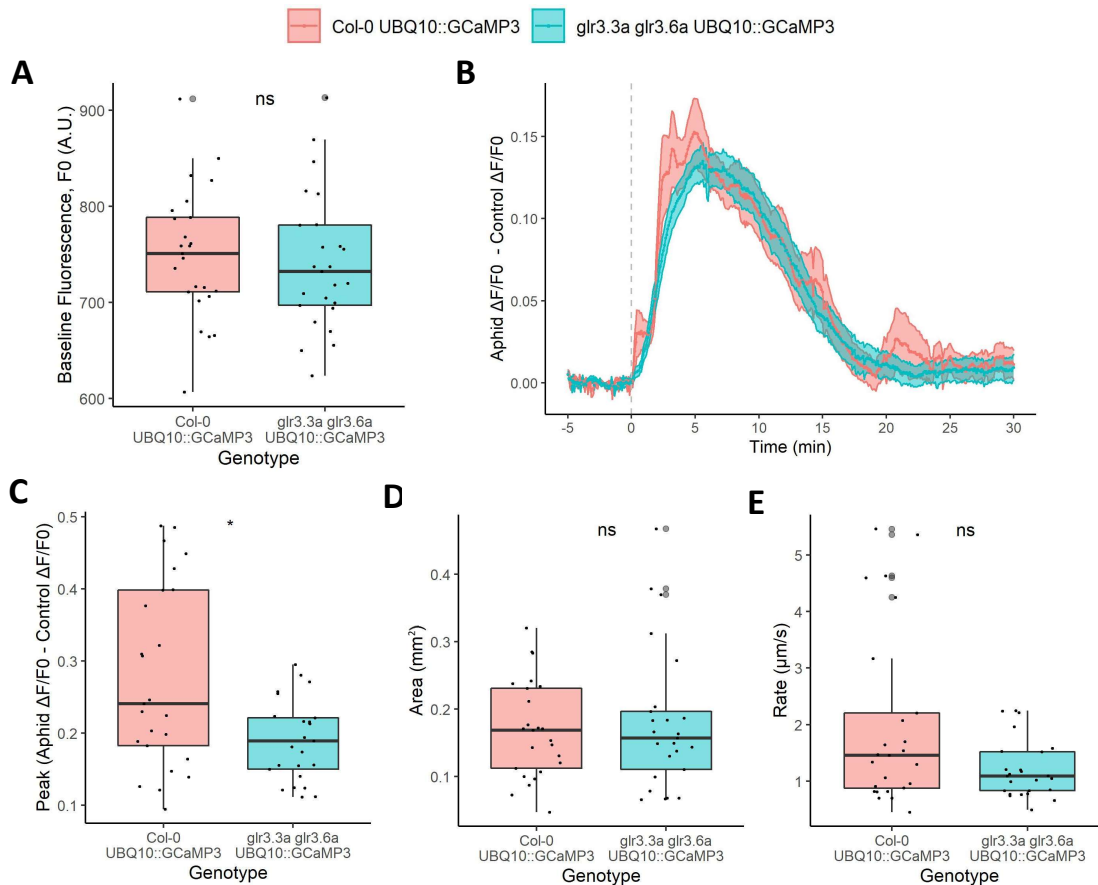


Figure 3.13 Properties of *M. persicae* feeding-induced GCaMP3 signals in Col-0 and *glr3.3a glr3.6a A. thaliana*.

Properties of *M. persicae* feeding-induced reporter signals in Col-0 and *glr3.3a glr3.6a UBQ10::GCaMP3 A. thaliana* ($n = 25$). Elevations were recorded by imaging (Axio Zoom.V16, HXP 120 V light source, 50 % excitation intensity) *A. thaliana* leaves subjected to *M. persicae* or no aphid control treatments. Non-corrected fluorescence intensity (F , A.U.) values were recorded over the area of the feeding-induced responses and at comparable control sites and transformed into $\Delta F/F_0$ values with F_0 being the mean F over the 5 min prior to feeding. **(B)** Traces for the mean \pm S.E.M. normalised $\Delta F/F_0$ values (Aphid $\Delta F/F_0$ - Control $\Delta F/F_0$) over time with feeding beginning at 0 min (grey dashed line). Boxplots are displayed for the **(A)** feeding site F_0 values (A.U.), **(C)** peak normalised $\Delta F/F_0$ values (Aphid $\Delta F/F_0$ - Control $\Delta F/F_0$), **(D)** signal areas (mm^2) and **(E)** signal propagation rates ($\mu\text{m s}^{-1}$), with grey dots associated with outliers. Statistical significance, tested using **(A)** a t-test or **(C, D, E)** a Wilcoxon rank-sum test, shown by ns: $p > 0.05$, *: $p \leq 0.05$.

3.3. Discussion

In this chapter, I re-evaluated the methods and key results from previous investigations into *M. persicae* feeding-induced $[Ca^{2+}]$ elevations by Vincent *et al.* (2017a) to ensure these could provide a foundation for further investigations into aphid and thrips perception in *A. thaliana*. Consistent with the results of Vincent *et al.* (2017a), *M. persicae* feeding induced $[Ca^{2+}]$ elevations localised to the feeding sites and these had similar areas and propagation rates to those previously reported (Then *et al.*, 2021; Vincent *et al.*, 2017a). However, I found that some of the mutant phenotypes reported in Vincent *et al.* (2017a) were likely caused by GCaMP3 expression differences between the compared lines. Empirical and modelling approaches highlighted how differences in reporter expression can give rise to artefactual differences in normalised intensimetric reporter signals if background corrections are absent. Moreover, a similar effect was demonstrated for the non-FRET ratiometric reporter, apo-pHusion, and is also expected for FRET-based ratiometric reporters (preliminary data, not shown). Methods for imaging all intensimetric and ratiometric genetically encoded fluorescent reporters were therefore developed to include checks for equal reporter expression between compared material and background corrections where appropriate and possible. Moreover, the improved methods avoid lines with low reporter expression and utilise higher resolution imaging equipment, fitted ROIs for analyses, and stricter criteria for retaining samples only if stimulus treated sites are visible. Aided by these improved methods, I identified that TPC1 and BAK1 do not contribute to *M. persicae* feeding-induced $[Ca^{2+}]$ elevations in contrast to previous findings (Vincent *et al.*, 2017a). Interestingly however, *glr3.3a glr3.6a* mutants displayed *M. persicae* feeding-induced GCaMP3 signals but did not produce the relatively high intensity or fast propagating signals that were found in the wildtype. As the *glr3.3a glr3.6a* mutant signals were superficially similar to a subset of the Col-0 signals, it appears that a subset of *M. persicae* feeding-induced $[Ca^{2+}]$ elevations are GLR3.3/3.6-dependent. These methods and results form a foundation for further investigations into *A. thaliana* responses to aphid and thrips feeding.

3.3.1. Causes and lessons: What has been learnt from investigating the effects of variation in fluorescent reporter expression on normalised reporter signals?

Through the present investigations, the methods for assessing stimulus-induced genetically encoded fluorescent reporter signals have been developed to limit variation in reporter expression and any effects of this variation on results. The lessons that have been learnt are valuable for any investigations utilising such reporters and are outlined below.

Silencing of reporter transgenes appeared to be the major cause of variation in reporter expression in Vincent *et al.* (2017a) and is a frequent challenge with transgenic reporter lines (Loro *et al.*, 2016; Behera *et al.*, 2015; Grenzi *et al.*, 2021). The nature of the reduced expression regions was characteristic of silencing with low expression regions being heterogeneous within seedlings, expanding through development and becoming more widespread in later generations (Napoli *et al.*, 1990; Amack and Antunes, 2020; Elmayan and Vaucheret, 1996). To limit the risk of reporter transgene silencing, it would be beneficial to avoid high expression levels with the 35S viral promoter and aim for more moderate reporter expression levels with, for example, the *A. thaliana* *UBQ10* promoter (DeBlasio *et al.*, 2010; Amack and Antunes, 2020; Schubert *et al.*, 2004; Elmayan and Vaucheret, 1996; Behera *et al.*, 2015). Additionally, avoiding multiple copies of a transgene or transgene sequences with high homology to the genomic background can help limit silencing (DeBlasio *et al.*, 2010). This was likely problematic for the mutant 35S::*GCaMP3* lines because there were two copies of the reporter transgene and because both the 35S::*GCaMP3* and SALK T-DNA mutant transgenes contain the 35S promoter and a kanamycin resistance gene (Daxinger *et al.*, 2008; Ülker *et al.*, 2008; Vincent *et al.*, 2017a; Alonso *et al.*, 2003). In conclusion, silencing seemed to cause the differences in reporter expression between lines in Vincent *et al.* (2017a). Such silencing could be limited by utilising single copy reporter lines and reporter transgenes that have a low homology to the genomic background as well as a moderate expression constitutive promoter such as the *UBQ10* promoter.

As differences in reporter expression may be subtle, unexpected or go unnoticed, it is important to assess the variation in reporter expression within experiments and consider its impacts. Many authors make attempts to do just this. For example, Matsumura *et al.* (2022) assessed *GCaMP3* protein levels via Western blots and concluded comparable reporter expression between *A. thaliana* lines. Meena *et al.* (2019) treated *GCaMP3* lines with ethanol and CaCl_2 to trigger maximal reporter signals and showed that they were similar between their lines suggesting comparable *GCaMP3* expression. A similar approach was used in Vincent (2016). These approaches are useful but can be difficult or costly to apply and challenging to standardise or reproduce. Additionally, they can overlook the impacts of other variables on reporter fluorescence such as pH. As such, a standardised, simple, and efficient way of assessing for equal reporter expression would be beneficial. This could be achieved by assessing and reporting the background-corrected baseline fluorescence (F_0) values as a proxy for expression. Whilst these values could be influenced by pH effects or other variables, this approach does not require any further experimentation and can highlight the need for further investigation or to exercise additional caution. Using this approach with the two FPs of ratiometric reporters can provide an even better indication of expression levels and the impacts of other variables such as pH. Therefore, assessing and reporting background-corrected baseline fluorescence is a useful

addition to methods for using genetically encoded intensimetric and ratiometric fluorescent reporters.

Even with the best effort, unavoidable differences in intensimetric or ratiometric reporter expression will exist within and between *A. thaliana* lines due to natural variation, biological effects, or time constraints. To limit the impact of this variation on results, analyses should include a suitable background correction which leaves only the reporter fluorescence to be analysed. In this context, this may be achieved by subtracting from all intensity values the intensity of an equivalent region in a non-transgenic sample. In some cases, such a background correction is described and applied (Gjetting *et al.*, 2012; Palmer and Tsien, 2006; Mou *et al.*, 2020). However, in many cases, it unclear whether appropriate background corrections have been performed as they are absent from methods descriptions (Matsumura *et al.*, 2022; Toyota *et al.*, 2018; Meena *et al.*, 2019; Luo *et al.*, 2020; Krogman *et al.*, 2020; DeFalco *et al.*, 2017; Matthus *et al.*, 2020; Xue *et al.*, 2022; Uemura *et al.*, 2021; Hagihara *et al.*, 2022) or not fully described (Kelner *et al.*, 2018; Leitão *et al.*, 2019; Waadt *et al.*, 2017; Matthus *et al.*, 2022). Background correction values used sometimes originate from regions in images outside of a reporter expressing sample (Bootman *et al.*, 2013; Himschoot *et al.*, 2018; Yoshinari *et al.*, 2021). These background values can misrepresent the true background intensity of a sample and thereby maintain a risk of expression artefacts in results. It seems much more common in studies of animal calcium signalling with GECIs to see great care paid to appropriate background corrections (Yasuda *et al.*, 2004; Shkryl, 2020; Zhang *et al.*, 2021c; Joucla *et al.*, 2013). Whilst it is unclear whether expression differences have influenced results beyond those in Vincent *et al.* (2017a), it appears beneficial to utilise a suitable background correction for analyses with intensimetric and ratiometric reporters and detail the correction in methods descriptions.

Whilst a background correction reduces the risk of expression artefacts when comparing normalised reporter signals, it does not overcome all the challenges caused by the presence of expression differences in comparisons or reduced expression levels. For example, background corrections were problematic with the low expression *tpc1-2 35S::GCaMP3* line here as small errors in the background correction value for each sample led to significant variation in $\Delta F/F_0$ values. Moreover, lower reporter expression generally results in lower SNR values for normalised reporter signals (Rose *et al.*, 2014) and signals which are less clear for analyses compared to those in a higher expression line imaged under equal conditions. As reporter expression can influence endogenous signalling and plant development through binding signalling species or disrupting molecular processes, variation in reporter expression can also make plant responses less comparable (Yang *et al.*, 2018; Rose *et al.*, 2014; Waadt *et al.*, 2017; Castro-Rodríguez *et al.*, 2022). As such, comparing results from lines with different expression

levels is of limited value even with background corrections and the limitations should be considered.

In conclusion, I identified that silencing likely caused the expression differences in Vincent *et al.* (2017a) which influenced some of the results reported. Steps can be taken to reduce silencing in *A. thaliana* reporter lines. Background corrections limit the risk of expression differences affecting results but comparing lines with significantly different or low expression levels is of limited value. Investigations here will report baseline fluorescence for comparisons between reporter expressing lines as a measure of expression levels and implement background corrections where possible. These steps will allow various genetically encoded fluorescent reporters to be robustly visualised to investigate plant responses to localised stimuli including aphid and thrips feeding.

3.3.2. Reassessing the role of BAK1, TPC1 and GLR3.3/3.6 in aphid-plant interactions

Having reassessed key results of Vincent *et al.* (2017a) with updated methods, I confirmed the presence of *M. persicae* feeding-induced $[Ca^{2+}]$ elevations restricted to the feeding site. However, in contrast to Vincent *et al.* (2017a), data here indicated that TPC1 and BAK1 do not contribute to these $[Ca^{2+}]$ elevations and that *glr3.3 glr3.6* mutants do display some *M. persicae* feeding-induced $[Ca^{2+}]$ elevations. Instead, the *glr3.3a glr3.6a UBQ10::GCaMP3 A. thaliana* mutants were impaired in GCaMP3 signals with relatively high intensities and/or fast propagation rates, revealing a novel role for GLR3.3/3.6 in *M. persicae* feeding-induced $[Ca^{2+}]$ elevations. With this, the role of TPC1, BAK1 and GLR3.3/3.6 in aphid-plant interactions shall be reconsidered here to form the foundations for further investigations into aphid and thrips perception in *A. thaliana*.

The contribution of TPC1 to aphid-induced defence responses has multiple lines of support. Beyond identifying reduced *M. persicae* feeding-induced $[Ca^{2+}]$ elevations in *tpc1-2*, Vincent *et al.* (2017a) revealed that the gain-of-function TPC1^{D454N} mutant, *fou2*, responds to *M. persicae* feeding with further propagating $[Ca^{2+}]$ elevations. This mutant has reduced TPC1 inhibition by elevated vacuolar $[Ca^{2+}]$ (Beyhl *et al.*, 2009; Bonaventure *et al.*, 2007b; Guo *et al.*, 2016). *fou2* mutants also display enhanced resistance against the aphids *B. brassicae* (Kusnierczyk *et al.*, 2011) and *A. pisum* (Vincent, 2016) along with enhanced JA-dependent resistance against *M. persicae* (Vincent *et al.*, 2017a). As such, TPC1 seemed likely to contribute to the perception of aphid feeding and aphid-induced defence responses. However, the enhanced aphid resistance of *fou2* mutants may derive entirely from the mutant's elevated basal JA signalling activity (Bonaventure *et al.*, 2007a) without the need for aphid perception or induced defence responses. Moreover, the further propagating *M. persicae* feeding-induced

[Ca²⁺] elevations in *fou2* (Vincent *et al.*, 2017a) may result from enhanced TPC1 activity without TPC1 functioning in endogenous aphid-plant interactions. With no role for TPC1 in responses to localised wounding here or in Bellandi *et al.* (2022), it may be that TPC1 function in leaves is restricted to mediating systemic Ca²⁺ signal propagations induced by large-scale wound events (Kiep *et al.*, 2015; Fichman *et al.*, 2020). Finally, *M. persicae* colonisation is not altered on *tpc1-2* mutants (Vincent *et al.*, 2017a). As a result, whilst *fou2* mutants display phenotypes in aphid-plant interactions, TPC1 does not clearly contribute to the endogenous plant perception of aphid feeding or subsequent signalling events.

Though data here indicates that BAK1 does not contribute to *M. persicae* feeding-induced [Ca²⁺] elevations, evidence suggests that BAK1 does function in aphid-plant interactions. This contribution focusses around the perception of aphid-derived HAMPs. Putative aphid HAMPs or HAMP-containing aphid extracts induce PTI-associated ROS signalling, gene expression, MAPK activation and aphid resistance, which are all impaired in *bak1-5* mutants (Prince *et al.*, 2014; Canham, 2022; Vincent, 2016; Chaudhary *et al.*, 2014). BAK1-dependent responses are also thought to be targeted by the Mp10 *M. persicae* effector as Mp10 promotes *M. persicae* colonisation in a BAK1-dependent manner (Bos *et al.*, 2010; Drurey *et al.*, 2019). Mp10 suppression of BAK1-dependent responses may explain why *M. persicae* fecundity is unaltered on *bak1-5* mutants (Prince *et al.*, 2014). In contrast, *bak1-5* mutants have impaired resistance against *A. pisum* which cannot colonise *A. thaliana* (Prince *et al.*, 2014). Therefore, BAK1 likely contributes to putative aphid HAMP perception and aphid resistance as well as a response mechanism targeted by an aphid effector. Effector suppression of BAK1-dependent responses may explain why *M. persicae* feeding-induced [Ca²⁺] elevations were not BAK1-dependent here. As Mp10 is delivered into cells probed by aphid stylets during feeding (Mugford *et al.*, 2016), it is possible that Mp10 or other effectors could act within minutes to suppress any BAK1-dependent aphid feeding-induced [Ca²⁺] elevations. Alternatively, it may be that BAK1-dependent aphid HAMP perception does not contribute to the induction of [Ca²⁺] elevations with *M. persicae* feeding. Further investigations into aphid effector activity and HAMP perception during aphid feeding could help test whether BAK1 functions in the initial perception of aphid feeding.

GLR3.3/3.6 contributed to *M. persicae* feeding-induced GCaMP3 signals with fast propagation rates and/or high peak intensities revealing a novel role for these channels in aphid feeding-induced [Ca²⁺] elevations. Whilst heavy *M. persicae* infestation may trigger systemic GLR3.3/3.6-dependent [Ca²⁺] signalling and defence responses (Xue *et al.*, 2022), individual *M. persicae* feeding events trigger [Ca²⁺] elevations that remain highly localised to the feeding site in epidermal and mesophyll cells (Vincent *et al.*, 2017a; Wang *et al.*, 2022b; Then *et al.*, 2021).

Therefore, a role for GLR3.3/3.6 here is in stark contrast to the GLR3.3/3.6-dependent rapid systemic signalling responses that propagate via the vascular tissue following large-scale wounding (Mousavi *et al.*, 2013; Toyota *et al.*, 2018; Nguyen *et al.*, 2018; Shao *et al.*, 2020; Salvador-Recatalà, 2016; Wu *et al.*; Moe-Lange *et al.*, 2021; Xue *et al.*, 2022). Furthermore, the majority of reports for GLR3.3/3.6 expression have identified their expression as predominantly in vascular bundles with only limited GLR3.3 expression elsewhere in trichome base cells, guard cells and leaf mesophyll cells (Moe-Lange *et al.*, 2021; Nguyen *et al.*, 2018; Toyota *et al.*, 2018; Wu *et al.*, 2022; Tenorio Berrío *et al.*, 2022). Recently GLR3.3 has been implicated in localised wound-induced $[Ca^{2+}]$ elevations in the epidermal and mesophyll cells of cotyledons (Bellandi *et al.*, 2022). As such, it may be that *M. persicae* feeding-induced $[Ca^{2+}]$ elevations in true leaves are also triggered by localised damage perception. As aphids do only limited damage with feeding and use gelling saliva that protects cells that stylets probe or pass by (Hewer *et al.*, 2011; Silva-Sanzana *et al.*, 2020; Nalam *et al.*, 2019), this could explain why *M. persicae* feeding-induced $[Ca^{2+}]$ elevations were only partially dependent on GLR3.3/3.6. Alternatively, mechanical stress perception could contribute to aphid feeding-induced GLR3.3/3.6-dependent responses because trichome touch induces hyponasty that is partially dependent on GLR3.3/3.6 (Pantazopoulou *et al.*, 2022). At present, there have been few investigations into GLR3.3/3.6 activity in responses to localised stimuli. As such, it is unclear how these channels could function in *M. persicae* feeding-induced $[Ca^{2+}]$ elevations. Nonetheless, *M. persicae* feeding-induced $[Ca^{2+}]$ elevations appear partially dependent on GLR3.3/3.6.

In summary, using improved reporter imaging methods, I have identified that BAK1 and TPC1 do not clearly contribute to *M. persicae* feeding-induced $[Ca^{2+}]$ elevations. Moreover, I have revealed that these elevations are partially dependent on GLR3.3/3.6. The GLR3.3/3.6-dependent $[Ca^{2+}]$ elevations could be triggered by damage or mechanical stress perception during aphid feeding. However, the roles of GLR3.3 and 3.6 in leaf epidermal and mesophyll cells in responses to localised stimuli are largely uncharacterised. Therefore, further investigations will aim to better characterise the contributions of GLR3.3 and 3.6 to the perception of localised damage and mechanical stress. Any findings will help appreciate how these channels could contribute to the perception of localised feeding from aphids and thrips and provide a platform for further investigations.

4. Exploring the Mechanisms of Localised Wound and Touch
Perception and the Contributions of GLR3.3/3.6

4.1. Introduction

The results in Chapter 3 show that *glr3.3a glr3.6a* mutants are impaired in *M. persicae* feeding-induced $[Ca^{2+}]$ elevations that give GCaMP3 signals with relatively high peak intensities and/or propagation rates. This contribution of GLR3.3/3.6 to *M. persicae* feeding-induced responses may derive from the plant perception of damage or mechanical stress during aphid feeding. In this chapter, I will explore GLR3.3/3.6 activity, starting with the existing knowledge, to consider how these channels may operate in responses to localised damage or mechanical stress. Findings will then inform further investigations into how GLR3.3/3.6 contribute to the plant perception of localised insect feeding from aphids and thrips.

Throughout this thesis and in particular this chapter, stimuli will be categorised based on their spatial scales. A 'large-scale' stimulus will refer to any stimulus that directly affects cells across many tissues. Large-scale wound events often induce rapid systemic signalling that propagates via the vascular tissue. 'Localised' stimuli are those which directly affect only the few cells contacted by the stimulus or closely neighbouring cells and these stimuli typically do not induce rapid systemic signalling. For example, localised insect feeding refers to thrips or aphid feeding whilst chewing insects do large-scale damage during feeding. In the absence of these terms, 'localised' stimuli should be assumed.

4.1.1. GLR3.3/3.6 contribute to various biological processes including responses to large-scale damage and touch

GLR3.3 and GLR3.6 can be present at the plasma membrane and form non-selective cation channels that preferentially transport Ca^{2+} (Alfieri *et al.*, 2020; Bellandi *et al.*, 2022; Toyota *et al.*, 2018; Shao *et al.*, 2020). Their expression in aerial tissues is predominantly in vascular bundles with additional GLR3.3 expression in trichome base cells, guard cells and leaf mesophyll cells (Nguyen *et al.*, 2018; Toyota *et al.*, 2018; Moe-Lange *et al.*, 2021; Tenorio Berrío *et al.*, 2022). GLR3.3 functions in the regulation of pollen tube $[Ca^{2+}]$ elevations and development (Wudick *et al.*, 2018b) as well as in resistance against *H. arabidopsidis* (Manzoor *et al.*, 2013) and *P. syringae* (Li *et al.*, 2013). GLR3.6 contributes to the developmental regulation of primary and lateral root growth (Singh *et al.*, 2016). However, the most studied functions of GLR3.3 and GLR3.6 are in signalling responses to large-scale wounding, touch and insect feeding. For instance, large-scale wounding triggers rapidly propagating systemic $[Ca^{2+}]$ elevations, ROS production, depolarisations and hydraulic pressure changes that are all dramatically impaired in *glr3.3 glr3.6* mutants (Fichman and Mittler, 2021a; Nguyen *et al.*, 2018; Mousavi *et al.*, 2013; Toyota *et al.*, 2018). Moreover, *glr3.3* and *glr3.6* single mutants display phenotypes in some

responses to large-scale wounding. *glr3.3* mutants, for example, lack the systemic hydraulic pressure changes (Fichman and Mittler, 2021a) and display reduced systemic $[Ca^{2+}]$ elevations (Nguyen *et al.*, 2018; Bellandi, 2021; Grenzi *et al.*, 2023). This contribution of GLR3.3/3.6 to large-scale wound-induced signalling leads them to function in defences against chewing insect pests (Nguyen *et al.*, 2018; Mousavi *et al.*, 2013). *glr3.3 glr3.6* double mutants are also impaired in large-scale touch responses such as touch-induced hyponasty which is associated with $[Ca^{2+}]$ elevations in the vascular tissue (Pantazopoulou *et al.*, 2022). As such, GLR3.3 and GLR3.6 perform various functions including in responses to large-scale touch and wounding. Through similar functions in damage or mechanical stress perception, GLR3.3/3.6 could contribute to the perception of localised insect feeding.

4.1.2. What factors determine GLR3.3/3.6 activation?

Understanding how GLR3.3 and GLR3.6 permeability is dynamically regulated is crucial for appreciating how they could operate in plant responses to localised insect feeding. There are many components to this regulation which will be explored here.

Several amino acids and related molecules (e.g. glutamate and glutathione) are considered the dominant GLR3.3/3.6 agonists *in planta* as they induce GLR3.3/3.6-dependent Ca^{2+} influxes and as some are known to directly bind to GLR3.3 (Alfieri *et al.*, 2020; Qi *et al.*, 2006; Li *et al.*, 2013; Shao *et al.*, 2020). Glu treatment, for example, can trigger GLR3.3/3.6-dependent $[Ca^{2+}]$ elevations in various plant tissues including systemically between leaves and between roots and shoots (Alfieri *et al.*, 2020; Qi *et al.*, 2006; Li *et al.*, 2013; Toyota *et al.*, 2018; Bellandi *et al.*, 2022; Shao *et al.*, 2020; Grenzi *et al.*, 2023). Localised Glu application onto cotyledons and within leaves also induces localised epidermal and mesophyll $[Ca^{2+}]$ elevations that are GLR3.3-dependent (Bellandi *et al.*, 2022; Grenzi *et al.*, 2023). *In planta*, GLR ligands are thought to operate as DAMPs passively released with cell damage. Support for this comes from investigations utilising the genetically-encoded [Glu] reporter, iGluSnFR (Marvin *et al.*, 2013), expressed in the *A. thaliana* apoplast. Large-scale wounding and leaf burning induce local and systemic iGluSnFR signals indicating increases in apoplastic [Glu] which are thought to activate GLR3.3/3.6-dependent $[Ca^{2+}]$ elevations (Toyota *et al.*, 2018; Bellandi *et al.*, 2022; Grenzi *et al.*, 2023). For propagation of large-scale wound-induced rapid systemic signalling, Glu may act as a mobile signal in the xylem travelling by bulk flow with further spread through mesophyll tissues by diffusion (Bellandi *et al.*, 2022). Interestingly, applying mechanical stress to trichomes through touch stimuli also induces iGluSnFR reporter signals and localised $[Ca^{2+}]$ elevations (Bellandi *et al.*, 2022). This suggests that apoplastic [Glu] elevations could occur without cell damage to activate GLRs though there are no known mechanisms for such Glu efflux. In any

case, there is significant evidence for GLR ligands in the apoplast acting as DAMPs or signals to activate GLR3.3/3.6 and these agonists could regulate GLR activity in responses to localised insect feeding.

Recently, extracellular pH gating of GLR3.3 and GLR3.6 has been revealed as their Glu-induced conductance in heterologous systems requires pH 6.5 or above and is greater at pH 8.5 than pH 7.5 (Shao *et al.*, 2020). In support of pH regulating GLR3.3/3.6 *in planta*, the GLR3.3/3.6-dependent large-scale wound-induced systemic depolarisations are negatively regulated by AHA1 which exports protons into the apoplast (Kumari *et al.*, 2019; Shao *et al.*, 2020). Moreover, overactivation of plasma membrane H⁺-ATPases by fusicoccin treatment curtails these depolarisations (Shao *et al.*, 2020; Kumari *et al.*, 2019). As such, GLR3.3 and GLR3.6 activities appear to be inhibited by lower apoplastic pH, as is the case for their animal homologs of NMDA Glu receptors (Traynelis and Cull-Candy, 1990; Wudick *et al.*, 2018a). Importantly, Shao *et al.* (2020) only found pH gating with [Glu] of 50 mM or more suggesting that any pH gating of GLR3.3/3.6 operates alongside gating by GLR ligands. It is unclear at present how apoplastic alkalinisations could occur to gate GLR3.3/3.6 though suppression of AHA activity has been proposed (Shao *et al.*, 2020). Moreover, apoplastic pH changes with GLR3.3/3.6-dependent responses are not well characterised. The apoplastic ratiometric pH reporter, apo-pHusion (Gjetting *et al.*, 2012), would provide a means to visualise any such pH changes. In summary, pH could be an important determinant of GLR3.3/3.6 activity and is currently understudied including in responses to localised stimuli such as insect feeding.

Large-scale wound-induced systemic hydraulic pressure changes and membrane depolarisations may also regulate GLR3.3/3.6 activity (Moe-Lange *et al.*, 2021). These depolarisations are significantly shortened in *glr3.3* and *glr3.6* mutants and are absent in *glr3.3 glr3.6* double mutants (Mousavi *et al.*, 2013; Nguyen *et al.*, 2018; Moe-Lange *et al.*, 2021; Salvador-Recatalà *et al.*, 2014; Wu *et al.*, 2022). Mutants in the plasma membrane mechanosensitive ion channel, MSL10, are also impaired in these systemic depolarisations and phenocopy *glr3.3* and *glr3.6* mutants, with no further phenotype in the *glr3.3 msl10* or *glr3.6 msl10* double mutants (Moe-Lange *et al.*, 2021). With a preference for anion efflux (Maksaev and Haswell, 2012; Basu and Haswell, 2020), MSL10 likely contributes directly to the large-scale wound-induced systemic depolarisations. Furthermore, *msl10* is impaired in large-scale wound-induced systemic [Ca²⁺] elevations (Moe-Lange *et al.*, 2021). Assuming GLR3.3/3.6 primarily conduct the Ca²⁺ for these [Ca²⁺] elevations, this implies that MSL10-dependent depolarisations are required for the full GLR3.3/3.6 activation (Moe-Lange *et al.*, 2021). In large-scale wound-induced systemic responses, MSL10 stretch activation may result from turgor pressure changes in the xylem increasing membrane tension in neighbouring xylem contact cells, as outlined in

the Squeeze Cell hypothesis (Farmer *et al.*, 2014; Moe-Lange *et al.*, 2021). Interestingly, MSL10 did not contribute to large-scale wound-induced $[Ca^{2+}]$ elevations in the local damaged tissue, potentially because agonist accumulation there is alone sufficient for full GLR3.3/3.6 activation without requiring depolarisations (Moe-Lange *et al.*, 2021). Nonetheless, depolarisations alongside ligand release may contribute to the regulation of GLR3.3/3.6 in plants.

The potential for pH, membrane potential and ligands to influence GLR3.3/3.6 activity makes appreciating GLR3.3/3.6 regulation complex. Furthermore, these regulatory components do not exist independently of one another and may interact (Suda and Toyota, 2022). For example, systemic turgor pressure changes, which may contribute to MSL10 activation, also appear capable of triggering systemic [Glu] increases (Grenzi *et al.*, 2023). Moreover, Ca^{2+} binding EF-hand motifs in MSL10 imply that the systemic large-scale wound-induced MSL10-dependent depolarisations may be influenced by the GLR3.3/3.6-dependent $[Ca^{2+}]$ elevations (Moe-Lange *et al.*, 2021). Finally, in response to turgor pressure changes, systemic iGluSnFR signals are reduced in *glr3.3* mutants suggesting that GLR3.3 activity may promote Glu efflux further activating GLR3.3 (Grenzi *et al.*, 2023). There are also less well characterised components that influence GLR activity in systemic responses to large-scale wounding. For instance, ISI1 interacts with GLR3.3 and negatively regulates its activity in these responses (Wu *et al.*, 2022). Additionally, large-scale wounding releases TGG thioglucosidase enzymes into the xylem as systemic mobile signals. These TGGs hydrolyse glucosinolates into unstable aglycones and their activity induces GLR3.3- and GLR3.6-dependent systemic signalling responses (Gao *et al.*, 2023). Whilst many of the GLR3.3/3.6 regulatory components have been investigated in systemic responses to large-scale wounding, the regulation of GLR3.3/3.6 in responses to localised stimuli is less well characterised. Deciphering localised GLR3.3/3.6 regulation will be key to appreciating how these channels might function in responses to localised insect feeding from aphids and thrips.

4.1.3. How do GLR3.3/3.6 contribute to plant defence responses?

To appreciate how GLR3.3/3.6 could contribute to aphid or thrips perception, it is important to explore any defence responses downstream of these channels. In responses to large-scale wounding, rapid systemic signalling is thought to drive the *in-situ* production of JAs in distal tissue with vascular connections within 120 s of wounding (Mousavi *et al.*, 2013; Chauvin *et al.*, 2013; Glauser *et al.*, 2009; Koo *et al.*, 2009; Glauser *et al.*, 2008). This production appears to be GLR3.3/3.6-dependent as systemic JA marker gene expression is severely reduced in *glr3.3 glr3.6* double mutants (Mousavi *et al.*, 2013; Fichman and Mittler, 2021a; Shao *et al.*, 2020) with smaller reductions in *glr3.3* and *glr3.6* single mutants (Mousavi *et al.*, 2013). Interestingly, $LaCl_3$

treatment suppresses the large-scale wound-induced systemic $[Ca^{2+}]$ elevations and JA marker gene expression (Toyota *et al.*, 2018). Therefore, GLR3.3/3.6-dependent $[Ca^{2+}]$ elevations may be required for systemic JA accumulation following large-scale wounding. $[Ca^{2+}]$ elevations could directly regulate JA signalling by promoting disassembly of the JAV1-JAZ8-WRKY51 complex which suppresses the expression of JA biosynthetic genes (Yan *et al.*, 2018). In responses to large-scale damage from chewing insects, systemic JA accumulation is also GLR3.3/3.6-dependent (Xue *et al.*, 2022). In many cases, genetically suppressing GLR3.3/3.6-dependent responses reduces chewing insect resistance whilst enhancing them has the opposite effect (Xue *et al.*, 2022; Nguyen *et al.*, 2018; Kumari *et al.*, 2019; Wu *et al.*, 2022). Therefore, GLR3.3/3.6 appear to promote systemic JA-mediated defence responses to large-scale wounding and chewing insects. As such, GLR3.3/3.6 could contribute to any localised insect feeding-induced JA signalling and JA-dependent insect resistance.

4.1.4. Current investigations

There is a good understanding of the functions of GLR3.3/3.6 in responses to large-scale wounding and chewing insect feeding as well as growing insights into GLR3.3/3.6 regulation in those contexts. However, there is a limited understanding of how GLR3.3/3.6 could function in responses to localised damage or mechanical stress during aphid or thrips feeding. The stylet bundle of *M. persicae* has a diameter of approximately 4.5 μm near the head that tapers to 2.7 μm near the tip (Forbes, 1969). The *F. occidentalis* mandibular stylet is approximately 2 μm in diameter as is the maxillary stylet bundle (Hunter and Ullman, 1992). The micropipette needles used for localised wound treatments in Chapter 3 had a diameter of $6.46 \pm 0.61 \mu\text{m}$ ($n = 6$). Here, micropipette wounding will be used to investigate the mechanisms of localised damage perception on a scale relevant to aphid and thrips feeding as well as the contributions of GLR3.3/3.6 to this perception. Furthermore, fire blunted versions of the micropipette needles, with broader diameters of $333 \pm 13 \mu\text{m}$ ($n = 7$), will be used to investigate the perception of localised mechanical stress or touch and whether GLR3.3/3.6 function in this perception. An improved understanding of localised wound and touch perception will provide the foundations for further investigations into GLR3.3/3.6 activity in the perception of aphid and thrips feeding.

To investigate plant responses to localised stimuli and the contributions of GLR3.3/3.6 with high spatiotemporal resolution, I acquired *A. thaliana* lines expressing various genetically encoded fluorescent reporters. These reporters included $35S::iGluSnFR$ (Toyota *et al.*, 2018) for assessing the potential of apoplastic $[Glu]$ increases to regulate GLR3.3/3.6 in responses to localised stimuli. Similarly, I acquired *A. thaliana* expressing $35S::Apo-pHusion$ to assess the potential for GLR3.3/3.6 regulation by apoplastic pH changes (Gjetting *et al.*, 2012). *A. thaliana*

lines expressing *UBQ10::GCaMP3* were available to visualise any localised wound- or touch-induced $[Ca^{2+}]$ elevations. As *GLR3.1*, *GLR3.3* and *GLR3.6* have all been implicated in large-scale wound-induced systemic responses (Nguyen *et al.*, 2018), *UBQ10::GCaMP3 A. thaliana* lines containing different combinations of mutations in these genes were acquired to assess their contributions to localised wound- and touch-induced responses. Finally, marker gene expression reporters were acquired for assessing hormone signalling responses to localised wounding and touch. These reporters utilised JA-, SA- and Et-activated promoters to drive the expression of a nuclear-localised 3xVENUS FP (Marhavý *et al.*, 2019). Together, these reporters will be used to explore localised wound- and touch-induced responses and how *GLR3.3/3.6* may contribute to these responses and be regulated. These investigations will provide insights into how *GLR3.3/3.6* could function in the perception of aphid or thrips feeding. With this, the research aims of this chapter are to:

1. Characterise any localised wound- or touch-induced $[Ca^{2+}]$ elevations and whether they are *GLR3.1/3.3/3.6*-dependent.
2. Explore the mechanisms that underpin the signalling responses to localised wound and touch stimuli including any *GLR3.1/3.3/3.6* activation.
3. Identify whether wound and touch stimuli induce hormone signalling that could influence insect resistance and whether these responses are dependent on any associated GLRs.

4.2. Results

4.2.1. The dynamics of wound-induced [Ca²⁺] elevations are altered on *glr3.3a* mutants

To test whether GLR3.1/3.3/3.6 contribute to localised wound-induced [Ca²⁺] elevations, I micropipette wounded ('wounded') *A. thaliana* UBQ10::GCaMP3 expressing lines containing mutations in one or more of these channels. The resulting reporter signals were analysed for their F0 values, peak normalised $\Delta F/F0$ values, areas, and propagation rates (Table 4.1). For *glr3.1a glr3.3a*, *glr3.3a glr3.6a* and *glr3.1a glr3.3a glr3.6a* mutants, the peak normalised $\Delta F/F0$ values and rate values were significantly lower than in their Col-0 controls. These properties did not differ between the triple mutant and the *glr3.3a* mutant. Comparing the single mutants, the *glr3.3a* signal propagation rates were significantly lower than in Col-0 with mean values of $1.11 \pm 0.16 \mu\text{m s}^{-1}$ and $2.33 \pm 0.13 \mu\text{m s}^{-1}$, respectively. The *glr3.3a* peak normalised $\Delta F/F0$ values were also significantly lower than in Col-0 with mean values of 0.75 ± 0.06 A.U. and 1.17 ± 0.07 A.U., respectively. *glr3.1a* and *glr3.6a* single mutants did not display reduced peak normalised $\Delta F/F0$ values or signal propagation rates compared to Col-0. Instead, *glr3.6a* peak normalised $\Delta F/F0$ values were significantly greater than in Col-0. These analyses revealed that *glr3.3a* mutants have altered wound-induced [Ca²⁺] elevations, detected by GCaMP3 signals with lower peak normalised $\Delta F/F0$ values and propagation rates, whilst GLR3.1 and GLR3.6 do not clearly contribute to these elevations.

Table 4.1 Properties of wound-induced GCaMP3 signals in *A. thaliana* with mutations in GLR3.1, GLR3.3 and/or GLR3.6 alongside wildtype Col-0 controls.

Statistical analyses were performed within experiments. For pairwise comparisons, tests were t-tests or Wilcoxon rank-sum tests. For comparing multiple genotypes, tests were one-way ANOVAs with Tukey post hoc tests or Kruskal-Wallis tests with Wilcoxon rank-sum post hoc tests. For pairwise comparisons to Col-0: No symbol: $p > 0.05$, *: $p \leq 0.05$, ****: $p \leq 0.0001$. For multi-group comparisons, superscript letters indicate significance levels.

Red - statistically significant properties for *A. thaliana* lines carrying the *glr3.3a* mutation. Data values represent mean \pm S.E.M. Grey highlight – background correction included in analyses.

Experiment	Genotype	F0 (A.U.)	Peak Normalised $\Delta F/F0$ (Wound $\Delta F/F0$ - Control $\Delta F/F0$)	Signal Rate ($\mu\text{m s}^{-1}$)	Signal Area (mm ²)	Sample size
Col-0 vs <i>glr3.3a glr3.6a</i> UBQ10::GCaMP3	Col-0	775 \pm 12	0.36 \pm 0.02	2.38 \pm 0.17	0.700 \pm 0.038	17
	<i>glr3.3a glr3.6a</i>	749 \pm 11	0.23 \pm 0.01****	0.81 \pm 0.04****	0.843 \pm 0.080	15
Col-0 vs <i>glr3.1a glr3.3a</i> UBQ10::GCaMP3	Col-0	713 \pm 12	0.37 \pm 0.02	2.14 \pm 0.11	0.617 \pm 0.048	17
	<i>glr3.1a glr3.3a</i>	705 \pm 13	0.19 \pm 0.01****	0.74 \pm 0.05****	0.616 \pm 0.061	16
Col-0 vs <i>glr3.1a glr3.3a glr3.6a</i> vs <i>glr3.3a</i> UBQ10::GCaMP3	Col-0	635 \pm 14	0.29 \pm 0.01 ^a	2.96 \pm 0.19 ^a	0.638 \pm 0.045	17
	<i>glr3.1a glr3.3a glr3.6a</i>	657 \pm 15	0.19 \pm 0.01 ^b	1.16 \pm 0.08 ^b	0.685 \pm 0.047	19
	<i>glr3.3a</i>	652 \pm 14	0.18 \pm 0.01 ^b	1.09 \pm 0.07 ^b	0.606 \pm 0.057	19
Col-0 vs <i>glr3.1a</i> vs <i>glr3.3a</i> vs <i>glr3.6a</i> UBQ10::GCaMP3	Col-0	698 \pm 46	1.17 \pm 0.07 ^b	2.33 \pm 0.13 ^{ab}	0.640 \pm 0.047	19
	<i>glr3.1a</i>	722 \pm 32	1.27 \pm 0.06 ^{ab}	2.56 \pm 0.10 ^a	0.621 \pm 0.041	21
	<i>glr3.3a</i>	737 \pm 46	0.75 \pm 0.06 ^c	1.11 \pm 0.16 ^c	0.615 \pm 0.045	21
	<i>glr3.6a</i>	666 \pm 35	1.38 \pm 0.07 ^a	2.22 \pm 0.10 ^b	0.690 \pm 0.052	18

To characterise the *glr3.3a* phenotype in more detail, I focussed on the Col-0 and *glr3.3a* comparison from the 'Col-0 vs *glr3.1a* vs *glr3.3a* vs *glr3.6a* UBQ10::GCaMP3' experiment in Table 4.1. In *glr3.3a* mutant samples, wound-induced GCaMP3 signal dynamics were dramatically different from those in Col-0 (Figure 4.1, Video S4.1). In Col-0, there was a single normalised $\Delta F/F_0$ peak around 2 min post-wounding (Figure 4.1A). This peak corresponded approximately to the maximum area of reporter signals ($0.640 \pm 0.047 \text{ mm}^2$) which propagated radially from each wound site as a ring travelling at a mean rate of $2.33 \pm 0.13 \mu\text{m s}^{-1}$ (Figure 4.1B). These reporter signals and $[\text{Ca}^{2+}]$ elevations were termed 'waves' and were analysed as the 'dominant signal' for rate, area, and intensity measurements. Following wave reporter signals, there were occasionally less defined, lower-intensity reporter signals that appeared to grow out from the wound site and then fade over approximately 15 min. In contrast, *glr3.3a* mutants displayed two phases of reporter signals with two peaks in the normalised $\Delta F/F_0$ traces (Figure 4.1, Video S4.1). As these two phases were not always clearly separable, they were analysed as one 'dominant signal' for overall rate, area, and intensity measurements. Initial *glr3.3a* mutant reporter signals, termed 'bursts', occurred at each wound site with a normalised $\Delta F/F_0$ peak within 40 s of wounding. Bursts then largely dissipated by $60.95 \pm 6.34 \text{ s}$ post-wounding (Figure 4.1A). Bursts propagated at a mean rate of $6.02 \pm 0.49 \mu\text{m s}^{-1}$ which was significantly faster than the wave propagation rates (Wilcoxon rank-sum, $W = 2$, $p \leq 0.0001$). However, burst signals only reached a mean area of $0.267 \pm 0.034 \text{ mm}^2$ and were significantly smaller than the wave signals of Col-0 (t-test, $t = 6.43$, $p \leq 0.0001$). Bursts in *glr3.3a* mutants were followed by 'secondary (2^0)' reporter signals that grew radially from wound sites giving a mean normalised $\Delta F/F_0$ peak around 5 min (Figure 4.1). Secondary reporter signal areas had a mean of $0.615 \pm 0.045 \text{ mm}^2$ which was not statistically different from the Col-0 wave signal areas (Table 4.1). After secondary $\Delta F/F_0$ peaks, *glr3.3a* normalised $\Delta F/F_0$ values were often greater than for Col-0 as *glr3.3a* secondary reporter signals faded over the next 25 min. For instance, at 12 min post-wounding, the *glr3.3a* normalised $\Delta F/F_0$ values were significantly greater than values for Col-0 samples (Wilcoxon rank-sum test, $W = 81$, $p = 0.00097$). The normalised $\Delta F/F_0$ traces were initially closely matched for Col-0 and *glr3.3a* mutants (Figure 4.1) indicating that the wound-induced burst and wave reporter signals may begin as the same response but that GLR3.3 is required for propagation of the wave. Additionally, the reporter signals behind the Col-0 wave front may represent suppressed versions of the secondary $[\text{Ca}^{2+}]$ elevations in the *glr3.3a* mutant. In summary, these data reveal that *glr3.3a* mutants display wound-induced burst and secondary $[\text{Ca}^{2+}]$ elevations with different dynamics to the Col-0 wave $[\text{Ca}^{2+}]$ elevations. These differences can be detected in normalised $\Delta F/F_0$ traces with *glr3.3a* GCaMP3 reporter signals having reduced signal propagation rates and peak normalised $\Delta F/F_0$ values compared to Col-0.

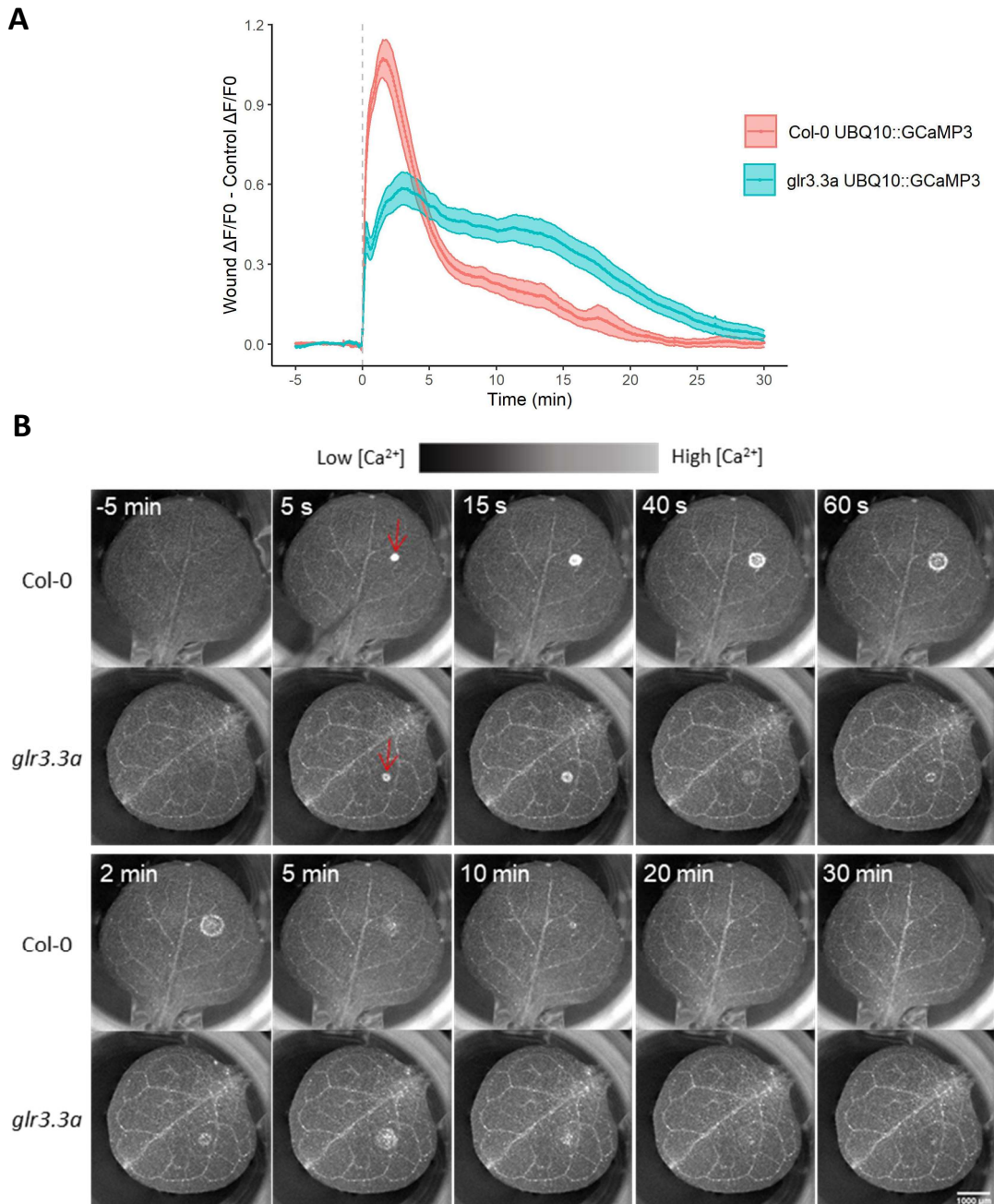


Figure 4.1 *glr3.3a* mutants display altered wound-induced GCaMP3 signals.

Comparisons of wound-induced GCaMP3 reporter signal dynamics between Col-0 ($n = 19$) and *glr3.3a* UBQ10::GCaMP3 ($n = 21$) *A. thaliana*. F (A.U.) values were the background corrected fluorescence intensities over the area of reporter signals and at comparable control sites which were transformed by $\Delta F/F_0$ with F_0 being the mean F over the 5 min prior to wounding. (A) Traces for the mean \pm S.E.M. normalised $\Delta F/F_0$ values (Wound $\Delta F/F_0$ – Control $\Delta F/F_0$) over time with wounding occurring at 0 min (grey dashed line). (B) Time series images from representative Col-0 and *glr3.3a* samples. Red arrows indicate wound sites at 0 s. Data taken from the comparison between Col-0, *glr3.1a*, *glr3.3a* and *glr3.6a* UBQ10::GCaMP3 *A. thaliana*.

4.2.2. Water infiltration perturbs wound-induced $[Ca^{2+}]$ elevations and provides insights into the underlying signalling mechanisms

To investigate the mechanisms underpinning wound-induced wave, burst and secondary $[Ca^{2+}]$ elevations as well as GLR3.3 activation, I attempted to manipulate the wound-induced GCaMP3 signals. To do so, I vacuum-infiltrated leaves expressing GCaMP3 with different solutions before micropipette wounding. Infiltrations included sterile dH₂O (pH 5.49 ± 0.08 , $n = 8$) as a negative control, (2R)-amino-5-phosphonopentanoate (AP5) as a competitive GLR antagonist (Li *et al.*, 2013), citrate buffer (pH 5) to buffer apoplastic alkalinisation, LaCl₃ to block plasma membrane Ca²⁺ channels, and EGTA to reduce free apoplastic $[Ca^{2+}]$. In these preliminary experiments (data not shown), all pre-treatments, including water, resulted in similarly altered wound-induced GCaMP3 reporter signals.

To better characterise the effect of water infiltration on wound-induced $[Ca^{2+}]$ elevations, I wounded Col-0 and *glr3.3a* *UBQ10::GCaMP3* *A. thaliana* leaves without pre-treatment ('uninfiltrated') and after water infiltration ('infiltrated'). Uninfiltrated *glr3.3a* leaves again displayed wound-induced burst and secondary reporter signals whilst Col-0 samples displayed wave signals (Figure 4.2A, Video S4.2). The *glr3.3a* GCaMP3 signals again had reduced peak normalised $\Delta F/F_0$ values (Figure 4.2B, Tukey test following ANOVA, $p \leq 0.0001$) and propagation rates (Figure 4.2C Tukey test following ANOVA, $p \leq 0.0001$). Wound-induced reporter signals in water-infiltrated Col-0 samples recapitulated this uninfiltrated *glr3.3a* phenotype with burst and secondary signals (Figure 4.2A) and reduced peak normalised $\Delta F/F_0$ values (Figure 4.2B, Tukey test following two-way ANOVA, $p = 0.0050$) and propagation rates compared to uninfiltrated Col-0 (Figure 4.2C, Tukey test following two-way ANOVA, $p = 0.031$). Across all groups, F_0 values (Figure 4.2D, two-way ANOVA, $F = 0.015$, $p = 0.90$) and signal areas were not statistically different (Figure 4.2E, two-way ANOVA, $F = 0.29$, $p = 0.60$). Whilst water-infiltrated Col-0 and *glr3.3a* mutants showed similar normalised $\Delta F/F_0$ traces, the burst peak values were significantly reduced in *glr3.3a* as seen at 10 s post-wounding (Figure 4.2A, Wilcoxon rank-sum, $W = 139$, $p = 0.0037$). Because GLR3.3 contributed to wound-induced wave reporter signals in uninfiltrated leaves and burst signals in infiltrated leaves, these data support the hypothesis that burst $[Ca^{2+}]$ elevations develop into waves via GLR3.3-dependent propagation. Moreover, water infiltration suppressed this GLR3.3-dependent propagation perhaps as it altered important apoplastic conditions for GLR3.3 activation. Interestingly, the secondary reporter signals were similar in water-infiltrated Col-0 and *glr3.3a* leaves (Figure 4.2A) suggesting that they are independent of burst signal properties. As such, these experiments have informed on the mechanics of wound-induced $[Ca^{2+}]$ elevations and revealed that burst signals likely develop into waves via GLR3.3-dependent propagation in uninfiltrated Col-0 leaves.

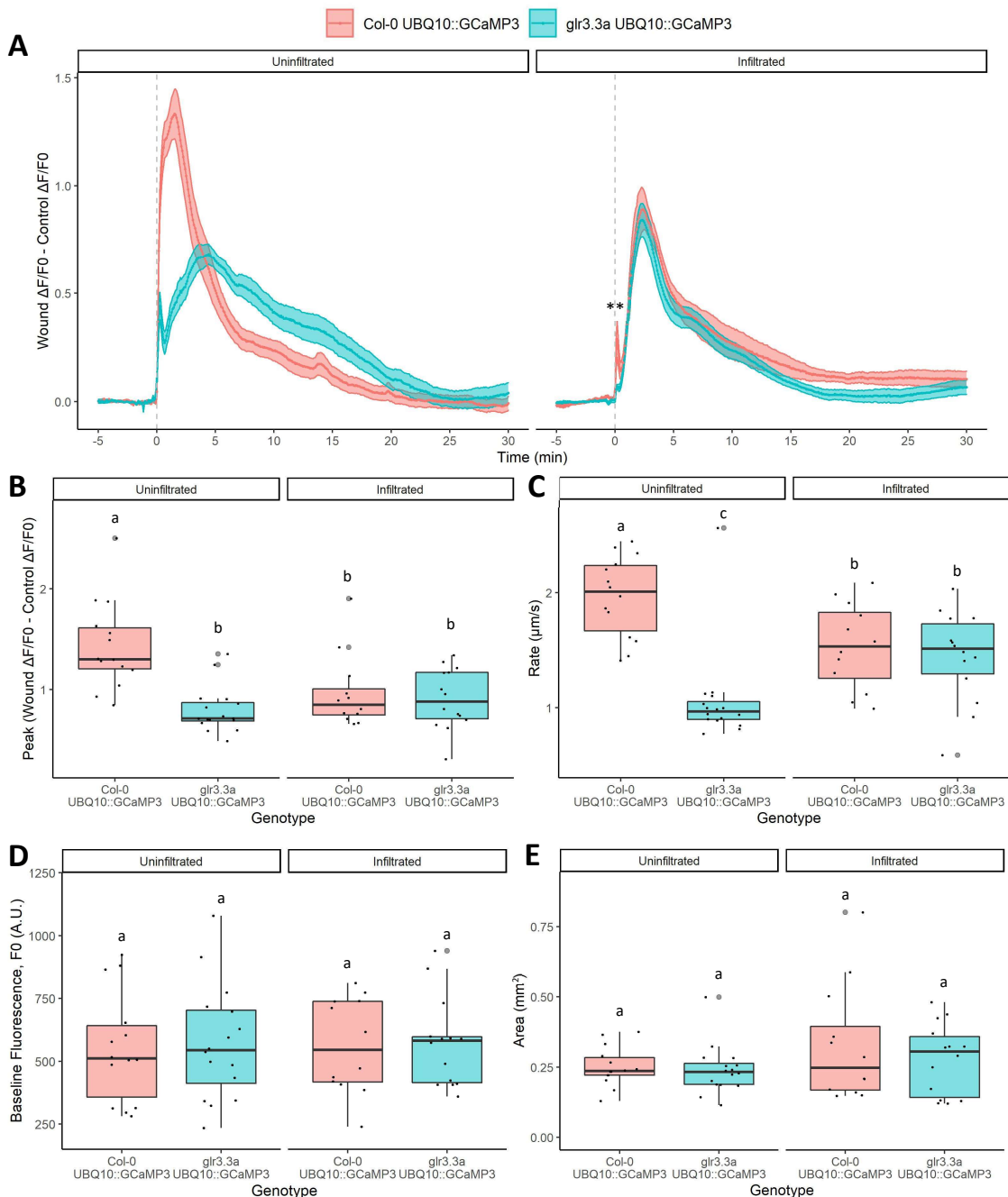


Figure 4.2 Wound-induced GCaMP3 signals are perturbed in water-infiltrated Col-0 and *glr3.3a* mutant *A. thaliana*.

Wound-induced GCaMP3 reporter signals in Col-0 and *glr3.3a* UBQ10::GCaMP3 *A. thaliana* leaves that had been pre-treated with water infiltration ('infiltrated') or had not been ('uninfiltreated'). Background corrected fluorescence intensities (F, A.U.) were calculated across the area of reporter signals and at comparable control sites. F values were transformed by $\Delta F/F_0$ with F0 being the mean F over the 5 min prior to wounding at 0 min (grey dashed line). (A) Traces for the mean \pm S.E.M. normalised $\Delta F/F_0$ values (Wound $\Delta F/F_0$ - Control $\Delta F/F_0$) over time. '**' indicates statistical significance as $p \leq 0.01$ at 10 s post-wounding between infiltrated Col-0 and *glr3.3a* mutant samples, as determined by a Wilcoxon rank-sum test. Boxplots for the (B) peak normalised $\Delta F/F_0$ values (Wound $\Delta F/F_0$ - Control $\Delta F/F_0$), (C) signal propagation rates ($\mu\text{m s}^{-1}$), (D) F0 values (A.U.) and (E) signal areas (mm^2) are shown with grey dots associated with outliers. Significance levels are indicated with letters and were calculated by two-way ANOVAs with Tukey post-hoc tests. Sample sizes were Col-0 uninfiltreated: $n = 14$, *glr3.3a* uninfiltreated: $n = 16$, Col-0 infiltrated: $n = 12$, *glr3.3a* infiltrated: $n = 14$.

4.2.3. Micropipette wounding induces iGluSnFR and apo-pHusion signals that are spatiotemporally correlated with GCaMP3 reporter signals

To investigate if wound-induced GLR3.3-dependent $[Ca^{2+}]$ elevations could be promoted by apoplastic [Glu] or pH increases, I wounded *A. thaliana* expressing *35S::iGluSnFR* and *35S::Apo-pHusion*, respectively. iGluSnFR plants displayed clear wound-induced reporter signals that began at the wound sites and propagated radially without notable decreases in intensity behind the leading fronts (Figure 4.3A, C, Video S4.3). These signals propagated at a mean rate of $2.01 \pm 0.20 \mu\text{m s}^{-1}$ to a mean maximum area of $0.570 \pm 0.041 \text{ mm}^2$ and gave a mean normalised $\Delta F/F_0$ peak around 4 min post-wounding (Figure 4.3A). At this point, wound site $\Delta F/F_0$ values were significantly greater than control site $\Delta F/F_0$ values (Figure 4.3B, paired Wilcoxon signed rank, $V = 0$, $p \leq 0.0001$). Apo-pHusion leaves also displayed clear wound-induced reporter signals that again propagated radially without clear intensity decreases behind the leading fronts. These signals propagated at a mean rate of $2.11 \pm 0.16 \mu\text{m s}^{-1}$ to a mean maximum area of $0.723 \pm 0.036 \text{ mm}^2$ and gave a mean normalised $\Delta R/R_0$ peak at approximately 3 min (Figure 4.4A, C, Video S4.4). At this time, wound site $\Delta R/R_0$ values were significantly greater than control site $\Delta R/R_0$ values (Figure 4.4B, paired Wilcoxon signed rank, $V = 0$, $p \leq 0.0001$). Leaves of both *35S::iGluSnFR* and *35S::Apo-pHusion* expressing *A. thaliana* displayed visually greater GFP emission from trichomes compared to surrounding tissues (Figure 4.3C, Figure 4.4C). As trichomes have elevated apoplastic pH values compared to surrounding tissue (Zhou *et al.*, 2017), and as the apo-pHusion GFP fluorescence should increase with higher pH within the apoplastic pH range, this supports apo-pHusion functioning as an apoplastic pH reporter here. However, it also strongly suggests that iGluSnFR is pH-sensitive in this context consistent with iGluSnFR being reported to be pH sensitive *in vitro* within the pH range of the apoplast (Marvin *et al.*, 2013; Geilfus, 2017). As it is difficult to disentangle the contribution of pH and [Glu] to iGluSnFR reporter signals here, iGluSnFR will be referred to here as a [Glu] reporter until further discussion in the context of all additional results. As such, data reveal that micropipette wounding induces iGluSnFR and apo-pHusion reporter signals indicative of apoplastic alkalinisations and putative [Glu] increases that could be linked to the GLR3.3-dependent $[Ca^{2+}]$ elevations.

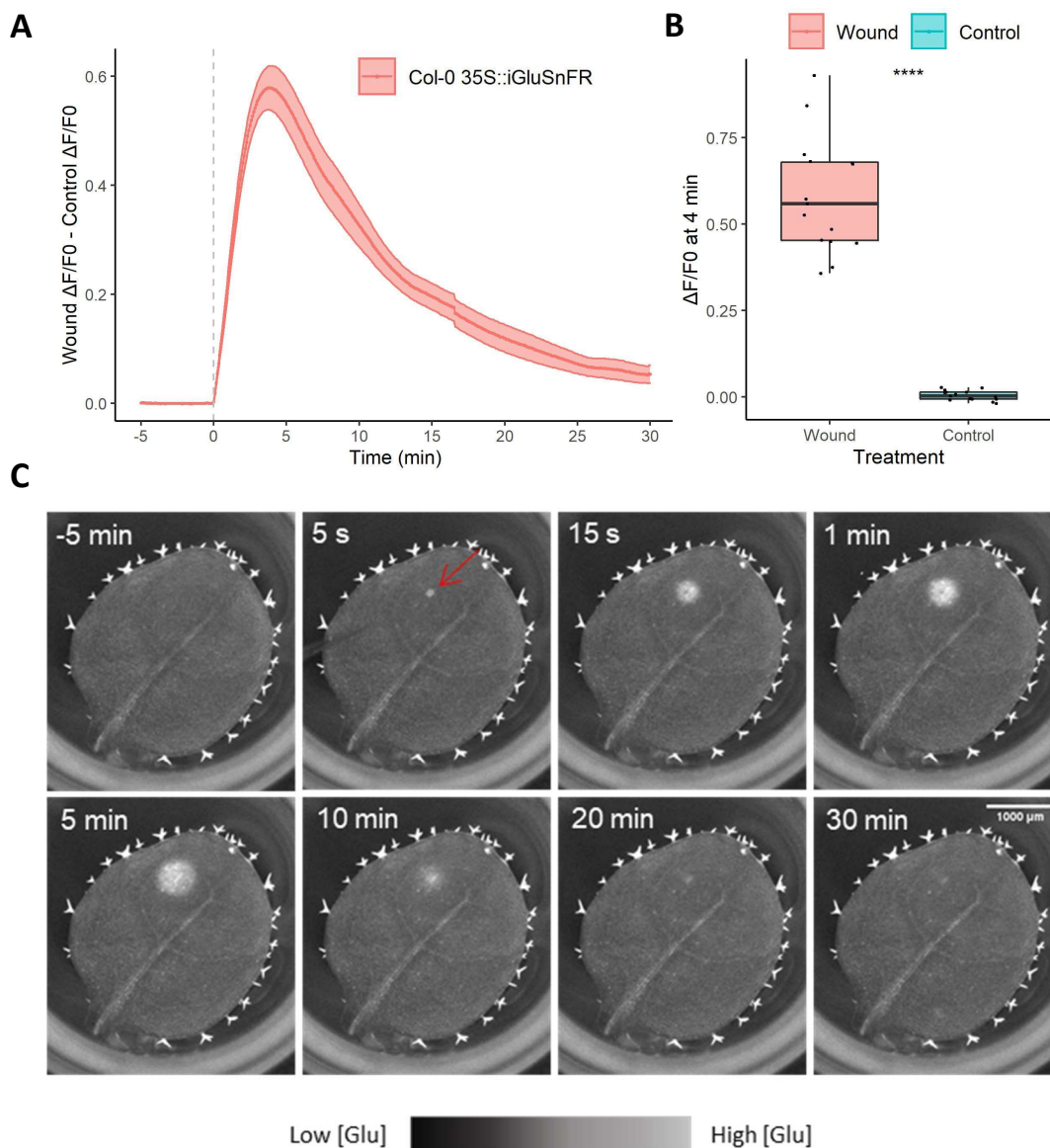


Figure 4.3 Wound-induced reporter signals in *A. thaliana* expressing *35S::iGluSnFR*

Properties of wound-induced reporter signals in Col-0 *35S::iGluSnFR A. thaliana* imaged with an Axio Zoom.V16 and a 120 V metal halide excitation lamp. (A) Traces for the mean \pm S.E.M. normalised $\Delta F/F_0$ (Wound $\Delta F/F_0$ – Control $\Delta F/F_0$) over time with wounding occurring at 0 min (grey dashed line). (B) Boxplots of the $\Delta F/F_0$ values for wound and control sites at 4 min post-wounding. Fluorescence intensity values (F, A.U.) were calculated as the mean intensity over the area of reporter signals and at comparable control sites and transformed by $\Delta F/F_0$ with F_0 being the mean F over the 5 min prior to wounding. F values were not background corrected. Statistical significance, tested using a paired Wilcoxon rank-sum test, shown by ****: $p < 0.0001$. (C) Time series of images from a representative wounded Col-0 *A. thaliana* sample expressing *35S::iGluSnFR*. Red arrow indicates wound site. Sample size: $n = 15$.

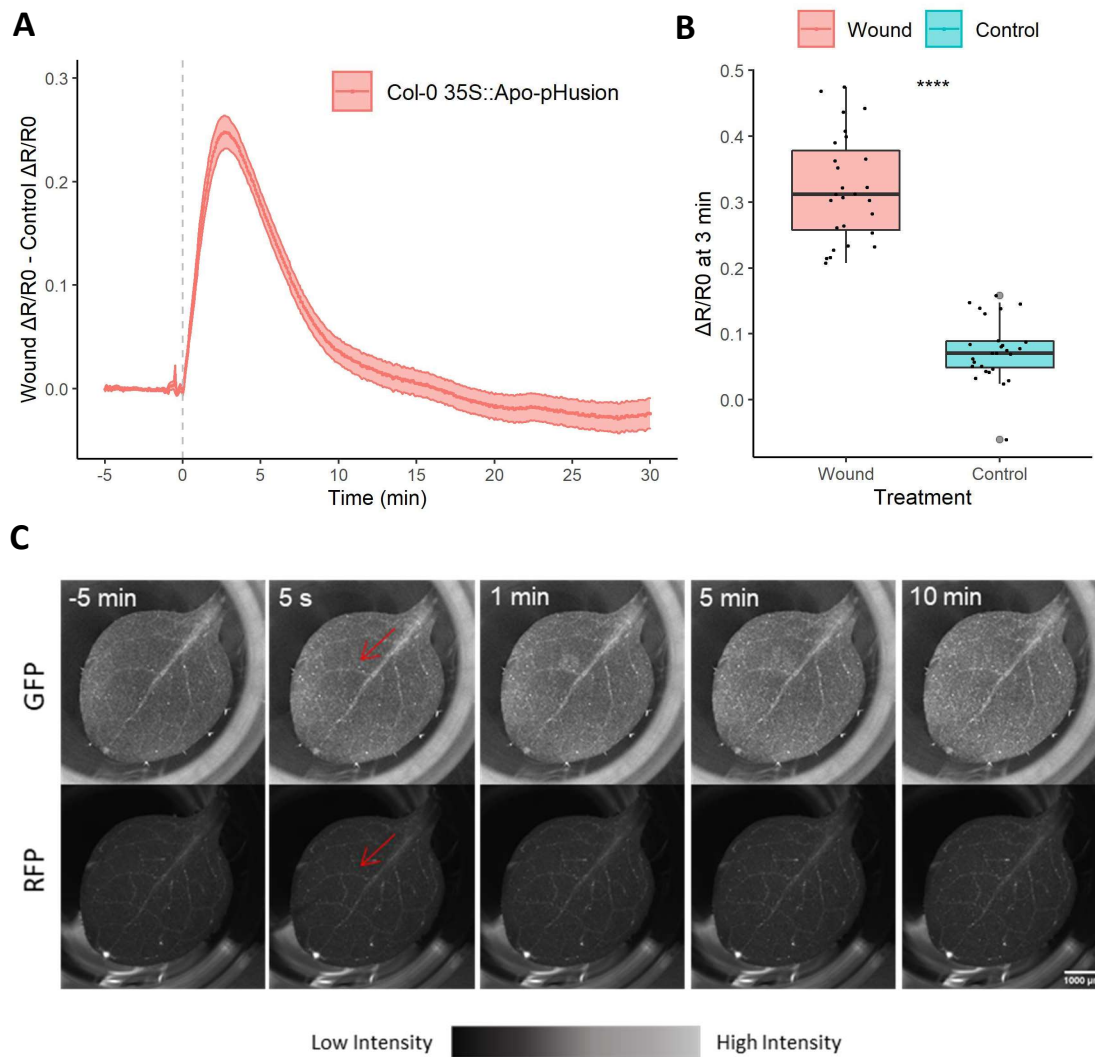


Figure 4.4 Wound-induced reporter signals in *A. thaliana* expressing 35S::Apo-pHusion

Properties of wound-induced reporter signals in Col-0 35S::Apo-pHusion *A. thaliana*. (A) Traces for the mean \pm S.E.M. normalised $\Delta R/R0$ (Wound $\Delta R/R0$ – Control $\Delta R/R0$) over time with wounding occurring at 0 min (grey dashed line). (B) Boxplots of $\Delta R/R0$ values for wound and control sites at 3 min post-wounding with grey dots associated with outliers. Background corrected fluorescence intensity (F, A.U.) values were calculated for both GFP and RFP over the area of reporter signals and at comparable control sites. The GFP/RFP ratio (R) values were calculated from F values and transformed by $\Delta R/R0$ with R0 values being the mean R over the 5 min prior to wounding. Statistical significance, tested using a paired Wilcoxon rank-sum test, shown by ****: $p < 0.0001$. (C) Time series of images from a representative wounded Col-0 *A. thaliana* sample expressing 35S::Apo-pHusion and shown for both the GFP and RFP channels. Red arrow indicates wound site. Sample size: $n = 27$.

To further investigate the correlations between apoplastic alkalinisations, potential [Glu] increases and GLR3.3-dependent [Ca²⁺] elevations, I compared the properties of the wound-induced GCaMP3, iGluSnFR and apo-pHusion reporter signals (Figure 4.5). Peak normalised $\Delta F/F_0$ values occurred later for iGluSnFR and apo-pHusion signals than for GCaMP3 signals (Figure 4.5A, Wilcoxon rank-sum tests following a Kruskal-Wallis test, $p \leq 0.0001$ for both). However, the signal propagation rates for each reporter were not statistically different (Figure 4.5B, Kruskal-Wallis rank-sum test, $df = 2$, $\chi^2 = 3.22$, $p = 0.2$). There were no significant differences in the iGluSnFR and apo-pHusion reporter signal areas compared to the GCaMP3 signal areas (Figure 4.5C, Wilcoxon rank-sum tests following a Kruskal-Wallis test, $p = 0.34$ for iGluSnFR and $p = 0.14$) though the iGluSnFR signal areas were significantly smaller than the apo-pHusion signal areas (Figure 4.5C, Wilcoxon rank-sum test following a Kruskal-Wallis test, $p = 0.0022$). Overall, all reporter signals were approximately spatially correlated and propagated at statistically similar rates. This is consistent with the wound-induced apoplastic pH and/or [Glu] increases being linked to the GLR3.3-dependent [Ca²⁺] elevations by being either upstream of, interacting with, or downstream of the [Ca²⁺] elevations.

I attempted to wound water-infiltrated and uninfiltrated *A. thaliana* leaves expressing the *35S::iGluSnFR* or *35S::Apo-pHusion* reporters to test if signals in these reporters remained correlated with the GCaMP3 signals. However, water infiltration caused a significant reduction in baseline GFP fluorescence in iGluSnFR and apo-pHusion samples as well as an even greater reduction in RFP baseline fluorescence in apo-pHusion samples (data not shown). These differences could have been caused by reporter dilution, ligand dilution and/or pH effects amongst other factors. In any case, data could not be interpreted to draw a conclusion.

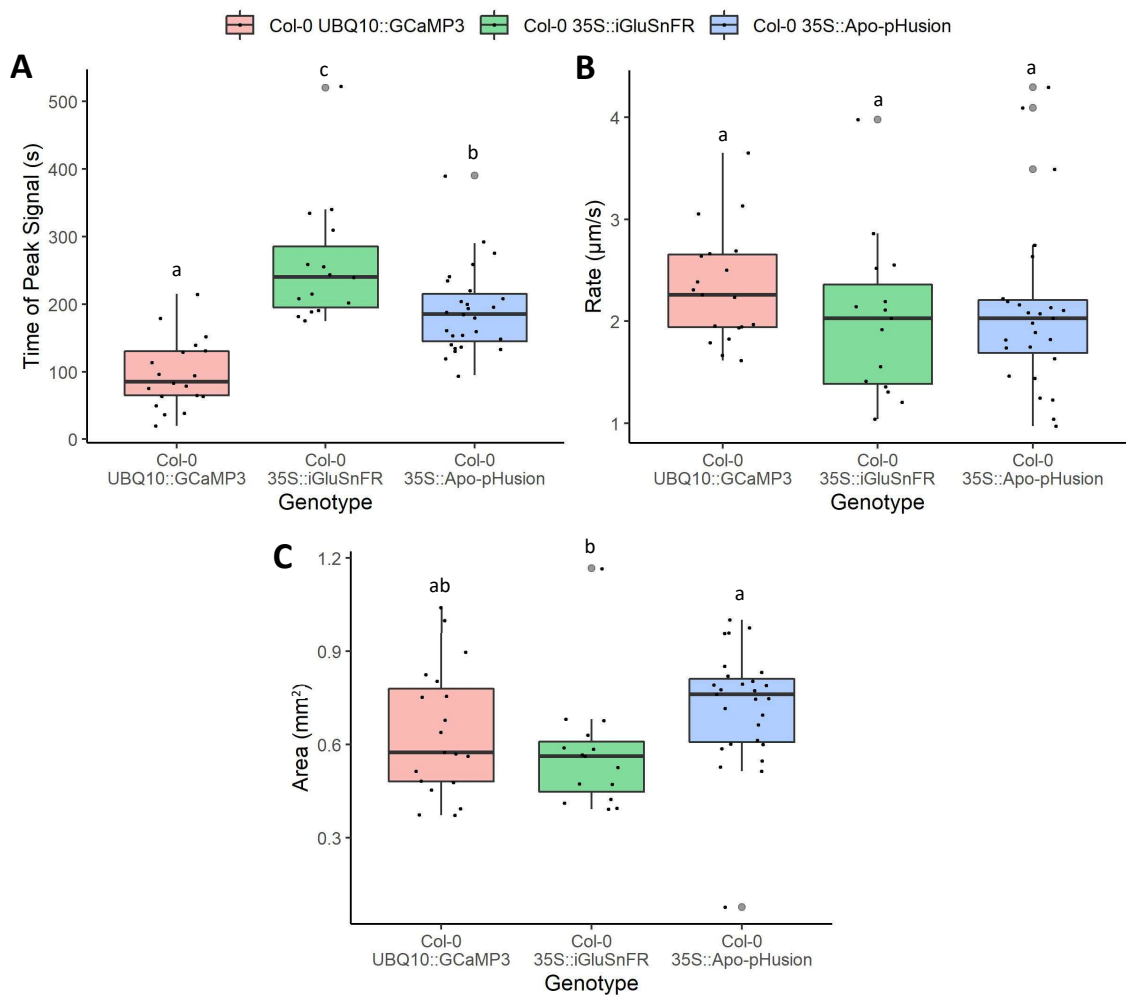


Figure 4.5 Comparisons of wound-induced reporter signal properties in *Col-0 A. thaliana* expressing *UBQ10::GCaMP3*, *35S::iGluSnFR* or *35S::Apo-pHusion*.

Comparisons of the (A) time of the peak normalised $\Delta F/F_0$ values post-wounding (s), (B) signal propagation rates ($\mu\text{m s}^{-1}$) and (C) signal areas (mm^2) shown in boxplots with grey dots associated with outliers. Data for *Col-0 UBQ10::GCaMP3* ($n = 19$) were taken from the comparison of wound-induced reporter signals in *Col-0*, *glr3.1a*, *glr3.3a* and *glr3.6a* *A. thaliana* expressing *UBQ10::GCaMP3*. Data for *Col-0 A. thaliana* expressing *35S::iGluSnFR* ($n = 15$) or *35S::Apo-pHusion* ($n = 27$) were taken from their respective wound vs control experiments. Statistical significance levels, calculated using a Kruskal-Wallis rank-sum test followed by pairwise Wilcoxon rank-sum tests, are indicated by letters.

4.2.4. Wound-induced apo-pHusion and iGluSnFR signals are altered in *glr3.3a* mutants

To further test the relationship between wound-induced $[Ca^{2+}]$ elevations and putative elevations in apoplastic pH and [Glu], I wounded Col-0 and *glr3.3a* mutant *A. thaliana* expressing *35S::Apo-pHusion* or *35S::iGluSnFR*. Data from three independent repeats, each with multiple replicates, were combined before comparing signal properties between the genotypes with ANOVAs (Repeat + Genotype). Between Col-0 and *glr3.3a* samples, F0 values were not statistically different for iGluSnFR or apo-pHusion (Figure 4.6A, iGluSnFR: $F = 0.40$, $p = 0.53$; Figure 4.7A, apo-pHusion: GFP: $F = 0.045$, $p = 0.83$, RFP: $F = 2.40$, $p = 0.13$), nor were peak normalised $\Delta F/F_0$ values for iGluSnFR or peak normalised $\Delta R/R_0$ values for apo-pHusion (Figure 4.6B, C, iGluSnFR: $F = 3.11$, $p = 0.080$; Figure 4.7B, C apo-pHusion: $F = 0.65$, $p = 0.42$). However, normalised $\Delta F/F_0$ and $\Delta R/R_0$ traces did differ between the genotypes for iGluSnFR (Figure 4.6B) and apo-pHusion, respectively (Figure 4.7B). Specifically, the Col-0 normalised $\Delta F/F_0$ and $\Delta R/R_0$ traces smoothly decreased after the peak whilst the *glr3.3a* traces displayed a secondary curve. As such, at 12 min post-wounding, the normalised $\Delta F/F_0$ and $\Delta R/R_0$ values were significantly greater in *glr3.3a* than in Col-0 (Figure 4.6D, iGluSnFR: $F = 9.87$, $p = 0.0021$; Figure 4.7D, apo-pHusion: $F = 12.05$, $p = 0.00073$). These wound-induced *glr3.3a* reporter signal dynamics for iGluSnFR and apo-pHusion were similar to the burst and secondary reporter signal dynamics of wounded *glr3.3a UBQ10::GCaMP3* samples. For both iGluSnFR and apo-pHusion, wound-induced *glr3.3a* mutant signals had significantly greater propagation rates (Figure 4.6E, iGluSnFR: $F = 13.01$, $p = 0.00045$; Figure 4.7E, apo-pHusion: $F = 45.78$, $p \leq 0.0001$) and lower signal areas than the Col-0 signals (Figure 4.6F, iGluSnFR: $F = 7.30$, $p = 0.0079$; Figure 4.7F, $F = 22.99$, $p \leq 0.0001$). This is alike the *glr3.3a UBQ10::GCaMP3* burst reporter signals which, compared to Col-0 wave GCaMP3 signals, had reduced signal areas and faster propagation rates. Therefore, these data reveal that there are strong correlations between wound-induced reporter signals in Col-0 and *glr3.3a A. thaliana* for GCaMP3, iGluSnFR and apo-pHusion. The dynamics, areas, and propagation rates of the wound-induced iGluSnFR and apo-pHusion reporter signals indicate that this correlation is most clear for burst or wave GCaMP3 signals and less so for secondary GCaMP3 signals, though the correlation does still hold for the secondary GCaMP3 signals. The strong correlations between all the wound-induced reporter signals suggest that the $[Ca^{2+}]$ elevations could be linked to the putative apoplastic [Glu] or pH increases. With *glr3.3a* phenotypes present in iGluSnFR and apo-pHusion reporter signals, wound-induced apoplastic [Glu] or pH increases are unlikely to solely be upstream of GLR3.3-dependent $[Ca^{2+}]$ elevations but may be downstream of, or interact with, the $[Ca^{2+}]$ elevations. In any case, wounding *glr3.3a A. thaliana* expressing *35S::iGluSnFR* or *35S::Apo-pHusion* has provided

insights into the potential relationships between the putative wound-induced apoplastic pH and [Glu] increases and the wound-induced $[Ca^{2+}]$ elevations.

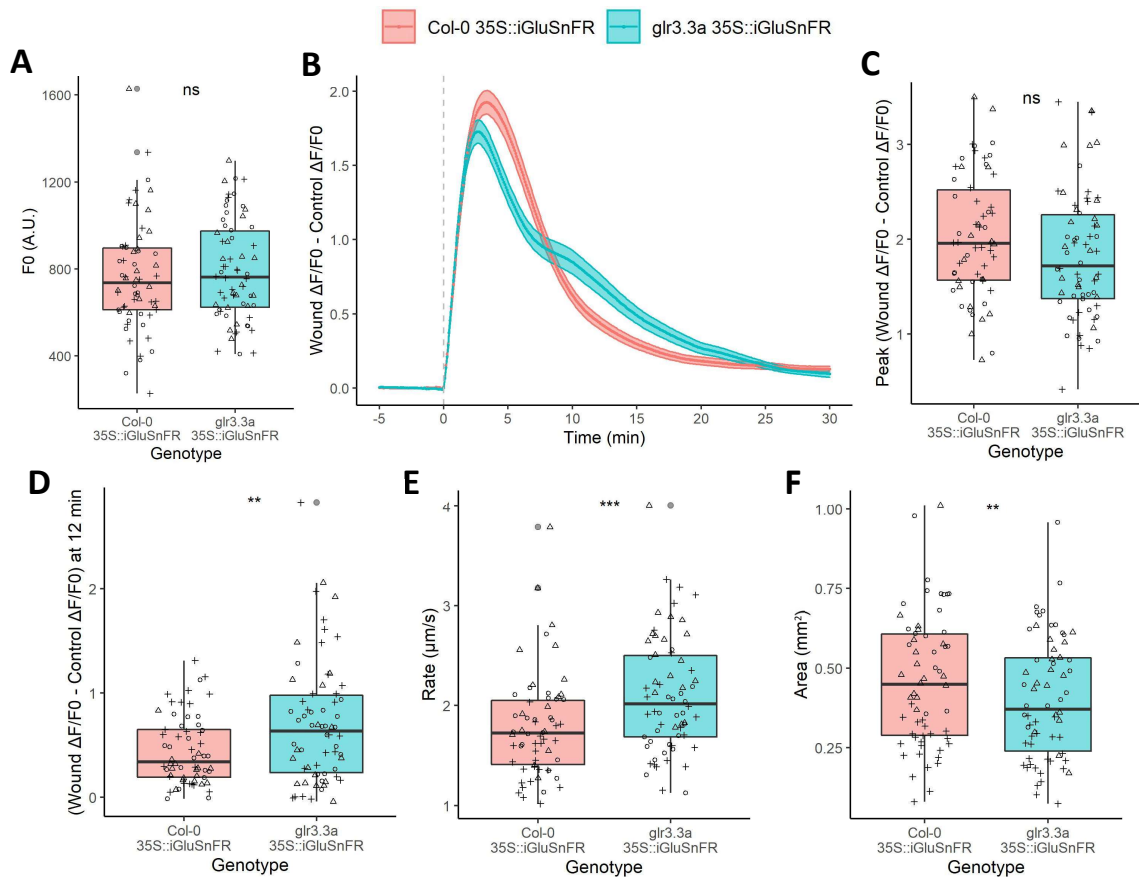


Figure 4.6 Wound-induced iGluSnFR signals are altered in *glr3.3a* mutants.

Comparisons of wound-induced reporter signals in Col-0 and *glr3.3a* mutant *A. thaliana* expressing *35S::iGluSnFR*. Background corrected fluorescence intensity (F , A.U.) values were calculated over the area of reporter signals and at comparable control sites. F values were transformed by $\Delta F/F_0$ with F_0 calculated as the mean F over the 5 min before wounding. (B) Traces for the mean \pm S.E.M. normalised $\Delta F/F_0$ values (Wound $\Delta F/F_0$ - Control $\Delta F/F_0$) over time with wounding at 0 min (grey dashed line). Boxplots for (A) F_0 values (A.U.), (C) peak normalised $\Delta F/F_0$ values (Wound $\Delta F/F_0$ - Control $\Delta F/F_0$) (D) normalised $\Delta F/F_0$ values (Wound $\Delta F/F_0$ - Control $\Delta F/F_0$) at 12 min post-wounding, (E) signal propagation rates ($\mu\text{m s}^{-1}$) and (F) signal areas (mm^2). Shapes indicate data points from each repeat (Repeat 1 (o): Col-0 $n = 21$, *glr3.3a* $n = 22$; Repeat 2 (Δ): Col-0 $n = 17$, *glr3.3a* $n = 19$; Repeat 3 (+): Col-0 $n = 24$, *glr3.3a* $n = 25$) and grey dots are associated with outliers. Statistical significance, calculated using an ANOVA (Repeat + Genotype) and a Tukey post hoc test, is shown for each boxplot by ns: $p > 0.05$, **: $p \leq 0.01$, ***: $p \leq 0.001$.

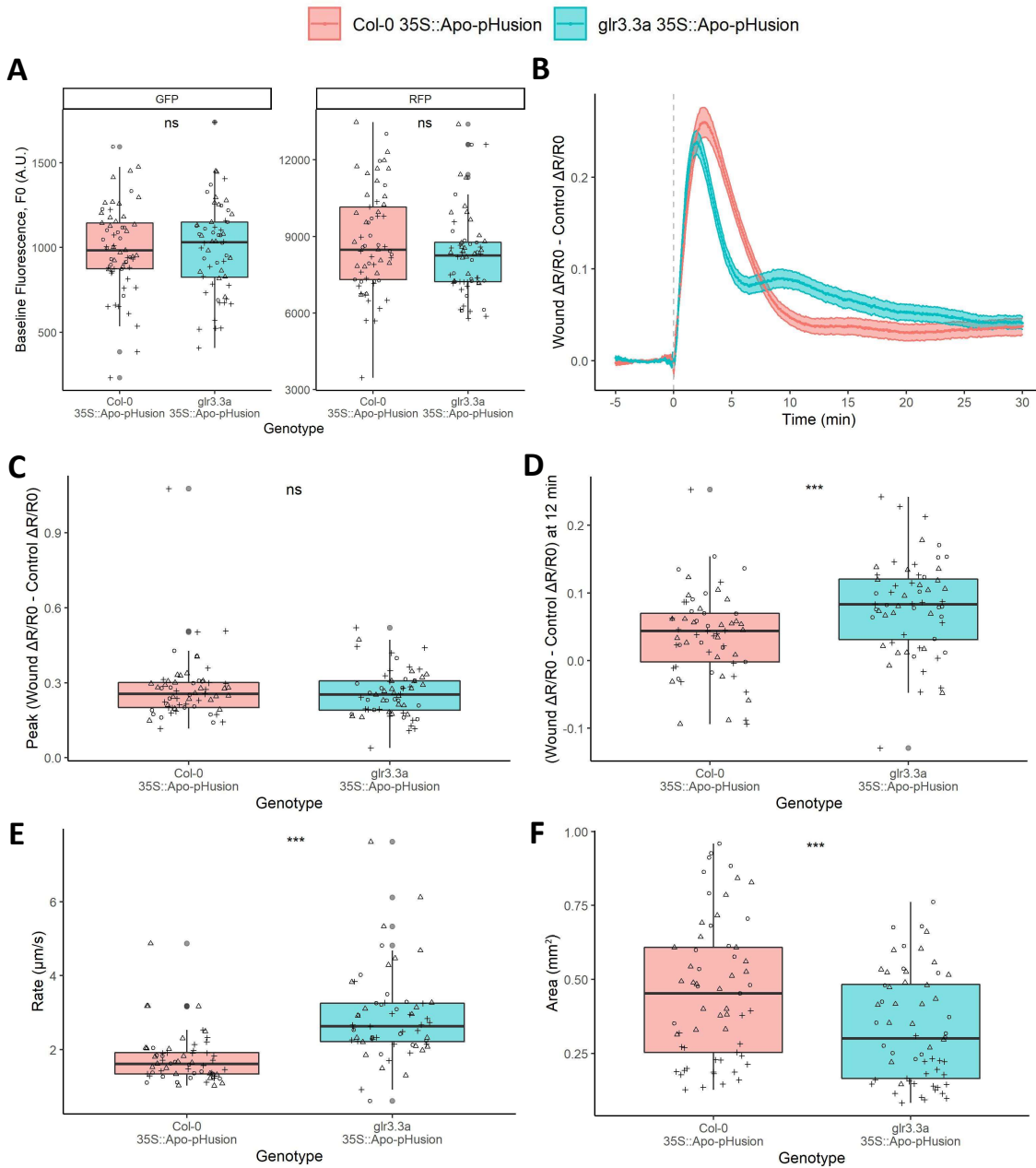


Figure 4.7 Wound-induced apo-pHusion signals are altered in *glr3.3a* mutants

Comparisons of wound-induced reporter signals in Col-0 and *glr3.3a* mutant *A. thaliana* expressing 35S::Apo-pHusion. Background corrected fluorescence intensity (F, A.U.) values were calculated for GFP and RFP across the area of reporter signals and at comparable control sites. F0 was the mean F over the 5 min prior to wounding. R values were the ratio of GFP/RFP F values and were transformed by $\Delta R/R0$ with R0 as the mean R over the 5 min prior to wounding. (B) Traces for the mean \pm S.E.M. normalised $\Delta R/R0$ values (Wound $\Delta R/R0$ - Control $\Delta R/R0$) over time with wounding at 0 min (grey dashed line). Boxplots for (A) F0 values (A.U.), (C) peak normalised $\Delta R/R0$ values (Wound $\Delta R/R0$ - Control $\Delta R/R0$), (D) normalised $\Delta R/R0$ values (Wound $\Delta R/R0$ - Control $\Delta R/R0$) at 12 min post-wounding, (E) signal propagation rates ($\mu\text{m s}^{-1}$) and (F) signal areas (mm^2). Shapes indicate data points from repeats (Repeat 1 (o): Col-0 $n = 16$, *glr3.3a* $n = 16$; Repeat 2 (Δ): Col-0 $n = 23$, *glr3.3a* $n = 21$; Repeat 3 (+): Col-0 $n = 22$, *glr3.3a* $n = 23$) and grey dots are associated with outliers. Statistical significance, calculated using an ANOVA on a linear model (Repeat + Genotype) and a Tukey test, are shown for each boxplot by ns: $p > 0.05$, ***: $p \leq 0.001$.

4.2.5. Wounding induces JA marker gene expression that shows partial dependency on GLR3.3

To examine if the localised wound-induced responses detected and GLR3.3 could contribute to plant defence responses, I first assessed wound-induced marker gene expression for several defence-related hormone signalling pathways. To do so with spatiotemporal resolution, I wounded 'expression reporter' *A. thaliana* lines which utilise promoters from JA (*pAOS*, *pJAZ10*), Et (*pACS6*, *pPR4*) and SA (*pPR1*) marker genes to drive the expression of a nuclear localised 3xVENUS FP (NLS-3xVENUS)(Marhavý *et al.*, 2019). The fluorescence intensity, *F*, at wound and control sites was monitored hourly over the 8 h post-wounding to calculate the change in *F*, ΔF , from 0 h. I then compared wound and control site ΔF values using ANOVAs (Repeat + Sample + Treatment). There were no differences between wound and control site ΔF values at 8 h post-wounding for *pACS6::NLS-3xVENUS* (Figure 4.8A, $F = 0.59$, $p = 0.45$), *pPR4::NLS-3xVENUS* (Figure 4.8B, $F = 1.91$, $p = 0.18$) or *pPR1::NLS-3xVENUS A. thaliana* (Figure 4.8C, $F = 0.30$, $p = 0.59$). However, ΔF values were significantly greater for wound sites than control sites at 8 h post-wounding for *pAOS::NLS-3xVENUS* (Figure 4.8D, $F = 210.84$, $p \leq 0.0001$) and *pJAZ10::NLS-3xVENUS A. thaliana* (Figure 4.8E, $F = 70.88$, $p \leq 0.0001$) with signals visible in 39/40 and 34/40 samples, respectively. All JA expression reporter signals were spatially restricted around wound sites with a mean area of $0.318 \pm 0.023 \text{ mm}^2$ for *pAOS::NLS-3xVENUS* (Figure 4.8D) and $0.367 \pm 0.023 \text{ mm}^2$ for *pJAZ10::NLS-3xVENUS* (Figure 4.8E). These reporter signals, therefore, fall within the mean area of 0.640 mm^2 for the wound-induced $[\text{Ca}^{2+}]$ elevations in Col-0 (Table 4.1). Thus, micropipette wounding induced the expression of JA marker genes but not SA or Et marker genes. The spatial patterns of the JA marker gene expression responses suggest that wound-induced $[\text{Ca}^{2+}]$ elevations, apoplastic alkalinisations and/or apoplastic [Glu] increases as well as GLR3.3 could promote JA marker gene expression.

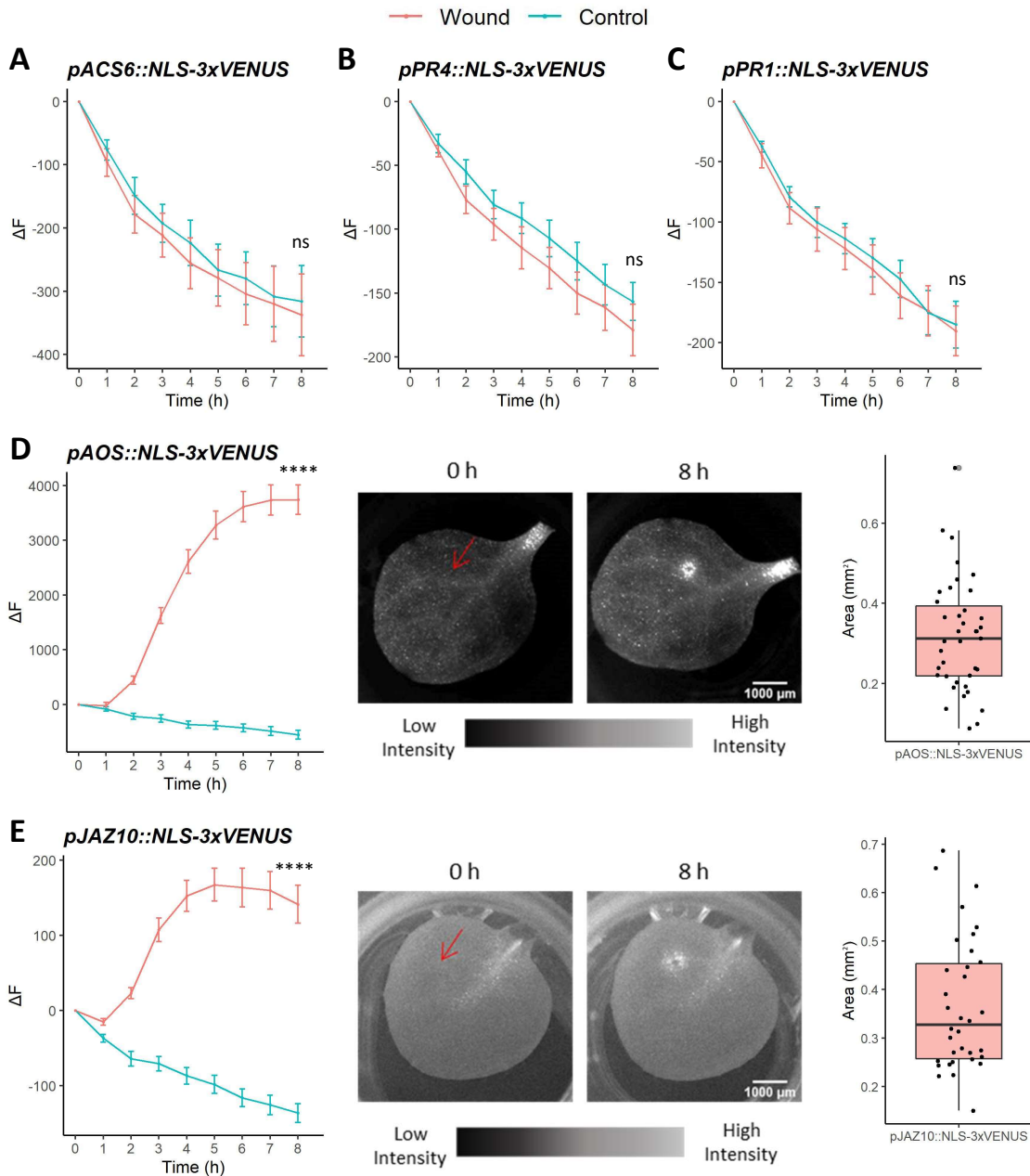


Figure 4.8 Wounding of *A. thaliana* induces JA, but not SA or Et, marker gene expression.

Wound-induced responses in Col-0 *A. thaliana* leaves containing the expression reporter transgenes of (A) *pACS6::NLS-3xVENUS*, (B) *pPR4::NLS-3xVENUS*, (C) *pPR1::NLS-3xVENUS* (D) *pAOS::NLS-3xVENUS* or (E) *pJAZ10::NLS-3xVENUS*. Fluorescence intensity (F, A.U.) was monitored across reporter signal areas or, in the absence of clear signals, around wound sites and at comparable control sites at hourly intervals from 0 h to 8 h. The change in F over time, ΔF , is shown in line graphs (mean \pm S.E.M.). For (D, E), this is accompanied by representative images of wound-induced responses at 8 h with red arrows marking the wound site at 0 h. Box plots display the signal area (mm²) for the (D) 39/40 and (E) 36/40 wound events that induced visible reporter signals. Statistical significance for all genotypes was assessed for the 8 h time point by ANOVAs on linear models (Repeat + Sample + Treatment) and is shown by ns: $p > 0.05$, ****: $p \leq 0.0001$. Sample sizes were $n = 44$ for *pACS6::NLS-3xVENUS* and $n = 40$ for all other expression reporter genotypes.

To assess if wound-induced JA marker gene expression was GLR3.3-dependent, I crossed *glr3.3a* mutants with Col-0 *A. thaliana* carrying the *pAOS::NLS-3xVENUS* or *pJAZ10::NLS-3xVENUS* transgenes to produce homozygous Col-0 and *glr3.3a* JA expression reporter lines. Col-0 and *glr3.3a* lines were chosen with statistically equal responses to mock and MeJA treatments (AOS: Figure 4.9A, Wilcoxon rank-sum, Mock: $W = 100$, $p = 0.45$, MeJA: $W = 87$, $p = 0.92$; JAZ10: Figure 4.10A, t-test, Mock: $t = 26.86$, $p = 0.44$, MeJA: $t = 23.23$, $p = 0.32$). These lines were then subjected to micropipette wounding and ΔF values were compared between the Col-0 and *glr3.3a* lines separately at wound and control sites at each time point using ANOVAs on linear models (Repeat + Position in Plate + Genotype). In *pAOS::NLS-3xVENUS*, ΔF values for Col-0 and *glr3.3a* mutant wound sites were only statistically different at 8 h post-wounding when the mutant ΔF was greater (Figure 4.9B, $F = 4.27$, $p = 0.041$). Additionally, the signal areas were not statistically different for Col-0 and *glr3.3a pAOS::NLS-3xVENUS* (Figure 4.9C, $F = 1.88$, $p = 0.17$). In contrast, wound-induced ΔF values were significantly reduced in *glr3.3a pJAZ10::NLS-3xVENUS A. thaliana* compared to Col-0 at all timepoints from 1 h post-wounding (Figure 4.10B, e.g. 4 h post wounding: $F = 14.48$, $p = 0.00020$). Furthermore, *glr3.3a pJAZ10::NLS-3xVENUS A. thaliana* displayed reduced signal areas compared to Col-0 (Figure 4.10C, $F = 8.79$, $p = 0.0035$). Therefore, *glr3.3a* mutants were impaired in wound induced *JAZ10* expression but not AOS expression. This suggests that GLR3.3 activity promotes some wound-induced JA-mediated gene expression and defence signalling.

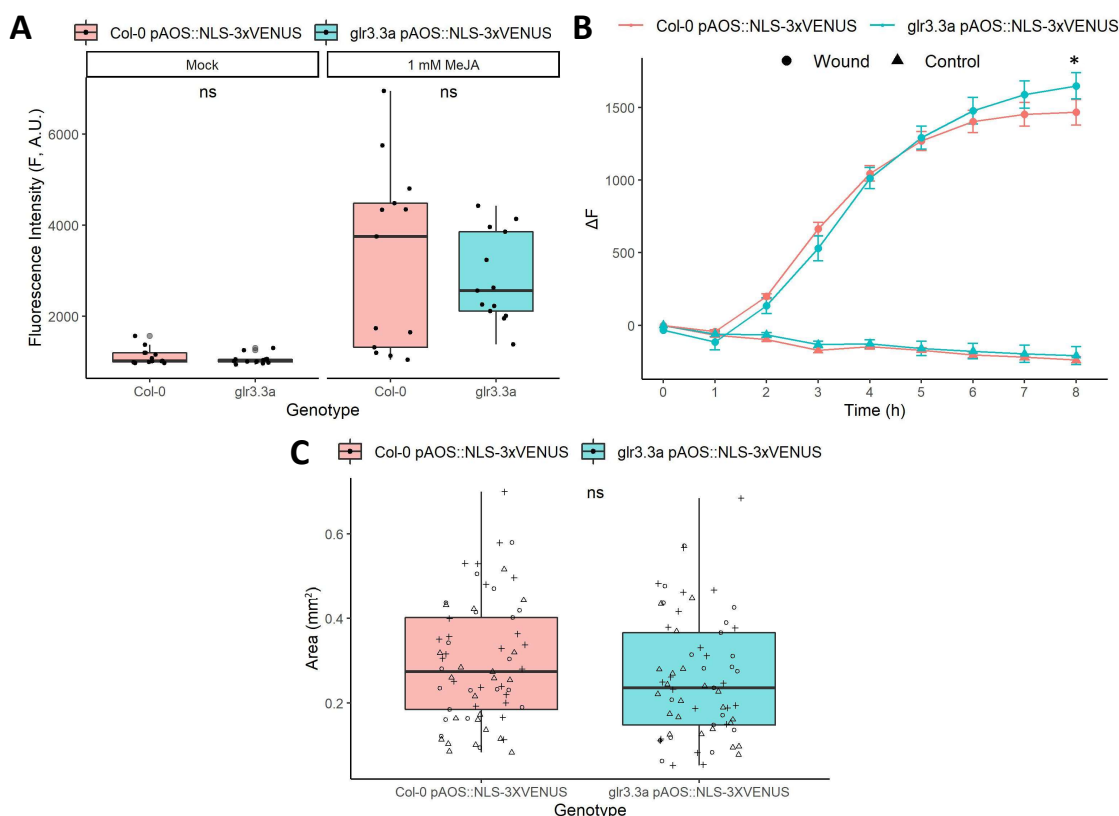


Figure 4.9 Developing and wounding *glr3.3a pAOS::NLS-3xVENUS A. thaliana* revealed that wound-induced AOS marker gene expression is not GLR3.3-dependent.

Col-0 and *glr3.3a pAOS::NLS-3xVENUS A. thaliana* expression reporter lines were subjected to treatments of (A) 1 mM methyl jasmonate (MeJA) or a mock solution and (B, C) micropipette wounding. (A) Boxplots of the mean fluorescence intensities (F, A.U.) across leaves in MeJA and mock-treated Col-0 and *glr3.3a* samples imaged 48 h after treatment. (B) Traces for the mean \pm S.E.M. change in fluorescence intensities over time, ΔF , over the area of wound-induced reporter signals and at comparable control sites for Col-0 and *glr3.3a* samples. (C) Boxplot of signal areas (mm^2) detected in response to wounding in Col-0 and *glr3.3a* samples with data points shown and different shapes representing samples from the three different repeats. Sample sizes were (A) $n = 13$ and (B, C) $n = 65$. Statistical analyses were (A) a Wilcoxon rank-sum test and (B, C) ANOVAs (Repeat + Position in Plate + Genotype). Statistical significance is shown by no symbol or ns: $p > 0.05$, *: $p \leq 0.05$.

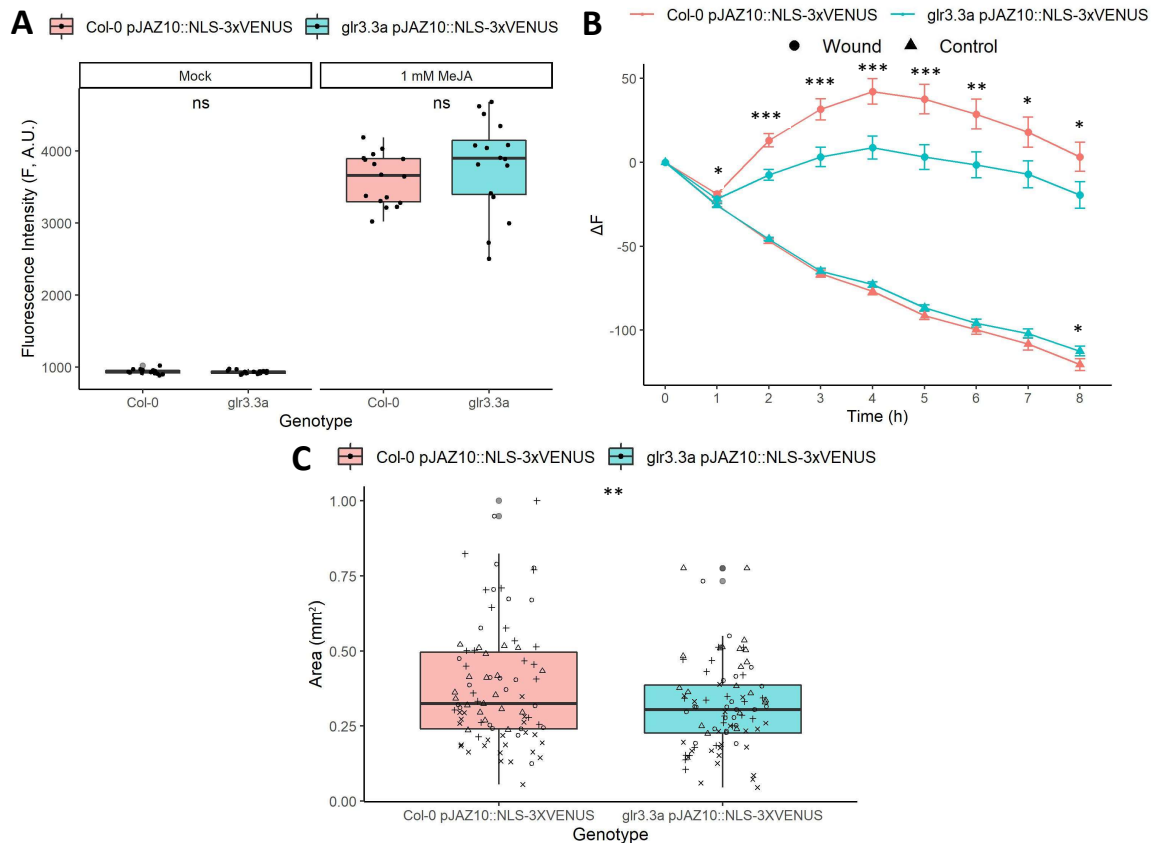


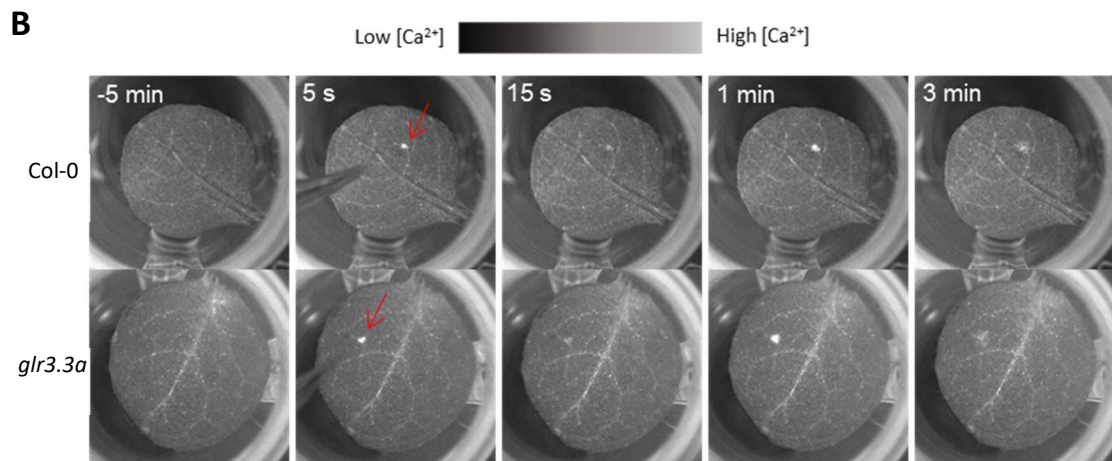
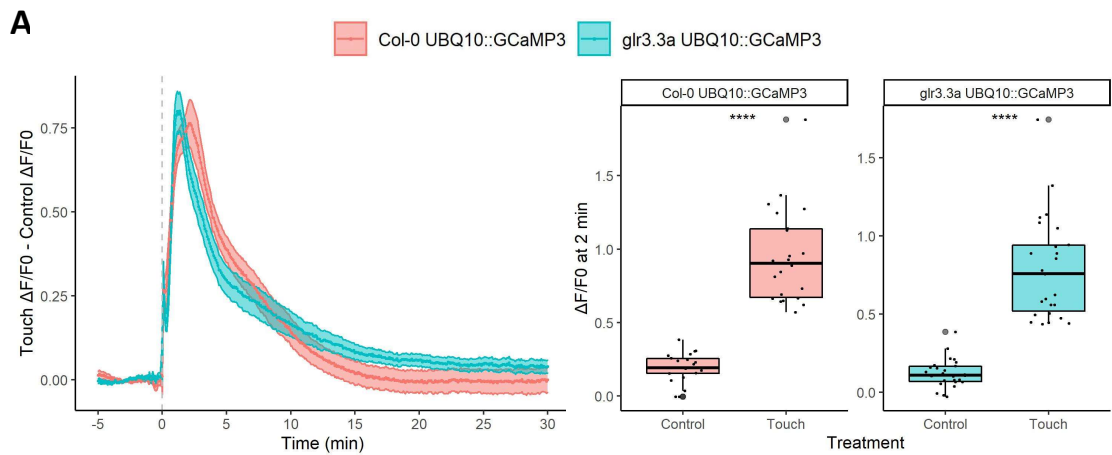
Figure 4.10 Developing and wounding *glr3.3a pJAZ10::NLS-3xVENUS A. thaliana* revealed that wound-induced *JAZ10* marker gene expression is reduced in *glr3.3a* mutants.

Col-0 and *glr3.3a pJAZ10::NLS-3xVENUS A. thaliana* expression reporter lines were subjected to treatments of (A) 1 mM methyl jasmonate (MeJA) or a mock solution and (B, C) micropipette wounding. (A) Boxplots of mean fluorescence intensities (F, A.U.) across leaves in MeJA and mock-treated Col-0 and *glr3.3a* samples imaged 48 h after treatment. (B) Traces for the mean \pm S.E.M. change in fluorescence intensities over time, ΔF , over the area of wound-induced reporter signals and at comparable control sites for Col-0 and *glr3.3a* samples. (C) Boxplot of signal areas (mm^2) detected in response to wounding in Col-0 and *glr3.3a* with datapoints shown and different shapes representing samples from the four different repeats. Grey dots are associated with outliers. Sample sizes were (A) $n = 16$ and (B, C) $n = 87$. Statistical analyses were (A) a t-test and (B, C) ANOVAs (Repeat + Position in Plate + Genotype). Statistical significance is shown by no symbol or ns: $p > 0.05$, *: $p \leq 0.05$, **: $p \leq 0.01$, ***: $p \leq 0.001$, ****: $p \leq 0.0001$.

4.2.6. Touch induces GLR3.3-independent [Ca²⁺] elevations similar to those induced by wounding in *glr3.3a* mutants

Mechanical stress perception could form an important part of GLR3.3-dependent or -independent responses to localised wounding or insect feeding. Therefore, I tested for touch induced GCaMP3 reporter signals and probed their dependency on GLR3.1/3.3/3.6. Firstly, I identified clear touch-induced elevations in normalised $\Delta F/F_0$ traces for Col-0 and *glr3.3a* *A. thaliana* expressing *UBQ10::GCaMP3* (Figure 4.11A, Video S4.5). There were significant differences between touch and control site $\Delta F/F_0$ values at 2 min post-touch for both genotypes (Figure 4.11A, Col-0: paired Wilcoxon signed rank, $V = 0$, $p \leq 0.0001$; *glr3.3a* paired Wilcoxon signed rank, $V = 0$, $p \leq 0.0001$). Both Col-0 and *glr3.3a* presented similar reporter signal dynamics (Figure 4.11A) and signal properties with the only statistical differences being in signal propagation rates (Figure 4.11C, Wilcoxon rank-sum, $W = 155$, $p = 0.0061$) and F_0 values (Figure 4.11C, Wilcoxon rank-sum, $W = 190$, $p = 0.047$). Comparing touch-induced reporter signals in Col-0 and *glr3.1a glr3.3a glr3.6a* *A. thaliana* expressing *UBQ10::GCaMP3* revealed similar normalised $\Delta F/F_0$ traces in both genotypes (Figure 4.12B) and no statistically significant differences in F_0 values (Figure 4.12A, Wilcoxon rank-sum, $W = 358$, $p = 0.25$), peak normalised $\Delta F/F_0$ values (Figure 4.12C, Wilcoxon rank-sum, $W = 282$, $p = 0.73$), signal areas (Figure 4.12D, Wilcoxon rank-sum, $W = 322$, $p = 0.67$) or signal propagation rates (Figure 4.12E, Wilcoxon rank-sum, $W = 313$, $p = 0.80$). Therefore, these data indicate that touch induces [Ca²⁺] elevations that appear to be GLR3.1/3.3/3.6-independent.

Interestingly, the Col-0 and *glr3.3a* mutant touch-induced GCaMP3 signals displayed initial burst signals before secondary signals (Figure 4.11A, B, Video S4.5), similar to the wound-induced *glr3.3a* GCaMP3 signals. However, compared to the wound-induced *glr3.3a* GCaMP3 signals (Section 4.2.1), touch-induced GCaMP3 signals had lower signal areas, lower burst signal areas and shorter burst durations with no or limited burst signal propagation from the touch sites (Figure 4.11C). Taken together, these data suggest that the touch-induced GCaMP3 signals represented lower magnitude versions of the GLR3.3-independent wound-induced GCaMP3 signals. Therefore, the regulation of touch- and wound-induced [Ca²⁺] elevations may involve shared mechanisms of mechanical stress perception.



C

Genotype	F0 (A.U.)	Peak Normalised $\Delta F/F_0$					Sample size
		(Wound $\Delta F/F_0$ - Control $\Delta F/F_0$)	Signal Rate ($\mu m/s$)	Signal Area (mm^2)	Burst Area (mm^2)	Burst Duration (s)	
Col-0	540 ± 23	0.90 ± 0.08	0.93 ± 0.05	0.132 ± 0.015	0.023 ± 0.005	23.63 ± 3.14	22
<i>glr3.3a</i>	$707 \pm 62^*$	0.89 ± 0.07	$1.27 \pm 0.10^{**}$	0.104 ± 0.017	0.015 ± 0.002	19.42 ± 0.93	26

Figure 4.11 Touch induces GCaMP3 signals with burst and secondary signal dynamics that appear GLR3.3-independent.

Analysis of touch-induced GCaMP3 signals in Col-0 and *glr3.3a A. thaliana* expressing UBQ10::GCaMP3. Background corrected fluorescence intensities (F, A.U.) were measured over the area of touch-induced reporter signals and at comparable control sites. F values were transformed by $\Delta F/F_0$ with F0 being the mean F over the 5 min before touch treatment. (A) Traces for the mean \pm S.E.M. normalised $\Delta F/F_0$ values (Touch $\Delta F/F_0$ - Control $\Delta F/F_0$) over time with touch occurring at 0 min (grey dashed line). Presented alongside boxplots for Col-0 and *glr3.3a* touch and control site $\Delta F/F_0$ values at 2 min post-touch with grey dots associated with outliers. (B) Time series images from representative touch-treated samples of Col-0 and *glr3.3a A. thaliana*. Red arrows indicate touch sites. (C) Properties of signals detected in Col-0 and *glr3.3a* samples for the initial rapid GCaMP3 signals ('Burst') and the overall properties of the burst and secondary signals ('Signal'). Sample sizes were Col-0: $n = 22$ and *glr3.3a* $n = 26$. Statistical significance is indicated by no symbol: $p > 0.05$, *: $p \leq 0.05$, **: $p \leq 0.01$, ****: $p \leq 0.0001$. Statistical analyses were (A) a paired Wilcoxon signed rank test and (C) Wilcoxon rank-sum tests or t-tests.

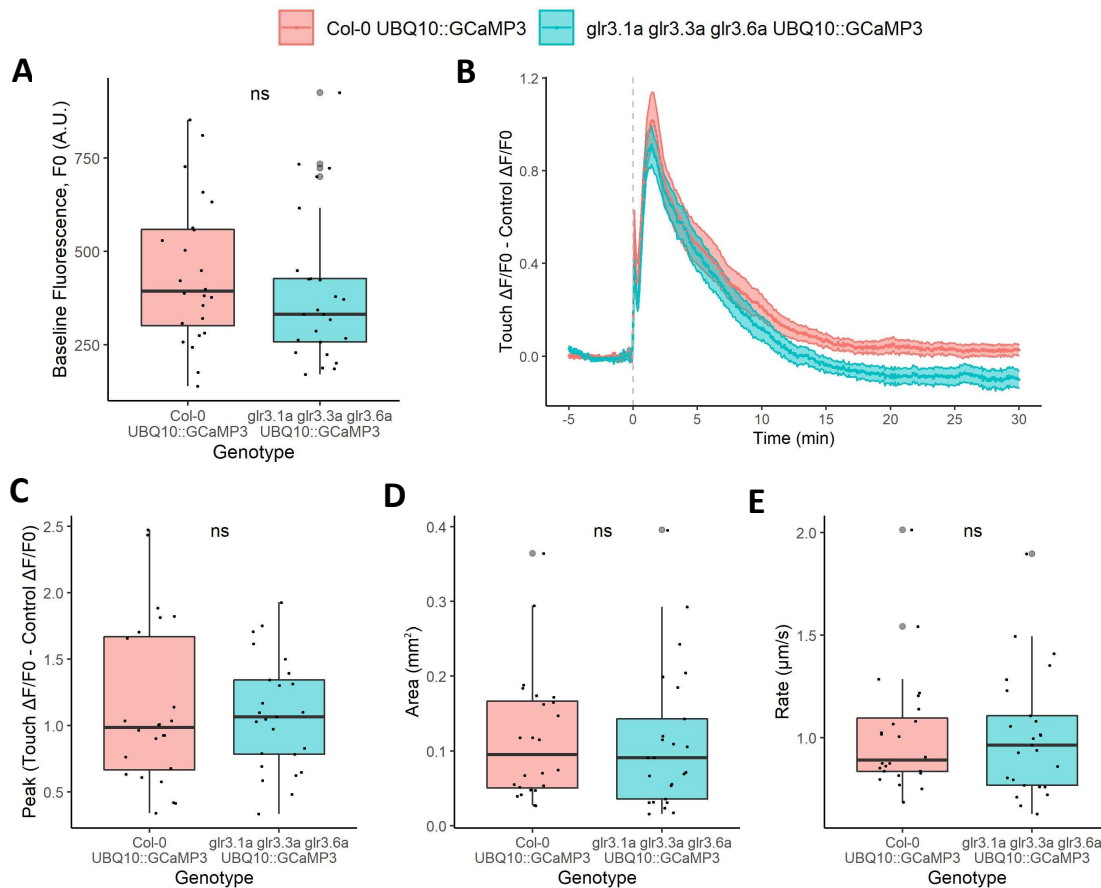


Figure 4.12 Touch-induced GCaMP3 signals in *A. thaliana* leaves are unaltered in the *glr3.1a glr3.3a glr3.6a* mutant.

Properties of touch-induced GCaMP3 signals in Col-0 and *glr3.1a glr3.3a glr3.6a* *A. thaliana* expressing *UBQ10::GCaMP3*. Background corrected fluorescence intensities (F , A.U.) were recorded over the area of reporter signals and at comparable control sites. F values were transformed by $\Delta F/F_0$ with F_0 being the mean F over the 5 min before touch treatment. (B) Traces for the mean \pm S.E.M. normalised $\Delta F/F_0$ (Touch $\Delta F/F_0$ - Control $\Delta F/F_0$) over time with touch occurring at 0 min (grey dashed line). Boxplots show the (A) F_0 values (A.U.) (C) peak normalised $\Delta F/F_0$ values (Touch $\Delta F/F_0$ - Control $\Delta F/F_0$), (D) signal areas (mm^2) and (E) signal propagation rates ($\mu\text{m s}^{-1}$), with grey dots associated with outliers. Sample sizes are Col-0 $n = 24$ and *glr3.3a* $n = 25$. Statistical significance, calculated using Wilcoxon rank-sum tests, is shown by ns: $p > 0.05$.

4.2.7. Touch can induce iGluSnFR and apo-pHusion signals that are associated with the touch-induced GCaMP3 signals

To explore the mechanisms of touch-induced $[Ca^{2+}]$ elevations and their relationship to wound-induced GLR3.3-dependent responses, I investigated whether touch could induce *35S::iGluSnFR* or *35S::Apo-pHusion* *A. thaliana* reporter signals. For both reporter lines, samples were grouped as those with visually clear touch-induced reporter signals ('signal' samples) and those without ('no signal' samples). These groups were analysed separately alongside a group for all samples ('all (samples)'). In the signal group, there were 15/30 samples for iGluSnFR and 9/38 samples for apo-pHusion. Touch-induced normalised $\Delta F/F_0$ elevations were present in the iGluSnFR signal samples group and all samples group but not in the no signal samples group (Figure 4.13A, C). This was reflected in statistically greater touch site $\Delta F/F_0$ values compared to control sites at 2 min post-touch for the all samples group (Figure 4.13B, paired Wilcoxon signed rank, $V = 429$, $p \leq 0.0001$) and the signal samples group (Figure 4.13B, paired Wilcoxon signed rank, $V = 119$, $p = 0.00012$) but not for the no signal samples group (Figure 4.13B, paired Wilcoxon signed rank, $V = 94$, $p = 0.055$). The iGluSnFR signals detected propagated at a mean rate of $1.35 \pm 0.12 \mu m s^{-1}$ to a mean area of $0.053 \pm 0.009 mm^2$. This same pattern was detected for touch-induced apo-pHusion responses with normalised $\Delta R/R_0$ elevations detected in the signal samples group but not in the no signal samples group (Figure 4.14A). Comparing touch and control site $\Delta R/R_0$ values at 5 min post-touch revealed statistically greater values at touch sites for the all samples group (Figure 4.14B, paired Wilcoxon signed rank, $V = 128$, $p = 0.00024$) and the signal samples group (Figure 4.14B, paired Wilcoxon signed rank, $V = 0$, $p = 0.0020$) but not for the no signal samples group (Figure 4.14B, paired Wilcoxon signed rank, $V = 127$, $p = 0.086$). The apo-pHusion signals detected propagated at a mean rate of $1.24 \pm 0.16 \mu m s^{-1}$ to a mean area of $0.046 \pm 0.006 mm^2$. In summary, touch treatment induced detectable apo-pHusion and iGluSnFR signals in some samples but not all samples.

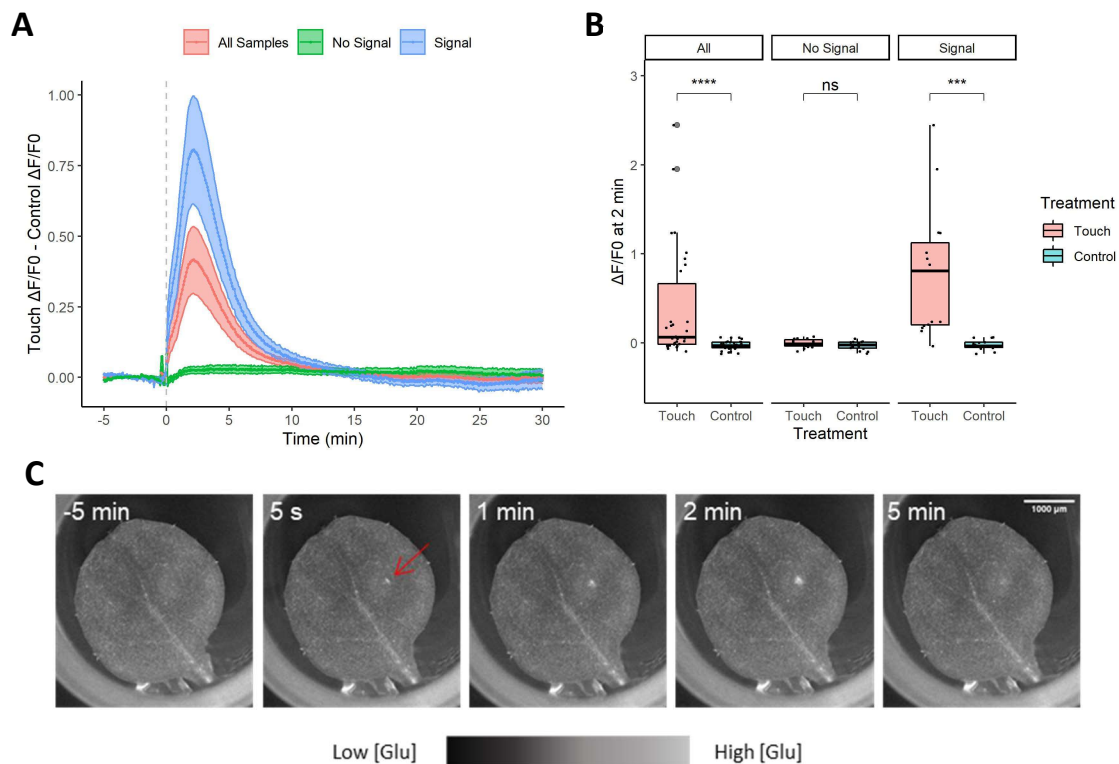


Figure 4.13 Touch can induce detectable iGluSnFR reporter signals in *A. thaliana* leaves.

Analysis of touch treated and control sites in Col-0 *A. thaliana* expressing *35S::iGluSnFR*. Background corrected fluorescence intensity (F, A.U.) values were measured over the area of reporter signals or, in the absence of clear reporter signals, around touch sites and at comparable control sites. F values were transformed by $\Delta F/F_0$ with F_0 being the mean F over the 5 min before touch treatment. Samples were analysed all together ('All (Samples)') and in subgroups of those with clear signals ('Signal') and those without clear reporter signals ('No Signal'). (A) Traces for the mean \pm S.E.M. normalised $\Delta F/F_0$ values (Touch $\Delta F/F_0$ - Control $\Delta F/F_0$) over time for the three groups with touch occurring at 0 min (grey dashed line). (B) Boxplots of $\Delta F/F_0$ values at 2 min post-touch for touch and control sites in each of the groups with grey dots associated with outliers. Statistical significance, assessed by paired Wilcoxon signed rank tests, shown by ns: $p \geq 0.05$, ***: $p \leq 0.001$, ****: $p \leq 0.0001$. (C) Time series images of a touch-induced iGluSnFR reporter signal in a representative 'Signal' sample with a red arrow indicating the touch site. Sample sizes were 'All Samples': $n = 30$, 'Signal': $n = 15$, 'No Signal': $n = 15$.

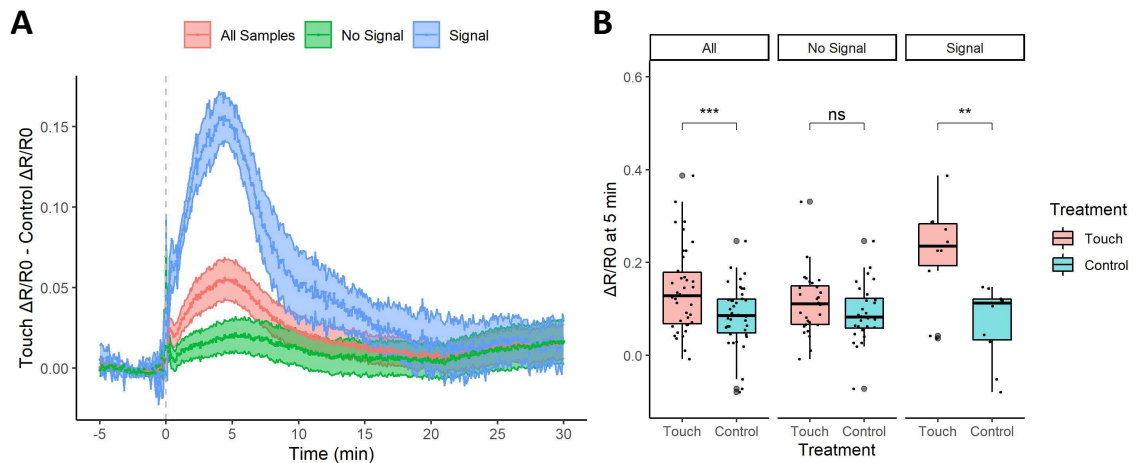


Figure 4.14 Touch can induce detectable apo-pHusion reporter signals in *A. thaliana* leaves.

Analysis of touch treated and control sites in Col-0 *A. thaliana* expressing 35S::Apo-pHusion. Background corrected fluorescence intensity (F, A.U.) values were measured for GFP and RFP over the area of reporter signals or, in the absence of clear reporter signals, around touch sites and at comparable control sites. The GFP/RFP ratios, R, were calculated from F values and transformed by $\Delta R/R_0$ with R_0 being the mean R value over the 5 min prior to wounding. Samples were analysed all together ('All (Samples)') and in subgroups of those with clear signals ('Signal') and those without clear reporter signals ('No Signal'). (A) Traces for the mean \pm S.E.M. normalised $\Delta R/R_0$ values (Touch $\Delta R/R_0$ - Control $\Delta R/R_0$) over time for the three groups with touch occurring at 0 min (grey dashed line). (B) Boxplots of $\Delta R/R_0$ values at 5 min post-touch for touch and control sites in each of the groups with grey dots associated with outliers. Statistical significance, assessed by paired Wilcoxon signed rank tests, shown by ns: $p \geq 0.05$, **: $p \leq 0.01$, ***: $p \leq 0.001$. Sample sizes were 'All Samples': $n = 38$, 'Signal': $n = 9$, 'No Signal': $n = 29$.

For wound-induced responses, data indicated that the iGluSnFR, apo-pHusion and GCaMP3 signals may be linked. Therefore, I assessed for correlations between touch-induced responses across these reporters. Firstly, visual touch-induced apo-pHusion and iGluSnFR signals were not always present whilst GCaMP3 signals were. Moreover, touch-induced GCaMP3 signals had larger areas than the signals in the other reporters (Figure 4.15A, Wilcoxon rank-sum after Kruskal-Wallis, $p \leq 0.001$), reached their peaks earlier (Figure 4.15B, Wilcoxon rank-sum after Kruskal-Wallis, iGluSnFR: $p = 0.040$; apo-pHusion: $p \leq 0.0001$) and had slower signal propagation rates (Figure 4.15C, Wilcoxon rank-sum after Kruskal-Wallis, iGluSnFR: $p = 0.0066$; apo-pHusion: $p = 0.021$). Whilst all the touch-induced reporter signals were approximately spatiotemporally associated, these data suggest that the touch-induced apo-pHusion and iGluSnFR signals were only weakly correlated with the GCaMP3 signals. However, support for the correlation being maintained comes from the touch-induced signals in all the reporters being of a lower amplitude and area than the signals induced by wounding. Additionally, the touch-induced apo-pHusion signals displayed an initial increase before a plateau and secondary signalling (Figure 4.14A), similar to the burst and secondary GCaMP3 signals induced by touch. Differences in the properties of the three different reporters likely contributed to some of the differences detected for the touch-induced reporter signal properties. Therefore, data here appears consistent with touch inducing spatiotemporally associated GCaMP3, apo-pHusion and iGluSnFR signals suggesting that touch-induced apoplastic [Glu] or pH increases could be linked with the $[Ca^{2+}]$ elevations.

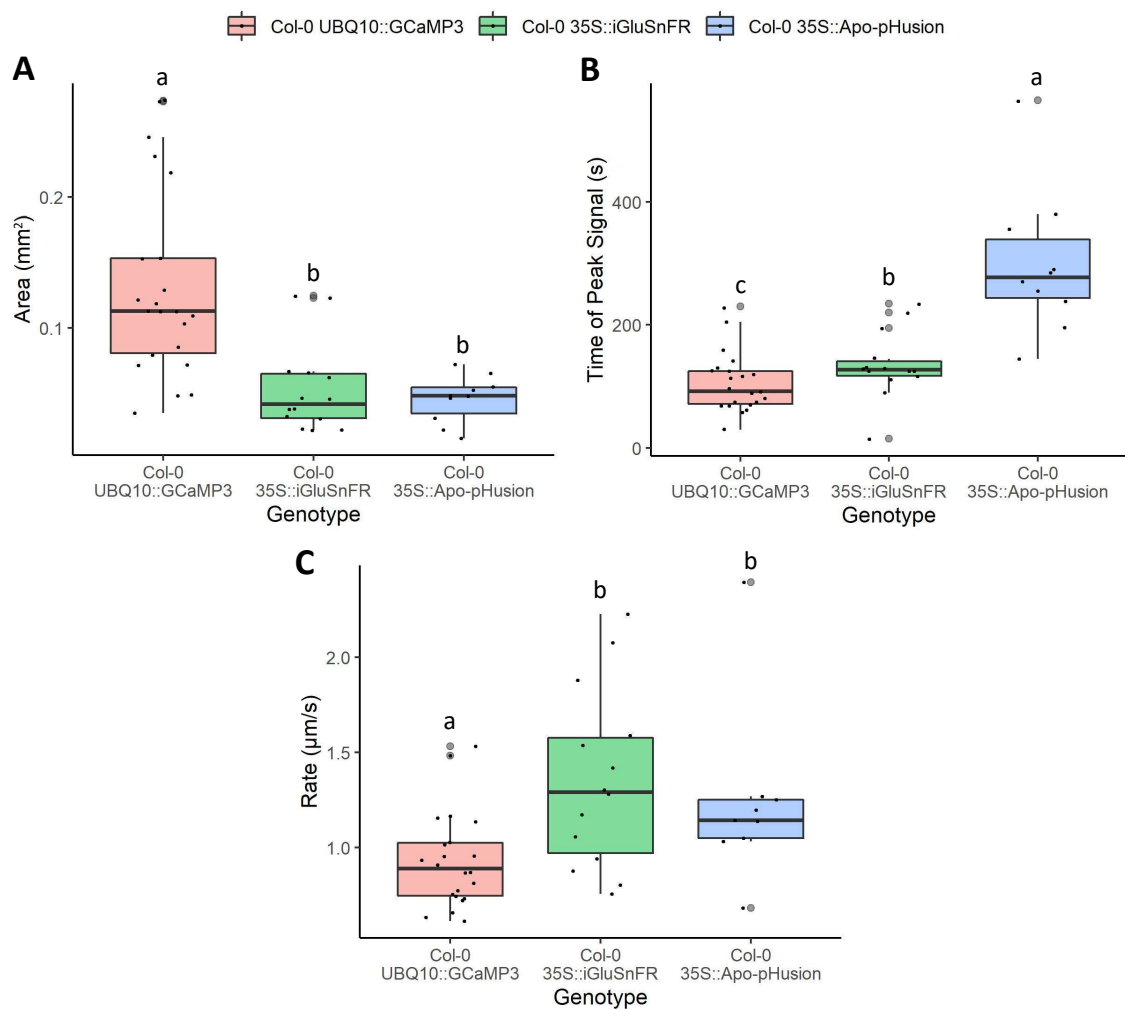


Figure 4.15 Comparisons of touch-induced reporter signal properties in Col-0 *A. thaliana* expressing *UBQ10::GCaMP3*, *35S::iGluSnFR* or *35S::Apo-pHusion*.

Comparisons of properties for touch-induced signals in Col-0 *UBQ10::GCaMP3*, *35S::iGluSnFR* and *35S::Apo-pHusion*. Boxplots for the (A) signal areas (mm²), (B) time of the peak normalised $\Delta F/F_0$ values post-touch (s) and (C) signal propagation rates (μm s⁻¹) are shown with grey dots associated with outlier data points. Data for Col-0 *UBQ10::GCaMP3* ($n = 22$) were taken from the comparison of Col-0 and *glr3.3a UBQ10::GCaMP3* touch-induced reporter signals. Data for Col-0 *35S::iGluSnFR* ($n = 15$) and *35S::Apo-pHusion* ($n = 9$) were taken from their respective touch vs control experiments. Statistical significance levels, calculated using a Kruskal-Wallis rank-sum test followed by pairwise Wilcoxon rank-sum tests, are indicated by letters.

4.2.8. Localised touch treatment does not induce *JAZ10* or *AOS* expression

Though touch does not trigger GLR3.3-dependent $[Ca^{2+}]$ elevations, mechanical stress perception could still contribute to any JA-mediated responses induced by localised wounding or insect feeding. Therefore, I tested if touch treatment induces signals in the expression reporter lines of *pAOS::NLS3x-VENUS* and *pJAZ10::NLS-3xVENUS* *A. thaliana*. Fluorescence intensity, *F*, was monitored at touch and control sites at hourly intervals over the 8 h after treatment to calculate change in fluorescence from the 0 h time point (ΔF). ΔF values were not statistically different between touch and control sites for either line as demonstrated at 8 h post-touch for *pAOS::NLS-3xVENUS* (Figure 4.16A, ANOVA on linear models (Repeat + Sample), $F = 2.02$, $p = 0.16$) and for *pJAZ10::NLS-3xVENUS* (Figure 4.16B, ANOVA on linear models (Repeat + Sample), $F = 1.51$, $p = 0.23$). Therefore, touch did not appear to induce *JAZ10* or *AOS* expression suggesting that touch perception does not contribute to this element of the wound response and that this touch perception is unlikely to contribute to any JA-mediated responses to localised insect feeding.

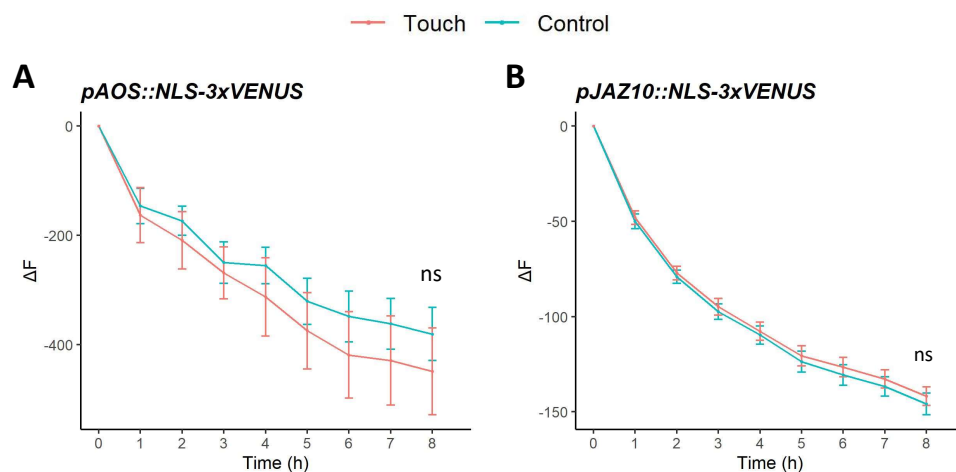


Figure 4.16 Touch treatment does not induce *AOS* or *JAZ10* marker gene expression within 8 h of treatment.

Assessment for touch-induced expression reporter signals in Col-0 *A. thaliana* carrying the (A) *pAOS::NLS-3xVENUS* or (B) *pJAZ10::NLS-3xVENUS* transgenes. Change in fluorescence intensity (A.U.), ΔF , was monitored around the touch site and at comparable control sites at hourly intervals for 8 h post-touch which occurred at 0 h. Data represent mean \pm S.E.M. for $n = 44$. Statistical significance, assessed with one-way ANOVAs on linear models (repeat + sample + treatment), shown by ns: $p > 0.05$.

4.3. Discussion

Here, I explored *A. thaliana* responses to localised wounding and touch stimuli and the contributions of GLR3.1/3.3/3.6 to these responses. These investigations aimed to provide insights into how the perception of damage or mechanical stress could function during aphid or thrips feeding and contribute to the activation of GLRs.

Wound events induced a highly localised $[Ca^{2+}]$ increase, termed the 'burst' here, that developed into a radially propagating $[Ca^{2+}]$ wave dependent on GLR3.3 but not GLR3.1 or GLR3.6. In the absence of GLR3.3, this burst remained spatiotemporally restricted before being replaced by secondary $[Ca^{2+}]$ elevations. Though secondary $[Ca^{2+}]$ elevations may have been present in wild-type wound responses, they appeared to be suppressed by the presence of GLR3.3. Wounding also induced iGluSnFR reporter signals and apo-pHusion reporter signals that were spatiotemporally associated with all the $[Ca^{2+}]$ elevations. The presence of correlated iGluSnFR and GLR3.3-dependent GCaMP3 signals in responses to localised wounding has also been reported in cotyledons adding support to the results identified here in *A. thaliana* leaves (Bellandi *et al.*, 2022). Finally, wound-induced increases in JA marker gene expression were spatially associated with the apo-pHusion, iGluSnFR and GCaMP3 reporter signals and showed partial GLR3.3-dependency. Therefore, wound induced responses included $[Ca^{2+}]$ elevations, apoplastic alkalinisations and JA marker gene expression increases which were all spatially correlated and partially dependent on GLR3.3 suggesting that they function in the same response mechanism.

Touch stimuli only induced GLR3.1/3.3/3.6-independent $[Ca^{2+}]$ elevations with burst and secondary elevation dynamics. The touch-induced burst and secondary $[Ca^{2+}]$ elevations were similar to the wound-induced GLR3.3-independent responses but were of a smaller area and had shorter durations. These findings suggest a shared response mechanism for touch and wounding that involves mechanical stress perception and responses that correlate with the degree of mechanical stress experienced. Touch also induced limited iGluSnFR and apo-pHusion reporter signals that correlated with the $[Ca^{2+}]$ elevations suggesting a link between these touch-induced responses. However, touch did not induce the expression of the selected JA marker genes. Therefore, the touch stimuli appeared not to activate GLR3.3-dependent responses.

The following will discuss major questions related to localised touch and wound perception and the contributions of GLR3.3. Then, I will propose a model by which mechanical stress perception and apoplastic alkalinisations could operate in wound and touch perception and determine GLR3.3 activation. This model and the findings of this chapter will form the

foundations for the next chapter investigating how damage or mechanical stress perception and GLR3.3 could contribute to the perception of localised insect feeding from aphids or thrips.

4.3.1. How could mechanical stress trigger burst $[Ca^{2+}]$ elevations?

The first responses detected to localised touch and wounding were the highly localised and short-lived burst $[Ca^{2+}]$ elevations that correlated with apoplastic alkalinisations. As these bursts are present in touch responses, they are likely a result of mechanical stress. Potential mechanisms for mechanical stress-induced burst $[Ca^{2+}]$ and apoplastic pH elevations in wound and touch responses will be explored here.

There are several ways in which mechanical stress perception could trigger burst $[Ca^{2+}]$ and apoplastic pH elevations in wound or touch responses and these could involve the perception of cell pressure changes. Similarly to laser ablation in roots, micropipette wounding bursts one or a few cells (Bellandi, 2021). Such laser ablation causes root cell collapse and pressure shocks in neighbouring cells as they rapidly bulge outwards (Hoermayer *et al.*, 2020). These pressure shocks are perceived by root cells, which also display propagating $[Ca^{2+}]$ elevations (Marhavý *et al.*, 2019), and appear to regulate regenerative cell divisions (Hoermayer *et al.*, 2020) and PAMP receptor expression (Zhou *et al.*, 2020). As such, wounding in leaves may cause burst $[Ca^{2+}]$ elevations in closely neighbouring cells that directly perceive pressure shocks as mechanical stress. As the touch needle is much broader than the wound needle and is unlikely to burst cells or penetrate the leaf cuticle, any pressure changes would be less severe than in wound responses and restricted to fewer cells. This may explain why touch-induced burst $[Ca^{2+}]$ and apoplastic pH elevations here were more spatially restricted and of a lower amplitude than those induced by wounding in *glr3.3a* mutants. In summary, mechanical stress perception with wounding and touch likely initiates burst $[Ca^{2+}]$ and apoplastic pH elevations and this perception may result from cell pressure changes.

There are many candidate molecular components that could function as receptors in the active perception of touch- or wound-induced mechanical stresses. Any machinery must rapidly facilitate the initial burst events of $[Ca^{2+}]$ elevations and/or apoplastic alkalinisations or be upstream of at least one of these responses. Candidates include mechanosensitive ion channels, such as MSLs, MCAs or PIEZO1, and components that perceive cell wall properties, such as FERONIA which contributes to root touch-induced $[Ca^{2+}]$ elevations (Shih *et al.*, 2014; Hamant and Haswell, 2017). Interestingly, FERONIA promotes the $[Ca^{2+}]$ -dependent suppression of H^+ -ATPase activity which drives apoplastic alkalinisations in responses to some RALFs (Gjetting *et al.*, 2020). Additionally, AHA1 has been implicated in GLR3.3/3.6-dependent responses to large-scale wounding with a hypothesised role in apoplastic alkalinisations following $[Ca^{2+}]$ -dependent

suppression of its activity (Shao *et al.*, 2020; Moe-Lange *et al.*, 2021; Kumari *et al.*, 2019). Therefore, it may be that bursts begin with a mechanical stress-induced receptor-mediated rapid $[Ca^{2+}]$ elevation that suppresses the activity of a H^+ -ATPase to induce apoplastic alkalinisations. Uncovering components involved in burst $[Ca^{2+}]$ and apoplastic pH elevations will be significant in appreciating the responses to touch and wounding.

Passive mechanisms could also underpin burst responses to wounding or touch. In laser ablation of *Drosophila melanogaster* epithelial cells, neighbouring cells experience cavitation-induced microtears allowing Ca^{2+} influx into cells. The resulting $[Ca^{2+}]$ elevations recapitulate the burst elevations in *A. thaliana* as they are rapid, spatially restricted to closely associated cells, shrink after 40 – 200 s and are replaced by secondary $[Ca^{2+}]$ elevations (Shannon *et al.*, 2017). Furthermore, larger-scale cavitation produces $[Ca^{2+}]$ elevations with a greater area alike how wound-induced burst $[Ca^{2+}]$ elevations in *glr3.3a* mutants were larger than those induced by touch. It is unknown whether similar microtears could occur in *A. thaliana* following localised wounding, especially with cell walls restricting any cell expansion. Interestingly, the rapid burst-like $[Ca^{2+}]$ elevations in *D. melanogaster* propagated via gap junctions (Shannon *et al.*, 2017). Whilst plasmodesmata do not contribute to the propagation of GLR3.3-dependent wave $[Ca^{2+}]$ elevations in cotyledons (Bellandi *et al.*, 2022), it is not known whether they are significant in burst $[Ca^{2+}]$ elevations. Moreover, passive responses to mechanical stress could alter apoplastic pH or responses upstream of the $[Ca^{2+}]$ elevations. Therefore, the burst $[Ca^{2+}]$ and apoplastic pH elevations induced by wounding and touch may result from passive processes rather than the active perception of mechanical stress.

In summary, touch- and wound-induced burst responses could result from active or passive mechanical stress perception mechanisms. In any case, a model in which mechanical stress causes burst $[Ca^{2+}]$ and apoplastic pH elevations following touch- or wound-induced pressure changes fits well with the findings here. Better characterising the cellular changes induced by localised touch and wounding will help appreciate how burst responses are initiated and how they could contribute to localised insect feeding-induced responses.

4.3.2. How is GLR3.3 permeability regulated in localised wound-induced responses?

Burst $[Ca^{2+}]$ elevations appeared to grow into GLR3.3-dependent $[Ca^{2+}]$ waves in wound responses but not touch responses. Identifying what determines the GLR3.3 activation in these localised responses will be key to appreciating GLR3.3 function in responses to localised insect feeding. Here, the potential for Glu/GLR agonists and pH to regulate GLR3.3 in localised wound-induced responses will be considered.

Glu and GLR ligands are candidates for localised wound-induced GLR3.3 activation as wound-induced GLR3.3-dependent $[Ca^{2+}]$ elevations correlated with iGluSnFR signals here. Moreover, $[Ca^{2+}]$ elevations and iGluSnFR signals are closely correlated in localised wound-induced responses in cotyledons and in trichome touch-induced responses (Bellandi *et al.*, 2022). These data have led to the hypothesis that localised wounding induces passive elevations of apoplastic [Glu] as a DAMP which spreads locally by diffusion to activate GLR3.3 (Bellandi *et al.*, 2022). However, as localised wound-induced iGluSnFR signals were perturbed in *glr3.3a* mutants, data here indicates that passive [Glu] release does not solely precede GLR3.3 activation. Recently, Grenzi *et al.* (2023) reported that *glr3.3* mutants also display altered systemic iGluSnFR signals following the hypo-osmotic stress of roots. Therefore, GLR3.3 activation may contribute to the regulation of apoplastic [Glu] explaining the results seen here. Alternatively, the wound-induced iGluSnFR signals seen here may have been influenced by the closely correlated apoplastic pH increases. This seems likely as iGluSnFR fluorescence increases with more alkaline pH values (Marvin *et al.*, 2013) within the physiological range of the apoplast (Geilfus, 2017). Moreover, both iGluSnFR and apo-pHusion plants displayed increased fluorescence in trichomes where apoplastic pH is known to be elevated thus demonstrating the pH sensitivity of both reporters (Zhou *et al.*, 2017). Therefore, apoplastic pH changes seem likely to have influenced the localised wound-induced iGluSnFR reporter signals detected making it challenging to assess whether increases in apoplastic [Glu] occurred and could have contributed to the activation of GLR3.3.

Wound-induced $[Ca^{2+}]$ elevations and apoplastic alkalinisations were closely correlated here suggesting a link between these responses and a potential role for pH in regulating GLR3.3. However, the wound-induced apoplastic alkalinisations were altered in *glr3.3a* mutants revealing that these alkalinisations cannot solely precede GLR3.3 activation. Instead, the wound-induced $[Ca^{2+}]$ and apoplastic pH elevations may interact with feedback between them. Interacting $[Ca^{2+}]$ and apoplastic pH elevations have been proposed for responses to trichome bending (Zhou *et al.*, 2017) and root bending (Monshausen *et al.*, 2009) with similar associations between cytosolic acidifications and $[Ca^{2+}]$ elevations in responses to large-scale wounding (Behera *et al.*, 2018). If this is the case here, then wound-induced GLR3.3-dependent $[Ca^{2+}]$ elevations and apoplastic alkalinisations could form a positive feedback loop. For instance, wound-induced GLR3.3-dependent $[Ca^{2+}]$ elevations could promote apoplastic alkalinisations which promote further GLR3.3 activity in neighbouring regions, thereby propagating the responses. For GLR3.3 activation, apoplastic pH must exceed 6.5 (Shao *et al.*, 2020). Such pH elevations seem feasible for wound-induced responses as root touch can alkalinise the apoplast from pH 5.6 to above pH 7.5 (Monshausen *et al.*, 2009). Furthermore, resting tobacco leaf epidermal apoplastic pH is approximately 6.5 at the plasma membrane (Martinière *et al.*, 2018).

However, it is unclear how the wound-induced apoplastic alkalinisations could be regulated. As with the burst responses, AHA suppression could cause the apoplastic alkalinisations. Importantly, it remains possible that apoplastic alkalinisation events are entirely downstream of the wound-induced $[Ca^{2+}]$ elevations and do not regulate GLR3.3 or that the responses are correlated but not causally linked. Further investigations to manipulate wound-induced apoplastic pH and $[Ca^{2+}]$ elevations whilst monitoring reporter signals could help clarify any relationships between these responses. Nonetheless, the tight correlations here suggest wound-induced apoplastic alkalinisations and GLR3.3-dependent $[Ca^{2+}]$ elevations are linked in some way with the potential for pH to regulate GLR3.3 by a feedback loop that promotes signal propagation.

In summary, iGluSnFR reporter data presented here is conflicted by coinciding apoplastic pH changes. Nonetheless, active and/or passive apoplastic [Glu] increases could still contribute to the activation of GLR3.3 in responses to localised wounding. Additionally, wound-induced apoplastic pH changes may interact with the closely correlated $[Ca^{2+}]$ elevations and contribute to the regulation of GLR3.3. Here, other components that influence GLR3.3 activity, such as MSL10 and membrane depolarisations (Moe-Lange *et al.*, 2021), ISI1 (Wu *et al.*, 2022), or TGG-mediated aglycone production from glucosinolates (Gao *et al.*, 2023), were not investigated. These components have only been implicated in systemic responses to large-scale wounding. TGG enzymes and their glucosinolate substrates are primarily stored within the vascular bundle (Andréasson *et al.*, 2001; Koroleva *et al.*, 2010; Shirakawa and Hara-Nishimura, 2018) making them unlikely to contribute to localised wound-induced responses. Additionally, MSL10 may be unlikely to function in localised responses because it does not contribute to local $[Ca^{2+}]$ elevations following large-scale wounding (Moe-Lange *et al.*, 2021). Nonetheless, it remains unknown if these additional GLR3.3 regulatory factors could contribute to localised wound-induced GLR3.3 activation. Further investigations into the mechanisms of GLR3.3 activation in localised responses will be important for understanding any contribution of GLR3.3 to the perception of localised wounding and insect feeding.

4.3.3. What determines the extent of GLR3.3 activation in localised responses?

To appreciate how GLR3.3 could function in responses to localised insect feeding, it is important to consider what determines the extent of GLR3.3 activation. As GLR3.3 was activated by wounding but not touch, comparing responses to these stimuli can provide insights into the factors that determine GLR3.3 activation.

The obvious candidate for explaining why wounding induced GLR3.3-dependent $[Ca^{2+}]$ elevations but touch did not is that GLR3.3 activation requires the damage-induced release of

GLR ligands as DAMPs. However, with iGluSnFR signals not clearly reporting apoplastic [Glu], it is unclear whether localised wounding elevates the apoplastic concentrations of GLR ligands. Moreover, emerging data reveals that GLR3.3 activation may not require cell damage. For example, hypo-osmotic stress-induced turgor pressure changes can activate systemic GLR3.3-dependent $[Ca^{2+}]$ elevations (Grenzi *et al.*, 2023). Moreover, trichome bending is capable of triggering wave $[Ca^{2+}]$ elevations and correlated apoplastic alkalinisations that appear to occur without cell damage (Zhou *et al.*, 2017; Bellandi *et al.*, 2022). In preliminary data (not shown), trichome touch-induced $[Ca^{2+}]$ waves seemed dependent on GLR3.3. Whilst GLR3.3 activation without damage could occur by the active release of GLR3.3 ligands, mechanisms for such stress-induced efflux of GLR3.3 ligands are not known. Therefore, it is not clear whether apoplastic GLR ligand concentrations increase with localised wounding or if damage-induced DAMP release is required for GLR3.3 activation.

Instead, the extent of mechanical stress experienced may be the key determinant of GLR3.3 activation. Mechanical stress perception during touch and wounding likely led to the GLR3.3-independent burst responses of $[Ca^{2+}]$ elevations and apoplastic alkalinisations that appeared to be linked. However, the touch-induced burst responses were of a smaller area and magnitude than those induced in the *glr3.3a* mutant by wounding. Moreover, only the wound-induced burst $[Ca^{2+}]$ elevations propagated as GLR3.3-dependent waves. It could be then, that the extent of the mechanical stress experienced determines the magnitude or size of the burst responses that subsequently determine the extent of GLR3.3 activation. For instance, greater mechanical stress could lead to larger area and magnitude burst responses. The burst apoplastic alkalinisations may then activate GLR3.3 in proportion to their magnitude or area. This may result in proportional activation of the proposed GLR3.3-dependent Ca^{2+} -pH positive feedback loop (Section 4.3.2.). Interestingly, this notion of mechanical stress activating GLRs is conceptually similar to the Squeeze Cell model for large-scale wound-induced systemic signalling. In this model, turgor pressure changes in the xylem are perceived in neighbouring cells as mechanical stress, potentially by MSL10, to activate GLR3.3/3.6 (Farmer *et al.*, 2014; Moe-Lange *et al.*, 2021). Additional support for mechanical stress determining localised GLR3.3 activation comes from comparing the localised touch-induced GLR3.3-independent responses with the trichome touch-induced responses of wave $[Ca^{2+}]$ elevations (Bellandi *et al.*, 2022) that appear to be GLR3.3-dependent (preliminary data, not shown). Compared to localised touch, trichome touch may lead to greater GLR3.3 activation as trichomes focus mechanical forces into neighbouring cells amplifying the mechanical stress experienced (Zhou *et al.*, 2017). Moreover, in preliminary experiments, less severe trichome touch stimuli appeared to induce $[Ca^{2+}]$ elevations with burst and secondary dynamics whilst firmer touch stimuli induced wave $[Ca^{2+}]$ elevations (data not shown). Therefore, the degree of mechanical stress experienced correlates

with, and could explain, the extent of GLR3.3 activation in localised responses to wounding and touch.

Further investigations are required to clarify whether localised GLR3.3 activity is determined by damage-induced DAMP release and/or mechanical stress perception. Data and considerations here fit well with a model for the extent of mechanical stress experienced determining GLR3.3 activation. Understanding the cellular processes that determine localised GLR3.3 activity will be important for appreciating the role of GLR3.3 in responses to localised stimuli including aphid or thrips feeding.

4.3.4. What drives secondary $[Ca^{2+}]$ elevations?

The mechanisms and functions of wound- and touch-induced secondary $[Ca^{2+}]$ elevations remain unclear from these investigations. However, as *glr3.3a* mutants display wound-induced JA marker gene expression, secondary $[Ca^{2+}]$ elevations may be significant in regulating plant JA responses. Therefore, the properties of these $[Ca^{2+}]$ elevations are of interest in the wound- and touch-induced responses and may be relevant to localised insect feeding-induced responses.

The dynamics of initial responses, such as burst $[Ca^{2+}]$ elevations, that precede delayed secondary $[Ca^{2+}]$ elevations suggest that the secondary responses may require a perception event, some processing event and then initiation. Such a mechanism could involve the burst perception event leading to active agonist release with propagation of the processing component or agonist to trigger propagating secondary $[Ca^{2+}]$ elevations. This kind of signalling mechanism is seen in some *D. melanogaster* damage-induced $[Ca^{2+}]$ elevations which display an initial burst-like increase before delayed secondary increases (Shannon *et al.*, 2017). These secondary $[Ca^{2+}]$ elevations are driven by protease diffusion from the wound site that liberates Growth-blocking peptides to bind Methuselah-like 10 upstream of the $[Ca^{2+}]$ elevations (O'Connor *et al.*, 2021). A similar mechanism has been proposed for signalling from the phytocytokine, PEP1, following cell damage in roots. A damage-induced loss of membrane integrity causes a Ca^{2+} influx that activates METACASPASE4 to release PEP1 from PROPEP1 at the tonoplast forming a mobile signal that induces $[Ca^{2+}]$ elevations via PEPR1/2 in surrounding cells (Hander *et al.*, 2019). Accumulation of PEP1 in this model occurs within 30 s of wounding suggesting that it could contribute to the wound-induced secondary $[Ca^{2+}]$ elevations that occur around 30 – 60 s post-wounding in *glr3.3a* leaves. However, because touch is unlikely to cause sufficient damage for this pathway, PEP1 signalling is not a strong candidate for touch-induced secondary $[Ca^{2+}]$ elevations. Other mechanisms that induce $[Ca^{2+}]$ elevations and require similar perception and ligand processing, such as signalling from other phytocytokines (Hou *et al.*, 2021a), could also be candidates for driving secondary $[Ca^{2+}]$ elevations.

The relationship of secondary $[Ca^{2+}]$ elevations to burst and wave $[Ca^{2+}]$ increases is also not well resolved. Secondary $[Ca^{2+}]$ elevations appeared suppressed after GLR3.3-dependent wave $[Ca^{2+}]$ elevations. As Ca^{2+} -ATPase activity can be $[Ca^{2+}]$ -dependent (Fuglsang and Palmgren, 2021), this suppression could result from wave $[Ca^{2+}]$ elevations promoting Ca^{2+} -ATPase activity before the secondary elevations. It may be then, that the greater the extent of GLR3.3 activation and wave $[Ca^{2+}]$ elevations, the greater the suppression of secondary $[Ca^{2+}]$ elevations. The secondary $[Ca^{2+}]$ elevations do not appear to be dependent on burst properties because wound-induced burst $[Ca^{2+}]$ elevations in water-infiltrated plants were reduced in the *glr3.3a* samples whilst the secondary $[Ca^{2+}]$ elevations were unaffected. Both touch-induced burst and secondary $[Ca^{2+}]$ elevations were of a shorter duration than those induced by wounding. Therefore, whilst the relationship between burst and secondary responses remains unclear, both responses correlate with the extent of mechanical stress experienced.

Exploring how secondary $[Ca^{2+}]$ elevations are driven may reveal additional mechanisms or components of localised damage or mechanical stress perception and help reveal the significance of these elevations in plant defence responses. Improving the understanding of the secondary responses could also be important for a mechanistic description of how *A. thaliana* perceives aphid and thrips feeding.

4.3.5. Do localised GLR3.3-dependent responses contribute to plant defences?

For considering the contribution of GLR3.3 to insect perception, it is important to assess whether GLR3.3 can promote plant defence responses to localised stimuli. Data here revealed that *JAZ10* and *AOS* JA marker gene expression was induced with wounding within the area of the rapid apoplastic alkalinisations and $[Ca^{2+}]$ elevations. Similarly, localised wounding in cotyledons induces localised *JAZ10* expression (Bellandi *et al.*, 2022). *JAZ10* expression was impaired in wound-induced responses in *glr3.3a* mutants. Furthermore, touch, which did not induce GLR3.3-dependent responses, also did not induce *JAZ10* or *AOS* expression within 8 h of wounding. Thus, wound-induced GLR3.3-dependent responses appear to contribute to JA-mediated gene expression which could contribute to insect resistance. However, wound-induced expression of *AOS* was unaltered in *glr3.3a* mutants. Similarly, in cotyledons, the *JOX3* and *VSP2* JA marker genes show unaltered localised wound-induced expression in *glr3.3a* mutants (Bellandi *et al.*, 2022). As such, it may be that GLR3.3 activity regulates only a subset of JA-inducible genes. Moreover, wound-induced *JAZ10* expression was only partially suppressed in *glr3.3a* mutants. This indicates that there is significant redundancy in the signalling mechanisms that regulate JA responses following localised wounding. For example, the remaining wound-induced JA-regulated gene expression in the *glr3.3a* mutants could be

mediated by the wound-induced GLR3.3-independent $[Ca^{2+}]$ and apoplastic pH elevations or alternative signalling components not investigated here. In any case, GLR3.3 activity appeared to contribute to the wound-induced expression of a JA marker gene indicating that GLR3.3 can promote JA-mediated responses to localised wounding.

4.3.6. A model for mechanical stress perception and GLR3.3 activation in responses to localised wounding and touch

Findings here have raised many questions regarding the perception of localised touch and wound stimuli in *A. thaliana* and the mechanisms of localised GLR3.3 activation. These include:

1. What mechanisms underpin the initiation of burst $[Ca^{2+}]$ elevations?
2. How is GLR3.3 permeability regulated in localised wound-induced responses?
3. Is the extent of GLR3.3 activation determined by the extent of damage/DAMP release or mechanical stress?
4. What mechanisms give rise to secondary $[Ca^{2+}]$ elevations?
5. What signalling components other than GLR3.3 contribute to wound-induced responses including JA-mediated gene expression changes?

Despite these outstanding questions, findings here have supported a role for mechanical stress perception in responses to localised wounding and touch. This perception seems to initiate burst and secondary $[Ca^{2+}]$ elevations with the former developing into wave $[Ca^{2+}]$ elevations with GLR3.3 activation. This GLR3.3 activation may require damage-induced DAMP/GLR ligand release. However, with the reports that GLR3.3 activation may be possible without cell damage (Grenzi *et al.*, 2023; Bellandi *et al.*, 2022), and with the comparisons of wound- and touch-induced responses, the favoured hypothesis here is that the extent of mechanical stress experienced during localised wounding or touch determines GLR3.3 activation. Burst, wave and secondary $[Ca^{2+}]$ elevations are closely correlated with apoplastic alkalinisations suggesting a link between these responses. Moreover, extracellular pH increases can activate GLR3.3 (Shao *et al.*, 2020). Therefore, it may be that larger mechanical stress events cause greater apoplastic alkalinisations which proportionally activate GLR3.3-dependent $[Ca^{2+}]$ elevations. These GLR3.3-dependent $[Ca^{2+}]$ elevations could drive further apoplastic pH increases in a Ca^{2+} -pH feedback loop that promotes signal propagation. Finally, GLR3.3 contributes to wound-induced JA marker gene expression. Whilst there are many outstanding questions here, these findings have been used to synthesise a model for how mechanical stress perception could contribute to localised wound- and touch-induced responses (Figure 4.17).

In Chapter 3, I identified that *M. persicae* feeding induced $[Ca^{2+}]$ elevations that were partially GLR3.3/3.6-dependent. The *M. persicae* feeding-induced GLR3.3/3.6 dependent GCaMP3 signals were alike the wound-induced GLR3.3-dependent GCaMP3 signals in that they both displayed relatively fast propagation rates and/or high peak intensities. Therefore, GLR3.3/3.6-dependent $[Ca^{2+}]$ elevations induced by *M. persicae* feeding may be alike those induced by wounding. Additionally, GLR3.3/3.6-independent *M. persicae* feeding-induced $[Ca^{2+}]$ elevations may be alike those induced by touch. The findings of this chapter will be used to provide a foundation for exploring aphid and thrips perception and the contributions of GLR3.3/3.6 to this perception in the next chapter.

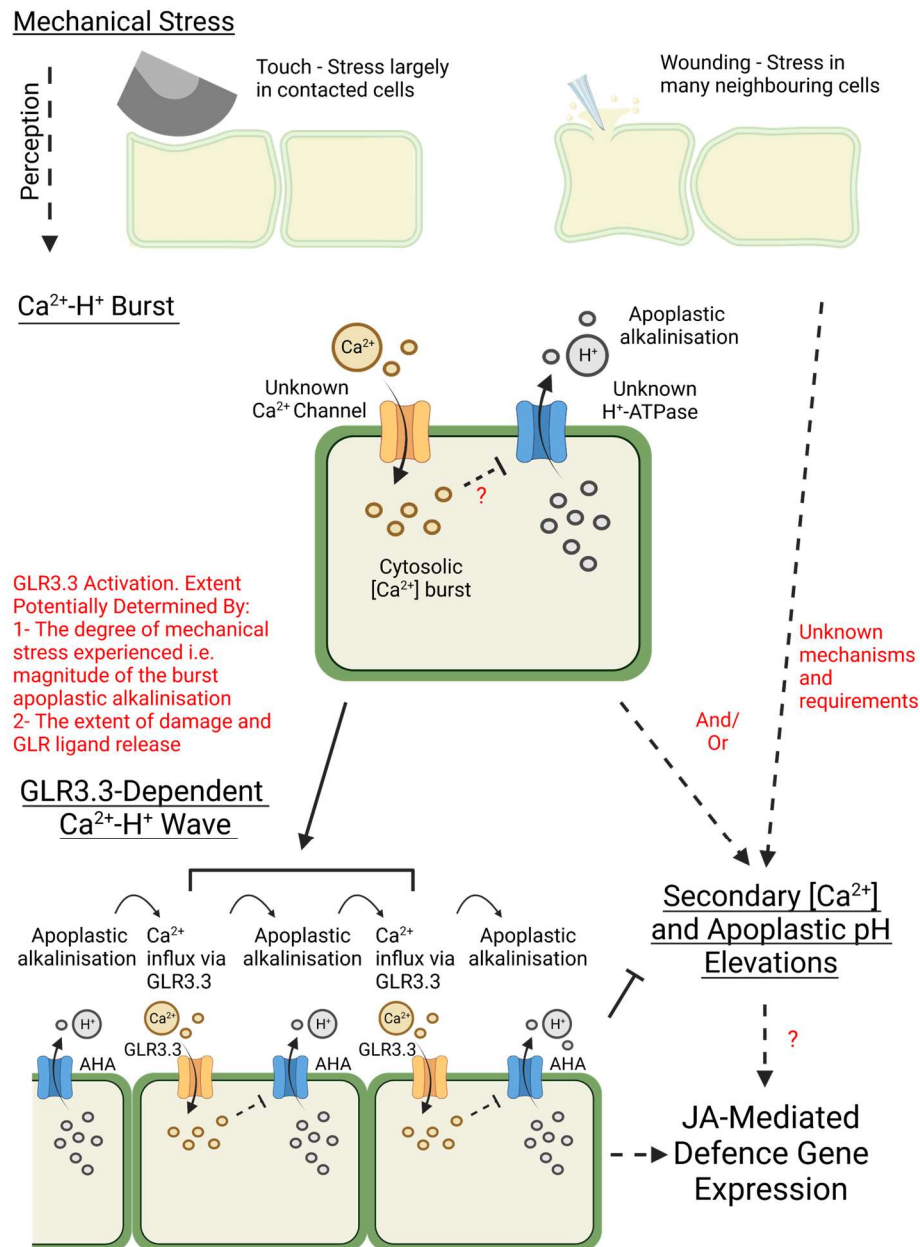


Figure 4.17 Hypothetical model for how mechanical stress perception and GLR3.3 could function in wound- and touch-induced responses.

An initial wound event causes lysis of a cell and pressure shocks in neighbouring cells resulting in mechanical stress. Touch triggers lower levels of mechanical stress restricted more to the contacted cell(s). Perturbed cells passively or actively perceive mechanical stress, potentially via mechanosensitive ion channels, resulting in [Ca²⁺] increases that are short-lived as 'burst' elevations. Apoplasmic alkalisations co-occur and may result from the suppression of plasma membrane H⁺-ATPase (AHA) activity, potentially in a [Ca²⁺]-dependent manner. The extent of GLR3.3 activation could then be determined by the magnitude of the mechanical stress and burst apoplasmic alkalisations or the damage-induced release of GLR3.3 ligands (e.g. Glu) as DAMPs. GLR3.3 may then function in a propagating Ca²⁺-H⁺ wave. In this wave, AHA suppression could alkalise the apoplast to activate GLR3.3-dependent [Ca²⁺] elevations that further suppress AHAs in neighbouring regions, thereby propagating the response. After bursts, secondary [Ca²⁺] and apoplasmic pH elevations occur as a result of the mechanical stress perception. GLR3.3-dependent wave responses suppress secondary [Ca²⁺] elevations. Finally, GLR3.3-dependent and -independent responses can contribute to JA-mediated defence gene expression. Arrows indicate positive regulation. Flat arrows indicate suppression. Dashed lines indicate indirect links. Red indicates queries. Created with BioRender.com

5. Exploring the Role of GLR3.3 in the Perception of Aphid and
Thrips Feeding

5.1. Introduction

There is a limited understanding of how plants perceive pests with localised feeding mechanisms such as aphids and thrips. Specifically, there are no known DAMPs or HAMPs associated with thrips feeding and no *A. thaliana* membrane receptors known to perceive thrips (Steenbergen *et al.*, 2018). For aphids, there is evidence of HAMP existence from aphid saliva and aphid extract but little is known about any specific candidate HAMPs or DAMPs or the receptors that perceive them (Elzinga *et al.*, 2014; Chaudhary *et al.*, 2014; Canham, 2022; Bos *et al.*, 2010; Prince *et al.*, 2014; Nalam *et al.*, 2019; De Vos and Jander, 2009). In the current work, I have identified that *glr3.3a glr3.6a* mutants are impaired in *M. persicae* feeding-induced $[Ca^{2+}]$ elevations detected by GCaMP3 signals with relatively fast propagation rates and/or high peak intensities. Additionally, I have identified that GLR3.3, but not GLR3.6, contributes to localised wound-induced responses including $[Ca^{2+}]$ elevations. Based on these findings, it may be that GLR3.3 contributes to *M. persicae* feeding-induced $[Ca^{2+}]$ elevations without GLR3.6 and that GLR3.3 functions more widely in *A. thaliana* responses to aphid and thrips feeding. Characterising any contribution of GLR3.3, with or without GLR3.6, to aphid and thrips feeding-induced responses could significantly advance the understanding of aphid and thrips perception in *A. thaliana*.

With mechanical stress and/or damage potentially important in determining localised GLR3.3 activation, the role of GLR3.3 in responses to localised insect feeding is likely to be heavily influenced by the insect feeding mechanisms. Thrips feeding behaviour involves localised piercing of epidermal and mesophyll cells using the mandibular stylet before salivation and then ingestion of the released cell contents through the maxillary stylets (Kindt *et al.*, 2006; Steenbergen *et al.*, 2018; Chisholm and Lewis, 1984). Thus, thrips feeding involves high levels of localised mechanical stress, damage and cell death. In direct contrast, aphids carefully navigate their stylets to the vascular bundle for feeding. The gelling saliva, which envelopes the stylets, protects plant cells along the stylet path from damage and can contribute to plugging pores following stylet penetration of sieve elements, mesophyll cells and epidermal cells (Walling, 2008; Miles, 1999; Tjallingii, 2006). Whilst aphid stylets pierce, probe and disrupt most mesophyll cells en route to the vascular bundles for feeding, very few cells die (Tjallingii and Esch, 1993; Tjallingii, 2006). Therefore, aphid feeding causes limited damage and mechanical stress compared to thrips feeding. As wound stimuli activated GLR3.3 but touch did not, and as GLR3.3 contributes to large-scale wound-induced responses (Nguyen *et al.*, 2018), it may be that thrips feeding activates GLR3.3 more than aphid feeding. However, GLR3.3 also contributes to pathogen resistance against *P. syringae* pv *tomato* DC3000 (Li *et al.*, 2013) and *H. arabidopsidis* (Manzoor *et al.*, 2013) where mechanical stress and damage are less apparent. This suggests

that the contribution of GLR3.3 to plant biotic stress responses may be determined by more complex factors than just the degree of mechanical stress or damage induced. Nonetheless, aphid and thrips differentially cause mechanical stress and damage when they feed which may influence the activation of GLR3.3 in feeding-induced responses.

The relationship that the thrips or aphid species has with the host plant may also influence the contribution of GLR3.3 to the feeding-induced responses. For example, GLR3.3 activity could be influenced by differences in feeding behaviour determined by the ability of the insect species to colonise the host plant species. In support of this, when aphids cannot colonise the host, feeding often becomes less efficient with increased probing of mesophyll cells and an impaired ability to initiate sustained feeding from the phloem (Escudero-Martinez *et al.*, 2021; Escudero-Martinez *et al.*, 2017; Kaloshian *et al.*, 2000; Jhou *et al.*, 2021). The relationship between the insect and host plant may also influence the contribution of GLR3.3 to plant responses as it may determine whether the insect has suitable effectors to manipulate the host responses. For example, some aphid species that have co-evolved with *A. thaliana* or related hosts may deploy effectors that target *A. thaliana* GLR3.3 activation. Other species that cannot colonise *A. thaliana* may not have evolved suitable effectors for this activity. These considerations indicate that the relationship of the insect species to *A. thaliana* seems more likely to influence GLR3.3 function in responses to aphid feeding than to thrips feeding. This is because individual aphid feeding events can last for hours and are more protracted than thrips feeding events (Tjallingii, 2006; Kindt *et al.*, 2003). As such, to appreciate the contribution of GLR3.3 to thrips and aphid perception, it will be important to assess whether GLR3.3 differentially contributes to feeding from aphid species with different *A. thaliana* colonisation abilities.

To explore the contribution of GLR3.3 to localised insect feeding-induced responses in *A. thaliana* and incorporate differences in the host colonisation abilities and feeding mechanisms, aphid species were carefully selected along with a thrips species for investigations. This selection included species for which JA is known to contribute to plant defences because GLR3.3 contributed to wound-induced *JAZ10* expression. With a known phenotype for *M. persicae* feeding-induced $[Ca^{2+}]$ elevations in *glr3.3a glr3.6a A. thaliana*, *M. persicae* was used as the focus for these investigations as a generalist aphid that can colonise *A. thaliana*. Next, the cabbage aphid, *B. brassicae*, was selected as a *Brassica* specialist which can also colonise *A. thaliana* (Kusnierczyk *et al.*, 2008). Whilst both *M. persicae* and *B. brassicae* colonisation induces JA-mediated responses in *A. thaliana* (Kusnierczyk *et al.*, 2007; Rubil *et al.*, 2022), *B. brassicae* can uniquely sequester certain JA-induced plant glucosinolates for its own defence responses against insect predators (Kazana *et al.*, 2007; Mewis *et al.*, 2005). The final aphid species selected

was *R. padi* which is a grass specialist (Peng *et al.*, 2019; Leather and Dixon, 1982). *R. padi* cannot colonise *A. thaliana* but does initiate feeding and probes *A. thaliana* leaf epidermal and mesophyll cells (Jaouannet *et al.*, 2015; Escudero-Martinez *et al.*, 2017). *R. padi* colonisation induces JA marker gene expression in *A. thaliana* (Jaouannet *et al.*, 2015) and barley (Escudero-Martinez *et al.*, 2020). Moreover, barley JA responses can limit *R. padi* colonisation (Losvik *et al.*, 2017) and are suppressed by *R. padi* effectors (Escudero-Martinez *et al.*, 2020). Finally, the thrips species, *F. occidentalis*, was selected as a serious pest species and generalist that can colonise over 240 host plants (He *et al.*, 2020; Tommasini and Maini, 1995). *F. occidentalis* can infest *A. thaliana* and induces JA-mediated defence responses (Abe *et al.*, 2008). This selection process gave three aphid species and a thrips species which covered variation in the feeding mechanism used and the ability to colonise *A. thaliana*. As such, investigating *A. thaliana* responses to these insects provides a unique opportunity to explore the contribution and mechanisms of GLR3.3 activity in responses to localised insect feeding.

To investigate the contribution of GLR3.3 to aphid and thrips feeding-induced responses and perception in *A. thaliana*, the methods and approaches developed in Chapters 3 and 4 can be utilised. Therefore, for the aphids *M. persicae*, *R. padi* and *B. brassicae*, and the thrips *F. occidentalis*, the research aims of this chapter are to:

- Identify whether localised insect feeding triggers GLR3.3-dependent $[Ca^{2+}]$ elevations along with apoplastic pH and/or [Glu] increases that could regulate GLR3.3 activity.
- Identify whether localised insect feeding induces JA marker gene expression that could be GLR3.3-dependent.
- Investigate whether GLR3.3 contributes to resistance against the selected aphid and thrips species.

5.2. Results

5.2.1. GLR3.3 contributes to $[Ca^{2+}]$ elevations induced by *M. persicae* feeding

With the *glr3.3a* mutant, but not *glr3.6a* mutant, impaired in wound-induced $[Ca^{2+}]$ elevations, I hypothesised that the *glr3.3a* mutation was responsible for the loss of relatively high intensity and/or fast propagating *M. persicae* feeding-induced GCaMP3 signals in the *glr3.3a glr3.6a* mutant. To test this hypothesis, I investigated *M. persicae* feeding-induced GCaMP3 signals in Col-0 and *glr3.3a UBQ10::GCaMP3 A. thaliana*. Whilst data could not be background corrected, F0 values were not significantly different between the genotypes (Figure 5.1A, t-test, $t = -0.31$, $p = 0.76$). *M. persicae* feeding induced GCaMP3 signals with normalised $\Delta F/F0$ elevations that appeared superficially similar in Col-0 and *glr3.3a* (Figure 5.1B). Col-0 and *glr3.3a* reporter signal areas were not significantly different and had mean values of $0.215 \pm 0.025 \text{ mm}^2$ and $0.178 \pm 0.020 \text{ mm}^2$, respectively (Figure 5.1E, Wilcoxon rank-sum, $W = 510$, $p = 0.38$). However, the *glr3.3a* mean normalised $\Delta F/F0$ trace appeared smoother than the Col-0 trace (Figure 5.1B). Moreover, the Col-0 peak normalised $\Delta F/F0$ values were statistically greater than the values for the *glr3.3a* samples (Figure 5.1C, Wilcoxon rank-sum, $W = 651$, $p = 0.0026$). Col-0 reporter signals had significantly faster propagation rates than the *glr3.3a* signals (Figure 5.1D, Wilcoxon rank-sum, $W = 654$, $p = 0.0022$). 9/30 Col-0 samples had reporter signal propagation rates exceeding the maximum rate detected in *glr3.3a* of $1.35 \mu\text{m s}^{-1}$. 7 of these responses were in a group of 12 Col-0 responses that displayed peak normalised $\Delta F/F0$ values exceeding the maximum detected in *glr3.3a* of 0.26 A.U. Therefore, *glr3.3a* mutants were impaired in *M. persicae* feeding-induced GCaMP3 signals with relatively fast propagation rates and/or high peak intensity values. This phenotype recapitulated that of the *glr3.3a glr3.6a* mutant revealing that the mutation in *GLR3.3* is sufficient for the *glr3.3a glr3.6a* phenotype.

The *M. persicae* feeding-induced GCaMP3 signals could be approximately grouped by their properties with some signals displaying similarities to those induced by wounding or touch (Figure 5.1F, Video S5.1). Firstly, *M. persicae* feeding-induced Col-0 signals with relatively high propagation rates or peak intensity values often propagated radially as rings. Thus, these signals were similar to the wound-induced GLR3.3-dependent wave GCaMP3 signals. Furthermore, 8/30 Col-0 and 11/30 *glr3.3a* samples displayed highly localised burst GCaMP3 signals at feeding sites that dissipated before secondary signalling of a lower intensity developed. These signals recapitulated the touch- and wound-induced GLR3.3-independent GCaMP3 signals. The other GCaMP3 reporter signals could not be visually placed into these categories. Whilst this categorisation is approximate, these data suggest that *M. persicae* feeding can induce GCaMP3 signals similar to the GLR3.3-independent touch responses or the GLR3.3-dependent wound responses.

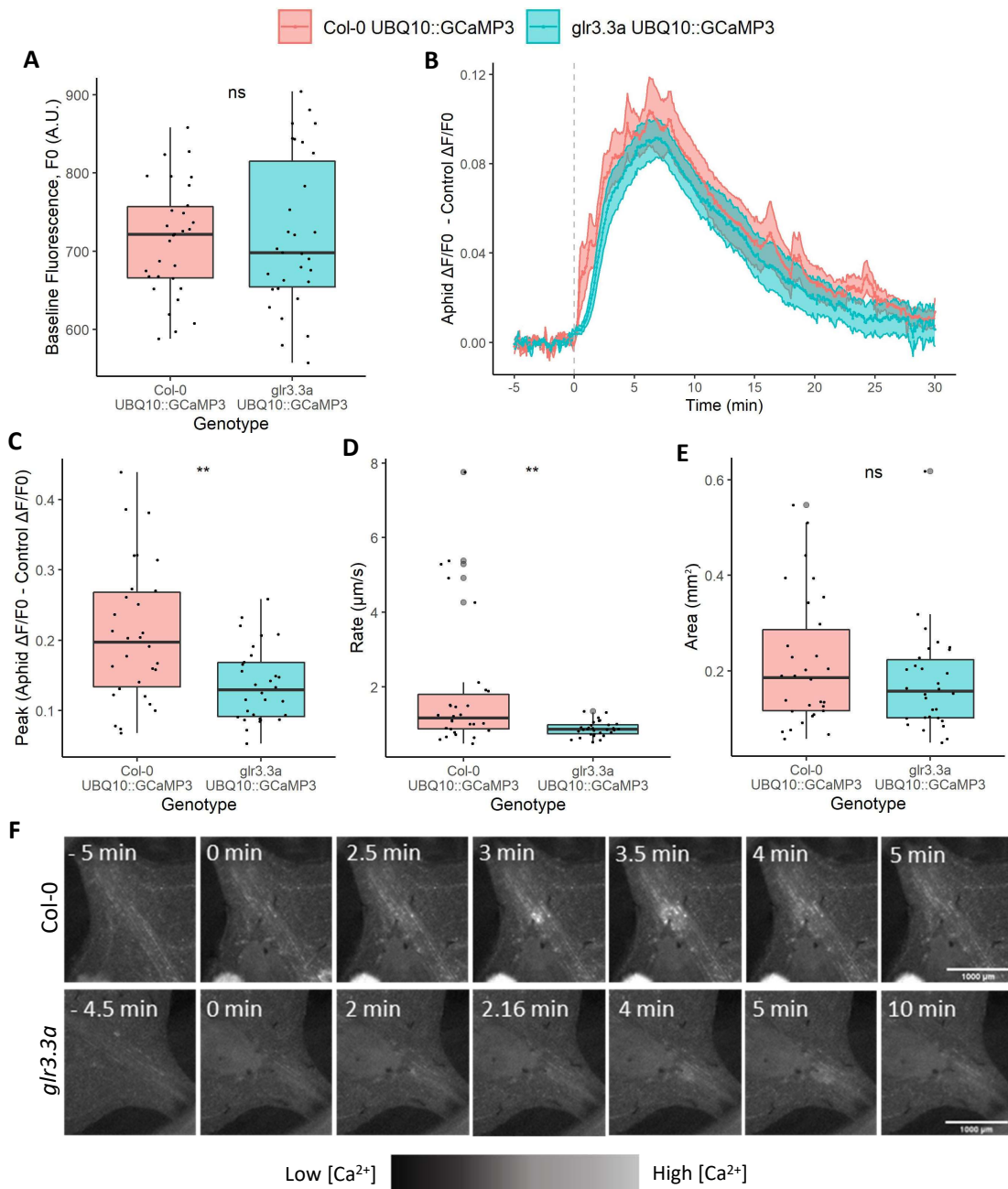


Figure 5.1 *glr3.3a* mutants are partially impaired in *M. persicae* feeding-induced GCaMP3 signals.

Properties of *M. persicae* feeding-induced GCaMP3 signals in *Col-0* and *glr3.3a* UBQ10::GCaMP3 *A. thaliana* ($n = 30$). Elevations were recorded by imaging (Axio Zoom.V16, HXP 120 V light source) *A. thaliana* leaves subjected to *M. persicae* or no aphid control treatments. Non-corrected fluorescence intensity (F, A.U.) values were recorded over the area of feeding-induced reporter signals and at comparable control sites and transformed into $\Delta F/F_0$ values with F_0 being the mean F over the 5 min prior to feeding. (B) Traces for the mean \pm S.E.M. normalised $\Delta F/F_0$ values (Aphid $\Delta F/F_0$ - Control $\Delta F/F_0$) over time with feeding beginning at 0 min (grey dashed line). Boxplots are displayed for the (A) feeding site F_0 values (A.U.), (C) peak normalised $\Delta F/F_0$ values (Aphid $\Delta F/F_0$ - Control $\Delta F/F_0$), (D) signal propagation rates ($\mu\text{m s}^{-1}$) and (E) signal areas (mm^2), with grey dots associated with outliers. Statistical significance, tested using a (A) t-test or a (C, D, E) Wilcoxon rank-sum test, shown by ns: $p > 0.05$, **: $p \leq 0.01$. (F) Representative time series images of a *Col-0* high intensity, fast propagating wave GCaMP3 signal and a *glr3.3a* burst and secondary GCaMP3 signal. Times are shown in relation to aphid feeding at 0 min with a 1000 μm scale bar.

To test if GLR3.1 contributes to *M. persicae* feeding-induced $[Ca^{2+}]$ elevations alongside GLR3.3, I imaged *M. persicae* feeding-induced GCaMP3 signals in Col-0 and *glr3.1a glr3.3a UBQ10::GCaMP3 A. thaliana*. Fluorescence intensity values could not be background-corrected but the F0 values were not significantly different between the genotypes (Figure 5.2A, Wilcoxon rank-sum, $W = 427$, $p = 0.74$). As with the *glr3.3a* mutant, the mean normalised $\Delta F/F0$ traces appeared superficially similar with reporter signals in both genotypes but with the *glr3.1a glr3.3a* trace seemingly smoother than the Col-0 trace (Figure 5.2B). Whilst there were no statistically significant differences in the peak normalised $\Delta F/F0$ values between the genotypes here (Figure 5.2C, Wilcoxon rank-sum, $W = 551$, $p = 0.14$), the signal propagation rates were significantly reduced in *glr3.1a glr3.3a* samples (Figure 5.2D, Wilcoxon rank-sum, $W = 726$, $p \leq 0.0001$). Moreover, 6 Col-0 responses had peak normalised $\Delta F/F0$ values exceeding the maximum value detected for *glr3.1a glr3.3a* and 4 of these had propagation rates beyond the upper limit detected in *glr3.1a glr3.3a*. As such, *glr3.1a glr3.3a* mutants appeared to be impaired in *M. persicae* feeding-induced GCaMP3 signals with relatively fast propagation rates and/or high peak normalised $\Delta F/F0$ values. There were no statistically significant differences in signal areas between the genotypes (Figure 5.2E, Wilcoxon rank-sum, $W = 381$, $p = 0.31$). In summary, the *glr3.1a glr3.3a* phenotype here can be explained by the *glr3.3a* mutation suggesting that GLR3.1 does not contribute to *M. persicae* feeding-induced $[Ca^{2+}]$ elevations beyond the role of GLR3.3.

Considering these two experiments along with that for *M. persicae* feeding-induced GCaMP3 signals in *glr3.3a glr3.6a A. thaliana* (Section 3.2.6), the ability to detect the *glr3.3a* phenotype in the signal properties by statistical significance clearly varied. From multiple independent experiments using *glr3.3a A. thaliana* (data not shown), this seemed to result from variation in the GLR3.3-dependency for individual *M. persicae* feeding-induced responses with most responses seemingly GLR3.3-independent. Therefore, identifying the *glr3.3a* phenotype for *M. persicae* feeding-induced GCaMP3 signals here required consideration of the signal propagation rates, intensities and dynamics.

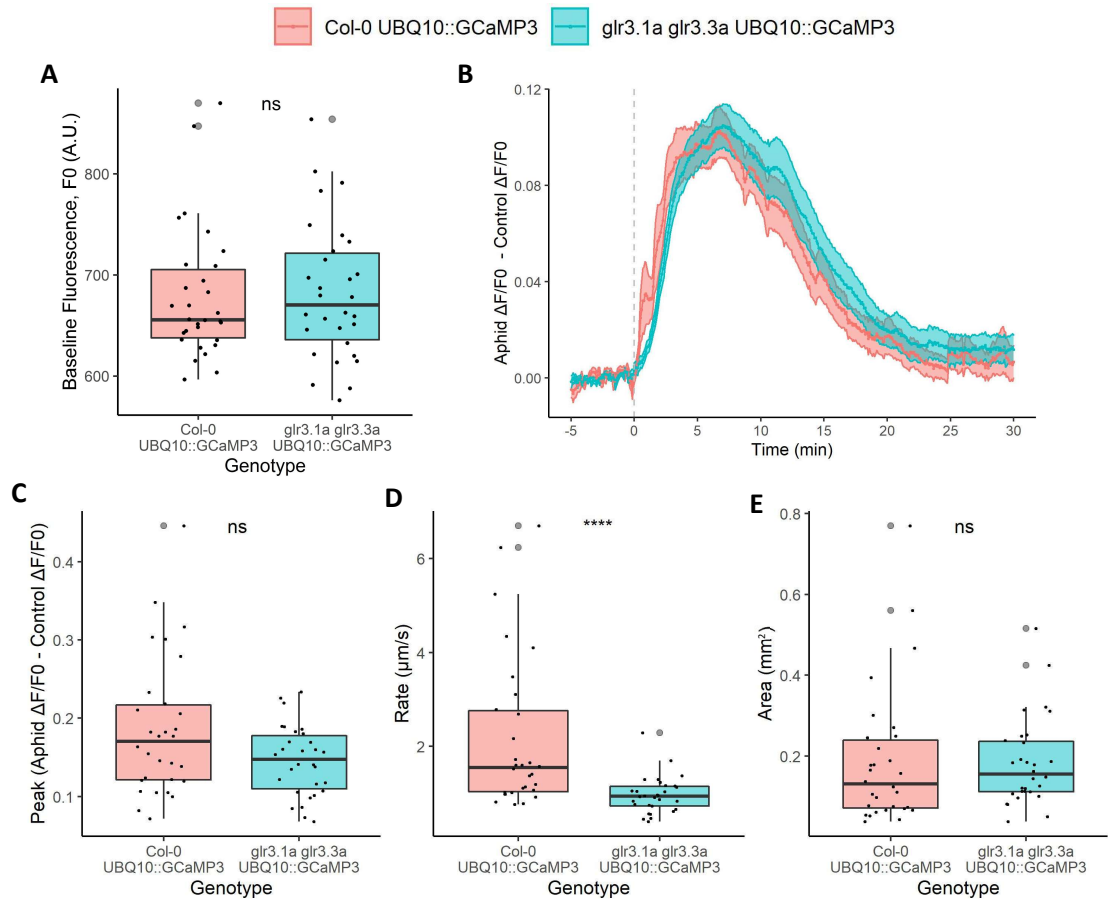


Figure 5.2 *glr3.1a glr3.3a* mutants are partially impaired in *M. persicae* feeding-induced GCaMP3 signals.

Properties of *M. persicae* feeding-induced GCaMP3 signals in Col-0 and *glr3.1a glr3.3a* *UBQ10::GCaMP3 A. thaliana* ($n = 30$). Elevations were recorded by imaging (Axio Zoom.V16, HXP 120 V light source) *A. thaliana* leaves subjected to *M. persicae* or no aphid control treatments. Non-corrected fluorescence intensity (F, A.U.) values were recorded over the area of feeding-induced reporter signals and at comparable control sites and transformed into $\Delta F/F_0$ values with F_0 being the mean F over the 5 min prior to feeding. (B) Traces for the mean \pm S.E.M. normalised $\Delta F/F_0$ values (Aphid $\Delta F/F_0$ - Control $\Delta F/F_0$) over time with feeding beginning at 0 min (grey dashed line). Boxplots are displayed for the (A) feeding site F_0 values (A.U.), (C) peak normalised $\Delta F/F_0$ values (Aphid $\Delta F/F_0$ - Control $\Delta F/F_0$), (D) signal propagation rates ($\mu\text{m s}^{-1}$) and (E) signal areas (mm^2), with grey dots associated with outliers. Statistical significance, tested using Wilcoxon rank-sum tests, shown by ns: $p > 0.05$, ****: $p \leq 0.0001$.

5.2.2. *R. padi* and *B. brassicae* feeding induces localised [Ca²⁺] elevations in *A. thaliana* that are altered in *glr3.3a* mutants

To test whether GLR3.3 activation differs in responses to aphid species with different abilities to colonise *A. thaliana*, I assessed GCaMP3 signals in Col-0 and *glr3.3a* *UBQ10::GCaMP3* *A. thaliana* in responses to feeding from *R. padi* and *B. brassicae*. These aphids cannot and can colonise *A. thaliana*, respectively. For both investigations, F0 values were not statistically different between the genotypes (*R. padi*: Figure 5.3A, t-test, $t = 0.90$, $p = 0.37$; *B. brassicae*: Figure 5.4A, t-test, $t = 0.38$, $p = 0.71$). Both aphid species induced localised reporter signals in Col-0 as visible in the mean normalised $\Delta F/F_0$ traces (Figure 5.3B, Figure 5.4B). For Col-0 responses, the mean signal area was 0.193 ± 0.024 mm² for *R. padi* and 0.186 ± 0.015 mm² for *B. brassicae*. The mean normalised $\Delta F/F_0$ traces for both aphid species revealed a change in the reporter signal dynamics in *glr3.3a* with a lower peak amplitude and longer duration of elevation compared with the Col-0 traces. Moreover, *R. padi* and *B. brassicae* feeding-induced GCaMP3 reporter signals in *glr3.3a* had significantly reduced peak normalised $\Delta F/F_0$ values (*R. padi*: Figure 5.3C, Wilcoxon rank-sum, $W = 674$, $p = 0.00073$; *B. brassicae*: Figure 5.4C, Wilcoxon rank-sum, $W = 746$, $p \leq 0.0001$) and propagation rates (*R. padi*: Figure 5.3D, Wilcoxon rank-sum, $W = 744$, $p \leq 0.0001$; *B. brassicae*: Figure 5.4D, Wilcoxon rank-sum, $W = 862$, $p \leq 0.0001$). There were no differences between the signal areas in Col-0 and *glr3.3a* for either aphid species (*R. padi*: Figure 5.3E, Wilcoxon rank-sum, $W = 416$, $p = 0.63$; *B. brassicae*: Figure 5.4E, Wilcoxon rank-sum, $W = 500$, $p = 0.46$). Finally, for both aphid species, Col-0 GCaMP3 signals with relatively high propagation rates or peak normalised $\Delta F/F_0$ values often propagated as waves whilst some other Col-0 and *glr3.3a* GCaMP3 signals displayed burst and secondary dynamics (Figure 5.3F, Figure 5.4F). Therefore, *R. padi* and *B. brassicae* feeding appeared to induce *A. thaliana* GCaMP3 signals that were GLR3.3-dependent and similar to wound responses along with some GLR3.3-independent responses that were more similar to touch-induced responses. Whilst data were not directly compared to the *M. persicae* feeding-induced GCaMP3 signals, *R. padi* and *B. brassicae* feeding-induced GCaMP3 signals appeared to be more heavily dependent on GLR3.3 than those induced by *M. persicae*. This was apparent because *R. padi* and *B. brassicae* feeding resulted in a more pronounced *glr3.3a* phenotype in normalised $\Delta F/F_0$ traces, peak normalised $\Delta F/F_0$ values and signal propagation rates, compared to *M. persicae* feeding. As such, various aphid species induce GLR3.3-dependent [Ca²⁺] elevations with feeding but the extent to which they are GLR3.3-dependent appears to vary between the species investigated.

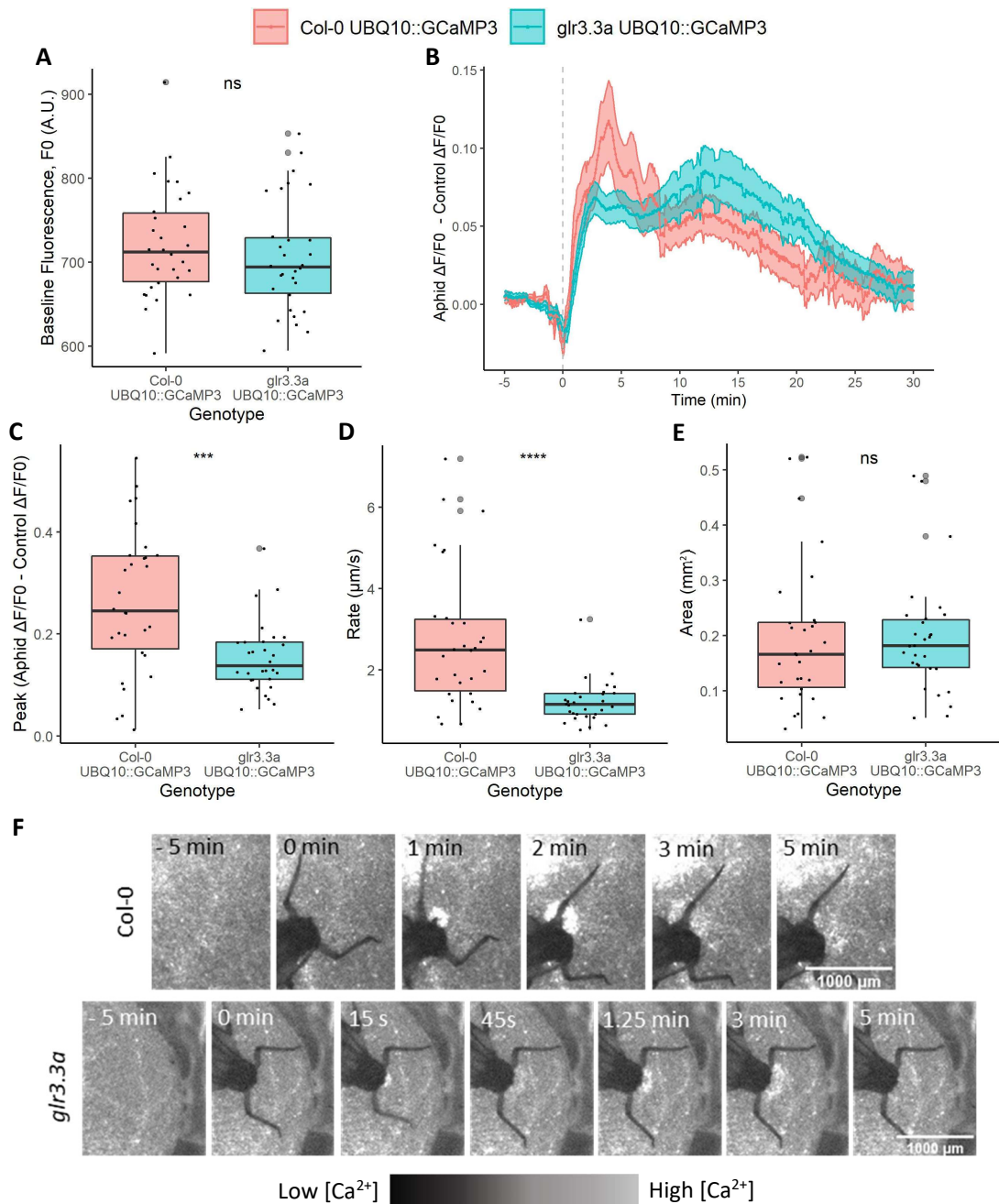


Figure 5.3 *R. padi* feeding induces GCaMP3 signals that are partially dependent on *glr3.3a*.

Properties of *R. padi* feeding-induced GCaMP3 signals in Col-0 and *glr3.3a* UBQ10::GCaMP3 *A. thaliana* ($n = 30$). Elevations were recorded by imaging (Axio Zoom.V16, HXP 120 V light source) *A. thaliana* leaves subjected to *R. padi* or no aphid control treatments. Non-corrected fluorescence intensity (F , A.U.) values were recorded over the area of feeding-induced reporter signals and at comparable control sites and transformed into $\Delta F/F_0$ values with F_0 being the mean F over the 5 min prior to feeding. (B) Traces for the mean \pm S.E.M. normalised $\Delta F/F_0$ values (Aphid $\Delta F/F_0$ - Control $\Delta F/F_0$) over time with feeding beginning at 0 min (grey dashed line). Boxplots are displayed for the (A) feeding site F_0 values (A.U.), (C) peak normalised $\Delta F/F_0$ values (Aphid $\Delta F/F_0$ - Control $\Delta F/F_0$), (D) signal propagation rates ($\mu\text{m s}^{-1}$) and (E) signal areas (mm^2), with grey dots associated with outliers. Statistical significance, tested using a (A) t-test or a (C, D, E) Wilcoxon rank-sum test, shown by ns: $p > 0.05$, ***: $p \leq 0.001$, ****: $p \leq 0.0001$. (F) Representative time series images of a Col-0 high intensity, fast propagating wave GCaMP3 signal and a *glr3.3a* burst and secondary signal. Times are shown in relation to aphid feeding at 0 min with a 1000 μm scale bar.

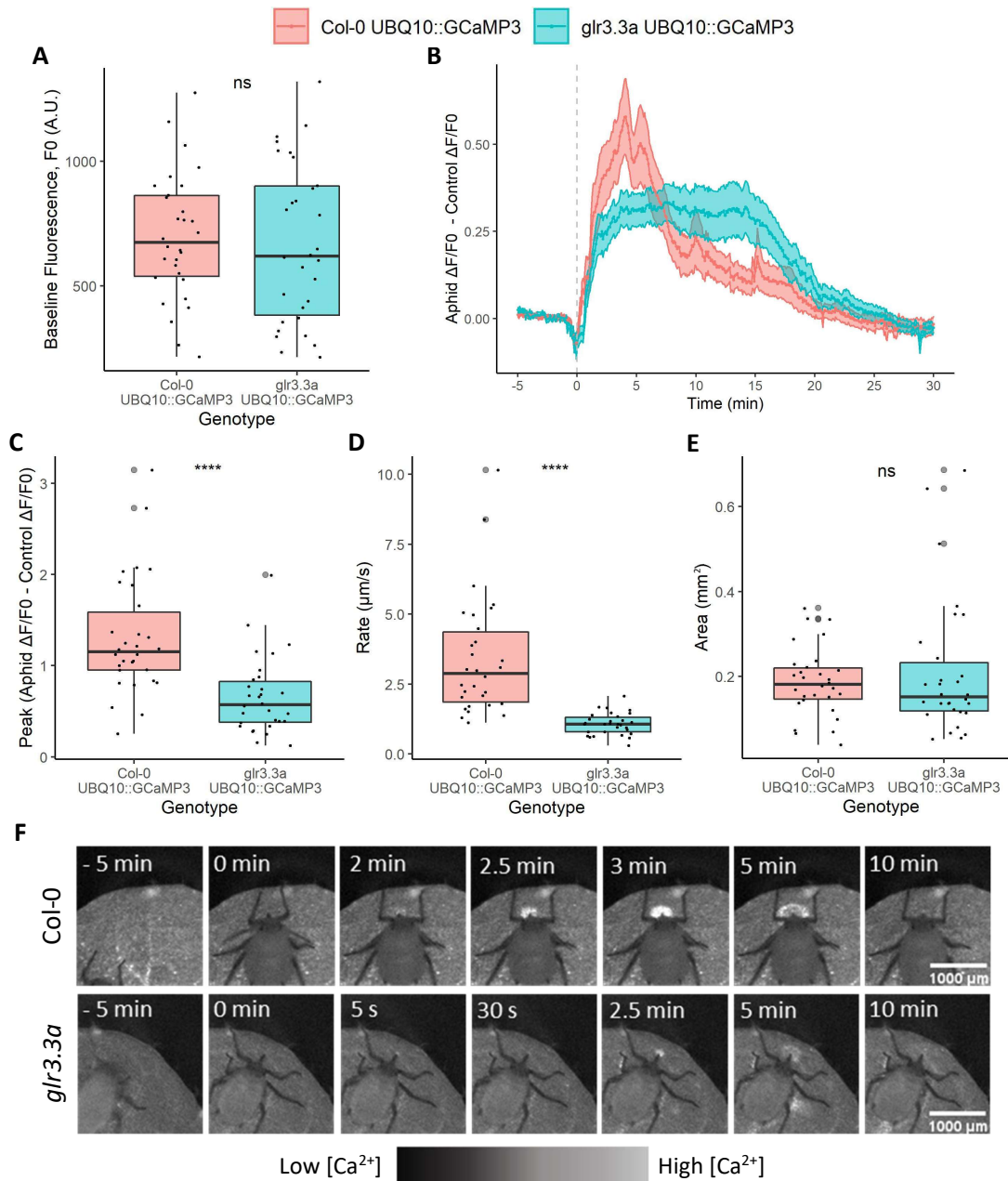


Figure 5.4 *B. brassicae* feeding induces *A. thaliana* GCaMP3 signals that are partially dependent on GLR3.3.

Properties of *B. brassicae* feeding-induced GCaMP3 signals in Col-0 and *glr3.3a* UBQ10::GCaMP3 *A. thaliana* ($n = 30$). Elevations were recorded by imaging *A. thaliana* leaves subjected to *B. brassicae* or no aphid control treatments. Background corrected fluorescence intensity (F , A.U.) values were recorded over the area of feeding-induced reporter signals and at comparable control sites and transformed into $\Delta F/F_0$ values with F_0 being the mean F over the 5 min prior to feeding. **(B)** Traces for the mean \pm S.E.M. normalised $\Delta F/F_0$ values (Aphid $\Delta F/F_0$ - Control $\Delta F/F_0$) over time with feeding beginning at 0 min (grey dashed line). Boxplots are displayed for the **(A)** feeding site F_0 values (A.U.), **(C)** peak normalised $\Delta F/F_0$ values (Aphid $\Delta F/F_0$ - Control $\Delta F/F_0$), **(D)** signal propagation rates ($\mu\text{m s}^{-1}$) and **(E)** signal areas (mm^2), with grey dots associated with outliers. Statistical significance, tested using a **(A)** t-test or a **(C, D, E)** Wilcoxon rank-sum test, shown by ns: $p > 0.05$, ****: $p \leq 0.01$. **(F)** Representative time series images of a Col-0 high intensity, fast propagating wave GCaMP3 signal and a *glr3.3a* burst and secondary GCaMP3 signal. Times are shown in relation to aphid feeding at 0 min with a 1000 μm scale bar.

5.2.3. *F. occidentalis* feeding induces localised GLR3.3-dependent [Ca²⁺] elevations in *A. thaliana*

Next, I investigated whether localised damage-based feeding from the generalist thrips, *F. occidentalis*, induces *A. thaliana* [Ca²⁺] elevations and whether these are GLR3.3-dependent. To do so, I imaged responses to *F. occidentalis* feeding on Col-0 and *glr3.3a* *UBQ10::GCaMP3* *A. thaliana*. F₀ values were not significantly different between the genotypes (Figure 5.5A, t-test, $t = -0.24$, $p = 0.81$). On leaves of both genotypes, thrips triggered multiple visible GCaMP3 signals. These localised reporter signals were considered to result from feeding events as they originated from the anterior of the thrips and often began with a visible downward movement of the head characteristic of feeding initiation (Kindt *et al.*, 2003). GCaMP3 responses to isolated feeding events were analysed and revealed that thrips feeding induced elevations in normalised $\Delta F/F_0$ values in Col-0 and *glr3.3a* (Figure 5.5B). The Col-0 samples displayed a single peak in normalised $\Delta F/F_0$ values associated with a GCaMP3 signal that propagated radially away from the feeding site as a wave elevation (Figure 5.5B, F, Video S5.2). In each *glr3.3a* sample, thrips feeding induced a highly restricted initial burst GCaMP3 signal that rapidly dissipated and was replaced by a secondary GCaMP3 signal that grew radially away from the feeding site (Figure 5.5B, F, Video S5.2). Moreover, thrips feeding-induced GCaMP3 signals in *glr3.3a* samples had reduced peak normalised $\Delta F/F_0$ values (Figure 5.5C, Wilcoxon rank-sum, $W = 774$, $p \leq 0.0001$) and signal propagation rates (Figure 5.5D, Wilcoxon rank-sum, $W = 884$, $p \leq 0.0001$). The signal areas were not statistically different between Col-0 and *glr3.3a* (Figure 5.5E, Wilcoxon test, $W = 525$, $p = 0.27$) and had mean values of 0.338 ± 0.032 mm² and 0.276 ± 0.019 mm², respectively. These data reveal that thrips feeding induces localised [Ca²⁺] elevations that are partially dependent on GLR3.3. Moreover, the signal dynamics and properties of the Col-0 and *glr3.3a* thrips feeding-induced [Ca²⁺] elevations recapitulate those of the wound-induced [Ca²⁺] elevations reported in Section 4.2.1.

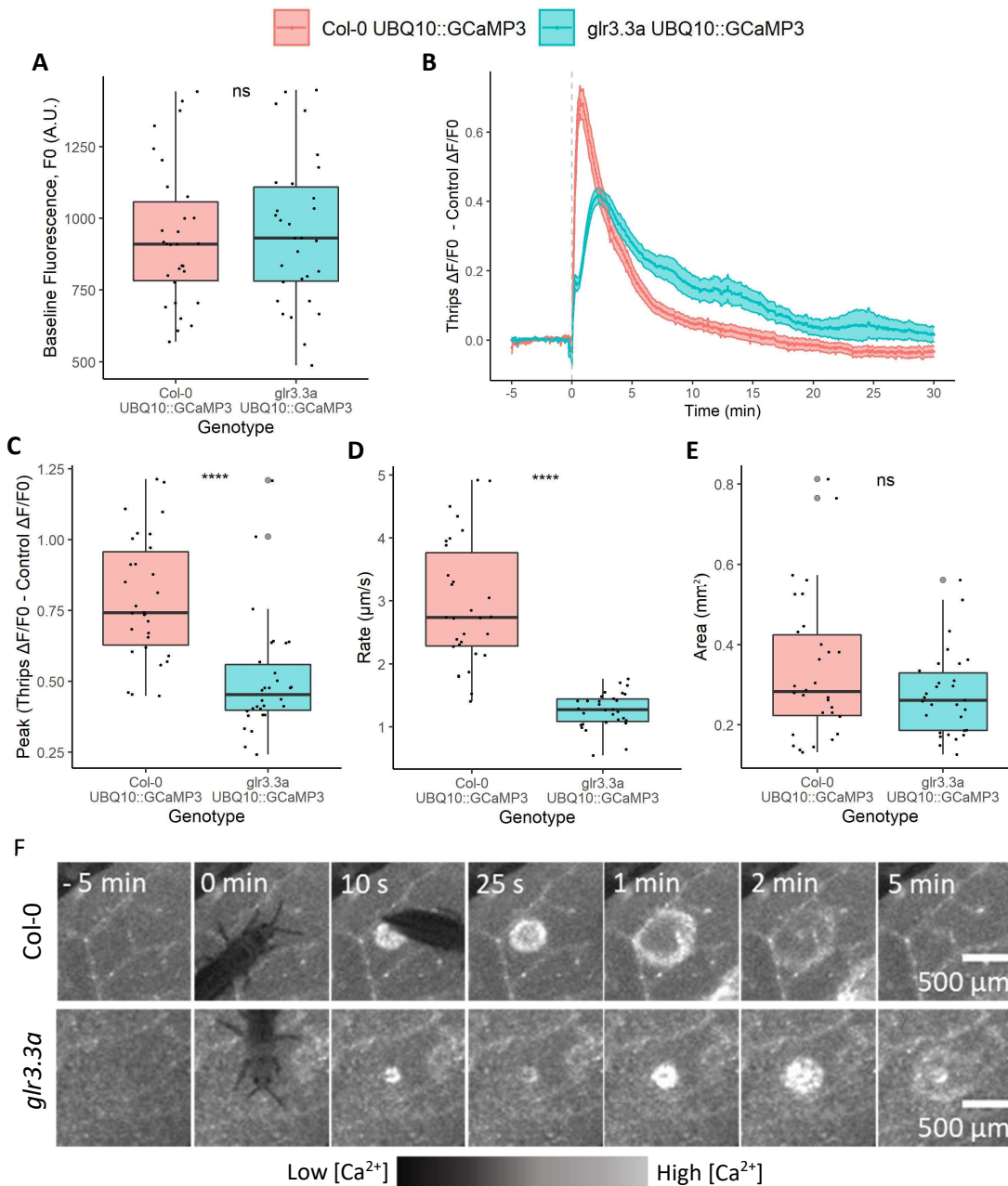
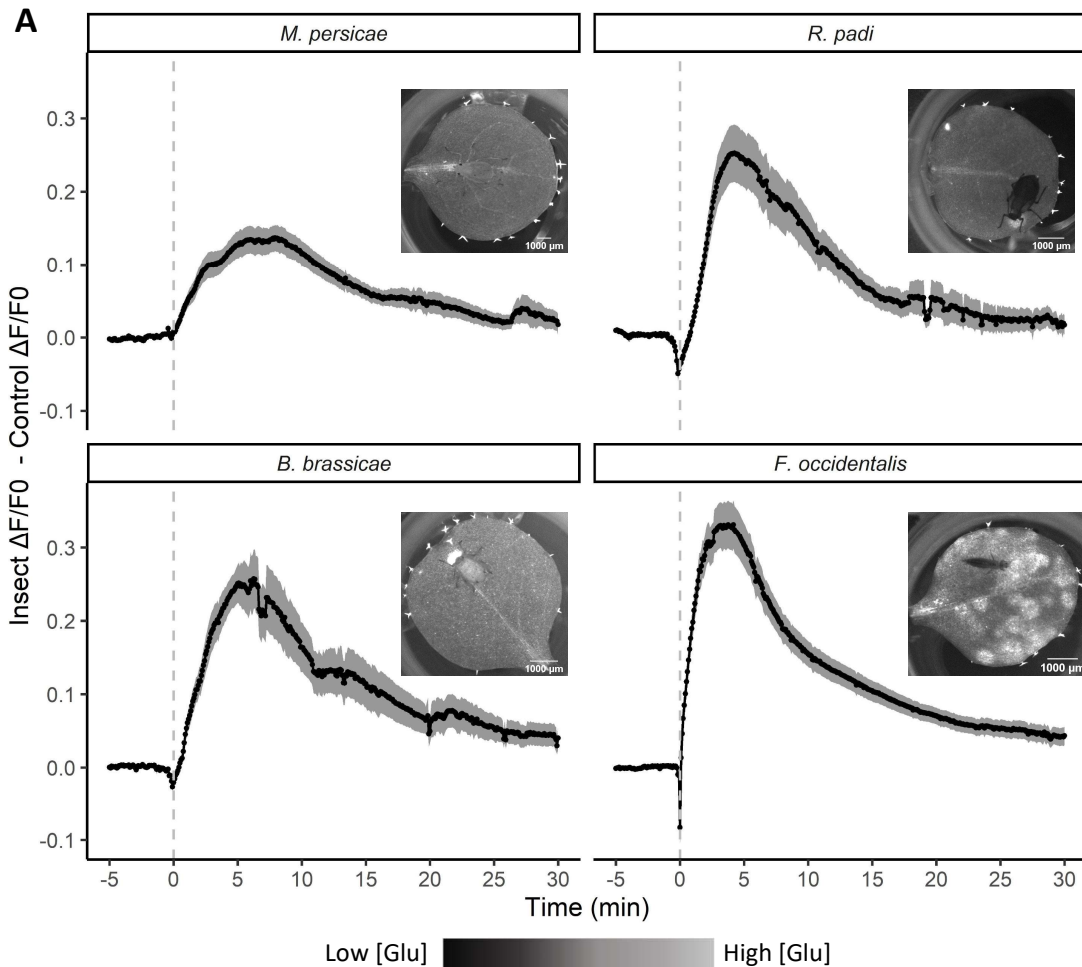


Figure 5.5 *F. occidentalis* feeding induces *A. thaliana* GCaMP3 signals that are partially dependent on GLR3.3.

Properties of *F. occidentalis* feeding-induced GCaMP3 signals in Col-0 and *glr3.3a* UBQ10::GCaMP3 *A. thaliana* ($n = 30$). Elevations were recorded by imaging *A. thaliana* leaves subjected to *F. occidentalis* or no thrips control treatments. Background-corrected fluorescence intensity (F, A.U.) values were recorded over the area of feeding-induced reporter signals and at comparable control sites and were transformed into $\Delta F/F_0$ values with F_0 being the mean F over the 5 min prior to feeding. (B) Traces for the mean \pm S.E.M. normalised $\Delta F/F_0$ values (Aphid $\Delta F/F_0$ - Control $\Delta F/F_0$) over time with feeding occurring at 0 min (grey dashed line). Boxplots are displayed for the (A) feeding site F_0 values (A.U.), (C) peak normalised $\Delta F/F_0$ values (Aphid $\Delta F/F_0$ - Control $\Delta F/F_0$), (D) signal propagation rates ($\mu\text{m s}^{-1}$) and (E) signal areas (mm^2), with grey dots associated with outliers. Statistical significance, tested using a (A) t-test or a (C, D, E) Wilcoxon rank-sum test, shown by ns: $p > 0.05$, ****: $p \leq 0.0001$. (F) Representative time series images of a Col-0 high intensity, fast propagating wave GCaMP3 signal and a *glr3.3a* burst and secondary GCaMP3 signal. Times are shown in relation to thrips feeding at 0 min with a 500 μm scale bar.

5.2.4. Localised feeding from aphids and thrips induces iGluSnFR and apo-pHusion reporter signals associated with the GCaMP3 signals

As localised feeding from the different insect species triggered GLR3.3-dependent $[Ca^{2+}]$ elevations, I investigated whether these stimuli also trigger apoplastic $[Glu]$ increases that could influence GLR3.3 activity. To do so, I imaged *35S::iGluSnFR A. thaliana* responses to feeding from *M. persicae*, *R. padi*, *B. brassicae* and *F. occidentalis* in separate experiments. All feeding events from all the insect species triggered visible iGluSnFR reporter signals except 1/30 *M. persicae* events and 2/30 *B. brassicae* events. For all species, the feeding-induced iGluSnFR reporter signals were spatially restricted to the feeding sites and gave elevations in normalised $\Delta F/F_0$ values with a peak in the mean traces around 5 min post-feeding initiation (Figure 5.6A). At this time, $\Delta F/F_0$ values at feeding sites were significantly greater than at control sites (Figure 5.6B) for *M. persicae* (Wilcoxon signed rank, $V = 3$, $p \leq 0.0001$), *R. padi* (Wilcoxon signed rank, $V = 1$, $p \leq 0.0001$), *B. brassicae* (Wilcoxon signed rank, $V = 464$, $p \leq 0.0001$) and *F. occidentalis* (paired Wilcoxon signed rank, $V = 0$, $p \leq 0.0001$). As the F_0 values appeared to differ between the experiments (Figure 5.6B) and F values were not background corrected, the normalised $\Delta F/F_0$ values could not be compared between the insect species. However, the properties of the localised iGluSnFR reporter signals (Figure 5.6B) revealed that these signals were approximately spatiotemporally correlated with the GCaMP3 reporter signals induced by feeding from each of the insect species. Therefore, if iGluSnFR reports apoplastic $[Glu]$ increases here, these increases could influence GLR3.3 activity and interact with the localised insect feeding-induced $[Ca^{2+}]$ elevations.



B

Species	Treatment	Signal Area (mm ²)	Signal Rate (μm s ⁻¹)	Peak Wound ΔF/F0 - Control ΔF/F0	Feeding Site FO (A.U.)	ΔF/F0 at 5 min
<i>M. persicae</i>	Insect	0.163 ± 0.023	2.25 ± 0.30	0.225 ± 0.022	704 ± 10	0.122 ± 0.019****
	Control					-0.005 ± 0.004
<i>R. padi</i>	Insect	0.200 ± 0.032	2.06 ± 0.21	0.331 ± 0.041	767 ± 16	0.242 ± 0.037****
	Control					-0.002 ± 0.004
<i>B. brassicae</i>	Insect	0.179 ± 0.018	1.89 ± 0.19	0.374 ± 0.041	745 ± 21	0.248 ± 0.026****
	Control					-0.003 ± 0.003
<i>F. occidentalis</i>	Insect	0.310 ± 0.018	1.95 ± 0.11	0.353 ± 0.033	734 ± 10	0.297 ± 0.032****
	Control					-0.007 ± 0.003

Figure 5.6 Localised feeding from aphids and thrips induces iGluSnFR reporter signals.

Properties of iGluSnFR signals in *A. thaliana* in responses to localised feeding from *M. persicae*, *R. padi*, *B. brassicae* and *F. occidentalis*. Reporter signals were recorded by imaging *35S::iGluSnFR A. thaliana* leaves subjected to insect or no insect control treatments. Imaging was performed with an Axio Zoom.V16 with an HXP 120 V light source for the aphid species and a Zeiss Lumenacor Spectra III light source for the thrips. Non-corrected fluorescence intensities (F, A.U.) were recorded over the area of feeding-induced reporter signals and at comparable control sites and transformed into $\Delta F/F_0$ values with F_0 being the mean F over the 5 min prior to feeding. (A) Traces for the mean \pm S.E.M. normalised $\Delta F/F_0$ values (Insect $\Delta F/F_0$ – Control $\Delta F/F_0$) over time with feeding beginning at 0 min (grey dashed line). Each trace is accompanied by a representative image of a reporter signal induced by the associated insect species (B) Table of mean \pm S.E.M. properties for the reporter signals detected in response to each species. $\Delta F/F_0$ values at 5 min after the initiation of feeding were compared between feeding and control sites using paired Wilcoxon signed rank tests with significance indicated by ****: $p \leq 0.0001$. For all experiments, $n = 30$. Visible signals were present in all samples for *R. padi* and *F. occidentalis* and in 29/30 *M. persicae* samples and 28/30 *B. brassicae* samples. Responses to feeding from each insect species were investigated in independent experiments.

Next, I explored whether feeding from the aphid and thrips species triggers apoplastic alkalinisations that could have influenced the iGluSnFR signals detected and could influence GLR3.3 activity. Through imaging *A. thaliana* expressing *35S::Apo-pHusion*, I found that feeding from each of the insect species induced visible apo-pHusion reporter signals with only 2/38 of the *M. persicae* feeding events not doing so (Figure 5.7A). For all the insect species tested, the mean normalised $\Delta R/R_0$ elevations peaked between 2- and 5-min post-feeding initiation. At 2.5 min post-feeding initiation, the $\Delta R/R_0$ values were significantly greater at feeding sites than at control sites (Figure 5.7B) for *M. persicae* (Wilcoxon signed rank, $V = 3$, $p \leq 0.0001$), *R. padi* (Wilcoxon signed rank, $V = 29$, $p \leq 0.0001$), *B. brassicae* (Wilcoxon signed rank, $V = 465$, $p \leq 0.0001$) and *F. occidentalis* (Wilcoxon signed rank, $V = 0$, $p \leq 0.0001$). The insect feeding-induced apo-pHusion reporter signal timings and properties (Figure 5.7) revealed that they spatiotemporally correlated approximately with the GCaMP3 signals induced by each species. Moreover, as F values were background corrected for apo-pHusion signals, the apo-pHusion responses to each species could be compared which revealed further correlations with the GCaMP3 signals. Specifically, *M. persicae* feeding induced apo-pHusion signals with the lowest mean peak normalised $\Delta R/R_0$ of the aphid species (Figure 5.7). This correlated with *M. persicae* seemingly inducing GLR3.3-dependent GCaMP3 signals with relatively high peak normalised $\Delta F/F_0$ values to a lesser extent than the other aphid species (Sections 5.2.1, 5.2.2). Additionally, *F. occidentalis* feeding induced both apo-pHusion and GCaMP3 reporter signals with a shorter duration than the aphid feeding-induced responses (Figure 5.7A, Sections 5.2.1-5.2.3). These comparisons suggest a close correlation between the localised insect feeding-induced apo-pHusion and GCaMP3 reporter signals. The apo-pHusion reporter signals (Figure 5.7) for each insect species were also approximately spatiotemporally correlated with those induced in iGluSnFR (Figure 5.6). Therefore, apoplastic alkalinisations likely influenced the iGluSnFR reporter signals detected in responses to localised insect feeding. In summary, localised insect feeding from the aphid and thrips species induces apoplastic alkalinisations. These alkalinisations probably influenced the iGluSnFR reporter signals detected and may interact with the feeding-induced $[Ca^{2+}]$ elevations and influence GLR3.3 activity.

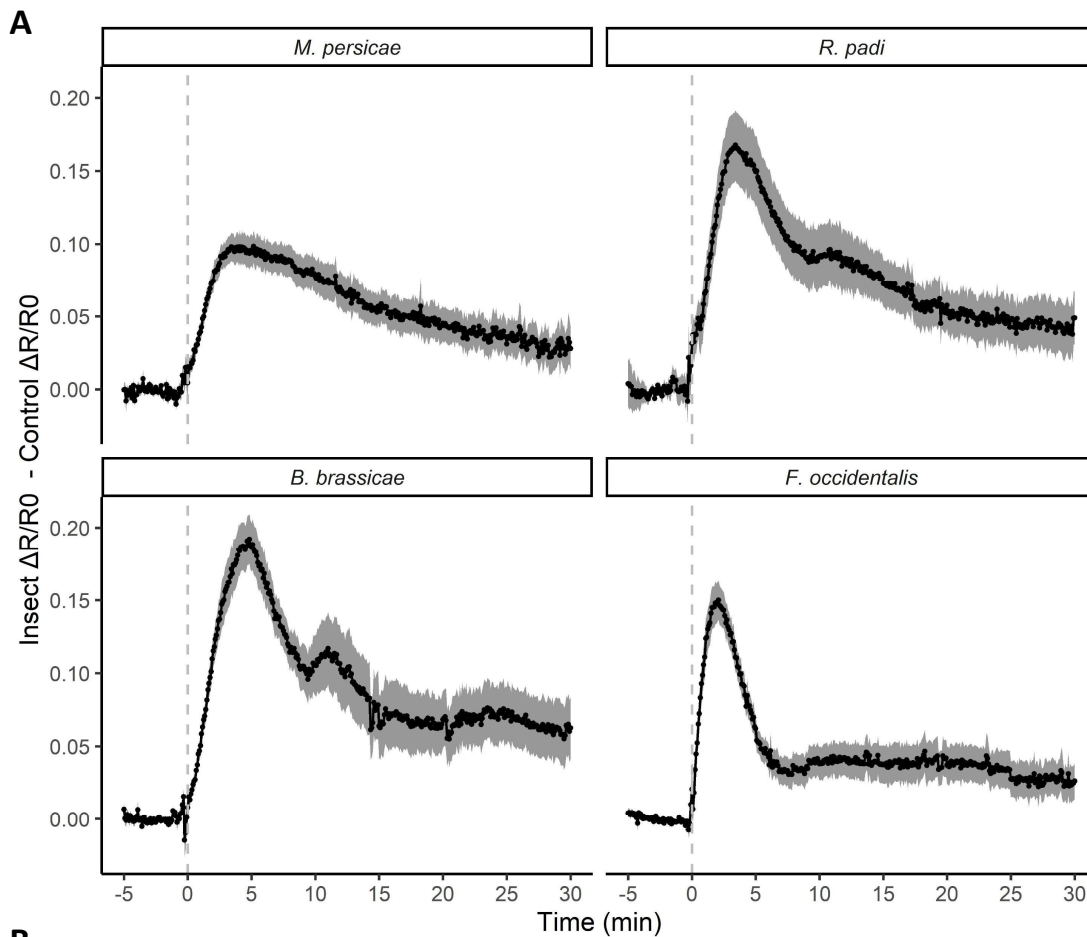


Figure 5.7 Localised feeding from aphids and thrips induces apo-pHusion reporter signals.

Properties of apo-pHusion signals in *A. thaliana* responses to localised feeding from *M. persicae*, *R. padi*, *B. brassicae* and *F. occidentalis*. Reporter signals were recorded by imaging *35S::Apo-pHusion A. thaliana* leaves subjected to insect or no insect control treatments. Background-corrected fluorescence intensities (F, A.U.) were recorded for both GFP and RFP over the area of feeding-induced reporter signals and at comparable control sites and transformed into R values by taking the GFP/RFP ratios. R0 and F0 values were the mean R and F values over the 5 min prior to feeding, respectively. R values were transformed by $\Delta R/R0$. (A) Traces for the mean \pm S.E.M. normalised $\Delta R/R0$ values (Insect $\Delta R/R0 - \text{Control } \Delta R/R0$) over time with feeding beginning at 0 min (grey dashed line). (B) Table of mean \pm S.E.M. properties for the reporter signals in response to each species. $\Delta R/R0$ values at 2.5 min after the initiation of feeding were compared using paired Wilcoxon signed rank tests with significance indicated by ****: $p \leq 0.0001$. For *M. persicae*, $n = 38$ and 36/38 feeding events induced visible signals. For all other experiments, $n = 30$ and all feeding events induced visible signals. Responses to each insect species were investigated in independent experiments.

5.2.5. Localised feeding from the aphid and thrips species differentially induces JA marker gene expression

To investigate whether feeding from the insect species induces JA-mediated responses that could be GLR3.3-dependent, I first investigated whether aphid feeding induces JA marker gene expression using the *A. thaliana* lines carrying the *pAOS::NLS-3xVENUS* or *pJAZ10::NLS-3xVENUS* transgenes. The change in fluorescence intensity (ΔF) from a pre-feeding timepoint was monitored for feeding and control sites at hourly intervals over the 8 h post-feeding. Feeding events were grouped into those that induced visible reporter signals ('Signal' group) and those that did not ('No Signal'). ΔF values were compared between feeding and control sites within these groups. For Signal samples, reporter fluorescence increased from approximately 2 h post-feeding and plateaued at around 6 h post-feeding. Only 4/48 *M. persicae* feeding events induced visible *pAOS::NLS-3xVENUS* reporter signals and there was no statistically significant difference in ΔF values between the feeding and control sites at 8 h post-feeding for these samples (Figure 5.8A, Wilcoxon signed rank, $V = 0$, $p = 0.13$). These signals had a mean area of 0.109 ± 0.028 mm². In contrast, 24/51 *R. padi* feeding events and 26/59 *B. brassicae* feeding events induced visible *pAOS::NLS-3xVENUS* reporter expression. These signals had mean areas of 0.061 ± 0.007 mm² and 0.109 ± 0.021 mm², respectively, and gave statistically greater ΔF values at feeding sites than at control sites at 8 h post-feeding (*R. padi*: Figure 5.8B, paired t-test, $t = -5.22$, $p \leq 0.0001$; *B. brassicae*: Figure 5.8C, paired t-test, $t = 5.58$, $p \leq 0.0001$). In *pJAZ10::NLS-3xVENUS A. thaliana*, 11/50 *M. persicae* feeding events and 25/56 *R. padi* feeding events induced visible reporter signals. These signals had mean areas of 0.162 ± 0.020 mm² and 0.084 ± 0.008 mm², respectively, and gave statistically greater ΔF values at feeding sites than at control sites at 8 h post-feeding (Figure 5.9A, *M. persicae*, paired t-test, $t = -4.78$, $p = 0.00074$; Figure 5.9B, *R. padi*, paired t-test, $t = -3.44$, $p = 0.0021$). In contrast, *B. brassicae* feeding induced visible *pJAZ10::NLS-3xVENUS* expression in only 1/46 feeding events (Figure 5.9C). In summary, aphid feeding induced JA marker gene expression in a subset of feeding events. AOS expression was most frequently induced by *R. padi* and *B. brassicae* feeding and rarely induced by *M. persicae* feeding. In contrast, *B. brassicae* feeding largely did not induce JAZ10 expression whilst JAZ10 expression was occasionally induced by *M. persicae* feeding and more frequently induced by *R. padi* feeding.

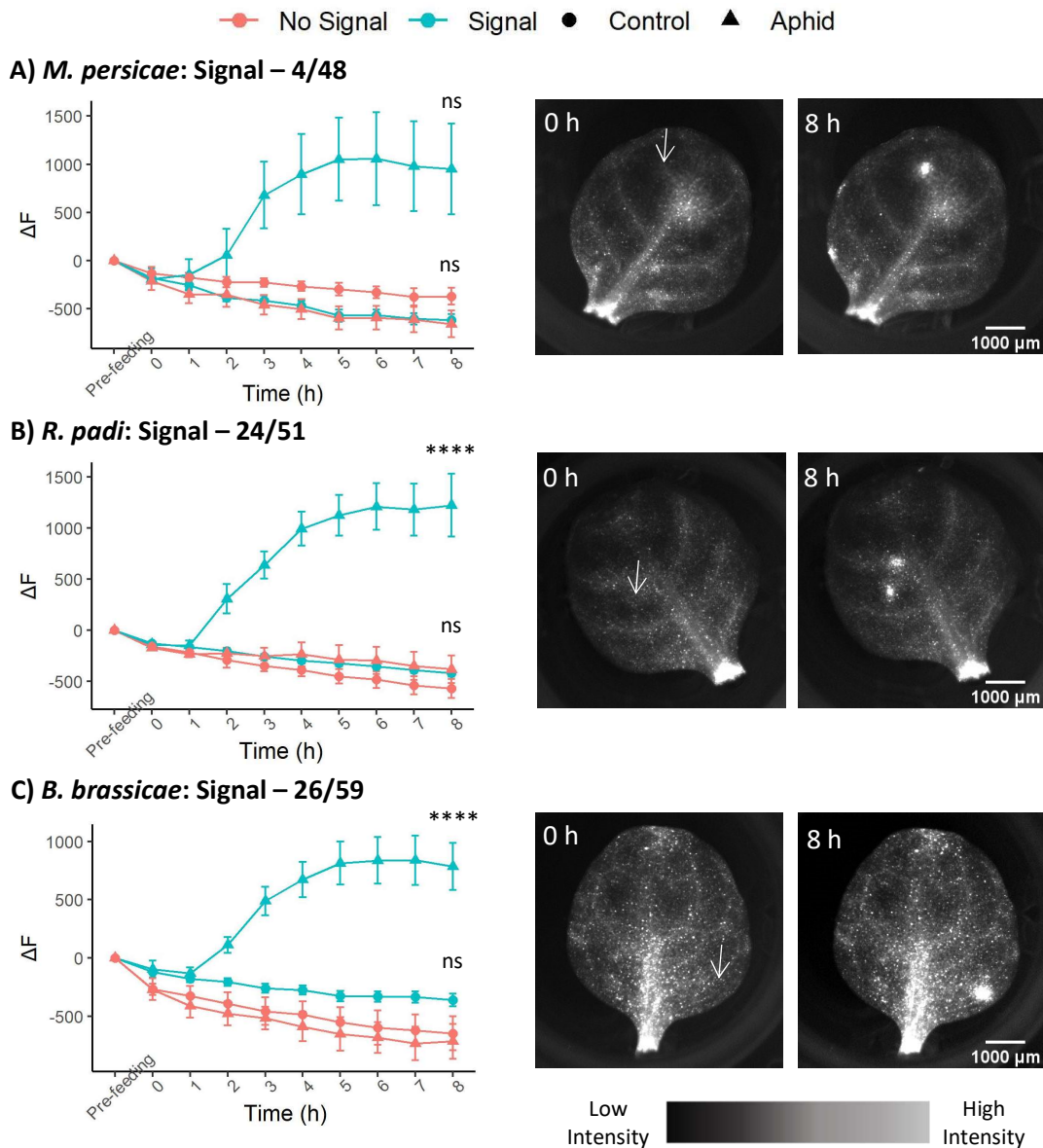


Figure 5.8 *pAOS::NLS-3xVENUS* expression in responses to feeding from different aphid species.

pAOS::NLS-3xVENUS expression in *A. thaliana* in responses to feeding from (A) *M. persicae* ($n = 48$), (B) *R. padi* ($n = 51$) and (C) *B. brassicae* ($n = 59$). Samples were categorised as those containing visible elevations in fluorescence around the feeding site over time ('Signal' samples) and those with no clear elevations ('No Signal' samples). The number of Signal samples is shown. Fluorescence intensity (F, A.U.) was monitored across reporter signal areas or, in the absence of clear signals, around feedings sites and at comparable control sites. F was measured before treatment ('Pre-feeding') and at hourly intervals from 0 h to 8 h after treatment. The mean \pm S.E.M. change in intensity over time, ΔF , is shown in traces (left) alongside images (right) from representative Signal samples at the 0 h and 8 h time points with feeding sites indicated by arrows in the 0 h images. ΔF values at 8 h were compared between feeding and control sites for the Signal and No Signal groups using paired t-tests for all comparisons except the Signal group of *M. persicae* for which a paired Wilcoxon signed rank test was used. Statistical significance is indicated by ns: $p > 0.05$, ****: $p \leq 0.0001$. Data were taken from independent investigations into each aphid species.

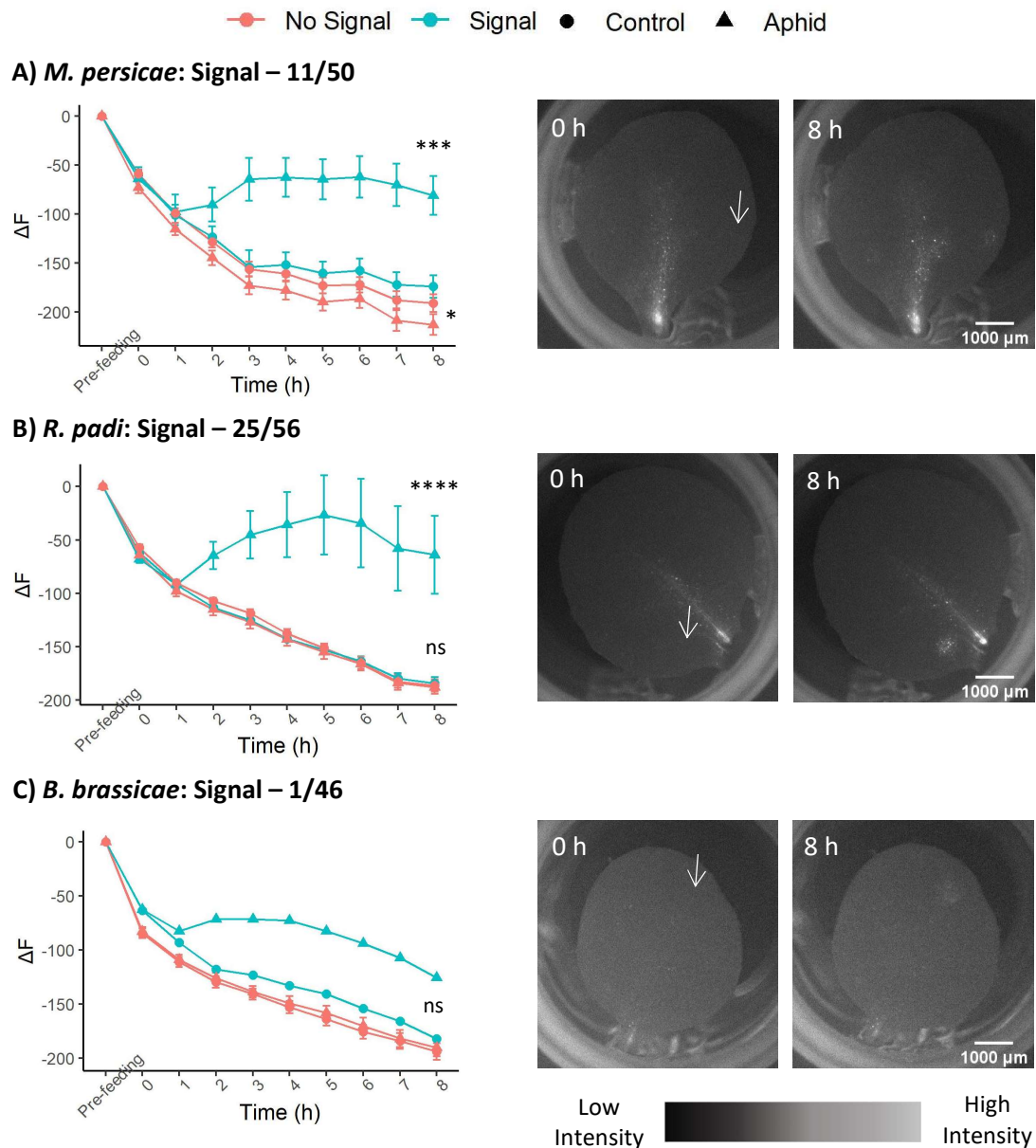


Figure 5.9 *pJAZ10::NLS-3xVENUS* expression in responses to feeding from different aphid species.

pJAZ10::NLS-3xVENUS expression in *A. thaliana* in responses to feeding from (A) *M. persicae* ($n = 50$), (B) *R. padi* ($n = 56$) and (C) *B. brassicae* ($n = 46$). Samples were categorised as those containing visible elevations in fluorescence around the feeding site over time ('Signal' samples) and those with no clear elevations ('No Signal' samples). The number of Signal samples is shown. Fluorescence intensity (F, A.U.) was monitored across reporter signal areas or, in the absence of a clear signal, around feedings sites and at comparable control sites. F was measured before treatment ('Pre-feeding') and at hourly intervals from 0 h to 8 h after treatment. The mean \pm S.E.M. change in intensity over time, ΔF , is shown in traces (left) alongside images (right) from representative Signal samples at the 0 h and 8 h time points with feeding sites indicated by arrows in the 0 h images. ΔF values at 8 h were compared between feeding and control sites for the Signal and No Signal groups using paired t-tests. Statistical significance is indicated by ns: $p > 0.05$, *: $p \leq 0.05$, ***: $p \leq 0.001$, ****: $p \leq 0.0001$. Data were taken from independent investigations into each aphid species.

Next, I investigated whether *F. occidentalis* feeding induces JA marker gene expression which could be GLR3.3-dependent by subjecting *pAOS::NLS-3xVENUS* and *pJAZ10::NLS-3xVENUS* *A. thaliana* leaves to *F. occidentalis* treatment. For treatment and control samples, the change in fluorescence (ΔF) from a pre-treatment timepoint was monitored hourly over the 8 h post-treatment. As thrips feeding sites could not easily be recorded, I first monitored the ΔF values over the area of the leaves ('Whole Leaves' in Figure 5.10) to assess for thrips-induced JA marker gene expression. At 8 h after thrips treatment, ΔF values across whole leaves were significantly greater in treated leaves than in untreated control leaves for *pAOS::NLS-3xVENUS* (Figure 5.10A, paired t-test, $t = -3.40$, $p = 0.0027$) and *pJAZ10::NLS-3xVENUS* (Figure 5.10B, paired t-test, $t = -6.03$, $p \leq 0.0001$). Treated leaves typically displayed multiple localised reporter signal increases (Figure 5.10C) which were consistent with expected patterns of thrips feeding from *A. thaliana* leaves. Therefore, the visible JA reporter signals were likely induced by thrips feeding events. Isolated reporter signals ('Isolated Responses' in Figure 5.10) were then identified and ΔF values were analysed to characterise thrips feeding-induced *AOS* and *JAZ10* gene expression changes. Individual responses could be identified in all the thrips treated *pAOS::NLS-3xVENUS* *A. thaliana* leaves and 21/23 of the thrips treated *pJAZ10::NLS-3xVENUS* *A. thaliana* leaves. For both reporters, fluorescence increased over the area of responses from 1 h after thrips treatment and plateaued at around 6 h after treatment. Compared to control sites, ΔF values were significantly greater at 8 h post-treatment at feeding sites for *pAOS::NLS-3xVENUS* (Figure 5.10A, paired t-test, $t = -5.65$, $p \leq 0.0001$) and *pJAZ10::NLS-3xVENUS* *A. thaliana* (Figure 5.10B, paired t-test, $t = -8.85$, $p \leq 0.0001$) with signals having mean areas of 0.168 ± 0.015 mm² and 0.206 ± 0.020 mm², respectively. Therefore, these data indicate that thrips feeding induces *AOS* and *JAZ10* JA marker gene expression localised to feeding sites.

For each insect species investigated, the areas of the feeding-induced *pAOS::NLS-3xVENUS* and *pJAZ10::NLS-3xVENUS* expression responses fell within the areas of the feeding-induced GCaMP3 signals (Sections 5.2.1, 5.2.2, 5.2.3). As GLR3.3 contributed to these insect feeding-induced GCaMP3 signals, these correlations suggest that GLR3.3 could also contribute to the JA marker gene expression responses induced by the insect feeding events.

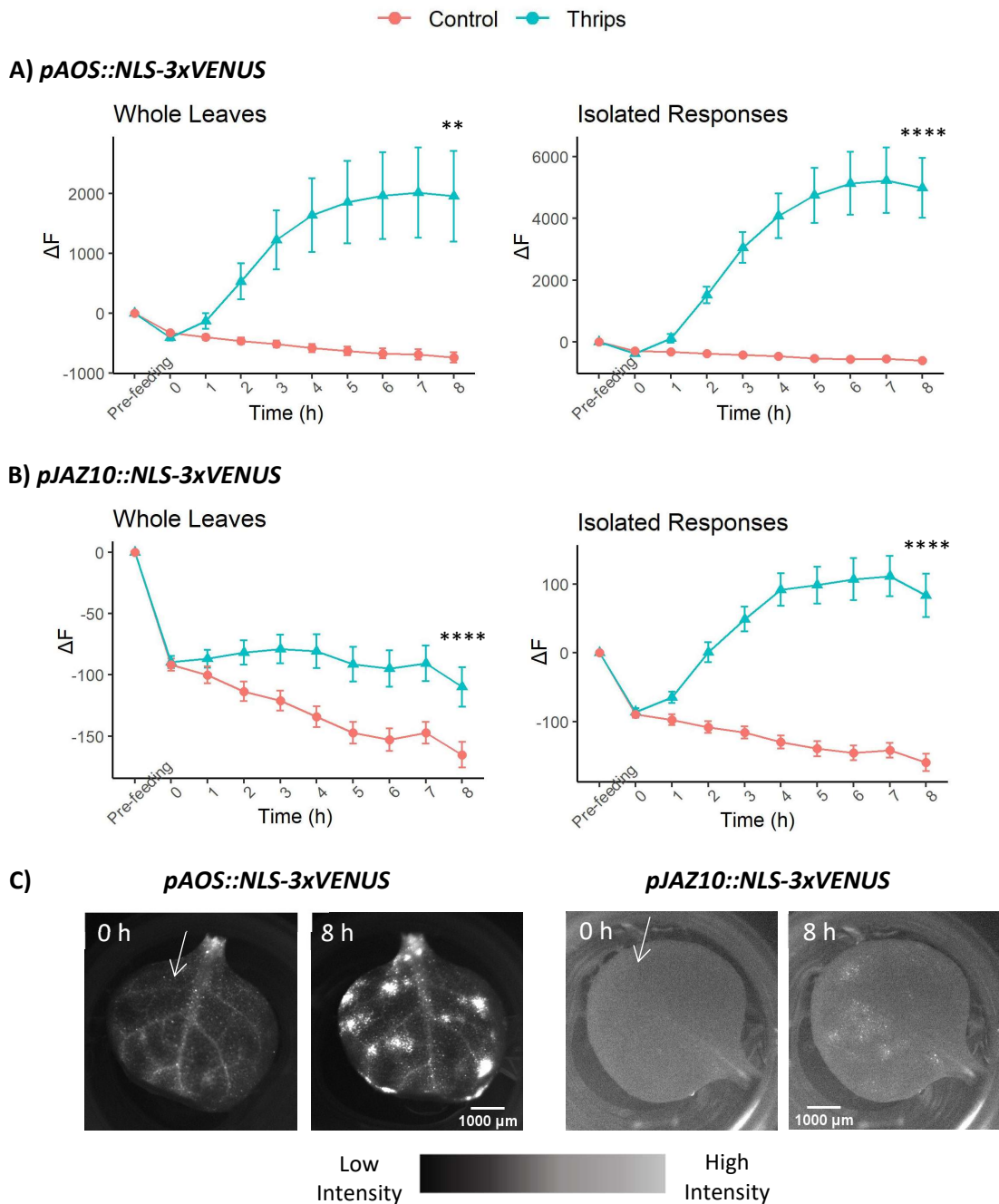


Figure 5.10 Feeding from *F. occidentalis* induces *AOS* and *JAZ10* JA marker gene expression.

F. occidentalis feeding-induced expression in *A. thaliana* of (A, C) *pAOS::NLS-3xVENUS* and (B, C) *pJAZ10::NLS-3xVENUS*. Mean fluorescence intensities (F, A.U.) were recorded before thrips treatment ('Pre-feeding') and at hourly intervals after treatment for 0 – 8 h. Samples were either thrips treated ('Thrips') with a single thrips added to the leaf or control ('Control') samples with no thrips added. F values were measured across the area of the leaves for treated and control leaves ('Whole Leaves') and, if reporter fluorescence elevations were clear, over the area of an isolated signal for each sample ('Isolated Responses'). The mean \pm S.E.M. change in F from pre-feeding, ΔF , over time is shown in traces for (A) *pAOS::NLS-3xVENUS* for whole leaves ($n = 22$) and isolated responses ($n = 22$) and for (B) *pJAZ10::NLS-3xVENUS* for whole leaves ($n = 23$) and isolated response ($n = 21$). Statistical significance was tested using paired t-tests and is shown by **: $p \leq 0.01$ and ****: $p \leq 0.0001$. (C) Representative images from 0 h and 8 h post-treatment for thrips-treated *pAOS::NLS-3xVENUS* and *pJAZ10::NLS-3xVENUS* samples. Arrows in the 0 h time point image indicate the origin of an isolated response used for analyses.

5.2.6. GLR3.3 contributes to limiting *R. padi* survival and *F. occidentalis* feeding but does not impact *M. persicae* or *B. brassicae* fecundity

Next, I investigated the contribution of GLR3.3 to resistance against each of the insect species. For *M. persicae* and *B. brassicae*, which can colonise *A. thaliana*, this was assessed by adding a single aphid nymph to individual Col-0 and *glr3.3a UBQ10::GCaMP3 A. thaliana* plants and scoring aphid fecundity (nymphs/adult) over time. There were no statistically significant differences in aphid fecundity between the genotypes for *M. persicae* (Figure 5.11A, ANOVA (Repeat + Time + Genotype), $F = 2.27$, $p = 0.13$) or *B. brassicae* (Figure 5.11B, ANOVA (Repeat + Time + Genotype), $F = 0.078$, $p = 0.78$). However, many *B. brassicae* individuals did not survive transfer to *A. thaliana* or did not produce nymphs after transfer. Of the 30 *B. brassicae* nymphs transferred to *A. thaliana*, 19 survived and produced nymphs on Col-0 whilst only 12 did so on *glr3.3a*. Further investigation would be required to determine if this difference in colonisation ability on the two genotypes is reproducible. As *R. padi* cannot colonise *A. thaliana*, resistance was assessed through survival assays on Col-0 and *glr3.3a UBQ10::GCaMP3 A. thaliana*. Survival out of 10 was scored from Day 0 to Day 6 with aphids added on Day 0. *R. padi* survival was only statistically different for Day 3 when it was greater on *glr3.3a* than on Col-0 (Figure 5.11C, ANOVA (Repeat + Time + Genotype) with Tukey post hoc, $p = 0.0026$). For assessing *F. occidentalis* resistance on Col-0 and *glr3.3a UBQ10::GCaMP3 A. thaliana*, scar damage after 8 days of colonisation from 8 adult female thrips was recorded as a measure of thrips feeding. The total area of scar damage was significantly greater on *glr3.3a* plants than on Col-0 plants after thrips treatment and was not statistically different between the genotypes on the control plants that were not treated with thrips (Figure 5.12, ANOVA (Repeat + Treatment * Genotype) with Tukey post hoc test, Thrips: $p = 0.0028$; No Thrips: $p = 0.98$). Therefore, these data provide evidence that GLR3.3 does not function in resistance against *M. persicae* or *B. brassicae* but does contribute to *F. occidentalis* resistance and performs a small but significant role in *R. padi* resistance.

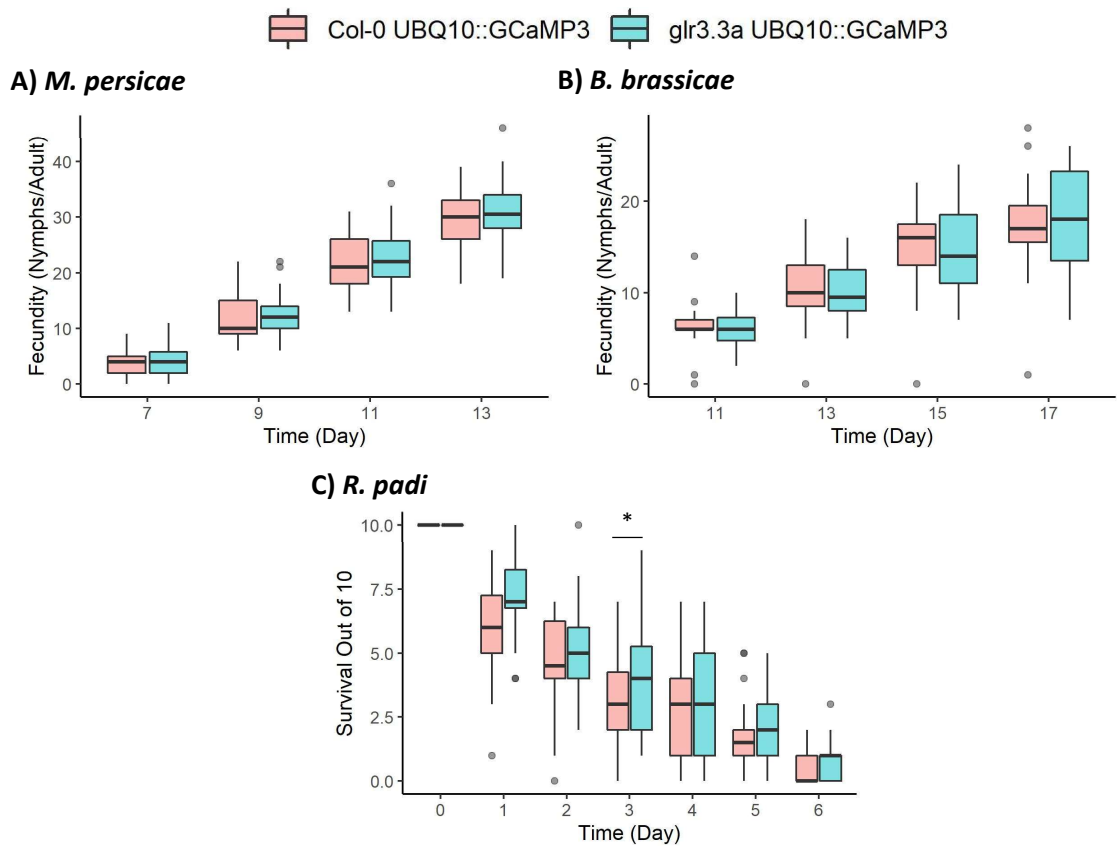


Figure 5.11 The *glr3.3a* mutation does not affect *M. persicae* or *B. brassicae* fecundity on *A. thaliana* but does increase *R. padi* survival.

Aphid performance on Col-0 and *glr3.3a UBQ10::GCaMP3 A. thaliana* measured as total fecundity (nymphs/adult) for (A) *M. persicae* and (B) *B. brassicae* and (C) survival for *R. padi*. For fecundity assays, a single nymph was caged on each *A. thaliana* plant at day 0 and total fecundity scored by removing and counting nymphs at each of the days shown. Data is reported only for aphids that survived transfer and reproduced during the experiments. For *R. padi* survival assays, 10 4-day-old aphids were caged on each *A. thaliana* plant and the number of aphids alive (Survival out of 10) was counted at each day shown. Sample sizes were (A) Col-0: $n = 29$, *glr3.3a* = 30, (B) Col-0: $n = 19$, *glr3.3a* = 12 and (C) Col-0: $n = 30$, *glr3.3a* = 30. Data were collected from three repeats and the fecundity or survival compared between the genotypes using an ANOVA on a linear model (Repeat + Time + Genotype). Statistical significance is indicated by *: $p \leq 0.05$.

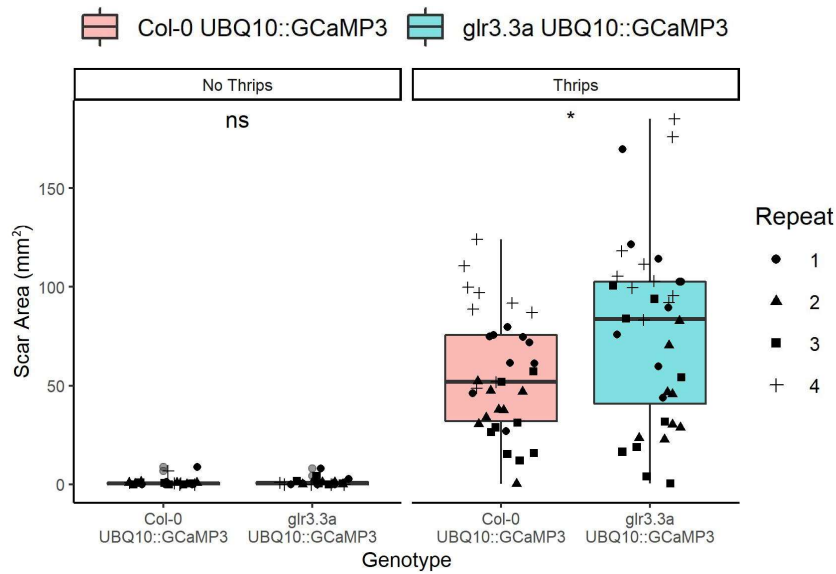


Figure 5.12 *F. occidentalis* feeding is increased on *glr3.3a* *A. thaliana*.

F. occidentalis feeding damage on Col-0 and *glr3.3a UBQ10::GCaMP3 A. thaliana* as measured by the area of scar damage. 4-week-old Col-0 and *glr3.3a UBQ10::GCaMP3 A. thaliana* plants were caged with either 8 adult female *F. occidentalis* individuals added ('Thrips') or no thrips added ('No Thrips') and left for 8 days. The leaves were then removed and the total area of scar damage for each plant was measured from leaf scans. Total scar areas (mm²) were compared between Col-0 and *glr3.3a* samples within the No Thrips and Thrips treatment groups across 4 independent repeats using an ANOVA on a linear model (Repeat + Treatment + Genotype). Data points from each repeat are shown with the shape indicating the repeat. Sample sizes were Col-0 No Thrips: $n = 25$, Col-0 Thrips: $n = 34$, *glr3.3a* No Thrips: $n = 24$ and *glr3.3a* Thrips: $n = 36$. Statistical significance is indicated by ns: $p > 0.05$, *: $p \leq 0.05$.

5.3. Discussion

In this chapter, I explored the contribution of GLR3.3 to the perception of localised feeding from *M. persicae*, *R. padi*, *B. brassicae* and *F. occidentalis*. To do so, I assessed whether feeding from each species induced GLR3.3-dependent $[Ca^{2+}]$ elevations, apoplastic pH or [Glu] increases that could influence GLR3.3 activity, and JA marker gene expression that could be GLR3.3-dependent. I also investigated whether GLR3.3 contributed to resistance against the insect species. All the insect species induced correlated apoplastic alkalinisations and $[Ca^{2+}]$ elevations. However, the extent that the $[Ca^{2+}]$ elevations were GLR3.3-dependent and the proportion of feeding events that induced JA marker gene expression varied for the different insect species, as did the contribution of GLR3.3 to *A. thaliana* resistance (Table 5.1). Specifically, *F. occidentalis* consistently induced GLR3.3-dependent $[Ca^{2+}]$ elevations along with JA marker gene expression and GLR3.3 restricted *F. occidentalis* feeding from *A. thaliana*. In contrast, aphid feeding-induced JA marker gene expression from only a subset of feeding events and feeding could induce $[Ca^{2+}]$ elevations that appeared GLR3.3-dependent or -independent. For *M. persicae*, GLR3.3 played a minor role in the aphid feeding-induced $[Ca^{2+}]$ elevations and JA marker gene expression was induced by only a limited number of feeding events. Moreover, GLR3.3 did not influence *M. persicae* fecundity. In contrast, *R. padi* seemingly induced GLR3.3-dependent $[Ca^{2+}]$ elevations and JA marker gene expression to a greater extent than *M. persicae* and *R. padi* survival increased on *glr3.3a* mutants. Finally, *B. brassicae* induced each of the responses other than *JAZ10* expression to a greater extent than *M. persicae* but *B. brassicae* fecundity was unaltered on *glr3.3a* mutants. As such, data presented here revealed that GLR3.3 functions in localised aphid and thrips feeding-induced $[Ca^{2+}]$ elevations that correlate with apoplastic alkalinisations. But, the extent that feeding activates GLR3.3 and induces JA marker gene expression, as well as the importance of GLR3.3 in insect resistance, varies between the insect species investigated.

Table 5.1 The relative presence of GLR3.3-dependent and associated responses in *A. thaliana* following feeding from the aphid and thrips species investigated.

Species	Apoplastic Alkalinisation	Role of GLR3.3 in $[Ca^{2+}]$ Elevations	<i>JAZ10</i> Induction	AOS Induction	GLR3.3-Dependent Resistance
<i>M. persicae</i>	Yes	Minor	Rare	Rare	No
<i>R. padi</i>	Yes	Moderate	Often	Often	Yes
<i>B. brassicae</i>	Yes	Moderate	Very Rare	Often	No
<i>F. occidentalis</i>	Yes	Strong	Always	Always	Yes

In Chapter 4, responses to localised wound and touch stimuli were explored along with the contribution of GLR3.3 to those responses. Considering the findings of Chapter 4 along with

those of this chapter, the mechanisms and importance of GLR3.3 in responses to localised feeding from the different aphid and thrips species will be explored here.

5.3.1. How is GLR3.3 activity regulated in responses to localised insect feeding?

As discussed in Chapter 4, the regulatory factors that determine localised GLR3.3 activation remain unclear. Here, localised insect feeding from aphids and thrips was found to induce iGluSnFR reporter signals which can indicate increases in the apoplastic concentrations of the GLR3.3 agonist and DAMP, glutamate (Toyota *et al.*, 2018; Bellandi *et al.*, 2022; Grenzi *et al.*, 2023). However, as these insect feeding-induced iGluSnFR signals were conflicted by spatiotemporally associated apoplastic alkalinisations, it is unclear whether Glu or GLR ligand release could contribute to activating GLR3.3 in these responses. The localised insect feeding-induced apoplastic alkalinisations could also contribute to GLR3.3 activation (Shao *et al.*, 2020). Almost all aphid and thrips feeding events induced spatiotemporally associated $[Ca^{2+}]$ and apoplastic pH elevations suggesting that these responses may be linked independently of GLR3.3 activation. Localised wounding and touch also induced closely correlated $[Ca^{2+}]$ elevations and apoplastic alkalinisations independently of GLR3.3 activation (Chapter 4). In Chapter 4, I proposed that localised wound-induced apoplastic alkalinisations could contribute to the activation of GLR3.3 and that this could result in a positive feedback loop between propagating apoplastic alkalinisations and GLR3.3-dependent $[Ca^{2+}]$ elevations. With the correlations between $[Ca^{2+}]$ and apoplastic pH elevations presented here, the insect feeding-induced apoplastic alkalinisations could also contribute to regulating GLR3.3 activity and do so by this same mechanism. Alternatively, the apoplastic alkalinisations may be solely downstream of the $[Ca^{2+}]$ elevations and not influence GLR3.3 activity or there could be no causal link between these two correlated responses. Further investigations will be required to understand how DAMPs and apoplastic pH contribute to the regulation of GLR3.3 activity in responses to localised insect feeding. Importantly, these investigations could identify if GLR3.3 is functioning as a DAMP receptor or a signalling component in the early responses to aphid and thrips feeding.

5.3.2. Why does localised feeding from the different insect species differentially activate GLR3.3?

F. occidentalis damage-based feeding consistently induced $[Ca^{2+}]$ elevations that were GLR3.3-dependent. In contrast, the contribution of GLR3.3 to aphid feeding-induced $[Ca^{2+}]$ elevations was less clear and varied in responses to the different aphid species. For instance, GLR3.3 appeared to contribute less to the $[Ca^{2+}]$ elevations induced by *M. persicae* than those induced by *R. padi* or *B. brassicae*. Here, factors that could determine differential GLR3.3

activation in responses to localised feeding from the three aphid species and *F. occidentalis* will be considered.

The degree of damage and/or mechanical stress caused by feeding could explain why GLR3.3 activation appeared to vary in responses to the different aphid and thrips species. As discussed in Chapter 4, this could be as GLR3.3 activation is determined by the extent of damage-induced DAMP release and/or mechanical stress experienced. As with micropipette wounding, *F. occidentalis* feeding pierces and kills epidermal and mesophyll cells (Kindt *et al.*, 2003). This feeding behaviour causes significant cell damage and mechanical stress and consistently induced GLR3.3-dependent $[Ca^{2+}]$ elevations. In contrast to thrips, aphid feeding behaviour causes limited mechanical stress and cell damage (Tjallingii, 2006) and the aphid feeding-induced $[Ca^{2+}]$ elevations were less heavily dependent on GLR3.3. Moreover, differences in the degree of mechanical stress or damage during aphid feeding from the different aphid species may explain why *M. persicae* appeared to activate GLR3.3 to a lesser extent than the other aphid species. For instance, *M. persicae* feeding may cause less mechanical stress or damage than *B. brassicae* feeding as, on some *Brassica* species, *B. brassicae* performs more probing than *M. persicae* (Cole, 1997). Moreover, *M. persicae* may cause less mechanical stress or damage than *R. padi* as *M. persicae* locates the *A. thaliana* phloem for feeding more quickly than *R. padi* with *R. padi* stylets in mesophyll and epidermal cell layers for a longer duration (Escudero-Martinez *et al.*, 2021). Other factors which can vary between aphid species, such as stylet dimensions (Harris and Maramorosch, 2014), may also influence the amount of mechanical stress or damage caused with aphid feeding and thus, GLR3.3 activation. Whilst it is not clear whether the extent damage or mechanical stress determines localised GLR3.3 activation (Section 4.3.3.), aphid feeding induced $[Ca^{2+}]$ elevations similar to those induced by touch and wounding. Therefore, mechanical stress appears significant in inducing at least some responses to aphid feeding and the extent of this stress may determine GLR3.3 activation. In any case, different extents of mechanical stress and/or damage during localised insect feeding could explain the differential GLR3.3 activation in responses to the different species investigated here.

Insects could also deliver effectors that suppress GLR3.3 activity which could contribute to determining the extent of GLR3.3 activation in responses to each of the insect species investigated here. Whilst *F. occidentalis* may possess effectors, thrips effectors have not yet been characterised (Abd-El-Haliem *et al.*, 2018; Steenbergen *et al.*, 2018; Rotenberg *et al.*, 2020). Moreover, the nature of thrips feeding makes their effectors unlikely to influence the rapid feeding-induced GLR3.3-dependent $[Ca^{2+}]$ elevations monitored here. In contrast, aphid feeding here was often maintained and triggered $[Ca^{2+}]$ elevations at various times over the 30 min after feeding initiation with some $[Ca^{2+}]$ elevations lasting most of this period. Thus, effector

delivery could occur and influence aphid feeding-induced $[Ca^{2+}]$ elevations. Indeed, various aphid effectors have been identified and characterised (Deshoux *et al.*, 2022; Chen *et al.*, 2020; Mugford *et al.*, 2016; Bos *et al.*, 2010; Liu *et al.*, 2022; Zhang *et al.*, 2022; Wang *et al.*, 2021b; Escudero-Martinez *et al.*, 2020; MacWilliams *et al.*, 2020; Dommel *et al.*, 2020; Cui *et al.*, 2019; Chaudhary *et al.*, 2018; Rodriguez *et al.*, 2017; Peng *et al.*, 2016; Wang *et al.*, 2015; Elzinga *et al.*, 2014; Atamian *et al.*, 2013; Drurey *et al.*, 2019). Whilst no aphid effectors have been specifically shown to manipulate GLR3.3 activity, *M. persicae* Mp10 is delivered into plants with feeding (Mugford *et al.*, 2016) and can suppress PTI responses induced by various elicitors, including aphid HAMPs (Bos *et al.*, 2010; Drurey *et al.*, 2019). Therefore, aphid effectors could reasonably suppress GLR3.3 activity. Effector repertoires and expression levels can vary for different aphid species and ecotypes as well as on different host plants (Boulain *et al.*, 2019; Thorpe *et al.*, 2016; Mathers *et al.*, 2017). Therefore, it may be that variation in the effectors present at feeding sites between the aphid species influences GLR3.3 activation. If this is the case, *M. persicae*, which can efficiently colonise *A. thaliana*, may be more likely to effectively suppress GLR3.3 activation than *R. padi* which cannot colonise *A. thaliana*. Many aphid effectors have been investigated in the context of PTI-like responses to aphid HAMPs (Bos *et al.*, 2010; Drurey *et al.*, 2019). The finding that mechanical stress and/or damage perception via GLR3.3 contributes to aphid feeding-induced $[Ca^{2+}]$ elevations could help search for effectors that influence GLR3.3 activity or GLR3.3-dependent responses.

In summary, the extent of mechanical stress and/or damage caused by localised insect feeding may determine the extent of GLR3.3 activation. Damage-based feeding by thrips consistently activated GLR3.3 whilst aphid feeding activated GLR3.3 to a lesser extent and causes relatively limited mechanical stress and damage. Moreover, *M. persicae* may activate GLR3.3 less than *R. padi* and *B. brassicae* because it causes less cell damage or mechanical stress during feeding or because of GLR3.3 suppression by *M. persicae* effector activity.

5.3.3. How could GLR3.3 contribute to *A. thaliana* resistance against aphids and thrips?

There were strong correlations here between GLR3.3-dependent $[Ca^{2+}]$ elevations, *JAZ10* marker gene expression and the contributions of GLR3.3 to insect resistance. For example, GLR3.3-dependent $[Ca^{2+}]$ elevations and *JAZ10* expression were consistently induced by *F. occidentalis* and *F. occidentalis* feeding was increased on *glr3.3a* mutants. Moreover, *R. padi* appeared to induce GLR3.3-dependent $[Ca^{2+}]$ elevations and JA marker gene expression to a greater extent than *M. persicae*, with GLR3.3 contributing to *R. padi* survival but not *M. persicae* fecundity. Taken together with the observation that wound-induced *JAZ10* expression is partially GLR3.3-dependent (Section 4.2.5), these correlations suggest that GLR3.3 activation likely

promotes JA-mediated defences against aphids and thrips. In support of this notion, JA-mediated defence responses can promote resistance against aphids (Ellis *et al.*, 2002; Gao *et al.*, 2007; Mewis *et al.*, 2006; Züst and Agrawal, 2016) and *F. occidentalis* (Abe *et al.*, 2008; De Vos *et al.*, 2005; Abe *et al.*, 2009; Chen *et al.*, 2023). As *B. brassicae* did not induce notable *JAZ10* expression despite inducing GLR3.3-dependent $[Ca^{2+}]$ elevations to a similar extent as *R. padi*, it may be that *B. brassicae* feeding does not induce GLR3.3-dependent JA signalling responses. This could be caused by *B. brassicae* effector activity targeting GLR3.3-dependent responses and may explain why *B. brassicae* fecundity was unaltered on *glr3.3a A. thaliana*. Interestingly, apoplastic alkalinisations can influence cell wall properties and plant defence responses (Geilfus *et al.*, 2017; Kesten *et al.*, 2019). With GLR3.3 contributing to wound-induced apoplastic alkalinisations (Section 4.2.4.), localised GLR3.3 activity could influence insect resistance through influencing apoplastic pH. Nonetheless, data here are consistent with localised GLR3.3 activation contributing to aphid and thrips resistance via the regulation of JA-mediated responses including *JAZ10* expression.

5.3.4. A piece in the puzzle of aphid and thrips perception in *A. thaliana*

Here, I identified that GLR3.3 contributes to *A. thaliana* $[Ca^{2+}]$ elevations induced by localised feeding from *M. persicae*, *R. padi*, *B. brassicae* and *F. occidentalis*. In these responses, GLR3.3 activation likely depends on the extent of mechanical stress and/or damage perceived and may be regulated by apoplastic pH and/or DAMP concentrations. GLR3.3 contributes to resistance against *R. padi* and *F. occidentalis* and likely does so through promoting JA-mediated defence responses. Therefore, strategies that limit GLR3.3 activation or suppress GLR3.3-dependent responses seem beneficial for insect colonisation. *M. persicae* may avoid or suppress GLR3.3 activation whilst *B. brassicae* may suppress GLR3.3-dependent responses. Using the model developed in Chapter 4 for localised GLR3.3 activity, the main findings of this Chapter are summarised in a model (Figure 5.13). With the regulatory mechanisms of GLR3.3 remaining unclear, it is not obvious whether GLR3.3 functions as a receptor that initially perceives localised insect feeding or as an important signalling component in responses. Nonetheless, implicating GLR3.3 in *A. thaliana* responses to thrips and aphid feeding forms a notable leap in the understanding of how *A. thaliana* perceives localised feeding from these insects.

Despite this progress, there are various unresolved components and mechanisms operating in the initial responses to aphid and thrips feeding. Specifically, the underlying mechanisms are largely uncharacterised for the GLR3.3-independent $[Ca^{2+}]$ elevations that are similar to those induced by touch. Moreover, additional regulatory or signalling components likely contribute to the GLR3.3-dependent $[Ca^{2+}]$ elevations that are alike the wound-induced

responses. Whilst mechanical stress or damage is likely important in initiating these responses, aphid feeding also triggered GLR3.3-independent $[Ca^{2+}]$ elevations that did not clearly display dynamics similar to the touch- or wound-induced responses. The perception event that initiates these $[Ca^{2+}]$ elevations is unknown. Therefore, components could contribute to the perception of aphid and thrips feeding and the subsequent $[Ca^{2+}]$ elevations by functioning in the perception of mechanical stress, DAMPs, HAMPs, effectors or phytochemicals. It will be important to identify and characterise any of these components to place them alongside GLR3.3 as pieces in the puzzle of how *A. thaliana* perceives localised aphid or thrips feeding.

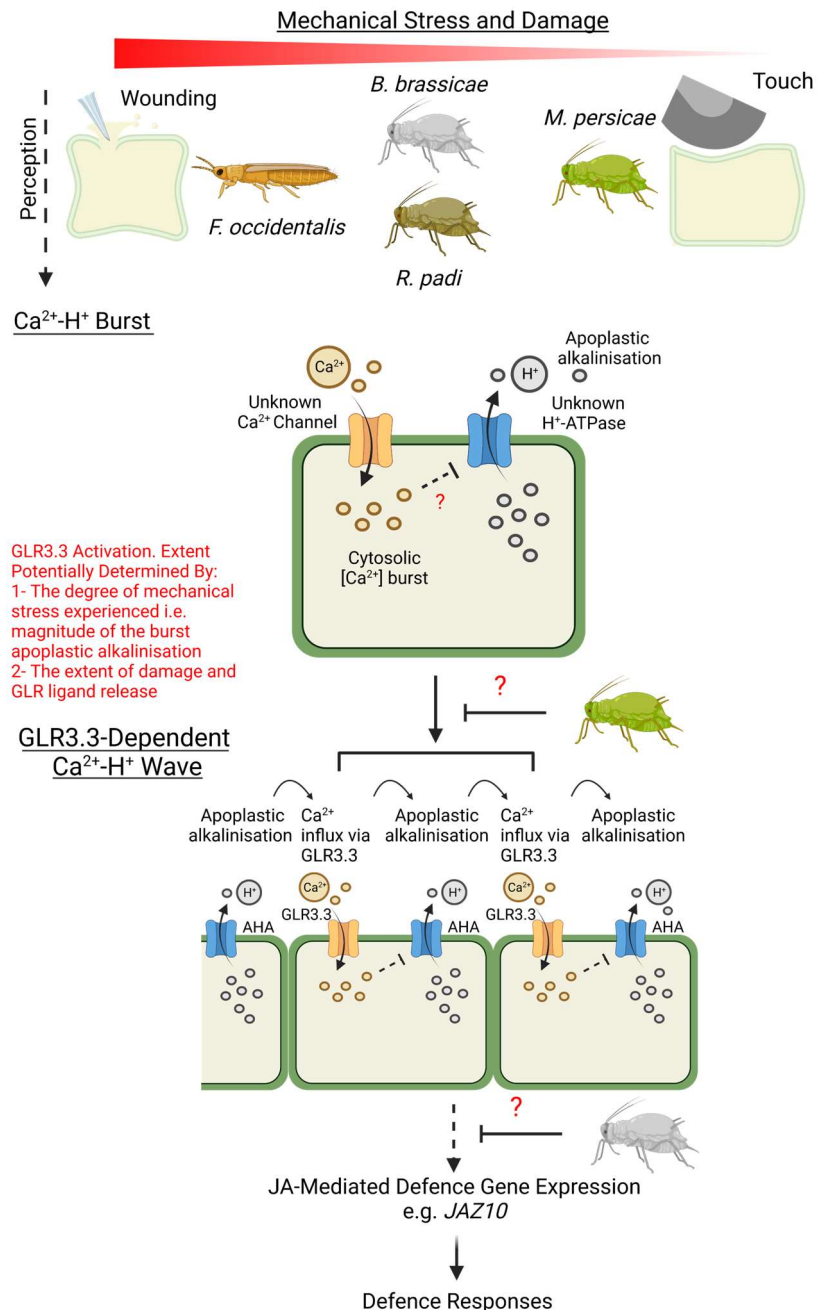


Figure 5.13 Hypothetical model for the contribution of GRL3.3 to aphid and thrips feeding-induced responses.

Model for the contribution of GRL3.3 to aphid and thrips feeding-induced responses compared to wounding- and touch-induced responses. Model based on the model presented in Figure 4.17. Here, the extent of cell damage and mechanical stress caused by the stimuli varies from high (wounding, *F. occidentalis*) to moderate (*R. padi*, *B. brassicae*) and low (touch, *M. persicae*). All stimuli can induce burst responses of [Ca²⁺] elevations and apoplasmic alkalisations. Subsequently, GRL3.3 activation can occur. The extent of GRL3.3 activation correlates with the extent of damage and mechanical stress caused by the stimuli. This correlation may result from the GRL3.3 activation being determined by the magnitude of the mechanical stress and burst apoplasmic alkalisation or the extent of damage-induced DAMP release. GRL3.3 activation results in wave [Ca²⁺] elevations which may promote further apoplasmic alkalisations in a positive feedback loop. GRL3.3 activation promotes some JA-mediated defence gene expression which in turn promotes defence responses. *M. persicae* may deploy effectors to limit GRL3.3 activation whilst *B. brassicae* may utilise effectors to suppress GRL3.3-dependent responses. This model results in effective GRL3.3-dependent defence responses against *F. occidentalis* and *R. padi* but not *M. persicae* or *B. brassicae*.

6. Screening Candidate Genes for Their Potential to Contribute to the Perception of Aphid or Thrips Feeding in *A. thaliana*

6.1. Introduction

In Chapter 4, I identified that GLR3.3 contributes to localised wound-induced responses through the perception of mechanical stress or damage. In Chapter 5, I revealed that GLR3.3 functions in responses to feeding from thrips and aphids with the extent of GLR3.3 activation potentially depending on the degree of mechanical stress or damage caused by each species. In this chapter, I focus on investigating additional components that could contribute to the perception of aphid or thrips feeding. Candidate components include those that function in GLR3.3 regulation or in responses to mechanical stress, damage, or HAMPs. In sections 6.1.1. through to 6.1.5., I categorise and outline candidate genes for contributing to the perception of aphid or thrips feeding in *A. thaliana* and summarise the rationale for their investigation in this chapter. In section 6.1.6., I outline the approaches taken to investigate these candidate components in section 6.2.

6.1.1. Candidate genes selected for their potential to regulate GLR3.3 activity

Several genes have been demonstrated to influence GLR3.3 activity and could do so in responses to localised insect feeding. These genes include *ISI1*, *AHA1* and *MSL10*.

IMPAIRED SUCROSE INDUCTION1, ISI1, was identified through its role in promoting the sugar-induced expression of starch biosynthesis genes with *isi1* mutants displaying altered carbohydrate allocation as well as reduced plant growth and seed set (Rook *et al.*, 2006). Whilst ISI1 function is not fully characterised, its expression is known to be predominantly in the phloem with some sugar-inducible expression demonstrated in leaf mesophyll cells (Rook *et al.*, 2006). Recently, ISI1 was found to interact with the GLR3.3 C-terminal domain and suppress large-scale wound-induced systemic electrical signalling and caterpillar resistance (Wu *et al.*, 2022). As ISI1 does not display any apparent functional domains, it may function as a scaffold protein for mediating GLR3.3 interactions with other unknown regulatory factors (Wu *et al.*, 2022). In this way, ISI1 could influence GLR3.3 activity in *A. thaliana* responses to thrips or aphid feeding.

H⁺-ATPase 1, AHA1, encodes a plasma membrane H⁺-ATPase that extrudes protons into the apoplast (Falhof *et al.*, 2016) with expression in various *A. thaliana* tissues including within leaves (Merlot *et al.*, 2007). AHA1 functions in the repolarisation phase of large-scale wound-induced systemic membrane depolarisations with *aha1* mutants displaying longer duration depolarisations and enhanced JA-mediated resistance against *S. littoralis* (Kumari *et al.*, 2019; Shao *et al.*, 2020). Interestingly, these membrane depolarisations are curtailed in the *glr3.3a* mutant and this phenotype is dominant to the *aha1-7* mutant phenotype (Kumari *et al.*, 2019).

Therefore, GLR3.3 and AHA1 appear to function in the same large-scale wound-induced response mechanism. As GLR3.3 activity is gated by apoplastic pH, AHA1 could influence GLR3.3 activity by determining apoplastic pH (Shao *et al.*, 2020). For example, with large-scale wounding, AHA1 may be suppressed resulting in apoplastic pH increases which promote GLR3.3 activity and depolarisations. AHA1 activity could then re-acidify the apoplast thereby limiting GLR3.3 activity and promoting repolarisation. Through this activity, AHA1 could regulate GLR3.3 activity in responses to aphid or thrips feeding.

MscS-LIKE 10, MSL10, encodes a plasma membrane mechanosensitive ion channel that preferentially transports anions and is primarily expressed in root cells and leaf vascular tissue (Maksaev and Haswell, 2012; Moe-Lange *et al.*, 2021; Haswell *et al.*, 2008). MSL10 modulates resistance to *P. syringae* (Basu *et al.*, 2022) and confers mechanosensitivity to root protoplasts (Haswell *et al.*, 2008). MSL10 also contributes to cell swelling-induced responses including $[Ca^{2+}]$ elevations, which are reduced in *msl10-1* null mutants but enhanced in *msl10-3G* gain-of-function mutants (Basu and Haswell, 2020). Recently, MSL10 has been proposed to perceive vascular pressure changes following large-scale wounding and to contribute to the systemic depolarisations (Moe-Lange *et al.*, 2021). These MSL10-dependent depolarisations are thought to be required for the full activation of GLR3.3/3.6 (Moe-Lange *et al.*, 2021). Though large-scale wound-induced $[Ca^{2+}]$ elevations in local tissue are not impaired in *msl10-1* mutants (Moe-Lange *et al.*, 2021), the properties of MSL10 suggest that it could perceive membrane tension changes during localised insect feeding and influence GLR3.3 activity.

6.1.2. Candidate genes investigated for their contributions to large-scale wound-induced rapid systemic signalling

The function of GLR3.3 in large-scale wound-induced rapid systemic signalling is well documented (Mousavi *et al.*, 2013; Nguyen *et al.*, 2018; Bellandi *et al.*, 2022; Grenzi *et al.*, 2023; Gao *et al.*, 2023). With GLR3.3 functioning in responses to localised insect feeding, other components implicated in this rapid systemic signalling may also function in *A. thaliana* responses to aphid or thrips feeding. Genes implicated in large-scale wound-induced rapid systemic signalling include *GLR3.2*, *TPC1* and *RBOHD*. *RBOHF* has been implicated in similar systemic signalling responses to high light stress.

GLUTAMATE RECEPTOR-LIKE 3.2, GLR3.2, encodes a Ca^{2+} -permeable GLR that can bind amino acid ligands including Gly and Met (Gangwar *et al.*, 2021). GLR3.2 localises at the plasma membrane and is predominantly expressed in roots and rapidly growing tissues with lower expression present in leaf vascular tissues (Vincill *et al.*, 2013; Turano *et al.*, 2002). Whilst GLR3.2 does not interact with GLR3.3 (Vincill *et al.*, 2013), *glr3.2* mutants are alike *glr3.3* mutants in that

they are impaired in large-scale wound-induced depolarisations in both local and systemic leaves (Mousavi *et al.*, 2013). This similarity suggests that GLR3.2 could, like GLR3.3, function in responses to aphid or thrips feeding.

TWO-PORE CHANNEL 1, TPC1, encodes a Ca^{2+} -, K^+ - and Na^+ -permeable cation channel that is responsible for large outward-rectifying conductance with slow activation kinetics at the tonoplast (Peiter *et al.*, 2005; Hedrich and Neher, 1987; Ward and Schroeder, 1994; Gradogna *et al.*, 2009; Guo *et al.*, 2016; Allen and Sanders, 1995). This TPC1 activity is regulated by voltage and $[\text{Ca}^{2+}]$ with elevated cytosolic $[\text{Ca}^{2+}]$ promoting opening and elevated vacuolar $[\text{Ca}^{2+}]$ limiting opening (Guo *et al.*, 2016; Beyhl *et al.*, 2009; Allen and Sanders, 1996; Hedrich and Neher, 1987). TPC1 has been proposed to mediate Ca^{2+} release from the vacuole and could contribute to a Ca^{2+} -induced- Ca^{2+} -release mechanism for Ca^{2+} signalling (Ward and Schroeder, 1994; Allen and Sanders, 1995). Moreover, *tpc1* mutants are impaired in ABA-induced repression of germination, Ca^{2+} -induced stomatal closure (Peiter *et al.*, 2005), propagating salt-induced $[\text{Ca}^{2+}]$ elevations (Evans *et al.*, 2016; Choi *et al.*, 2014c) and tonoplast excitability (Jašlan *et al.*, 2019). Additionally, TPC1 functions in the propagation of large-scale wound-induced $[\text{Ca}^{2+}]$ elevations (Kiep *et al.*, 2015). Though TPC1 did not appear to contribute to *M. persicae*- or wound-induced $[\text{Ca}^{2+}]$ elevations in Chapter 3, these functions of TPC1 suggest that it could contribute to $[\text{Ca}^{2+}]$ elevations induced by aphid or thrips feeding thereby warranting further investigation.

RESPIRATORY BURST OXIDASE HOMOLOG D & F, RBOHD & F, are expressed in leaves amongst other locations and encode plasma membrane enzymes that produce ROS important in many plant stress responses including immune responses (Morales *et al.*, 2016; Kadota *et al.*, 2014; Kadota *et al.*, 2015; Torres *et al.*, 2002; Otulak-Kozieł *et al.*, 2020). High light stress and large-scale wounding induce systemic ROS and $[\text{Ca}^{2+}]$ elevations which are RBOHD-dependent and GLR3.3/3.6-dependent in adult *A. thaliana* (Fichman and Mittler, 2021a; Fichman and Mittler, 2021b; Fichman *et al.*, 2019; Miller *et al.*, 2009). RBOHF also contributes to systemic ROS elevations induced by high light stress but not by wounding (Zandalinas *et al.*, 2020; Miller *et al.*, 2009). These findings have led to models for rapid systemic signalling involving GLR3.3/3.6 and RBOHD/F in which systemic ROS and $[\text{Ca}^{2+}]$ elevations interact to promote signal propagation (Johns *et al.*, 2021; Gilroy *et al.*, 2016). A similar model has been proposed for root salt stress-induced propagating ROS and $[\text{Ca}^{2+}]$ elevations (Evans *et al.*, 2016). The links between RBOHD/F and GLR3.3 in systemic signalling suggests that they could all function in responses to localised insect feeding in leaves. Moreover, *M. persicae* resistance is reduced on mutants in *RBOHD* (Miller *et al.*, 2009) and *RBOHF* (Jaouannet *et al.*, 2015). Therefore, *RBOHD* and *RBOHF* form candidates for investigations here.

6.1.3. Candidate genes for perceiving mechanical stress during thrips or aphid feeding

Mechanical stress perception appeared to be significant in $[Ca^{2+}]$ elevations induced by touch, wounding and localised insect feeding. Along with MSL10, there are various components that could mediate this perception via different mechanisms. One mechanism could involve ion channel opening upon increased membrane tension or with increased tension between an ion channel and other proteins (Hamant and Haswell, 2017). Secondary mechanoreceptors can also perceive mechanical stress by detecting changes in cell wall properties that can occur without plasma membrane damage (Rui and Dinneny, 2020; Hamant and Haswell, 2017). Candidate genes for contributing to mechanical stress perception during aphid or thrips feeding include *TPK1*, *MCA1*, *MCA2*, *PIEZO1*, *GL1* and *FER*.

TWO-PORE K^+ CHANNEL 1, *TPK1*, encodes a tonoplast localised K^+ channel expressed in many tissues, including the leaf mesophyll, with permeability regulated by cytosolic $[Ca^{2+}]$ and pH (Czempinski *et al.*, 2002; Bihler *et al.*, 2005; Gobert *et al.*, 2007). *TPK1* has functions in K^+ homeostasis (Gobert *et al.*, 2007), tonoplast depolarisation (Jašlan *et al.*, 2019) and ABA- and CO_2 -induced stomatal closure (Isner *et al.*, 2018). With *TPK1* also thought to function as a mechanosensitive ion channel important in osmosensing (Maathuis, 2011), *TPK1* could contribute to the perception of mechanical stresses during aphid or thrips feeding.

MID1-COMPLEMENTING ACTIVITY 1 & 2, *MCA1* & 2, encode Ca^{2+} -permeable plasma membrane channels with *MCA1* expressed primarily in leaf vascular tissue and *MCA2* expressed throughout leaves (Nakagawa *et al.*, 2007; Yoshimura *et al.*, 2021; Yamanaka *et al.*, 2010). These channels have overlapping but distinct functions including in the ability of roots to sense the hardness of growth media (Yamanaka *et al.*, 2010), in responses to chilling and freezing (Mori *et al.*, 2018) and in responses to hypergravity (Hattori *et al.*, 2020). Recently, *MCA2* activity has been shown to be regulated by membrane tension and voltage with *MCA1* thought to be regulated similarly (Yoshimura *et al.*, 2021). These properties suggest that *MCA1* and/or *MCA2* could contribute to thrips- or aphid-induced $[Ca^{2+}]$ elevations as mechanosensitive Ca^{2+} -permeable channels.

PIEZO genes were first identified in mammals where PIEZO proteins function as plasma membrane mechanosensitive cation channels with a slight preference for calcium transport (Coste *et al.*, 2010). One *PIEZO* gene, *PIEZO1*, has been identified in the *A. thaliana* genome. *PIEZO1* is thought to function as a tonoplast-localised mechanosensitive ion channel expressed in various *A. thaliana* tissues including in trichomes (Mousavi *et al.*, 2021; Radin *et al.*, 2021; Fang *et al.*, 2021). *PIEZO1* suppresses the systemic movement of plant viruses (Zhang *et al.*, 2019). *PIEZO1* also contributes to mechanical stress perception in roots including in the

associated $[Ca^{2+}]$ elevations and ability to penetrate harder media (Mousavi *et al.*, 2021; Fang *et al.*, 2021). Therefore, PIEZO1 could contribute to mechanical stress perception during thrips or aphid feeding.

GLABROUS 1, GL1, encodes a Myb transcription factor most heavily studied for being required in trichome development (Larkin *et al.*, 1994). However, *gl1* mutants also display impaired leaf cuticle development which is associated with reduced resistance to fungal pathogens (Xia *et al.*, 2010). Moreover, *gl1* mutants are impaired in the ability to trigger mechanical stress-induced $[Ca^{2+}]$ elevations in leaves (Matsumura *et al.*, 2022) that recapitulate those induced by localised wounding. Whilst this phenotype is thought to be due to the loss of trichomes, it could instead be caused by an impaired ability to perceive mechanical stresses due to the cuticle defects. If this is the case, then GL1 could influence mechanical stress perception in epidermal or mesophyll cells during feeding from aphids or thrips.

FERONIA, FER, encodes a plasma membrane RLK which is a member of a family of RLKs that contain extracellular domains homologous to the diglucose-binding protein, malectin (Li *et al.*, 2016b). This property of FER may facilitate binding to cell wall carbohydrates and an ability to respond to changes in cell wall properties (Cheung and Wu, 2011). Indeed, FER contributes to the sensing of cell wall properties during cell elongation (Dünser *et al.*, 2019). However, *FER* is also broadly expressed and *fer* mutants display highly pleiotropic phenotypes (Li *et al.*, 2016b). These *fer* phenotypes include impaired female fertility (Huck *et al.*, 2003), growth (Li *et al.*, 2015), root hair development (Duan *et al.*, 2010) and epidermal pavement cell patterning (Li *et al.*, 2015). FER pleiotropy may derive from its activity as a scaffold protein for several RLKs, including FLS2, that results in it modulating immune signalling (Stegmann *et al.*, 2017). Importantly here, FER has been found to contribute to mechanosensing during root bending and root touch with *fer* mutants impaired in the downstream $[Ca^{2+}]$ elevations and gene expression changes (Shih *et al.*, 2014). Moreover, FER can bind the RALF1 growth regulator peptide and subsequently inhibit AHA2 leading to apoplastic alkalinisations (Haruta *et al.*, 2014). These functions of FER make it a candidate for contributing to aphid and thrips feeding-induced $[Ca^{2+}]$ and apoplastic pH elevations, potentially by perceiving mechanical stress through changes in cell wall properties.

6.1.4. Candidates genes selected for their role in damage perception

Cell damage is fundamental in thrips feeding and can occur with aphid feeding but to a lesser extent. Therefore, damage perception may be significant in responses to aphid and thrips feeding. Various genes have been implicated in the perception of damage, DAMPs or damage-associated phytochemicals including *PEPR1*, *PEPR2*, *MIK2*, *DORN1*, *ACA8* and *ACA10*.

PLANT ELICITOR PEPTIDE RECEPTOR 1 & 2, PEPR1 & 2, encode plasma membrane RLKs with overlapping functions as receptors for the 8 *A. thaliana* PLANT ELICITOR PEPTIDES (PEPs) which they bind with differing affinities (Krol *et al.*, 2010; Yamaguchi *et al.*, 2010; Yamaguchi *et al.*, 2006). There is variation in PEP expression and localisation pattern throughout *A. thaliana* (Bartels *et al.*, 2013). However, all PEPs function as phytoytokines expressed as precursor PROPEPs and then liberated by [Ca²⁺]-dependent metacaspase (MC) activity (Shen *et al.*, 2019; Hou *et al.*, 2021a). Following PEP binding, PEPR1 and 2 trigger PTI-like responses including MAPK activation, resistance to several pathogens and [Ca²⁺] elevations that are dependent on CNGC2, 4 and 19 (Bartels *et al.*, 2013; Yamaguchi *et al.*, 2010; Qi *et al.*, 2010; Huffaker *et al.*, 2006; Liu *et al.*, 2013b; Tian *et al.*, 2019; Meena *et al.*, 2019). PEP signalling can function in damage perception with PEPR1/2 promoting responses to large-scale wounding and *S. littoralis* feeding (Meena *et al.*, 2019; Klausner *et al.*, 2015). Interestingly, a damage-induced loss of membrane integrity in roots causes Ca²⁺ influxes which activate MC4 to release PEP1 to surrounding cells within 1 min of damage (Hander *et al.*, 2019). Such a mechanism could underpin the burst and secondary GLR3.3-independent [Ca²⁺] elevations that were detected in responses to localised stimuli in leaves (Chapter 4 & 5). Therefore, damage induced by aphid or thrips feeding may trigger PEPR1/2-mediated responses.

MDIS1-INTERACTING RECEPTOR-LIKE KINASE 2, MIK2, encodes a plasma membrane-localised RLK that perceives *A. thaliana* SCOOP phytoytokine peptides with binding demonstrated for SCOOP12 (Rhodes *et al.*, 2021; Hou *et al.*, 2021b). MIK2 functions include in salt stress tolerance (Van der Does *et al.*, 2017; Julkowska *et al.*, 2016) and the perception of *Fusarium oxysporum* (Van der Does *et al.*, 2017; Coleman *et al.*, 2021) which may occur through the binding of SCOOP-like peptides produced by the pathogen (Rhodes *et al.*, 2021). Interestingly, SCOOP12 induces many damage-associated responses (Gully *et al.*, 2019) with MIK2 also implicated in cell wall damage sensing (Van der Does *et al.*, 2017; Julkowska *et al.*, 2016) and responses to large scale wounding and caterpillar feeding (Stahl *et al.*, 2022). As such, MIK2 and SCOOP signalling could contribute to localised damage perception. Moreover, SCOOPs are thought to be released from PROSCOOP peptides as mobile ligands (Gully *et al.*, 2019) and can induce MIK2-dependent [Ca²⁺] elevations (Rhodes *et al.*, 2021). Therefore, as with PEP signalling, SCOOP signalling could drive the delayed GLR3.3-independent secondary [Ca²⁺] elevations induced by aphid feeding or thrips feeding. Therefore, MIK2 is a candidate for contributing to aphid or thrips feeding-induced responses through the perception of SCOOPs and/or damage.

DOES NOT RESPOND TO NUCLEOTIDES 1, DORN1, encodes a plasma membrane extracellular ATP (eATP) receptor required for ATP-induced [Ca²⁺] elevations, MAPK activation

and gene expression (Choi *et al.*, 2014a; Matthus *et al.*, 2020; Bouwmeester *et al.*, 2011). Whilst intracellular ATP levels are highly regulated in plants, eATP is thought to act as DAMP in damage perception (Choi *et al.*, 2014b). Consistent with this, eATP concentrations can be elevated around wound sites (Song *et al.*, 2006). Moreover, DORN1 ectopic expression enhances wound-induced responses (Choi *et al.*, 2014a) and eATP treatment reinforces JA signalling (Chivasa *et al.*, 2009). Interestingly, eATP concentrations can also be elevated by treatment with the proposed DAMP, L-Glu (Dark *et al.*, 2011), and touch (Weerasinghe *et al.*, 2009). Therefore, both mechanical stress or damage during aphid or thrips feeding could elevate eATP levels and activate DORN1-dependent responses including $[Ca^{2+}]$ elevations. As ATP treatment induces $[Ca^{2+}]$ elevations that are tightly linked to cytosolic acidification events (Behera *et al.*, 2018), it could be that DORN1 contributes to both the localised insect feeding-induced $[Ca^{2+}]$ elevations and apoplastic alkalinisations.

AUTOINHIBITED Ca^{2+} -ATPase 8 & 10, ACA8 & 10, are considered to encode plasma membrane Ca^{2+} -ATPases with broad expression throughout *A. thaliana* including in adult leaves (Bonza *et al.*, 2000; George *et al.*, 2008; Costa *et al.*, 2017). ACA8 and 10 have overlapping and distinct functions including in *A. thaliana* development, stomatal closure, fertility, and immunity (George *et al.*, 2008; Yang *et al.*, 2017; Yu *et al.*, 2018; Frei dit Frey *et al.*, 2012; Li *et al.*, 2018). Importantly here, *aca8 aca10* double mutants are impaired in the linked cytosolic $[Ca^{2+}]$ elevations and acidifications induced by ATP (Behera *et al.*, 2018). Moreover, *aca8* single mutants display altered $[Ca^{2+}]$ elevations in responses to ATP and large-scale wounding (Costa *et al.*, 2017). Interestingly, *aca10 aca12* double mutants are impaired in the ability to produce large-scale wound-induced systemic depolarisations following prior large-scale wounding, *S. littoralis* feeding or *B. brassicae* feeding (Fotouhi *et al.*, 2022). These mutants are also impaired in *S. littoralis* and *B. brassicae* resistance (Fotouhi *et al.*, 2022). These functions of ACA8 and ACA10 in responses to ATP, large-scale wounding and insect feeding, make them candidates for contributing to aphid or thrips feeding-induced $[Ca^{2+}]$ and apoplastic pH elevations.

6.1.5. Candidate genes that function in perceiving putative aphid HAMPs

Additional candidate genes that could function in the perception of aphid feeding are those that facilitate aphid HAMP-induced responses. Whilst aphid HAMPs have been challenging to characterise, ***BRI1-ASSOCIATED KINASE 1 (BAK1)*** and ***SUPPRESSOR OF BIR1-1 (SOBIR1)*** have been implicated in the perception of *M. persicae* aphid extract which is thought to contain proteinaceous aphid HAMPs (Canham, 2022). These two LRR-RLK co-receptors contribute widely to immune and developmental signalling with SOBIR1 essential for RLP receptor function and BAK1 important in responses mediated by many RLP and RLK receptors (Liebrand *et al.*, 2014).

For example, the RLP23-SOBIR1-BAK1 complex mediates plant immune responses to the nlp20 elicitor found in multiple pathogens (Albert *et al.*, 2015). Canham (2022) found that *bak1-5* and *sobir1* mutants were impaired in *M. persicae* aphid extract-induced MAPK phosphorylation, defence gene expression and seedling growth inhibition. Moreover, BAK1 contributes to ROS elevations and defence gene expression induced by aphid extracts (Prince *et al.*, 2014) and by the putative aphid HAMP, GroEL (Chaudhary *et al.*, 2014). Whilst in Chapter 3, BAK1 did not clearly contribute to *M. persicae* feeding-induced $[Ca^{2+}]$ elevations, it may be that its contribution was masked by the GLR3.3-dependent responses to *M. persicae* feeding. Therefore, the evidence for BAK1 and SOBIR1 contributing to aphid HAMP-induced responses warrants further investigation of their contributions to aphid feeding-induced responses.

6.1.6. Screening components for their potential to contribute to aphid or thrips feeding-induced responses

The list of genes and proteins outlined here form a subset of candidate components that could contribute to aphid or thrips feeding-induced responses in *A. thaliana*. To investigate whether this is the case, a reverse genetics approach will be used here. For this, it is necessary to have a known and predictable measure of early plant responses to localised stimuli that could reveal potentially subtle differences in responses. These criteria can be met by visualising $[Ca^{2+}]$ reporter signals in real time. Moreover, there were correlations between the localised insect feeding-induced $[Ca^{2+}]$ elevations, JA marker gene expression and insect resistance (Chapter 5). These correlations indicate that visualising the $[Ca^{2+}]$ elevations can provide a valuable measure of the early plant defence responses to localised stimuli. Insect behaviour can be highly variable which limits throughput and reproducibility in experiments. *A. thaliana* responses to aphid and thrips feeding appeared to involve damage and/or mechanical stress perception and showed many similarities to localised wound- and touch-induced responses (Chapters 4 & 5). These factors allow the likelihood of candidate genes to contribute to localised insect feeding-induced responses to first be assessed by the more reproducible, higher throughput stimuli of localised touch and wounding. To assess if aphid HAMP perception contributes to *M. persicae* feeding-induced $[Ca^{2+}]$ elevations, *M. persicae* aphid extract-induced responses can first be assessed to see if they include $[Ca^{2+}]$ elevations. These elevations can then be tested for dependency on BAK1 and SOBIR1 as well as GLR3.1/3.3/3.6 to assess if these components could contribute to HAMP perception during aphid feeding. Any components that function in responses to wounding, touch or aphid extract will be assessed for their role in aphid or thrips feeding-induced $[Ca^{2+}]$ elevations and, if any role is identified, aphid or thrips resistance. Therefore, the research aims of this chapter are to:

- Investigate the contribution of candidate genes to localised wound- and touch-induced $[Ca^{2+}]$ elevations in *A. thaliana*.
- Identify if *M. persicae* aphid extract treatment induces $[Ca^{2+}]$ elevations that are dependent on BAK1, SOBIR1 or GLR3.1/3.3/3.6.
- Test any genes that contribute to wound-, touch- or aphid extract-induced $[Ca^{2+}]$ elevations for their contributions to aphid or thrips feeding-induced $[Ca^{2+}]$ elevations.
- Test any genes involved in the localised insect feeding-induced responses for their contribution to aphid or thrips resistance.

6.2. Results

6.2.1. Screening candidate mutants for a phenotype in wound- or touch-induced responses

To investigate $[Ca^{2+}]$ elevations in responses to wounding and touch in candidate gene *A. thaliana* mutants, I first established homozygous reporter-expressing *A. thaliana* mutant lines by either acquiring published seed (*aha1-7*, *piezo-1*, *gl1* and *aca8 aca10*) or by performing crosses (*isi1-3*, *glr3.2a*, *msl10-1/3G*, *tpk1-1*, *mca1 mca2*, *fer-4*, *pepr1-1 pepr2-3*, *dorn1-3*, *tpc1-2*, *rbohD rbohF*, *mik2-6*, *bak1-5* and *sobir1-12*). Whilst acquired material utilised a range of $[Ca^{2+}]$ reporters, crosses were performed to produce mutant lines expressing *35S::GCaMP3* in the wild-type background or *UBQ10::GCaMP3* in the wild-type or *glr3.3a* background. As *FER* has been implicated in apoplastic pH changes (Haruta *et al.*, 2014), *fer-4 A. thaliana* expressing *35S::ApopHusion* was also produced. Mutant and control *A. thaliana* reporter lines were then subjected to localised touch or wound treatments and reporter signals were compared between the genotypes by their baseline intensities, peak intensities, propagation rates and signal areas. Additionally, reporter signal dynamics were compared by visually assessing the normalised reporter signal traces. Therefore, using $[Ca^{2+}]$ reporter imaging as the primary measure, these experiments allowed the contributions of candidate genes to localised touch- and/or wound-induced responses to be assessed. The reporter signal properties for each candidate gene and experiment are summarised in Table 6.1 with accompanying figures in Appendix I.

For most of the candidate genes and responses investigated, most of the signal properties were not statistically different between the control and mutant lines. There were also no clear differences detected in the wound- or touch-induced signal dynamics between any of the compared mutant and control lines. The differences that were detected in signal properties can be grouped into three categories: those likely caused by reduced baseline fluorescence in mutant samples (1), those likely caused by an altered resting state or indirect effects in mutant samples (2), and those which could represent direct mutant phenotypes in wound- or touch-induced responses but that require further investigation (3).

1. Reporter baseline fluorescence was significantly reduced in the *tpk1-1* and *gl1* wound- and touch-treated samples. The wound- and touch-induced signals in these mutants displayed significantly faster propagation rates than signals in their Col-0 controls. Signal areas were significantly increased in the *gl1* touch treated samples as were peak normalised $\Delta F/F_0$ values in the touch treated *tpk1-1* and *gl1* samples. The reduced baseline fluorescence in these mutant lines, however, suggests that all

these differences are unreliable. This is because the reduced reporter baseline fluorescence was likely caused by reduced reporter expression. Reduced reporter expression usually results in a reduced signal-to-noise ratio which can bias measurements of signal properties and reduce their accuracy. Additionally, reduced reporter baseline fluorescence increases the error in background corrections (Chapter 3) which can make differences detected in peak normalised $\Delta F/F_0$ values unreliable. This is reflected in the increased variation in peak normalised $\Delta F/F_0$ values for the *gl1* and *tpk1-1* touch treated samples. With wound- and touch-induced reporter signal dynamics unaltered in *tpk1-1* and *gl1* samples, it seems likely that these mutants display wild-type touch- and wound-induced $[Ca^{2+}]$ elevations. Further investigations into these candidate genes with mutant and control lines that display equal reporter baseline fluorescence could better this hypothesis.

2. Wound treated *fer-4 (glr3.3a)*, *rbohD rbohF* and *aca8 aca10* samples displayed altered resting states. *fer-4 (glr3.3a)* and *rbohD rbohF* samples displayed elevated baseline GCaMP3 fluorescence compared to their controls. GFP baseline fluorescence from apo-pHusion was also elevated in the *fer-4* mutant whilst RFP baseline fluorescence was unaltered. Whilst baseline YFP and CFP fluorescence was not significantly altered in wound treated *aca8 aca10 UBQ10::NES-YC3.6* samples, these samples did display reduced resting YFP/CFP fluorescence intensity (R0) values (Appendix I.XXVIII, Wilcoxon rank-sum, $W = 649$, $p = 0.0093$). *rbohD rbohF*, *fer-4 (glr3.3a)* and *aca8 aca10* samples also displayed statistically significant differences in various wound-induced reporter signal properties compared to their controls. For example, the GCaMP3 signals in the *rbohD rbohF* and *fer-4* samples and the YC3.6 signals in the *aca8 aca10* samples all had significantly reduced signal areas. For the YC3.6 and apo-pHusion reporter samples, the altered resting states could indicate changes in resting $[Ca^{2+}]$ and apoplasmic pH, respectively. However, what caused the differences detected in resting GCaMP3 fluorescence cannot be determined. Nevertheless, the changes in baseline properties probably affected the measurement of other signal properties in all these mutant lines. All these mutant lines also displayed dramatic developmental phenotypes (data not shown) which may have indirectly influenced the wound-induced responses or the ability to assay them. As reporter signal dynamics were unaltered in the mutants, and as *rbohD* and *rbohF* single mutants displayed wildtype wound-induced GCaMP3 signals, it seems likely that RBOHD, RBOHF, FER, ACA8 and ACA10 do not directly perform major functions in the localised wound-induced responses assessed.

3. In touch and wound responses, there were some differences detected between mutants and their controls that could represent direct phenotypes in these responses. These occurred without differences in baseline fluorescence and were the following:

- a. *isi1-3*: Reduced GCaMP3 signal propagation rates in touch responses.
- b. *msl10-3G*: Increased GCaMP3 peak normalised $\Delta F/F_0$ values in wound responses.
- c. *tpc1-2*: Reduced GCaMP3 signal areas in touch responses.
- d. *mca1 mca2*: Reduced GCaMP3 signal propagation rates in touch responses.
- e. *dorn1-3*: Reduced GCaMP3 signal propagation rates in wound responses.
- f. *bak1-5*: Increased GCaMP3 peak normalised $\Delta F/F_0$ in touch responses.
- g. *sobir1-12*: Increased GCaMP3 peak normalised $\Delta F/F_0$ in wound responses.

Probabilistically, with 31 experiments performed and 4 variables quantified, some statistically significant differences were expected with a significance level of $p \leq 0.05$. Indeed, setting a higher significance threshold of $p \leq 0.01$ would have rendered all of these differences nonsignificant except from the differences detected for *dorn1-3* and *msl10-3G*. As the *msl10-1* null mutant displayed wild-type wound-induced GCaMP3 signals, MSL10 does not appear to be required for localised wound-induced $[Ca^{2+}]$ elevations. With none of these mutants displaying altered wound- or touch-induced GCaMP3 signal dynamics, the associated genes are all unlikely to perform major functions in the responses to these stimuli. Repeating the experiments for these genes would test whether the differences detected are robust and represent mutant phenotypes.

In summary, none of the candidate genes demonstrated clear contributions to wound- or touch-induced $[Ca^{2+}]$ elevations. Therefore, without further investigations, the candidate genes assessed seem unlikely to contribute significantly to damage or mechanical stress perception during aphid or thrips feeding.

Table 6.1 Properties of wound- and touch-induced reporter signals in mutant *A. thaliana* lines.

Properties of stimulus-induced reporter signals assessed in mutant and control *A. thaliana* lines expressing transgenic fluorescent reporters. All fluorescence intensity (F, A.U.) values were recorded at 5 s intervals for 5 min prior to treatment with localised touch or wounding and for 30 min after treatment. F0 values were the mean F over the 5 min pre-treatment. F values were background corrected for all experiments other than for *piezo-1* experiments in which the GCaMP6s baseline intensity was too low for correction. Each investigation has an accompanying figure in Appendix I which was used to assess if signal dynamics were altered in mutants. Experiments were performed independently for each mutant and stimulus. Peak Normalised $\Delta F/F_0$ and $\Delta R/R_0$ are displayed with units of 'Stimulus $\Delta F/F_0$ – Control $\Delta F/F_0$ ' and 'Stimulus $\Delta R/R_0$ – Control $\Delta R/R_0$ ', respectively. Statistical analyses were performed with t-tests or Wilcoxon rank-sum tests for pairwise comparisons. For comparing multiple groups, ANOVAs or Kruskal-Wallis tests were used with Tukey and Wilcoxon post hoc tests, respectively. Statistical significance is indicated by *: $p \leq 0.05$, **: $p \leq 0.01$, ***: $p \leq 0.001$, ****: $p \leq 0.0001$, or superscript letters with different letters for statistically different groups. Any comparison between a mutant and its control that gave a $p \leq 0.05$ is indicated in yellow.

Mutant	Reporter	Stimulus	Genotype	Baseline Intensity, F0 (A.U.)	Peak Normalised $\Delta F/F_0$ or $\Delta R/R_0$	Rate ($\mu\text{m s}^{-1}$)	Area (mm^2)	Dynamics Altered?	Sample Size (n)	Figure
<i>isi1-3</i>	<i>UBQ10::GCaMP3</i>	Wound	Col-0	589 ± 58	1.73 ± 0.16	2.46 ± 0.15	0.578 ± 0.046		25	I
			<i>isi1-3</i>	442 ± 26	1.70 ± 0.09	2.27 ± 0.09	0.662 ± 0.038		25	
		Touch	Col-0	462 ± 35	1.01 ± 0.10	0.76 ± 0.04	0.092 ± 0.011		22	II
			<i>isi1-3</i>	534 ± 34	0.83 ± 0.06	0.64 ± 0.03*	0.099 ± 0.012		22	
<i>aha1-7</i>	<i>UBQ10::GCaMP3</i>	Wound	Col-0	937 ± 55	1.15 ± 0.05	2.08 ± 0.13	0.708 ± 0.039		17	III
			<i>aha1-7</i>	934 ± 86	1.21 ± 0.09	2.37 ± 0.13	0.641 ± 0.039		15	
<i>msl10-1</i>	<i>UBQ10::GCaMP3</i>	Wound	Col-0	758 ± 49	1.19 ± 0.07	2.17 ± 0.13	0.712 ± 0.038		23	IV
			<i>msl10-1</i>	736 ± 38	1.16 ± 0.07	1.93 ± 0.11	0.703 ± 0.034		23	
		Touch	Col-0	440 ± 29	0.94 ± 0.12	0.96 ± 0.06	0.105 ± 0.012		29	V
			<i>msl10-1</i>	459 ± 23	0.79 ± 0.07	1.07 ± 0.15	0.095 ± 0.011		26	
<i>msl10-3G</i>	<i>UBQ10::GCaMP3</i>	Wound	Col-0	677 ± 49	1.18 ± 0.06	2.23 ± 0.10	0.594 ± 0.025		25	VI
			<i>msl10-3G</i>	750 ± 48	1.37 ± 0.06**	2.33 ± 0.21	0.610 ± 0.043		19	
<i>glr3.2a</i>	<i>UBQ10::GCaMP3</i>	Wound	Col-0	704 ± 56	1.32 ± 0.10	2.06 ± 0.10	0.627 ± 0.034		20	VII
			<i>glr3.2a</i>	762 ± 60	1.34 ± 0.09	1.95 ± 0.11	0.638 ± 0.043		21	
		Touch	Col-0	436 ± 42	0.99 ± 0.12	0.89 ± 0.24	0.109 ± 0.014		24	VIII
			<i>glr3.2a</i>	488 ± 35	0.82 ± 0.07	0.87 ± 0.06	0.112 ± 0.016		24	

Table 6.1 Continued

<i>tpc1-2</i>	<i>UBQ10::GCaMP3</i>	Wound	Col-0	862 ± 52	1.00 ± 0.11 ^{ab}	2.16 ± 0.19 ^a	0.673 ± 0.081		13	
			<i>tpc1-2</i>	743 ± 37	0.99 ± 0.06 ^a	2.12 ± 0.12 ^a	0.546 ± 0.037		14	
			<i>glr3.3a</i>	736 ± 43	0.65 ± 0.04 ^c	0.80 ± 0.08 ^b	0.672 ± 0.085		11	
			<i>tpc1-2 glr3.3a</i>	761 ± 51	0.74 ± 0.06 ^{bc}	0.78 ± 0.04 ^b	0.661 ± 0.074	No	12	IX
		Touch	Col-0	363 ± 33	1.21 ± 0.13	0.97 ± 0.07	0.081 ± 0.012		23	
		<i>tpc1-2</i>	404 ± 30	0.90 ± 0.07	1.00 ± 0.16	0.050 ± 0.006 [*]	No	25	X	
<i>rbohD, rbohF, rbohD rbohF</i>	<i>35S::GCaMP3</i>	Wound	Col-0	735 ± 58 ^b	1.36 ± 0.08	2.05 ± 0.14	0.584 ± 0.035 ^a		14	
			<i>rbohD</i>	801 ± 54 ^b	1.19 ± 0.06	2.25 ± 0.10	0.599 ± 0.033 ^a		15	
			<i>rbohF</i>	863 ± 45 ^b	1.12 ± 0.05	2.27 ± 0.11	0.581 ± 0.046 ^a		15	
		<i>rbohD rbohF</i>	1191 ± 102 ^a	1.25 ± 0.11	2.39 ± 0.19	0.359 ± 0.062 ^b	No	13	XI	
<i>tpk1-1</i>	<i>35S::GCaMP3</i>	Wound	Col-0	1028 ± 54	1.09 ± 0.05	2.31 ± 0.12	0.604 ± 0.035		24	
			<i>tpk1-1</i>	338 ± 26 ^{****}	1.09 ± 0.08	2.66 ± 0.11 [*]	0.603 ± 0.037	No	26	XII
		Touch	Col-0	638 ± 41	0.89 ± 0.05	0.70 ± 0.03	0.104 ± 0.020		19	
		<i>tpk1-1</i>	106 ± 29 ^{****}	4.87 ± 1.14 ^{****}	1.06 ± 0.14 ^{**}	0.096 ± 0.015	No	15	XIII	
<i>mca1 mca2</i>	<i>UBQ10::GCaMP3</i>	Wound	Col-0	539 ± 47	1.54 ± 0.15	2.77 ± 0.13	0.575 ± 0.058		12	
			<i>mca1 mca2</i>	510 ± 24	1.56 ± 0.08	2.61 ± 0.11	0.540 ± 0.035	No	16	XIV
		Touch	Col-0	629 ± 65	0.92 ± 0.10	1.09 ± 0.06	0.307 ± 0.043		19	
		<i>mca1 mca2</i>	527 ± 44	0.76 ± 0.06	0.97 ± 0.07 [*]	0.281 ± 0.037	No	22	XV	
<i>piezo-1</i>	<i>UBQ10::GCaMP6s</i>	Wound	Col-0	2257 ± 32	0.22 ± 0.01	2.20 ± 0.12	0.859 ± 0.047		22	
			<i>piezo-1</i>	2271 ± 31	0.22 ± 0.01	2.22 ± 0.10	0.871 ± 0.041	No	17	XVI
		Touch	Col-0	2034 ± 23	0.11 ± 0.00	0.82 ± 0.07	0.144 ± 0.016		25	
		<i>piezo-1</i>	2084 ± 20	0.11 ± 0.01	0.70 ± 0.03	0.174 ± 0.024	No	25	XVII	
<i>gl1</i>	<i>35S::GCaMP3</i>	Wound	Col-0	1157 ± 52	1.04 ± 0.05	2.09 ± 0.08	0.570 ± 0.034		21	
			<i>gl1</i>	671 ± 23 ^{****}	0.93 ± 0.07	2.45 ± 0.12 [*]	0.627 ± 0.041	No	21	XVIII
		Touch	Col-0	809 ± 44	0.71 ± 0.04	0.68 ± 0.02	0.104 ± 0.014		24	
		<i>gl1</i>	287 ± 17 ^{****}	1.21 ± 0.19 ^{**}	1.11 ± 0.15 ^{****}	0.142 ± 0.012 [*]	No	25	XIX	

Table 6.1 Continued

fer-4	<i>UBQ10::GCaMP3</i>	Wound	Col-0	577 ± 46 ^b	1.36 ± 0.08 ^a	1.91 ± 0.15 ^a	0.263 ± 0.016 ^a		25		
			<i>fer-4</i>	1026 ± 74 ^a	0.90 ± 0.06 ^b	1.99 ± 0.16 ^a	0.194 ± 0.010 ^b		24		
			<i>glr3.3a</i>	545 ± 30 ^b	0.79 ± 0.06 ^{bc}	1.10 ± 0.11 ^b	0.208 ± 0.013 ^b		29		
			<i>fer-4 glr3.3a</i>	895 ± 40 ^a	0.71 ± 0.05 ^c	1.59 ± 0.17 ^a	0.166 ± 0.013 ^b	No	20	XX	
	Touch	Col-0	573 ± 38	0.86 ± 0.07	0.85 ± 0.04	0.100 ± 0.015		24			
		<i>fer-4</i>	894 ± 49 ^{****}	0.73 ± 0.08	0.93 ± 0.09	0.077 ± 0.014	No	13	XXI		
	<i>35S::Apo-pHusion</i>	Wound	Col-0	RFP: 8114 ± 301 GFP: 904 ± 49	0.30 ± 0.02	2.01 ± 0.13	0.207 ± 0.010		26		
			<i>fer-4</i>	RFP: 7914 ± 305 GFP: 1432 ± 67 ^{****}	0.23 ± 0.01 ^{**}	2.99 ± 0.23 ^{***}	0.149 ± 0.012 ^{****}	No	23	XXII	
	pepr1-1 pepr2-3	<i>UBQ10::GCaMP3</i>	Wound	Col-0	597 ± 45	1.44 ± 0.12	2.13 ± 0.14	0.727 ± 0.058		17	
				<i>pepr1-1 pepr2-3</i>	601 ± 34	1.40 ± 0.09	2.16 ± 0.08	0.672 ± 0.037	No	20	XXIII
Touch		Col-0	451 ± 34	0.77 ± 0.06	0.85 ± 0.04	0.109 ± 0.015		20			
		<i>pepr1-1 pepr2-3</i>	469 ± 31	0.81 ± 0.10	0.78 ± 0.03	0.123 ± 0.014	No	22	XXIV		
mik2-6	<i>UBQ10::GCaMP3</i>	Wound	Col-0	518 ± 72	1.56 ± 0.13 ^a	2.02 ± 0.09 ^a	0.273 ± 0.014 ^a		21		
			<i>mik2-6</i>	610 ± 56	1.45 ± 0.06 ^a	2.01 ± 0.10 ^a	0.228 ± 0.019 ^{ab}		20		
			<i>glr3.3a</i>	577 ± 74	0.98 ± 0.12 ^b	1.11 ± 0.015 ^b	0.201 ± 0.012 ^b		26		
			<i>mik2-6 glr3.3a</i>	655 ± 65	0.87 ± 0.07 ^b	1.02 ± 0.06 ^b	0.201 ± 0.017 ^b	No	22	XXV	
dorn1-3	<i>UBQ10::GCaMP3</i>	Wound	Col-0	491 ± 31	1.49 ± 0.10 ^a	2.02 ± 0.08 ^a	0.317 ± 0.018 ^a		19		
			<i>dorn1-3</i>	493 ± 34	1.56 ± 0.11 ^a	1.67 ± 0.09 ^b	0.322 ± 0.018 ^a		19		
			<i>glr3.3a</i>	547 ± 55	0.98 ± 0.08 ^b	0.89 ± 0.10 ^c	0.255 ± 0.016 ^b		21		
			<i>dorn1-3 glr3.3a</i>	487 ± 29	1.11 ± 0.09 ^b	0.92 ± 0.08 ^c	0.291 ± 0.025 ^{ab}	No	25	XXVI	
		Touch	Col-0	502 ± 52	1.25 ± 0.24	1.00 ± 0.14	0.119 ± 0.017		23		
<i>dorn1-3</i>	425 ± 18	0.89 ± 0.07	1.10 ± 0.18	0.092 ± 0.014	No	23	XXVII				
aca8 aca10	<i>UBQ10::NES-YC3.6</i>	Wound	Col-0	YFP: 480 ± 16 CFP: 2848 ± 27	0.30 ± 0.01	5.89 ± 0.21	0.395 ± 0.019		36		
			<i>aca8 aca10</i>	YFP: 423 ± 31 CFP: 2869 ± 47	0.26 ± 0.02	7.05 ± 0.33 ^{**}	0.311 ± 0.020 ^{**}	No	28	XXVIII	

Table 6.1 Continued

<i>bak1-5</i>	<i>UBQ10:: GCaMP3</i>	Wound	Col-0	646 ± 37	1.30 ± 0.06 ^a	2.28 ± 0.11 ^a	0.609 ± 0.024		27	
			<i>bak1-5</i>	708 ± 40	1.26 ± 0.05 ^a	2.37 ± 0.10 ^a	0.660 ± 0.036		27	
			<i>glr3.3a</i>	764 ± 41	0.69 ± 0.04 ^b	1.13 ± 0.08 ^b	0.561 ± 0.032		33	
			<i>bak1-5 glr3.3a</i>	683 ± 33	0.71 ± 0.05 ^b	1.06 ± 0.05 ^b	0.553 ± 0.031	No	30	XXIX
		Touch	Col-0	458 ± 28	0.74 ± 0.05	0.76 ± 0.03	0.116 ± 0.012		27	
			<i>bak1-5</i>	422 ± 18	0.91 ± 0.07*	0.79 ± 0.03	0.109 ± 0.014	No	23	XXX
<i>sobir1-12</i>	<i>UBQ10:: GCaMP3</i>	Wound	Col-0	805 ± 46	1.21 ± 0.05	2.23 ± 0.09	0.626 ± 0.033		21	
			<i>sobir1-12</i>	781 ± 54	1.38 ± 0.05*	2.10 ± 0.10	0.593 ± 0.032	No	19	XXXI

6.2.2. Aphid extract induces $[Ca^{2+}]$ elevations in *A. thaliana*

Next, I aimed to investigate whether aphid HAMP perception could contribute to *M. persicae* feeding-induced $[Ca^{2+}]$ elevations in *A. thaliana* by assessing if *M. persicae* aphid extract ('aphid extract') induces *A. thaliana* $[Ca^{2+}]$ elevations. To do so, I used a plate reader to monitor fluorescence intensity from *A. thaliana* seedlings expressing *UBQ10::GCaMP3*. The immunogenic flagellin peptide, flg22, was used as a positive control and induced GCaMP3 signals (Figure 6.1A) which gave significantly greater peak $\Delta F/F_0$ values than those for the H₂O-treated controls (Figure 6.1B, Wilcoxon rank-sum after Kruskal-Wallis, $p \leq 0.0001$). Aphid extract treatment induced GCaMP3 reporter signals (Figure 6.1A) that gave significantly greater peak $\Delta F/F_0$ values than those for the 0.25% v/v PBS-treated controls (Figure 6.1B, Wilcoxon rank-sum after Kruskal-Wallis, $p \leq 0.0001$). As such, aphid extract induces $[Ca^{2+}]$ elevations in *A. thaliana* seedlings suggesting that aphid HAMP perception could contribute to *M. persicae* feeding-induced $[Ca^{2+}]$ elevations and the perception of aphid feeding in *A. thaliana*.

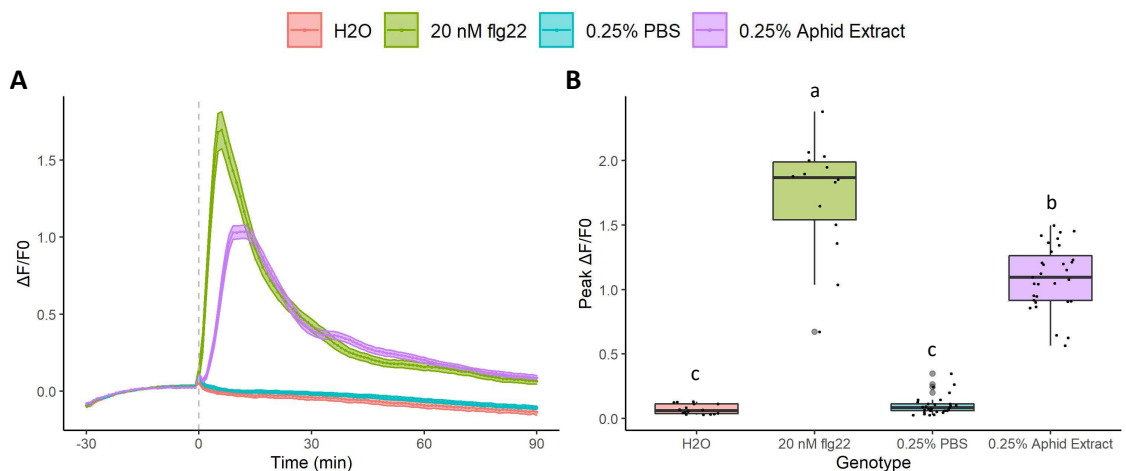


Figure 6.1 Aphid extract from *M. persicae* induces GCaMP3 signals in *A. thaliana* seedlings.

GCaMP3 reporter signals in 10-day-old *A. thaliana* seedlings expressing *UBQ10::GCaMP3* treated with 20 nM flg22 ($n = 14$), H₂O (flg22 negative control, $n = 16$), 0.25% v/v aphid extract ($n = 32$) or 0.25% v/v 1 x PBS (aphid extract negative control, $n = 29$). Background corrected fluorescence intensity (F, A.U.) values were recorded at 1 min intervals for 30 min prior to treatment and 90 min after treatment. F values were then transformed into $\Delta F/F_0$ values with F₀ for each sample being the mean F over the 30 min prior to treatment. (A) Mean \pm S.E.M. $\Delta F/F_0$ traces over time with treatment occurring at 0 min (grey dashed line). (B) Boxplots for the peak $\Delta F/F_0$ values with grey dots associated with outliers. Statistical significance was assessed using a Kruskal-Wallis test with pairwise Wilcoxon post hoc tests. Significantly different groups are indicated by the different letters.

6.2.3. BAK1 and SOBIR1 contribute to aphid extract-induced [Ca²⁺] elevations which are GLR3.1/3.3/3.6-independent

Next, I investigated whether specific candidate genes, namely *GLR3.1/3.3/3.6*, *BAK1* and *SOBIR1*, contribute to aphid extract-induced [Ca²⁺] elevations. To do so, I monitored aphid extract-induced reporter signals in the *glr3.1a glr3.3a glr3.6a*, *bak1-5* and *sobir1-12* *A. thaliana* mutants expressing *UBQ10::GCaMP3* alongside Col-0 control samples. For all three genotypes, there were no differences in baseline intensities between the mutant and Col-0 samples (*glr3.1a glr3.3a glr3.6a*: Figure 6.2A, ANOVA, $F = 0.70$, $p = 0.56$; *bak1-5*: Figure 6.3A, Kruskal-Wallis, $\chi^2 = 8.78$, $p = 0.06$; *sobir1-12*: Figure 6.4A, ANOVA, $F = 0.28$, $p = 0.84$). Aphid extract-induced GCaMP3 signals in the Col-0 and *glr3.1a glr3.3a glr3.6a* samples also displayed similar $\Delta F/F_0$ traces (Figure 6.2B) with no statistically significant differences in the peak $\Delta F/F_0$ values (Figure 6.2C, Tukey post hoc test following ANOVA, $p = 0.98$). However, compared with Col-0, the *bak1-5* and *sobir1-12* mutants displayed aphid extract-induced GCaMP3 signals with reduced amplitude $\Delta F/F_0$ elevations (Figure 6.3B, Figure 6.4B) and reduced peak $\Delta F/F_0$ values (*bak1-5*: Figure 6.3C, pairwise Wilcoxon rank-sum following Kruskal-Wallis, $p \leq 0.0001$; *sobir1-12*: Figure 6.4C, pairwise Wilcoxon rank-sum following Kruskal-Wallis, $p \leq 0.0001$). The reduction in aphid extract-induced $\Delta F/F_0$ elevations appeared more severe in the *sobir1-12* mutants (Figure 6.4B) than in the *bak1-5* mutants (Figure 6.3B). These data indicate that GLR3.1/3.3/3.6 do not function in aphid extract-induced [Ca²⁺] elevations whilst BAK1 and SOBIR1 do. As such, BAK1 and SOBIR1 could contribute to *M. persicae* feeding-induced [Ca²⁺] elevations by mediating HAMP perception.

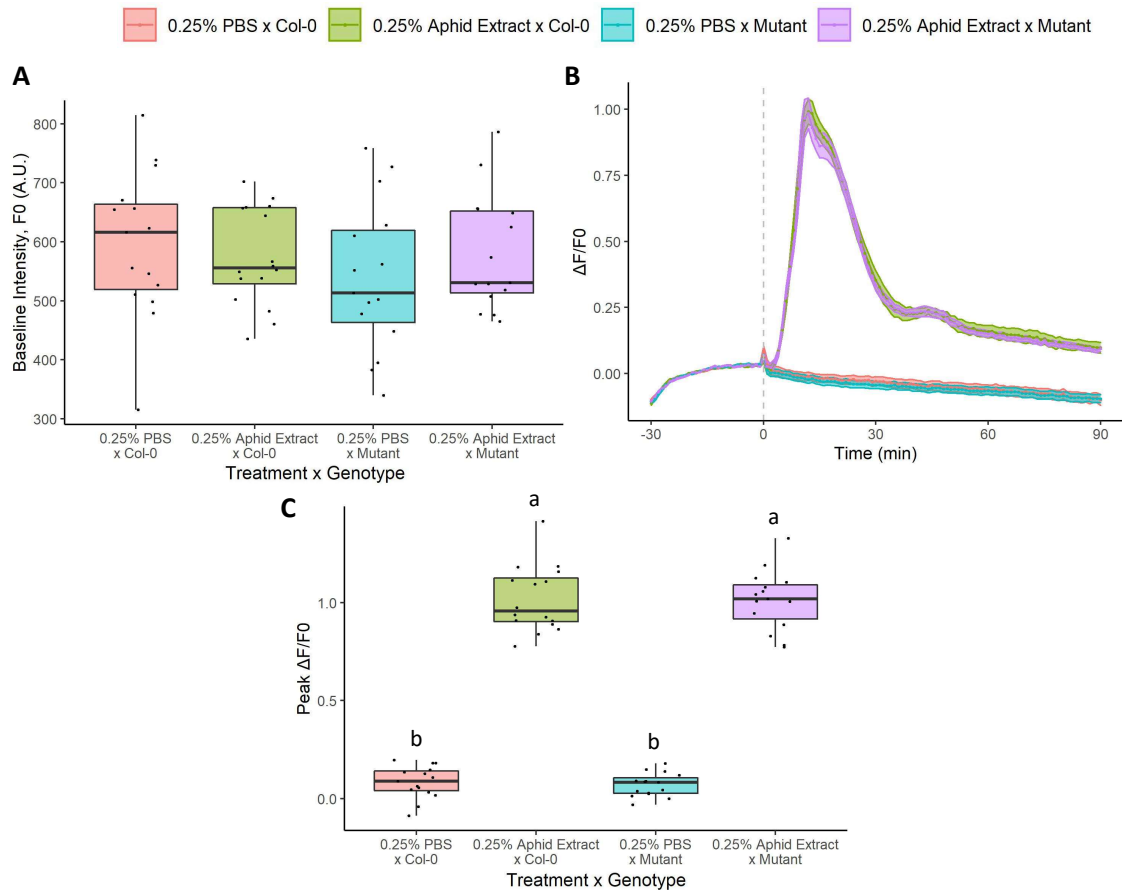


Figure 6.2 Aphid extract-induced GCaMP3 signals are not altered in *glr3.1 glr3.3a glr3.6a* mutants.

GCaMP3 reporter signals in 10-day-old Col-0 or *glr3.1a glr3.3a glr3.6a* ('Mutant') *A. thaliana* seedlings expressing *UBQ10::GCaMP3* treated with 0.25% v/v aphid extract or 0.25% v/v 1 x PBS (negative control). Background corrected fluorescence intensity (F, A.U.) values were recorded at 1 min intervals for 30 min prior to treatment and 90 min after treatment. F values were then transformed into $\Delta F/F_0$ values with F_0 for each sample being the mean F over the 30 min prior to treatment. Boxplots are shown for the (A) F_0 values (A.U.) and (C) peak $\Delta F/F_0$ values. Statistical significance was assessed using an (A) ANOVA with a Tukey post hoc test or a (C) Kruskal-Wallis test with post hoc pairwise Wilcoxon rank-sum tests. Significantly different groups are indicated by the different letters. (B) Mean \pm S.E.M. $\Delta F/F_0$ traces over time with treatment occurring at 0 min (grey dashed line). Sample sizes were 0.25% PBS x Col-0: $n = 15$, 0.25% Aphid Extract x Col-0: $n = 16$, 0.25% PBS x Mutant: $n = 15$, 0.25% Aphid Extract x Mutant: $n = 15$.

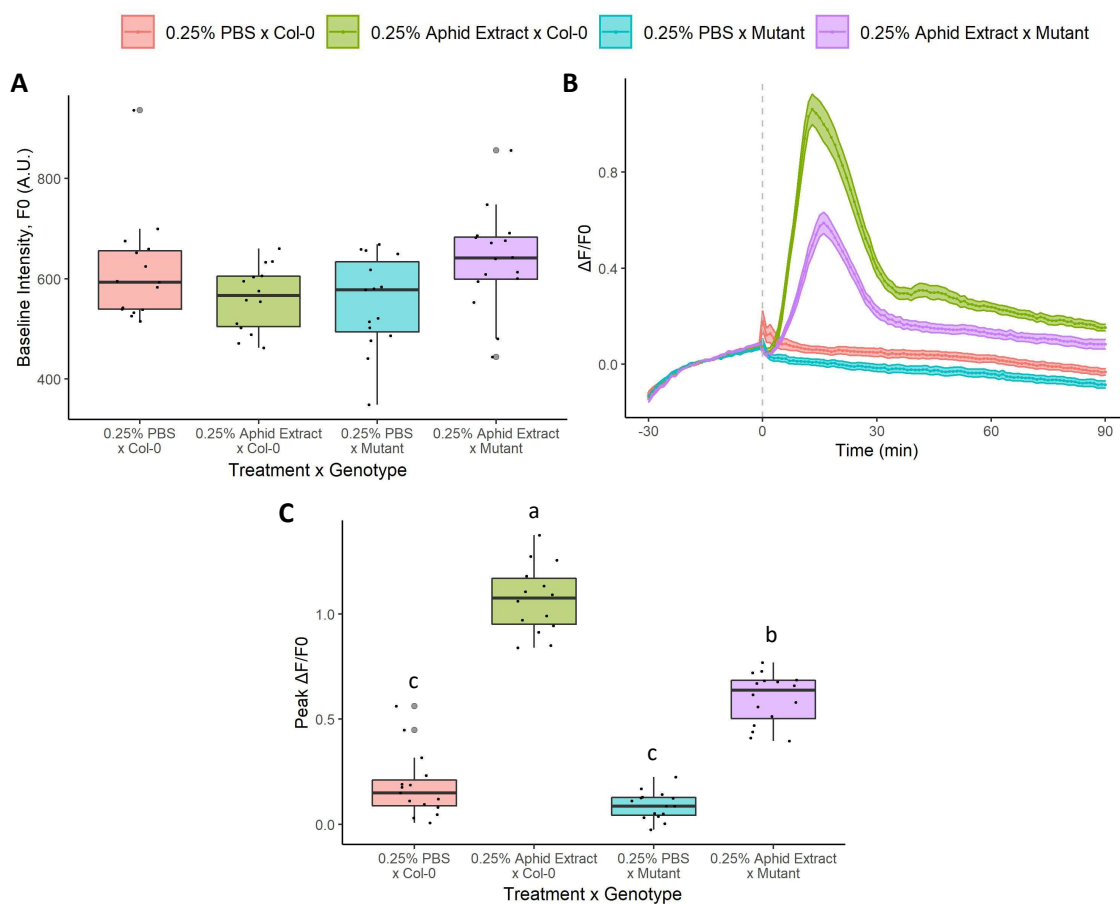


Figure 6.3 Aphid extract-induced GCaMP3 signals are reduced in *bak1-5* mutant *A. thaliana*.

GCaMP3 reporter signals in 10-day-old Col-0 or *bak1-5* ('Mutant') *A. thaliana* seedlings expressing *UBQ10::GCaMP3* treated with 0.25% v/v aphid extract or 0.25% v/v 1 x PBS (negative control). Background corrected fluorescence intensity (F, A.U.) values were recorded at 1 min intervals for 30 min prior to treatment and 90 min after treatment. F values were then transformed into $\Delta F/F_0$ values with F₀ for each sample being the mean F over the 30 min prior to treatment. Boxplots are shown for the (A) F₀ values (A.U.) and (C) peak $\Delta F/F_0$ values, with grey dots associated with outliers. Statistical significance was assessed using Kruskal-Wallis tests with post hoc pairwise Wilcoxon rank-sum tests and significantly different groups are indicated by the different letters. (B) Mean \pm S.E.M. $\Delta F/F_0$ traces over time with treatment occurring at 0 min (grey dashed line). Sample sizes were 0.25% PBS x Col-0: $n = 15$, 0.25% Aphid Extract x Col-0: $n = 14$, 0.25% PBS x Mutant: $n = 15$, 0.25% Aphid Extract x Mutant: $n = 16$.

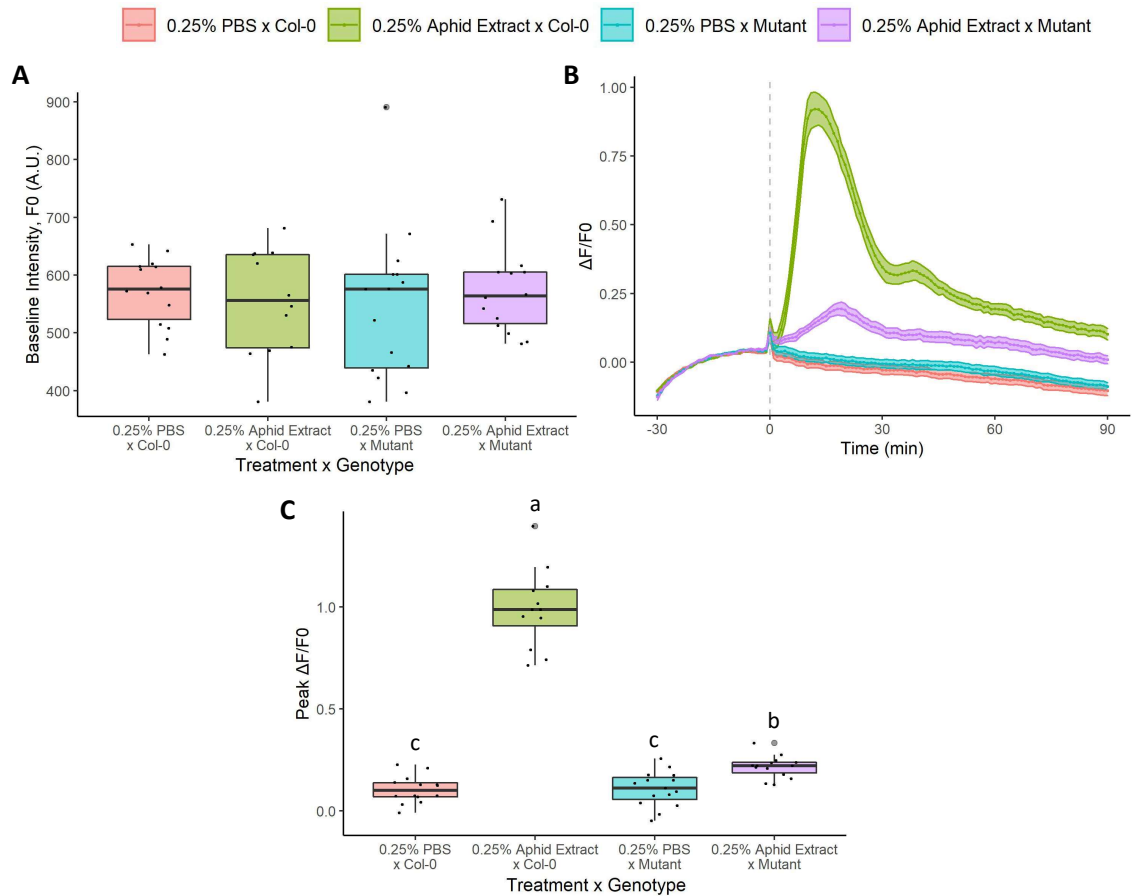


Figure 6.4 Aphid extract-induced GCaMP3 signals are severely reduced in *sobir1-12* mutant *A. thaliana*.

GCaMP3 reporter signals in 10-day-old Col-0 or *sobir1-12* ('Mutant') *A. thaliana* seedlings expressing *UBQ10::GCaMP3* treated with 0.25% v/v aphid extract or 0.25% v/v 1 x PBS (negative control). Background corrected fluorescence intensity (F , A.U.) values were recorded at 1 min intervals for 30 min prior to treatment and 90 min after treatment. F values were then transformed into $\Delta F/F_0$ values with F_0 for each sample being the mean F over the 30 min prior to treatment. Boxplots are shown for the (A) F_0 values (A.U.) and (C) peak $\Delta F/F_0$ values, with grey dots associated with outliers. Statistical significance was assessed using an (A) ANOVA with a post hoc Tukey test and (C) a Kruskal-Wallis test with post hoc pairwise Wilcoxon rank-sum tests. Significantly different groups are indicated by the different letters. (B) Mean \pm S.E.M. $\Delta F/F_0$ traces over time with treatment occurring at 0 min (grey dashed line). Sample sizes were 0.25% PBS x Col-0: $n = 14$, 0.25% Aphid Extract x Col-0: $n = 12$, 0.25% PBS x Mutant: $n = 15$, 0.25% Aphid Extract x Mutant: $n = 14$.

6.2.4. BAK1 does not appear to contribute to *M. persicae* feeding-induced $[Ca^{2+}]$ elevations in the *glr3.3a* background

In Chapter 3, *bak1-5 UBQ10::GCaMP3* mutants were found to display wildtype *M. persicae* feeding-induced GCaMP3 reporter signals. As *bak1-5* mutants were impaired in aphid extract-induced responses which were GLR3.1/3.3/3.6-independent, I hypothesised that the contribution of BAK1 to aphid feeding-induced $[Ca^{2+}]$ elevations may only be visible in the *glr3.3a* mutant background. Therefore, I assessed *M. persicae* feeding-induced $[Ca^{2+}]$ elevations in Col-0 and *bak1-5 glr3.3a A. thaliana* expressing *UBQ10::GCaMP3*. F0 values were not statistically different between these genotypes (Figure 6.5A, t-test, $t = -0.84$, $p = 0.41$). GCaMP3 reporter signals were clear in both genotypes as reflected in the normalised $\Delta F/F_0$ traces but the *bak1-5 glr3.3a* mutant trace appeared smoother than the Col-0 trace (Figure 6.5B). There was no statistically significant difference in the peak values between the genotypes (Figure 6.5C, Wilcoxon rank-sum, $W = 349$, $p = 0.14$) but the signal propagation rates were significantly reduced in *bak1-5 glr3.3a* samples compared to in Col-0 samples (Figure 6.5D, Wilcoxon rank-sum, $W = 662$, $p = 0.0014$). Signal areas did not differ significantly between the genotypes (Figure 6.5E, Wilcoxon rank-sum, $W = 483$, $p = 0.64$). As the approaches used only facilitated the imaging of two genotypes in parallel, *M. persicae* feeding-induced GCaMP3 signals in the *bak1-5 glr3.3a* mutant were not directly compared to those in the *glr3.3a* mutant. However, the phenotype detected for the *bak1-5 glr3.3a* mutant recapitulated the phenotype demonstrated for *A. thaliana* carrying the *glr3.3a* mutation. Therefore, BAK1 appears not to contribute to *M. persicae* feeding-induced $[Ca^{2+}]$ elevations in the *glr3.3a* background. Directly comparing *M. persicae* feeding-induced GCaMP3 signals in the *bak1-5 glr3.3a* and *glr3.3a A. thaliana* mutants could further test this conclusion.

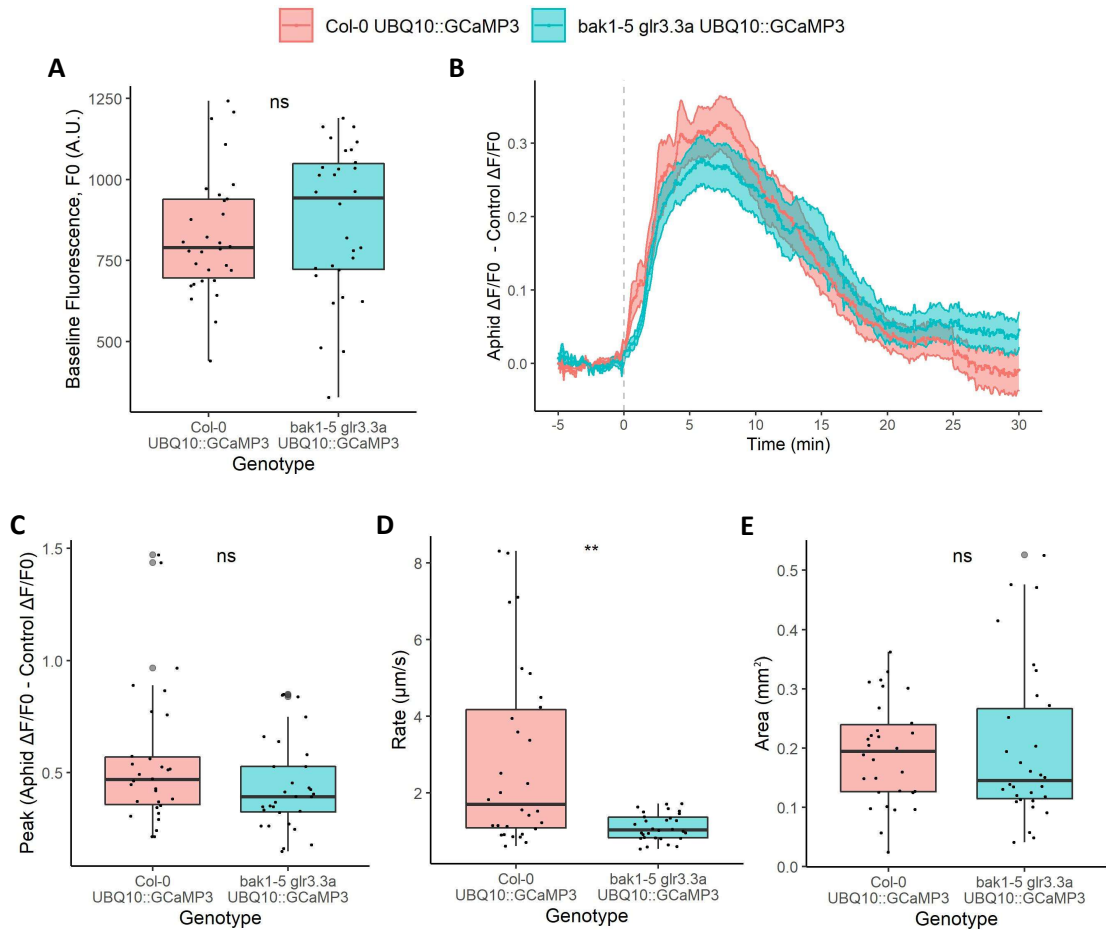


Figure 6.5 BAK1 does not appear to contribute to *M. persicae* feeding-induced GCaMP3 signals in *glr3.3a* mutant *A. thaliana*.

Properties of *M. persicae* feeding-induced GCaMP3 signals in Col-0 and *bak1-5 glr3.3a* *A. thaliana* expressing *UBQ10::GCaMP3* ($n = 30$). Elevations were recorded by imaging *A. thaliana* leaves subjected to *M. persicae* or no aphid control treatments. Background-corrected fluorescence intensity (F, A.U.) values were recorded over the area of feeding-induced responses and at comparable control sites and transformed into $\Delta F/F_0$ values with F_0 being the mean F over the 5 min prior to feeding. (B) Traces for the mean \pm S.E.M. normalised $\Delta F/F_0$ values (Aphid $\Delta F/F_0$ - Control $\Delta F/F_0$) over time with feeding beginning at 0 min (grey dashed line). Boxplots are displayed for the (A) feeding site F_0 values (A.U.), (C) peak normalised $\Delta F/F_0$ values (Aphid $\Delta F/F_0$ - Control $\Delta F/F_0$), (D) signal propagation rates ($\mu\text{m s}^{-1}$) and (E) signal areas (mm^2), with grey dots associated with outliers. Statistical significance, tested using a (A) t-test or a (C, D, E) Wilcoxon rank-sum test, shown by ns: $p > 0.05$, **: $p \leq 0.01$.

6.2.5. SOBIR1 does not appear to contribute to *M. persicae* feeding-induced [Ca²⁺] elevations in the Col-0 or *glr3.3a* background

To assess if SOBIR1 contributes to *M. persicae* feeding-induced [Ca²⁺] elevations, I investigated *M. persicae* feeding-induced GCaMP3 signals in *sobir1-12* and *sobir1-12 glr3.3a* *A. thaliana* expressing *UBQ10::GCaMP3* alongside Col-0 controls. For both genotypes, F0 values were not statistically different from those in their Col-0 controls (*sobir1-12*: Figure 6.6A, t-test, $t = 0.42$, $p = 0.68$; *sobir1-12 glr3.3a*: Figure 6.7A, Wilcoxon rank-sum, $W = 375$, $p = 0.27$). *M. persicae* feeding induced GCaMP3 reporter signals in both the *sobir1-12* and *sobir1-12 glr3.3a* mutants and in their Col-0 controls. For the *sobir1-12* mutant, the mean normalised $\Delta F/F_0$ trace was similar to the Col-0 trace (Figure 6.6B). However, as with the *glr3.3a* single mutant, the *sobir1-12 glr3.3a* mutant mean normalised $\Delta F/F_0$ trace was visibly smoother than the Col-0 trace (Figure 6.7B). There were no statistically significant differences between Col-0 and *sobir1-12* samples in peak normalised $\Delta F/F_0$ values (Figure 6.6C, Wilcoxon rank-sum, $W = 733$, $p = 0.73$), signal propagation rates (Figure 6.6D, Wilcoxon rank-sum, $W = 680$, $W = 0.84$) or signal areas (Figure 6.6E, Wilcoxon rank-sum, $W = 715$, $p = 0.88$). Reporter signals in Col-0 and *sobir1-12 glr3.3a* samples were not statistically different in their peak normalised $\Delta F/F_0$ values (Figure 6.7C, Wilcoxon rank-sum, $W = 510$, $p = 0.38$) or signal areas (Figure 6.7E, Wilcoxon rank-sum, $W = 378$, $p = 0.29$) but mutant signals did display reduced signal propagation rates (Figure 6.7D, Wilcoxon rank-sum, $W = 705$, $p = 0.0001$). As such, *sobir1-12* mutants were not impaired in *M. persicae* feeding-induced GCaMP3 signals and the phenotype of the *sobir1-12 glr3.3a* mutant GCaMP3 signals could be fully explained by the *glr3.3a* mutation. Therefore, SOBIR1 does not appear to contribute to *M. persicae* feeding-induced [Ca²⁺] elevations in the Col-0 or *glr3.3a* background. Directly comparing *M. persicae* feeding-induced GCaMP3 signals in the *sobir1-12 glr3.3a* and *glr3.3a* *A. thaliana* mutants could further test this conclusion.

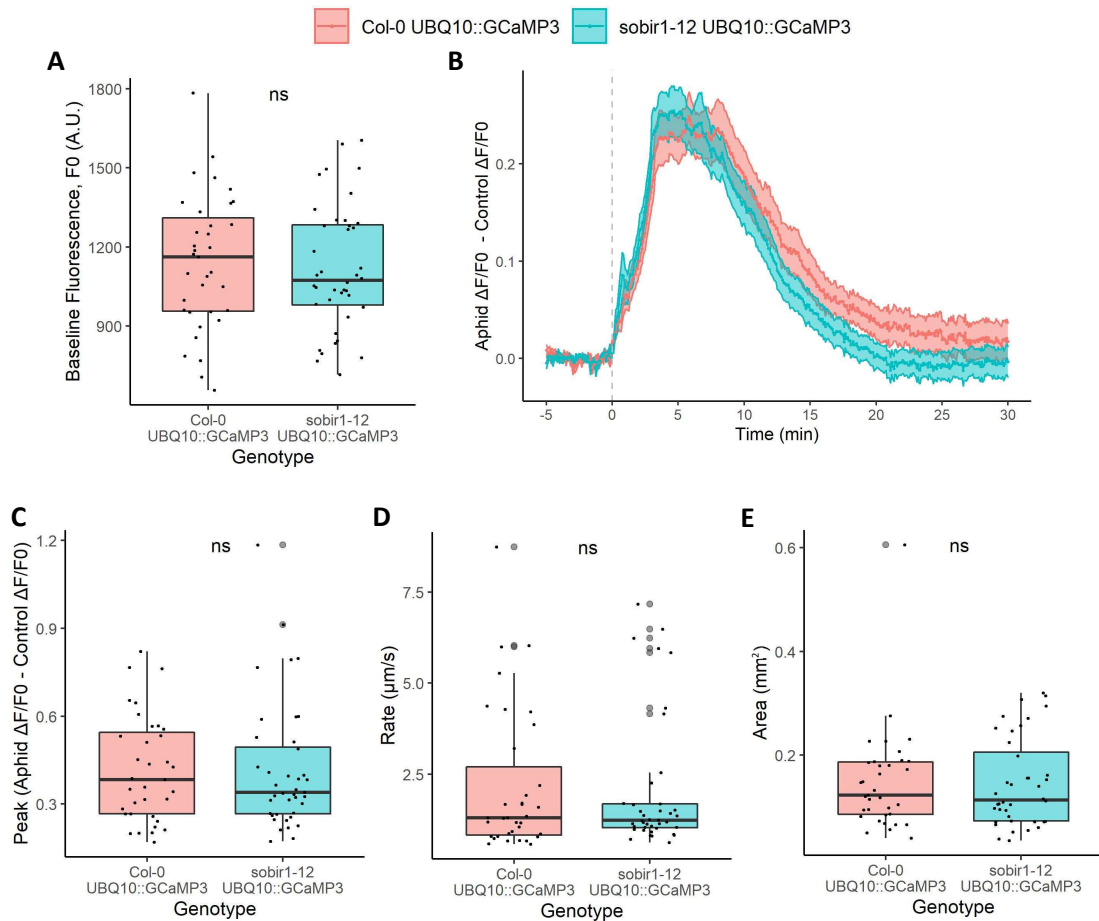


Figure 6.6 The *sobir1-12* mutation does not affect *M. persicae* feeding-induced GCaMP3 signals in Col-0 *A. thaliana*.

Properties of *M. persicae* feeding-induced GCaMP3 signals in Col-0 ($n = 35$) and *sobir1-12* ($n = 40$) *A. thaliana* expressing *UBQ10::GCaMP3*. Elevations were recorded by imaging *A. thaliana* leaves subjected to *M. persicae* or no aphid control treatments. Background-corrected fluorescence intensity (F, A.U.) values were recorded over the area of feeding-induced responses and at comparable control sites and transformed into $\Delta F/F_0$ values with F_0 being the mean F over the 5 min prior to feeding. (B) Traces for the mean \pm S.E.M. normalised $\Delta F/F_0$ values (Aphid $\Delta F/F_0$ - Control $\Delta F/F_0$) over time with feeding beginning at 0 min (grey dashed line). Boxplots are displayed for the (A) feeding site F_0 values (A.U.), (C) peak normalised $\Delta F/F_0$ values (Aphid $\Delta F/F_0$ - Control $\Delta F/F_0$), (D) signal propagation rates ($\mu\text{m s}^{-1}$) and (E) signal areas (mm^2), with grey dots associated with outliers. Statistical significance, tested using a (A) t-test or a (C, D, E) Wilcoxon rank-sum test, shown by ns: $p > 0.05$.

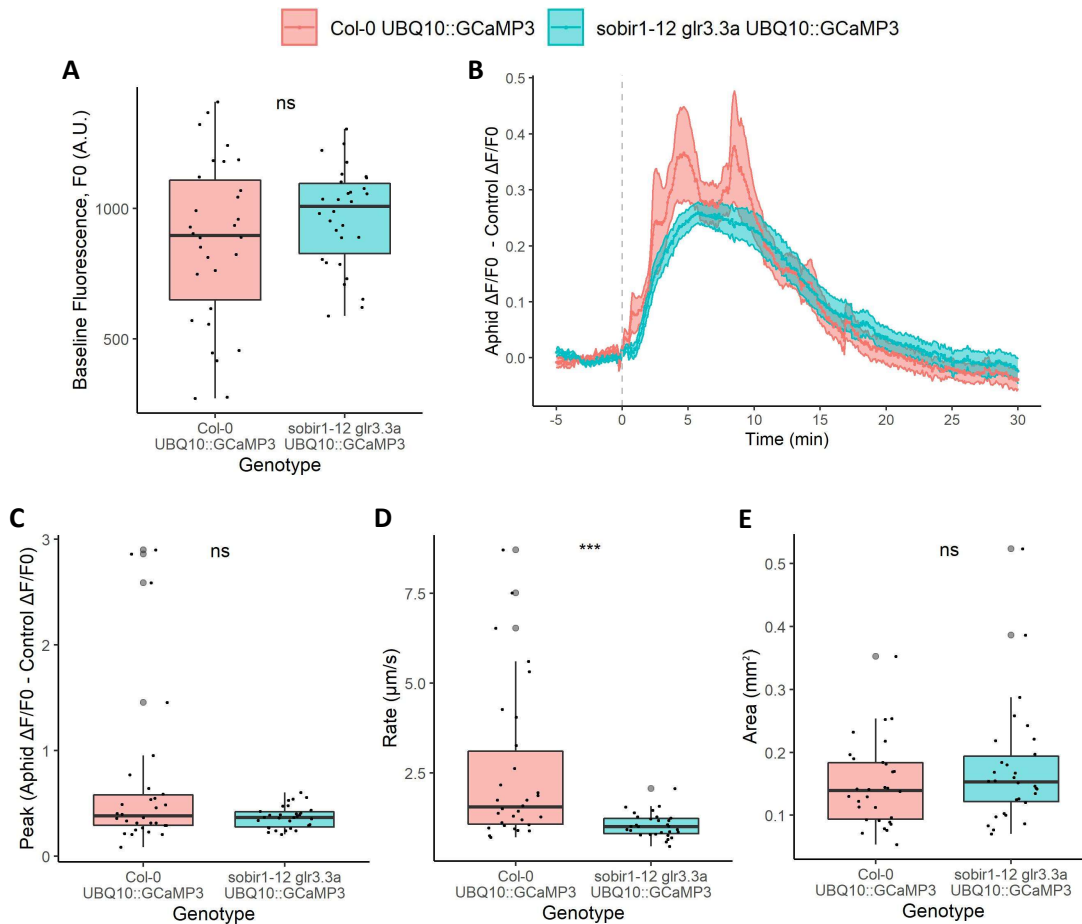


Figure 6.7 SOBIR1 does not appear to contribute to *M. persicae* feeding-induced GCaMP3 signals in the *glr3.3a* background.

Properties of *M. persicae* feeding-induced GCaMP3 signals in Col-0 and *sobir1-12 glr3.3a A. thaliana* expressing *UBQ10::GCaMP3* ($n = 30$). Elevations were recorded by imaging *A. thaliana* leaves subjected to *M. persicae* or no aphid control treatments. Background-corrected fluorescence intensity (F , A.U.) values were recorded over the area of feeding-induced responses and at comparable control sites and transformed into $\Delta F/F_0$ values with F_0 being the mean F over the 5 min prior to feeding. (B) Traces for the mean \pm S.E.M. normalised $\Delta F/F_0$ values (Aphid $\Delta F/F_0 -$ Control $\Delta F/F_0$) over time with feeding beginning at 0 min (grey dashed line). Boxplots are displayed for the (A) feeding site F_0 values (A.U.), (C) peak normalised $\Delta F/F_0$ values (Aphid $\Delta F/F_0 -$ Control $\Delta F/F_0$), (D) signal propagation rates ($\mu\text{m s}^{-1}$) and (E) signal areas (mm^2), with grey dots associated with outliers. Statistical significance, tested using a Wilcoxon rank-sum test, shown by ns: $p > 0.05$, ***: $p \leq 0.001$.

6.3. Discussion

Live imaging of genetically encoded fluorescent reporters has provided insights into how *A. thaliana* recognises and responds to aphid and thrips feeding and the role of GLR3.3 in these responses. Coupling a reverse genetics approach with reporter imaging here facilitated investigations into additional candidate genes that could contribute to the perception of aphid and thrips feeding in *A. thaliana*. The potential of candidate genes to function in responses to localised aphid or thrips feeding was first assessed by testing whether they function in responses to wounding, touch, or aphid HAMP treatments.

With the perception of mechanical stress and/or damage seemingly significant in aphid and thrips feeding-induced responses, many genes were investigated here for their known roles in damage or mechanical stress perception. Despite this, no candidate mutants were clearly impaired in wound- or touch-induced $[Ca^{2+}]$ elevations with only some differences identified that would require further investigation to evaluate definitively. For *tpc1-2* and single or double mutants in *RBOHD* and *RBOHF*, recent data in cotyledons have supported that they do not contribute to localised wound-induced $[Ca^{2+}]$ elevations (Bellandi *et al.*, 2022). The absence of strong phenotypes in investigations here may have resulted from the candidate genes not contributing to the responses investigated. However, functional redundancy in candidate gene function or epistatic interactions may have masked some contributions. This could have been particularly influential in wound responses in the wild-type background as GLR3.3-dependent wave $[Ca^{2+}]$ elevations appeared to suppress the GLR3.3-independent secondary $[Ca^{2+}]$ elevations (Chapter 4). To avoid this effect hiding the contributions of candidate genes to wound-induced $[Ca^{2+}]$ elevations, *bak1-5*, *dorn1-3*, *fer-4*, *mik2-6*, and *tpc1-2* mutants were wounded in the wild-type and *glr3.3a* backgrounds. As touch responses recapitulate GLR3.3-independent wound responses, touch stimuli provided the opportunity to investigate candidate gene function in mechanical stress-induced responses in the absence of GLR3.3 activation. Even with these efforts, no clear mutant phenotypes were identified in the touch- or wound-induced $[Ca^{2+}]$ elevations. Therefore, the genes investigated were deemed unlikely to contribute to damage or mechanical stress perception during aphid or thrips feeding.

As aphid extract contains putative HAMPs that induce PTI-like responses through the BAK1 and SOBIR1 co-receptors (Prince *et al.*, 2014; Canham, 2022), I tested whether aphid HAMP perception could contribute to *M. persicae* feeding-induced $[Ca^{2+}]$ elevations via BAK1 or SOBIR1. Aphid extract induced $[Ca^{2+}]$ elevations that were GLR3.1/3.3/3.6-independent suggesting that HAMP perception could contribute to aphid feeding-induced $[Ca^{2+}]$ elevations independently of these GLRs. Furthermore, aphid extract-induced $[Ca^{2+}]$ elevations were

partially BAK1- and SOBIR1-dependent. Despite this, neither protein clearly contributed to the $[Ca^{2+}]$ elevations induced by *M. persicae* feeding in the wild-type or *glr3.3a* background. This may be because the perception of aphid extract-associated HAMPs involves multiple redundant receptors. Alternatively, aphid HAMP perception may not significantly contribute to the aphid feeding-induced $[Ca^{2+}]$ elevations detected. In the latter case, it could be that *M. persicae* effectors suppress SOBIR1- and BAK1-dependent responses reducing their contribution to the feeding-induced $[Ca^{2+}]$ elevations. A candidate effector for this would be Mp10 which is delivered into plants with feeding, suppresses aphid extract-induced responses and targets BAK1-dependent responses (Mugford *et al.*, 2016; Drurey *et al.*, 2019). Nevertheless, BAK1 and SOBIR1 do not appear to influence *M. persicae* resistance in *A. thaliana* as *M. persicae* fecundity is unaltered on *bak1* and *sobir1* mutants (Prince *et al.*, 2014; Canham, 2022; Drurey *et al.*, 2019). Therefore, BAK1- and SOBIR1-dependent HAMP perception does not clearly contribute to *M. persicae* feeding-induced $[Ca^{2+}]$ elevations or determine *M. persicae* resistance in *A. thaliana*.

The work presented here revealed that various candidate genes do not clearly contribute to localised wound- or touch-induced $[Ca^{2+}]$ elevations. Nonetheless, the approaches taken were not successful in identifying genes that function in the perception of aphid or thrips feeding in *A. thaliana*. Here, I will consider the approaches taken along with potential options for future efforts to identify components that underpin the perception of aphid or thrips feeding in *A. thaliana*.

6.3.1. Outstanding candidates components for functioning in localised damage or mechanical stress perception in *A. thaliana*

Using the reverse genetics approach taken here, many genes that could contribute to localised damage or mechanical stress perception were not investigated. These genes could form candidates for future investigations into aphid or thrips perception in *A. thaliana*.

One group of candidates could focus on those linked to GLR3.3 regulation or activity. For example, GLR3.5 plays an intriguing role in systemic wound-induced action potential (AP) propagation as it prevents AP transmission to non-neighbouring leaves (Salvador-Recatalà, 2016). As GLR3.3 contributes to this AP transmission (Salvador-Recatalà, 2016), it may be that GLR3.5 influences GLR3.3 activity and could do so in *A. thaliana* responses to aphid or thrips feeding. One way GLR3.5 could influence GLR3.3 activity may be through hetero-tetrameric complex formation as GLRs can form homo- or hetero-tetrameric channel complexes (Wudick *et al.*, 2018a). Recently, the TGG1 and TGG2 thioglucosidase enzymes were implicated in large-scale wound-induced systemic signalling responses (Gao *et al.*, 2023). These enzymes appear to travel rapidly via the xylem and mediate glucosinolate hydrolysis upstream of systemic signalling

responses, including membrane depolarisations and $[Ca^{2+}]$ elevations, that are partially dependent on GLR3.3 (Gao *et al.*, 2023). Whilst this TGG signalling is thought to be restricted to the vascular tissue (Gao *et al.*, 2023), it may be possible that TGG activity indirectly or directly activates GLR3.3 in localised damage-induced responses. Additionally, IMPORTIN SUBUNIT α -2, IMPA2, was found in yeast to interact with GLR3.3 (Wu *et al.*, 2022). Whilst *impa2-1* mutants were not impaired in large-scale wound-induced systemic depolarisations (Wu *et al.*, 2022), IMPA2 could still influence GLR3.3 activity in localised responses. Finally, the Cornichon family proteins, CNIH1 and 4, interact with GLR3.3 and can influence its conductance in COS-7 cells and its localisation in *A. thaliana* sperm (Wudick *et al.*, 2018b). Therefore, CNIH proteins could influence GLR3.3 activity in leaf mesophyll or epidermal tissue. In summary, GLR3.5, TGG1/2, IMPA2 and CNIH proteins could influence GLR3.3 activity in *A. thaliana* responses to aphid or thrips feeding.

Though many candidate genes were investigated for their contributions to large-scale wound-induced responses alongside *GLR3.3*, some candidates were not examined. For example, *ANNEXIN1* has been implicated in large-scale wound-induced rapid systemic $[Ca^{2+}]$ elevations and in resistance against *S. littoralis* (Malabarba *et al.*, 2021). Additionally, *CNGC19* functions in the vascular propagation of large-scale wound-induced $[Ca^{2+}]$ elevations in wounded leaves and in JA-mediated resistance against *S. littura* (Meena *et al.*, 2019). Mutants in *CNGC19* are also impaired in PEP perception (Meena *et al.*, 2019). Though *pepr1 pepr2* mutants displayed wild-type localised wound- and touch-induced $[Ca^{2+}]$ elevations here, *CNGC19* could still function in these responses. Therefore, *ANNEXIN1* and *CNGC19* could function in *A. thaliana* responses to localised wounding or insect feeding alongside *GLR3.3*.

Some mechanosensitive ion channels were not investigated here but could function in aphid or thrips feeding-induced responses. In addition to *MSL10* which was investigated, there are 9 *MSL* proteins thought to function as stretch-activated ion-permeable channels (Hamilton *et al.*, 2015b). *MSL4*, *5*, *6* and *9* are unlikely candidates here as wound- and touch-induced gene expression was unaltered on quintuple *A. thaliana* mutants in these genes and *MSL10* (Haswell *et al.*, 2008). *MSL8* is thought to be localised to pollen (Hamilton *et al.*, 2015a) also making it an unlikely candidate for contributing to aphid or thrips feeding-induced responses in leaves. However, because *MSLs* have diverse functions that have been difficult to characterise (Basu and Haswell, 2017), they could reasonably contribute to *A. thaliana* responses to aphid or thrips feeding. The *A. thaliana* genome also encodes 15 *OSCA* proteins with some members known to function as mechanosensitive ion channels (Murthy *et al.*, 2018) and be Ca^{2+} -permeable (Yuan *et al.*, 2014; Thor *et al.*, 2020). Known *A. thaliana* *OSCA* functions are largely in root cells and guard cells (Guichard *et al.*, 2022), with roles in osmosensing (Yuan *et al.*, 2014) and stomatal

immunity (Thor *et al.*, 2020). However, many OSCA proteins have poorly characterised functions (Hartmann *et al.*, 2021) and some, such as OSCA1.1, have been identified in leaf mesophyll cells (Tenorio Berrío *et al.*, 2022). With the potential then to mediate mechanosensing in leaves, OSCAs could be candidates for mechanical stress perception during aphid or thrips feeding along with MSLs.

Additional candidate components that could contribute to perceiving aphid or thrips feeding include those that perceive mechanical stresses or cell wall damage through sensing physicochemical changes in the cell wall (Rui and Dinneny, 2020). Many of these are RLKs including THESEUS1 that binds RALF34 (Gonneau *et al.*, 2018) and functions in responses to cell wall damage (Engelsdorf *et al.*, 2018b). Wall-associated kinases (WAKs) are also RLKs that form cell wall integrity sensors. WAKs perceive the pectin derivatives of homogalacturonan and oligogalacturonides (OGs) to mediate responses such as to the pathogen, *Botrytis cinerea* (Brutus *et al.*, 2010; Kohorn *et al.*, 2009; Decreux and Messiaen, 2005). Beyond RLKs, other plasma membrane proteins can contribute to sensing mechanical stresses via cell wall changes including GPI-anchored proteins, Leucine-rich Repeat Extensins (LRXs) and proteins that link the cell wall and cytoskeleton (Rui and Dinneny, 2020). Whilst FER functions in sensing cell wall properties (Dünser *et al.*, 2019) and did not show any clear contribution to wound- or touch-induced responses here, other cell wall sensing components could still contribute to these responses. Therefore, proteins that sense cell wall properties may form candidates for functioning in *A. thaliana* responses to aphid or thrips feeding.

Whilst not an exhaustive list, the proteins and genes outlined here are interesting candidates that may function in *A. thaliana* mechanical stress or damage perception during aphid or thrips feeding. These candidates could be considered for any future reverse genetics investigations into aphid or thrips feeding-induced responses in *A. thaliana*, especially if additional evidence supports their potential to contribute to these responses.

6.3.2. Limitations of the reverse genetics approach

Here, the screening approach taken focussed on coupling reverse genetics with genetically encoded $[Ca^{2+}]$ reporter imaging to assess the contribution of candidate genes to touch- and/or wound-induced responses. The $[Ca^{2+}]$ reporter imaging allowed rapid *A. thaliana* responses to be assessed with high spatiotemporal resolution and relevance to aphid and thrips feeding-induced responses. However, the approach taken experienced limitations which should be considered for future reverse genetics efforts to investigate plant responses to localised wounding, touch, aphid feeding or thrips feeding.

The approach taken here assumed that the $[Ca^{2+}]$ elevations imaged were actively regulated by *A. thaliana* proteins and were not passive responses to cell damage or mechanical stress. Support for active regulation comes from the contribution of GLR3.3 to some components of the $[Ca^{2+}]$ elevations induced by thrips feeding, aphid feeding and wounding. However, localised wounding by laser ablation in roots is thought to cause a loss of membrane integrity and a passive Ca^{2+} influx that drives MC4-dependent PEP1 release (Hander *et al.*, 2019). Moreover, laser ablation in *D. melanogaster* epithelial cells causes cavitation induced microtears in neighbouring cells that allow Ca^{2+} influx and passive $[Ca^{2+}]$ elevations that spread via gap junctions (Shannon *et al.*, 2017). Therefore, it could be that components of the $[Ca^{2+}]$ elevations induced by localised insect feeding, wounding, or even touch, are passive consequences of a loss of membrane integrity. Monitoring passive responses in candidate mutants would not reveal genes that actively and directly regulate responses to localised insect feeding, wounding or touch. An improved understanding of the cellular processes behind the $[Ca^{2+}]$ elevations induced by these localised stimuli would help establish whether any components are passive and aid the design of further investigations.

The need to introduce reporter transgenes into the desired mutant backgrounds limited both the number of genes and mutant alleles that could be investigated and the ability to investigate higher-order mutants. To overcome this limitation with a reverse genetics approach, mutants could have been transformed with reporter transgenes or produced in a reporter expressing background by gene editing, as was performed to produce *glr2.7 glr2.8 glr2.9 A. thaliana* expressing YC3.6 (Bjornson *et al.*, 2021). However, these approaches require further characterisation of reporter expression or mutation success, respectively, limiting their benefits. Alternatively, virus-induced gene silencing (VIGS), or other gene knockdown methods, could be used to silence candidate genes for investigation in *A. thaliana* plants expressing a reporter transgene (Fernandez and Gilroy, 2023). For each mutant of interest, VIGS plasmids must be developed, and the gene expression knockdown must be validated. Therefore, whilst this method eliminates the need for crossing, it can still be time consuming and challenging. To visualise $[Ca^{2+}]$ elevations in known mutant backgrounds without using a transgenic reporter, fluorescent $[Ca^{2+}]$ reporter dyes can be used. Loading $[Ca^{2+}]$ reporter dyes can be difficult and hard to standardise (Grenzi *et al.*, 2021). However, a method has recently been developed for the reproducible and efficient loading of a ROS dye, H₂DCFDA, into plants by fumigation (Fichman *et al.*, 2019). This method has also been adapted to the $[Ca^{2+}]$ reporter dye, Fluo-4-AM, and both dyes have been used to investigate large-scale wound-induced rapid systemic signalling (Fichman and Mittler, 2021a; Fichman *et al.*, 2020; Fichman *et al.*, 2019). Loading fluorescent reporter dyes into *A. thaliana* in this way could facilitate the visualisation of $[Ca^{2+}]$ elevations for a reverse genetics approach. However, this method has not yet been utilised to

visualise localised responses to stimuli and it is unclear whether it can provide a sufficient SNR and spatiotemporal resolution to do so. Therefore, whilst alternative methods exist that could facilitate a reverse genetics approach with $[Ca^{2+}]$ imaging, it is not clear whether these methods would be suitable and more efficient than the approaches taken here.

In summary, the approaches taken here were based on the need for a high spatiotemporal resolution output, the knowledge of aphid and thrips feeding-induced responses and the proven techniques available. These approaches were limited in their throughput and did not identify novel genes involved in localised wound or touch perception. Future reverse genetics investigations into the responses induced by localised wounding, touch or insect feeding, may benefit from characterising the cellular responses to these stimuli and exploring alternative approaches to those used here.

6.3.3. Alternative approaches to reverse genetics

There are alternative approaches to reverse genetics that could help to identify components that function in the perception of aphid or thrips feeding in *A. thaliana*. These approaches could be screens broader in scope or methods that use existing information to focus investigations on relevant genes.

A forward genetics screen could be used to search for components that function in *A. thaliana* responses to aphid or thrips feeding. The best read out for these localised responses may be $[Ca^{2+}]$ reporter signals. Therefore, a $[Ca^{2+}]$ reporter expressing *A. thaliana* population could be mutagenized for such a screen. *A. thaliana* expressing the $[Ca^{2+}]$ reporter, aequorin, has been used for forward genetics screens to identify genes involved in responses to various stimuli including pathogen exudates (Michal Johnson *et al.*, 2014). Optimised protocols for forward genetics screens using aequorin have been developed (Sun *et al.*, 2021). For the forward genetics screen proposed here, a non-FRET, ratiometric fluorescent $[Ca^{2+}]$ reporter could provide sufficient resolution for imaging whilst also helping to identify variation in reporter expression or background variables. Screening responses to aphid feeding would be challenging due to variation in aphid feeding behaviour and the responses induced. However, the wounding or touch stimuli could be amenable for the proposed screen. These stimuli were applied manually for data presented here and wounding occasionally caused damage to veins. For reproducibility in a screen, it may be beneficial to automate the wound and touch stimuli. Interestingly, thrips could be used for a forward genetics screen as thrips feeding reliably induced wave $[Ca^{2+}]$ elevations and often produced multiple responses on one leaf allowing any phenotypes to be assessed with higher confidence. In summary, a search to find components

involved in *A. thaliana* responses to aphid or thrips feeding may benefit from a forward genetics screen.

The knowledge of components involved in responses to localised wounding, touch or insect feeding could be used to identify associated components that also function in these responses. For example, components that interact with GLR3.3 may also be implicated in responses to localised aphid or thrips feeding. A yeast-two-hybrid (Y2H) screen can be used to identify interactors of target proteins. This approach revealed that ISI1 interacts with GLR3.3 and led to the discovery that ISI1 influences GLR3.3 activity in large-scale wound-induced responses (Wu *et al.*, 2022). *In planta*, GLR3.3 interactors could be identified by performing GLR3.3 immunoprecipitation before mass spectrometry (IP-MS) on interacting proteins. For this, tagged GLR3.3 expressing *A. thaliana* lines could be used (Nguyen *et al.*, 2018; Toyota *et al.*, 2018). This approach has recently been performed successfully for MSL10 (Codjoe *et al.*, 2022). However, to derive the most relevant insights with IP-MS, it is necessary to perform investigations in the context of the stimuli or responses of interest. With the stimuli and responses here being localised, it may be challenging to acquire samples for investigation with IP-MS. Nonetheless, any components found to function in the perception of aphid feeding, thrips feeding, wounding or touch, could be built upon to identify associated components that also function in the perception of these stimuli.

6.3.4. The search can continue

This chapter aimed to identify additional components that function in responses to aphid or thrips feeding in *A. thaliana*. Of the candidate genes investigated, none were found to clearly contribute to localised wound- or touch-induced $[Ca^{2+}]$ elevations. Therefore, the genes investigated were deemed unlikely to function in *A. thaliana* responses to aphid or thrips feeding through damage or mechanical stress perception. Moreover, BAK1 and SOBIR1 were found not to contribute to *M. persicae* feeding-induced $[Ca^{2+}]$ elevations despite functioning in aphid extract-induced $[Ca^{2+}]$ elevations. Whilst there are remaining candidate genes that could be investigated with the same approaches used here, future investigations may benefit from utilising an alternative reverse genetics approach or a forward genetics screen. It may also benefit investigations to better understand the cellular processes that underpin the GLR3.3-dependent wave $[Ca^{2+}]$ elevations and the burst and secondary $[Ca^{2+}]$ elevations in responses to localised stimuli. This will help identify any candidate genes that could be involved and whether any components of the $[Ca^{2+}]$ elevations are passively regulated. The results and material generated here should help guide future investigations that continue to search for molecular components involved in the perception of aphid or thrips feeding.

7. General Discussion

7.1. Summary and Discussion of Research Findings

Plants must specifically perceive biotic stresses to be able to launch appropriate defence responses. Characterising inducible plant defence responses is of growing importance for efforts to enhance crop resistance against pests and pathogens. The mechanisms by which plants perceive and signal attack from chewing insect pests, such as caterpillars, have been heavily studied. In contrast, the mechanisms by which plants recognise and respond to insect pests with localised feeding behaviours, such as aphids and thrips, are less well characterised. In this thesis, I aimed to address the question of how plants initially perceive localised feeding from aphids and thrips.

7.1.1. Developing methods for investigating plant responses to localised stimuli

To facilitate investigations into how plants perceive aphid and thrips feeding, I first developed methods for assessing plant responses to localised stimuli (Chapter 3). These methods had to provide high spatiotemporal resolution insights into early plant responses whilst coping with the variability of insect behaviour. Imaging genetically encoded fluorescent reporters in real-time provides a unique opportunity to meet these demands. Therefore, I adapted existing methods for imaging aphid feeding-induced $[Ca^{2+}]$ elevations with GCaMP3 (Vincent *et al.*, 2017b) to be more robust and work with various intensimetric and ratiometric reporters as well as multiple stimuli.

To ensure methods of genetically encoded fluorescent reporter imaging are robust, it is important to address any limitations in the methods. As intensimetric reporters utilise only a single fluorescent protein to report analyte levels, they are considered to be more likely than ratiometric reporters to produce artefacts as a result of variation in reporter expression (Grenzi *et al.*, 2021). However, I demonstrated that differences in reporter expression between compared material can give rise to artefactual differences in normalised reporter signals from both intensimetric and ratiometric non-FRET reporters. The size of this effect was not compared between the reporter types nor were FRET-based reporters directly investigated. Nonetheless, methods for imaging any intensimetric and ratiometric reporters were adapted to limit the risk of reporter expression differences impacting comparisons of normalised reporter signals. To do so, methods incorporated checks for equal baseline fluorescence between compared material and background corrections wherever possible. These steps are not widely reported in investigations utilising genetically encoded fluorescent reporters. Moreover, differences in reporter expression between compared *A. thaliana* lines appeared to impact data that previously implicated BAK1 and TPC1 in *M. persicae* feeding-induced $[Ca^{2+}]$ elevations

(Vincent *et al.*, 2017a). With the advanced methods, I found no phenotype for *M. persicae* feeding-induced GCaMP3 signals in *bak1* or *tpc1* mutant *A. thaliana*. Therefore, data presented here demonstrated the importance of ensuring equal reporter expression between compared material and of performing appropriate background corrections when possible.

Using ratiometric rather than intensimetric reporters can help detect and control for variation in background variables, such as pH. Imaging methods developed here were adapted for the YC3.6 FRET-based ratiometric $[Ca^{2+}]$ reporter in investigations reported in Section 6.2.1. However, the limited dynamic range and more complex imaging requirements of YC3.6 compared to GCaMP3 made the former reporter less favourable for investigations here (Grenzi *et al.*, 2021; Rose *et al.*, 2014). Ratiometric non-FRET $[Ca^{2+}]$ reporters, often formed of an intensimetric reporter and a linked reference FP, can combine the benefits of ratiometric and intensimetric reporters. For example, R-GECO1-mTurquoise employs the R-GECO1 $[Ca^{2+}]$ reporter with mTurquoise acting as a reference FP for ratiometry (Waadt *et al.*, 2017). Whilst R-GECO1-mTurquoise requires dual excitation, MatryoshCaMP6s is based on a similar principle but requires only one excitation wavelength for both the $[Ca^{2+}]$ reporter of GCaMP6s and the reference FP of LSSmOrange (Ast *et al.*, 2017). MatryoshCaMP6s has been used to detect large-scale wound-induced systemic $[Ca^{2+}]$ elevations (Moe-Lange *et al.*, 2021) and seems suitable for visualising plant responses to localised stimuli. By utilising ratiometric non-FRET $[Ca^{2+}]$ reporters with the methods developed here, future investigations will be better equipped to identify and control for variation in background variables.

In Chapters 4 and 5, imaging methods were adapted for the iGluSnFR intensimetric reporter and the apo-pHusion ratiometric reporter. These reporters were imaged along with GCaMP3 to investigate how GLR3.3 functions in responses to localised wounding, touch and insect feeding. However, because all three reporters contained a GFP-based protein, they had to be imaged independently. Such independent imaging of reporters limits the ability to directly compare signal properties between reporters and test for correlations in the associated plant responses. Deploying the methods developed here to simultaneously image multiple reporters with distinct emission spectra could help appreciate the correlations and interactions between multiple plant responses. The simultaneous imaging of co-expressed iGluSnFR and R-GECO has revealed a close relationship between signals from both reporters in responses to large-scale and localised wounding, trichome touch, and turgor pressure changes (Bellandi *et al.*, 2022; Grenzi *et al.*, 2023). Multi-parameter imaging can also be achieved by expressing a single protein that reports on multiple signalling species (Waadt *et al.*, 2021). For instance, R-GECO1-GSL-E²GFP simultaneously reports on intracellular $[Ca^{2+}]$ (R-GECO1), pH and $[Cl^-]$ (E²GFP) (Waadt *et al.*, 2020). Similarly, the CapHensor reporter combines the R-GECO1 and PRpHluorin reporters

to allow simultaneous monitoring of intracellular $[Ca^{2+}]$ and pH, respectively (Li *et al.*, 2021a). Even with simultaneous reporter imaging, differences in reporter properties, such as ligand binding and dissociation rates (Grenzi *et al.*, 2021), can make interpreting the relationship between reporter signals challenging. Nonetheless, an improved understanding of plant responses to aphid or thrips feeding could be gained by adapting the methods developed here to perform simultaneous multi-parameter imaging.

Identifying and monitoring additional plant responses that occur rapidly with aphid or thrips feeding will also help appreciate the plant perception of these insects and the corresponding function of any genes. There is an expanding toolbox of genetically encoded reporters that could facilitate such investigations. Infestation with some aphid species is known to cause elevations in ROS (Goggin and Fischer, 2022). Aphid and thrips feeding-induced ROS elevations could be assessed using genetically encoded ROS reporters such as roGFP2-Orp1 (Nietzel *et al.*, 2019) or HyPer7 (Ugalde *et al.*, 2021). Additionally, as GLR3.3 contributes to large-scale wound-induced systemic depolarisations (Mousavi *et al.*, 2013), it may be informative to assess aphid or thrips feeding-induced membrane potential changes with reporters such as ArcLight (Matzke and Matzke, 2015). There is a wide range of genetically encoded reporters that have been expressed in *A. thaliana* allowing various signalling events to be monitored (Colin *et al.*, 2021). Any reporters of interest will need to be assessed for their suitability for each stimulus and the imaging approaches available. The imaging methods developed here provide a foundation for imaging additional reporters to investigate the perception of aphid and thrips feeding in *A. thaliana*.

In summary, the methods developed here facilitated investigations into the plant perception of aphid and thrips feeding. Future investigations may benefit from adapting these methods to image non-FRET ratiometric $[Ca^{2+}]$ reporters, to image more reporters or to monitor multiple parameters simultaneously. The use of genetically encoded fluorescent reporters to study wider plant-insect interactions is gaining popularity. For example, they have been used to investigate caterpillar feeding-induced responses in *A. thaliana* (Toyota *et al.*, 2018; Nguyen *et al.*, 2018), Venus flytrap leaf closure (Suda *et al.*, 2020) and leaf movements in *Mimosa pudica* following grasshopper attack (Hagihara *et al.*, 2022). The advances and considerations presented here can help ensure such investigations are effective and robust.

7.1.2. GLR3.3 functions in localised wound-induced responses

Using the improved methods, I identified that *M. persicae* feeding-induced $[Ca^{2+}]$ elevations are altered in *glr3.3a glr3.6a* mutant *A. thaliana* (Chapter 3). This led to an exploration

of how GLR3.3 and GLR3.6 contribute to the perception of localised damage and mechanical stress that could occur during aphid or thrips feeding (Chapter 4).

Localised wound-induced $[Ca^{2+}]$ elevations in *A. thaliana* leaves were found to propagate radially as a wave dependent on GLR3.3 but not GLR3.6. In *glr3.3a* mutants, wounding induced an initial $[Ca^{2+}]$ elevation that remained highly spatiotemporally restricted as a 'burst' before being replaced by a lower intensity and radially propagating 'secondary' $[Ca^{2+}]$ elevation. Data indicated that the burst likely developed into the wave with the activation of GLR3.3. Moreover, the secondary $[Ca^{2+}]$ elevations appeared to be suppressed by the GLR3.3-dependent responses in wildtype plants. Therefore, localised wounding seems to induce three phases of $[Ca^{2+}]$ elevation: an initial burst elevation; a GLR3.3-dependent wave that develops from the burst; and a secondary $[Ca^{2+}]$ elevation that is suppressed in wildtype plants. At the time the investigations reported here begun, the only characterised function of GLR3.3 in wound responses was in large-scale wound-induced systemic signalling that propagates rapidly via the vascular tissue (Nguyen *et al.*, 2018). However, since then collaborators have reported that GLR3.3 functions in responses to localised wounding in cotyledons providing support for the findings here (Bellandi, 2021; Bellandi *et al.*, 2022). Moreover, GLR3.3 has been found to be necessary for localised glutamate-induced $[Ca^{2+}]$ elevations in *A. thaliana* leaves and cotyledons (Grenzi *et al.*, 2023; Bellandi *et al.*, 2022). Whilst not directly studied, the large-scale wounding of *glr3.3a* mutants appears to induce $[Ca^{2+}]$ elevations with burst and secondary dynamics at the wound site (Nguyen *et al.*, 2018). Therefore, GLR3.3 seems to function in the localised $[Ca^{2+}]$ elevations induced by large-scale and localised wounding as well as glutamate application.

Localised touch-induced $[Ca^{2+}]$ elevations were GLR3.3-independent and displayed burst and secondary dynamics. These $[Ca^{2+}]$ elevations were similar to those induced by wounding in the *glr3.3a* mutant but were of a lower magnitude. Therefore, mechanical stress appears to be responsible for triggering burst and secondary $[Ca^{2+}]$ elevations in responses to wounding and touch. This thesis proposes two hypotheses regarding the factors that determine the degree of GLR3.3 activation and GLR3.3-dependent propagation of burst $[Ca^{2+}]$ elevations: 1) the extent of cell damage-induced DAMP release and 2) the extent of mechanical stress experienced. Localised wounding, but not touch, induced GLR3.3-dependent responses. Therefore, data might suggest that cell damage-induced DAMP release is required for GLR3.3 activation. This notion is consistent with the hypothesis that localised damage leads to the release of Glu and other GLR3.3 amino acid agonists that spread by diffusion to propagate wave $[Ca^{2+}]$ elevations (Bellandi *et al.*, 2022). However, GLR3.3 activation appears to be possible without cell damage in responses to mechanical stresses that are likely more severe than the touch stimuli applied here. For example, vascular turgor pressure changes can induce GLR3.3-dependent $[Ca^{2+}]$

elevations (Grenzi *et al.*, 2023) and larger leaf touch stimuli can induce GLR3.3/3.6-dependent hyponasty (Pantazopoulou *et al.*, 2022). Moreover, trichome bending can induce wave-like $[Ca^{2+}]$ elevations (Bellandi *et al.*, 2022; Matsumura *et al.*, 2022) that appear to be GLR3.3-dependent whilst lighter trichome touch only induces burst and secondary $[Ca^{2+}]$ elevations (preliminary data, not shown). These data suggest that the extent of mechanical stress experienced may determine the extent of GLR3.3 activation with wounding causing greater mechanical stress than touch. Resolving whether the extent of mechanical stress or damage-induced DAMP release determines localised GLR3.3 activation will be important for a mechanistic understanding of its role in responses to localised touch and wounding.

Localised wounding induced iGluSnFR reporter signals that spatiotemporally correlated with the GLR3.3-dependent $[Ca^{2+}]$ elevations. These findings suggest that the damage caused by localised wounding induces a release of glutamate as a DAMP that may contribute to the activation of GLR3.3. Similar apoplastic [Glu] increases have been reported in responses to large-scale and localised wounding (Toyota *et al.*, 2018; Bellandi *et al.*, 2022; Grenzi *et al.*, 2023). Consistent with apoplastic [Glu] increases activating GLR3.3, exogenously applied Glu can induce localised or systemic GLR3.3-dependent $[Ca^{2+}]$ elevations and GLR3.3 can be gated by Glu when expressed in the heterologous system of HEK293T cells (Toyota *et al.*, 2018; Qi *et al.*, 2006; Bellandi *et al.*, 2022; Grenzi *et al.*, 2023; Shao *et al.*, 2020; Gao *et al.*, 2023). Additionally, important ligand binding residues in GLR3.3 are required for $[Ca^{2+}]$ elevations induced by Glu treatment or induced systemically by leaf burning (Grenzi *et al.*, 2023). However, in the localised wound-induced responses reported here, iGluSnFR signals were likely influenced by coinciding apoplastic alkalinisations. Therefore, it is unclear whether localised wounding induces apoplastic [Glu] increases that could activate GLR3.3. Similarly, apoplastic pH changes may have influenced other reported iGluSnFR signals. For example, trichome bending induces apoplastic alkalinisations that appear to correlate with reported iGluSnFR signals and $[Ca^{2+}]$ waves (Bellandi *et al.*, 2022; Zhou *et al.*, 2017). Interestingly, when expressed in HEK293T cells, relatively high Glu concentrations of 50 mM or above are required to activate GLR3.3 (Shao *et al.*, 2020). Therefore, whilst GLR3.3 can be activated by exogenously applied Glu and its key ligand binding residues are important for activation, it is unclear whether localised damage causes a release of Glu that is sufficient to activate GLR3.3.

Apoplastic alkalinisations closely correlated with all phases of the wound- and touch-induced $[Ca^{2+}]$ elevations and similar extracellular pH increases can activate GLR3.3 in HEK293T cells (Shao *et al.*, 2020). As the touch-induced burst alkalinisations were of a lower magnitude than those induced by wounding, apoplastic alkalinisations could play a significant role in activating GLR3.3 in proportion to the extent of mechanical stress experienced. Moreover,

because $[Ca^{2+}]$ elevations can promote apoplastic alkalinisations (Monshausen *et al.*, 2009), GLR3.3-dependent $[Ca^{2+}]$ and apoplastic pH elevations could form a positive feedback loop that promotes GLR3.3-dependent propagation. $[Ca^{2+}]$ elevations have been linked to cytosolic acidifications in responses to large-scale wounding in leaves (Behera *et al.*, 2018). However, data presented here form the first report of apoplastic alkalinisations coinciding with GLR3.3-dependent wound-induced responses. In support of GLR3.3 being gated by apoplastic pH *in planta*, H^+ -ATPase overactivation acidifies the apoplast and negatively regulates large-scale wound-induced GLR3.3/3.6-dependent systemic responses (Kumari *et al.*, 2019; Shao *et al.*, 2020). Additionally, these GLR3.3/3.6-dependent responses are negatively regulated by the AHA1 H^+ -ATPase (Kumari *et al.*, 2019; Shao *et al.*, 2020). Despite this role, AHA1 did not appear to function in responses to localised wounding (Chapter 6). It is unclear whether pH gating could activate GLR3.3 without concurrent elevations in apoplastic GLR3.3 ligand concentrations. This uncertainty is because pH gating of GLR3.3 conductance in HEK293T cells requires at least 50 mM glutamate (Shao *et al.*, 2020). However, less than 100 μ M [Glu] can induce GLR3.3-dependent $[Ca^{2+}]$ elevations in *A. thaliana* leaves (Grenzi *et al.*, 2023). With *A. thaliana* apoplastic [Glu] reported at 414.8 μ M (Hirner *et al.*, 2006), apoplastic pH changes may alone be sufficient to gate GLR3.3 without requiring elevated GLR3.3 ligand concentrations. Therefore, findings here are consistent with a model in which the extent of mechanical stress experienced determines the magnitude of the burst apoplastic alkalinisations, that subsequently determine the extent of localised GLR3.3 activation (Figure 7.1).

In responses to localised wounding, *glr3.3a* mutants were impaired in *JAZ10* JA marker gene expression. Moreover, systemic *JAZ10* expression induced by large-scale wounding is impaired in *glr3.3a* mutants (Mousavi *et al.*, 2013; Wu *et al.*, 2022). Therefore, GLR3.3 appears to promote JA-mediated responses to both localised and large-scale wounding. However, localised wound-induced *VSP2* and *JOX3* JA marker gene expression in *glr3.3a* cotyledons is unaltered (Bellandi *et al.*, 2022). As localised wound-induced *AOS* expression was also unaltered in *glr3.3a* mutants here, it appears that GLR3.3 promotes the localised wound-induced expression of a subset of JA-inducible genes. This finding indicates that GLR3.3 functions as an important component in the regulation of localised wound-induced JA defence signalling.

In summary, I identified that localised wounding induces burst $[Ca^{2+}]$ elevations that can develop to propagate as waves via GLR3.3. In contrast, touch induces GLR3.3-independent burst and secondary $[Ca^{2+}]$ elevations. All the localised wound and touch-induced $[Ca^{2+}]$ elevations coincide with apoplastic alkalinisations. The extent of localised GLR3.3 activation could be determined by the extent of damage-induced DAMP release and/or mechanical stress experienced. Data presented here support a model in which the extent of mechanical stress

experienced determines the magnitude of the burst apoplastic alkalinisations that proportionally promote GLR3.3 activity (Figure 7.1). If the GLR3.3-dependent $[Ca^{2+}]$ elevations promote apoplastic alkalinisations, GLR3.3-dependent signal propagation may occur by a Ca^{2+} - H^+ positive feedback loop. As GLR3.3 appears to promote JA-mediated defence gene expression, it could be that progressive GLR3.3 activation with increasing mechanical stress allows plants to tailor the extent of JA responses to the severity of the mechanical stress experienced. There is significant interest in how GLR3.3 functions in localised and large-scale wound-induced responses (Toyota *et al.*, 2018; Shao *et al.*, 2020; Moe-Lange *et al.*, 2021; Bellandi *et al.*, 2022; Grenzi *et al.*, 2023; Gao *et al.*, 2023). The model and data presented here highlight the potential for mechanical stress and apoplastic alkalinisations to determine GLR3.3 activity *in planta*, as well as the need for caution when utilising the iGluSnFR reporter to monitor apoplastic [Glu]. These findings could significantly support efforts to understand how GLR3.3 functions more broadly in plant responses to wounding and biotic stresses.

7.1.3. GLR3.3 functions in responses to localised feeding from aphids and thrips

With an improved understanding of how GLR3.3 contributes to localised damage and mechanical stress perception, I explored the role of GLR3.3 in the perception of aphid and thrips feeding (Chapter 5). For this, I investigated responses to three aphid species with contrasting abilities to colonise *A. thaliana*: the generalist aphid *M. persicae* and the specialist aphid *B. brassicae*, both of which readily colonise *A. thaliana*, and the specialist aphid *R. padi*, which cannot colonise *A. thaliana*.

Thrips feeding induced apoplastic alkalinisations and iGluSnFR signals that correlated with wave $[Ca^{2+}]$ elevations. These wave $[Ca^{2+}]$ elevations were abolished in the *glr3.3a* mutant and were replaced with burst and secondary $[Ca^{2+}]$ elevations. Therefore, thrips feeding-induced $[Ca^{2+}]$ elevations recapitulated those induced by localised wounding. This similarity is consistent with both stimuli causing localised cell damage (Hunter and Ullman, 1989; Kindt *et al.*, 2003). Furthermore, thrips feeding induced JA marker gene expression and thrips resistance was reduced in *glr3.3a* mutants. With the role identified for GLR3.3 in wound-induced *JAZ10* expression, these data suggest that GLR3.3 contributes to JA-mediated defence responses against thrips. This notion is consistent with JA signalling promoting thrips resistance in *A. thaliana* (Abe *et al.*, 2008; Steenbergen, 2022). Taken together, these findings indicate that GLR3.3 performs a significant role in the perception of thrips feeding similarly to how it functions in the perception of localised wounding.

Aphid feeding from all the aphid species induced correlated apoplastic alkalinisations, iGluSnFR reporter signals and $[Ca^{2+}]$ elevations. The aphid feeding-induced $[Ca^{2+}]$ elevations

included some that recapitulated those induced by touch and some that recapitulated the wave $[Ca^{2+}]$ elevations induced by wounding. The aphid feeding-induced wave $[Ca^{2+}]$ elevations appeared to be GLR3.3-dependent. Additionally, GLR3.3 appeared to contribute to the $[Ca^{2+}]$ elevations induced by each aphid species to different extents with a more major role in those induced by *B. brassicae* and *R. padi* than those induced by *M. persicae*. *M. persicae* feeding also rarely induced detectable *JAZ10* expression and GLR3.3 did not contribute to *M. persicae* resistance. In contrast, *JAZ10* expression was detectable in response to a higher proportion of *R. padi* feeding events than *M. persicae* feeding events and *R. padi* survival was increased on *glr3.3a* mutants. Finally, despite inducing GLR3.3-dependent $[Ca^{2+}]$ elevations to a similar extent as *R. padi*, *B. brassicae* rarely induced *JAZ10* expression and GLR3.3 did not appear to contribute to *B. brassicae* resistance. Therefore, the signalling mechanism proposed here for localised GLR3.3 activity seems to function in responses to aphid feeding but the contribution of GLR3.3 to the responses appears to vary depending on the aphid species involved.

As with wound- and touch-induced responses, the extent of GLR3.3 activation induced by each of the insect species investigated may positively correlate with the extent of damage and/or mechanical stress that occurs during feeding. This is consistent with thrips feeding causing more mechanical stress and damage than aphid feeding as well as a greater extent of GLR3.3 activation. The extent of damage or mechanical stress caused by feeding may also differ between the aphid species, since their feeding behaviours are known to differ and can vary with the ability to colonise the host (Cole, 1997; Escudero-Martinez *et al.*, 2021). To assess whether feeding behaviours differ between the aphid species and cause differences in cell damage or mechanical stress in *A. thaliana*, it would be informative to monitor the feeding behaviour for each aphid species with the electrical penetration graph (EPG) technology (Tjallingii, 1985; Tjallingii, 1978; Tjallingii and Esch, 1993). Moreover, coupling EPG with $[Ca^{2+}]$ reporter imaging could help identify what cellular events lead to GLR3.3 activation. As an alternative to this challenging combined approach, aphid feeding behaviour and the damage caused could be assessed after $[Ca^{2+}]$ imaging by visualising stylet tracks (Brennan *et al.*, 2001) together with any cell death (Lei *et al.*, 2014). These experiments could help identify if the extent of mechanical stress and/or damage caused with aphid or thrips feeding determines the extent of GLR3.3 activation.

The influence of aphid effectors on GLR3.3 activity or downstream signalling may also differ for the aphid species investigated. For example, *M. persicae* may deploy effectors that suppress GLR3.3 activation and GLR3.3-dependent $[Ca^{2+}]$ elevations. A candidate effector for this would be Mp10 which can suppress immune signalling (Bos *et al.*, 2010; Drurey *et al.*, 2019) and is delivered into mesophyll cells with aphid feeding (Mugford *et al.*, 2016). *R. padi* may be

less effective at suppressing GLR3.3 activity since it has not evolved to colonise *A. thaliana*. Whilst *B. brassicae* can colonise *A. thaliana*, *B. brassicae* feeding induced GLR3.3-dependent $[Ca^{2+}]$ elevations to a similar extent as *R. padi*. However, *B. brassicae* did not induce *JAZ10* expression and *B. brassicae* resistance in *A. thaliana* did not seem to be GLR3.3-dependent. Interestingly, *B. brassicae* has specialised on Brassicas to sequester plant defensive glucosinolates, which then function in the aphids own defence responses (Kazana *et al.*, 2007; Pratt *et al.*, 2008). As many glucosinolates are JA regulated and can be induced by damage (Textor and Gershenzon, 2009), *B. brassicae* may have evolved to induce glucosinolate production by causing damage, which also activates GLR3.3. To limit GLR3.3-dependent plant defence responses, *B. brassicae* may have evolved effectors that suppress events downstream of GLR3.3 activation, such as *JAZ10* expression. Whilst no *B. brassicae* effectors are yet known to display this activity, some caterpillar species can deliver the HARP1 effector that suppresses JA-dependent gene expression by preventing the degradation of JAZ repressor proteins (Chen *et al.*, 2019). The newly discovered role of GLR3.3 in plant responses to aphid feeding could facilitate the identification of aphid effectors that target GLR3.3 activation or GLR3.3-dependent defence responses.

In summary, I identified a novel role for GLR3.3 in responses to aphid and thrips feeding. The contribution of GLR3.3 to the perception of these insects is likely dependent on the extent of damage and/or mechanical stress that occurs with feeding. Therefore, GLR3.3 activation may provide a means for plants to tailor certain defence responses against these insects to the extent of mechanical stress and/or damage experienced. Additionally, aphid effectors could limit GLR3.3 activity or GLR3.3-dependent responses to promote colonisation. Without detailed knowledge of GLR3.3 gating *in planta*, it cannot be determined whether GLR3.3 functions as a receptor for DAMPs or as a signalling component in responses to localised insect feeding. Nonetheless, implicating GLR3.3 in the perception of damage and/or mechanical stress during aphid and thrips feeding advances the understanding of how plants perceive these insects. With this, the findings of this thesis have been synthesised into a summary model for how GLR3.3 activation and mechanical stress perception could function in *A. thaliana* responses to localised wounding, touch, aphid feeding and thrips feeding (Figure 7.1).

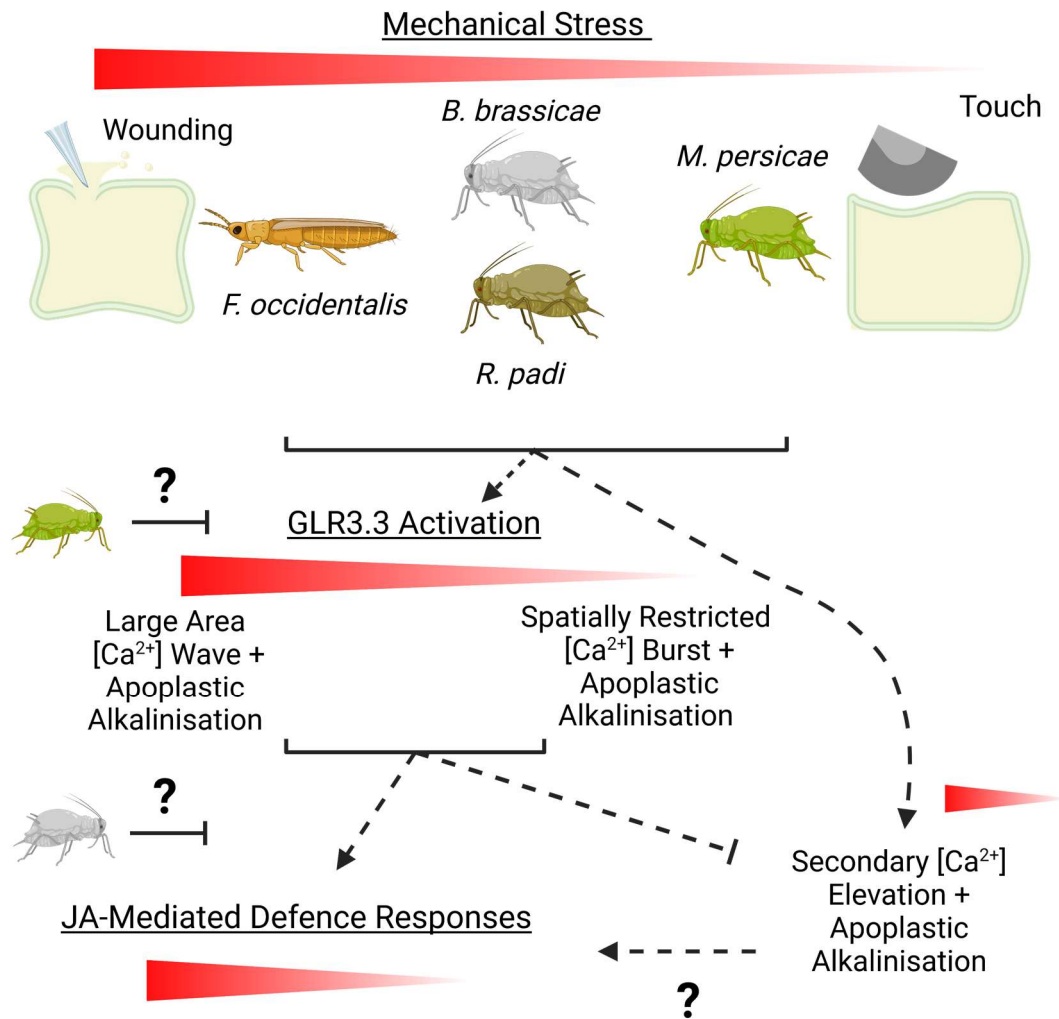


Figure 7.1 Proposed model for the function of mechanical stress perception and GLR3.3 in responses to localised wounding, touch, aphid feeding, and thrips feeding.

A proposed model for the mechanical stress perception of localised stimuli leading to $[Ca^{2+}]$ elevations, apoplastic alkalinisations and JA-mediated defence responses. In this model, the stimuli shown cause different degrees of mechanical stress: localised wounding > *F. occidentalis* (thrips) > *B. brassicae* = *R. padi* > *M. persicae* > touch. The extent of mechanical stress determines the extent of GLR3.3 activation. A greater extent of GLR3.3 activation with more mechanical stress leads to further propagating wave $[Ca^{2+}]$ elevations and larger area apoplastic alkalinisations, whilst a lesser extent leads to more spatially restricted burst responses. The greater the GLR3.3 activation, the greater the extent that GLR3.3-dependent signalling can promote JA-mediated defence responses. Mechanical stress perception also proportionally triggers secondary $[Ca^{2+}]$ elevations and apoplastic alkalinisations. Secondary responses appeared to be suppressed by GLR3.3 activity. It is unclear whether secondary responses can promote JA-defence signalling. *M. persicae* may deposit effectors that suppress GLR3.3 activation whilst *B. brassicae* may deploy effectors that impair GLR3.3-dependent JA-mediated defence responses. Arrows indicate promotional effects. Flat arrows indicate suppressive effects. Dashed lines indicate unknown intermediate steps. Question marks indicate low confidence interactions. Red to white graded triangles indicate gradients of stimuli and responses.

7.1.4. The search for additional components involved in the perception of aphid or thrips feeding

In Chapter 6, reverse genetics was combined with genetically encoded reporter imaging to search for additional components that function in responses to aphid or thrips feeding. Whilst touch and wound stimuli were used to increase throughput, efforts were limited by the need to introgress reporter transgenes into mutant backgrounds of interest. This resulted in a limited number of genes and alleles that could be investigated as well as limitations on investigating higher order mutants. Nonetheless, it emerged that many candidate components for the perception of damage or mechanical stress in *A. thaliana* showed no major contribution to the perception of localised wounding or touch. These components were therefore deemed unlikely to function in responses to aphid or thrips feeding.

BAK1 and SOBIR1 have been implicated in the perception of putative aphid HAMPs (Prince *et al.*, 2014; Drurey *et al.*, 2019; Chaudhary *et al.*, 2014; Canham, 2022). Moreover, aphid extract-induced $[Ca^{2+}]$ elevations were impaired in *bak1-5* and *sobir1-12* *A. thaliana*. However, data presented here found no clear contribution of BAK1 or SOBIR1 to *M. persicae* feeding-induced $[Ca^{2+}]$ elevations. This may be because the putative aphid HAMPs that trigger BAK1- or SOBIR1-dependent responses are not sufficiently present at the aphid feeding site to induce detectable responses within the 30 min post-feeding period that was monitored here. Alternatively, it could be that aphid effectors delivered by *M. persicae* can suppress BAK1/SOBIR1-dependent HAMP-induced responses. In support of this, the *M. persicae* effector, Mp10, is delivered with aphid feeding and appears to suppress BAK1-dependent defence responses (Drurey *et al.*, 2019; Mugford *et al.*, 2016). Moreover, *M. persicae* performance is unaltered on *bak1-5* mutants (Prince *et al.*, 2014; Vincent, 2016). In contrast, *bak1-5* mutants display reduced resistance against the pea aphid, *A. pisum*, which cannot colonise *A. thaliana* (Prince *et al.*, 2014; Vincent, 2016). Testing whether BAK1 or SOBIR1 can function in $[Ca^{2+}]$ elevations induced by aphid species which cannot colonise *A. thaliana*, such as *A. pisum*, would help identify whether BAK1/SOBIR1-dependent HAMP perception can function in the initial responses to aphid feeding. Nonetheless, data presented here do not identify a role for BAK1 or SOBIR1 in the early plant responses to *M. persicae* feeding.

7.2. Focus for future investigations

7.2.1. What determines GLR3.3 activation *in planta*?

The understanding of how GLR3.3 contributes to the perception of localised wounding, aphid feeding, and thrips feeding is hindered by the lack of clarity around GLR3.3 activation. Specifically, whilst pH and glutamate gating of GLR3.3 has been demonstrated by electrophysiology in heterologous systems (Shao *et al.*, 2020), further investigations are required to understand the cellular and molecular processes that determine GLR3.3 activation *in planta*. Such investigations will help identify whether GLR3.3 functions as a DAMP receptor or a signalling component in plant responses to localised wounding, aphid feeding and thrips feeding.

Investigations could assess whether the extent of mechanical stress or damage-induced DAMP release determines localised GLR3.3 activation in *A. thaliana*. An informative experiment would be to assess the dependency of $[Ca^{2+}]$ elevations on GLR3.3 in responses to localised stimuli that cause damage or mechanical stress without damage, with varying degrees of severity. If the extent of mechanical stress determines GLR3.3 activation, the GLR3.3 dependency for the $[Ca^{2+}]$ elevations would positively correlate with the degree of mechanical stress applied. If damage is required for GLR3.3 activation, larger damage events may trigger GLR3.3-dependent $[Ca^{2+}]$ elevations with greater areas but mechanical stress without damage would not induce GLR3.3-dependent responses. For these experiments, it would be beneficial to be able to apply localised mechanical stress or damage stimuli reproducibly and quantitatively. Experimental design may therefore benefit from automating stimuli and utilising sensors that record each stimulus event. Interestingly, protruding trichome cells may provide an accessible system to apply different levels of mechanical stress. In preliminary experiments (data not shown), a light trichome touch induced burst and secondary $[Ca^{2+}]$ elevations whilst firmer touch induced wave-like GLR3.3-dependent $[Ca^{2+}]$ elevations revealing the tractability of this system. Laser ablation, which can induce wave-like $[Ca^{2+}]$ elevations in *A. thaliana* leaf epidermal cells (Guo *et al.*, 2022), could be appropriate to apply graded damage stimuli to leaves. For all these experiments, it would be beneficial to perform higher resolution imaging than was performed here to reveal the effects of each stimulus on cells and identify any cell damage. These experiments would help reveal the cellular processes that determine GLR3.3 activation in responses to aphid and thrips feeding.

Identifying whether amino acid ligands gate GLR3.3 *in planta* will be crucial for understanding GLR3.3 function in the perception of aphid and thrips feeding. To identify whether these ligands, such as glutamate, could activate GLR3.3, it would be beneficial to

advance the reporters available for visualising apoplastic [Glu]. For example, a [Glu]-insensitive iGluSnFR would help assess pH effects on iGluSnFR and test whether localised stimuli cause apoplastic [Glu] increases which could activate GLR3.3. This approach is similar to the HyPer ROS reporter being used alongside its ROS-insensitive partner, SypHer, to test for pH effects (Poburko *et al.*, 2011; Smolyarova *et al.*, 2022). Additionally, a FRET-based [Glu] reporter could be relatively insensitive to pH effects and thus help assess apoplastic [Glu] changes. FLIPEs are FRET-based [Glu] reporters which have been expressed freely in the apoplast and anchored at the extracellular face of the plasma membrane (Castro-Rodríguez *et al.*, 2022). Whilst several FLIPE variants with different glutamate binding affinities have been developed, many cause developmental phenotypes which may make them unsuitable for use. Because glutamate performs many key roles in plants, including as an amino acid for protein synthesis (Liao *et al.*, 2022), apoplastic [Glu] cannot easily be significantly and specifically manipulated to investigate its importance in GLR3.3 activation. Therefore, characterising apoplastic [Glu] changes in responses to aphid or thrips feeding will be crucial for understanding their contribution to GLR3.3 gating.

The potential for apoplastic pH to regulate GLR3.3 activity *in planta* is not well characterised. Quantifying the magnitude of the apoplastic alkalinisations associated with localised GLR3.3-dependent responses could help identify whether the pH changes are likely to activate GLR3.3. Such pH estimates could be achieved by calibrating the apo-pHusion reporter as has been done *ex vivo* for estimates of apoplastic alkalinisations during leaf senescence (Borniego *et al.*, 2020). Additionally, there are other pH reporters that can be used quantitatively in the apoplast (Martinière *et al.*, 2018; Bell *et al.*, 2022; Moreau *et al.*, 2022). For example, the ratiometric pHluorin pH reporter has been used in roots and revealed that the apoplastic pH can be elevated at the plasma membrane surface (~ pH 6.0-6.3) compared to the general apoplastic space (~ pH 5.0) (Martinière *et al.*, 2018). Similarly, heterogeneity in apoplastic pH has been demonstrated for tobacco leaf epidermal cells with the Acidin pH reporters (Moreau *et al.*, 2022). These findings suggest that it may be necessary to monitor apoplastic pH specifically at the plasma membrane to assess the potential for any apoplastic pH increases to gate GLR3.3. Manipulating apoplastic pH genetically or pharmacologically could also help reveal whether pH can gate GLR3.3 in responses to localised stimuli. To buffer apoplastic pH in the present study, leaves were vacuum infiltrated pre-wounding with a citrate buffer (pH 5, Chapter 4). However, the infiltration process appeared to suppress GLR3.3 activation independently of the infiltrated solution. Whilst this suppression of GLR3.3 could have resulted from effects on apoplastic pH, it was not possible using this method to specifically manipulate apoplastic pH and assess the effects on GLR3.3 activation. Further efforts to manipulate and visualise apoplastic pH will help

reveal whether apoplastic alkalinisations can contribute to regulating GLR3.3 activity in responses to aphid or thrips feeding.

The regulation of GLR3.3 activity in systemic responses to large-scale wounding is thought to involve several components in addition to pH and amino acid ligands. ISI1 interacts with GLR3.3 and suppresses large-scale wound-induced systemic responses (Wu *et al.*, 2022). MSL10 contributes to large-scale wound-induced systemic membrane depolarisations which are thought to promote GLR3.3/3.6 activity (Moe-Lange *et al.*, 2021). However, neither ISI1 nor MSL10 contributed to localised wound-induced $[Ca^{2+}]$ elevations here (Chapter 6). Recently, the thioglucosidase (TGG) enzymes, TGG1 and TGG2, have been implicated as the dominant mobile signals for mediating large-scale wound-induced rapid systemic signalling (Gao *et al.*, 2023). These TGGs are released from myrosin cells in the phloem parenchyma and are required for the large-scale wound-induced systemic depolarisations and $[Ca^{2+}]$ elevations (Gao *et al.*, 2023). Additionally, this function of TGG1/2 requires their enzymatic activity to cleave glucosinolates into reactive aglycones, which are also required for the responses (Gao *et al.*, 2023). TGG1-induced responses are partially dependent on GLR3.3 and fully dependent on GLR3.6 (Gao *et al.*, 2023). This suggests that GLR3.3 and GLR3.6 function as signalling components downstream of TGGs in large-scale wound-induced systemic responses. However, it is unknown at present how GLR3.3 and GLR3.6 are activated by TGG activity. It is possible that apoplastic pH could contribute to this regulation of GLR3.3/3.6 because AHA activity, that reduces apoplastic pH, can negatively regulate large-scale wound-induced rapid systemic signalling (Kumari *et al.*, 2019; Shao *et al.*, 2020). Storage of TGGs in the vascular bundle implies that they are unlikely to regulate localised wound-induced responses. Nonetheless, identifying how TGGs can activate GLR3.3/3.6 could help reveal how GLR3.3 functions in responses to localised stimuli.

The further characterisation of factors that determine GLR3.3 activity *in planta* will be significant for understanding how plants perceive localised feeding from aphids and thrips. Moreover, this characterisation will help understand the functions of GLR3.3 in responses to localised and large-scale wounding (Toyota *et al.*, 2018; Shao *et al.*, 2020; Moe-Lange *et al.*, 2021; Bellandi *et al.*, 2022; Grenzi *et al.*, 2023; Gao *et al.*, 2023) and pathogens such as *H. arabidopsidis* and *P. syringae* (Manzoor *et al.*, 2013; Li *et al.*, 2013). With an improved understanding of GLR3.3 regulation, novel functions for GLR3.3 in plant stress responses may also become apparent. For example, if GLR3.3 functions in mechanical stress perception, it could underpin the apoplastic alkalinisations and $[Ca^{2+}]$ elevations induced by mechanical stress in roots (Monshausen *et al.*, 2009). Therefore, the outlined experiments could build on data presented here to significantly advance the understanding how GLR3.3 functions more broadly in plant biotic stress responses.

7.2.2. How significant is GLR3.3 in promoting JA-mediated defence responses to localised stimuli?

GLR3.3 promoted localised wound-induced *JAZ10* expression indicating that localised GLR3.3 activation promotes JA defence signalling (Chapter 4). However, the investigations into the role of GLR3.3 in wound-induced JA-mediated responses were limited by assessing the expression of only two JA marker genes. Moreover, the role of GLR3.3 in aphid and thrips feeding-induced JA marker gene expression was not directly assessed. Therefore, whilst GLR3.3 did contribute to *F. occidentalis* and *R. padi* resistance, it remains unclear how significant GLR3.3 activity is in promoting JA-mediated defence responses to aphids and thrips. To further characterise this function of GLR3.3, investigations could assay various responses in Col-0 and *glr3.3a* *A. thaliana* following localised wounding, aphid feeding or thrips feeding. For example, the role of GLR3.3 in JA-mediated defence gene expression could be further assessed by RNAseq. Moreover, the accumulation of JA species could be monitored to test for GLR3.3-dependency. Desorption electrospray ionisation mass spectrometry can allow the quantification of metabolites across the leaf surface and could be used to assess the accumulation of JAs with spatial resolution (Zhang *et al.*, 2021a). Additionally, the Jas9-VENUS genetically encoded fluorescent reporter, which is degraded with elevated JA levels, could allow JA levels to be monitored with high spatiotemporal resolution (Larrieu *et al.*, 2015). Finally, the role of GLR3.3 in JA-mediated defence outputs, such as the production of some glucosinolate species (Mitreiter and Gigolashvili, 2020), could be tested. Various methods exist for assaying glucosinolate profiles including methods using liquid chromatography and mass spectrometry (Glauser *et al.*, 2012). Quantifying JA-mediated responses to aphid or thrips feeding may prove challenging due to the highly localised and variable nature of the insect feeding behaviours. Nevertheless, it will be crucial to characterise the role of localised GLR3.3 activation in JA-mediated defence responses to better understand how GLR3.3 functions in plant resistance against aphids or thrips.

7.2.3. What is the contribution of GLR3.3 to the perception of feeding from other insect pests?

With data presented here indicating that GLR3.3 functions in responses to aphid and thrips feeding through damage or mechanical stress perception, it would be interesting to assess how GLR3.3 contributes to responses induced by other insect pests. Like aphids and thrips, spider mites display localised feeding behaviours. However, unlike aphids and thrips, spider mites navigate their stylets between epidermal cells to mesophyll cells, which they feed on by extracting the cell contents (Bensoussan *et al.*, 2016). This spider mite feeding behaviour causes

death for a limited number of mesophyll cells (Bensoussan *et al.*, 2016) and likely causes greater damage and mechanical stress than aphid feeding. Therefore, GLR3.3 may play a more dominant role in responses to spider mites than to aphids. Spider mite feeding is thought to induce JA signalling (Bruinsma, 2014; Santamaría *et al.*, 2018) which could show dependency on GLR3.3. Chewing insects may also induce GLR3.3-dependent responses in epidermal and mesophyll cell layers because they cause damage to these cells during feeding. Indeed, preliminary data (not shown) indicated that feeding from the cabbage stem flea beetle induces GLR3.3-dependent $[Ca^{2+}]$ elevations in the non-vascular tissue of *A. thaliana* leaves. Characterising the function of GLR3.3 in plant responses to other insect pests may help determine how those insects are perceived and more broadly how GLR3.3 functions in plant-insect interactions.

7.2.4. What other components contribute to the perception of aphid and thrips feeding?

There are many factors that remain unknown in the perception of localised aphid and thrips feeding. Additional components may function in the perception of mechanical stress, damage, HAMPs, or effectors. To identify components involved in mechanical stress or damage perception, forward genetics or reverse genetics screens could be performed. These screens could be aided by the methods developed in this thesis and the considerations of Chapter 6. Whilst there have already been significant efforts to purify and characterise aphid HAMPs (De Vos and Jander, 2009; Prince *et al.*, 2014; Chaudhary *et al.*, 2014; Canham, 2022), the knowledge of aphid and thrips HAMPs remains highly limited. As these HAMPs may be present in saliva and interact with plants during the early phases of feeding, characterising any aphid or thrips HAMPs will be important for understanding how plants initially perceive aphid or thrips feeding. Finally, characterising aphid or thrips effectors, their activities and plant NLRs will be significant in understanding how plants perceive these insects and how the insects can manipulate hosts to promote colonisation. Any additional components characterised will help build the knowledge of how plants can perceive aphids and thrips and what factors determine the success of the plant defence responses.

7.3. Conclusions

This thesis has explored the mechanisms by which plants perceive the localised and intricate feeding behaviours of aphids and thrips. By developing methods for reporter imaging, I have established a foundation to robustly visualise plant responses to localised insect feeding. Moreover, I have deployed these methods to identify and characterise a role for GLR3.3 in responses to localised wounding. Although GLR3.3 activation in localised wound-induced responses may require damage-induced DAMP release, I have proposed a novel signalling

mechanism that links the extent of mechanical stress and the magnitude of initial apoplastic alkalinisations to the degree of GLR3.3 activation. With these findings, I have characterised the role of GLR3.3 in the perception of three aphid species and a thrips species. Efforts to identify additional components that function in the early plant responses to aphid or thrips feeding revealed that many candidate genes are unlikely to do so.

Aphid and thrips perception in plants is complex and challenging to investigate. The discovery that GLR3.3 contributes to this perception is a significant advance and highlights the importance of mechanical stress and damage in early plant responses to aphid and thrips feeding. This thesis can now guide further investigations in exploring GLR3.3 activity and additional elements that allow plants to perceive insects with highly localised feeding mechanisms. Combined with the advances presented here, such investigations can help build a more complete understanding of how plants perceive aphids and thrips. This knowledge will support crucial efforts to enhance plant resistance against significant aphid and thrips pests.

Appendix I

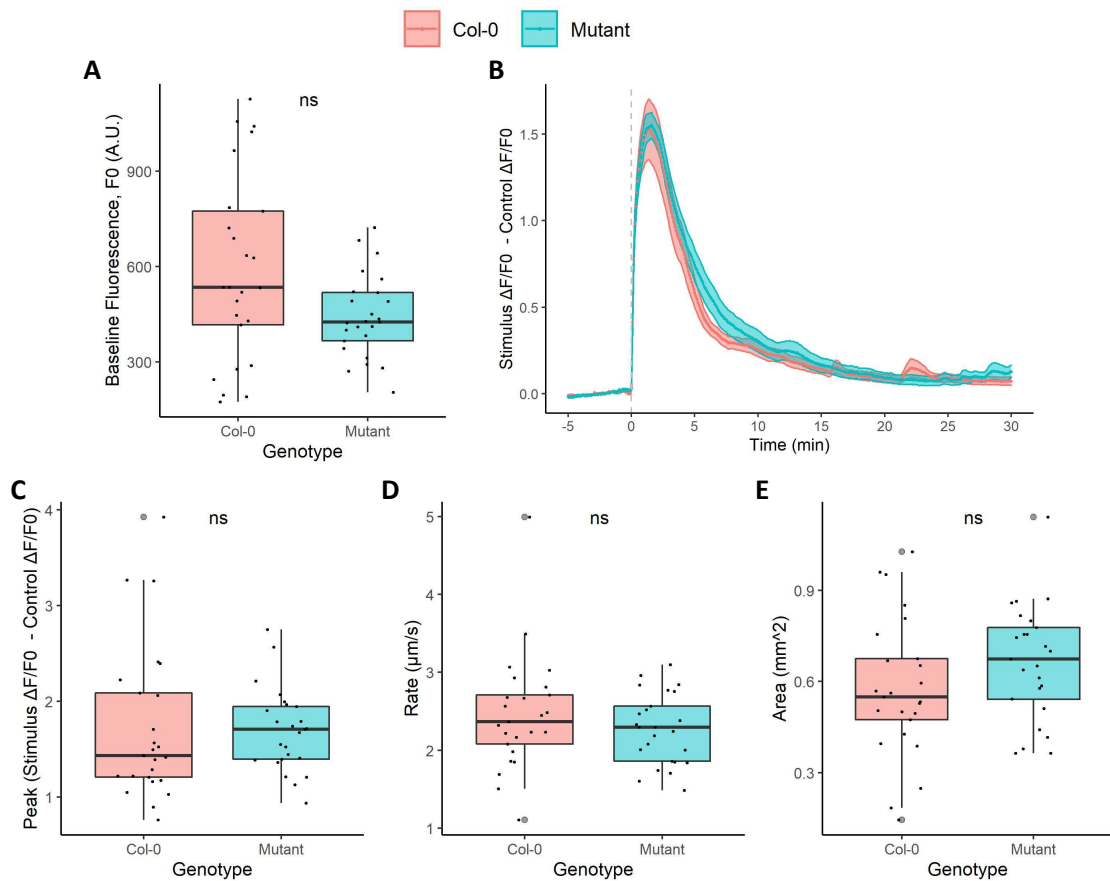


Figure I.I Wound-induced GCaMP3 reporter signals in Col-0 and *isi1-3 A. thaliana*.

Properties of wound-induced GCaMP3 signals in Col-0 and *isi1-3 A. thaliana* expressing *UBQ10::GCaMP3* ($n = 25$). Background-corrected fluorescence intensity (F , A.U.) values were recorded over the area of the stimulus-induced responses and at comparable control sites. F values were transformed into $\Delta F/F_0$ values with F_0 being the mean F over the 5 min prior to stimulus treatment. (B) Traces for the mean \pm S.E.M. normalised $\Delta F/F_0$ values (Stimulus $\Delta F/F_0$ - Control $\Delta F/F_0$) over time with stimulus treatment at 0 min (grey dashed line). Boxplots are displayed for the (A) stimulus-treated site F_0 values (A.U.), (C) peak normalised $\Delta F/F_0$ values (Stimulus $\Delta F/F_0$ - Control $\Delta F/F_0$), (D) signal propagation rates ($\mu\text{m s}^{-1}$) and (E) signal areas (mm^2), with grey dots associated with outliers. Statistical significance, calculated using a t-test or a Wilcoxon rank-sum test, is shown by ns: $p > 0.05$, *: $p \leq 0.05$, **: $p \leq 0.01$, ***: $p \leq 0.001$, ****: $p \leq 0.0001$.

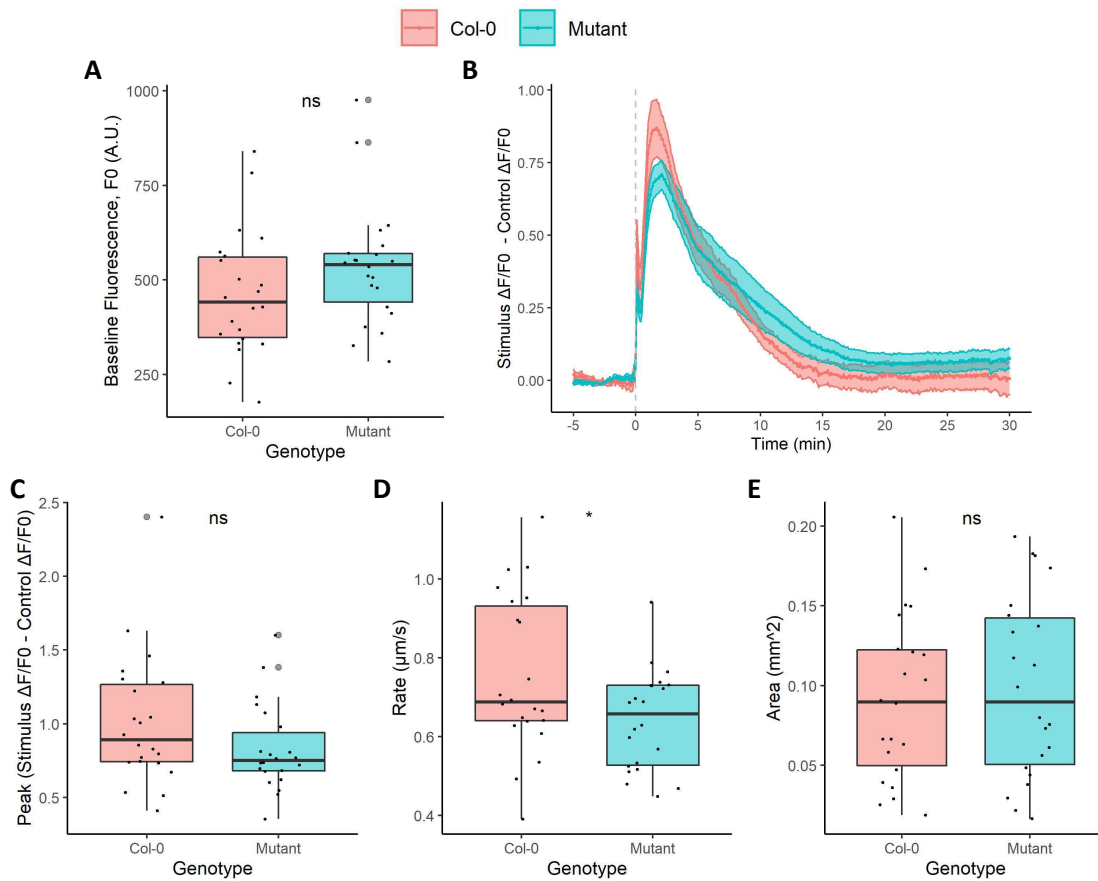


Figure I.II Touch-induced GCaMP3 reporter signals in Col-0 and *isi1-3 A. thaliana*.

Properties of touch-induced GCaMP3 signals in Col-0 and *isi1-3 A. thaliana* expressing *UBQ10::GCaMP3* ($n = 22$). Background-corrected fluorescence intensity (F , A.U.) values were recorded over the area of the stimulus-induced responses and at comparable control sites. F values were transformed into $\Delta F/F_0$ values with F_0 being the mean F over the 5 min prior to stimulus treatment. (B) Traces for the mean \pm S.E.M. normalised $\Delta F/F_0$ values (Stimulus $\Delta F/F_0$ - Control $\Delta F/F_0$) over time with stimulus treatment at 0 min (grey dashed line). Boxplots are displayed for the (A) stimulus-treated site F_0 values (A.U.), (C) peak normalised $\Delta F/F_0$ values (Stimulus $\Delta F/F_0$ - Control $\Delta F/F_0$), (D) signal propagation rates ($\mu\text{m s}^{-1}$) and (E) signal areas (mm^2), with grey dots associated with outliers. Statistical significance, calculated using a t-test or a Wilcoxon rank-sum test, is shown by ns: $p > 0.05$, *: $p \leq 0.05$, **: $p \leq 0.01$, ***: $p \leq 0.001$, ****: $p \leq 0.0001$.

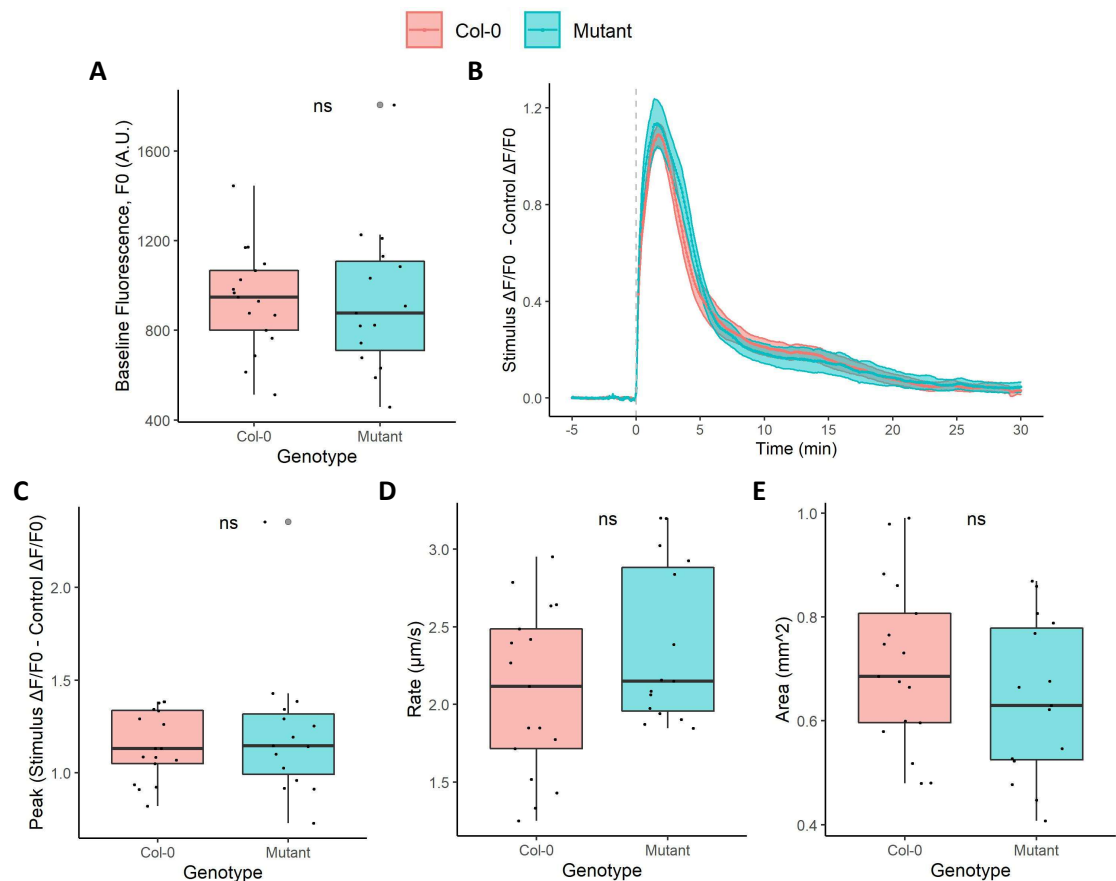


Figure I.III Wound-induced GCaMP3 reporter signals in Col-0 and *aha1-7* *A. thaliana*.

Properties of wound-induced GCaMP3 signals in Col-0 ($n = 17$) and *aha1-7* ($n = 15$) *A. thaliana* expressing *UBQ10::GCaMP3*. Background-corrected fluorescence intensity (F , A.U.) values were recorded over the area of the stimulus-induced responses and at comparable control sites. F values were transformed into $\Delta F/F_0$ values with F_0 being the mean F over the 5 min prior to stimulus treatment. **(B)** Traces for the mean \pm S.E.M. normalised $\Delta F/F_0$ values (Stimulus $\Delta F/F_0$ - Control $\Delta F/F_0$) over time with stimulus treatment at 0 min (grey dashed line). Boxplots are displayed for the **(A)** stimulus-treated site F_0 values (A.U.), **(C)** peak normalised $\Delta F/F_0$ values (Stimulus $\Delta F/F_0$ - Control $\Delta F/F_0$), **(D)** signal propagation rates ($\mu\text{m s}^{-1}$) and **(E)** signal areas (mm^2), with grey dots associated with outliers. Statistical significance, calculated using a t-test or a Wilcoxon rank-sum test, is shown by ns: $p > 0.05$, *: $p \leq 0.05$, **: $p \leq 0.01$, ***: $p \leq 0.001$, ****: $p \leq 0.0001$.

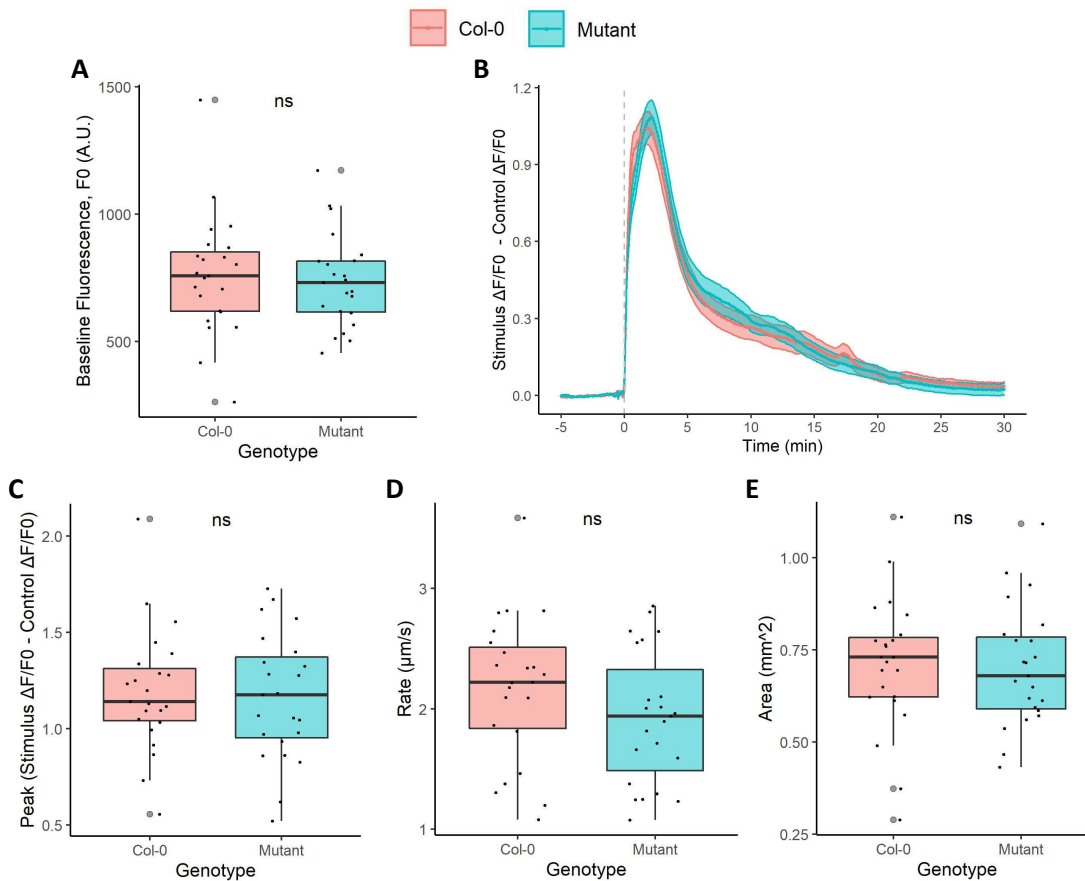


Figure I.IV Wound-induced GCaMP3 reporter signals in Col-0 and *ms10-1 A. thaliana*.

Properties of wound-induced GCaMP3 signals in Col-0 and *ms10-1 A. thaliana* expressing *UBQ10::GCaMP3* ($n = 23$). Background-corrected fluorescence intensity (F , A.U.) values were recorded over the area of the stimulus-induced responses and at comparable control sites. F values were transformed into $\Delta F/F_0$ values with F_0 being the mean F over the 5 min prior to stimulus treatment. (B) Traces for the mean \pm S.E.M. normalised $\Delta F/F_0$ values (Stimulus $\Delta F/F_0 -$ Control $\Delta F/F_0$) over time with stimulus treatment at 0 min (grey dashed line). Boxplots are displayed for the (A) stimulus-treated site F_0 values (A.U.), (C) peak normalised $\Delta F/F_0$ values (Stimulus $\Delta F/F_0 -$ Control $\Delta F/F_0$), (D) signal propagation rates ($\mu\text{m s}^{-1}$) and (E) signal areas (mm^2), with grey dots associated with outliers. Statistical significance, calculated using a t-test or a Wilcoxon rank-sum test, is indicated by ns: $p > 0.05$, *: $p \leq 0.05$, **: $p \leq 0.01$, ***: $p \leq 0.001$, ****: $p \leq 0.0001$.

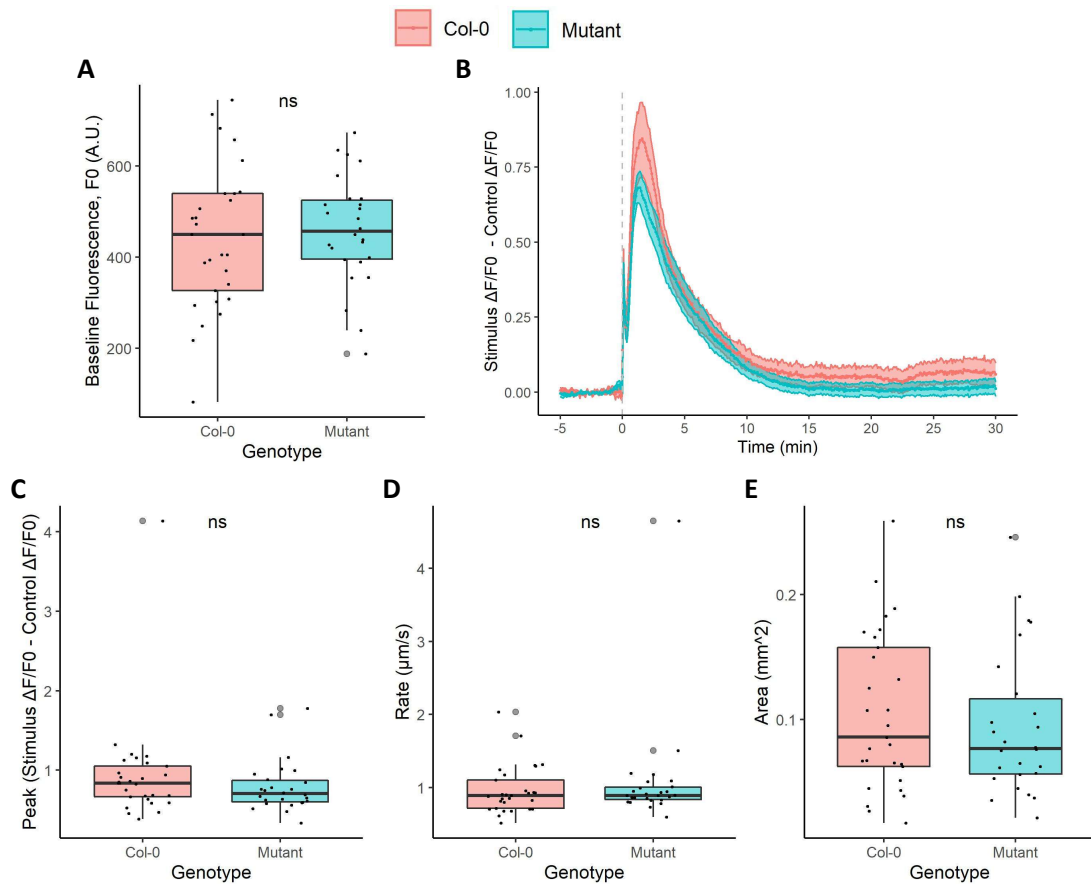


Figure I.V Touch-induced GCaMP3 reporter signals in Col-0 and *msl10-1 A. thaliana*.

Properties of touch-induced GCaMP3 signals in Col-0 ($n = 29$) and *msl10-1* ($n = 26$) *A. thaliana* expressing *UBQ10::GCaMP3*. Background-corrected fluorescence intensity (F , A.U.) values were recorded over the area of the stimulus-induced responses and at comparable control sites. F values were transformed into $\Delta F/F_0$ values with F_0 being the mean F over the 5 min prior to stimulus treatment. (B) Traces for the mean \pm S.E.M. normalised $\Delta F/F_0$ values (Stimulus $\Delta F/F_0$ - Control $\Delta F/F_0$) over time with stimulus treatment at 0 min (grey dashed line). Boxplots are displayed for the (A) stimulus-treated site F_0 values (A.U.), (C) peak normalised $\Delta F/F_0$ values (Stimulus $\Delta F/F_0$ - Control $\Delta F/F_0$), (D) signal propagation rates ($\mu\text{m s}^{-1}$) and (E) signal areas (mm^2), with grey dots associated with outliers. Statistical significance, calculated using a t-test or a Wilcoxon rank-sum test, is shown by ns: $p > 0.05$, *: $p \leq 0.05$, **: $p \leq 0.01$, ***: $p \leq 0.001$, ****: $p \leq 0.0001$.

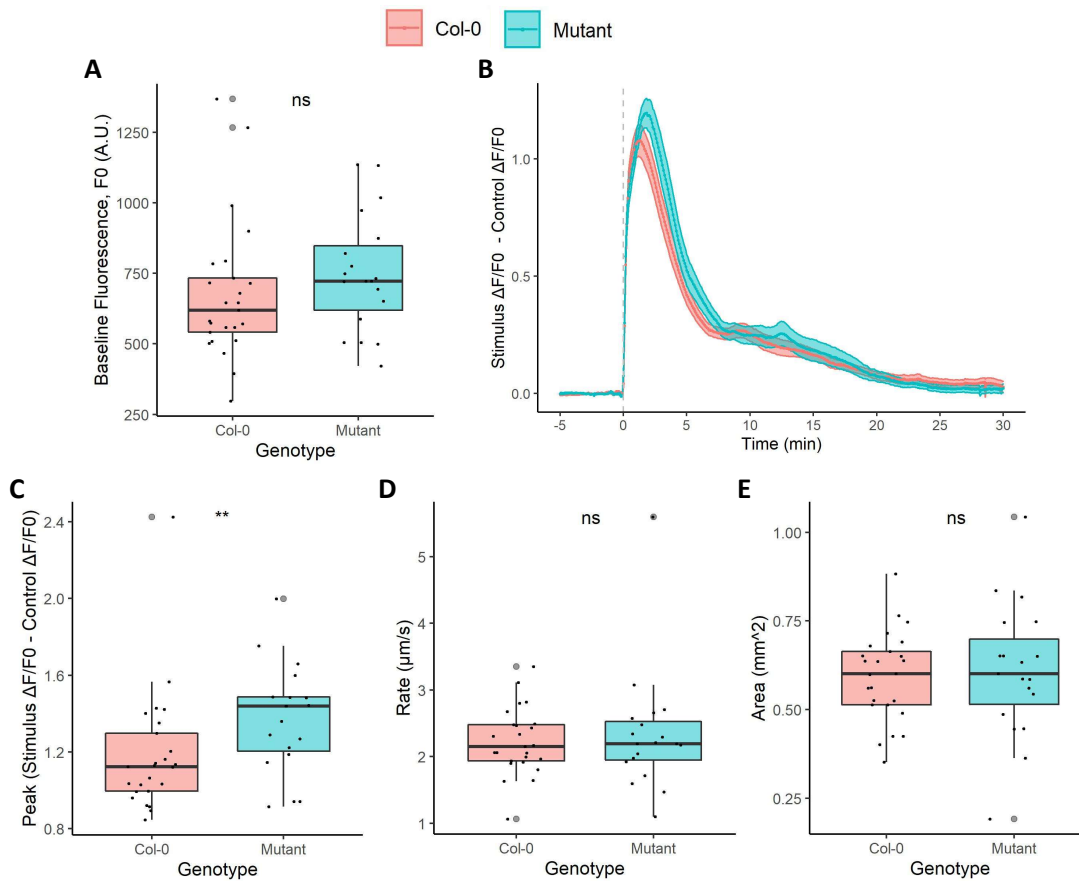


Figure I.VI Wound-induced GCaMP3 reporter signals in Col-0 and *ms10-3G A. thaliana*.

Properties of wound-induced GCaMP3 signals in Col-0 ($n = 25$) and *ms10-3G* ($n = 19$) *A. thaliana* expressing *UBQ10::GCaMP3*. Background-corrected fluorescence intensity (F , A.U.) values were recorded over the area of the stimulus-induced responses and at comparable control sites. F values were transformed into $\Delta F/F_0$ values with F_0 being the mean F over the 5 min prior to stimulus treatment. (B) Traces for the mean \pm S.E.M. normalised $\Delta F/F_0$ values (Stimulus $\Delta F/F_0 -$ Control $\Delta F/F_0$) over time with stimulus treatment at 0 min (grey dashed line). Boxplots are displayed for the (A) stimulus-treated site F_0 values (A.U.), (C) peak normalised $\Delta F/F_0$ values (Stimulus $\Delta F/F_0 -$ Control $\Delta F/F_0$), (D) signal propagation rates ($\mu\text{m s}^{-1}$) and (E) signal areas (mm^2), with grey dots associated with outliers. Statistical significance, calculated using a t-test or a Wilcoxon rank-sum test, is shown by ns: $p > 0.05$, *: $p \leq 0.05$, **: $p \leq 0.01$, ***: $p \leq 0.001$, ****: $p \leq 0.0001$.

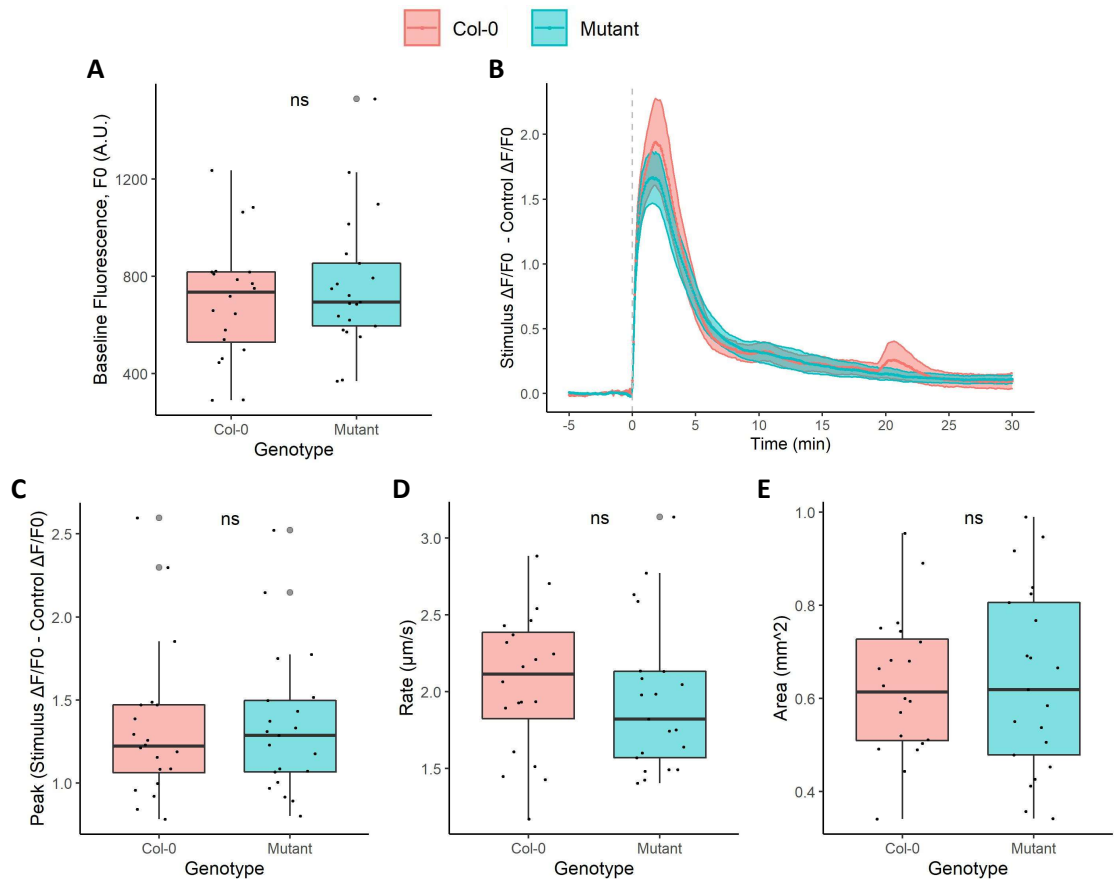


Figure I.VII Wound-induced GCaMP3 reporter signals in Col-0 and *glr3.2a* *A. thaliana*.

Properties of wound-induced GCaMP3 signals in Col-0 ($n = 20$) and *glr3.2a* ($n = 21$) *A. thaliana* expressing *UBQ10::GCaMP3*. Background-corrected fluorescence intensity (F , A.U.) values were recorded over the area of the stimulus-induced responses and at comparable control sites. F values were transformed into $\Delta F/F_0$ values with F_0 being the mean F over the 5 min prior to stimulus treatment. (B) Traces for the mean \pm S.E.M. normalised $\Delta F/F_0$ values (Stimulus $\Delta F/F_0$ - Control $\Delta F/F_0$) over time with stimulus treatment at 0 min (grey dashed line). Boxplots are displayed for the (A) stimulus-treated site F_0 values (A.U.), (C) peak normalised $\Delta F/F_0$ values (Stimulus $\Delta F/F_0$ - Control $\Delta F/F_0$), (D) signal propagation rates ($\mu\text{m s}^{-1}$) and (E) signal areas (mm^2), with grey dots associated with outliers. Statistical significance, calculated using a t-test or a Wilcoxon rank-sum test, is shown by ns: $p > 0.05$, *: $p \leq 0.05$, **: $p \leq 0.01$, ***: $p \leq 0.001$, ****: $p \leq 0.0001$.

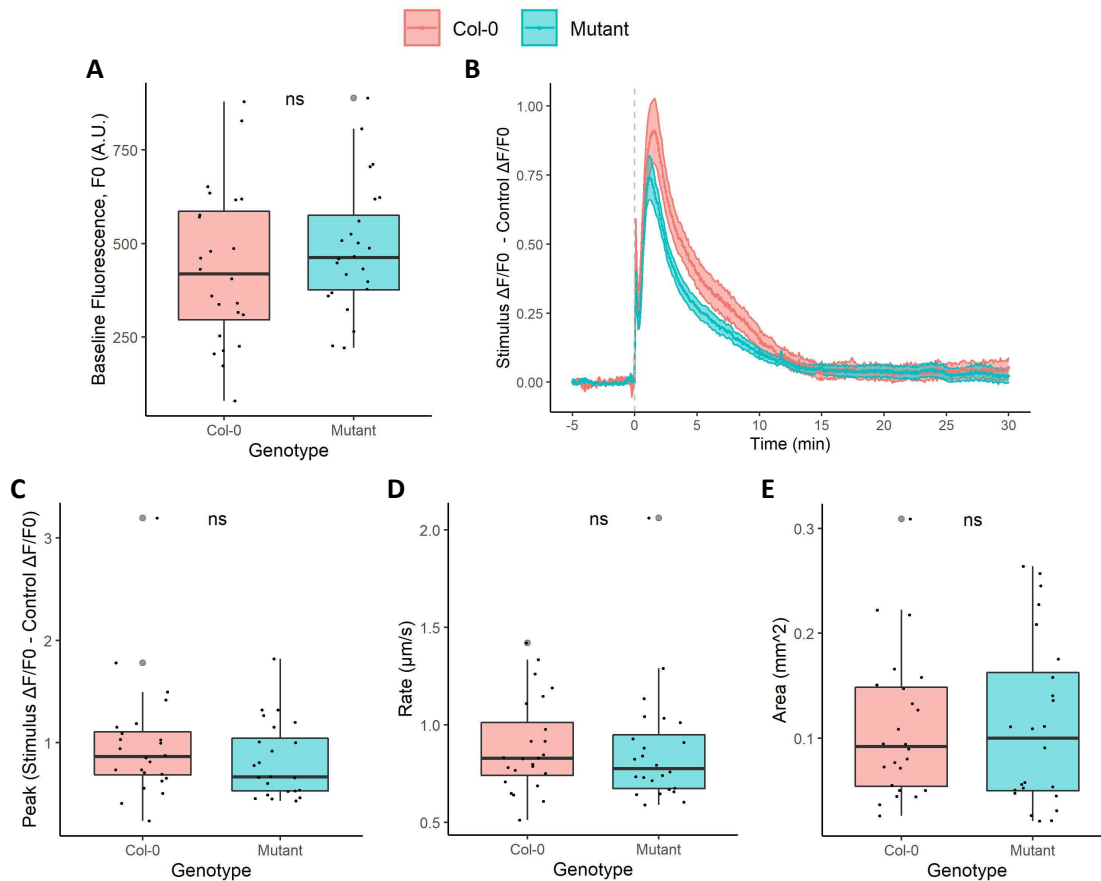


Figure I.VIII Touch-induced GCaMP3 reporter signals in Col-0 and *glr3.2a A. thaliana*.

Properties of touch-induced GCaMP3 signals in Col-0 and *glr3.2a A. thaliana* expressing *UBQ10::GCaMP3* ($n = 24$). Background-corrected fluorescence intensity (F , A.U.) values were recorded over the area of the stimulus-induced responses and at comparable control sites. F values were transformed into $\Delta F/F_0$ values with F_0 being the mean F over the 5 min prior to stimulus treatment. (B) Traces for the mean \pm S.E.M. normalised $\Delta F/F_0$ values (Stimulus $\Delta F/F_0 -$ Control $\Delta F/F_0$) over time with stimulus treatment at 0 min (grey dashed line). Boxplots are displayed for the (A) stimulus-treated site F_0 values (A.U.), (C) peak normalised $\Delta F/F_0$ values (Stimulus $\Delta F/F_0 -$ Control $\Delta F/F_0$), (D) signal propagation rates ($\mu\text{m s}^{-1}$) and (E) signal areas (mm^2), with grey dots associated with outliers. Statistical significance, calculated using a t-test or a Wilcoxon rank-sum test, is shown by ns: $p > 0.05$, *: $p \leq 0.05$, **: $p \leq 0.01$, ***: $p \leq 0.001$, ****: $p \leq 0.0001$.

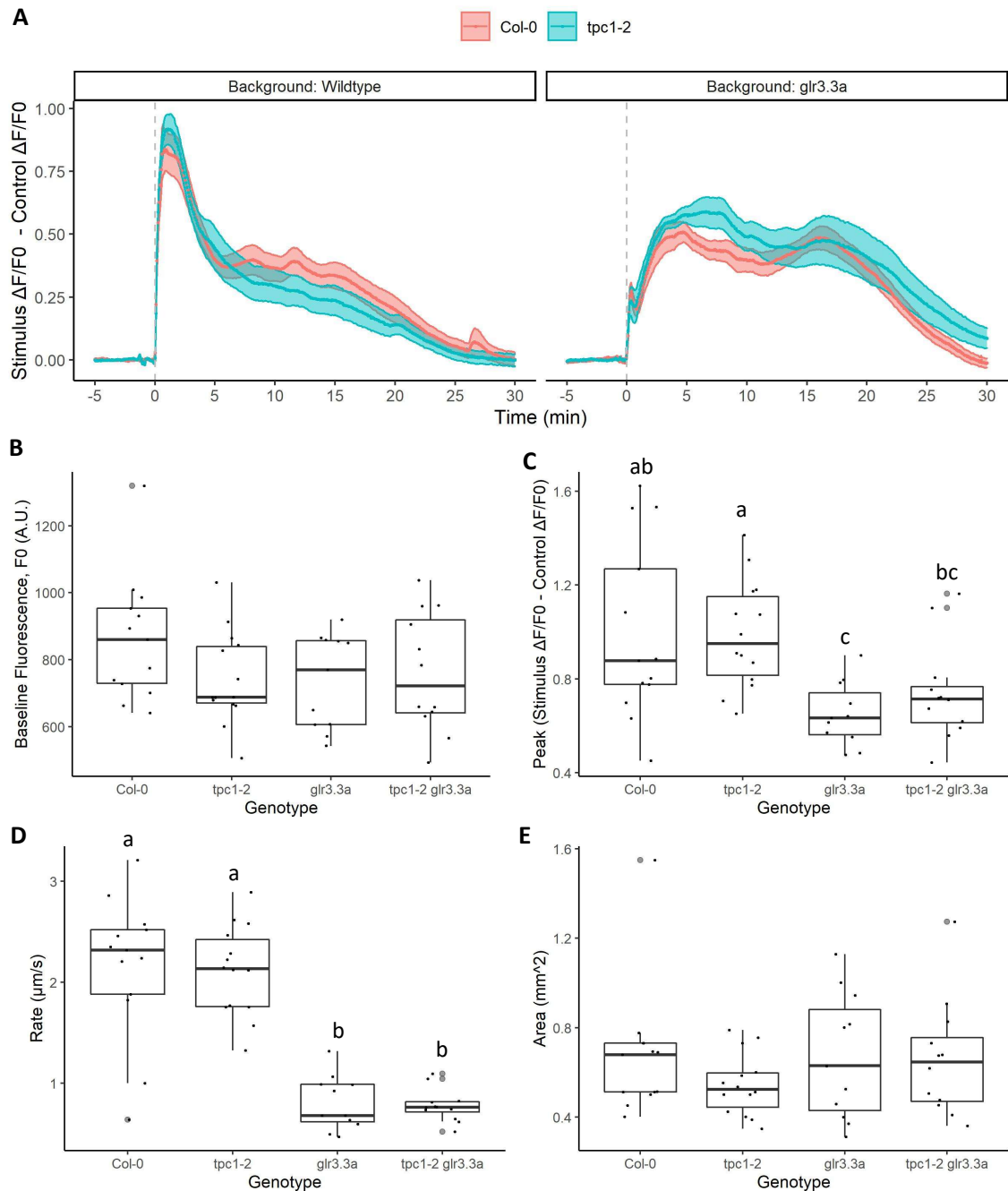


Figure 1.IX Wound-induced GCaMP3 reporter signals in Col-0, *tpc1-2*, *glr3.3a* and *tpc1-2 glr3.3a* *A. thaliana*.

Properties of wound-induced GCaMP3 signals in Col-0 ($n = 13$), *tpc1-2* ($n = 14$), *glr3.3a* ($n = 11$) and *tpc1-2 glr3.3a* ($n = 12$) *A. thaliana* expressing *UBQ10::GCaMP3*. Background-corrected fluorescence intensity (F , A.U.) values were recorded over the area of the stimulus-induced responses and at comparable control sites. F values were transformed into $\Delta F/F_0$ values with F_0 being the mean F over the 5 min prior to stimulus treatment. (A) Traces for the mean \pm S.E.M. normalised $\Delta F/F_0$ values (Stimulus $\Delta F/F_0$ - Control $\Delta F/F_0$) over time with stimulus treatment at 0 min (grey dashed line). Traces are displayed for Col-0 and *tpc1-2* in the wildtype *A. thaliana* background ('Wildtype') and in the *glr3.3a* *A. thaliana* background ('*glr3.3a*'). Boxplots are displayed for the (B) stimulus-treated site F_0 values (A.U.), (C) peak normalised $\Delta F/F_0$ values (Stimulus $\Delta F/F_0$ - Control $\Delta F/F_0$), (D) signal propagation rates ($\mu\text{m s}^{-1}$) and (E) signal areas (mm^2), with grey dots associated with outliers. Statistical significance levels are indicated by letters if genotypes significantly differed. Significance was assessed using an ANOVA with a Tukey post hoc test or a Kruskal-Wallis test with post hoc pairwise Wilcoxon rank-sum tests.

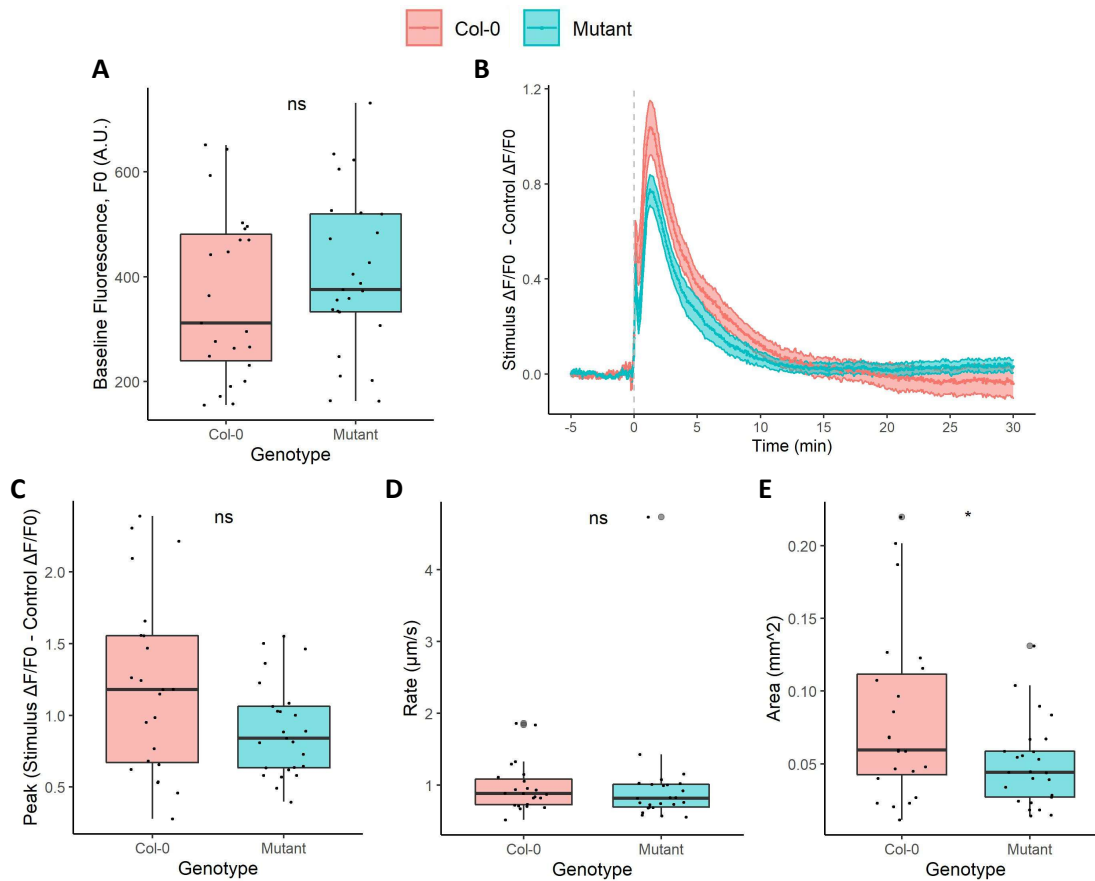


Figure I.X Touch-induced GCaMP3 reporter signals in Col-0 and *tpc1-2* *A. thaliana*.

Properties of touch-induced GCaMP3 signals in Col-0 ($n = 23$) and *tpc1-2* ($n = 25$) *A. thaliana* expressing *UBQ10::GCaMP3*. Background-corrected fluorescence intensity (F , A.U.) values were recorded over the area of the stimulus-induced responses and at comparable control sites. F values were transformed into $\Delta F/F_0$ values with F_0 being the mean F over the 5 min prior to stimulus treatment. (B) Traces for the mean \pm S.E.M. normalised $\Delta F/F_0$ values (Stimulus $\Delta F/F_0$ - Control $\Delta F/F_0$) over time with stimulus treatment at 0 min (grey dashed line). Boxplots are displayed for the (A) stimulus-treated site F_0 values (A.U.), (C) peak normalised $\Delta F/F_0$ values (Stimulus $\Delta F/F_0$ - Control $\Delta F/F_0$), (D) signal propagation rates ($\mu\text{m s}^{-1}$) and (E) signal areas (mm^2), with grey dots associated with outliers. Statistical significance, calculated using a t-test or a Wilcoxon rank-sum test, is shown by ns: $p > 0.05$, *: $p \leq 0.05$, **: $p \leq 0.01$, ***: $p \leq 0.001$, ****: $p \leq 0.0001$.

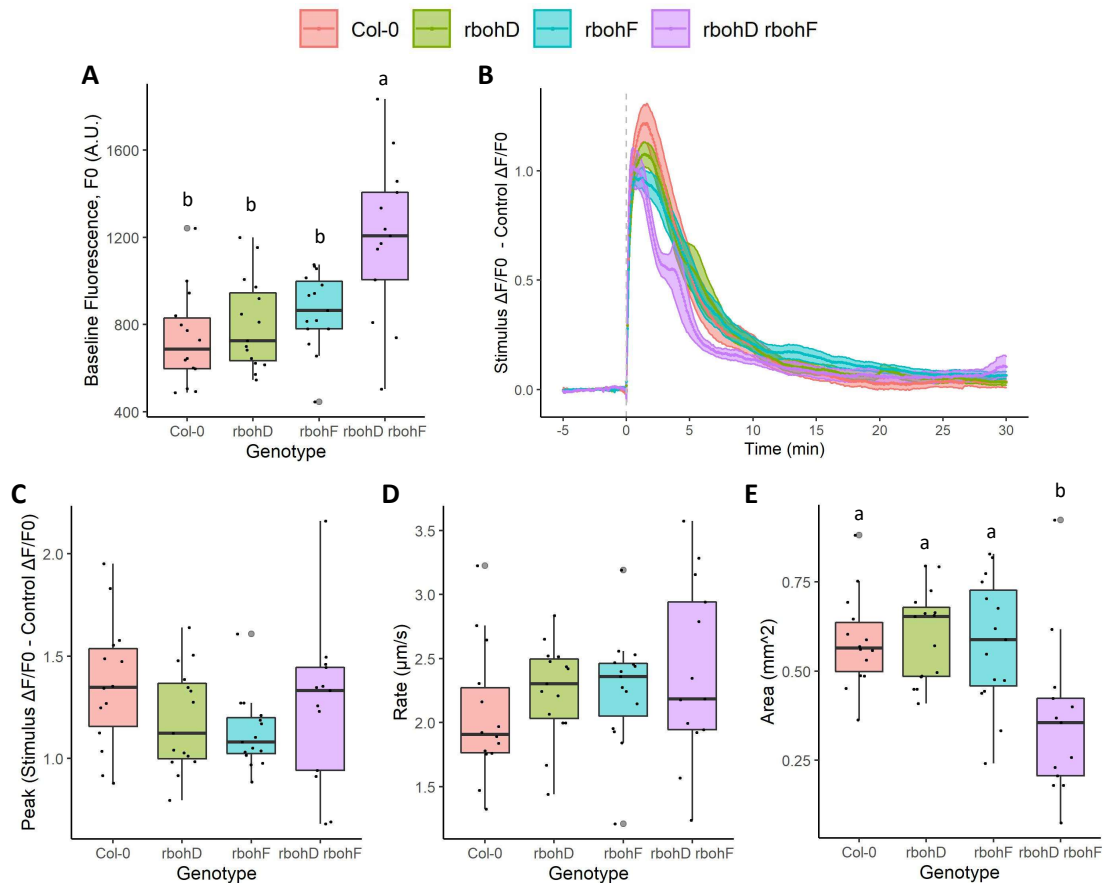


Figure I.XI Wound-induced GCaMP3 reporter signals in Col-0, *rbohD*, *rbohF* and *rbohD rbohF* *A. thaliana*.

Properties of wound-induced GCaMP3 signals in Col-0 ($n = 14$), *rbohD* ($n = 15$), *rbohF* ($n = 15$) and *rbohD rbohF* ($n = 13$) *A. thaliana* expressing *35S::GCaMP3*. Background-corrected fluorescence intensity (F , A.U.) values were recorded over the area of the stimulus-induced responses and at comparable control sites. F values were transformed into $\Delta F/F_0$ values with F_0 being the mean F over the 5 min prior to stimulus treatment. **(B)** Traces for the mean \pm S.E.M. normalised $\Delta F/F_0$ values (Stimulus $\Delta F/F_0$ - Control $\Delta F/F_0$) over time with stimulus treatment at 0 min (grey dashed line). Boxplots are displayed for the **(A)** stimulus-treated site F_0 values (A.U.), **(C)** peak normalised $\Delta F/F_0$ values (Stimulus $\Delta F/F_0$ - Control $\Delta F/F_0$), **(D)** signal propagation rates ($\mu\text{m s}^{-1}$) and **(E)** signal areas (mm^2), with grey dots associated with outliers. Statistical significance levels are indicated by letters if genotypes significantly differed. Significance was assessed using an ANOVA with a Tukey post hoc test or a Kruskal-Wallis test with post hoc pairwise Wilcoxon rank-sum tests.

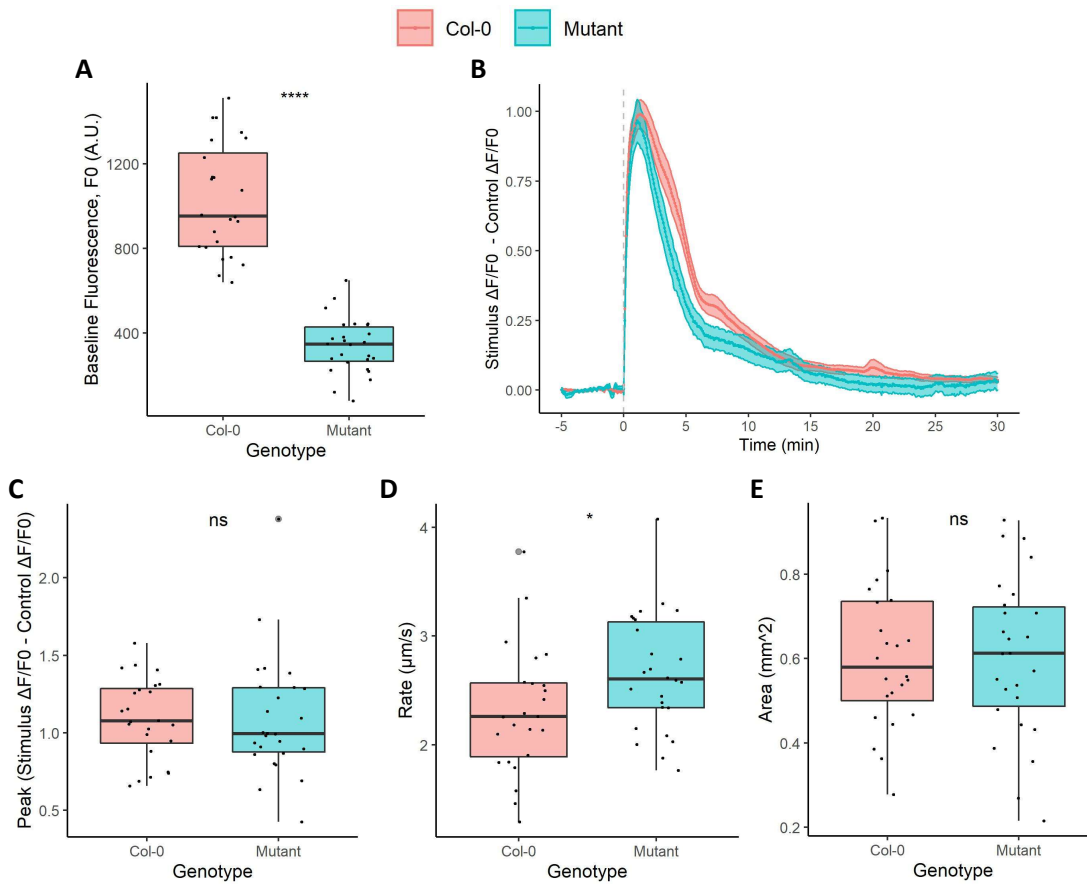


Figure I.XII Wound-induced GCaMP3 reporter signals in Col-0 and *tpk1-1* *A. thaliana*.

Properties of wound-induced GCaMP3 signals in Col-0 ($n = 24$) and *tpk1-1* ($n = 26$) *A. thaliana* expressing *35S::GCaMP3*. Background-corrected fluorescence intensity (F , A.U.) values were recorded over the area of the stimulus-induced responses and at comparable control sites. F values were transformed into $\Delta F/F_0$ values with F_0 being the mean F over the 5 min prior to stimulus treatment. (B) Traces for the mean \pm S.E.M. normalised $\Delta F/F_0$ values (Stimulus $\Delta F/F_0$ – Control $\Delta F/F_0$) over time with stimulus treatment at 0 min (grey dashed line). Boxplots are displayed for the (A) stimulus-treated site F_0 values (A.U.), (C) peak normalised $\Delta F/F_0$ values (Stimulus $\Delta F/F_0$ – Control $\Delta F/F_0$), (D) signal propagation rates ($\mu\text{m s}^{-1}$) and (E) signal areas (mm^2), with grey dots associated with outliers. Statistical significance, calculated using a t-test or a Wilcoxon rank-sum test, is shown by ns: $p > 0.05$, *: $p \leq 0.05$, **: $p \leq 0.01$, ***: $p \leq 0.001$, ****: $p \leq 0.0001$.

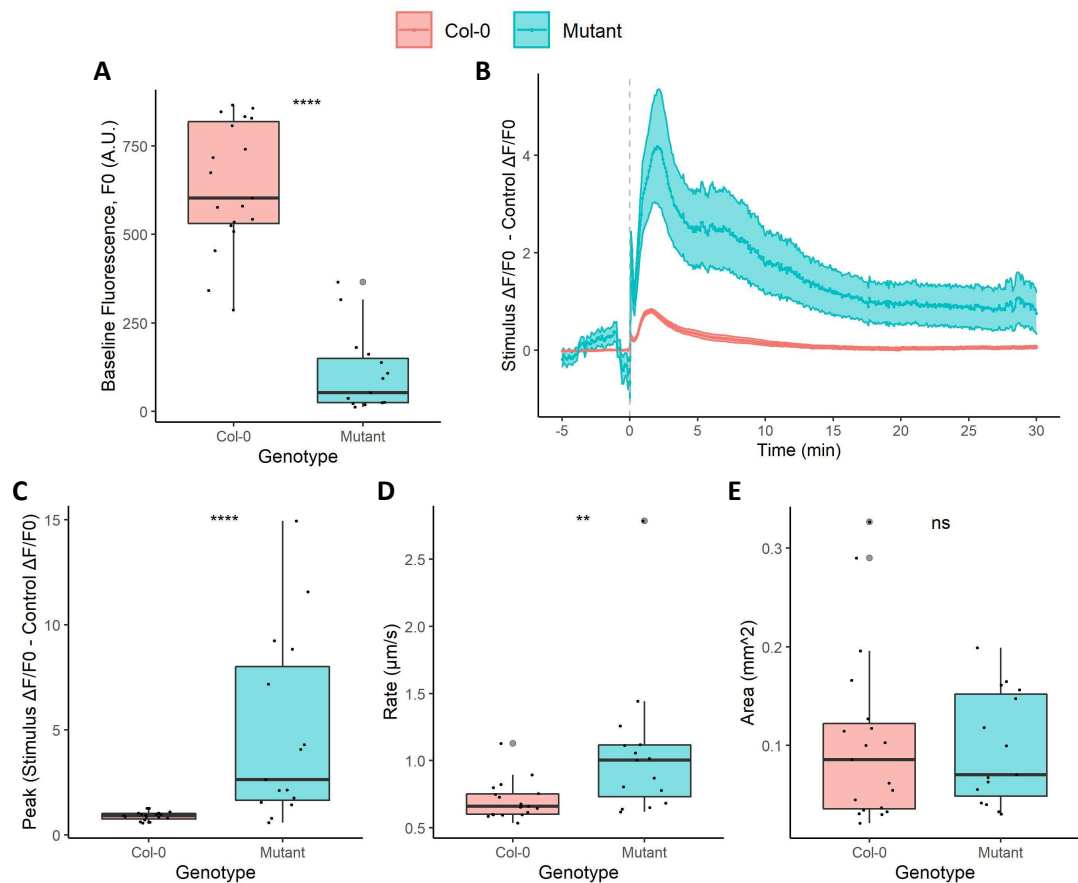


Figure I.XIII Touch-induced GCaMP3 reporter signals in Col-0 and *tpk1-1* *A. thaliana*.

Properties of touch-induced GCaMP3 signals in Col-0 ($n = 19$) and *tpk1-1* ($n = 15$) *A. thaliana* expressing *35S::GCaMP3*. Background-corrected fluorescence intensity (F , A.U.) values were recorded over the area of the stimulus-induced responses and at comparable control sites. F values were transformed into $\Delta F/F_0$ values with F_0 being the mean F over the 5 min prior to stimulus treatment. (B) Traces for the mean \pm S.E.M. normalised $\Delta F/F_0$ values (Stimulus $\Delta F/F_0 -$ Control $\Delta F/F_0$) over time with stimulus treatment at 0 min (grey dashed line). Boxplots are displayed for the (A) stimulus-treated site F_0 values (A.U.), (C) peak normalised $\Delta F/F_0$ values (Stimulus $\Delta F/F_0 -$ Control $\Delta F/F_0$), (D) signal propagation rates ($\mu\text{m s}^{-1}$) and (E) signal areas (mm^2), with grey dots associated with outliers. Statistical significance, calculated using a t-test or a Wilcoxon rank-sum test, is shown by ns: $p > 0.05$, *: $p \leq 0.05$, **: $p \leq 0.01$, ***: $p \leq 0.001$, ****: $p \leq 0.0001$.

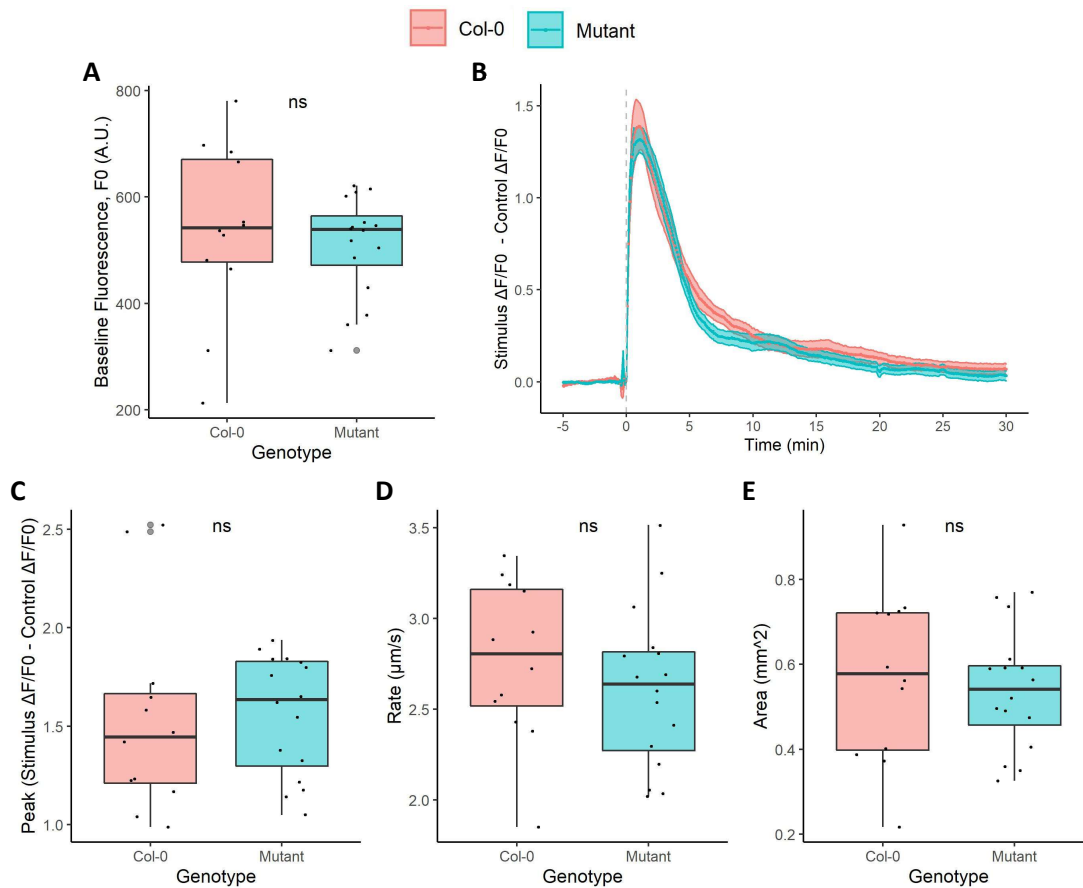


Figure I.XIV Wound-induced GCaMP3 reporter signals in Col-0 and *mca1 mca2* *A. thaliana*.

Properties of wound-induced GCaMP3 signals in Col-0 ($n = 12$) and *mca1 mca2* ($n = 16$) *A. thaliana* expressing *UBQ10::GCaMP3*. Background-corrected fluorescence intensity (F , A.U.) values were recorded over the area of the stimulus-induced responses and at comparable control sites. F values were transformed into $\Delta F/F_0$ values with F_0 being the mean F over the 5 min prior to stimulus treatment. (B) Traces for the mean \pm S.E.M. normalised $\Delta F/F_0$ values (Stimulus $\Delta F/F_0 -$ Control $\Delta F/F_0$) over time with stimulus treatment at 0 min (grey dashed line). Boxplots are displayed for the (A) stimulus-treated site F_0 values (A.U.), (C) peak normalised $\Delta F/F_0$ values (Stimulus $\Delta F/F_0 -$ Control $\Delta F/F_0$), (D) signal propagation rates ($\mu\text{m s}^{-1}$) and (E) signal areas (mm^2), with grey dots associated with outliers. Statistical significance, calculated using a t-test or a Wilcoxon rank-sum test, is shown by ns: $p > 0.05$, *: $p \leq 0.05$, **: $p \leq 0.01$, ***: $p \leq 0.001$, ****: $p \leq 0.0001$.

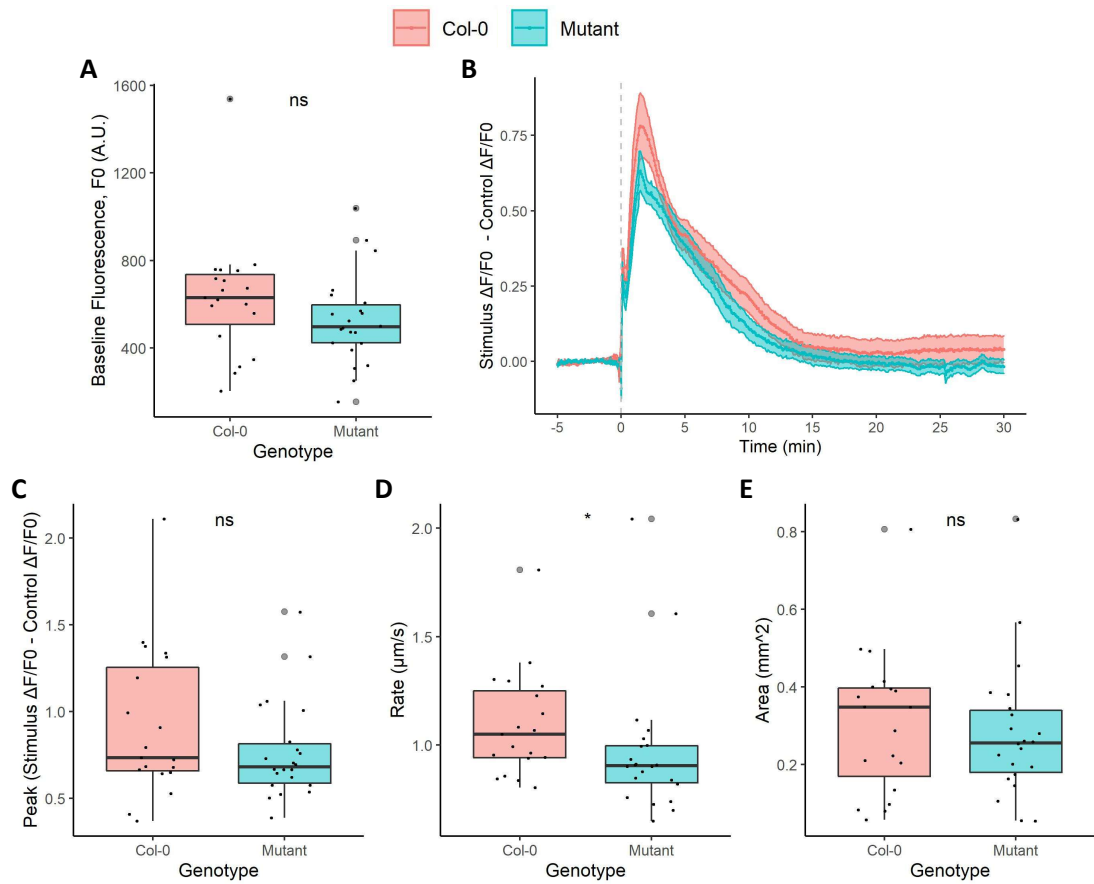


Figure I.XV Touch-induced GCaMP3 reporter signals in Col-0 and *mca1 mca2 A. thaliana*.

Properties of touch-induced GCaMP3 signals in Col-0 ($n = 19$) and *mca1 mca2* ($n = 22$) *A. thaliana* expressing *UBQ10::GCaMP3*. Background-corrected fluorescence intensity (F, A.U.) values were recorded over the area of the stimulus-induced responses and at comparable control sites. F values were transformed into $\Delta F/F_0$ values with F_0 being the mean F over the 5 min prior to stimulus treatment. (B) Traces for the mean \pm S.E.M. normalised $\Delta F/F_0$ values (Stimulus $\Delta F/F_0$ – Control $\Delta F/F_0$) over time with stimulus treatment at 0 min (grey dashed line). Boxplots are displayed for the (A) stimulus-treated site F_0 values (A.U.), (C) peak normalised $\Delta F/F_0$ values (Stimulus $\Delta F/F_0$ – Control $\Delta F/F_0$), (D) signal propagation rates ($\mu\text{m s}^{-1}$) and (E) signal areas (mm^2), with grey dots associated with outliers. Statistical significance, calculated using a t-test or a Wilcoxon rank-sum test, is shown by ns: $p > 0.05$, *: $p \leq 0.05$, **: $p \leq 0.01$, ***: $p \leq 0.001$, ****: $p \leq 0.0001$.

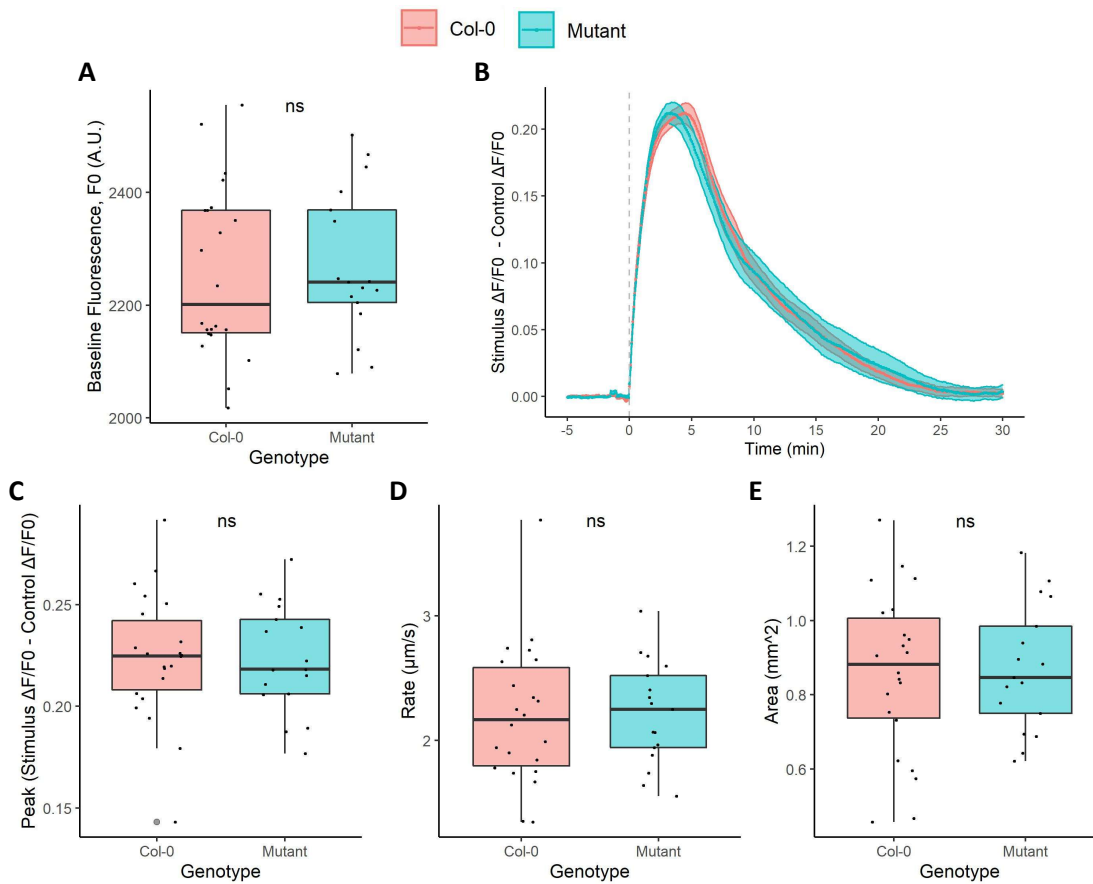


Figure I.XVI Wound-induced GCaMP6s reporter signals in Col-0 and *piezo-1 A. thaliana*.

Properties of wound-induced GCaMP6s signals in Col-0 ($n = 22$) and *piezo-1* ($n = 17$) *A. thaliana* expressing *UBQ10::GCaMP6s*. Non-corrected fluorescence intensity (F , A.U.) values were recorded over the area of the stimulus-induced responses and at comparable control sites. F values were transformed into $\Delta F/F_0$ values with F_0 being the mean F over the 5 min prior to stimulus treatment. **(B)** Traces for the mean \pm S.E.M. normalised $\Delta F/F_0$ values (Stimulus $\Delta F/F_0 -$ Control $\Delta F/F_0$) over time with stimulus treatment at 0 min (grey dashed line). Boxplots are displayed for the **(A)** stimulus-treated site F_0 values (A.U.), **(C)** peak normalised $\Delta F/F_0$ values (Stimulus $\Delta F/F_0 -$ Control $\Delta F/F_0$), **(D)** signal propagation rates ($\mu\text{m s}^{-1}$) and **(E)** signal areas (mm^2), with grey dots associated with outliers. Statistical significance, calculated using a t-test or a Wilcoxon rank-sum test, is shown by ns: $p > 0.05$, *: $p \leq 0.05$, **: $p \leq 0.01$, ***: $p \leq 0.001$, ****: $p \leq 0.0001$.

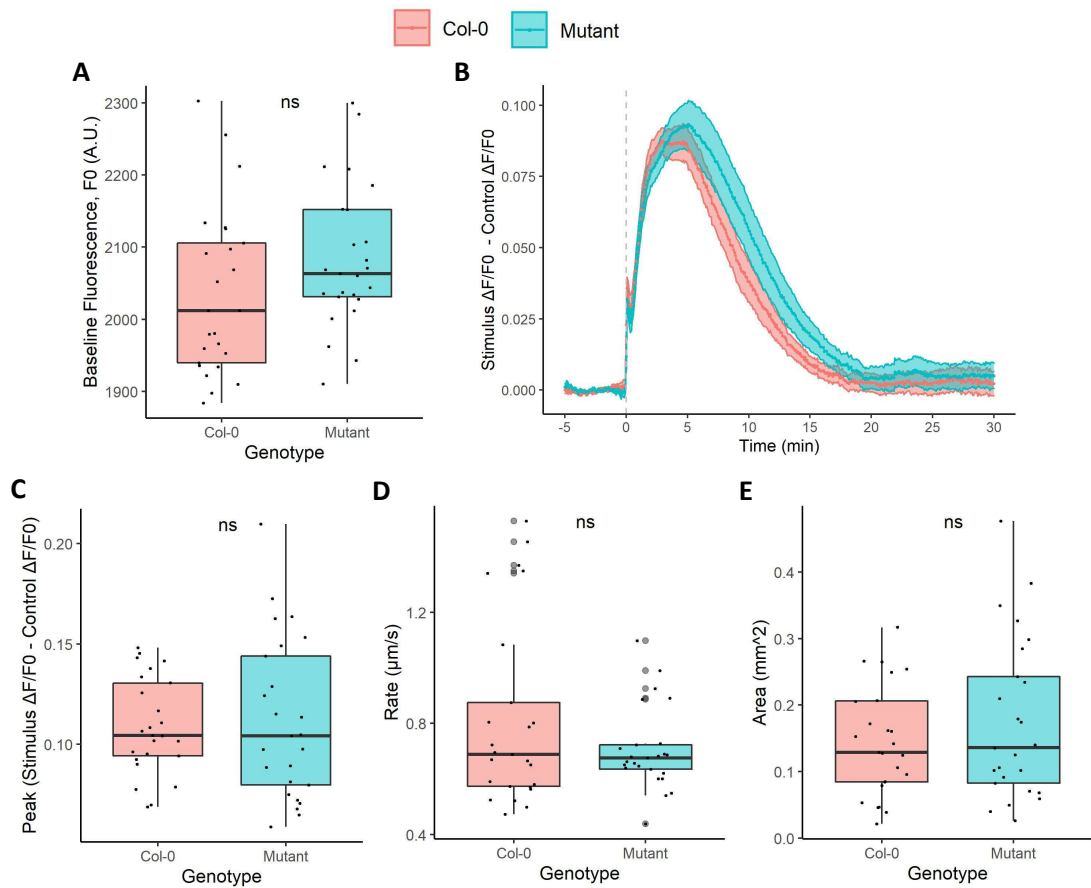


Figure I.XVII Touch-induced GCaMP6s reporter signals in Col-0 and *piezo-1 A. thaliana*.

Properties of touch-induced GCaMP6s signals in Col-0 and *piezo-1 A. thaliana* expressing *UBQ10::GCaMP6s* ($n = 25$). Non-corrected fluorescence intensity (F , A.U.) values were recorded over the area of the stimulus-induced responses and at comparable control sites. F values were transformed into $\Delta F/F_0$ values with F_0 being the mean F over the 5 min prior to stimulus treatment. (B) Traces for the mean \pm S.E.M. normalised $\Delta F/F_0$ values (Stimulus $\Delta F/F_0$ - Control $\Delta F/F_0$) over time with stimulus treatment at 0 min (grey dashed line). Boxplots are displayed for the (A) stimulus-treated site F_0 values (A.U.), (C) peak normalised $\Delta F/F_0$ values (Stimulus $\Delta F/F_0$ - Control $\Delta F/F_0$), (D) signal propagation rates ($\mu\text{m s}^{-1}$) and (E) signal areas (mm^2), with grey dots associated with outliers. Statistical significance, calculated using a t-test or a Wilcoxon rank-sum test, is shown by ns: $p > 0.05$, *: $p \leq 0.05$, **: $p \leq 0.01$, ***: $p \leq 0.001$, ****: $p \leq 0.0001$.

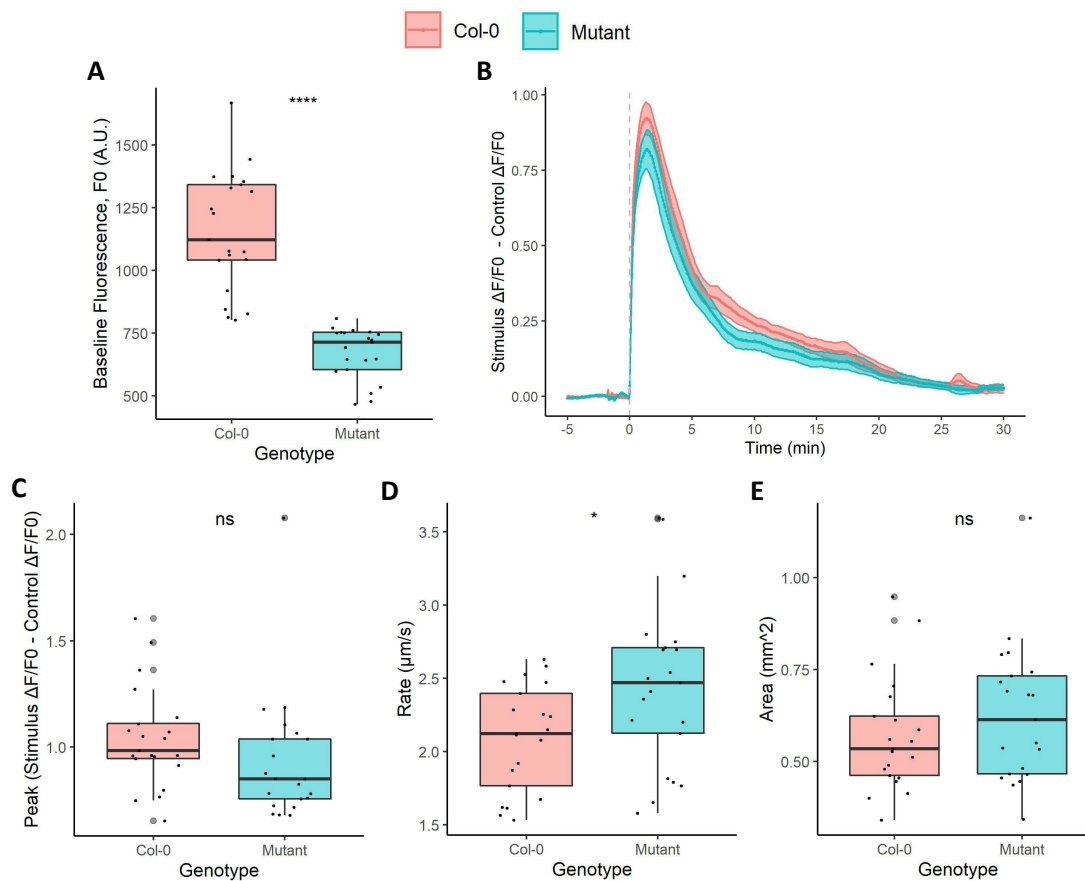


Figure I.XVIII Wound-induced GCaMP3 reporter signals in Col-0 and *gl1 A. thaliana*.

Properties of wound-induced GCaMP3 signals in Col-0 and *gl1 A. thaliana* expressing *35S::GCaMP3* ($n = 21$). Background-corrected fluorescence intensity (F , A.U.) values were recorded over the area of the stimulus-induced responses and at comparable control sites. F values were transformed into $\Delta F/F_0$ values with F_0 being the mean F over the 5 min prior to stimulus treatment. (B) Traces for the mean \pm S.E.M. normalised $\Delta F/F_0$ values (Stimulus $\Delta F/F_0 -$ Control $\Delta F/F_0$) over time with stimulus treatment at 0 min (grey dashed line). Boxplots are displayed for the (A) stimulus-treated site F_0 values (A.U.), (C) peak normalised $\Delta F/F_0$ values (Stimulus $\Delta F/F_0 -$ Control $\Delta F/F_0$), (D) signal propagation rates ($\mu\text{m s}^{-1}$) and (E) signal areas (mm^2), with grey dots associated with outliers. Statistical significance, calculated using a t-test or a Wilcoxon rank-sum test, is shown by ns: $p > 0.05$, *: $p \leq 0.05$, **: $p \leq 0.01$, ***: $p \leq 0.001$, ****: $p \leq 0.0001$.

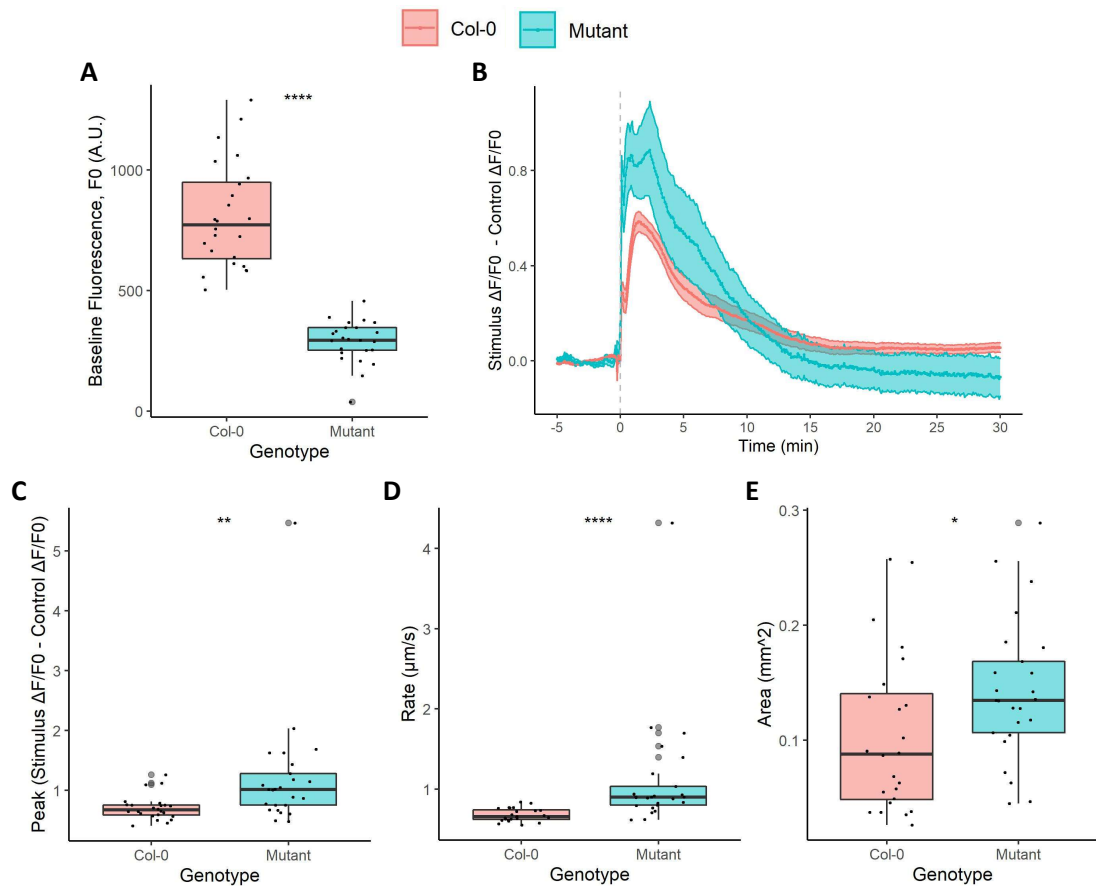


Figure I.XIX Touch-induced GCaMP3 reporter signals in Col-0 and *gl1* *A. thaliana*.

Properties of touch-induced GCaMP3 signals in Col-0 ($n = 24$) and *gl1* ($n = 25$) *A. thaliana* expressing *35S::GCaMP3*. Background-corrected fluorescence intensity (F, A.U.) values were recorded over the area of the stimulus-induced responses and at comparable control sites. F values were transformed into $\Delta F/F_0$ values with F_0 being the mean F over the 5 min prior to stimulus treatment. (B) Traces for the mean \pm S.E.M. normalised $\Delta F/F_0$ values (Stimulus $\Delta F/F_0$ - Control $\Delta F/F_0$) over time with stimulus treatment at 0 min (grey dashed line). Boxplots are displayed for the (A) stimulus-treated site F_0 values (A.U.), (C) peak normalised $\Delta F/F_0$ values (Stimulus $\Delta F/F_0$ - Control $\Delta F/F_0$), (D) signal propagation rates ($\mu\text{m s}^{-1}$) and (E) signal areas (mm^2), with grey dots associated with outliers. Statistical significance, calculated using a t-test or a Wilcoxon rank-sum test, is shown by ns: $p > 0.05$, *: $p \leq 0.05$, **: $p \leq 0.01$, ***: $p \leq 0.001$, ****: $p \leq 0.0001$.

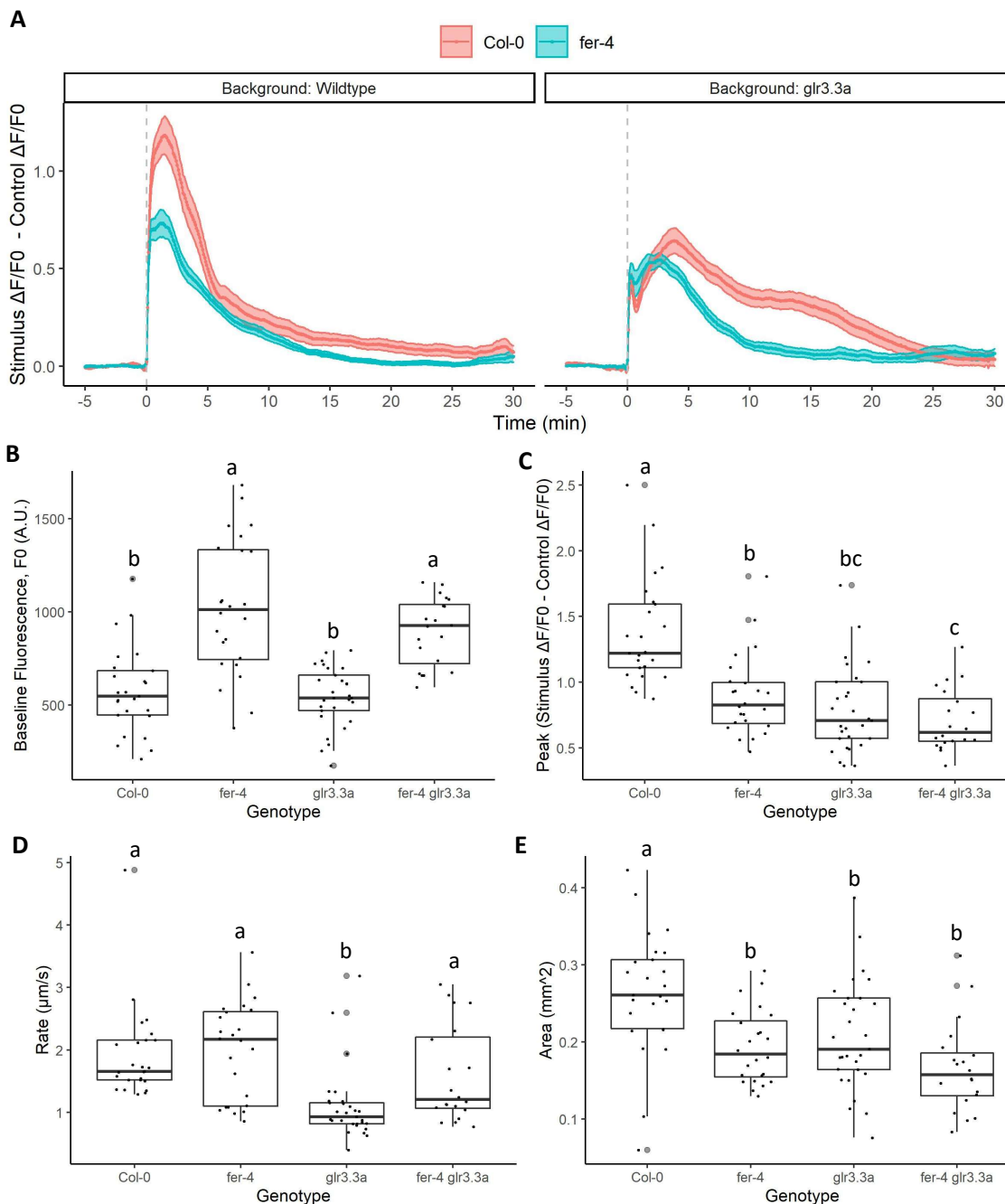


Figure I.XX Wound-induced GCaMP3 reporter signals in Col-0, *fer-4*, *glr3.3a* and *fer-4 glr3.3a* *A. thaliana*.

Properties of wound-induced GCaMP3 signals in Col-0 ($n = 25$), *fer-4* ($n = 24$), *glr3.3a* ($n = 29$) and *fer-4 glr3.3a* ($n = 20$) *A. thaliana* expressing *UBQ10::GCaMP3*. Background-corrected fluorescence intensity (F , A.U.) values were recorded over the area of the stimulus-induced responses and at comparable control sites. F values were transformed into $\Delta F/F_0$ values with F_0 being the mean F over the 5 min prior to stimulus treatment. (A) Traces for the mean \pm S.E.M. normalised $\Delta F/F_0$ values (Stimulus $\Delta F/F_0$ – Control $\Delta F/F_0$) over time with stimulus treatment at 0 min (grey dashed line). Traces are displayed for Col-0 and *fer-4* in the wildtype *A. thaliana* background ('Wildtype') and in the *glr3.3a* *A. thaliana* background ('*glr3.3a*'). Boxplots are displayed for the (B) stimulus-treated site F_0 values (A.U.), (C) peak normalised $\Delta F/F_0$ values (Stimulus $\Delta F/F_0$ – Control $\Delta F/F_0$), (D) signal propagation rates ($\mu\text{m s}^{-1}$) and (E) signal areas (mm^2), with grey dots associated with outliers. Statistical significance levels are indicated by letters if genotypes significantly differed. Significance was assessed using an ANOVA with a Tukey post hoc test or a Kruskal-Wallis test with post hoc pairwise Wilcoxon rank-sum tests.

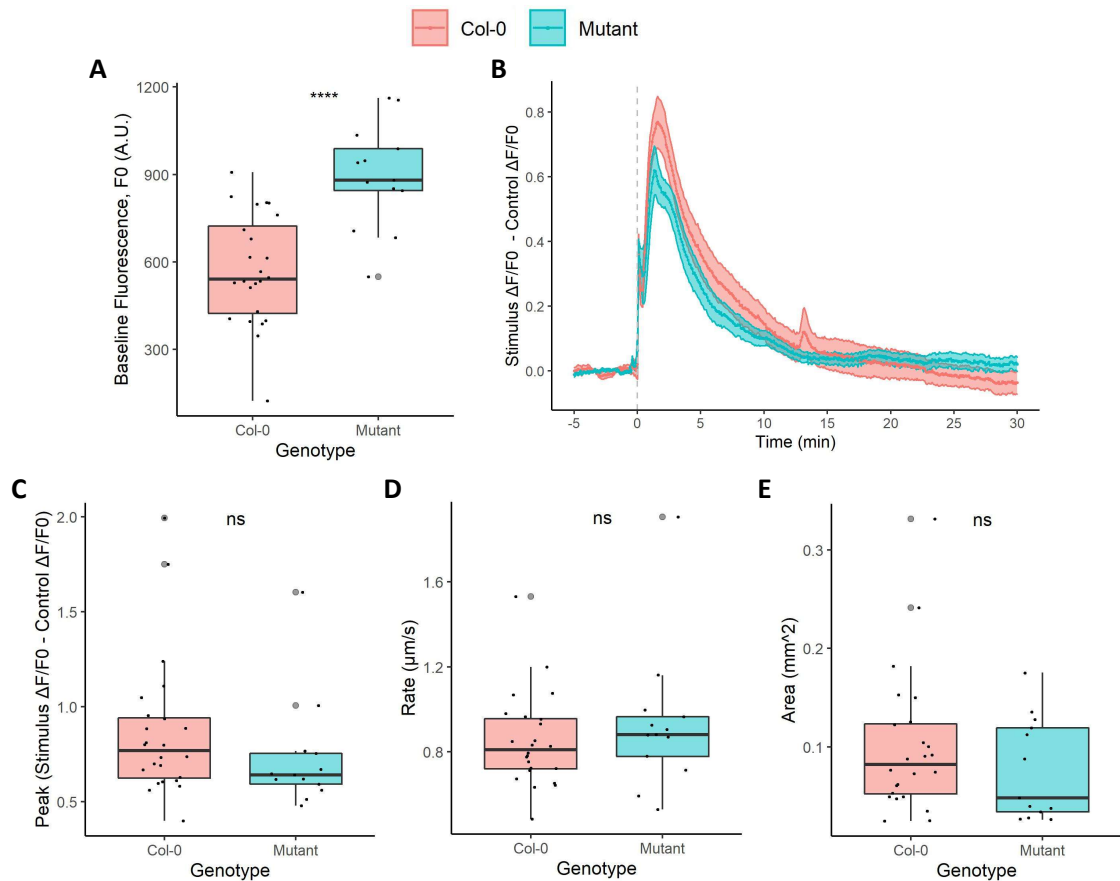


Figure I.XXI Touch-induced GCaMP3 reporter signals in Col-0 and *fer-4 A. thaliana*.

Properties of touch-induced GCaMP3 signals in Col-0 ($n = 24$) and *fer-4* ($n = 13$) *A. thaliana* expressing *UBQ10::GCaMP3*. Background-corrected fluorescence intensity (F, A.U.) values were recorded over the area of the stimulus-induced responses and at comparable control sites. F values were transformed into $\Delta F/F_0$ values with F_0 being the mean F over the 5 min prior to stimulus treatment. (B) Traces for the mean \pm S.E.M. normalised $\Delta F/F_0$ values (Stimulus $\Delta F/F_0$ - Control $\Delta F/F_0$) over time with stimulus treatment at 0 min (grey dashed line). Boxplots are displayed for the (A) stimulus-treated site F_0 values (A.U.), (C) peak normalised $\Delta F/F_0$ values (Stimulus $\Delta F/F_0$ - Control $\Delta F/F_0$), (D) signal propagation rates ($\mu\text{m s}^{-1}$) and (E) signal areas (mm^2), with grey dots associated with outliers. Statistical significance, calculated using a t-test or a Wilcoxon rank-sum test, is shown by ns: $p > 0.05$, *: $p \leq 0.05$, **: $p \leq 0.01$, ***: $p \leq 0.001$, ****: $p \leq 0.0001$.

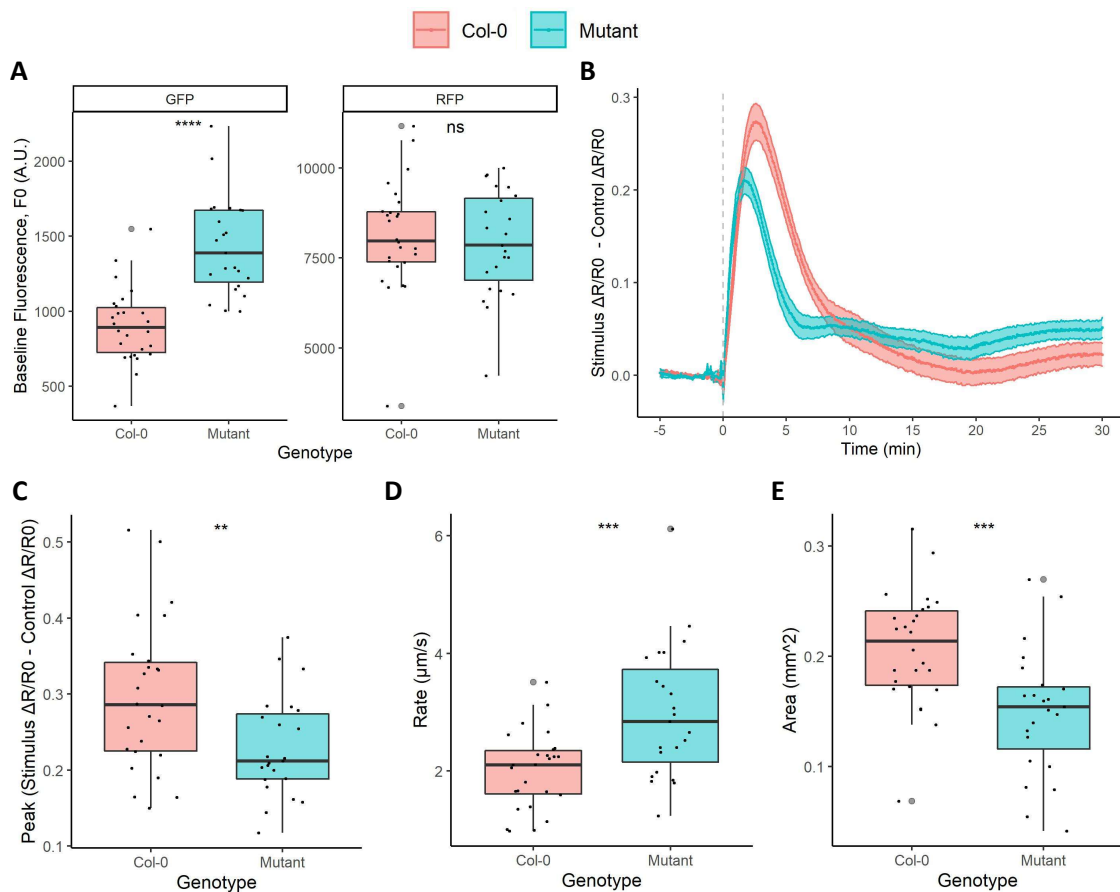


Figure I.XXII Wound-induced apo-pHusion reporter signals in Col-0 and *fer-4 A. thaliana*.

Properties of wound-induced apo-pHusion signals in Col-0 ($n = 26$) and *fer-4* ($n = 23$) *A. thaliana* expressing *35S::Apo-pHusion*. Background-corrected fluorescence intensity (F , A.U.) values were recorded over the area of the stimulus-induced responses and at comparable control sites for GFP and RFP. The GFP/ RFP ratio (R) values were calculated from the F values and transformed into $\Delta R/R_0$ values. R_0 and F_0 were the mean R and F values, respectively, over the 5 min prior to stimulus treatment. **(B)** Traces for the mean \pm S.E.M. normalised $\Delta R/R_0$ values (Stimulus $\Delta R/R_0$ - Control $\Delta R/R_0$) over time with stimulus treatment at 0 min (grey dashed line). Boxplots are displayed for the **(A)** stimulus-treated site F_0 values (A.U.) for GFP and RFP, **(C)** peak normalised $\Delta R/R_0$ values (Stimulus $\Delta R/R_0$ - Control $\Delta R/R_0$), **(D)** signal propagation rates ($\mu\text{m s}^{-1}$) and **(E)** signal areas (mm^2), with grey dots associated with outliers. Statistical significance, calculated using a t-test or a Wilcoxon rank-sum test, is shown by ns: $p > 0.05$, *: $p \leq 0.05$, **: $p \leq 0.01$, ***: $p \leq 0.001$, ****: $p \leq 0.0001$.

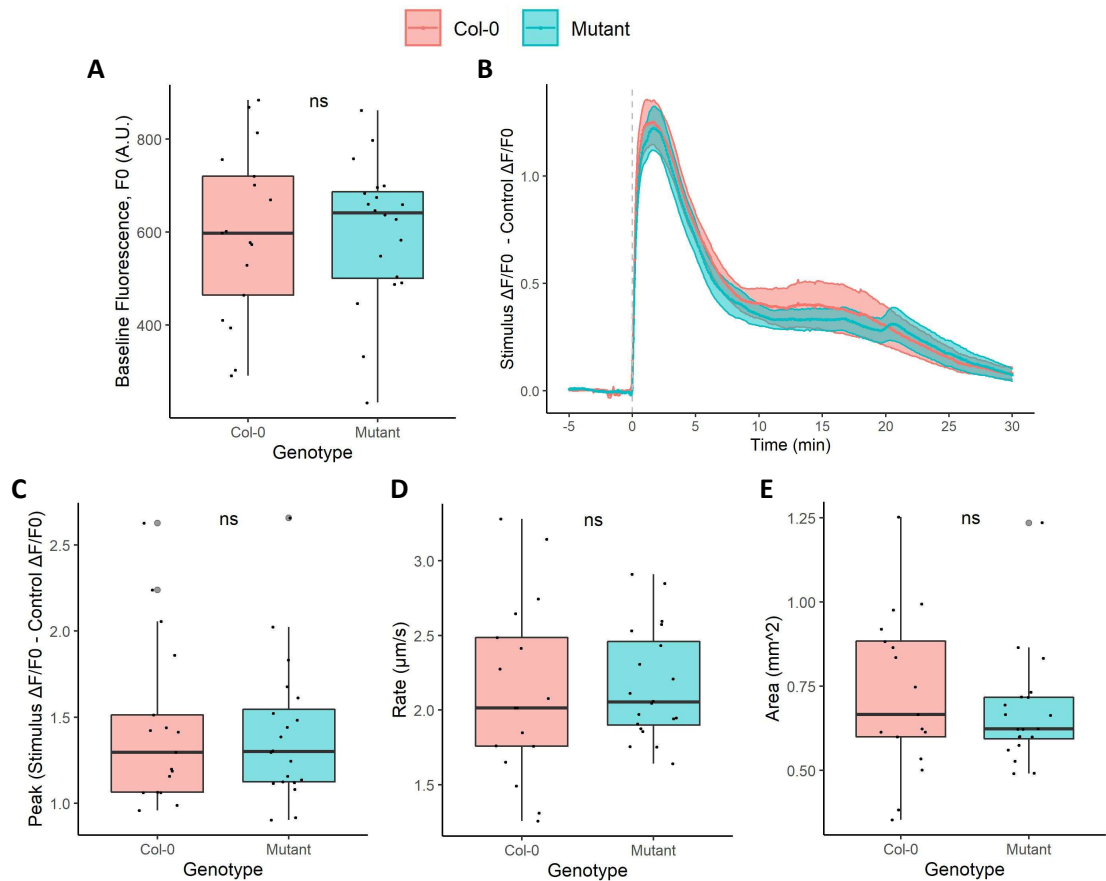


Figure I.XXIII Wound-induced GCaMP3 reporter signals in Col-0 and *pepr1-1 pepr2-3* *A. thaliana*.

Properties of wound-induced GCaMP3 signals in Col-0 ($n = 17$) and *pepr1-1 pepr2-3* ($n = 20$) *A. thaliana* expressing *UBQ10::GCaMP3*. Background-corrected fluorescence intensity (F, A.U.) values were recorded over the area of the stimulus-induced responses and at comparable control sites. F values were transformed into $\Delta F/F_0$ values with F_0 being the mean F over the 5 min prior to stimulus treatment. (B) Traces for the mean \pm S.E.M. normalised $\Delta F/F_0$ values (Stimulus $\Delta F/F_0$ - Control $\Delta F/F_0$) over time with stimulus treatment at 0 min (grey dashed line). Boxplots are displayed for the (A) stimulus-treated site F_0 values (A.U.), (C) peak normalised $\Delta F/F_0$ values (Stimulus $\Delta F/F_0$ - Control $\Delta F/F_0$), (D) signal propagation rates ($\mu\text{m s}^{-1}$) and (E) signal areas (mm^2), with grey dots associated with outliers. Statistical significance, calculated using a t-test or a Wilcoxon rank-sum test, is shown by ns: $p > 0.05$, *: $p \leq 0.05$, **: $p \leq 0.01$, ***: $p \leq 0.001$, ****: $p \leq 0.0001$.

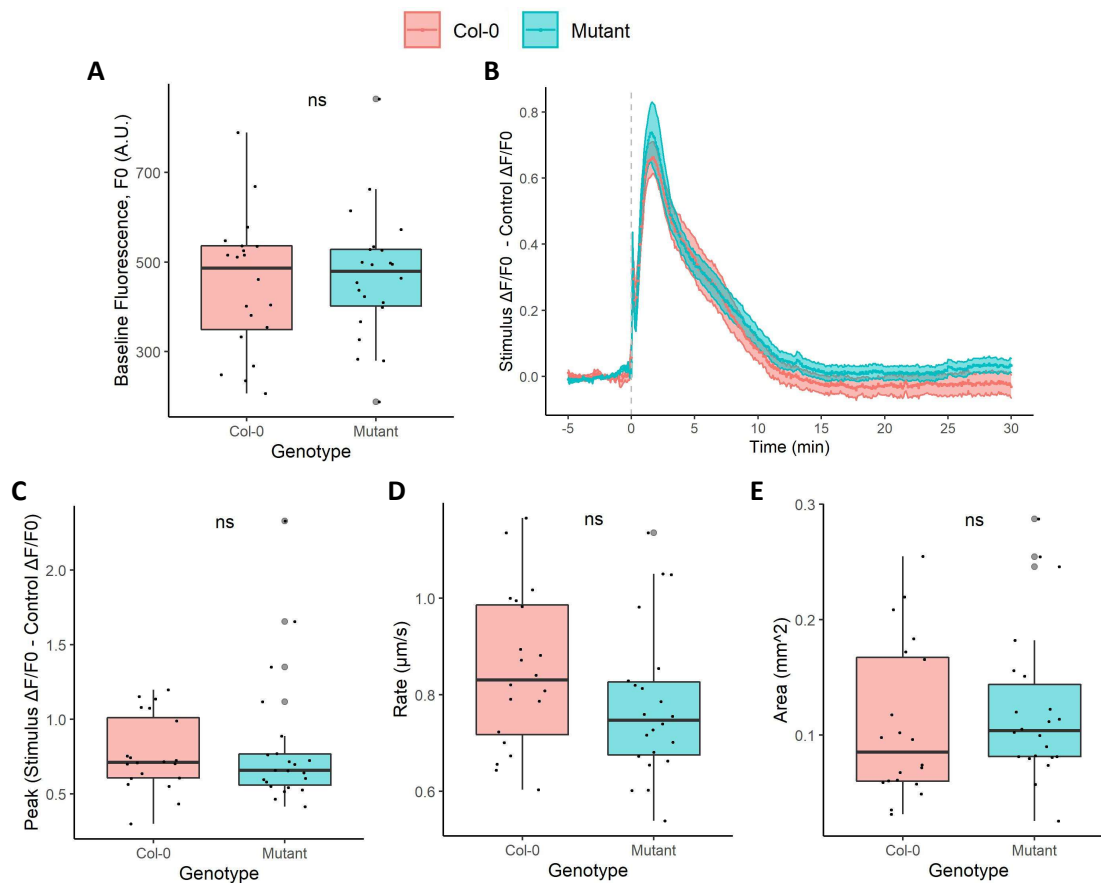


Figure I.XXIV Touch-induced GCaMP3 reporter signals in Col-0 and *pepr1-1 pepr2-3 A. thaliana*.

Properties of touch-induced GCaMP3 signals in Col-0 ($n = 20$) and *pepr1-1 pepr2-3* ($n = 22$) *A. thaliana* expressing *UBQ10::GCaMP3*. Background-corrected fluorescence intensity (F , A.U.) values were recorded over the area of the stimulus-induced responses and at comparable control sites. F values were transformed into $\Delta F/F_0$ values with F_0 being the mean F over the 5 min prior to stimulus treatment. (B) Traces for the mean \pm S.E.M. normalised $\Delta F/F_0$ values (Stimulus $\Delta F/F_0$ - Control $\Delta F/F_0$) over time with stimulus treatment at 0 min (grey dashed line). Boxplots are displayed for the (A) stimulus-treated site F_0 values (A.U.), (C) peak normalised $\Delta F/F_0$ values (Stimulus $\Delta F/F_0$ - Control $\Delta F/F_0$), (D) signal propagation rates ($\mu\text{m s}^{-1}$) and (E) signal areas (mm^2), with grey dots associated with outliers. Statistical significance, calculated using a t-test or a Wilcoxon rank-sum test, is shown by ns: $p > 0.05$, *: $p \leq 0.05$, **: $p \leq 0.01$, ***: $p \leq 0.001$, ****: $p \leq 0.0001$.

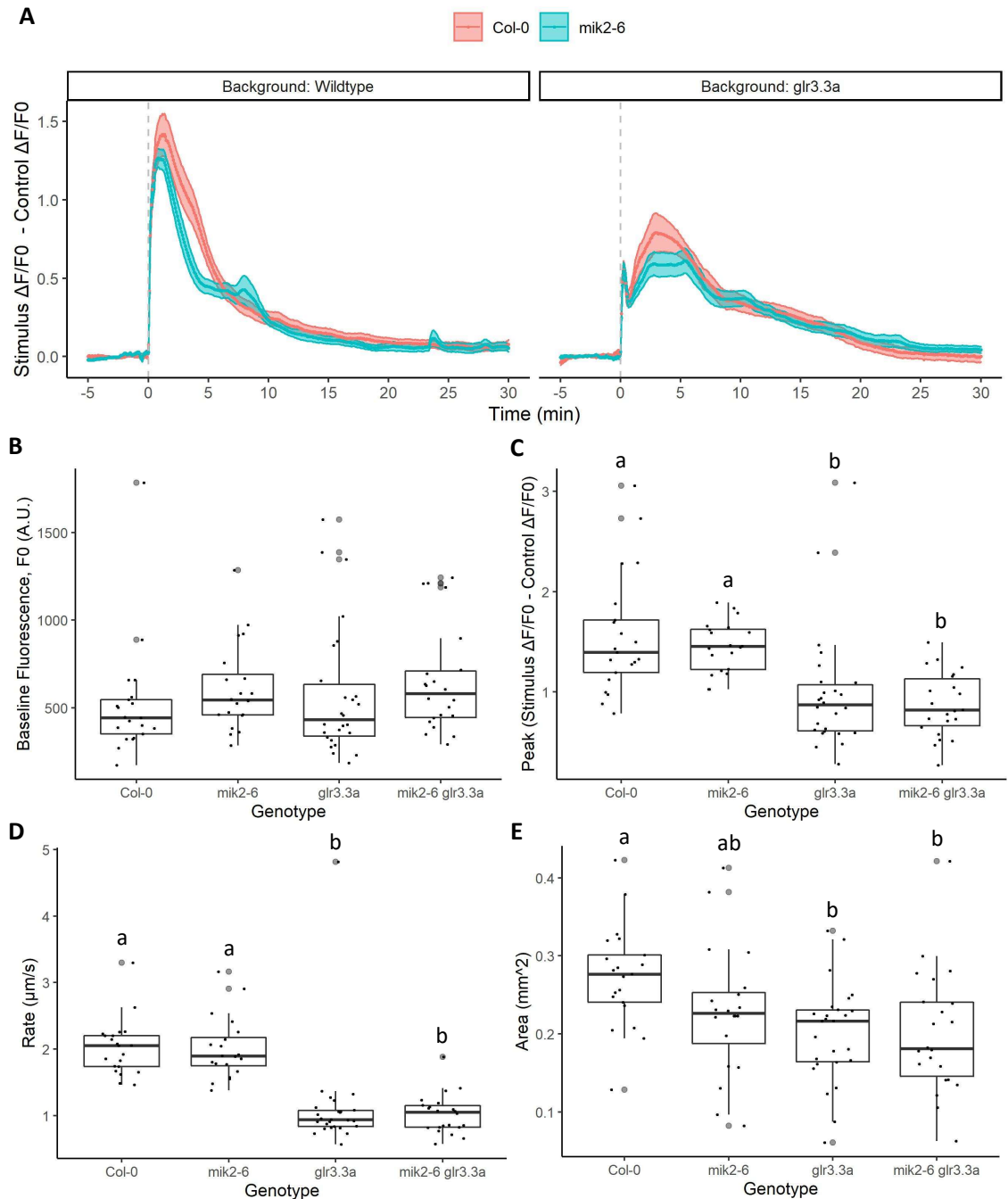


Figure I.XXV Wound-induced GCaMP3 reporter signals in Col-0, *mik2-6*, *glr3.3a* and *mik2-6 glr3.3a* *A. thaliana*.

Properties of wound-induced GCaMP3 signals in Col-0 ($n = 21$), *mik2-6* ($n = 20$), *glr3.3a* ($n = 26$) and *mik2-6 glr3.3a* ($n = 22$) *A. thaliana* expressing *UBQ10::GCaMP3*. Background-corrected fluorescence intensity (F , A.U.) values were recorded over the area of the stimulus-induced responses and at comparable control sites. F values were transformed into $\Delta F/F_0$ values with F_0 being the mean F over the 5 min prior to stimulus treatment. (A) Traces for the mean \pm S.E.M. normalised $\Delta F/F_0$ values (Stimulus $\Delta F/F_0$ - Control $\Delta F/F_0$) over time with stimulus treatment at 0 min (grey dashed line). Traces are displayed for Col-0 and *mik2-6* in the wildtype *A. thaliana* background ('Wildtype') and in the *glr3.3a* *A. thaliana* background ('*glr3.3a*'). Boxplots are displayed for the (B) stimulus-treated site F_0 values (A.U.), (C) peak normalised $\Delta F/F_0$ values (Stimulus $\Delta F/F_0$ - Control $\Delta F/F_0$), (D) signal propagation rates ($\mu\text{m s}^{-1}$) and (E) signal areas (mm^2), with grey dots associated with outliers. Statistical significance levels are indicated by letters if genotypes significantly differed. Significance was assessed using an ANOVA with a Tukey post hoc test or a Kruskal-Wallis test with post hoc pairwise Wilcoxon rank-sum tests.

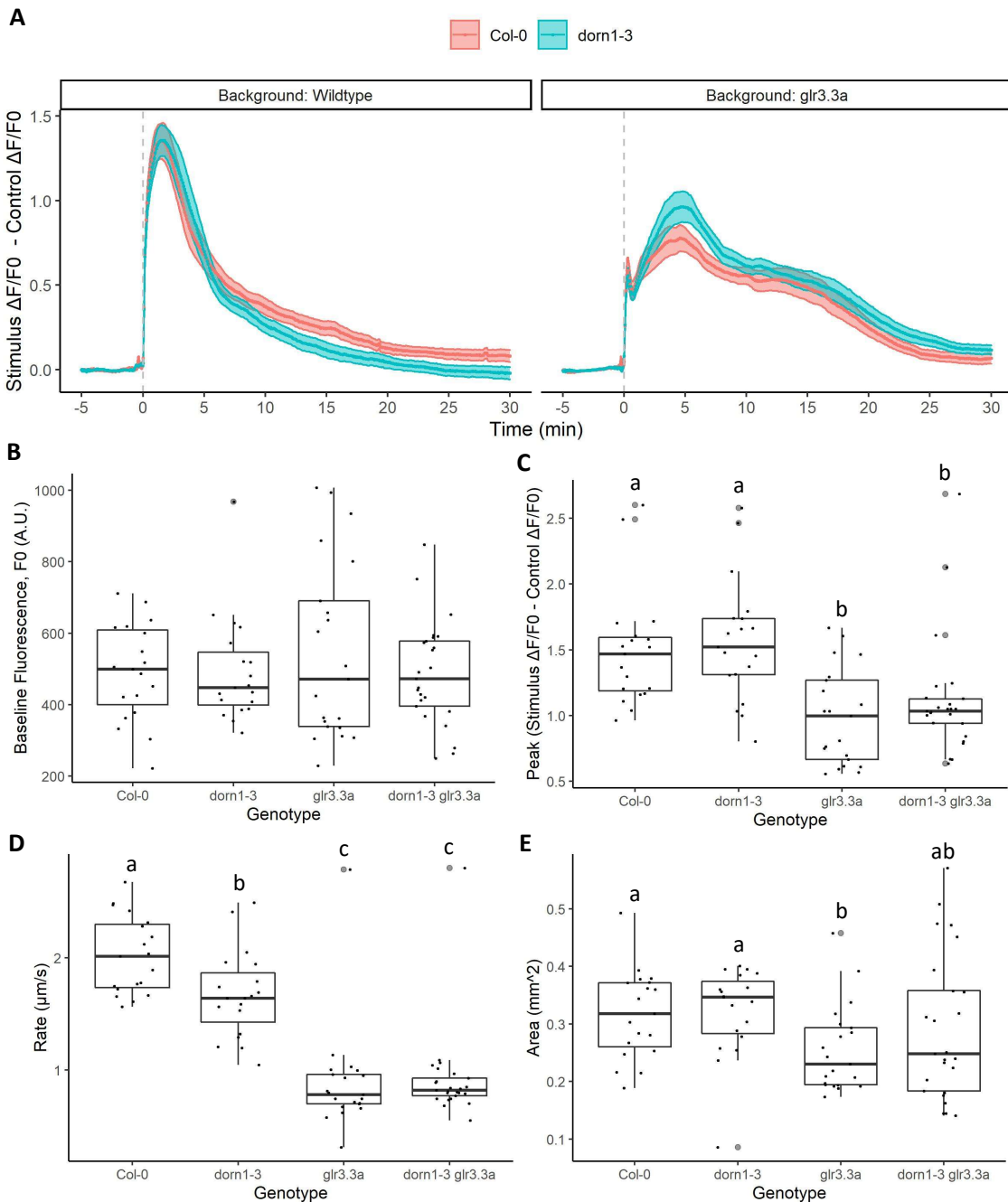


Figure I.XXVI Wound-induced GCaMP3 reporter signals in *Col-0*, *dorn1-3*, *glr3.3a* and *dorn1-3 glr3.3a* *A. thaliana*.

Properties of wound-induced GCaMP3 signals in *Col-0* ($n = 19$), *dorn1-3* ($n = 19$), *glr3.3a* ($n = 21$) and *dorn1-3 glr3.3a* ($n = 25$) *A. thaliana* expressing *UBQ10::GCaMP3*. Background-corrected fluorescence intensity (F , A.U.) values were recorded over the area of the stimulus-induced responses and at comparable control sites. F values were transformed into $\Delta F/F_0$ values with F_0 being the mean F over the 5 min prior to stimulus treatment. (A) Traces for the mean \pm S.E.M. normalised $\Delta F/F_0$ values (Stimulus $\Delta F/F_0$ - Control $\Delta F/F_0$) over time with stimulus treatment at 0 min (grey dashed line). Traces are displayed for *Col-0* and *dorn1-3* in the wildtype *A. thaliana* background ('Wildtype') and in the *glr3.3a* *A. thaliana* background ('*glr3.3a*'). Boxplots are displayed for the (B) stimulus-treated site F_0 values (A.U.), (C) peak normalised $\Delta F/F_0$ values (Stimulus $\Delta F/F_0$ - Control $\Delta F/F_0$), (D) signal propagation rates ($\mu\text{m s}^{-1}$) and (E) signal areas (mm^2), with grey dots associated with outliers. Statistical significance levels are indicated by letters if genotypes significantly differed. Significance was assessed using an ANOVA with a Tukey post hoc test or a Kruskal-Wallis test with post hoc pairwise Wilcoxon rank-sum tests.

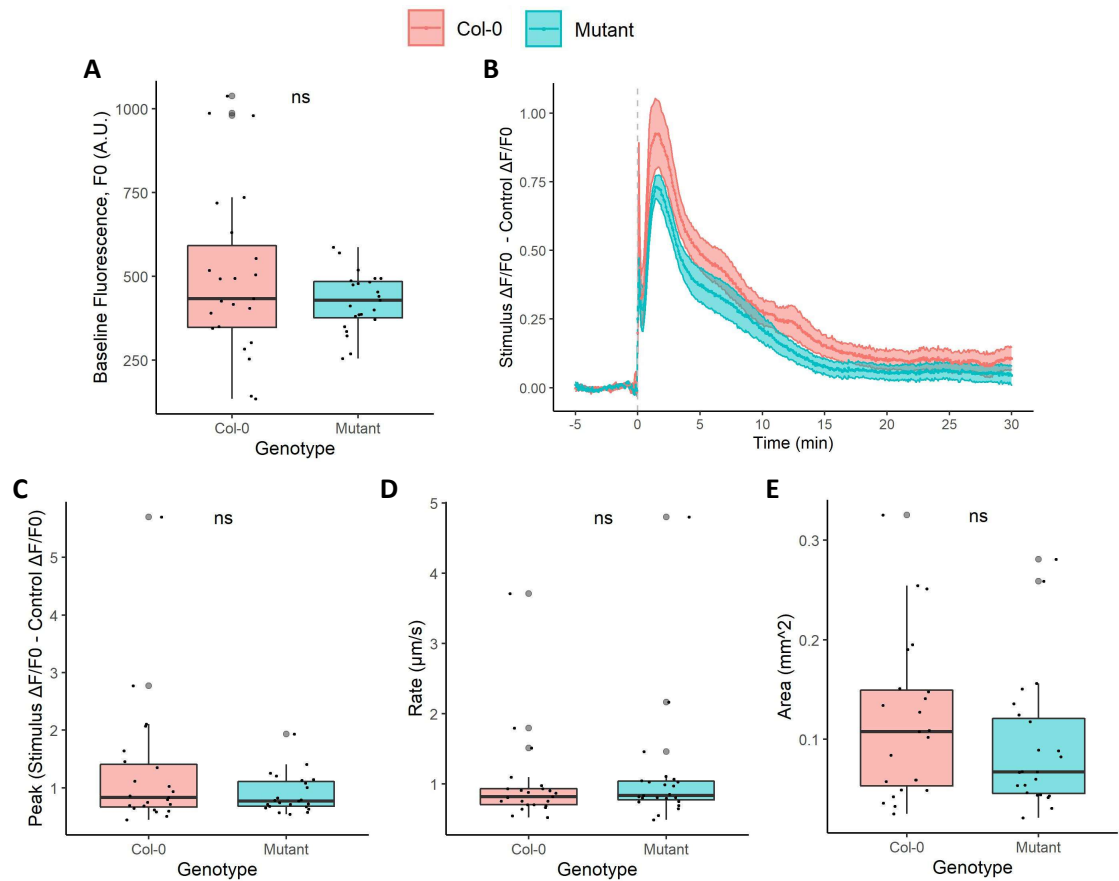


Figure I.XXVII Touch-induced GCaMP3 reporter signals in Col-0 and *dorn1-3 A. thaliana*.

Properties of touch-induced GCaMP3 signals in Col-0 and *dorn1-3 A. thaliana* expressing *UBQ10::GCaMP3* ($n = 23$). Background-corrected fluorescence intensity (F , A.U.) values were recorded over the area of the stimulus-induced responses and at comparable control sites. F values were transformed into $\Delta F/F_0$ values with F_0 being the mean F over the 5 min prior to stimulus treatment. (B) Traces for the mean \pm S.E.M. normalised $\Delta F/F_0$ values (Stimulus $\Delta F/F_0$ – Control $\Delta F/F_0$) over time with stimulus treatment at 0 min (grey dashed line). Boxplots are displayed for the (A) stimulus-treated site F_0 values (A.U.), (C) peak normalised $\Delta F/F_0$ values (Stimulus $\Delta F/F_0$ – Control $\Delta F/F_0$), (D) signal propagation rates ($\mu\text{m s}^{-1}$) and (E) signal areas (mm^2), with grey dots associated with outliers. Statistical significance, calculated using a t-test or a Wilcoxon rank-sum test, is shown by ns: $p > 0.05$, *: $p \leq 0.05$, **: $p \leq 0.01$, ***: $p \leq 0.001$, ****: $p \leq 0.0001$.

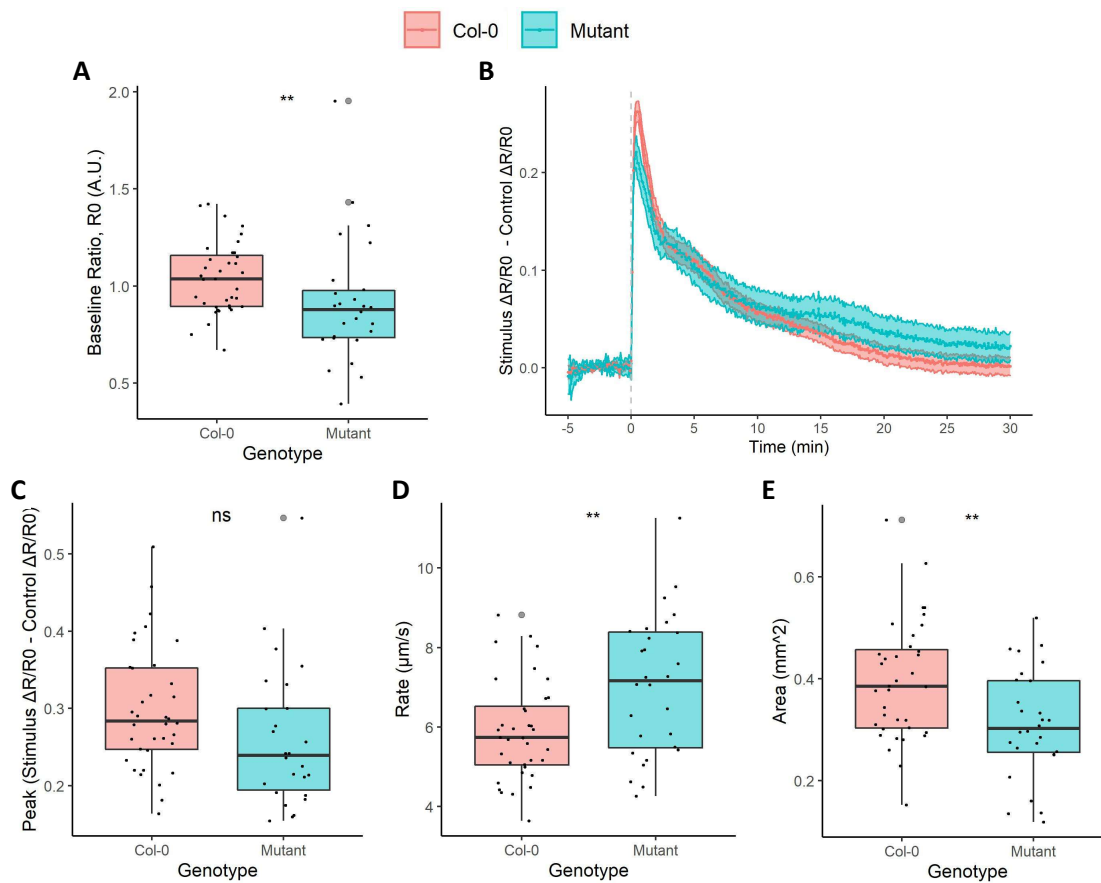


Figure I.XXVIII Wound-induced YC3.6 reporter signals in Col-0 and *aca8 aca10* *A. thaliana*.

Properties of wound-induced YC3.6 signals in Col-0 ($n = 36$) and *aca8 aca10* ($n = 28$) *A. thaliana* expressing *UBQ10::NES-YC3.6*. Background-corrected fluorescence intensity (F, A.U.) values were recorded over the area of the stimulus-induced responses and at comparable control sites for cpVENUS and eCFP. F values were then converted into cpVENUS/eCFP ratio (R) values and transformed into $\Delta R/R0$ values. R0 and F0 values were the mean R and F values, respectively, for the 5 min prior to stimulus treatment. (B) Traces for the mean \pm S.E.M. normalised $\Delta R/R0$ values (Stimulus $\Delta R/R0$ - Control $\Delta R/R0$) over time with stimulus treatment at 0 min (grey dashed line). Boxplots are displayed for the (A) stimulus-treated site R0 values (A.U.), (C) peak normalised $\Delta R/R0$ values (Stimulus $\Delta R/R0$ - Control $\Delta R/R0$), (D) signal propagation rates ($\mu\text{m s}^{-1}$) and (E) signal areas (mm^2), with grey dots associated with outliers. Statistical significance, calculated using a (A) Wilcoxon rank-sum test and (C, D, E) an ANOVA (Repeat + Genotype), is shown by ns: $p > 0.05$, *: $p \leq 0.05$, **: $p \leq 0.01$, ***: $p \leq 0.001$, ****: $p \leq 0.0001$.

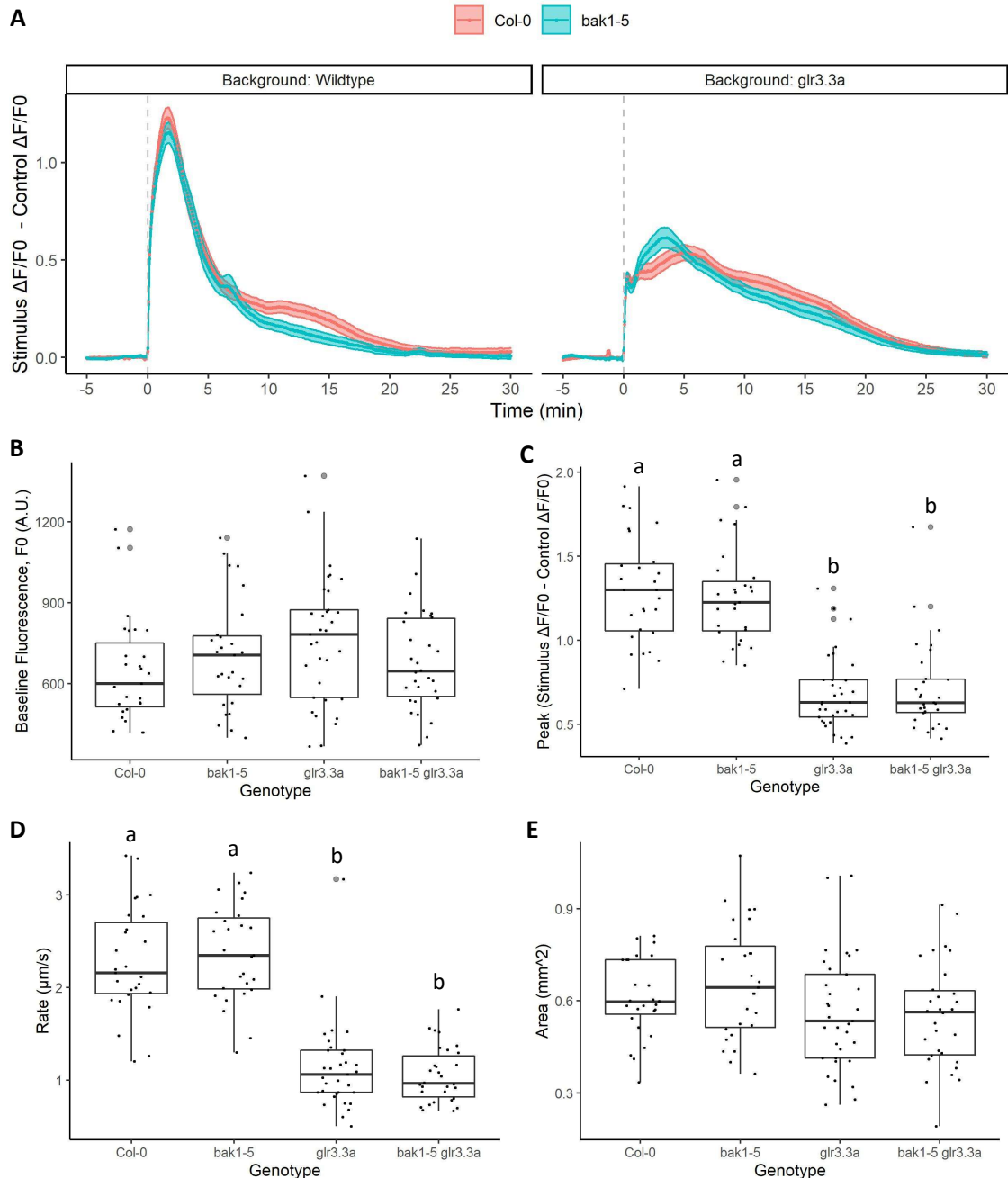


Figure I.XXIX Wound-induced GCaMP3 reporter signals in Col-0, *bak1-5*, *glr3.3a* and *bak1-5 glr3.3a* *A. thaliana*.

Properties of wound-induced GCaMP3 signals in Col-0 ($n = 27$), *bak1-5* ($n = 27$), *glr3.3a* ($n = 33$) and *bak1-5 glr3.3a* ($n = 33$) *A. thaliana* expressing *UBQ10::GCaMP3*. Background-corrected fluorescence intensity (F, A.U.) values were recorded over the area of the stimulus-induced responses and at comparable control sites. F values were transformed into $\Delta F/F_0$ values with F_0 being the mean F over the 5 min prior to stimulus treatment. (A) Traces for the mean \pm S.E.M. normalised $\Delta F/F_0$ values (Stimulus $\Delta F/F_0$ - Control $\Delta F/F_0$) over time with stimulus treatment at 0 min (grey dashed line). Traces are displayed for Col-0 and *bak1-5* in the wildtype *A. thaliana* background ('Wildtype') and in the *glr3.3a* *A. thaliana* background ('*glr3.3a*'). Boxplots are displayed for the (B) stimulus-treated site F_0 values (A.U.), (C) peak normalised $\Delta F/F_0$ values (Stimulus $\Delta F/F_0$ - Control $\Delta F/F_0$), (D) signal propagation rates ($\mu\text{m s}^{-1}$) and (E) signal areas (mm^2), with grey dots associated with outliers. Statistical significance levels are indicated by letters if genotypes significantly differed. Significance was assessed using an ANOVA with a Tukey post hoc test or a Kruskal-Wallis test with post hoc pairwise Wilcoxon rank-sum tests.

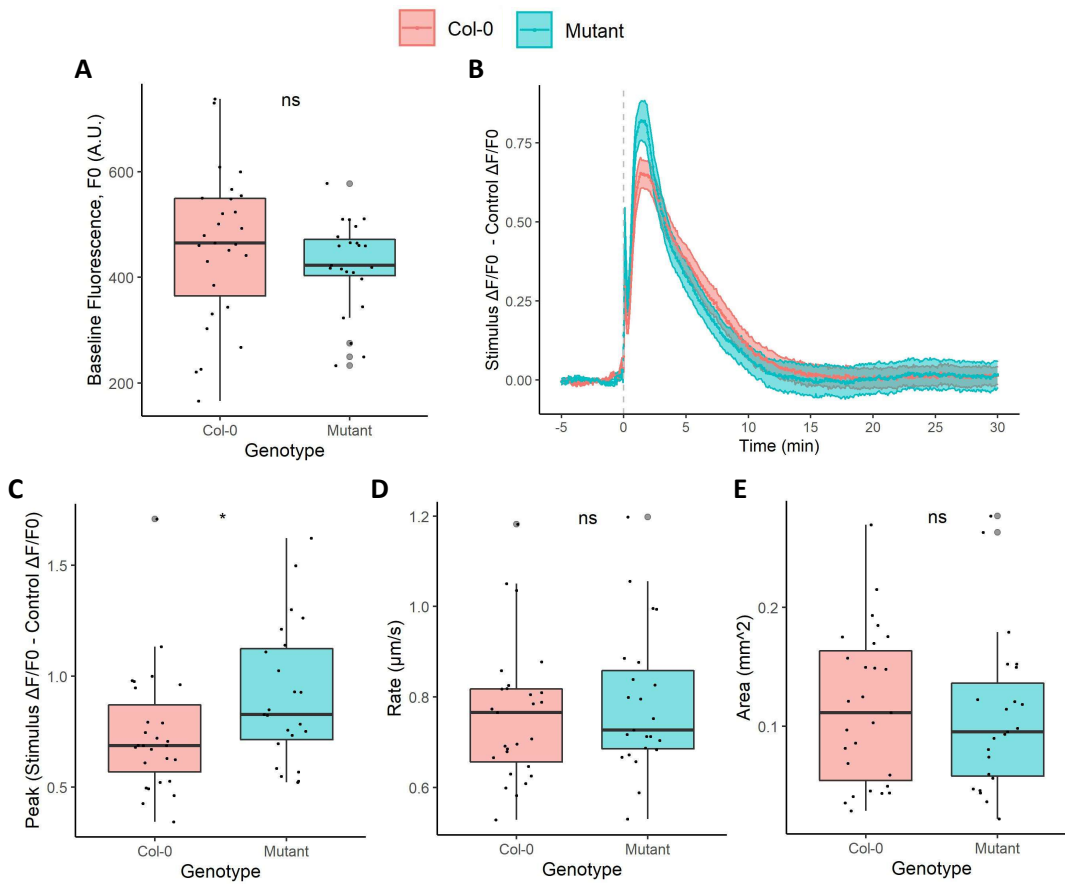


Figure I.XXX Touch-induced GCaMP3 reporter signals in Col-0 and *bak1-5 A. thaliana*.

Properties of touch-induced GCaMP3 signals in Col-0 ($n = 27$) and *bak1-5* ($n = 23$) *A. thaliana* expressing *UBQ10::GCaMP3*. Background-corrected fluorescence intensity (F , A.U.) values were recorded over the area of the stimulus-induced responses and at comparable control sites. F values were transformed into $\Delta F/F_0$ values with F_0 being the mean F over the 5 min prior to stimulus treatment. (B) Traces for the mean \pm S.E.M. normalised $\Delta F/F_0$ values (Stimulus $\Delta F/F_0 -$ Control $\Delta F/F_0$) over time with stimulus treatment at 0 min (grey dashed line). Boxplots are displayed for the (A) stimulus-treated site F_0 values (A.U.), (C) peak normalised $\Delta F/F_0$ values (Stimulus $\Delta F/F_0 -$ Control $\Delta F/F_0$), (D) signal propagation rates ($\mu\text{m s}^{-1}$) and (E) signal areas (mm^2), with grey dots associated with outliers. Statistical significance, calculated using a t-test or a Wilcoxon rank-sum test, is shown by ns: $p > 0.05$, *: $p \leq 0.05$, **: $p \leq 0.01$, ***: $p \leq 0.001$, ****: $p \leq 0.0001$.

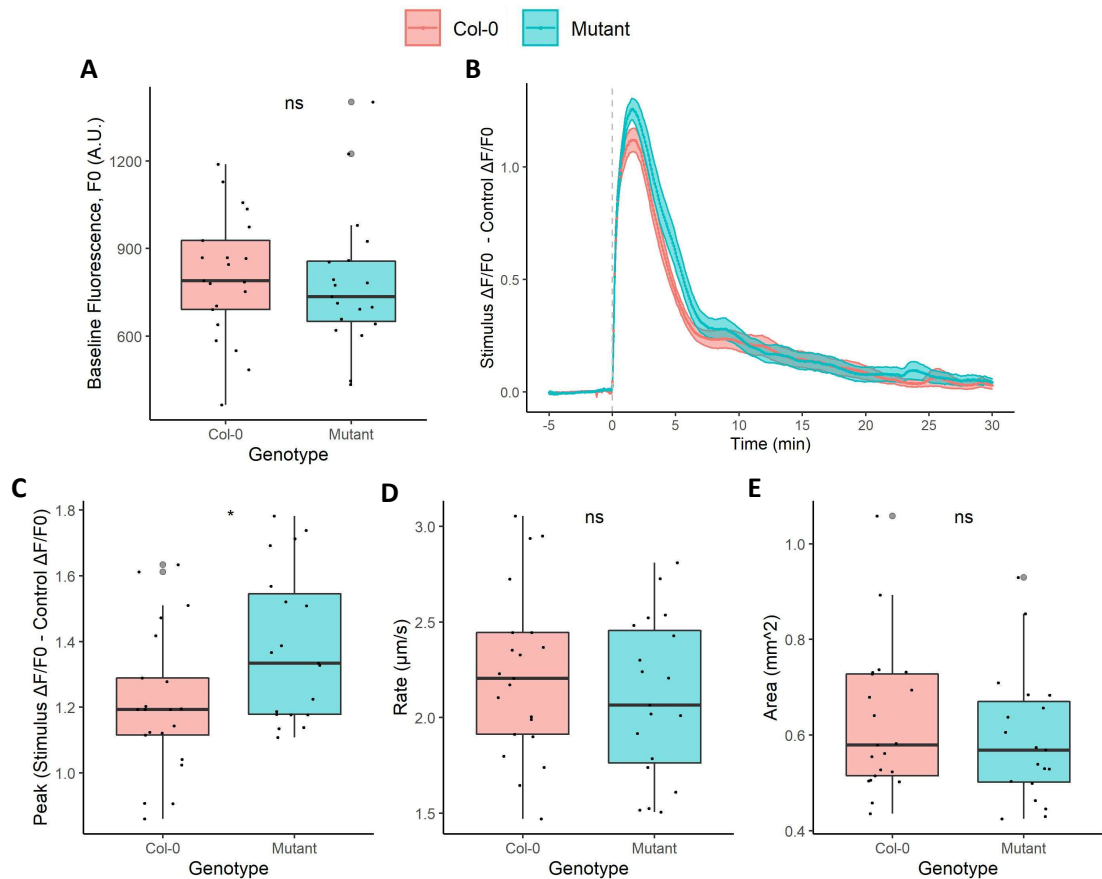


Figure I.XXXI Wound-induced GCaMP3 reporter signals in Col-0 and *sobir1-12 A. thaliana*.

Properties of wound-induced GCaMP3 signals in Col-0 ($n = 21$) and *sobir1-12* ($n = 19$) *A. thaliana* expressing *UBQ10::GCaMP3*. Background-corrected fluorescence intensity (F, A.U.) values were recorded over the area of the stimulus-induced responses and at comparable control sites. F values were transformed into $\Delta F/F_0$ values with F_0 being the mean F over the 5 min prior to stimulus treatment. (B) Traces for the mean \pm S.E.M. normalised $\Delta F/F_0$ values (Stimulus $\Delta F/F_0$ – Control $\Delta F/F_0$) over time with stimulus treatment at 0 min (grey dashed line). Boxplots are displayed for the (A) stimulus-treated site F_0 values (A.U.), (C) peak normalised $\Delta F/F_0$ values (Stimulus $\Delta F/F_0$ – Control $\Delta F/F_0$), (D) signal propagation rates ($\mu\text{m s}^{-1}$) and (E) signal areas (mm^2), with grey dots associated with outliers. Statistical significance, calculated using a t-test or a Wilcoxon rank-sum test, is shown by ns: $p > 0.05$, *: $p \leq 0.05$, **: $p \leq 0.01$, ***: $p \leq 0.001$, ****: $p \leq 0.0001$.

Reference List

- Abd-El-Haliem, A. M., Hoogstrate, S. W. & Schuurink, R. C. (2018) A robust functional genomics approach to identify effector genes required for thrips (*Frankliniella occidentalis*) reproductive performance on tomato leaf discs. *Frontiers in Plant Science*, 9.
- Abe, H., Ohnishi, J., Narusaka, M., Seo, S., Narusaka, Y., Tsuda, S. & Kobayashi, M. (2008) Function of jasmonate in response and tolerance of Arabidopsis to thrip feeding. *Plant & Cell Physiology*, 49, 68-80.
- Abe, H., Shimoda, T., Ohnishi, J., Kugimiya, S., Narusaka, M., Seo, S., Narusaka, Y., Tsuda, S. & Kobayashi, M. (2009) Jasmonate-dependent plant defense restricts thrips performance and preference. *BMC Plant Biology*, 9, 97.
- Abe, H., Tomitaka, Y., Shimoda, T., Seo, S., Sakurai, T., Kugimiya, S., Tsuda, S. & Kobayashi, M. (2012) Antagonistic plant defense system regulated by phytohormones assists interactions among vector insect, thrips and a tospovirus. *Plant & Cell Physiology*, 53, 204-212.
- Acevedo, F. E., Peiffer, M., Tan, C. W., Stanley, B. A., Stanley, A., Wang, J., Jones, A. G., Hoover, K., Rosa, C., Luthe, D. & Felton, G. (2017) Fall armyworm-associated gut bacteria modulate plant defense responses. *Molecular Plant-Microbe Interactions*, 30, 127-137.
- Acevedo, F. E., Rivera-Vega, L. J., Chung, S. H., Ray, S. & Felton, G. W. (2015) Cues from chewing insects — the intersection of DAMPs, HAMPs, MAMPs and effectors. *Current Opinion in Plant Biology*, 26, 80-86.
- Acosta, I. F., Gasperini, D., Chételat, A., Stolz, S., Santuari, L. & Farmer, E. E. (2013) Role of NINJA in root jasmonate signaling. *Proceedings of the National Academy of Sciences*, 110, 15473-15478.
- Albert, I., Böhm, H., Albert, M., Feiler, C. E., Imkampe, J., Wallmeroth, N., Brancato, C., Raaymakers, T. M., Oome, S., Zhang, H., Krol, E., Grefen, C., Gust, A. A., Chai, J., Hedrich, R., Van Den Ackerveken, G. & Nürnberger, T. (2015) An RLP23–SOBIR1–BAK1 complex mediates NLP-triggered immunity. *Nature Plants*, 1, 15140.
- Albert, I., Hua, C., Nürnberger, T., Pruitt, R. N. & Zhang, L. (2020) Surface sensor systems in plant immunity. *Plant Physiology*, 182, 1582-1596.
- Alfieri, A., Doccula, F. G., Pederzoli, R., Grenzi, M., Bonza, M. C., Luoni, L., Candeo, A., Romano Armada, N., Barbiroli, A., Valentini, G., Schneider, T. R., Bassi, A., Bolognesi, M., Nardini, M. & Costa, A. (2020) The structural bases for agonist diversity in an *Arabidopsis thaliana* glutamate receptor-like channel. *Proceedings of the National Academy of Sciences*, 117, 752-760.
- Allen, G. J. & Sanders, D. (1995) Calcineurin, a type 2B protein phosphatase, modulates the Ca²⁺-permeable slow vacuolar ion channel of stomatal guard cells. *The Plant Cell*, 7, 1473-1483.
- Allen, G. J. & Sanders, D. (1996) Control of ionic currents in guard cell vacuoles by cytosolic and luminal calcium. *The Plant Journal*, 10, 1055-1069.
- Alonso, J. M., Stepanova, A. N., Leisse, T. J., Kim, C. J., Chen, H., Shinn, P., Stevenson, D. K., Zimmerman, J., Barajas, P., Cheuk, R., Gadriab, C., Heller, C., Jeske, A., Koesema, E., Meyers, C. C., Parker, H., Prednis, L., Ansari, Y., Choy, N., Deen, H., Geralt, M., Hazari, N., Hom, E., Karnes, M., Mulholland, C., Ndubaku, R., Schmidt, I., Guzman, P., Aguilar-Henonin, L., Schmid, M., Weigel, D., Carter, D. E., Marchand, T., Risseuw, E., Brogden, D., Zeko, A., Crosby, W. L., Berry, C. C. & Ecker, J. R. (2003) Genome-wide insertional mutagenesis of *Arabidopsis thaliana*. *Science*, 301, 653-657.
- Amack, S. C. & Antunes, M. S. (2020) CaMV35S promoter – a plant biology and biotechnology workhorse in the era of synthetic biology. *Current Plant Biology*, 24, 9.
- Amano, Y., Tsubouchi, H., Shinohara, H., Ogawa, M. & Matsubayashi, Y. (2007) Tyrosine-sulfated glycopeptide involved in cellular proliferation and expansion in Arabidopsis. *Proceedings of the National Academy of Sciences*, 104, 18333-18338.

- Andréasson, E., Bolt Jørgensen, L., Höglund, A. S., Rask, L. & Meijer, J. (2001) Different myrosinase and idioblast distribution in *Arabidopsis* and *Brassica napus*. *Plant Physiology*, 127, 1750-1763.
- Archer, L., Mondal, H. A., Behera, S., Twayana, M., Louis, J., Nalam, V. J., Keereetaweep, J., Chowdhury, Z. & Shah, J. (2022) Interplay between MYZUS PERSICAE-INDUCED LIPASE 1 and OPDA signaling in controlling green peach aphid infestation on *Arabidopsis thaliana*. *bioRxiv*, 2022.2007.2008.499389.
- Arnaiz, A., Talavera-Mateo, L., Gonzalez-Melendi, P., Martinez, M., Diaz, I. & Santamaria, M. E. (2018) *Arabidopsis* kunitz trypsin inhibitors in defense against spider mites. *Frontiers in Plant Science*, 9, 986.
- Ast, C., Foret, J., Oltrogge, L. M., De Michele, R., Kleist, T. J., Ho, C.-H. & Frommer, W. B. (2017) Ratiometric Matryoshka biosensors from a nested cassette of green- and orange-emitting fluorescent proteins. *Nature Communications*, 8, 431-444.
- Atamian, H. S., Chaudhary, R., Cin, V. D., Bao, E., Girke, T. & Kaloshian, I. (2013) *In planta* expression or delivery of potato aphid *Macrosiphum euphorbiae* effectors Me10 and Me23 enhances aphid fecundity. *Molecular Plant-Microbe Interactions*, 26, 67-74.
- Badillo-Vargas, I. E., Rotenberg, D., Schneewis, B. A. & Whitfield, A. E. (2015) RNA interference tools for the western flower thrips, *Frankliniella occidentalis*. *Journal of Insect Physiology*, 76, 36-46.
- Baez, I., Reitz, S. R., Funderburk, J. E. & Olson, S. M. (2011) Variation within and between *Frankliniella* thrips species in host plant utilization. *Journal of Insect Science*, 11, 41.
- Bartels, S., Lori, M., Mbengue, M., Van Verk, M., Klausner, D., Hander, T., Boni, R., Robatzek, S. & Boller, T. (2013) The family of Peps and their precursors in *Arabidopsis*: Differential expression and localization but similar induction of pattern-triggered immune responses. *Journal of Experimental Botany*, 64, 5309-5321.
- Bass, C., Puinean, A. M., Zimmer, C. T., Denholm, I., Field, L. M., Foster, S. P., Gutbrod, O., Nauen, R., Slater, R. & Williamson, M. S. (2014) The evolution of insecticide resistance in the peach potato aphid, *Myzus persicae*. *Insect Biochemistry and Molecular Biology*, 51, 41-51.
- Basu, D., Codjoe, J. M., Velez, K. M. & Haswell, E. S. (2022) The Mechanosensitive Ion Channel MSL10 modulates susceptibility to *Pseudomonas syringae* in *Arabidopsis thaliana*. *Molecular Plant-Microbe Interactions*, 35, 567-582.
- Basu, D. & Haswell, E. S. (2017) Plant mechanosensitive ion channels: An ocean of possibilities. *Current Opinion in Plant Biology*, 40, 43-48.
- Basu, D. & Haswell, E. S. (2020) The Mechanosensitive Ion Channel MSL10 potentiates responses to cell swelling in *Arabidopsis* seedlings. *Current Biology*, 30, R804-R806.
- Behera, S., Wang, N., Zhang, C., Schmitz-Thom, I., Strohkamp, S., Schültke, S., Hashimoto, K., Xiong, L. & Kudla, J. (2015) Analyses of Ca²⁺ dynamics using a ubiquitin-10 promoter-driven Yellow Cameleon 3.6 indicator reveal reliable transgene expression and differences in cytoplasmic Ca²⁺ responses in *Arabidopsis* and rice (*Oryza sativa*) roots. *New Phytologist*, 206, 751-760.
- Behera, S., Xu, Z., Luoni, L., Bonza, C., Doccula, F. G., Demichelis, M. I., Morris, R. J., Schwarzländer, M. & Costa, A. (2018) Cellular Ca²⁺ signals generate defined pH signatures in plants. *The Plant Cell*, 30, 2704-2719.
- Bell, C., Multhoff, J. & Schwarzländer, M. (2022) Biosensing on acid: Fluorescent protein probes for low pH environments. *Journal of Experimental Botany*, 73, 7199-7203.
- Bellandi, A. (2021) *Dynamics and cell-to-cell transmission of wound-induced calcium waves in plants*. Doctoral, University of East Anglia.
- Bellandi, A., Papp, D., Breakspear, A., Joyce, J., Johnston, M. G., De Keijzer, J., Raven, E. C., Ohtsu, M., Vincent, T. R., Miller, A. J., Sanders, D., Hogenhout, S. A., Morris, R. J. & Faulkner, C. (2022) Diffusion and bulk flow of amino acids mediate calcium waves in plants. *Science Advances*, 8, eabo6693.

- Bellincampi, D., Dipierro, N., Salvi, G., Cervone, F. & De Lorenzo, G. (2000) Extracellular H₂O₂ induced by oligogalacturonides is not involved in the inhibition of the auxin-regulated rolb gene expression in tobacco leaf explants. *Plant Physiology*, 122, 1379-1386.
- Benedetti, M., Pontiggia, D., Raggi, S., Cheng, Z., Scaloni, F., Ferrari, S., Ausubel, F. M., Cervone, F. & De Lorenzo, G. (2015) Plant immunity triggered by engineered in vivo release of oligogalacturonides, damage-associated molecular patterns. *Proceedings of the National Academy of Sciences*, 112, 5533-5538.
- Benikhlef, L., L'haridon, F., Abou-Mansour, E., Serrano, M., Binda, M., Costa, A., Lehmann, S. & Métraux, J.-P. (2013) Perception of soft mechanical stress in Arabidopsis leaves activates disease resistance. *BMC Plant Biology*, 13, 133.
- Bensoussan, N., Santamaria, M. E., Zhurov, V., Diaz, I., Grbić, M. & Grbić, V. (2016) Plant-herbivore interaction: Dissection of the cellular pattern of *Tetranychus urticae* feeding on the host plant. *Frontiers in Plant Science*, 7, 1105.
- Betsuyaku, S., Katou, S., Takebayashi, Y., Sakakibara, H., Nomura, N. & Fukuda, H. (2018) Salicylic acid and jasmonic acid pathways are activated in spatially different domains around the infection site during effector-triggered immunity in *Arabidopsis thaliana*. *Plant & Cell Physiology*, 59, 8-16.
- Beyhl, D., Hortensteiner, S., Martinoia, E., Farmer, E. E., Fromm, J., Marten, I. & Hedrich, R. (2009) The *fou2* mutation in the major vacuolar cation channel *TPC1* confers tolerance to inhibitory luminal calcium. *The Plant Journal*, 58, 715-723.
- Bi, G., Su, M., Li, N., Liang, Y., Dang, S., Xu, J., Hu, M., Wang, J., Zou, M., Deng, Y., Li, Q., Huang, S., Li, J., Chai, J., He, K., Chen, Y.-H. & Zhou, J.-M. (2021) The ZAR1 resistosome is a calcium-permeable channel triggering plant immune signaling. *Cell*, 184, 3528-3541.e3512.
- Bi, G., Zhou, Z., Wang, W., Li, L., Rao, S., Wu, Y., Zhang, X., Menke, F. L. H., Chen, S. & Zhou, J. M. (2018) Receptor-Like cytoplasmic kinases directly link diverse pattern recognition receptors to the activation of mitogen-activated protein kinase cascades in Arabidopsis. *Plant Cell*, 30, 1543-1561.
- Bigear, J., Colcombet, J. & Hirt, H. (2015) Signaling mechanisms in pattern-triggered immunity (pti). *Molecular Plant*, 8, 521-539.
- Bihler, H., Eing, C., Hebeisen, S., Roller, A., Czempinski, K. & Bertl, A. (2005) TPK1 is a vacuolar ion channel different from the slow-vacuolar cation channel. *Plant Physiology*, 139, 417-424.
- Bjornson, M., Pimprikar, P., Nürnberger, T. & Zipfel, C. (2021) The transcriptional landscape of *Arabidopsis thaliana* pattern-triggered immunity. *Nature Plants*, 7, 579-586
- Blackman, R. & Eastop, V. (2017) *Aphids as crop pests: Taxonomic issues*, CABI International.
- Blackman, R. L. (1974) Life-cycle variation of *Myzus persicae* (sulz.) (hom., Aphididae) in different parts of the world, in relation to genotype and environment. *Bulletin of Entomological Research*, 63, 595-607.
- Blackman, R. L. & Eastop, V. F. (2000) *Aphids on the world's crops: An identification and information guide*, John Wiley & Sons Ltd.
- Böhm, H., Albert, I., Oome, S., Raaymakers, T. M., Van Den Ackerveken, G. & Nürnberger, T. (2014) A conserved peptide pattern from a widespread microbial virulence factor triggers pattern-induced immunity in Arabidopsis. *PLoS Pathogens*, 10, e1004491.
- Bonaventure, G., Gfeller, A., Proebsting, W. M., Hortensteiner, S., Chetelat, A., Martinoia, E. & Farmer, E. E. (2007a) A gain-of-function allele of *TPC1* activates oxylipin biogenesis after leaf wounding in Arabidopsis. *The Plant Journal*, 49, 889-898.
- Bonaventure, G., Gfeller, A., Rodriguez, V. M., Armand, F. & Farmer, E. E. (2007b) The *fou2* gain-of-function allele and the wild-type allele of *Two Pore Channel 1* contribute to different extents or by different mechanisms to defense gene expression in Arabidopsis. *Plant & Cell Physiology*, 48, 1775-1789.
- Bonza, M. C., Morandini, P., Luoni, L., Geisler, M., Palmgren, M. G. & De Michelis, M. I. (2000) *At-ACA8* encodes a plasma membrane-localized calcium-ATPase of Arabidopsis with a calmodulin-binding domain at the N terminus. *Plant Physiology* 123, 1495-1506.

- Bootman, M. D., Rietdorf, K., Collins, T., Walker, S. & Sanderson, M. (2013) Ca²⁺-sensitive fluorescent dyes and intracellular Ca²⁺ imaging. *Cold Spring Harbor Protocols*.
- Borniego, M. L., Molina, M. C., Guiamét, J. J. & Martinez, D. E. (2020) Physiological and proteomic changes in the apoplast accompany leaf senescence in Arabidopsis. *Frontiers in Plant Science*, 10.
- Bos, J. I. B., Prince, D., Pitino, M., Maffei, M. E., Win, J. & Hogenhout, S. A. (2010) A functional genomics approach identifies candidate effectors from the aphid species *Myzus persicae* (green peach aphid). *PLoS Genetics*, 6, e1001216.
- Boudsocq, M., Willmann, M. R., McCormack, M., Lee, H., Shan, L., He, P., Bush, J., Cheng, S.-H. & Sheen, J. (2010) Differential innate immune signalling via Ca(2+) sensor protein kinases. *Nature*, 464, 418-422.
- Boulain, H., Legeai, F., Jaquiéry, J., Guy, E., Morlière, S., Simon, J.-C. & Sugio, A. (2019) Differential expression of candidate salivary effector genes in pea aphid biotypes with distinct host plant specificity. *Frontiers in Plant Science*, 10.
- Boursiac, Y., Lee, S. M., Romanowsky, S., Blank, R., Sladek, C., Chung, W. S. & Harper, J. F. (2010) Disruption of the vacuolar calcium-ATPases in Arabidopsis results in the activation of a salicylic acid-dependent programmed cell death pathway. *Plant Physiology*, 154, 1158-1171.
- Bouwmeester, K., De Sain, M., Weide, R., Gouget, A., Klamer, S., Canut, H. & Govers, F. (2011) The lectin receptor kinase LecRK-I.9 is a novel *Phytophthora* resistance component and a potential host target for a RXLR effector. *PLoS Pathogens*, 7, e1001327.
- Bredow, M. & Monaghan, J. (2019) Regulation of plant immune signaling by calcium-dependent protein kinases. *Molecular Plant-Microbe Interactions*, 32, 6-19.
- Brennan, E. B., Weinbaum, S. A. & Pinney, K. (2001) A new technique for studying the stylet tracks of homopteran insects in hand-sectioned plant tissue using light or epifluorescence microscopy. *Biotechnic and Histochemistry*, 76, 59-66.
- Bricchi, I., Leitner, M., Foti, M., Mithöfer, A., Boland, W. & Maffei, M. E. (2010) Robotic mechanical wounding (MecWorm) versus herbivore-induced responses: Early signaling and volatile emission in lima bean (*Phaseolus lunatus* L.). *Planta*, 232, 719-729.
- Bruinsma, K. A. (2014) *Arabidopsis thaliana-spider mite interaction: Plant perception, signalling, and response*. Masters, The University of Western Ontario.
- Brutus, A., Sicilia, F., Macone, A., Cervone, F. & De Lorenzo, G. (2010) A domain swap approach reveals a role of the plant wall-associated kinase 1 (WAK1) as a receptor of oligogalacturonides. *Proceedings of the National Academy of Sciences*, 107, 9452-9457.
- Bürger, M. & Chory, J. (2019) Stressed out about hormones: How plants orchestrate immunity. *Cell Host Microbe*, 26, 163-172.
- Buscaill, P., Chandrasekar, B., Sanguankiatichai, N., Kourelis, J., Kaschani, F., Thomas, E. L., Morimoto, K., Kaiser, M., Preston, G. M., Ichinose, Y. & Van Der Hoorn, R. a. L. (2019) Glycosidase and glycan polymorphism control hydrolytic release of immunogenic flagellin peptides. *Science*, 364, eaav0748.
- Bush, D. S. & Jones, R. L. (1987) Measurement of cytoplasmic calcium in aleurone protoplasts using indo-1 and fura-2. *Cell Calcium*, 8, 455-472.
- Bush, D. S. & Jones, R. L. (1990) Measuring intracellular Ca levels in plant cells using the fluorescent probes, indo-1 and fura-2 : Progress and prospects. *Plant Physiology*, 93, 841-845.
- Cabi (2015) *Myzus persicae* (green peach aphid). Invasive Species Compendium. Wallingford: CAB International.
- Canham, J. (2022) *Characterisation of aphid-derived components involved in plant innate immune responses*. Doctoral, University of East Anglia.
- Cantero, A., Barthakur, S., Bushart, T. J., Chou, S., Morgan, R. O., Fernandez, M. P., Clark, G. B. & Roux, S. J. (2006) Expression profiling of the Arabidopsis annexin gene family during germination, de-etiolation and abiotic stress. *Plant Physiology and Biochemistry*, 44, 13-24.

- Cao, Y., Liang, Y., Tanaka, K., Nguyen, C. T., Jedrzejczak, R. P., Joachimiak, A. & Stacey, G. (2014) The kinase LYK5 is a major chitin receptor in *Arabidopsis* and forms a chitin-induced complex with related kinase CERK1. *eLife*, 3, e03766.
- Castro-Rodríguez, V., Kleist, T. J., Gappel, N. M., Atanjaoui, F., Okumoto, S., Machado, M., Denyer, T., Timmermans, M. C. P., Frommer, W. B. & Wudick, M. M. (2022) Sponging of glutamate at the outer plasma membrane surface reveals roles for glutamate in development. *The Plant Journal*, 109, 664-674.
- Chae, H. B., Kim, M. G., Kang, C. H., Park, J. H., Lee, E. S., Lee, S.-U., Chi, Y. H., Paeng, S. K., Bae, S. B., Wi, S. D., Yun, B.-W., Kim, W.-Y., Yun, D.-J., Mackey, D. & Lee, S. Y. (2021) Redox sensor QSOX1 regulates plant immunity by targeting GSNOR to modulate ROS generation. *Molecular Plant*, 14, 1312-1327.
- Charpentier, M., Sun, J., Vaz Martins, T., Radhakrishnan, G. V., Findlay, K., Soumpourou, E., Thouin, J., Véry, A. A., Sanders, D., Morris, R. J. & Oldroyd, G. E. (2016) Nuclear-localized cyclic nucleotide-gated channels mediate symbiotic calcium oscillations. *Science*, 352, 1102-1105.
- Chaudhary, R., Atamian, H. S., Shen, Z., Briggs, S. P. & Kaloshian, I. (2014) GroEL from the endosymbiont *Buchnera aphidicola* betrays the aphid by triggering plant defense. *Proceedings of the National Academy of Sciences*, 111, 8919-8924.
- Chaudhary, R., Peng, H.-C., He, J., Macwilliams, J., Teixeira, M., Tsuchiya, T., Chesnais, Q., Mudgett, M. B. & Kaloshian, I. (2018) Aphid effector Me10 interacts with tomato TFT7, a 14-3-3 isoform involved in aphid resistance. *New Phytologist*, 221, 1518-1528.
- Chauvin, A., Caldelari, D., Wolfender, J. L. & Farmer, E. E. (2013) Four 13-lipoxygenases contribute to rapid jasmonate synthesis in wounded *Arabidopsis thaliana* leaves: A role for lipoxygenase 6 in responses to long-distance wound signals. *New Phytologist*, 197, 566-575.
- Chen, C.-Y., Liu, Y.-Q., Song, W.-M., Chen, D.-Y., Chen, F.-Y., Chen, X.-Y., Chen, Z.-W., Ge, S.-X., Wang, C.-Z., Zhan, S., Chen, X.-Y. & Mao, Y.-B. (2019) An effector from cotton bollworm oral secretion impairs host plant defense signaling. *Proceedings of the National Academy of Sciences*, 116, 14331-14338.
- Chen, D., Cao, Y., Li, H., Kim, D., Ahsan, N., Thelen, J. & Stacey, G. (2017) Extracellular ATP elicits DORN1-mediated RBOHD phosphorylation to regulate stomatal aperture. *Nature Communications*, 8, 2265.
- Chen, J., Zhang, X., Rathjen, J. P. & Dodds, P. N. (2022) Direct recognition of pathogen effectors by plant NLR immune receptors and downstream signalling. *Essays in Biochemistry*, 66, 471-483.
- Chen, J., Zhao, Y., Luo, X., Hong, H., Yang, T., Huang, S., Wang, C., Chen, H., Qian, X., Feng, M., Chen, Z., Dong, Y., Ma, Z., Li, J., Zhu, M., He, S. Y., Dinesh-Kumar, S. P. & Tao, X. (2023) NLR surveillance of pathogen interference with hormone receptors induces immunity. *Nature*, 613, 145-152.
- Chen, Y.-C., Holmes, E. C., Rajniak, J., Kim, J.-G., Tang, S., Fischer, C. R., Mudgett, M. B. & Sattely, E. S. (2018) N-hydroxy-pipecolic acid is a mobile metabolite that induces systemic disease resistance in *Arabidopsis*. *Proceedings of the National Academy of Sciences*, 115, E4920-E4929.
- Chen, Y., Singh, A., Kaithakottil, G. G., Mathers, T. C., Gravino, M., Mugford, S. T., Van Oosterhout, C., Swarbreck, D. & Hogenhout, S. A. (2020) An aphid RNA transcript migrates systemically within plants and is a virulence factor. *Proceedings of the National Academy of Sciences*, 117, 12763-12771.
- Cheung, A. Y. & Wu, H. M. (2011) THESEUS 1, FERONIA and relatives: A family of cell wall-sensing receptor kinases? *Current Opinion in Plant Biology*, 14, 632-641.
- Childers, C. & Brecht, J. (1996) Colored sticky traps for monitoring *Frankliniella bispinosa* (Morgan)(Thysanoptera: Thripidae) during flowering cycles in citrus. *Journal of Economic Entomology*, 89, 1240-1249.

- Chin, K., Defalco, T. A., Moeder, W. & Yoshioka, K. (2013) The Arabidopsis cyclic nucleotide-gated ion channels AtCNGC2 and AtCNGC4 work in the same signaling pathway to regulate pathogen defense and floral transition. *Plant Physiology*, 163, 611-624.
- Chinchilla, D., Bauer, Z., Regenass, M., Boller, T. & Felix, G. (2006) The Arabidopsis receptor kinase FLS2 binds flg22 and determines the specificity of flagellin perception. *The Plant Cell*, 18, 465-476.
- Chinchilla, D., Shan, L., He, P., De Vries, S. & Kemmerling, B. (2009) One for all: The receptor-associated kinase BAK1. *Trends in Plant Science*, 14, 535-541.
- Chisholm, I. F. & Lewis, T. (1984) A new look at thrips (*Thysanoptera*) mouthparts, their action and effects of feeding on plant tissue. *Bulletin of Entomological Research*, 74, 663-675.
- Chiu, J. C., Brenner, E. D., Desalle, R., Nitabach, M. N., Holmes, T. C. & Coruzzi, G. M. (2002) Phylogenetic and expression analysis of the glutamate-receptor-like gene family in *Arabidopsis thaliana*. *Molecular Biology and Evolution*, 19, 1066-1082.
- Chivasa, S., Murphy, A. M., Hamilton, J. M., Lindsey, K., Carr, J. P. & Slabas, A. R. (2009) Extracellular ATP is a regulator of pathogen defence in plants. *The Plant Journal*, 60, 436-448.
- Cho, J.-H., Swanson, C. J., Chen, J., Li, A., Lippert, L. G., Boye, S. E., Rose, K., Sivaramakrishnan, S., Chuong, C.-M. & Chow, R. H. (2017) The GCaMP-R family of genetically encoded ratiometric calcium indicators. *ACS Chemical Biology*, 12, 1066-1074.
- Choi, H. W., Manohar, M., Manosalva, P., Tian, M., Moreau, M. & Klessig, D. F. (2016) Activation of plant innate immunity by extracellular High Mobility Group Box 3 and its inhibition by salicylic acid. *PLoS Pathogens*, 12, e1005518.
- Choi, J., Tanaka, K., Cao, Y., Qi, Y., Qiu, J., Liang, Y., Lee, S. Y. & Stacey, G. (2014a) Identification of a plant receptor for extracellular ATP. *Science*, 343, 290-294.
- Choi, J., Tanaka, K., Liang, Y., Cao, Y., Lee, Sang y. & Stacey, G. (2014b) Extracellular ATP, a danger signal, is recognized by DORN1 in Arabidopsis. *Biochemical Journal*, 463, 429-437.
- Choi, W.-G., Toyota, M., Kim, S.-H., Hilleary, R. & Gilroy, S. (2014c) Salt stress-induced Ca²⁺ waves are associated with rapid, long-distance root-to-shoot signaling in plants. *Proceedings of the National Academy of Sciences*, 111, 6497-6502.
- Cloyd, R. A. (2009) Western flower thrips (*Frankliniella occidentalis*) management on ornamental crops grown in greenhouses: Have we reached an impasse. *Pest Technology*, 3, 1-9.
- Codjoe, J. M., Richardson, R. A., Mcloughlin, F., Vierstra, R. D. & Haswell, E. S. (2022) Unbiased proteomic and forward genetic screens reveal that mechanosensitive ion channel MSL10 functions at er-plasma membrane contact sites in *Arabidopsis thaliana*. *eLife*, 11, e80501.
- Cole, R. A. (1997) Comparison of feeding behaviour of two Brassica pests *Brevicoryne brassicae* and *Myzus persicae* on wild and cultivated brassica species. *Entomologia Experimentalis et Applicata*, 85, 135-143.
- Coleman, A. D., Maroschek, J., Raasch, L., Takken, F. L. W., Ranf, S. & Hückelhoven, R. (2021) The Arabidopsis leucine-rich repeat receptor-like kinase MIK2 is a crucial component of early immune responses to a fungal-derived elicitor. *New Phytologist*, 229, 3453-3466.
- Coleman, A. D., Wouters, R. H., Mugford, S. T. & Hogenhout, S. A. (2015) Persistence and transgenerational effect of plant-mediated RNAi in aphids. *Journal of Experimental Botany*, 66, 541-548.
- Colin, L., Martin-Arevalillo, R., Bovio, S., Bauer, A., Vernoux, T., Caillaud, M.-C., Landrein, B. & Jaillais, Y. (2021) Imaging the living plant cell: From probes to quantification. *The Plant Cell*, 34, 247-272.
- Consales, F., Schweizer, F., Erb, M., Gouhier-Darimont, C., Bodenhausen, N., Bruessow, F., Sobhy, I. & Reymond, P. (2011) Insect oral secretions suppress wound-induced responses in Arabidopsis. *Journal of Experimental Botany*, 63, 727-737.
- Coppola, M., Lelio, I. D., Romanelli, A., Gualtieri, L., Molisso, D., Ruocco, M., Avitabile, C., Natale, R., Cascone, P., Guerrieri, E., Pennacchio, F. & Rao, R. (2019) Tomato plants treated with systemin peptide show enhanced levels of direct and indirect defense associated with increased expression of defense-related genes. *Plants*, 8, 395.

- Costa, A., Luoni, L., Marrano, C. A., Hashimoto, K., Köster, P., Giacometti, S., De Michelis, M. I., Kudla, J. & Bonza, M. C. (2017) Ca²⁺-dependent phosphoregulation of the plasma membrane Ca²⁺-ATPase ACA8 modulates stimulus-induced calcium signatures. *Journal of Experimental Botany*, 68, 3215-3230.
- Coste, B., Mathur, J., Schmidt, M., Earley, T. J., Ranade, S., Petrus, M. J., Dubin, A. E. & Patapoutian, A. (2010) Piezo1 and Piezo2 are essential components of distinct mechanically activated cation channels. *Science*, 330, 55-60.
- Cui, N., Lu, H., Wang, T., Zhang, W., Kang, L. & Cui, F. (2019) Armet, an aphid effector protein, induces pathogen resistance in plants by promoting the accumulation of salicylic acid. *Philosophical Transactions of the Royal Society B: Biological Sciences*, 374, 20180314.
- Czempinski, K., Frachisse, J.-M., Maurel, C., Barbier-Brygoo, H. & Mueller-Roeber, B. (2002) Vacuolar membrane localization of the Arabidopsis 'two-pore' K⁺ channel KCO1. *The Plant Journal*, 29, 809-820.
- Dark, A., Demidchik, V., Richards, S. L., Shabala, S. & Davies, J. M. (2011) Release of extracellular purines from plant roots and effect on ion fluxes. *Plant Signaling & Behavior*, 6, 1855-1857.
- Daxinger, L., Hunter, B., Sheikh, M., Jauvion, V., Gascioli, V., Vaucheret, H., Matzke, M. & Furner, I. (2008) Unexpected silencing effects from T-DNA tags in Arabidopsis. *Trends in Plant Science*, 13, 4-6.
- De Vos, M. & Jander, G. (2009) *Myzus persicae* (green peach aphid) salivary components induce defence responses in *Arabidopsis thaliana*. *Plant, Cell & Environment*, 32, 1548-1560.
- De Vos, M., Van Oosten, V. R., Van Poecke, R. M. P., Van Pelt, J. A., Pozo, M. J., Mueller, M. J., Buchala, A. J., Métraux, J.-P., Van Loon, L. C., Dicke, M. & Pieterse, C. M. J. (2005) Signal signature and transcriptome changes of Arabidopsis during pathogen and insect attack. *Molecular Plant-Microbe Interactions*, 18, 923-937.
- De Vriese, K., Costa, A., Beeckman, T. & Vanneste, S. (2018) Pharmacological strategies for manipulating plant Ca²⁺ signalling. *International journal of molecular sciences*, 19, 1506.
- Deblasio, S. L., Sylvester, A. W. & Jackson, D. (2010) Illuminating plant biology: Using fluorescent proteins for high-throughput analysis of protein localization and function in plants. *Briefings in Functional Genomics*, 9, 129-138.
- Decreux, A. & Messiaen, J. (2005) Wall-associated kinase WAK1 interacts with cell wall pectins in a calcium-induced conformation. *Plant and Cell Physiology*, 46, 268-278.
- Dedryver, C.-A., Le Ralec, A. & Fabre, F. (2010) The conflicting relationships between aphids and men: A review of aphid damage and control strategies. *Comptes Rendus Biologies*, 333, 539-553.
- Defalco, T. A., Toyota, M., Phan, V., Karia, P., Moeder, W., Gilroy, S. & Yoshioka, K. (2017) Using GCaMP3 to study Ca²⁺ signaling in Nicotiana species. *Plant and Cell Physiology*, 58, 1173-1184.
- Deshoux, M., Monsion, B., Pichon, E., Jiménez, J., Moreno, A., Cayrol, B., Thébaud, G., Mugford, S. T., Hogenhout, S. A., Blanc, S., Fereres, A. & Uzest, M. (2022) Role of acrostyle cuticular proteins in the retention of an aphid salivary effector. *International journal of molecular sciences*, 23, 15337.
- Després, C., DeLong, C., Glaze, S., Liu, E. & Fobert, P. R. (2000) The Arabidopsis NPR1/NIM1 protein enhances the DNA binding activity of a subgroup of the TGA family of bZIP transcription factors. *The Plant Cell*, 12, 279-290.
- Dewar, A. M. (2017) The adverse impact of the neonicotinoid seed treatment ban on crop protection in oilseed rape in the united kingdom. *Pest Management Science*, 73, 1305-1309.
- Ding, Y., Sun, T., Ao, K., Peng, Y., Zhang, Y., Li, X. & Zhang, Y. (2018) Opposite roles of salicylic acid receptors NPR1 and NPR3/NPR4 in transcriptional regulation of plant immunity. *Cell*, 173, 1454-1467.e1415.
- Divekar, P. A., Narayana, S., Divekar, B. A., Kumar, R., Gadratagi, B. G., Ray, A., Singh, A. K., Rani, V., Singh, V., Singh, A. K., Kumar, A., Singh, R. P., Meena, R. S. & Behera, T. K. (2022) Plant

- secondary metabolites as defense tools against herbivores for sustainable crop protection. *International Journal of Molecular Sciences* 23, 2690.
- Dixon, A. F. G. (2012) *Aphid ecology an optimization approach*, Springer Science & Business Media.
- Dodd, A. N., Kudla, J. & Sanders, D. (2010) The language of calcium signaling. *Annual Review of Plant Biology*, 61, 593-620.
- Dogimont, C., Chovelon, V., Pauquet, J., Boualem, A. & Bendahmane, A. (2014) The *Vat* locus encodes for a CC-NBS-LRR protein that confers resistance to *Aphis gossypii* infestation and *Aphis gossypii*-mediated virus resistance. *The Plant Journal*, 80, 993-1004.
- Dombrecht, B., Xue, G. P., Sprague, S. J., Kirkegaard, J. A., Ross, J. J., Reid, J. B., Fitt, G. P., Sewelam, N., Schenk, P. M., Manners, J. M. & Kazan, K. (2007) MYC2 differentially modulates diverse jasmonate-dependent functions in Arabidopsis. *Plant Cell*, 19, 2225-2245.
- Dommel, M., Oh, J., Hugueta-Tapia, J. C., Guy, E., Boulain, H., Sugio, A., Murugan, M., Legeai, F., Heck, M. & Smith, C. M. (2020) Big genes, small effectors: Pea aphid cassette effector families composed from miniature exons. *Frontiers in Plant Science*, 11, 1230.
- Dongus, J. A. & Parker, J. E. (2021) EDS1 signalling: At the nexus of intracellular and surface receptor immunity. *Current Opinion in Plant Biology*, 62, 102039.
- Döring, T. F. (2014) How aphids find their host plants, and how they don't. *Annals of Applied Biology*, 165, 3-26.
- Douglas, A. E. (2006) Phloem-sap feeding by animals: Problems and solutions. *Journal of Experimental Botany*, 57, 747-754.
- Dreyer, D. & Campbell, B. (1987) Chemical basis of host-plant resistance to aphids. *Plant, Cell & Environment*, 10, 353-361.
- Drurey, C. (2015) *The dynamics of molecular components that regulate aphid-plant interactions*. Doctoral, University of East Anglia.
- Drurey, C., Mathers, T. C., Prince, D. C., Wilson, C., Caceres-Moreno, C., Mugford, S. T. & Hogenhout, S. A. (2019) Chemosensory proteins in the CSP4 clade evolved as plant immunity suppressors before two suborders of plant-feeding hemipteran insects diverged. *bioRxiv*, 173278.
- Duan, Q., Kita, D., Li, C., Cheung, A. Y. & Wu, H. M. (2010) FERONIA receptor-like kinase regulates RHO GTPase signaling of root hair development. *Proceedings of the National Academy of Sciences*, 107, 17821-17826.
- Dubiella, U., Seybold, H., Durian, G., Komander, E., Lassig, R., Witte, C.-P., Schulze, W. X. & Romeis, T. (2013) Calcium-dependent protein kinase/NADPH oxidase activation circuit is required for rapid defense signal propagation. *Proceedings of the National Academy of Sciences*, 110, 8744-8749.
- Dubos, C., Huggins, D., Grant, G. H., Knight, M. R. & Campbell, M. M. (2003) A role for glycine in the gating of plant NMDA-like receptors. *The Plant Journal*, 35, 800-810.
- Dünser, K., Gupta, S., Herger, A., Feraru, M. I., Ringli, C. & Kleine-Vehn, J. (2019) Extracellular matrix sensing by FERONIA and leucine-rich repeat extensins controls vacuolar expansion during cellular elongation in *Arabidopsis thaliana*. *The EMBO Journal*, 38, e100353.
- Edel, K. H., Marchadier, E., Brownlee, C., Kudla, J. & Hetherington, A. M. (2017) The evolution of calcium-based signalling in plants. *Current Biology*, 27, R667-R679.
- Ellis, C., Karafyllidis, I. & Turner, J. G. (2002) Constitutive activation of jasmonate signaling in an Arabidopsis mutant correlates with enhanced resistance to *Erysiphe cichoracearum*, *Pseudomonas syringae*, and *Myzus persicae*. *Molecular Plant-Microbe Interactions*, 15, 1025-1030.
- Elmayan, T. & Vaucheret, H. (1996) Expression of single copies of a strongly expressed 35S transgene can be silenced post-transcriptionally. *The Plant Journal*, 9, 787-797.
- Elmore, J. M. & Coaker, G. (2011) The role of the plasma membrane H⁺-ATPase in plant-microbe interactions. *Molecular Plant*, 4, 416-427.

- Elzinga, D. A., De Vos, M. & Jander, G. (2014) Suppression of plant defenses by a *Myzus persicae* (green peach aphid) salivary effector protein. *Molecular Plant-Microbe Interactions*, 27, 747-756.
- Engelsdorf, T., Gigli-Bisceglia, N., Veerabagu, M., Mckenna, J. F., Vaahtera, L., Augstein, F., Does, D. V. D., Zipfel, C. & Hamann, T. (2018a) The plant cell wall integrity maintenance and immune signaling systems cooperate to control stress responses in *Arabidopsis thaliana*. *Science Signaling*, 11, eaao3070.
- Engelsdorf, T., Gigli-Bisceglia, N., Veerabagu, M., Mckenna, J. F., Vaahtera, L., Augstein, F., Van Der Does, D., Zipfel, C. & Hamann, T. (2018b) The plant cell wall integrity maintenance and immune signaling systems cooperate to control stress responses in *Arabidopsis thaliana*. *Science Signaling*, 11, eaao3070.
- Erb, M. & Kliebenstein, D. J. (2020) Plant secondary metabolites as defenses, regulators, and primary metabolites: The blurred functional trichotomy. *Plant Physiology*, 184, 39-52.
- Erb, M., Meldau, S. & Howe, G. A. (2012) Role of phytohormones in insect-specific plant reactions. *Trends in Plant Science*, 17, 250-259.
- Erickson, J., Weckwerth, P., Romeis, T. & Lee, J. (2022) What's new in protein kinase/phosphatase signalling in the control of plant immunity? *Essays in Biochemistry*, 66, 621-634.
- Escobar-Bravo, R., Klinkhamer, P. G. L. & Leiss, K. A. (2017) Induction of jasmonic acid-associated defenses by thrips alters host suitability for conspecifics and correlates with increased trichome densities in tomato. *Plant and Cell Physiology*, 58, 622-634.
- Escudero-Martinez, C., Leybourne, D. J. & Bos, J. I. B. (2021) Plant resistance in different cell layers affects aphid probing and feeding behaviour during non-host and poor-host interactions. *Bulletin of Entomological Research*, 111, 31-38.
- Escudero-Martinez, C., Rodriguez, P. A., Liu, S., Santos, P. A., Stephens, J. & Bos, J. I. B. (2020) An aphid effector promotes barley susceptibility through suppression of defence gene expression. *Journal of Experimental Botany*, 71, 2796-2807.
- Escudero-Martinez, C. M., Morris, J. A., Hedley, P. E. & Bos, J. I. B. (2017) Barley transcriptome analyses upon interaction with different aphid species identify thionins contributing to resistance. *Plant, Cell & Environment*, 40, 2628-2643.
- Espinoza, C., Liang, Y. & Stacey, G. (2017) Chitin receptor CERK1 links salt stress and chitin-triggered innate immunity in *Arabidopsis*. *The Plant Journal*, 89, 984-995.
- Evans, M. J., Choi, W. G., Gilroy, S. & Morris, R. J. (2016) A ROS-assisted calcium wave dependent on the AtrBOHD NADPH oxidase and TPC1 cation channel propagates the systemic response to salt stress. *Plant Physiology*, 171, 1771-1784.
- Falhof, J., Pedersen, Jesper t., Fuglsang, Anja t. & Palmgren, M. (2016) Plasma membrane H⁺-ATPase regulation in the center of plant physiology. *Molecular Plant*, 9, 323-337.
- Fang, X., Liu, B., Shao, Q., Huang, X., Li, J., Luan, S. & He, K. (2021) AtPiezo plays an important role in root cap mechanotransduction. *International journal of molecular sciences*, 22, 467-480.
- Farmer, E. E., Gasperini, D. & Acosta, I. F. (2014) The squeeze cell hypothesis for the activation of jasmonate synthesis in response to wounding. *New Phytologist*, 204, 282-288.
- Farmer, E. E., Mousavi, S. A. & Lenglet, A. (2013) Leaf numbering for experiments on long distance signalling in *Arabidopsis*. *Protocol Exchange*.
- Feehan, J. M., Castel, B., Bentham, A. R. & Jones, J. D. (2020) Plant NLRs get by with a little help from their friends. *Current Opinion in Plant Biology*, 56, 99-108.
- Felix, G., Duran, J. D., Volko, S. & Boller, T. (1999) Plants have a sensitive perception system for the most conserved domain of bacterial flagellin. *The Plant Journal*, 18, 265-276.
- Feng, W., Kita, D., Peaucelle, A., Cartwright, H. N., Doan, V., Duan, Q., Liu, M.-C., Maman, J., Steinhorst, L., Schmitz-Thom, I., Yvon, R., Kudla, J., Wu, H.-M., Cheung, A. Y. & Dinneny, J. R. (2018) The FERONIA receptor kinase maintains cell-wall integrity during salt stress through Ca²⁺ signaling. *Current Biology*, 28, 666-675.e665.
- Fernández-Calvo, P., Chini, A., Fernández-Barbero, G., Chico, J. M., Gimenez-Ibanez, S., Geerinck, J., Eeckhout, D., Schweizer, F., Godoy, M., Franco-Zorrilla, J. M., Pauwels, L., Witters, E.,

- Puga, M. I., Paz-Ares, J., Goossens, A., Reymond, P., De Jaeger, G. & Solano, R. (2011) The Arabidopsis bHLH transcription factors MYC3 and MYC4 are targets of JAZ repressors and act additively with MYC2 in the activation of jasmonate responses. *Plant Cell*, 23, 701-715.
- Fernandez, J. C. & Gilroy, S. (2023) Chapter sixteen - imaging systemic calcium response and its molecular dissection using virus-induced gene silencing. In: JEZ, J. (ed.) *Methods in enzymology*. Academic Press.
- Ferrari, S., Galletti, R., Denoux, C., De Lorenzo, G., Ausubel, F. M. & Dewdney, J. (2007) Resistance to *Botrytis cinerea* induced in Arabidopsis by elicitors is independent of salicylic acid, ethylene, or jasmonate signaling but requires PHYTOALEXIN DEFICIENT3. *Plant Physiology*, 144, 367-379.
- Fichman, Y., Miller, G. & Mittler, R. (2019) Whole-plant live imaging of reactive oxygen species. *Molecular Plant*, 12, 1203-1210.
- Fichman, Y. & Mittler, R. (2021a) Integration of electric, calcium, reactive oxygen species and hydraulic signals during rapid systemic signaling in plants. *The Plant Journal*, 107, 7-20.
- Fichman, Y. & Mittler, R. (2021b) A systemic whole-plant change in redox levels accompanies the rapid systemic response to wounding. *Plant Physiology*, 186, 4-8.
- Fichman, Y., Myers, R. J., Grant, D. G. & Mittler, R. (2020) Plasmodesmata-localized proteins and reactive oxygen species orchestrate light-induced rapid systemic signaling in Arabidopsis. *bioRxiv*.
- Fonseca, S., Chini, A., Hamberg, M., Adie, B., Porzel, A., Kramell, R., Miersch, O., Wasternack, C. & Solano, R. (2009) (+)-7-iso-jasmonoyl-l-isoleucine is the endogenous bioactive jasmonate. *Nature Chemical Biology*, 5, 344-350.
- Forbes, A. R. (1966) Electron microscope evidence for nerves in the mandibular stylets of the green peach aphid. *Nature*, 212, 726-726.
- Forbes, A. R. (1969) The stylets of the green peach aphid, *Myzus persicae* (Homoptera, Aphididae) *The Canadian Entomologist*, 101, 31-41.
- Forbes, A. R. (1977) Chapter 3 - the mouthparts and feeding mechanism of aphids. In: HARRIS, K. F. & MARAMOROSCH, K. (eds.) *Aphids as virus vectors*. Academic Press.
- Fotouhi, N., Fischer-Stettler, M., Lenzone, G., Stolz, S., Glauser, G., Zeeman, S. C. & Farmer, E. E. (2022) ACA pumps maintain leaf excitability during herbivore onslaught. *Current Biology*, 32, 2517-2528.
- Frei Dit Frey, N., Mbengue, M., Kwaaitaal, M., Nitsch, L., Altenbach, D., Häweker, H., Lozano-Duran, R., Njo, M. F., Beeckman, T., Huettel, B., Borst, J. W., Panstruga, R. & Robertzek, S. (2012) Plasma membrane calcium ATPases are important components of receptor-mediated signaling in plant immune responses and development. *Plant Physiology*, 159, 798-809.
- Fu, Z. Q., Yan, S., Saleh, A., Wang, W., Ruble, J., Oka, N., Mohan, R., Spoel, S. H., Tada, Y. & Zheng, N. (2012) NPR3 and NPR4 are receptors for the immune signal salicylic acid in plants. *Nature*, 486, 228-232.
- Fuglsang, A. T. & Palmgren, M. (2021) Proton and calcium pumping P-type ATPases and their regulation of plant responses to the environment. *Plant Physiology*, 187, 1856-1875.
- Galletti, R., Denoux, C., Gambetta, S., Dewdney, J., Ausubel, F. M., De Lorenzo, G. & Ferrari, S. (2008) The AtrbohD-mediated oxidative burst elicited by oligogalacturonides in Arabidopsis is dispensable for the activation of defense responses effective against *Botrytis cinerea*. *Plant Physiology*, 148, 1695-1706.
- Galletti, R., Ferrari, S. & De Lorenzo, G. (2011) Arabidopsis MPK3 and MPK6 play different roles in basal and oligogalacturonide- or flagellin-induced resistance against *Botrytis cinerea*. *Plant Physiology*, 157, 804-814.
- Galon, Y., Nave, R., Boyce, J. M., Nachmias, D., Knight, M. R. & Fromm, H. (2008) Calmodulin-binding transcription activator (CAMTA) 3 mediates biotic defense responses in Arabidopsis. *FEBS Letters*, 582, 943-948.

- Gangwar, S. P., Green, M. N., Michard, E., Simon, A. A., Feijó, J. A. & Sobolevsky, A. I. (2021) Structure of the *Arabidopsis* glutamate receptor-like channel GLR3.2 ligand-binding domain. *Structure*, 29, 161-169.
- Gao, L. L., Anderson, J. P., Klingler, J. P., Nair, R. M., Edwards, O. R. & Singh, K. B. (2007) Involvement of the octadecanoid pathway in bluegreen aphid resistance in *Medicago truncatula*. *Molecular Plant-Microbe Interactions*, 20, 82-93.
- Gao, M., Wang, X., Wang, D., Xu, F., Ding, X., Zhang, Z., Bi, D., Cheng, Y. T., Chen, S., Li, X. & Zhang, Y. (2009) Regulation of cell death and innate immunity by two receptor-like kinases in *Arabidopsis*. *Cell Host Microbe*, 6, 34-44.
- Gao, Y.-Q., Jimenez-Sandoval, P., Tiwari, S., Stolz, S., Wang, J., Glauser, G., Santiago, J. & Farmer, E. E. (2023) Ricca's factors as mobile proteinaceous effectors of electrical signaling. *Cell*.
- Gao, Y., Lei, Z. & Reitz, S. R. (2012) Western flower thrips resistance to insecticides: Detection, mechanisms and management strategies. *Pest Management Science*, 68, 1111-1121.
- Gao, Y., Li, Z., Yang, C., Li, G., Zeng, H., Li, Z., Zhang, Y. & Yang, X. (2022) *Pseudomonas syringae* activates ZAT18 to inhibit salicylic acid accumulation by repressing EDS1 transcription for bacterial infection. *New Phytologist*, 233, 1274-1288.
- García Bossi, J., Kumar, K., Barberini, M. L., Domínguez, G. D., Rondón Guerrero, Y. D. C., Marino-Buslje, C., Obertello, M., Muschiatti, J. P. & Estevez, J. M. (2019) The role of P-type IIA and P-type IIB Ca²⁺-ATPases in plant development and growth. *Journal of Experimental Botany*, 71, 1239-1248.
- Gasparini, D., Chauvin, A., Acosta, I. F., Kurenda, A., Stolz, S., Chételat, A., Wolfender, J.-L. & Farmer, E. E. (2015) Axial and radial oxylipin transport. *Plant Physiology*, 169, 2244-2254.
- Geilfus, C.-M. (2017) The pH of the apoplast: Dynamic factor with functional impact under stress. *Molecular Plant*, 10, 1371-1386.
- Geilfus, C. M., Tenhaken, R. & Carpentier, S. C. (2017) Transient alkalization of the leaf apoplast stiffens the cell wall during onset of chloride salinity in corn leaves. *The Journal of biological chemistry*, 292, 18800-18813.
- George, L., Romanowsky, S. M., Harper, J. F. & Sharrock, R. A. (2008) The ACA10 Ca²⁺-ATPase regulates adult vegetative development and inflorescence architecture in *Arabidopsis*. *Plant Physiology* 146, 716-728.
- Ghosh, S., Bheri, M., Bisht, D. & Pandey, G. K. (2022) Calcium signaling and transport machinery: Potential for development of stress tolerance in plants. *Current Plant Biology*, 29, 100235.
- Gilroy, S., Białasek, M., Suzuki, N., Górecka, M., Devireddy, A. R., Karpiński, S. & Mittler, R. (2016) ROS, calcium, and electric signals: Key mediators of rapid systemic signaling in plants. *Plant Physiology*, 171, 1606-1615.
- Giolai, M. (2019) *Spatially resolved transcriptomics reveals plant host responses to the aphid pest Myzus persicae*. Doctor of Philosophy (PhD), University of East Anglia.
- Gjetting, S. K., Mahmood, K., Shabala, L., Kristensen, A., Shabala, S., Palmgren, M. & Fuglsang, A. T. (2020) Evidence for multiple receptors mediating RALF-triggered Ca²⁺ signaling and proton pump inhibition. *The Plant Journal*, 104, 433-446.
- Gjetting, S. K., Ytting, C. K., Schulz, A. & Fuglsang, A. T. (2012) Live imaging of intra- and extracellular pH in plants using pHusion, a novel genetically encoded biosensor. *Journal of Experimental Botany*, 63, 3207-3218.
- Glauser, G., Dubugnon, L., Mousavi, S. A., Rudaz, S., Wolfender, J. L. & Farmer, E. E. (2009) Velocity estimates for signal propagation leading to systemic jasmonic acid accumulation in wounded *Arabidopsis*. *Journal of Biological Chemistry*, 284, 34506-34513.
- Glauser, G., Grata, E., Dubugnon, L., Rudaz, S., Farmer, E. E. & Wolfender, J. L. (2008) Spatial and temporal dynamics of jasmonate synthesis and accumulation in *Arabidopsis* in response to wounding. *The Journal of biological chemistry*, 283, 16400-16407.

- Glauser, G., Schweizer, F., Turlings, T. C. & Reymond, P. (2012) Rapid profiling of intact glucosinolates in *Arabidopsis* leaves by UHPLC-QTOFMS using a charged surface hybrid column. *Phytochem Analysis*, 23, 520-528.
- Gleason, C., Leelarasamee, N., Meldau, D. & Feussner, I. (2016) OPDA has key role in regulating plant susceptibility to the root-knot nematode *Meloidogyne hapla* in *Arabidopsis*. *Frontiers in Plant Science*, 7, 1565.
- Gobert, A., Isayenkov, S., Voelker, C., Czempinski, K. & Maathuis, F. J. M. (2007) The two-pore channel *TPK1* gene encodes the vacuolar K⁺ conductance and plays a role in K⁺ homeostasis. *Proceedings of the National Academy of Sciences*, 104, 10726-10731.
- Goggin, F. L. & Fischer, H. D. (2022) Reactive oxygen species in plant interactions with aphids. *Frontiers in Plant Science*, 12, 3255.
- Goggin, F. L., Jia, L., Shah, G., Hebert, S., Williamson, V. M. & Ullman, D. E. (2006) Heterologous expression of the *Mi-1.2* gene from tomato confers resistance against nematodes but not aphids in eggplant. *Molecular Plant-Microbe Interactions*, 19, 383-388.
- Gómez-Gómez, L., Felix, G. & Boller, T. (1999) A single locus determines sensitivity to bacterial flagellin in *Arabidopsis thaliana*. *The Plant Journal: For Cell and Molecular Biology*, 18, 277-284.
- Gonneau, M., Desprez, T., Martin, M., Doblaz, V. G., Bacete, L., Miart, F., Sormani, R., Hématy, K., Renou, J., Landrein, B., Murphy, E., Van De Cotte, B., Vernhettes, S., De Smet, I. & Höfte, H. (2018) Receptor kinase THESEUS1 is a Rapid Alkalinization Factor 34 receptor in *Arabidopsis*. *Current Biology*, 28, 2452-2458.e2454.
- Goto, Y., Maki, N., Ichihashi, Y., Kitazawa, D., Igarashi, D., Kadota, Y. & Shirasu, K. (2020) Exogenous treatment with glutamate induces immune responses in *Arabidopsis*. *Molecular Plant-Microbe Interactions*, 33, 474-487.
- Gradogna, A., Scholz-Starke, J., Gutla, P. V. K. & Carpaneto, A. (2009) Fluorescence combined with excised patch: Measuring calcium currents in plant cation channels. *The Plant Journal*, 58, 175-182.
- Gravino, M., Locci, F., Tundo, S., Cervone, F., Savatin, D. V. & De Lorenzo, G. (2017) Immune responses induced by oligogalacturonides are differentially affected by AvrPto and loss of BAK1/BKK1 and PEPR1/PEPR2. *Molecular Plant Pathology*, 18, 582-595.
- Green, M. N., Gangwar, S. P., Michard, E., Simon, A. A., Portes, M. T., Barbosa-Caro, J., Wudick, M. M., Lizzio, M. A., Klykov, O., Yelshanskaya, M. V., Feijó, J. A. & Sobolevsky, A. I. (2021) Structure of the *Arabidopsis thaliana* glutamate receptor-like channel GLR3.4. *Molecular Cell*, 81, 3216-3226.
- Green, T. R. & Ryan, C. A. (1972) Wound-induced proteinase inhibitor in plant leaves: A possible defense mechanism against insects. *Science*, 175, 776-777.
- Grenzi, M., Buratti, S., Parmagnani, A. S., Abdel Aziz, I., Bernacka-Wojcik, I., Resentini, F., Šimura, J., Doccula, F. G., Alfieri, A., Luoni, L., Ljung, K., Bonza, M. C., Stavrinidou, E. & Costa, A. (2023) Long-distance turgor pressure changes induce local activation of plant glutamate receptor-like channels. *Current Biology*.
- Grenzi, M., Resentini, F., Vanneste, S., Zottini, M., Bassi, A. & Costa, A. (2021) Illuminating the hidden world of calcium ions in plants with a universe of indicators. *Plant Physiology*, 187, 550-571.
- Griffiths, G. (2020) Jasmonates: Biosynthesis, perception and signal transduction. *Essays in Biochemistry*, 64, 501-512.
- Guerrieri, E. & Digilio, M. C. (2008) Aphid-plant interactions: A review. *Journal of Plant Interactions*, 3, 223-232.
- Guichard, M., Thomine, S. & Frachisse, J.-M. (2022) Mechanotransduction in the spotlight of mechano-sensitive channels. *Current Opinion in Plant Biology*, 68, 102252.
- Gully, K., Pelletier, S., Guillou, M. C., Ferrand, M., Aligon, S., Pokotylo, I., Perrin, A., Vergne, E., Fagard, M., Ruelland, E., Grappin, P., Bucher, E., Renou, J. P. & Aubourg, S. (2019) The SCOOP12 peptide regulates defense response and root elongation in *Arabidopsis thaliana*. *Journal of Experimental Botany*, 70, 1349-1365.

- Guo, H., Nolan, T. M., Song, G., Liu, S., Xie, Z., Chen, J., Schnable, P. S., Walley, J. W. & Yin, Y. (2018) FERONIA receptor kinase contributes to plant immunity by suppressing jasmonic acid signaling in *Arabidopsis thaliana*. *Current Biology*, 28, 3316-3324.
- Guo, J., He, J., Dehesh, K., Cui, X. & Yang, Z. (2022) Camellia-based simultaneous imaging of Ca²⁺ dynamics in subcellular compartments. *Plant Physiology*, 188, 2253-2271.
- Guo, J., Zeng, W., Chen, Q., Lee, C., Chen, L., Yang, Y., Cang, C., Ren, D. & Jiang, Y. (2016) Structure of the voltage-gated two-pore channel TPC1 from *Arabidopsis thaliana*. *Nature*, 531, 196-201.
- Gupta, A., Bhardwaj, M. & Tran, L. P. (2020) Jasmonic acid at the crossroads of plant immunity and *Pseudomonas syringae* virulence. *International Journal of Molecular Sciences* 21, 7482.
- Gust, A. A., Biswas, R., Lenz, H. D., Rauhut, T., Ranf, S., Kemmerling, B., Götz, F., Glawischnig, E., Lee, J., Felix, G. & Nürnberger, T. (2007) Bacteria-derived peptidoglycans constitute pathogen-associated molecular patterns triggering innate immunity in *Arabidopsis*. *Journal of Biological Chemistry*, 282, 32338-32348.
- Hagihara, T., Mano, H., Miura, T., Hasebe, M. & Toyota, M. (2022) Calcium-mediated rapid movements defend against herbivorous insects in *Mimosa pudica*. *Nature Communications*, 13, 6412-6421.
- Hamant, O. & Haswell, E. S. (2017) Life behind the wall: Sensing mechanical cues in plants. *BMC Biology*, 15.
- Hamilton, E. S., Jensen, G. S., Maksaev, G., Katims, A., Shero, A. M. & Haswell, E. S. (2015a) Mechanosensitive channel MSL8 regulates osmotic forces during pollen hydration and germination. *Science*, 350, 438-441.
- Hamilton, E. S., Schlegel, A. M. & Haswell, E. S. (2015b) United in diversity: Mechanosensitive ion channels in plants. *Annual Review of Plant Biology*, 66, 113-137.
- Hander, T., Fernández-Fernández, Á. D., Kumpf, R. P., Willems, P., Schatowitz, H., Rombaut, D., Staes, A., Nolf, J., Pottier, R., Yao, P., Gonçalves, A., Pavie, B., Boller, T., Gevaert, K., Van Breusegem, F., Bartels, S. & Stael, S. (2019) Damage on plants activates Ca²⁺-dependent metacaspases for release of immunomodulatory peptides. *Science*, 363, eaar7486.
- Hardy, N. B., Peterson, D. A. & Von Dohlen, C. D. (2015) The evolution of life cycle complexity in aphids: Ecological optimization or historical constraint? *Evolution*, 69, 1423-1432.
- Harris, K. F. & Maramorosch, K. (2014) *Aphids as virus vectors*, Elsevier Science.
- Hartmann, F. P., Tinturier, E., Julien, J.-L. & Leblanc-Fournier, N. (2021) Between stress and response: Function and localization of mechanosensitive Ca²⁺ channels in herbaceous and perennial plants. *International journal of molecular sciences*, 22, 11043.
- Hartmann, M., Zeier, T., Bernsdorff, F., Reichel-Deland, V., Kim, D., Hohmann, M., Scholten, N., Schuck, S., Bräutigam, A. & Hölzel, T. (2018) Flavin monooxygenase-generated N-hydroxypipicolinic acid is a critical element of plant systemic immunity. *Cell*, 173, 456-469. e416.
- Haruta, M., Sabat, G., Stecker, K., Minkoff, B. B. & Sussman, M. R. (2014) A peptide hormone and its receptor protein kinase regulate plant cell expansion. *Science*, 343, 408-411.
- Haswell, E. S., Peyronnet, R., Barbier-Brygoo, H., Meyerowitz, E. M. & Frachisse, J.-M. (2008) Two MscS homologs provide mechanosensitive channel activities in the *Arabidopsis* root. *Current Biology*, 18, 730-734.
- Hatsugai, N., Igarashi, D., Mase, K., Lu, Y., Tsuda, Y., Chakravarthy, S., Wei, H. L., Foley, J. W., Collmer, A. & Glazebrook, J. (2017) A plant effector-triggered immunity signaling sector is inhibited by pattern-triggered immunity. *The EMBO Journal*, 36, 2758-2769.
- Hattori, T., Otomi, Y., Nakajima, Y., Soga, K., Wakabayashi, K., Iida, H. & Hoson, T. (2020) MCA1 and MCA2 are involved in the response to hypergravity in *Arabidopsis* hypocotyls. *Plants* 9, 590.
- Havko, N. E., Kapali, G., Das, M. R. & Howe, G. A. (2020) Stimulation of insect herbivory by elevated temperature outweighs protection by the jasmonate pathway. *Plants*, 9, 172.

- Havshøi, N. W. & Fuglsang, A. T. (2022) A critical review on natural compounds interacting with the plant plasma membrane H⁺-ATPase and their potential as biologicals in agriculture. *Journal of Integrative Plant Biology*, 64, 268-286.
- He, Z., Guo, J. F., Reitz, S. R., Lei, Z. R. & Wu, S. Y. (2020) A global invasion by the thrip, *Frankliniella occidentalis*: Current virus vector status and its management. *Insect Science*, 27, 626-645.
- Hedrich, R. & Neher, E. (1987) Cytoplasmic calcium regulates voltage-dependent ion channels in plant vacuoles. *Nature*, 329, 833-836.
- Heming, B. S. (1978) Structure and function of the mouthparts in larvae of *Haplothrips verbasci* (Osborn) (Thysanoptera, Tubulifera, Phlaeothripidae). *Journal of Morphology*, 156, 1-37.
- Hewer, A., Becker, A. & Van Bel, A. J. E. (2011) An aphid's odyssey – the cortical quest for the vascular bundle. *Journal of Experimental Biology*, 214, 3868-3879.
- Hewer, A., Will, T. & Van Bel, A. J. E. (2010) Plant cues for aphid navigation in vascular tissues. *Journal of Experimental Biology*, 213, 4030-4042.
- Hilleary, R. & Gilroy, S. (2018) Systemic signaling in response to wounding and pathogens. *Current Opinion in Plant Biology*, 43, 57-62.
- Hilleary, R., Paez-Valencia, J., Vens, C., Toyota, M., Palmgren, M. & Gilroy, S. (2020) Tonoplast-localized Ca²⁺ pumps regulate Ca²⁺ signals during pattern-triggered immunity in *Arabidopsis thaliana*. *Proceedings of the National Academy of Sciences*, 117, 18849-18857.
- Himschoot, E., Krebs, M., Costa, A., Beeckman, T. & Vanneste, S. (2018) Calcium ion dynamics in roots: Imaging and analysis. In: RISTOVA, D. & BARBEZ, E. (eds.) *Root development: Methods and protocols*. New York, NY: Springer New York.
- Hirner, A., Ladwig, F., Stransky, H., Okumoto, S., Keinath, M., Harms, A., Frommer, W. B. & Koch, W. (2006) Arabidopsis LHT1 is a high-affinity transporter for cellular amino acid uptake in both root epidermis and leaf mesophyll. *The Plant Cell*, 18, 1931-1946.
- Hocking, B., Conn, S. J., Manohar, M., Xu, B., Athman, A., Stancombe, M. A., Webb, A. R., Hirschi, K. D. & Gilliam, M. (2017) Heterodimerization of Arabidopsis calcium/proton exchangers contributes to regulation of guard cell dynamics and plant defense responses. *Journal of Experimental Botany*, 68, 4171-4183.
- Hoermayer, L., Montesinos, J. C., Marhava, P., Benková, E., Yoshida, S. & Friml, J. (2020) Wounding-induced changes in cellular pressure and localized auxin signalling spatially coordinate restorative divisions in roots. *Proceedings of the National Academy of Sciences*, 117, 15322-15331.
- Hong, F., Han, H.-L., Pu, P., Wei, D., Wang, J. & Liu, Y. (2019) Effects of five host plant species on the life history and population growth parameters of *Myzus persicae* (Hemiptera: Aphididae). *Journal of Insect Science*, 19, 15.
- Horsefield, S., Burdett, H., Zhang, X., Manik, M. K., Shi, Y., Chen, J., Qi, T., Gilley, J., Lai, J. S., Rank, M. X., Casey, L. W., Gu, W., Ericsson, D. J., Foley, G., Hughes, R. O., Bosanac, T., Von Itzstein, M., Rathjen, J. P., Nanson, J. D., Boden, M., Dry, I. B., Williams, S. J., Staskawicz, B. J., Coleman, M. P., Ve, T., Dodds, P. N. & Kobe, B. (2019) NAD(+) cleavage activity by animal and plant TIR domains in cell death pathways. *Science*, 365, 793-799.
- Hou, S., Liu, D. & He, P. (2021a) Phytocytokines function as immunological modulators of plant immunity. *Stress Biology*, 1, 8.
- Hou, S., Liu, D., Huang, S., Luo, D., Liu, Z., Xiang, Q., Wang, P., Mu, R., Han, Z., Chen, S., Chai, J., Shan, L. & He, P. (2021b) The Arabidopsis MIK2 receptor elicits immunity by sensing a conserved signature from phytocytokines and microbes. *Nature Communications*, 12, 5494.
- Hou, S. & Tsuda, K. (2022) Salicylic acid and jasmonic acid crosstalk in plant immunity. *Essays in Biochemistry*, 66, 647-656.
- Hou, S., Wang, X., Chen, D., Yang, X., Wang, M., Turrà, D., Di Pietro, A. & Zhang, W. (2014) The secreted peptide PIP1 amplifies immunity through Receptor-Like kinase 7. *PLoS Pathogens*, 10, e1004331.

- Hsu, P. K., Takahashi, Y., Munemasa, S., Merilo, E., Laanemets, K., Waadt, R., Pater, D., Kollist, H. & Schroeder, J. I. (2018) Abscisic acid-independent stomatal CO₂ signal transduction pathway and convergence of CO₂ and ABA signaling downstream of OST1 kinase. *Proceedings of the National Academy of Sciences*, 115, E9971-e9980.
- Hu, M., Qi, J., Bi, G. & Zhou, J.-M. (2020) Bacterial effectors induce oligomerization of immune receptor ZAR1 in vivo. *Molecular Plant*, 13, 793-801.
- Huang, W., Wang, Y., Li, X. & Zhang, Y. (2020) Biosynthesis and regulation of salicylic acid and N-Hydroxypipicolinic acid in plant immunity. *Molecular Plant*, 13, 31-41.
- Huck, N., Moore, J. M., Federer, M. & Grossniklaus, U. (2003) The Arabidopsis mutant *feronia* disrupts the female gametophytic control of pollen tube reception. *Development*, 130, 2149-2159.
- Huep, G., Kleinboelting, N. & Weisshaar, B. (2014) An easy-to-use primer design tool to address paralogous loci and T-DNA insertion sites in the genome of *Arabidopsis thaliana*. *Plant Methods*, 10, 28.
- Huffaker, A., Pearce, G. & Ryan, C. A. (2006) An endogenous peptide signal in Arabidopsis activates components of the innate immune response. *Proceedings of the National Academy of Sciences*, 103, 10098-10103.
- Hunter, W. B. & Ullman, D. E. (1989) Analysis of mouthpart movements during feeding of *Frankliniella occidentalis* (Pergande) and *F. schultzei* Trybom (Thysanoptera: Thripidae). *International Journal of Insect Morphology and Embryology*, 18, 161-171.
- Hunter, W. B. & Ullman, D. E. (1992) Anatomy and ultrastructure of the piercing-sucking mouthparts and paraglossal sensilla of *Frankliniella occidentalis* (Pergande) (Thysanoptera: Thripidae). *International Journal of Insect Morphology and Embryology*, 21, 17-35.
- Hunter, W. B. & Ullman, D. E. (1994) Precibarial and cibarial chemosensilla in the western flower thrips, *Frankliniella occidentalis* (Pergande) (Thysanoptera: Thripidae). *International Journal of Insect Morphology and Embryology*, 23, 69-83.
- Huot, B., Yao, J., Montgomery, B. L. & He, S. Y. (2014) Growth–defense tradeoffs in plants: A balancing act to optimize fitness. *Molecular Plant*, 7, 1267-1287.
- Iizasa, E., Mitsutomi, M. & Nagano, Y. (2010) Direct binding of a plant LysM receptor-like kinase, LysM RLK1/CERK1, to chitin in vitro. *The Journal of Biological Chemistry* 285, 2996-3004.
- Isner, J. C., Begum, A., Nuehse, T., Hetherington, A. M. & Maathuis, F. J. M. (2018) KIN7 kinase regulates the vacuolar TPK1 K⁺ channel during stomatal closure. *Current Biology*, 28, 466-472.e464.
- Jacob, P., Kim, N. H., Wu, F., El-Kasbi, F., Chi, Y., Walton, W. G., Furzer, O. J., Lietzan, A. D., Sunil, S., Kempthorn, K., Redinbo, M. R., Pei, Z. M., Wan, L. & Dangl, J. L. (2021) Plant "helper" immune receptors are Ca²⁺-permeable nonselective cation channels. *Science*, 373, 420-425.
- Jaouannet, M., Morris, J. A., Hedley, P. E. & Bos, J. I. B. (2015) Characterization of Arabidopsis transcriptional responses to different aphid species reveals genes that contribute to host susceptibility and non-host resistance. *PLoS Pathogens*, 11, e1004918.
- Jarratt-Barnham, E., Wang, L., Ning, Y. & Davies, J. M. (2021) The complex story of plant cyclic nucleotide-gated channels. *International Journal of Molecular Sciences* 22, 874.
- Jašlan, D., Dreyer, I., Lu, J., O'malley, R., Dindas, J., Marten, I. & Hedrich, R. (2019) Voltage-dependent gating of SV channel TPC1 confers vacuole excitability. *Nature Communications*, 10, 2659-2768.
- Jayaraman, D., Gilroy, S. & Ané, J.-M. (2014) Staying in touch: Mechanical signals in plant–microbe interactions. *Current Opinion in Plant Biology*, 20, 104-109.
- Jeworutzki, E., Roelfsema, M. R. G., Anschutz, U., Krol, E., Elzenga, J. T. M., Felix, G., Boller, T., Hedrich, R. & Becker, D. (2010) Early signaling through the Arabidopsis pattern recognition receptors FLS2 and EFR involves Ca²⁺-associated opening of plasma membrane anion channels. *The Plant Journal*, 62, 367-378.

- Jhou, Y. S., Poovendhan, S., Huang, L. H. & Tsai, C. W. (2021) Host acceptance and plant resistance: A comparative behavioral study of *Myzus persicae* and *Acyrtosiphon pisum*. *Insects*, 12.
- Jiang, X., Hoehenwarter, W., Scheel, D. & Lee, J. (2020) Phosphorylation of the CAMTA3 transcription factor triggers its destabilization and nuclear export. *Plant Physiology*, 184, 1056-1071.
- Jiang, Y. & Ding, P. (2023) Calcium signaling in plant immunity: A spatiotemporally controlled symphony. *Trends in Plant Science*, 28, 74-89.
- Jiao, C., Li, K., Zuo, Y., Gong, J., Guo, Z. & Shen, Y. (2022) CALMODULIN1 and WRKY53 function in plant defense by negatively regulating the jasmonic acid biosynthesis pathway in Arabidopsis. *International journal of molecular sciences*, 23, 7718.
- Johns, S., Hagihara, T., Toyota, M. & Gilroy, S. (2021) The fast and the furious: Rapid long-range signaling in plants. *Plant Physiology*, 185, 694–706.
- Jojoa-Cruz, S., Saotome, K., Murthy, S. E., Tsui, C. C. A., Sansom, M. S. P., Patapoutian, A. & Ward, A. B. (2018) Cryo-EM structure of the mechanically activated ion channel OSCA1.2. *eLife*, 7, e41845.
- Jones, A. C., Felton, G. W. & Tumlinson, J. H. (2022) The dual function of elicitors and effectors from insects: Reviewing the ‘arms race’ against plant defenses. *Plant Molecular Biology*, 109, 427-445.
- Jones, D. R. (2005) Plant viruses transmitted by thrips. *European Journal of Plant Pathology*, 113, 119-157.
- Jones, J. D. & Dangl, J. L. (2006) The plant immune system. *Nature*, 444, 323-329.
- Jongsma, M. A., Thoen, M. P. M., Poleij, L. M., Wiegers, G. L., Goedhart, P. W., Dicke, M., Noldus, L. P. J. J. & Kruisselbrink, J. W. (2019) An integrated system for the automated recording and analysis of insect behavior in T-maze arrays. *Frontiers in Plant Science*, 10.
- Jose, J., Ghantasala, S. & Roy Choudhury, S. (2020) Arabidopsis transmembrane Receptor-Like kinases (RLKs): A bridge between extracellular signal and intracellular regulatory machinery. *International journal of molecular sciences*, 21, 4000.
- Joucla, S., Franconville, R., Pippow, A., Kloppenburg, P. & Pouzat, C. (2013) Estimating background-subtracted fluorescence transients in calcium imaging experiments: A quantitative approach. *Cell Calcium*, 54, 71-85.
- Julkowska, M. M., Klei, K., Fokkens, L., Haring, M. A., Schranz, M. E. & Testerink, C. (2016) Natural variation in rosette size under salt stress conditions corresponds to developmental differences between Arabidopsis accessions and allelic variation in the LRR-KISS gene. *Journal of Experimental Botany*, 67, 2127-2138.
- Kadota, Y., Shirasu, K. & Zipfel, C. (2015) Regulation of the NADPH oxidase RBOHD during plant immunity. *Plant and Cell Physiology*, 56, 1472-1480.
- Kadota, Y., Sklenar, J., Derbyshire, P., Stransfeld, L., Asai, S., Ntoukakis, V., Jones, J. D., Shirasu, K., Menke, F., Jones, A. & Zipfel, C. (2014) Direct regulation of the NADPH oxidase RBOHD by the PRR-associated kinase BIK1 during plant immunity. *Molecular Cell*, 54, 43-55.
- Kaloshian, I., Kinsey, M. G., Williamson, V. M. & Ullman, D. E. (2000) Mi-mediated resistance against the potato aphid *Macrosiphum euphorbiae* (Hemiptera: Aphididae) limits sieve element ingestion. *Environmental Entomology*, 29, 690-695.
- Kamano, S., Kume, S., Iida, K., Lei, K. J., Nakano, M., Nakayama, Y. & Iida, H. (2015) Transmembrane topologies of Ca²⁺-permeable mechanosensitive channels MCA1 and MCA2 in *Arabidopsis thaliana*. *The Journal of Biological Chemistry* 290, 30901-30909.
- Kamphuis, L., Guo, S.-M., Gao, L.-L. & Singh, K. (2016) Genetic mapping of a major resistance gene to pea aphid (*Acyrtosiphon pisum*) in the model legume *Medicago truncatula*. *International journal of molecular sciences*, 17, 1224.
- Kanvil, S., Collins, C. M., Powell, G. & Turnbull, C. G. (2015) Cryptic virulence and avirulence alleles revealed by controlled sexual recombination in pea aphids. *Genetics*, 199, 581-593.

- Kato, H., Nemoto, K., Shimizu, M., Abe, A., Asai, S., Ishihama, N., Matsuoka, S., Daimon, T., Ojika, M., Kawakita, K., Onai, K., Shirasu, K., Yoshida, M., Ishiura, M., Takemoto, D., Takano, Y. & Terauchi, R. (2022) Recognition of pathogen-derived sphingolipids in Arabidopsis. *Science*, 376, 857-860.
- Kazan, K. & Manners, J. M. (2013) MYC2: The master in action. *Molecular Plant*, 6, 686-703.
- Kazana, E., Pope, T. W., Tibbles, L., Bridges, M., Pickett, J. A., Bones, A. M., Powell, G. & Rossiter, J. T. (2007) The cabbage aphid: A walking mustard oil bomb. *Proceedings. Biological sciences*, 274, 2271-2277.
- Keinath, N. F., Kierszniowska, S., Lorek, J., Bourdais, G., Kessler, S. A., Shimosato-Asano, H., Grossniklaus, U., Schulze, W. X., Robatzek, S. & Panstruga, R. (2010) PAMP (pathogen-associated molecular pattern)-induced changes in plasma membrane compartmentalization reveal novel components of plant immunity. *The Journal of Biological Chemistry* 285, 39140-39149.
- Keinath, N. F., Waadt, R., Brugman, R., Schroeder, Julian i., Grossmann, G., Schumacher, K. & Krebs, M. (2015) Live cell imaging with R-GECO1 sheds light on flg22- and chitin-induced transient [Ca²⁺]_{cyt} patterns in Arabidopsis. *Molecular Plant*, 8, 1188-1200.
- Kelner, A., Leitão, N., Chabaud, M., Charpentier, M. & De Carvalho-Niebel, F. (2018) Dual color sensors for simultaneous analysis of calcium signal dynamics in the nuclear and cytoplasmic compartments of plant cells. *Frontiers in Plant Science*, 9.
- Kesarwani, M., Yoo, J. & Dong, X. (2007) Genetic interactions of TGA transcription factors in the regulation of pathogenesis-related genes and disease resistance in Arabidopsis. *Plant Physiology*, 144, 336-346.
- Kesten, C., Gámez-Arjona, F. M., Menna, A., Scholl, S., Dora, S., Huerta, A. I., Huang, H.-Y., Tintor, N., Kinoshita, T., Rep, M., Krebs, M., Schumacher, K. & Sánchez-Rodríguez, C. (2019) Pathogen-induced pH changes regulate the growth-defense balance in plants. *The EMBO Journal*, 38, e101822.
- Kettles, G. J., Drurey, C., Schoonbeek, H.-J., Maule, A. J. & Hogenhout, S. A. (2013) Resistance of *Arabidopsis thaliana* to the green peach aphid, *Myzus persicae*, involves camalexin and is regulated by microRNAs. *The New Phytologist*, 198, 1178-1190.
- Khan, A. M., Khan, A. A., Afzal, M. & Iqbal, M. S. (2012) Wheat crop yield losses caused by the aphids infestation. *Journal of Biofertilizers & Biopesticides* 3, 1-7.
- Kiep, V., Vadassery, J., Lattke, J., Maass, J. P., Boland, W., Peiter, E. & Mithofer, A. (2015) Systemic cytosolic Ca²⁺ elevation is activated upon wounding and herbivory in Arabidopsis. *New Phytologist*, 207, 996-1004.
- Kim, J. H. & Jander, G. (2007) *Myzus persicae* (green peach aphid) feeding on Arabidopsis induces the formation of a deterrent indole glucosinolate. *The Plant Journal*, 49, 1008-1019.
- Kindt, F., Joosten, N. N., Peters, D. & Tjallingii, W. F. (2003) Characterisation of the feeding behaviour of western flower thrips in terms of electrical penetration graph (EPG) waveforms. *Journal of Insect Physiology*, 49, 183-191.
- Kindt, F., Joosten, N. N. & Tjallingii, W. F. (2006) Electrical penetration graphs of thrips revised: Combining DC- and AC-EPG signals. *Journal of Insect Physiology*, 52, 1-10.
- Kinoshita, N. & Betsuyaku, S. (2018) The effects of lepidopteran oral secretion on plant wounds: A case study on the interaction between *Spodoptera litura* and *Arabidopsis thaliana*. *Plant Biotechnology*, 35, 237-242.
- Klauser, D., Flury, P., Boller, T., Bartels, S., Vallat, A., Glauser, G., Desurmont, G. A. & Turlings, T. C. J. (2015) The Arabidopsis Pep-PEPR system is induced by herbivore feeding and contributes to JA-mediated plant defence against herbivory. *Journal of Experimental Botany*, 66, 5327-5336.
- Klingauf, F. A. (1987) Feeding, adaptation and excretion. *Aphids: Their Biology, Natural Enemies, and Control*, 225-253.
- Kluyver, T., Ragan-Kelley, B., Pérez, F., Granger, B. E., Bussonnier, M., Frederic, J., Kelley, K., Hamrick, J. B., Grout, J. & Corlay, S. (2016) *Jupyter notebooks-a publishing format for reproducible computational workflows*.

- Knight, M. R., Campbell, A. K., Smith, S. M. & Trewavas, A. J. (1991) Transgenic plant aequorin reports the effects of touch and cold-shock and elicitors on cytoplasmic calcium. *Nature*, 352, 524-526.
- Kohorn, B. D., Johansen, S., Shishido, A., Todorova, T., Martinez, R., Defeo, E. & Obregon, P. (2009) Pectin activation of MAP kinase and gene expression is WAK2 dependent. *The Plant Journal*, 60, 974-982.
- Koo, A. J., Gao, X., Jones, A. D. & Howe, G. A. (2009) A rapid wound signal activates the systemic synthesis of bioactive jasmonates in Arabidopsis. *The Plant Journal*, 59, 974-986.
- Koo, A. J. & Howe, G. A. (2009) The wound hormone jasmonate. *Phytochemistry*, 70, 1571-1580.
- Koroleva, O. A., Gibson, T. M., Cramer, R. & Stain, C. (2010) Glucosinolate-accumulating s-cells in Arabidopsis leaves and flower stalks undergo programmed cell death at early stages of differentiation. *The Plant Journal*, 64, 456-469.
- Koschier, E., Hoffmann, D. & Riefler, J. (2007) Influence of salicylaldehyde and methyl salicylate on post-landing behaviour of *Frankliniella occidentalis* Pergande. *Journal of Applied Entomology*, 131, 362-367.
- Koschier, E. H., De Kogel, W. J. & Visser, J. H. (2000) Assessing the attractiveness of volatile plant compounds to western flower thrips *Frankliniella occidentalis*. *Journal of Chemical Ecology*, 26, 2643-2655.
- Kostyuk, A. I., Demidovich, A. D., Kotova, D. A., Belousov, V. V. & Bilan, D. S. (2019) Circularly permuted fluorescent protein-based indicators: History, principles, and classification. *International journal of molecular sciences*, 20, 4200.
- Kranti, W., Nivedita, G. & Shindikar, M. (2021) Understanding the plant aphid interaction: A review. *European Journal of Biology and Biotechnology*, 2, 1-6.
- Krebs, M., Held, K., Binder, A., Hashimoto, K., Den Herder, G., Parniske, M., Kudla, J. & Schumacher, K. (2012) FRET-based genetically encoded sensors allow high-resolution live cell imaging of Ca²⁺ dynamics. *The Plant Journal*, 69, 181-192.
- Krogman, W., Sparks, J. A. & Blancaflor, E. B. (2020) Cell type-specific imaging of calcium signaling in *Arabidopsis thaliana* seedling roots using GCaMP3. *International journal of molecular sciences*, 21, 6385.
- Krol, E., Mentzel, T., Chinchilla, D., Boller, T., Felix, G., Kemmerling, B., Postel, S., Arents, M., Jeworutzki, E., Al-Rasheid, K. a. S., Becker, D. & Hedrich, R. (2010) Perception of the Arabidopsis danger signal peptide 1 involves the pattern recognition receptor AtPEPR1 and its close homologue AtPEPR2. *The Journal of biological chemistry*, 285, 13471-13479.
- Kumari, A., Chételat, A., Nguyen, C. T. & Farmer, E. E. (2019) Arabidopsis H⁺-ATPase AHA1 controls slow wave potential duration and wound-response jasmonate pathway activation. *Proceedings of the National Academy of Sciences*, 116, 20226-20231.
- Kusnierczyk, A., Tran, D. H., Winge, P., Jorstad, T. S., Reese, J. C., Troczynska, J. & Bones, A. M. (2011) Testing the importance of jasmonate signalling in induction of plant defences upon cabbage aphid (*Brevicoryne brassicae*) attack. *BMC Genomics*, 12, 423.
- Kusnierczyk, A., Winge, P., Jorstad, T. S., Troczynska, J., Rossiter, J. T. & Bones, A. M. (2008) Towards global understanding of plant defence against aphids--timing and dynamics of early Arabidopsis defence responses to cabbage aphid (*Brevicoryne brassicae*) attack. *Plant, Cell & Environment*, 31, 1097-1115.
- Kuśnierczyk, A., Winge, P., Midelfart, H., Armbruster, W. S., Rossiter, J. T. & Bones, A. M. (2007) Transcriptional responses of *Arabidopsis thaliana* ecotypes with different glucosinolate profiles after attack by polyphagous *Myzus persicae* and oligophagous *Brevicoryne brassicae*. *Journal of Experimental Botany*, 58, 2537-2552.
- Lal, N. K., Nagalakshmi, U., Hurlburt, N. K., Flores, R., Bak, A., Sone, P., Ma, X., Song, G., Walley, J., Shan, L., He, P., Casteel, C., Fisher, A. J. & Dinesh-Kumar, S. P. (2018) The receptor-like cytoplasmic kinase BIK1 localizes to the nucleus and regulates defense hormone expression during plant innate immunity. *Cell Host Microbe*, 23, 485-497.e485.
- Lamb, C. & Dixon, R. A. (1997) The oxidative burst in plant disease resistance. *Annual Review of Plant Physiology and Plant Molecular Biology*, 48, 251-275.

- Laohavisit, A. & Davies, J. M. (2011) Annexins. *New Phytologist*, 189, 40-53.
- Laohavisit, A., Shang, Z., Rubio, L., Cuin, T. A., Véry, A. A., Wang, A., Mortimer, J. C., Macpherson, N., Coxon, K. M., Battey, N. H., Brownlee, C., Park, O. K., Sentenac, H., Shabala, S., Webb, A. A. & Davies, J. M. (2012) Arabidopsis Annexin1 mediates the radical-activated plasma membrane Ca²⁺- and K⁺-permeable conductance in root cells. *Plant Cell*, 24, 1522-1533.
- Larkin, J. C., Oppenheimer, D. G., Lloyd, A. M., Papparozzi, E. T. & Marks, M. D. (1994) Roles of the GLABROUS1 and TRANSPARENT TESTA GLABRA genes in Arabidopsis trichome development. *Plant Cell*, 6, 1065-1076.
- Larrieu, A., Champion, A., Legrand, J., Lavenus, J., Mast, D., Brunoud, G., Oh, J., Guyomarc'h, S., Pizot, M., Farmer, E. E., Turnbull, C., Vernoux, T., Bennett, M. J. & Laplace, L. (2015) A fluorescent hormone biosensor reveals the dynamics of jasmonate signalling in plants. *Nature Communications*, 6, 6043.
- Le Trionnaire, G., Hardie, J., Jaubert-Possamai, S., Simon, J. C. & Tagu, D. (2008) Shifting from clonal to sexual reproduction in aphids: Physiological and developmental aspects. *Biology of the Cell*, 100, 441-451.
- Leather, S. R. & Dixon, A. F. G. (1982) Secondary host preferences and reproductive activity of the bird cherry-oat aphid, *Rhopalosiphum padi*. *Annals of Applied Biology*, 101, 219-228.
- Lecourieux, D., Lamotte, O., Bourque, S., Wendehenne, D., Mazars, C., Ranjeva, R. & Pugin, A. (2005) Proteinaceous and oligosaccharidic elicitors induce different calcium signatures in the nucleus of tobacco cells. *Cell Calcium*, 38, 527-538.
- Lee, D., Lal, N. K., Lin, Z.-J. D., Ma, S., Liu, J., Castro, B., Toruño, T., Dinesh-Kumar, S. P. & Coaker, G. (2020) Regulation of reactive oxygen species during plant immunity through phosphorylation and ubiquitination of RBOHD. *Nature Communications*, 11, 1838.
- Léger, O., Garcia, F., Khafif, M., Carrere, S., Leblanc-Fournier, N., Duclos, A., Tournat, V., Badel, E., Didelon, M., Le Ru, A., Raffaele, S. & Barbacci, A. (2022) Pathogen-derived mechanical cues potentiate the spatio-temporal implementation of plant defense. *BMC Biology*, 20, 292.
- Lei, J., S, A. F., Salzman, R. A., Shan, L. & Zhu-Salzman, K. (2014) BOTRYTIS-INDUCED KINASE1 modulates Arabidopsis resistance to green peach aphids via PHYTOALEXIN DEFICIENT4. *Plant Physiology*, 165, 1657-1670.
- Leiss, K. A., Cristofori, G., Van Steenis, R., Verpoorte, R. & Klinkhamer, P. G. (2013) An eco-metabolomic study of host plant resistance to western flower thrips in cultivated, biofortified and wild carrots. *Phytochemistry*, 93, 63-70.
- Leiss, K. A., Maltese, F., Choi, Y. H., Verpoorte, R. & Klinkhamer, P. G. (2009) Identification of chlorogenic acid as a resistance factor for thrips in chrysanthemum. *Plant Physiology*, 150, 1567-1575.
- Leitão, N., Dangeville, P., Carter, R. & Charpentier, M. (2019) Nuclear calcium signatures are associated with root development. *Nature Communications*, 10, 4865-4874.
- Leybourne, D. J., Valentine, T. A., Robertson, J. a. H., Pérez-Fernández, E., Main, A. M., Karley, A. J. & Bos, J. I. B. (2018) Partial-resistance against aphids in wild barley involves phloem and mesophyll-based defences. *bioRxiv*, 502476.
- Li, B., Meng, X., Shan, L. & He, P. (2016a) Transcriptional regulation of pattern-triggered immunity in plants. *Cell Host Microbe*, 19, 641-650.
- Li, C., Wu, H. M. & Cheung, A. Y. (2016b) FERONIA and her pals: Functions and mechanisms. *Plant Physiology*, 171, 2379-2392.
- Li, C., Yeh, F. L., Cheung, A. Y., Duan, Q., Kita, D., Liu, M. C., Maman, J., Luu, E. J., Wu, B. W., Gates, L., Jalal, M., Kwong, A., Carpenter, H. & Wu, H. M. (2015) Glycosylphosphatidylinositol-anchored proteins as chaperones and co-receptors for FERONIA receptor kinase signaling in Arabidopsis. *eLife*, 4, e06587.
- Li, F., Wang, J., Ma, C., Zhao, Y., Wang, Y., Hasi, A. & Qi, Z. (2013) Glutamate receptor-like channel3.3 is involved in mediating glutathione-triggered cytosolic calcium transients, transcriptional changes, and innate immunity responses in Arabidopsis. *Plant Physiology*, 162, 1497-1509.

- Li, G., Bartram, S., Guo, H., Mithöfer, A., Kunert, M. & Boland, W. (2019) Spitworm, a herbivorous robot: Mechanical leaf wounding with simultaneous application of salivary components. *Plants*, 8, 318.
- Li, K., Prada, J., Damineli, D. S. C., Liese, A., Romeis, T., Dandekar, T., Feijó, J. A., Hedrich, R. & Konrad, K. R. (2021a) An optimized genetically encoded dual reporter for simultaneous ratio imaging of Ca²⁺ and H⁺ reveals new insights into ion signaling in plants. *New Phytologist*, 230, 2292-2310.
- Li, L., Li, M., Yu, L., Zhou, Z., Liang, X., Liu, Z., Cai, G., Gao, L., Zhang, X., Wang, Y., Chen, S. & Zhou, J. M. (2014) The FLS2-associated kinase BIK1 directly phosphorylates the NADPH oxidase RbohD to control plant immunity. *Cell Host Microbe*, 15, 329-338.
- Li, M., Wang, F., Li, S., Yu, G., Wang, L., Li, Q., Zhu, X., Li, Z., Yuan, L. & Liu, P. (2020) Importers drive leaf-to-leaf transmission of jasmonic acid in wound induced systemic immunity. *Molecular Plant*, 13, 1485-1498.
- Li, M., Yu, G., Ma, J. & Liu, P. (2021b) Interactions of importers in long-distance transmission of wound-induced jasmonate. *Plant Signaling & Behavior*, 16, 1886490.
- Li, Q., Zheng, J., Li, S., Huang, G., Skilling, S. J., Wang, L., Li, L., Li, M., Yuan, L. & Liu, P. (2017) Transporter-mediated nuclear entry of jasmonoyl-isoleucine is essential for jasmonate signaling. *Molecular Plant*, 10, 695-708.
- Li, Y., Guo, J., Yang, Z. & Yang, D.-L. (2018) Plasma membrane-localized calcium pumps and copines coordinately regulate pollen germination and fertility in Arabidopsis. *International journal of molecular sciences*, 19, 1774.
- Liang, X., Ma, M., Zhou, Z., Wang, J., Yang, X., Rao, S., Bi, G., Li, L., Zhang, X., Chai, J., Chen, S. & Zhou, J.-M. (2018) Ligand-triggered de-repression of Arabidopsis heterotrimeric G proteins coupled to immune receptor kinases. *Cell Research*, 28, 529-543.
- Liang, X. & Zhou, J.-M. (2018) Receptor-Like cytoplasmic kinases: Central players in plant receptor kinase-mediated signaling. *Annual Review of Plant Biology*, 69, 267-299.
- Liao, H.-S., Chung, Y.-H. & Hsieh, M.-H. (2022) Glutamate: A multifunctional amino acid in plants. *Plant Science*, 318, 111238.
- Liebrand, T. W. H., Van Den Berg, G. C. M., Zhang, Z., Smit, P., Cordewener, J. H. G., America, A. H. P., Sklenar, J., Jones, A. M. E., Tameling, W. I. L., Robatzek, S., Thomma, B. P. H. J. & Joosten, M. H. a. J. (2013) Receptor-like kinase SOBIR1/EVR interacts with receptor-like proteins in plant immunity against fungal infection. *Proceedings of the National Academy of Sciences*, 110, 10010-10015.
- Liebrand, T. W. H., Van Den Burg, H. A. & Joosten, M. H. a. J. (2014) Two for all: Receptor-associated kinases SOBIR1 and BAK1. *Trends in Plant Science*, 19, 123-132.
- Lin, W., Tang, W., Anderson, C. & Yang, Z. (2018) FERONIA's sensing of cell wall pectin activates ROP GTPase signaling in Arabidopsis. *bioRxiv*, 269647.
- Linkert, M., Rueden, C. T., Allan, C., Burel, J.-M., Moore, W., Patterson, A., Loranger, B., Moore, J., Neves, C., Macdonald, D., Tarkowska, A., Sticco, C., Hill, E., Rossner, M., Eliceiri, K. W. & Swedlow, J. R. (2010) Metadata matters: Access to image data in the real world. *Journal of Cell Biology*, 189, 777-782.
- Liu, J., Ding, P., Sun, T., Nitta, Y., Dong, O., Huang, X., Yang, W., Li, X., Botella, J. R. & Zhang, Y. (2013a) Heterotrimeric G proteins serve as a converging point in plant defense signaling activated by multiple receptor-like kinases. *Plant Physiology*, 161, 2146-2158.
- Liu, L., Sonbol, F. M., Huot, B., Gu, Y., Withers, J., Mwimba, M., Yao, J., He, S. Y. & Dong, X. (2016) Salicylic acid receptors activate jasmonic acid signalling through a non-canonical pathway to promote effector-triggered immunity. *Nature Communications*, 7, 13099.
- Liu, S., Lenoir, C. J. G., Amaro, T. M. M., Rodriguez, P. A., Huitema, E. & Bos, J. I. B. (2022) Virulence strategies of an insect herbivore and oomycete plant pathogen converge on a host E3 SUMO ligase. *bioRxiv*, 2020.2006.2018.159178.
- Liu, X., Wang, J. & Sun, L. (2018) Structure of the hyperosmolality-gated calcium-permeable channel OSCA1.2. *Nature Communications*, 9, 5060.

- Liu, Y., Wang, W.-L., Guo, G.-X. & Ji, X.-L. (2009) Volatile emission in wheat and parasitism by *Aphidius avenae* after exogenous application of salivary enzymes of *Sitobion avenae*. *Entomologia Experimentalis et Applicata*, 130, 215-221.
- Liu, Z., Wu, Y., Yang, F., Zhang, Y., Chen, S., Xie, Q., Tian, X. & Zhou, J.-M. (2013b) BIK1 interacts with PEPRs to mediate ethylene-induced immunity. *Proceedings of the National Academy of Sciences*, 110, 6205-6210.
- Logan, D. C. & Knight, M. R. (2003) Mitochondrial and cytosolic calcium dynamics are differentially regulated in plants. *Plant Physiology*, 133, 21-24.
- Loon, L. C. V., Rep, M. & Pieterse, C. M. J. (2006) Significance of inducible defense-related proteins in infected plants. *Annual Review of Phytopathology*, 44, 135-162.
- Lorenzo, O., Chico, J. M., Sánchez-Serrano, J. J. & Solano, R. (2004) JASMONATE-INSENSITIVE1 encodes a MYC transcription factor essential to discriminate between different jasmonate-regulated defense responses in Arabidopsis. *The Plant Cell*, 16, 1938-1950.
- Loro, G., Drago, I., Pozzan, T., Schiavo, F. L., Zottini, M. & Costa, A. (2012) Targeting of cameleons to various subcellular compartments reveals a strict cytoplasmic/mitochondrial Ca²⁺ handling relationship in plant cells. *The Plant Journal*, 71, 1-13.
- Loro, G., Ruberti, C., Zottini, M. & Costa, A. (2013) The D3cpv Cameleon reports Ca²⁺ dynamics in plant mitochondria with similar kinetics of the YC3.6 Cameleon, but with a lower sensitivity. *Journal of Microscopy*, 249, 8-12.
- Loro, G., Wagner, S., Doccula, F. G., Behera, S., Weinl, S., Kudla, J., Schwarzländer, M., Costa, A. & Zottini, M. (2016) Chloroplast-specific *in vivo* Ca²⁺ imaging using yellow cameleon fluorescent protein sensors reveals organelle-autonomous Ca²⁺ signatures in the stroma. *Plant Physiology*, 171, 2317-2330.
- Losvik, A., Beste, L., Glinwood, R., Ivarson, E., Stephens, J., Zhu, L.-H. & Jonsson, L. (2017) Overexpression and down-regulation of barley lipoxygenase LOX2.2 affects jasmonate-regulated genes and aphid fecundity. *International journal of molecular sciences*, 18, 2765.
- Lu, D., Wu, S., Gao, X., Zhang, Y., Shan, L. & He, P. (2010) A receptor-like cytoplasmic kinase, BIK1, associates with a flagellin receptor complex to initiate plant innate immunity. *Proceedings of the National Academy of Sciences*, 107, 496-501.
- Luo, J., Chen, L., Huang, F., Gao, P., Zhao, H., Wang, Y. & Han, S. (2020) Intraorganellar calcium imaging in Arabidopsis seedling roots using the GCaMP variants GCaMP6m and R-CEPIA1er. *Journal of Plant Physiology*, epub March 2020, 246-247.
- Ma, R., Reese, J. C., Black Iv, W. C. & Bramel-Cox, P. (1990) Detection of pectinesterase and polygalacturonase from salivary secretions of living greenbugs, *Schizaphis graminum* (Homoptera: Aphididae). *Journal of Insect Physiology*, 36, 507-512.
- Ma, S., Lapin, D., Liu, L., Sun, Y., Song, W., Zhang, X., Logemann, E., Yu, D., Wang, J., Jirschtzka, J., Han, Z., Schulze-Lefert, P., Parker, J. E. & Chai, J. (2020a) Direct pathogen-induced assembly of an NLR immune receptor complex to form a holoenzyme. *Science*, 370, eabe3069.
- Ma, X., Li, Q.-H., Yu, Y.-N., Qiao, Y.-M., Haq, S. U. & Gong, Z.-H. (2020b) The CBL–CIPK pathway in plant response to stress signals. *International journal of molecular sciences*, 21, 5668.
- Maathuis, F. J. M. (2011) Vacuolar two-pore K⁺ channels act as vacuolar osmosensors. *New Phytologist*, 191, 84-91.
- Macwilliams, J. R., Dingwall, S., Chesnais, Q., Sugio, A. & Kaloshian, I. (2020) AcDCXR is a cowpea aphid effector with putative roles in altering host immunity and physiology. *Frontiers in Plant Science*, 11.
- Maksaev, G. & Haswell, E. S. (2012) MscS-like10 is a stretch-activated ion channel from *Arabidopsis thaliana* with a preference for anions. *Proceedings of the National Academy of Sciences*, 109, 19015-19020.
- Malabarba, J., Meents, A. K., Reichelt, M., Scholz, S. S., Peiter, E., Rachowka, J., Konopka-Postupolska, D., Wilkins, K. A., Davies, J. M., Oelmüller, R. & Mithöfer, A. (2021) ANNEXIN1 mediates calcium-dependent systemic defense in Arabidopsis plants upon herbivory and wounding. *New Phytologist*, 231, 243-254.

- Manzoor, H., Chiltz, A., Madani, S., Vatsa, P., Schoefs, B., Pugin, A. & Garcia-Brugger, A. (2012) Calcium signatures and signaling in cytosol and organelles of tobacco cells induced by plant defense elicitors. *Cell Calcium*, 51, 434-444.
- Manzoor, H., Kelloniemi, J., Chiltz, A., Wendehenne, D., Pugin, A., Poinssot, B. & Garcia-Brugger, A. (2013) Involvement of the glutamate receptor AtGLR3.3 in plant defense signaling and resistance to *Hyaloperonospora arabidopsidis*. *The Plant Journal*, 76, 466-480.
- Marhavý, P., Kurenda, A., Siddique, S., Dénervaud Tendon, V., Zhou, F., Holbein, J., Hasan, M. S., Grundler, F. M., Farmer, E. E. & Geldner, N. (2019) Single-cell damage elicits regional, nematode-restricting ethylene responses in roots. *The EMBO Journal*, 38, e100972.
- Markovic, D., Glinwood, R., Olsson, U. & Ninkovic, V. (2014) Plant response to touch affects the behaviour of aphids and ladybirds. *Arthropod-Plant Interactions*, 8, 171-181.
- Martín, B., Collar, J. L., Tjallingii, W. F. & Fereres, A. (1997) Intracellular ingestion and salivation by aphids may cause the acquisition and inoculation of non-persistently transmitted plant viruses. *Journal of General Virology*, 78, 2701-2705.
- Martin, R., Qi, T., Zhang, H., Liu, F., King, M., Toth, C., Nogales, E. & Staskawicz, B. J. (2020) Structure of the activated ROQ1 resistosome directly recognizing the pathogen effector XopQ. *Science*, 370.
- Martinière, A., Gibrat, R., Sentenac, H., Dumont, X., Gaillard, I. & Paris, N. (2018) Uncovering pH at both sides of the root plasma membrane interface using noninvasive imaging. *Proceedings of the National Academy of Sciences*, 115, 6488-6493.
- Marvin, J. S., Borghuis, B. G., Tian, L., Cichon, J., Harnett, M. T., Akerboom, J., Gordus, A., Renninger, S. L., Chen, T.-W., Bargmann, C. I., Orger, M. B., Schreiter, E. R., Demb, J. B., Gan, W.-B., Hires, S. A. & Looger, L. L. (2013) An optimized fluorescent probe for visualizing glutamate neurotransmission. *Nature Methods*, 10, 162-170.
- Mathers, T. C., Chen, Y., Kaithakottil, G., Legeai, F., Mugford, S. T., Baa-Puyoulet, P., Bretaudeau, A., Clavijo, B., Colella, S., Collin, O., Dalmay, T., Derrien, T., Feng, H., Gabaldón, T., Jordan, A., Julca, I., Kettles, G. J., Kowitwanich, K., Lavenier, D., Lenzi, P., Lopez-Gomollon, S., Loska, D., Mapleson, D., Maumus, F., Moxon, S., Price, D. R. G., Sugio, A., Van Munster, M., Uzest, M., Waite, D., Jander, G., Tagu, D., Wilson, A. C. C., Van Oosterhout, C., Swarbreck, D. & Hogenhout, S. A. (2017) Rapid transcriptional plasticity of duplicated gene clusters enables a clonally reproducing aphid to colonise diverse plant species. *Genome biology*, 18, 27-27.
- Matsubayashi, Y., Ogawa, M., Kihara, H., Niwa, M. & Sakagami, Y. (2006) Disruption and overexpression of Arabidopsis phytosulfokine receptor gene affects cellular longevity and potential for growth. *Plant Physiology*, 142, 45-53.
- Matsumura, M., Nomoto, M., Itaya, T., Aratani, Y., Iwamoto, M., Matsuura, T., Hayashi, Y., Mori, T., Skelly, M. J., Yamamoto, Y. Y., Kinoshita, T., Mori, I. C., Suzuki, T., Betsuyaku, S., Spoel, S. H., Toyota, M. & Tada, Y. (2022) Mechanosensory trichome cells evoke a mechanical stimuli-induced immune response in *Arabidopsis thaliana*. *Nature Communications*, 13, 1216-1231.
- Matthus, E., Sun, J., Wang, L., Bhat, M. G., Mohammad-Sidik, A. B., Wilkins, K. A., Leblanc-Fournier, N., Legué, V., Moulia, B., Stacey, G. & Davies, J. M. (2020) DORN1/P2K1 and purino-calcium signalling in plants: Making waves with extracellular ATP. *Annals of Botany*, 124, 1227-1242.
- Matthus, E., Wilkins, K. A., Mohammad-Sidik, A., Ning, Y. & Davies, J. M. (2022) Spatial origin of the extracellular ATP-induced cytosolic calcium signature in *Arabidopsis thaliana* roots; wave formation and variation with phosphate nutrition. *Plant Biology*, 24, 863-873.
- Matzke, A. J. & Matzke, M. (2015) Expression and testing in plants of ArcLight, a genetically-encoded voltage indicator used in neuroscience research. *BMC Plant Biology*, 15, 245.
- Mcainsh, M. R. & Pittman, J. K. (2009) Shaping the calcium signature. *New Phytologist*, 181, 275-294.
- Mcallan, J. & Adams, J. B. (1961) The significance of pectinase in plant penetration by aphids. *Canadian Journal of Zoology*, 39, 305-310.

- Mccombe, Carl I., Greenwood, Julian r., Solomon, Peter s. & Williams, Simon j. (2022) Molecular plant immunity against biotrophic, hemibiotrophic, and necrotrophic fungi. *Essays in Biochemistry*, 66, 581-593.
- Meena, M. K., Prajapati, R., Krishna, D., Divakaran, K., Pandey, Y., Reichelt, M., Mathew, M., Boland, W., Mithöfer, A. & Vadassery, J. (2019) The Ca²⁺ channel CNGC19 regulates Arabidopsis defense against Spodoptera herbivory. *The Plant Cell*, 31, 1539–1562.
- Meijering, E., Dzyubachyk, O. & Smal, I. (2012) Methods for cell and particle tracking. *Methods in Enzymology*, 504, 183-200.
- Meng, X., Shan, L. & He, P. (2015) Stack heterotrimeric G proteins and MAPK cascades on a RACK. *Molecular Plant*, 8, 1691-1693.
- Merlot, S., Leonhardt, N., Fenzi, F., Valon, C., Costa, M., Piette, L., Vavasseur, A., Genty, B., Boivin, K., Müller, A., Giraudat, J. & Leung, J. (2007) Constitutive activation of a plasma membrane H⁺-ATPase prevents abscisic acid-mediated stomatal closure. *The EMBO Journal*, 26, 3216-3226.
- Mewis, I., Appel, H. M., Hom, A., Raina, R. & Schultz, J. C. (2005) Major signaling pathways modulate Arabidopsis glucosinolate accumulation and response to both phloem-feeding and chewing insects. *Plant Physiology*, 138, 1149-1162.
- Mewis, I., Tokuhisa, J. G., Schultz, J. C., Appel, H. M., Ulrichs, C. & Gershenzon, J. (2006) Gene expression and glucosinolate accumulation in *Arabidopsis thaliana* in response to generalist and specialist herbivores of different feeding guilds and the role of defense signaling pathways. *Phytochemistry*, 67, 2450-2462.
- Michal Johnson, J., Reichelt, M., Vadassery, J., Gershenzon, J. & Oelmüller, R. (2014) An Arabidopsis mutant impaired in intracellular calcium elevation is sensitive to biotic and abiotic stress. *BMC Plant Biology*, 14, 162.
- Miles, P. W. (1999) Aphid saliva. *Biological Reviews*, 74, 41-85.
- Miller, G., Schlauch, K., Tam, R., Cortes, D., Torres, M. A., Shulaev, V., Dangl, J. L. & Mittler, R. (2009) The plant NADPH oxidase RBOHD mediates rapid systemic signaling in response to diverse stimuli. *Science Signaling*, 2, ra45-ra45.
- Mitreiter, S. & Gigolashvili, T. (2020) Regulation of glucosinolate biosynthesis. *Journal of Experimental Botany*, 72, 70-91.
- Miya, A., Albert, P., Shinya, T., Desaki, Y., Ichimura, K., Shirasu, K., Narusaka, Y., Kawakami, N., Kaku, H. & Shibuya, N. (2007) CERK1, a LysM receptor kinase, is essential for chitin elicitor signaling in Arabidopsis. *Proceedings of the National Academy of Sciences*, 104, 19613-19618.
- Miyawaki, A., Llopis, J., Heim, R., Mccaffery, J. M., Adams, J. A., Ikura, M. & Tsien, R. Y. (1997) Fluorescent indicators for Ca²⁺ based on green fluorescent proteins and calmodulin. *Nature*, 388, 882-887.
- Moe-Lange, J., Gappel, N. M., Machado, M., Wudick, M. M., Sies, C. S. A., Schott-Verdugo, S. N., Bonus, M., Mishra, S., Hartwig, T., Bezruczyk, M., Basu, D., Farmer, E. E., Gohlke, H., Malkovskiy, A., Haswell, E. S., Lercher, M. J., Ehrhardt, D. W., Frommer, W. B. & Kleist, T. J. (2021) Interdependence of a mechanosensitive anion channel and glutamate receptors in distal wound signaling. *Science Advances*, 7, eabg4298.
- Mohammad-Sidik, A., Sun, J., Shin, R., Song, Z., Ning, Y., Matthus, E., Wilkins, K. A. & Davies, J. M. (2021) Annexin 1 is a component of eATP-induced cytosolic calcium elevation in *Arabidopsis thaliana* roots. *International journal of molecular sciences*, 22, 494.
- Mondal, H. A. (2020) Aphid saliva: A powerful recipe for modulating host resistance towards aphid clonal propagation. *Arthropod-Plant Interactions*, 14, 547-558.
- Monshausen, G. B., Bibikova, T. N., Weisenseel, M. H. & Gilroy, S. (2009) Ca²⁺ regulates reactive oxygen species production and pH during mechanosensing in *Arabidopsis* roots. *The Plant Cell*, 21, 2341-2356.
- Morales Bello, J. (2015) *New insights into the regulation of NADPH oxidase dependent reactive oxygen species signalling during plant immune responses*. PhD in Biology, Universidad Politecnica de Madrid.

- Morales, J., Kadota, Y., Zipfel, C., Molina, A. & Torres, M.-A. (2016) The Arabidopsis NADPH oxidases RbohD and RbohF display differential expression patterns and contributions during plant immunity. *Journal of Experimental Botany*, 67, 1663-1676.
- Moran, P. J., Cheng, Y., Cassell, J. L. & Thompson, G. A. (2002) Gene expression profiling of *Arabidopsis thaliana* in compatible plant-aphid interactions. *Archives of Insect Biochemistry and Physiology*, 51, 182-203.
- Moran, P. J. & Thompson, G. A. (2001) Molecular responses to aphid feeding in Arabidopsis in relation to plant defense pathways. *Plant Physiology*, 125, 1074-1085.
- Moreau, H., Gaillard, I. & Paris, N. (2022) Genetically encoded fluorescent sensors adapted to acidic pH highlight subdomains within the plant cell apoplast. *Journal of Experimental Botany*, 73, 6744-6757.
- Morel, J.-B. & Dangl, J. L. (1997) The hypersensitive response and the induction of cell death in plants. *Cell Death & Differentiation*, 4, 671-683.
- Moreno, I., Norambuena, L., Maturana, D., Toro, M., Vergara, C., Orellana, A., Zurita-Silva, A. & Ordenes, V. R. (2008) AtHMA1 is a thapsigargin-sensitive Ca²⁺/heavy metal pump *Journal of Biological Chemistry*, 283, 9633-9641.
- Mori, K., Renhu, N., Naito, M., Nakamura, A., Shiba, H., Yamamoto, T., Suzuki, T., Iida, H. & Miura, K. (2018) Ca(2+)-permeable mechanosensitive channels MCA1 and MCA2 mediate cold-induced cytosolic Ca(2+) increase and cold tolerance in Arabidopsis. *Scientific Reports*, 8, 550-550.
- Mosher, S., Seybold, H., Rodriguez, P., Stahl, M., Davies, K. A., Dayaratne, S., Morillo, S. A., Wierzba, M., Favery, B., Keller, H., Tax, F. E. & Kemmerling, B. (2013) The tyrosine-sulfated peptide receptors PSKR1 and PSY1R modify the immunity of Arabidopsis to biotrophic and necrotrophic pathogens in an antagonistic manner. *The Plant Journal*, 73, 469-482.
- Mou, W., Kao, Y.-T., Michard, E., Simon, A. A., Li, D., Wudick, M. M., Lizzio, M. A., Feijó, J. A. & Chang, C. (2020) Ethylene-independent signaling by the ethylene precursor ACC in Arabidopsis ovular pollen tube attraction. *Nature Communications*, 11, 4082-4083.
- Mou, Z., Fan, W. & Dong, X. (2003) Inducers of plant systemic acquired resistance regulate NPR1 function through redox changes. *Cell*, 113, 935-944.
- Mouden, S., Sarmiento, K. F., Klinkhamer, P. G. & Leiss, K. A. (2017) Integrated pest management in western flower thrips: Past, present and future. *Pest Management Science*, 73, 813-822.
- Mound, L. A. (2005) Thysanoptera: Diversity and interactions. *Annual Review of Entomology*, 50, 247-269.
- Mousavi, S. A., Chauvin, A., Pascaud, F., Kellenberger, S. & Farmer, E. E. (2013) GLUTAMATE RECEPTOR-LIKE genes mediate leaf-to-leaf wound signalling. *Nature*, 500, 422-426.
- Mousavi, S. a. R., Dubin, A. E., Zeng, W.-Z., Coombs, A. M., Do, K., Ghadiri, D. A., Keenan, W. T., Ge, C., Zhao, Y. & Patapoutian, A. (2021) PIEZO ion channel is required for root mechanotransduction in *Arabidopsis thaliana*. *Proceedings of the National Academy of Sciences*, 118, e2102188118.
- Mugford, S. T., Barclay, E., Drurey, C., Findlay, K. C. & Hogenhout, S. A. (2016) An immunosuppressive aphid saliva protein is delivered into the cytosol of plant mesophyll cells during feeding. *Molecular Plant-Microbe Interactions*, 29, 854-861.
- Mur, L. A., Kenton, P., Atzorn, R., Miersch, O. & Wasternack, C. (2006) The outcomes of concentration-specific interactions between salicylate and jasmonate signaling include synergy, antagonism, and oxidative stress leading to cell death. *Plant Physiology*, 140, 249-262.
- Murashige, T. & Skoog, F. (1962) A revised medium for rapid growth and bio assays with tobacco tissue cultures. *Physiologia Plantarum*, 15, 473-497.
- Murthy, S., Dubin, A., Whitwam, T., Jojoa Cruz, S., Cahalan, S., Mosavi, S. a. R., Ward, A. & Patapoutian, A. (2018) OSCA/TMEM63 are an evolutionarily conserved family of mechanically activated ion channels. *bioRxiv*, 408732.

- Mutti, N. S., Louis, J., Pappan, L. K., Pappan, K., Begum, K., Chen, M.-S., Park, Y., Dittmer, N., Marshall, J. & Reese, J. C. (2008) A protein from the salivary glands of the pea aphid, *Acyrtosiphon pisum*, is essential in feeding on a host plant. *Proceedings of the National Academy of Sciences*, 105, 9965-9969.
- Naessens, E., Dubreuil, G., Giordanengo, P., Baron, O. L., Minet-Kebdani, N., Keller, H. & Coustau, C. (2015) A secreted MIF cytokine enables aphid feeding and represses plant immune responses. *Current Biology*, 25, 1898-1903.
- Nagai, T., Yamada, S., Tominaga, T., Ichikawa, M. & Miyawaki, A. (2004) Expanded dynamic range of fluorescent indicators for Ca²⁺ by circularly permuted yellow fluorescent proteins. *Proceedings of the National Academy of Sciences*, 101, 10554-10559.
- Nakagawa, Y., Katagiri, T., Shinozaki, K., Qi, Z., Tatsumi, H., Furuichi, T., Kishigami, A., Sokabe, M., Kojima, I., Sato, S., Kato, T., Tabata, S., Iida, K., Terashima, A., Nakano, M., Ikeda, M., Yamanaka, T. & Iida, H. (2007) Arabidopsis plasma membrane protein crucial for Ca²⁺ influx and touch sensing in roots. *Proceedings of the National Academy of Sciences*, 104, 3639-3644.
- Nakai, J., Ohkura, M. & Imoto, K. (2001) A high signal-to-noise Ca²⁺ probe composed of a single green fluorescent protein. *Nature Biotechnology*, 19, 137-141.
- Nakano, M., Iida, K., Nyunoya, H. & Iida, H. (2011) Determination of structural regions important for Ca(2+) uptake activity in Arabidopsis MCA1 and MCA2 expressed in yeast. *Plant & Cell Physiology*, 52, 1915-1930.
- Nalam, V., Louis, J. & Shah, J. (2019) Plant defense against aphids, the pest extraordinaire. *Plant Science*, 279, 96-107.
- Napoli, C., Lemieux, C. & Jorgensen, R. (1990) Introduction of a chimeric chalcone synthase gene into petunia results in reversible co-suppression of homologous genes in trans. *The Plant Cell*, 2, 279-289.
- Ng, J. C. & Perry, K. L. (2004) Transmission of plant viruses by aphid vectors. *Molecular Plant Pathology*, 5, 505-511.
- Ngou, B. P. M., Ahn, H.-K., Ding, P. & Jones, J. D. G. (2021) Mutual potentiation of plant immunity by cell-surface and intracellular receptors. *Nature*, 592, 110-115.
- Nguyen, C. T., Kurenda, A., Stolz, S., Chételat, A. & Farmer, E. E. (2018) Identification of cell populations necessary for leaf-to-leaf electrical signaling in a wounded plant. *Proceedings of the National Academy of Sciences*, 115, 10178-10183.
- Nicolis, V. & Venter, E. (2018) Silencing of a unique integrated domain nucleotide-binding leucine-rich repeat gene in wheat abolishes *Diuraphis noxia* resistance. *Molecular Plant-Microbe Interactions*, 31, 940-950.
- Nietzel, T., Elsässer, M., Ruberti, C., Steinbeck, J., Ugalde, J. M., Fuchs, P., Wagner, S., Ostermann, L., Moseler, A., Lemke, P., Fricker, M. D., Müller-Schüssele, S. J., Moerschbacher, B. M., Costa, A., Meyer, A. J. & Schwarzländer, M. (2019) The fluorescent protein sensor roGFP2-Orp1 monitors in vivo H₂O₂ and thiol redox integration and elucidates intracellular H₂O₂ dynamics during elicitor-induced oxidative burst in Arabidopsis. *New Phytologist*, 221, 1649-1664.
- Nomoto, M., Skelly, M. J., Itaya, T., Mori, T., Suzuki, T., Matsushita, T., Tokizawa, M., Kuwata, K., Mori, H., Yamamoto, Y. Y., Higashiyama, T., Tsukagoshi, H., Spoel, S. H. & Tada, Y. (2021) Suppression of MYC transcription activators by the immune cofactor NPR1 fine-tunes plant immune responses. *Cell Rep*, 37, 110125.
- Nühse, T. S., Bottrill, A. R., Jones, A. M. E. & Peck, S. C. (2007) Quantitative phosphoproteomic analysis of plasma membrane proteins reveals regulatory mechanisms of plant innate immune responses. *The Plant Journal*, 51, 931-940.
- O'Connor, J. T., Stevens, A. C., Shannon, E. K., Akbar, F. B., Lafever, K. S., Narayanan, N. P., Gailey, C. D., Hutson, M. S. & Page-McCaw, A. (2021) Proteolytic activation of growth-blocking peptides triggers calcium responses through the GPCR Mthl10 during epithelial wound detection. *Developmental Cell*, 56, 2160-2175.
- Ogasawara, Y., Kaya, H., Hiraoka, G., Yumoto, F., Kimura, S., Kadota, Y., Hishinuma, H., Senzaki, E., Yamagoe, S., Nagata, K., Nara, M., Suzuki, K., Tanokura, M. & Kuchitsu, K. (2008)

- Synergistic activation of the Arabidopsis NADPH oxidase AtrbohD by Ca²⁺ and phosphorylation. *Journal of Biological Chemistry*, 283, 8885-8892.
- Ogawa, K. & Miura, T. (2014) Aphid polyphenisms: Trans-generational developmental regulation through viviparity. *Frontiers in Physiology*, 5.
- Oome, S. & Van Den Ackerveken, G. (2014) Comparative and functional analysis of the widely occurring family of nep1-like proteins. *Molecular Plant-Microbe Interactions*, 27, 1081-1094.
- Oppenheimer, D. G., Herman, P. L., Sivakumaran, S., Esch, J. & Marks, M. D. (1991) A myb gene required for leaf trichome differentiation in Arabidopsis is expressed in stipules. *Cell*, 67, 483-493.
- Orozco-Cardenas, M., Mcgurl, B. & Ryan, C. A. (1993) Expression of an antisense prosystemin gene in tomato plants reduces resistance toward *Manduca sexta* larvae. *Proceedings of the National Academy of Sciences*, 90, 8273-8276.
- Otulak-Kozieł, K., Kozieł, E., Bujarski, J. J., Frankowska-Łukawska, J. & Torres, M. A. (2020) Respiratory burst oxidase homologs RBOHD and RBOHF as key modulating components of response in Turnip Mosaic Virus—*Arabidopsis thaliana* (L.) Heyhn system. *International journal of molecular sciences*, 21, 8510.
- Outchkourov, N. S., De Kogel, W. J., Schuurman-De Bruin, A., Abrahamson, M. & Jongsma, M. A. (2004) Specific cysteine protease inhibitors act as deterrents of western flower thrips, *Frankliniella occidentalis* (Pergande), in transgenic potato. *Plant Biotechnology Journal*, 2, 439-448.
- Palmer, A. E. & Tsien, R. Y. (2006) Measuring calcium signaling using genetically targetable fluorescent indicators. *Nature Protocols*, 1, 1057-1065.
- Pantazopoulou, C. K., Buti, S., Nguyen, C. T., Oskam, L., Farmer, E. E., Kajala, K. & Pierik, R. (2022) Mechanodetection of neighbor plants elicits adaptive leaf movements through calcium dynamics. *bioRxiv*.
- Parisy, V., Poinssot, B., Owsianowski, L., Buchala, A., Glazebrook, J. & Mauch, F. (2007) Identification of PAD2 as a γ-glutamylcysteine synthetase highlights the importance of glutathione in disease resistance of Arabidopsis. *The Plant Journal*, 49, 159-172.
- Parmagnani, A. S. & Maffei, M. E. (2022) Calcium signaling in plant-insect interactions. *Plants* 11, 2689-2705.
- Patra, N., Hariharan, S., Gain, H., Maiti, M. K., Das, A. & Banerjee, J. (2021) Typical but delicate Ca⁺⁺: Dissecting the essence of calcium signaling network as a robust response coordinator of versatile abiotic and biotic stimuli in plants. *Frontiers in Plant Science*, 12.
- Pauwels, L., Barbero, G. F., Geerinck, J., Tilleman, S., Grunewald, W., Pérez, A. C., Chico, J. M., Bossche, R. V., Sewell, J., Gil, E., García-Casado, G., Witters, E., Inzé, D., Long, J. A., De Jaeger, G., Solano, R. & Goossens, A. (2010) NINJA connects the co-repressor TOPLESS to jasmonate signalling. *Nature*, 464, 788-791.
- Pearce, G. (2011) Systemin, hydroxyproline-rich systemin and the induction of protease inhibitors. *Current Protein and Peptide Science*, 12, 399-408.
- Pearce, G., Strydom, D., Johnson, S. & Ryan, C. A. (1991) A polypeptide from tomato leaves induces wound-inducible proteinase inhibitor proteins. *Science*, 253, 895-897.
- Pegadaraju, V., Knepper, C., Reese, J. & Shah, J. (2005) Premature leaf senescence modulated by the Arabidopsis PHYTOALEXIN DEFICIENT4 gene is associated with defense against the phloem-feeding green peach aphid. *Plant Physiology*, 139, 1927-1934.
- Peiter, E., Maathuis, F. J., Mills, L. N., Knight, H., Pelloux, J., Hetherington, A. M. & Sanders, D. (2005) The vacuolar Ca²⁺-activated channel TPC1 regulates germination and stomatal movement. *Nature*, 434, 404-408.
- Peng, H.-C., Mantelin, S., Hicks, G. R., Takken, F. L. & Kaloshian, I. (2016) The conformation of a plasma membrane-localized somatic embryogenesis receptor kinase complex is altered by a potato aphid-derived effector. *Plant Physiology*, 171, 2211-2222.
- Peng, X., Liu, L., Guo, X., Wang, P., Song, C., Su, S., Fang, G. & Chen, M. (2019) The survival and reproduction of *Rhopalosiphum padi* (Hemiptera: Aphididae) on different plants:

- Exploring the possible host range for a serious wheat pest. *Journal of Economic Entomology*, 113, 185-193.
- Peng, Y., Van Wersch, R. & Zhang, Y. (2018) Convergent and divergent signaling in PAMP-triggered immunity and effector-triggered immunity. *Molecular Plant-Microbe Interactions*, 31, 403-409.
- Petutschnig, E. K., Jones, A. M. E., Serazetdinova, L., Lipka, U. & Lipka, V. (2010) The lysin motif receptor-like kinase (LysM-RLK) CERK1 is a major chitin-binding protein in *Arabidopsis thaliana* and subject to chitin-induced phosphorylation. *Journal of Biological Chemistry*, 285, 28902-28911.
- Pham, A. Q., Cho, S.-H., Nguyen, C. T. & Stacey, G. (2020) Arabidopsis lectin receptor kinase P2K2 is a second plant receptor for extracellular ATP and contributes to innate immunity. *Plant Physiology*, 183, 1364-1375.
- Phelan, P. L. & Miller, J. R. (1982) Post-landing behavior of alate *Myzus persicae* as altered by (e)- β -farnesen and three carboxylic acids. *Entomologia Experimentalis et Applicata*, 32, 46-53.
- Piasecka, A., Jedrzejczak-Rey, N. & Bednarek, P. (2015) Secondary metabolites in plant innate immunity: Conserved function of divergent chemicals. *New Phytologist*, 206, 948-964.
- Pitino, M. & Hogenhout, S. A. (2013) Aphid protein effectors promote aphid colonization in a plant species-specific manner. *Molecular Plant-Microbe Interactions*, 26, 130-139.
- Pitsili, E., Phukan, U. J. & Coll, N. S. (2020) Cell death in plant immunity. *Cold Spring Harb Perspect Biol*, 12, a036483.
- Pobożniak, M. & Koschier, E. (2014) Effects of pea (*Pisum sativum* L.) cultivars on *Thrips tabaci* Lindeman preference and performance. *The Journal of Agricultural Science*, 152, 885-893.
- Poburko, D., Santo-Domingo, J. & Demaurex, N. (2011) Dynamic regulation of the mitochondrial proton gradient during cytosolic calcium elevations. *Journal of Biological Chemistry*, 286, 11672-11684.
- Pollard, D. (1973) Plant penetration by feeding aphids (Hemiptera, Aphidoidea): A review. *Bulletin of Entomological Research*, 62, 631-714.
- Poncini, L., Wyrsh, I., Dénervaud Tendon, V., Vorley, T., Boller, T., Geldner, N., Métraux, J. P. & Lehmann, S. (2017) In roots of *Arabidopsis thaliana*, the damage-associated molecular pattern AtPep1 is a stronger elicitor of immune signalling than flg22 or the chitin heptamer. *PLoS ONE*, 12, e0185808.
- Porcar, M., Grenier, A.-M., Federici, B. & Rahbé, Y. (2009) Effects of *Bacillus thuringiensis* δ -endotoxins on the pea aphid (*Acyrtosiphon pisum*). *Applied and Environmental Microbiology*, 75, 4897-4900.
- Powell, G., Tosh, C. R. & Hardie, J. (2006) Host plant selection by aphids: Behavioral, evolutionary, and applied perspectives. *Annual Review of Entomology*, 51, 309-330.
- Pratt, C., Pope, T. W., Powell, G. & Rossiter, J. T. (2008) Accumulation of glucosinolates by the cabbage aphid *Brevicoryne brassicae* as a defense against two coccinellid species. *Journal of Chemical Ecology*, 34, 323-329.
- Prince, D. C., Drurey, C., Zipfel, C. & Hogenhout, S. A. (2014) The leucine-rich repeat receptor-like kinase BRASSINOSTEROID INSENSITIVE1-ASSOCIATED KINASE1 and the cytochrome P450 PHYTOALEXIN DEFICIENT3 contribute to innate immunity to aphids in Arabidopsis. *Plant Physiology* 164, 2207-2219.
- Qi, J., Wang, J., Gong, Z. & Zhou, J.-M. (2017) Apoplastic ROS signaling in plant immunity. *Current Opinion in Plant Biology*, 38, 92-100.
- Qi, Z., Stephens, N. R. & Spalding, E. P. (2006) Calcium entry mediated by GLR3.3, an Arabidopsis glutamate receptor with a broad agonist profile. *Plant Physiology*, 142, 963-971.
- Qi, Z., Verma, R., Gehring, C., Yamaguchi, Y., Zhao, Y., Ryan, C. A. & Berkowitz, G. A. (2010) Ca²⁺ signaling by plant *Arabidopsis thaliana* Pep peptides depends on AtPepR1, a receptor with guanylyl cyclase activity, and cGMP-activated Ca²⁺ channels. *Proceedings of the National Academy of Sciences*, 107, 21193-21198.

- Rabbinge, R., Drees, E. M., Van Der Graaf, M., Verberne, F. C. M. & Wesselo, A. (1981) Damage effects of cereal aphids in wheat. *Netherlands Journal of Plant Pathology*, 87, 217-232.
- Radin, I., Richardson, R. A., Coomey, J. H., Weiner, E. R., Bascom, C. S., Li, T., Bezanilla, M. & Haswell, E. S. (2021) Plant PIEZO homologs modulate vacuole morphology during tip growth. *Science*, 373, 586-590.
- Ranf, S., Eschen-Lippold, L., Fröhlich, K., Westphal, L., Scheel, D. & Lee, J. (2014) Microbe-associated molecular pattern-induced calcium signaling requires the receptor-like cytoplasmic kinases, PBL1 and BIK1. *BMC Plant Biology*, 14, 374.
- Rasool, B., MCGowan, J., Pastok, D., Marcus, S. E., Morris, J. A., Verrall, S. R., Hedley, P. E., Hancock, R. D. & Foyer, C. H. (2017) Redox control of aphid resistance through altered cell wall composition and nutritional quality. *Plant Physiology*, 175, 259-271.
- Rassizadeh, L., Cervero, R., Flors, V. & Gamir, J. (2021) Extracellular DNA as an elicitor of broad-spectrum resistance in *Arabidopsis thaliana*. *Plant Science*, 312, 111036.
- Ray, S., Alves, P. C., Ahmad, I., Gaffoor, I., Acevedo, F. E., Peiffer, M., Jin, S., Han, Y., Shakeel, S., Felton, G. W. & Luthe, D. S. (2016) Turnabout is fair play: Herbivory-induced plant chitinases excreted in fall armyworm frass suppress herbivore defenses in maize. *Plant Physiology*, 171, 694-706.
- Rekhter, D., Lüdke, D., Ding, Y., Feussner, K., Zienkiewicz, K., Lipka, V., Wiermer, M., Zhang, Y. & Feussner, I. (2019) Isochorismate-derived biosynthesis of the plant stress hormone salicylic acid. *Science*, 365, 498-502.
- Remaudiere, G. & Remaudiere, M. (1997) *Catalogue of the world's Aphididae: Homoptera aphidoidea*, Paris, Institut National de la Recherche Agronomique (INRA).
- Reymond, P., Bodenhausen, N., Van Poecke, R. M. P., Krishnamurthy, V., Dicke, M. & Farmer, E. E. (2004) A conserved transcript pattern in response to a specialist and a generalist herbivore. *The Plant Cell*, 16, 3132-3147.
- Rhodes, J., Yang, H., Moussu, S., Boutrot, F., Santiago, J. & Zipfel, C. (2021) Perception of a divergent family of phytocytokines by the Arabidopsis receptor kinase MIK2. *Nature Communications*, 12, 705.
- Richards, S. L., Laohavisit, A., Mortimer, J. C., Shabala, L., Swarbreck, S. M., Shabala, S. & Davies, J. M. (2014) Annexin 1 regulates the H₂O₂-induced calcium signature in *Arabidopsis thaliana* roots. *The Plant Journal*, 77, 136-145.
- Riley, D. G., Joseph, S. V., Srinivasan, R. & Diffie, S. (2011) Thrips vectors of tospoviruses. *Journal of Integrated Pest Management*, 2, 11-110.
- Rodriguez, P., Escudero-Martinez, C. & Bos, J. (2017) An aphid effector targets trafficking protein VPS52 in a host-specific manner to promote virulence. *Plant Physiology*, 173, 1892-1903.
- Rodriguez, P. A., Stam, R., Warbroek, T. & Bos, J. I. (2014) Mp10 and Mp42 from the aphid species *Myzus persicae* trigger plant defenses in *Nicotiana benthamiana* through different activities. *Molecular Plant-Microbe Interactions*, 27, 30-39.
- Rook, F., Corke, F., Baier, M., Holman, R., May, A. G. & Bevan, M. W. (2006) Impaired sucrose induction1 encodes a conserved plant-specific protein that couples carbohydrate availability to gene expression and plant growth. *The Plant Journal*, 46, 1045-1058.
- Rose, T., Goltstein, P. M., Portugues, R. & Griesbeck, O. (2014) Putting a finishing touch on GECs. *Frontiers in Molecular Neuroscience*, 7, 15.
- Rossi, M., Goggin, F. L., Milligan, S. B., Kaloshian, I., Ullman, D. E. & Williamson, V. M. (1998) The nematode resistance gene Mi of tomato confers resistance against the potato aphid. *Proceedings of the National Academy of Sciences*, 95, 9750-9754.
- Rotenberg, D., Baumann, A. A., Ben-Mahmoud, S., Christiaens, O., Dermauw, W., Ioannidis, P., Jacobs, C. G. C., Vargas Jentzsch, I. M., Oliver, J. E., Poelchau, M. F., Rajarapu, S. P., Schneweis, D. J., Snoeck, S., Taning, C. N. T., Wei, D., Widana Gamage, S. M. K., Hughes, D. S. T., Murali, S. C., Bailey, S. T., Beijerman, N. E., Holmes, C. J., Jennings, E. C., Rosendale, A. J., Rosselot, A., Hervey, K., Schneweis, B. A., Cheng, S., Childers, C., Simão, F. A., Dietzgen, R. G., Chao, H., Dinh, H., Doddapaneni, H. V., Dugan, S., Han, Y., Lee, S. L., Muzny, D. M., Qu, J., Worley, K. C., Benoit, J. B., Friedrich, M., Jones, J. W., Panfilio,

- K. A., Park, Y., Robertson, H. M., Smagghe, G., Ullman, D. E., Van Der Zee, M., Van Leeuwen, T., Veenstra, J. A., Waterhouse, R. M., Weirauch, M. T., Werren, J. H., Whitfield, A. E., Zdobnov, E. M., Gibbs, R. A. & Richards, S. (2020) Genome-enabled insights into the biology of thrips as crop pests. *BMC Biology*, 18, 142.
- Rotenberg, D. & Whitfield, A. E. (2018) Molecular interactions between tospoviruses and thrips vectors. *Current Opinion in Virology*, 33, 191-197.
- Roudaire, T., Héloir, M. C., Wendehenne, D., Zadoroznyj, A., Dubrez, L. & Poinssot, B. (2020) Cross kingdom immunity: The role of immune receptors and downstream signaling in animal and plant cell death. *Front Immunol*, 11, 612452.
- Rstudio Team (2020) Rstudio: Integrated development for R. Boston, MA: RStudio, PBC.
- Ruan, J., Zhou, Y., Zhou, M., Yan, J., Khurshid, M., Weng, W., Cheng, J. & Zhang, K. (2019) Jasmonic acid signaling pathway in plants. *International Journal of Molecular Sciences* 20, 2479.
- Rubil, N., Kalachova, T., Hauser, T. P. & Burketová, L. (2022) Specialist aphids feeding causes local activation of salicylic and jasmonic acid signaling in Arabidopsis veins. *Molecular Plant-Microbe Interactions*, 35, 119-124.
- Rudd, J. J. & Franklin-Tong, V. E. (1999) Calcium signaling in plants. *Cellular and Molecular Life Sciences CMLS*, 55, 214-232.
- Rudolf, R., Mongillo, M., Rizzuto, R. & Pozzan, T. (2003) Looking forward to seeing calcium. *Nature Reviews Molecular Cell Biology*, 4, 579-586.
- Rui, Y. & Dinneny, J. R. (2020) A wall with integrity: Surveillance and maintenance of the plant cell wall under stress. *New Phytologist*, 225, 1428-1439.
- Rzemieniewski, J. & Stegmann, M. (2022) Regulation of pattern-triggered immunity and growth by phytoytokines. *Current Opinion in Plant Biology*, 68, 102230.
- Salvador-Recatalà, V. (2016) New roles for the GLUTAMATE RECEPTOR-LIKE 3.3, 3.5, and 3.6 genes as on/off switches of wound-induced systemic electrical signals. *Plant Signaling & Behavior*, 11, e1161879.
- Salvador-Recatalà, V., Tjallingii, W. F. & Farmer, E. E. (2014) Real-time, in vivo intracellular recordings of caterpillar-induced depolarization waves in sieve elements using aphid electrodes. *New Phytologist*, 203, 674-684.
- Santamaría, M. E., Arnaiz, A., Velasco-Arroyo, B., Grbic, V., Diaz, I. & Martinez, M. (2018) Arabidopsis response to the spider mite *Tetranychus urticae* depends on the regulation of reactive oxygen species homeostasis. *Scientific Reports*, 8, 9432.
- Santamaria, M. E., Garcia, A., Arnaiz, A., Rosa-Diaz, I., Romero-Hernandez, G., Diaz, I. & Martinez, M. (2021) Comparative transcriptomics reveals hidden issues in the plant response to arthropod herbivores. *Journal of Integrative Plant Biology*, 63, 312-326.
- Sardar, A., Nandi, A. K. & Chattopadhyay, D. (2017) CBL-interacting protein kinase 6 negatively regulates immune response to *Pseudomonas syringae* in Arabidopsis. *Journal of Experimental Botany*, 68, 3573-3584.
- Sarde, S. J. (2019) *Dynamics of transcriptional responses of plants to thrips feeding*. Doctoral, Wageningen University
- Savary, S., Willocquet, L., Pethybridge, S. J., Esker, P., McRoberts, N. & Nelson, A. (2019) The global burden of pathogens and pests on major food crops. *Nature, Ecology & Evolutions*, 3, 430-439.
- Schindelin, J., Arganda-Carreras, I., Frise, E., Kaynig, V., Longair, M., Pietzsch, T., Preibisch, S., Rueden, C., Saalfeld, S., Schmid, B., Tinevez, J.-Y., White, D. J., Hartenstein, V., Eliceiri, K., Tomancak, P. & Cardona, A. (2012) Fiji: An open-source platform for biological-image analysis. *Nature Methods*, 9, 676-682.
- Schmelz, E. A., Carroll, M. J., Leclere, S., Phipps, S. M., Meredith, J., Chourey, P. S., Alborn, H. T. & Teal, P. E. (2006) Fragments of ATP synthase mediate plant perception of insect attack. *Proceedings of the National Academy of Sciences*, 103, 8894-8899.
- Schmelz, E. A., Huffaker, A., Carroll, M. J., Alborn, H. T., Ali, J. G. & Teal, P. E. A. (2012) An amino acid substitution inhibits specialist herbivore production of an antagonist effector and recovers insect-induced plant defenses. *Plant Physiology*, 160, 1468-1478.

- Scholl, R. L., May, S. T. & Ware, D. H. (2000) Seed and molecular resources for Arabidopsis. *Plant Physiology*, 124, 1477-1480.
- Schubert, D., Lechtenberg, B., Forsbach, A., Gils, M., Bahadur, S. & Schmidt, R. (2004) Silencing in Arabidopsis T-DNA transformants: The predominant role of a gene-specific RNA sensing mechanism versus position effects. *Plant Cell*, 16, 2561-2572.
- Schulze, A., Zimmer, M., Mielke, S., Stellmach, H., Melnyk, C. W., Hause, B. & Gasperini, D. (2019) Wound-induced shoot-to-root relocation of JA-Ile precursors coordinates Arabidopsis growth. *Molecular Plant*, 12, 1383-1394.
- Schweizer, F., Bodenhausen, N., Lassueur, S., Masclaux, F. & Reymond, P. (2013) Differential contribution of transcription factors to *Arabidopsis thaliana* defense against *Spodoptera littoralis*. *Frontiers in Plant Science*, 4.
- Schwessinger, B., Roux, M., Kadota, Y., Ntoukakis, V., Sklenar, J., Jones, A. & Zipfel, C. (2011) Phosphorylation-dependent differential regulation of plant growth, cell death, and innate immunity by the regulatory receptor-like kinase BAK1. *PLoS Genetics*, 7, e1002046.
- Seigneurin-Berny, D., Gravot, A., Auroy, P., Mazard, C., Kraut, A., Finazzi, G., Grunwald, D., Rappaport, F., Vavasseur, A., Joyard, J., Richaud, P. & Rolland, N. (2006) HMA1, a new Cu-ATPase of the chloroplast envelope, is essential for growth under adverse light conditions. *Journal of Biological Chemistry* 281, 2882-2892.
- Sessions, A., Burke, E., Presting, G., Aux, G., McElver, J., Patton, D., Dietrich, B., Ho, P., Bacwaden, J., Ko, C., Clarke, J. D., Cotton, D., Bullis, D., Snell, J., Miguel, T., Hutchison, D., Kimmerly, B., Mitzel, T., Katagiri, F., Glazebrook, J., Law, M. & Goff, S. A. (2002) A high-throughput Arabidopsis reverse genetics system. *Plant Cell*, 14, 2985-2894.
- Shannon, E. K., Stevens, A., Edrington, W., Zhao, Y., Jayasinghe, A. K., Page-Mccaw, A. & Hutson, M. S. (2017) Multiple mechanisms drive calcium signal dynamics around laser-induced epithelial wounds. *Biophysical Journal*, 113, 1623-1635.
- Shao, Q., Gao, Q., Lhamo, D., Zhang, H. & Luan, S. (2020) Two glutamate- and pH-regulated Ca²⁺ channels are required for systemic wound signaling in Arabidopsis. *Science Signaling*, 13, eaba1453.
- Shen, Q., Bourdais, G., Pan, H., Robatzek, S. & Tang, D. (2017) Arabidopsis glycosylphosphatidylinositol-anchored protein LLG1 associates with and modulates FLS2 to regulate innate immunity. *Proceedings of the National Academy of Sciences*, 114, 5749-5754.
- Shen, W., Liu, J. & Li, J. F. (2019) Type-II metacaspases mediate the processing of plant elicitor peptides in Arabidopsis. *Molecular Plant*, 12, 1524-1533.
- Shigematsu, H., Iida, K., Nakano, M., Chaudhuri, P., Iida, H. & Nagayama, K. (2014) Structural characterization of the mechanosensitive channel candidate MCA2 from *Arabidopsis thaliana*. *PLoS ONE*, 9, e87724.
- Shih, H.W., Miller, N.D., Dai, C., Spalding, E.P. & Monshausen, G.B. (2014) The receptor-like kinase FERONIA is required for mechanical signal transduction in Arabidopsis seedlings. *Current Biology*, 24, 1887-1892.
- Shirakawa, M. & Hara-Nishimura, I. (2018) Specialized vacuoles of myrosin cells: Chemical defense strategy in Brassicales plants. *Plant & Cell Physiology*, 59, 1309-1316.
- Shkryl, V. M. (2020) Error correction due to background subtraction in ratiometric calcium measurements with ccd camera. *Heliyon*, 6, e04180-e04188.
- Silva-Sanzana, C., Estevez, J. M. & Blanco-Herrera, F. (2020) Influence of cell wall polymers and their modifying enzymes during plant-aphid interactions. *Journal of Experimental Biology*, 71, 3854-3864.
- Silva-Sanzana, C., Zavala, D., Moraga, F., Herrera-Vásquez, A. & Blanco-Herrera, F. (2022) Oligogalacturonides enhance resistance against aphids through pattern-triggered immunity and activation of salicylic acid signaling. *International Journal of Molecular Sciences* 23, 9753.

- Silva, A. X., Jander, G., Samaniego, H., Ramsey, J. S. & Figueroa, C. C. (2012) Insecticide resistance mechanisms in the green peach aphid *Myzus persicae* (Hemiptera: Aphididae) i: A transcriptomic survey. *PLoS ONE*, 7, e36366.
- Simon, A. A., Navarro-Retamal, C. & Feijó, J. A. (2023) Merging signaling with structure: Functions and mechanisms of plant glutamate receptor ion channels. *Annual Review of Plant Biology*, 74.
- Simon, J.-C., Rispé, C. & Sunnucks, P. (2002) Ecology and evolution of sex in aphids. *Trends in Ecology & Evolution*, 17, 34-39.
- Singh, N. & Pandey, G. K. (2020) Calcium signatures and signal transduction schemes during microbe interactions in *Arabidopsis thaliana*. *Journal of Plant Biochemistry and Biotechnology*, 29, 675-686.
- Singh, S. K., Chien, C.-T. & Chang, I.-F. (2016) The *Arabidopsis* glutamate receptor-like gene GLR3.6 controls root development by repressing the Kip-related protein gene KRP4. *Journal of Experimental Botany*, 67, 1853-1869.
- Smolyarova, D. D., Podgorny, O. V., Bilan, D. S. & Belousov, V. V. (2022) A guide to genetically encoded tools for the study of H₂O₂. *The FEBS journal*, 289, 5382-5395.
- Snoeck, S., Guayazán-Palacios, N. & Steinbrener, A. D. (2022) Molecular tug-of-war: Plant immune recognition of herbivory. *The Plant Cell*, 34, 1497-1513.
- Song, C. J., Steinebrunner, I., Wang, X., Stout, S. C. & Roux, S. J. (2006) Extracellular ATP induces the accumulation of superoxide via NADPH oxidases in *Arabidopsis*. *Plant Physiology*, 140, 1222-1232.
- Song, S., Huang, H., Gao, H., Wang, J., Wu, D., Liu, X., Yang, S., Zhai, Q., Li, C., Qi, T. & Xie, D. (2014) Interaction between MYC2 and ETHYLENE INSENSITIVE3 modulates antagonism between jasmonate and ethylene signaling in *Arabidopsis*. *Plant Cell*, 26, 263-279.
- Stael, S., Wurzing, B., Mair, A., Mehlmer, N., Voithknecht, U. C. & Teige, M. (2012) Plant organellar calcium signalling: An emerging field. *Journal of Experimental Botany*, 63, 1525-1542.
- Stafford-Banks, C. A., Rotenberg, D., Johnson, B. R., Whitfield, A. E. & Ullman, D. E. (2014) Analysis of the salivary gland transcriptome of *Frankliniella occidentalis*. *PLoS ONE*, 9, e94447.
- Stafford, C. A., Walker, G. P. & Ullman, D. E. (2011) Infection with a plant virus modifies vector feeding behavior. *Proceedings of the National Academy of Sciences*, 108, 9350-9355.
- Stahl, E., Fernandez Martin, A., Glauser, G., Guillou, M.-C., Aubourg, S., Renou, J.-P. & Reymond, P. (2022) The MIK2/SCOOP signaling system contributes to *Arabidopsis* resistance against herbivory by modulating jasmonate and indole glucosinolate biosynthesis. *Frontiers in Plant Science*, 13.
- Staswick, P. E. & Tiryaki, I. (2004) The oxylipin signal jasmonic acid is activated by an enzyme that conjugates it to isoleucine in *Arabidopsis*. *The Plant Cell*, 16, 2117-2127.
- Steenbergen, M. (2022) *Gene regulatory network induced by western flower thrips in Arabidopsis: Effect of hormone signaling, thrips development and spatial context*. Doctoral, Utrecht University.
- Steenbergen, M., Abd-El-Halim, A., Bleeker, P., Dicke, M., Escobar-Bravo, R., Cheng, G., Haring, M. A., Kant, M. R., Kappers, I., Klinkhamer, P. G. L., Leiss, K. A., Legarrea, S., Macel, M., Mouden, S., Pieterse, C. M. J., Sarde, S. J., Schuurink, R. C., De Vos, M., Van Wees, S. C. M. & Broekgaarden, C. (2018) Thrips advisor: Exploiting thrips-induced defences to combat pests on crops. *Journal of Experimental Botany*, 69, 1837-1848.
- Stegmann, M., Monaghan, J., Smakowska-Luzan, E., Rovenich, H., Lehner, A., Holton, N., Belkadir, Y. & Zipfel, C. (2017) The receptor kinase FER is a RALF-regulated scaffold controlling plant immune signaling. *Science*, 355, 287-289.
- Steinbrener, A. D., Muñoz-Amatriaín, M., Chaparro, A. F., Aguilar-Venegas, J. M., Lo, S., Okuda, S., Glauser, G., Dongiovanni, J., Shi, D., Hall, M., Crubaugh, D., Holton, N., Zipfel, C., Abagyan, R., Turlings, T. C. J., Close, T. J., Huffaker, A. & Schmelz, E. A. (2020) A receptor-like protein mediates plant immune responses to herbivore-associated molecular patterns. *Proceedings of the National Academy of Sciences*, 117, 31510-31518.

- Stewart, S. A., Hodge, S., Ismail, N., Mansfield, J. W., Feys, B. J., Prospéri, J.-M., Huguet, T., Ben, C., Gentzbittel, L. & Powell, G. (2009) The RAP1 gene confers effective, race-specific resistance to the pea aphid in *Medicago truncatula* independent of the hypersensitive reaction. *Molecular Plant-Microbe Interactions*, 22, 1645-1655.
- Su, J., Xu, J. & Zhang, S. (2015) RACK1, scaffolding a heterotrimeric G protein and a MAPK cascade. *Trends in Plant Science*, 20, 405-407.
- Suda, H., Mano, H., Toyota, M., Fukushima, K., Mimura, T., Tsutsui, I., Hedrich, R., Tamada, Y. & Hasebe, M. (2020) Calcium dynamics during trap closure visualized in transgenic Venus flytrap. *Nature Plants*, 6, 1219–1224.
- Suda, H. & Toyota, M. (2022) Integration of long-range signals in plants: A model for wound-induced Ca²⁺, electrical, ROS, and glutamate waves. *Current Opinion in Plant Biology*, 69, 102270.
- Sun, S., Zhang, X., Chen, K., Zhu, X. & Zhao, Y. (2021) Screening for Arabidopsis mutants with altered Ca²⁺ signal response using aequorin-based Ca²⁺ reporter system. *STAR Protocols*, 2, 100558.
- Sun, T., Busta, L., Zhang, Q., Ding, P., Jetter, R. & Zhang, Y. (2018) TGACG-BINDING FACTOR 1 (TGA1) and TGA4 regulate salicylic acid and pipelicolic acid biosynthesis by modulating the expression of systemic acquired resistance deficient 1 (SARD1) and calmodulin-binding protein 60g (CBP60g). *New Phytologist*, 217, 344-354.
- Sun, T., Huang, J., Xu, Y., Verma, V., Jing, B., Sun, Y., Orduna, A. R., Tian, H., Huang, X. & Xia, S. (2020) Redundant CAMTA transcription factors negatively regulate the biosynthesis of salicylic acid and N-hydroxypipelicolic acid by modulating the expression of SARD1 and CBP60g. *Molecular Plant*, 13, 144-156.
- Sun, T. & Zhang, Y. (2021) Short- and long-distance signaling in plant defense. *The Plant Journal*, 105, 505-517.
- Sun, T., Zhang, Y., Li, Y., Zhang, Q., Ding, Y. & Zhang, Y. (2015) ChIP-seq reveals broad roles of SARD1 and CBP60g in regulating plant immunity. *Nature Communications*, 6, 10159.
- Sun, Y., Li, L., Macho, A. P., Han, Z., Hu, Z., Zipfel, C., Zhou, J.-M. & Chai, J. (2013) Structural basis for flg22-induced activation of the Arabidopsis FLS2-BAK1 immune complex. *Science*, 342, 624-628.
- Taki, N., Sasaki-Sekimoto, Y., Obayashi, T., Kikuta, A., Kobayashi, K., Aina, T., Yagi, K., Sakurai, N., Suzuki, H., Masuda, T., Takamiya, K., Shibata, D., Kobayashi, Y. & Ohta, H. (2005) 12-oxo-phytodienoic acid triggers expression of a distinct set of genes and plays a role in wound-induced gene expression in Arabidopsis. *Plant Physiology*, 139, 1268-1283.
- Tang, D., Wang, G. & Zhou, J.-M. (2017) Receptor kinases in plant-pathogen interactions: More than pattern recognition. *The Plant Cell*, 29, 618-637.
- Tang, R.-J., Wang, C., Li, K. & Luan, S. (2020) The CBL–CIPK calcium signaling network: Unified paradigm from 20 years of discoveries. *Trends in Plant Science*, 25, 604-617.
- Tapken, D. & Hollmann, M. (2008) *Arabidopsis thaliana* glutamate receptor ion channel function demonstrated by ion pore transplantation. *Journal of Molecular Biology*, 383, 36-48.
- Teardo, E., Carraretto, L., Moscatiello, R., Cortese, E., Vicario, M., Festa, M., Maso, L., De Bortoli, S., Cali, T., Vothknecht, U. C., Formentin, E., Cendron, L., Navazio, L. & Szabo, I. (2019) A chloroplast-localized mitochondrial calcium uniporter transduces osmotic stress in Arabidopsis. *Nature Plants*, 5, 581-588.
- Tenorio Berrío, R., Verstaen, K., Vandamme, N., Pevernagie, J., Achon, I., Van Duyse, J., Van Isterdael, G., Saeys, Y., De Veylder, L., Inzé, D. & Dubois, M. (2022) Single-cell transcriptomics sheds light on the identity and metabolism of developing leaf cells. *Plant Physiology*, 188, 898-918.
- Teulon, D. A., Hollister, B., Butler, R. C. & Cameron, E. A. (1999) Colour and odour responses of flying western flower thrips: Wind tunnel and greenhouse experiments. *Entomologia Experimentalis et Applicata*, 93, 9-19.
- Textor, S. & Gershenzon, J. (2009) Herbivore induction of the glucosinolate–myrosinase defense system: Major trends, biochemical bases and ecological significance. *Phytochemistry Reviews*, 8, 149-170.

- Then, C., Bellegarde, F., Schivre, G., Martinière, A., Macia, J.-L., Xiong, T. C. & Drucker, M. (2021) Plant viruses can alter aphid-triggered calcium elevations in infected leaves. *Cells*, 10, 3534.
- Thoen, M. P., Kloth, K. J., Wiegers, G. L., Krips, O. E., Noldus, L. P., Dicke, M. & Jongsma, M. A. (2016) Automated video tracking of thrips behavior to assess host-plant resistance in multiple parallel two-choice setups. *Plant Methods*, 12, 1.
- Thomma, B. P. H. J., Nürnberger, T. & Joosten, M. H. a. J. (2011) Of PAMPs and effectors: The blurred PTI-ETI dichotomy. *The Plant Cell*, 23, 4-15.
- Thor, K., Jiang, S., Michard, E., George, J., Scherzer, S., Huang, S., Dindas, J., Derbyshire, P., Leitão, N., Defalco, T. A., Köster, P., Hunter, K., Kimura, S., Gronnier, J., Stransfeld, L., Kadota, Y., Bücherl, C. A., Charpentier, M., Wrzaczek, M., Maclean, D., Oldroyd, G. E. D., Menke, F. L. H., Roelfsema, M. R. G., Hedrich, R., Feijó, J. & Zipfel, C. (2020) The calcium-permeable channel OSCA1.3 regulates plant stomatal immunity. *Nature*, 585, 569-573.
- Thorpe, P., Cock, P. J. A. & Bos, J. (2016) Comparative transcriptomics and proteomics of three different aphid species identifies core and diverse effector sets. *BMC Genomics*, 17, 172.
- Thulasi Devendrakumar, K., Li, X. & Zhang, Y. (2018) MAP kinase signalling: Interplays between plant PAMP-and effector-triggered immunity. *Cellular and Molecular Life Sciences*, 75, 2981-2989.
- Tian, L., Hires, S. A., Mao, T., Huber, D., Chiappe, M. E., Chalasani, S. H., Petreanu, L., Akerboom, J., Mckinney, S. A., Schreiter, E. R., Bargmann, C. I., Jayaraman, V., Svoboda, K. & Looger, L. L. (2009) Imaging neural activity in worms, flies and mice with improved GCaMP calcium indicators. *Nature Methods*, 6, 875-881
- Tian, W., Hou, C., Ren, Z., Wang, C., Zhao, F., Dahlbeck, D., Hu, S., Zhang, L., Niu, Q., Li, L., Staskawicz, B. J. & Luan, S. (2019) A calmodulin-gated calcium channel links pathogen patterns to plant immunity. *Nature*, 572, 131-135.
- Tichá, M., Richter, H., Ovečka, M., Maghelli, N., Hrbáčková, M., Dvořák, P., Šamaj, J. & Šamajová, O. (2020) Advanced microscopy reveals complex developmental and subcellular localization patterns of ANNEXIN 1 in Arabidopsis. *Frontiers in Plant Science*, 11.
- Tissier, A. F., Marillonnet, S., Klimyuk, V., Patel, K., Torres, M. A., Murphy, G. & Jones, J. D. (1999) Multiple independent defective suppressor-mutator transposon insertions in Arabidopsis: A tool for functional genomics. *The Plant Cell*, 11, 1841-1852.
- Tjallingii, W. F. (1978) Electronic recording of penetration behaviour by aphids. *Entomologia Experimentalis et Applicata*, 24, 721-730.
- Tjallingii, W. F. (1985) Membrane potentials as an indication for plant cell penetration by aphid stylets. *Entomologia Experimentalis et Applicata*, 38, 187-193.
- Tjallingii, W. F. (1995) Regulation of phloem sap feeding by aphids. In: CHAPMAN, R. F. & DE BOER, G. (eds.) *Regulatory mechanisms in insect feeding*. Boston, MA: Springer US.
- Tjallingii, W. F. (2006) Salivary secretions by aphids interacting with proteins of phloem wound responses. *Journal of Experimental Botany*, 57, 739-745.
- Tjallingii, W. F. & Esch, T. H. (1993) Fine structure of aphid stylet routes in plant tissues in correlation with EPG signals. *Physiological Entomology*, 18, 317-328.
- Tomas-Grau, R. H., Requena-Serra, F. J., Hael-Conrad, V., Martínez-Zamora, M. G., Guerrero-Molina, M. F. & Díaz-Ricci, J. C. (2018) Soft mechanical stimulation induces a defense response against *Botrytis cinerea* in strawberry. *Plant Cell Reports*, 37, 239-250.
- Tommasini, M. & Maini, S. (1995) *Frankliniella occidentalis* and other thrips harmful to vegetable and ornamental crops in Europe. *Wageningen Agricultural University Papers*, 95, 1-42.
- Torrens-Spence, M. P., Bobokalonova, A., Carballo, V., Glinkerman, C. M., Pluskal, T., Shen, A. & Weng, J.-K. (2019) PBS3 and EPS1 complete salicylic acid biosynthesis from isochorismate in Arabidopsis. *Molecular Plant*, 12, 1577-1586.
- Torres, M. A., Dangl, J. L. & Jones, J. D. (2002) Arabidopsis gp91phox homologues AtrbohD and atrbohF are required for accumulation of reactive oxygen intermediates in the plant defense response. *Proceedings of the National Academy of Sciences*, 99, 517-522.

- Toyota, M., Spencer, D., Sawai-Toyota, S., Jiaqi, W., Zhang, T., Koo, A. J., Howe, G. A. & Gilroy, S. (2018) Glutamate triggers long-distance, calcium-based plant defense signaling. *Science*, 361, 1112-1115.
- Traynelis, S. F. & Cull-Candy, S. G. (1990) Proton inhibition of N-methyl-D-aspartate receptors in cerebellar neurons. *Nature*, 345, 347-350.
- Tsuda, K. & Katagiri, F. (2010) Comparing signaling mechanisms engaged in pattern-triggered and effector-triggered immunity. *Current Opinion in Plant Biology*, 13, 459-465.
- Tunc-Ozdemir, M. & Jones, A. M. (2017) Ligand-induced dynamics of heterotrimeric G protein-coupled receptor-like kinase complexes. *PLoS ONE*, 12, e0171854.
- Turano, F. J., Muhitch, M. J., Felker, F. C. & McMahon, M. B. (2002) The putative glutamate receptor 3.2 from *Arabidopsis thaliana* (AtGLR3.2) is an integral membrane peptide that accumulates in rapidly growing tissues and persists in vascular-associated tissues. *Plant Science*, 163, 43-51.
- Turlings, T. C. J., Alborn, H. T., Loughrin, J. H. & Tumlinson, J. H. (2000) Volicitin, an elicitor of maize volatiles in oral secretion of *Spodoptera exigua*: Isolation and bioactivity. *Journal of Chemical Ecology*, 26, 189-202.
- Uemura, T., Wang, J., Aratani, Y., Gilroy, S. & Toyota, M. (2021) Wide-field, real-time imaging of local and systemic wound signals in *Arabidopsis*. *Journal of Visualized Experiments : JoVE*, e62114.
- Ugalde, J. M., Schlößer, M., Dongois, A., Martinière, A. & Meyer, A. J. (2021) The latest HyPe(r) in plant H₂O₂ biosensing. *Plant Physiology*, 187, 480-484.
- Ülker, B., Peiter, E., Dixon, D. P., Moffat, C., Capper, R., Bouché, N., Edwards, R., Sanders, D., Knight, H. & Knight, M. R. (2008) Getting the most out of publicly available T-DNA insertion lines. *The Plant Journal*, 56, 665-677.
- Uzest, M., Gargani, D., Dombrovsky, A., Cazevielle, C., Cot, D. & Blanc, S. (2010) The “acrostyle”: A newly described anatomical structure in aphid stylets. *Arthropod Structure & Development*, 39, 221-229.
- Valenzuela, I. & Hoffmann, A. A. (2015) Effects of aphid feeding and associated virus injury on grain crops in Australia. *Austral Entomology*, 54, 292-305.
- Van Butselaar, T. & Van Den Ackerveken, G. (2020) Salicylic acid steers the growth & immunity tradeoff. *Trends in Plant Science*, 25, 566-576.
- Van Der Does, D., Boutrot, F., Engelsdorf, T., Rhodes, J., Mckenna, J. F., Vernhettes, S., Koevoets, I., Tintor, N., Veerabagu, M., Miedes, E., Segonzac, C., Roux, M., Breda, A. S., Hardtke, C. S., Molina, A., Rep, M., Testerink, C., Mouille, G., Höfte, H., Hamann, T. & Zipfel, C. (2017) The *Arabidopsis* leucine-rich repeat receptor kinase MIK2/LRR-KISS connects cell wall integrity sensing, root growth and response to abiotic and biotic stresses. *PLoS Genetics*, 13, e1006832.
- Van Rossum, G. & Drake Jr, F. L. (2009) Python 3 reference manual. Scotts Valley, CA: CreateSpace.
- Vanacker, H., Carver, T. L. & Foyer, C. H. (2000) Early H₂O₂ accumulation in mesophyll cells leads to induction of glutathione during the hyper-sensitive response in the barley-powdery mildew interaction. *Plant Physiology*, 123, 1289-1300.
- Vincent, T. R. (2016) *The role of calcium signalling in plant-aphid interactions*. Doctor of Philosophy, University of East Anglia.
- Vincent, T. R., Avramova, M., Canham, J., Higgins, P., Bilkey, N., Mugford, S. T., Pitino, M., Toyota, M., Gilroy, S., Miller, T. J., Hogenhout, S. & Sanders, D. (2017a) Interplay of plasma membrane and vacuolar ion channels, together with BAK1, elicits rapid cytosolic calcium elevations in *Arabidopsis* during aphid feeding. *The Plant Cell*, 29, 1460–1479.
- Vincent, T. R., Canham, J., Toyota, M., Avramova, M., Mugford, S. T., Gilroy, S., Miller, A. J., Hogenhout, S. & Sanders, D. (2017b) Real-time *in vivo* recording of *Arabidopsis* calcium signals during insect feeding using a fluorescent biosensor. *Journal of Visualized Experiments : JoVE*, 56142.

- Vincill, E. D., Clarin, A. E., Molenda, J. N. & Spalding, E. P. (2013) Interacting glutamate receptor-like proteins in phloem regulate lateral root initiation in *Arabidopsis*. *The Plant Cell*, 25, 1304-1313.
- Visschers, I. G. S., Van Dam, N. M. & Peters, J. L. (2018) An objective high-throughput screening method for thrips damage quantitation using Ilastik and ImageJ. *Entomologia Experimentalis et Applicata*, 166, 508-515.
- Voigt, C. A. (2014) Callose-mediated resistance to pathogenic intruders in plant defense-related papillae. *Frontiers in Plant Science*, 5, 168-168.
- Vos, P., Simons, G., Jesse, T., Wijbrandi, J., Heinen, L., Hogers, R., Frijters, A., Groenendijk, J., Diergaarde, P. & Reijans, M. (1998) The tomato Mi-1 gene confers resistance to both root-knot nematodes and potato aphids. *Nature Biotechnology*, 16, 1365-1369.
- Waadt, R., Köster, P., Andrés, Z., Waadt, C., Bradamante, G., Lampou, K., Kudla, J. & Schumacher, K. (2020) Dual-reporting transcriptionally linked genetically encoded fluorescent indicators resolve the spatiotemporal coordination of cytosolic abscisic acid and second messenger dynamics in *Arabidopsis*. *The Plant Cell*, 32, 2582-2601.
- Waadt, R., Krebs, M., Kudla, J. & Schumacher, K. (2017) Multiparameter imaging of calcium and abscisic acid and high-resolution quantitative calcium measurements using R-GECO1-mTurquoise in *Arabidopsis*. *New Phytologist*, 216, 303-320.
- Waadt, R., Kudla, J. & Kollist, H. (2021) Multiparameter in vivo imaging in plants using genetically encoded fluorescent indicator multiplexing. *Plant Physiology*, 187, 537-549.
- Walia, A., Waadt, R. & Jones, A. M. (2018) Genetically encoded biosensors in plants: Pathways to discovery. *Annual Review of Plant Biology*, 69, 497-524.
- Walling, L. L. (2008) Avoiding effective defenses: Strategies employed by phloem-feeding insects. *Plant Physiology*, 146, 859-866.
- Wan, L., Essuman, K., Anderson, R. G., Sasaki, Y., Monteiro, F., Chung, E. H., Osborne Nishimura, E., Diantonio, A., Milbrandt, J., Dangl, J. L. & Nishimura, M. T. (2019) TIR domains of plant immune receptors are NAD(+)-cleaving enzymes that promote cell death. *Science*, 365, 799-803.
- Wang, C., Zhou, M., Zhang, X., Yao, J., Zhang, Y. & Mou, Z. (2017a) A lectin receptor kinase as a potential sensor for extracellular nicotinamide adenine dinucleotide in *Arabidopsis thaliana*. *eLife*, 6, e25474.
- Wang, F., Yu, G. & Liu, P. (2019a) Transporter-mediated subcellular distribution in the metabolism and signaling of jasmonates. *Frontiers in Plant Science*, 10, 390.
- Wang, J., Hu, M., Wang, J., Qi, J., Han, Z., Wang, G., Qi, Y., Wang, H.-W., Zhou, J.-M. & Chai, J. (2019b) Reconstitution and structure of a plant NLR resistosome conferring immunity. *Science*, 364, eaav5870.
- Wang, J., Peiffer, M., Hoover, K., Rosa, C., Zeng, R. & Felton, G. W. (2017b) *Helicoverpa zea* gut-associated bacteria indirectly induce defenses in tomato by triggering a salivary elicitor(s). *New Phytologist*, 214, 1294-1306.
- Wang, J., Song, W. & Chai, J. (2023) Structure, biochemical function, and signaling mechanism of plant NLRs. *Molecular Plant*, 16, 75-95.
- Wang, J., Wang, J., Hu, M., Wu, S., Qi, J., Wang, G., Han, Z., Qi, Y., Gao, N., Wang, H.-W., Zhou, J.-M. & Chai, J. (2019c) Ligand-triggered allosteric ADP release primes a plant NLR complex. *Science*, 364, eaav5868.
- Wang, L., Einig, E., Almeida-Trapp, M., Albert, M., Fliegmann, J., Mithöfer, A., Kalbacher, H. & Felix, G. (2018) The systemin receptor SYR1 enhances resistance of tomato against herbivorous insects. *Nature Plants*, 4, 152-156.
- Wang, L., Ning, Y., Sun, J., Wilkins, K. A., Matthus, E., Mcnelly, R. E., Dark, A., Rubio, L., Moeder, W., Yoshioka, K., Véry, A.-A., Stacey, G., Leblanc-Fournier, N., Legué, V., Mouliá, B. & Davies, J. M. (2022a) *Arabidopsis thaliana* CYCLIC NUCLEOTIDE-GATED CHANNEL2 mediates extracellular ATP signal transduction in root epidermis. *New Phytologist*, 234, 412-421.

- Wang, L., Tsuda, K., Sato, M., Cohen, J. D., Katagiri, F. & Glazebrook, J. (2009) Arabidopsis cam binding protein CBP60g contributes to MAMP-induced SA accumulation and is involved in disease resistance against *Pseudomonas syringae*. *PLoS Pathogens*, 5, e1000301.
- Wang, L., Tsuda, K., Truman, W., Sato, M., Nguyen, L. V., Katagiri, F. & Glazebrook, J. (2011) CBP60g and SARD1 play partially redundant critical roles in salicylic acid signaling. *The Plant Journal*, 67, 1029-1041.
- Wang, W., Dai, H., Zhang, Y., Chandrasekar, R., Luo, L., Hiromasa, Y., Sheng, C., Peng, G., Chen, S., Tomich, J. M., Reese, J., Edwards, O., Kang, L., Reeck, G. & Cui, F. (2015) Armet is an effector protein mediating aphid–plant interactions. *The FASEB Journal*, 29, 2032-2045.
- Wang, X.-S., Yang, C.-L., Wang, S.-S. & Hu, G.-X. (2014a) Changes of phenols and lignin contents in alfalfa leaf damaged by *Odontothrips loti*. *The Journal of Applied Ecology*, 25, 1688-1692.
- Wang, Y., Gong, Q., Huang, F., He, L. & Liu, Y. (2022b) Live imaging and quantitation of insect feeding-induced Ca²⁺ signal using GCaMP3-based system in *Nicotiana benthamiana*. *STAR Protocols*, 3, 101040.
- Wang, Y., Li, Z., Liu, D., Xu, J., Wei, X., Yan, L., Yang, C., Lou, Z. & Shui, W. (2014b) Assessment of BAK1 activity in different plant receptor-like kinase complexes by quantitative profiling of phosphorylation patterns. *Journal of Proteomics*, 108, 484-493.
- Wang, Y., Mostafa, S., Zeng, W. & Jin, B. (2021a) Function and mechanism of jasmonic acid in plant responses to abiotic and biotic stresses. *International journal of molecular sciences*, 22, 8568.
- Wang, Y., Pruitt, R. N., Nürnberger, T. & Wang, Y. (2022c) Evasion of plant immunity by microbial pathogens. *Nature Reviews Microbiology*, 20, 449-464.
- Wang, Z., Lü, Q., Zhang, L., Zhang, M., Chen, L., Zou, S., Zhang, C. & Dong, H. (2021b) Aphid salivary protein Mp1 facilitates infestation by binding phloem protein 2-A1 in Arabidopsis. *Biochemical and Biophysical Research Communications*, 572, 105-111.
- War, A. R., Paulraj, M. G., Ahmad, T., Buhroo, A. A., Hussain, B., Ignacimuthu, S. & Sharma, H. C. (2012) Mechanisms of plant defense against insect herbivores. *Plant Signaling & Behavior*, 7, 1306-1320.
- Ward, J. M. & Schroeder, J. I. (1994) Calcium-activated K⁺ channels and calcium-induced calcium release by slow vacuolar ion channels in guard cell vacuoles implicated in the control of stomatal closure. *Plant Cell*, 6, 669-683.
- Watanabe, S., Murakami, Y. & Hasegawa, E. (2018) Effects of aphid parasitism on host plant fitness in an aphid-host relationship. *PLoS ONE*, 13, e0202411.
- Webster, C. G., Thillier, M., Piroles, E., Cayrol, B., Blanc, S. & Uzest, M. (2017) Proteomic composition of the acrostyle: Novel approaches to identify cuticular proteins involved in virus-insect interactions. *Insect Science*, 24, 990-1002.
- Weech, M.-H., Chapleau, M., Pan, L., Ide, C. & Bede, J. C. (2008) Caterpillar saliva interferes with induced *Arabidopsis thaliana* defence responses via the systemic acquired resistance pathway. *Journal of Experimental Botany*, 59, 2437-2448.
- Weerasinghe, R. R., Swanson, S. J., Okada, S. F., Garrett, M. B., Kim, S. Y., Stacey, G., Boucher, R. C., Gilroy, S. & Jones, A. M. (2009) Touch induces ATP release in Arabidopsis roots that is modulated by the heterotrimeric G-protein complex. *FEBS Letters*, 583, 2521-2526.
- Wijkamp, I., Almarza, N., Goldbach, R. & Peters, D. (1995) Distinct levels of specificity in thrips transmission of tospoviruses. *Phytopathology*, 85, 1069-1074.
- Will, T., Kornemann, S. R., Furch, A. C. U., Tjallingii, W. F. & Van Bel, A. J. E. (2009) Aphid watery saliva counteracts sieve-tube occlusion: A universal phenomenon? *Journal of Experimental Biology*, 212, 3305-3312.
- Will, T., Steckbauer, K., Hardt, M. & Van Bel, A. J. (2012) Aphid gel saliva: Sheath structure, protein composition and secretory dependence on stylet-tip milieu. *PLoS ONE*, 7, e46903.
- Will, T., Tjallingii, W. F., Thönnessen, A. & Van Bel, A. J. E. (2007) Molecular sabotage of plant defense by aphid saliva. *Proceedings of the National Academy of Sciences*, 104, 10536-10541.

- Wingate, V. P., Lawton, M. A. & Lamb, C. J. (1988) Glutathione causes a massive and selective induction of plant defense genes. *Plant Physiology*, 87, 206-210.
- Wu, C. H., Abd-El-Halim, A., Bozkurt, T. O., Belhaj, K., Terauchi, R., Vossen, J. H. & Kamoun, S. (2017) NLR network mediates immunity to diverse plant pathogens. *Proceedings of the National Academy of Sciences*, 114, 8113-8118.
- Wu, Q., Stolz, S., Kumari, A. & Farmer, E. E. (2022) The carboxy-terminal tail of GLR3.3 is essential for wound-response electrical signaling. *New Phytologist*, 236, 2189-2201.
- Wu, X., Xu, S., Zhao, P., Zhang, X., Yao, X., Sun, Y., Fang, R. & Ye, J. (2019) The orthotospovirus nonstructural protein NSs suppresses plant MYC-regulated jasmonate signaling leading to enhanced vector attraction and performance. *PLoS Pathogens*, 15, e1007897.
- Wu, Y., Zhang, D., Chu, J. Y., Boyle, P., Wang, Y., Brindle, I. D., De Luca, V. & Després, C. (2012) The Arabidopsis NPR1 protein is a receptor for the plant defense hormone salicylic acid. *Cell Rep*, 1, 639-647.
- Wudick, M. M., Michard, E., Oliveira Nunes, C. & Feijó, J. A. (2018a) Comparing plant and animal glutamate receptors: Common traits but different fates? *Journal of Experimental Botany*, 69, 4151-4163.
- Wudick, M. M., Portes, M. T., Michard, E., Rosas-Santiago, P., Lizzio, M. A., Nunes, C. O., Campos, C., Santa Cruz Damineli, D., Carvalho, J. C., Lima, P. T., Pantoja, O. & Feijó, J. A. (2018b) CORNICHON sorting and regulation of GLR channels underlie pollen tube Ca²⁺ homeostasis. *Science*, 360, 533-536.
- Xia, Y., Yu, K., Navarre, D., Seebold, K., Kachroo, A. & Kachroo, P. (2010) The *glabra1* mutation affects cuticle formation and plant responses to microbes. *Plant Physiology* 154, 833-846.
- Xiao, Y., Stegmann, M., Han, Z., Defalco, T. A., Parys, K., Xu, L., Belkhadir, Y., Zipfel, C. & Chai, J. (2019) Mechanisms of RALF peptide perception by a heterotypic receptor complex. *Nature*, 572, 270-274.
- Xu, J., Meng, J., Meng, X., Zhao, Y., Liu, J., Sun, T., Liu, Y., Wang, Q. & Zhang, S. (2016) Pathogen-responsive MPK3 and MPK6 reprogram the biosynthesis of indole glucosinolates and their derivatives in Arabidopsis immunity. *The Plant Cell*, 28, 1144-1162.
- Xu, L., Yao, X., Zhang, N., Gong, B. Q. & Li, J. F. (2017) Dynamic G protein alpha signaling in Arabidopsis innate immunity. *Biochemical and Biophysical Research Communications*, 516, 1039-1045.
- Xue, D. X., Li, C. L., Xie, Z. P. & Staehelin, C. (2019) LYK4 is a component of a tripartite chitin receptor complex in *Arabidopsis thaliana*. *Journal of Experimental Botany*, 70, 5507-5516.
- Xue, J., Gong, B.-Q., Yao, X., Huang, X. & Li, J.-F. (2020) BAK1-mediated phosphorylation of canonical G protein alpha during flagellin signaling in Arabidopsis. *Journal of Integrative Plant Biology*, 62, 690-701.
- Xue, N., Zhan, C., Song, J., Li, Y., Zhang, J., Qi, J. & Wu, J. (2022) The glutamate receptor-like 3.3 and 3.6 mediate systemic resistance to insect herbivores in Arabidopsis. *Journal of Experimental Biology*, 73, 7611-7627.
- Yamada, K., Yamaguchi, K., Shirakawa, T., Nakagami, H., Mine, A., Ishikawa, K., Fujiwara, M., Narusaka, M., Narusaka, Y., Ichimura, K., Kobayashi, Y., Matsui, H., Nomura, Y., Nomoto, M., Tada, Y., Fukao, Y., Fukamizo, T., Tsuda, K., Shirasu, K., Shibuya, N. & Kawasaki, T. (2016) The Arabidopsis CERK1-associated kinase PBL27 connects chitin perception to MAPK activation. *The EMBO Journal*, 35, 2468-2483.
- Yamaguchi, Y., Huffaker, A., Bryan, A. C., Tax, F. E. & Ryan, C. A. (2010) PEPR2 is a second receptor for the Pep1 and Pep2 peptides and contributes to defense responses in Arabidopsis. *The Plant Cell*, 22, 508-522.
- Yamaguchi, Y., Pearce, G. & Ryan, C. A. (2006) The cell surface leucine-rich repeat receptor for AtPep1, an endogenous peptide elicitor in Arabidopsis, is functional in transgenic tobacco cells. *Proceedings of the National Academy of Sciences*, 103, 10104-10109.
- Yamanaka, T., Nakagawa, Y., Mori, K., Nakano, M., Imamura, T., Kataoka, H., Terashima, A., Iida, K., Kojima, I., Katagiri, T., Shinozaki, K. & Iida, H. (2010) MCA1 and MCA2 that mediate

- Ca²⁺ uptake have distinct and overlapping roles in Arabidopsis. *Plant Physiology*, 152, 1284-1296.
- Yamasaki, Y., Sumioka, H., Takiguchi, M., Uemura, T., Kihara, Y., Shinya, T., Galis, I. & Arimura, G. I. (2021) Phytohormone-dependent plant defense signaling orchestrated by oral bacteria of the herbivore *Spodoptera litura*. *New Phytologist*, 231, 2029-2038.
- Yan, C., Fan, M., Yang, M., Zhao, J., Zhang, W., Su, Y., Xiao, L., Deng, H. & Xie, D. (2018) Injury activates Ca²⁺/calmodulin-dependent phosphorylation of JAV1-JAZ8-WRKY51 complex for jasmonate biosynthesis. *Molecular Cell*, 70, 136-149.
- Yan, J., Zhang, C., Gu, M., Bai, Z., Zhang, W., Qi, T., Cheng, Z., Peng, W., Luo, H., Nan, F., Wang, Z. & Xie, D. (2009) The Arabidopsis CORONATINE INSENSITIVE1 protein is a jasmonate receptor. *Plant Cell*, 21, 2220-2236.
- Yang, D.-L., Shi, Z., Bao, Y., Yan, J., Yang, Z., Yu, H., Li, Y., Gou, M., Wang, S., Zou, B., Xu, D., Ma, Z., Kim, J. & Hua, J. (2017) Calcium pumps and interacting BON1 protein modulate calcium signature, stomatal closure, and plant immunity. *Plant Physiology*, 175, 424-437.
- Yang, Y., Liu, N., He, Y., Liu, Y., Ge, L., Zou, L., Song, S., Xiong, W. & Liu, X. (2018) Improved calcium sensor GCaMP-X overcomes the calcium channel perturbations induced by the calmodulin in GCaMP. *Nature Communications*, 9.
- Yasuda, R., Nimchinsky, E. A., Scheuss, V., Pologruto, T. A., Oertner, T. G., Sabatini, B. L. & Svoboda, K. (2004) Imaging calcium concentration dynamics in small neuronal compartments. *Science's STKE*, 2004, pl5-pl5.
- Yoshimura, K., Iida, K. & Iida, H. (2021) MCAs in Arabidopsis are Ca²⁺-permeable mechanosensitive channels inherently sensitive to membrane tension. *Nature Communications*, 12, 6074.
- Yoshinaga, N., Alborn, H. T., Nakanishi, T., Suckling, D. M., Nishida, R., Tumlinson, J. H. & Mori, N. (2010) Fatty acid-amino acid conjugates diversification in lepidopteran caterpillars. *Journal of Chemical Ecology*, 36, 319-325.
- Yoshinari, A., Moe-Lange, J., Kleist, T. J., Cartwright, H. N., Quint, D. A., Ehrhardt, D. W., Frommer, W. B. & Nakamura, M. (2021) Using genetically encoded fluorescent biosensors for quantitative in vivo imaging. In: SANCHEZ-SERRANO, J. J. & SALINAS, J. (eds.) *Arabidopsis protocols*. New York, NY: Springer US.
- Yoshioka, K., Moeder, W., Kang, H. G., Kachroo, P., Masmoudi, K., Berkowitz, G. & Klessig, D. F. (2006) The chimeric Arabidopsis CYCLIC NUCLEOTIDE-GATED ION CHANNEL11/12 activates multiple pathogen resistance responses. *Plant Cell*, 18, 747-763.
- Yu, H., Yan, J., Du, X. & Hua, J. (2018) Overlapping and differential roles of plasma membrane calcium ATPases in Arabidopsis growth and environmental responses. *Journal of Experimental Botany*, 69, 2693-2703.
- Yu, K., Liu, Y., Tichelaar, R., Savant, N., Lagendijk, E., Van Kuijk, S. J. L., Stringlis, I. A., Van Dijken, A. J. H., Pieterse, C. M. J., Bakker, P. a. H. M., Haney, C. H. & Berendsen, R. L. (2019a) Rhizosphere-associated *Pseudomonas* suppress local root immune responses by gluconic acid-mediated lowering of environmental pH. *Current Biology*, 29, 3913-3920.e3914.
- Yu, X., Xu, G., Li, B., De Souza Vespoli, L., Liu, H., Moeder, W., Chen, S., De Oliveira, M. V. V., Ariádina De Souza, S., Shao, W., Rodrigues, B., Ma, Y., Chhaged, S., Xue, S., Berkowitz, G. A., Yoshioka, K., He, P. & Shan, L. (2019b) The receptor kinases BAK1/SERK4 regulate Ca²⁺ channel-mediated cellular homeostasis for cell death containment. *Current Biology*, 29, 3778-3790.e3778.
- Yu, X. D., Liu, Z. C., Huang, S. L., Chen, Z. Q., Sun, Y. W., Duan, P. F., Ma, Y. Z. & Xia, L. Q. (2016) RNAi-mediated plant protection against aphids. *Pest Management Science*, 72, 1090-1098.
- Yuan, F., Yang, H., Xue, Y., Kong, D., Ye, R., Li, C., Zhang, J., Theprungsirikul, L., Shrift, T., Krichilsky, B., Johnson, D. M., Swift, G. B., He, Y., Siedow, J. N. & Pei, Z.-M. (2014) OSCA1 mediates osmotic-stress-evoked Ca²⁺ increases vital for osmosensing in Arabidopsis. *Nature*, 514, 367-371.

- Yuan, H. M., Liu, W. C. & Lu, Y. T. (2017) CATALASE2 coordinates SA-mediated repression of both auxin accumulation and JA biosynthesis in plant defenses. *Cell Host Microbe*, 21, 143-155.
- Yuan, M., Jiang, Z., Bi, G., Nomura, K., Liu, M., He, S. Y., Zhou, J.-M. & Xin, X.-F. (2020) Pattern-recognition receptors are required for NLR-mediated plant immunity. *bioRxiv*, 2020.2004.2010.031294.
- Yuan, M., Ngou, B. P. M., Ding, P. & Xin, X.-F. (2021) PTI-ETI crosstalk: An integrative view of plant immunity. *Current Opinion in Plant Biology*, 62, 102030.
- Zandalinas, S. I., Fichman, Y. & Mittler, R. (2020) Vascular bundles mediate systemic reactive oxygen signaling during light stress in Arabidopsis. *The Plant Cell*, 32, 3425-3435.
- Zelman, A. K., Dawe, A., Berkowitz, G. A. & Gehring, C. (2012) Evolutionary and structural perspectives of plant cyclic nucleotide-gated cation channels. *Frontiers in Plant Science*, 3, 95.
- Zhang, C., Žukauskaitė, A., Petřík, I., Pěňčík, A., Höning, M., Grúz, J., Šíroká, J., Novák, O. & Doležal, K. (2021a) *In situ* characterisation of phytohormones from wounded Arabidopsis leaves using desorption electrospray ionisation mass spectrometry imaging. *Analyst*, 146, 2653-2663.
- Zhang, H., Xie, P., Xu, X., Xie, Q. & Yu, F. (2021b) Heterotrimeric G protein signalling in plant biotic and abiotic stress response. *Plant Biology*, 23, 20-30.
- Zhang, H., Zhang, H. & Lin, J. (2020) Systemin-mediated long-distance systemic defense responses. *New Phytologist*, 226, 1573-1582.
- Zhang, M., Wang, D., Kang, Y., Wu, J.-X., Yao, F., Pan, C., Yan, Z., Song, C. & Chen, L. (2018) Structure of the mechanosensitive OSCA channels. *Nature Structural & Molecular Biology*, 25, 850-858.
- Zhang, M. & Zhang, S. (2022) Mitogen-activated protein kinase cascades in plant signaling. *Journal of Integrative Plant Biology*, 64, 301-341.
- Zhang, Y., Fan, W., Kinkema, M., Li, X. & Dong, X. (1999) Interaction of NPR1 with basic leucine zipper protein transcription factors that bind sequences required for salicylic acid induction of the PR-1 gene. *Proceedings of the National Academy of Sciences*, 96, 6523-6528.
- Zhang, Y., Liu, X., Francis, F., Xie, H., Fan, J., Wang, Q., Liu, H., Sun, Y. & Chen, J. (2022) The salivary effector protein Sg2204 in the greenbug *Schizaphis graminum* suppresses wheat defence and is essential for enabling aphid feeding on host plants. *Plant Biotechnology Journal*, 20, 2187-2201.
- Zhang, Y., Rózsa, M., Liang, Y., Bushey, D., Wei, Z., Zheng, J., Reep, D., Broussard, G. J., Tsang, A., Tsegaye, G., Narayan, S., Obara, C. J., Lim, J.-X., Patel, R., Zhang, R., Ahrens, M. B., Turner, G. C., Wang, S. S.-H., Korff, W. L., Schreiter, E. R., Svoboda, K., Hasseman, J. P., Kolb, I. & Looger, L. L. (2021c) Fast and sensitive GCaMP calcium indicators for imaging neural populations. *bioRxiv*, 2021.11.08.467793.
- Zhang, Y., Tessaro, M. J., Lassner, M. & Li, X. (2003) Knockout analysis of Arabidopsis transcription factors TGA2, TGA5, and TGA6 reveals their redundant and essential roles in systemic acquired resistance. *The Plant Cell*, 15, 2647-2653.
- Zhang, Y., Xu, S., Ding, P., Wang, D., Cheng, Y. T., He, J., Gao, M., Xu, F., Li, Y. & Zhu, Z. (2010) Control of salicylic acid synthesis and systemic acquired resistance by two members of a plant-specific family of transcription factors. *Proceedings of the National Academy of Sciences*, 107, 18220-18225.
- Zhang, Z., Tong, X., Liu, S.-Y., Chai, L.-X., Zhu, F.-F., Zhang, X.-P., Zou, J.-Z. & Wang, X.-B. (2019) Genetic analysis of a Piezo-like protein suppressing systemic movement of plant viruses in *Arabidopsis thaliana*. *Scientific Reports*, 9, 3187.
- Zhao, C., Tang, Y., Wang, J., Zeng, Y., Sun, H., Zheng, Z., Su, R., Schneeberger, K., Parker, J. E. & Cui, H. (2021a) A mis-regulated cyclic nucleotide-gated channel mediates cytosolic calcium elevation and activates immunity in Arabidopsis. *New Phytologist*, 230, 1078-1094.

- Zhao, J., Li, L., Liu, Q., Liu, P., Li, S., Yang, D., Chen, Y., Pagnotta, S., Favery, B., Abad, P. & Jian, H. (2019) A MIF-like effector suppresses plant immunity and facilitates nematode parasitism by interacting with plant annexins. *Journal of Experimental Botany*, 70, 5943-5958.
- Zhao, Y., Araki, S., Wu, J., Teramoto, T., Chang, Y. F., Nakano, M., Abdelfattah, A. S., Fujiwara, M., Ishihara, T., Nagai, T. & Campbell, R. E. (2011) An expanded palette of genetically encoded Ca²⁺ indicators. *Science*, 333, 1888-1891.
- Zhao, Y., Zhang, S., Luo, J.-Y., Wang, C.-Y., Lv, L.-M., Wang, X.-P., Cui, J.-J. & Lei, C.-L. (2016) Bt proteins Cry1Ah and Cry2Ab do not affect cotton aphid *Aphis gossypii* and ladybeetle *Propylea japonica*. *Scientific Reports*, 6, 20368-20368.
- Zhao, Z.-X., Xu, Y.-J., Lei, Y., Li, Q., Zhao, J.-Q., Li, Y., Fan, J., Xiao, S. & Wang, W.-M. (2021b) ANNEXIN 8 negatively regulates RPW8.1-mediated cell death and disease resistance in Arabidopsis. *Journal of Integrative Plant Biology*, 63, 378-392.
- Zhao, Z., Fan, J., Gao, Y. G., Wang, Z., Yang, P., Liang, Y., Opiyo, S. & Xia, Y. (2022) Arabidopsis plasma membrane ATPase AHA5 is negatively involved in PAMP-triggered immunity. *International journal of molecular sciences*, 23, 3857.
- Zheng, X. Y., Spivey, N. W., Zeng, W., Liu, P. P., Fu, Z. Q., Klessig, D. F., He, S. Y. & Dong, X. (2012) Coronatine promotes *Pseudomonas syringae* virulence in plants by activating a signaling cascade that inhibits salicylic acid accumulation. *Cell Host Microbe*, 11, 587-596.
- Zheng, Y., Wang, L.-B., Sun, S.-F., Liu, S.-Y., Liu, M.-J. & Lin, J. (2021) Phylogenetic and ion-response analyses reveal a relationship between gene expansion and functional divergence in the Ca²⁺/cation antiporter family in angiosperms. *Plant Molecular Biology*, 105, 303-320.
- Zhou, F., Emonet, A., Dénervaud Tendon, V., Marhavy, P., Wu, D., Lahaye, T. & Geldner, N. (2020) Co-incidence of damage and microbial patterns controls localized immune responses in roots. *Cell*, 180, 440-453.
- Zhou, J.-M., Trifa, Y., Silva, H., Pontier, D., Lam, E., Shah, J. & Klessig, D. F. (2000) NPR1 differentially interacts with members of the TGA/OBF family of transcription factors that bind an element of the PR-1 gene required for induction by salicylic acid. *Molecular Plant-Microbe Interactions*, 13, 191-202.
- Zhou, L. H., Liu, S. B., Wang, P. F., Lu, T. J., Xu, F., Genin, G. M. & Pickard, B. G. (2017) The Arabidopsis trichome is an active mechanosensory switch. *Plant, Cell & Environment*, 40, 611-621.
- Zhou, S. & Jander, G. (2021) Molecular ecology of plant volatiles in interactions with insect herbivores. *Journal of Experimental Botany*, 73, 449-462.
- Zou, Y., Chintamanani, S., He, P., Fukushige, H., Yu, L., Shao, M., Zhu, L., Hildebrand, D. F., Tang, X. & Zhou, J.-M. (2016) A gain-of-function mutation in Msl10 triggers cell death and wound-induced hyperaccumulation of jasmonic acid in Arabidopsis. *Journal of Integrative Plant Biology*, 58, 600-609.
- Züst, T. & Agrawal, A. A. (2016) Mechanisms and evolution of plant resistance to aphids. *Nature Plants*, 2, 16206.